# Radar remote sensing to support tropical forest management

J.J. van der Sanden



Tropenbos - Guyana Series 5



# Radar remote sensing to support tropical forest management

Promotoren: Dr.ir. R.A. Feddes
Hoogleraar bodemnatuurkunde, agrohydrologie en grondwaterbeheer

Dr.ir. R.A.A. Oldeman
Hoogleraar bosteelt en bosecologie

Co-promotor: Dr.ir. D.H. Hoekman
Universitair hoofddocent bij het departement omgevingswetenschappen

J.J. van der Sanden

# Radar remote sensing to support tropical forest management

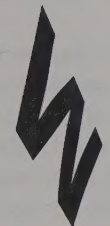
Proefschrift
ter verkrijging van de graad van doctor
op gezag van de rector magnificus
van de Landbouwuniversiteit Wageningen,
Dr. C.M. Karssen,
in het openbaar te verdedigen
op dinsdag 9 december 1997,
des namiddags te 16.00 uur in de Aula

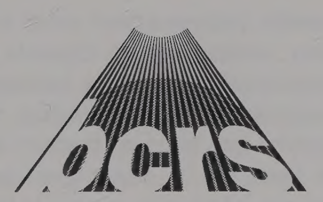
The Tropenbos-Guyana Series publishes results of research projects carried out in the framework of the Tropenbos-Guyana Programme. The Tropenbos-Guyana Programme operates within the framework of the international Programme of the Tropenbos Foundation. The multi-disciplinary Tropenbos-Guyana Programme contributes to conservation and wise utilisation of forest resources in Guyana by conducting strategic and applied research and upgrading Guyanese capabilities in the field of forest-related sciences.

J.J. van der Sanden
Radar remote sensing to support tropical forest management
Tropenbos-Guyana Series 5
Tropenbos-Guyana Programme, Georgetown, Guyana
ISBN 90 - 5485 - 778 - 1
Keywords: remote sensing, radar, tropical rain forest, forest resource assessment, forest resource monitoring, sustainable forest management



Printed by Ponsen & Looijen bv, Wageningen
Cover: C-, L-, P-band colour composite radar image showing the West Pibiri compartment in Mabura Hill, Guyana. Images acquired by the NASA/JPL AIRSAR system. P-band total power image shown in red, L-band total power image shown in green and C-band total power image shown in blue. Image processing by Martin Vissers.









The investigations reported in this text were carried out at the Department of Water Resources of the Wageningen Agricultural University, with funding from the Netherlands Remote Sensing Board (BCRS) and within the framework of the Tropenbos-Guyana Programme.

Department of Water Resources, Wageningen Agricultural University, Nieuwe Kanaal 11, 6709 PA Wageningen, The Netherlands, http://www.slm.wau.nl/whh/rs/ .
Netherlands Remote Sensing Board (BCRS), P.O. Box 5023, 2600 GA Delft, The Netherlands, http://www.minvenw.nl/rws/mdi/bcrs/en/ .
Tropenbos-Guyana Programme, Lot 12 E Garnettstreet, Campbellville, Georgetown, Guyana, http://www.tropenbos.nl/ .

Publication was made possible by the financial support of the Tropenbos-Guyana Programme and the Wageningen Agricultural University.

## Abstract

van der Sanden, J.J., 1997. *Radar remote sensing to support tropical forest management*. Wageningen, The Netherlands (Wageningen Agricultural University), Tropenbos-Guyana Series 5, doctoral thesis, 330 p.

This text describes an investigation into the potential of radar remote sensing for application to tropical forest management. The information content of various radar images is compared and assessed with regard to the information requirements of parties involved in tropical forest management at the global, national and local spatial levels. The study distinguishes between the use of radar remote sensing for application to forest resource assessment and forest resource monitoring. Both assessment and monitoring are essential components of procedures for sustainable forest management. The radar data studied are of tropical forest areas near the township of Mabura Hill in Guyana and the city of San José del Guaviare in Colombia. Mabura Hill is comprised of differing intact, primary forest types and forests that have been subjected to industrial selective logging. San José del Guaviare, on the other hand, is characterised by the presence of secondary forests and a variety of non-forest cover types. The available radar data set includes high resolution airborne radar images with differing wavelengths (i.e. X-, C-, L- and P-band) and polarizations, time-series images acquired by the first European remote sensing satellite ERS-1 and a collection of low altitude, nadir-looking, X-band scatterometer measurements.

The study makes use of three fundamentally different information sources from the radar return signal: its strength or backscatter, polarization and phase, and spatial variability or texture. Results show that backscatter values computed from L- and P-band radar data and textural attributes computed from high resolution X- and C-band radar data make modest to good and complementary bases for region-based classification of tropical land cover at the level of primary forest types. Textural attributes and backscatter values computed per region from mono-temporal ERS-1 images make modest bases for classifying at the levels of primary forest, logged-over forest, secondary forest and non-forest and poor bases for classifying at the level of primary forest types. Roads are usually the most easily observable indicators of foregoing and/or forthcoming (selective) logging and other human activities in ERS-1 images. Detection of change in road networks by means of ERS-1 images would make a good first step in forest resource monitoring at the national spatial level, in particular. Textural attributes enable the ranking of forest types according to the degree of canopy roughness. Specific textural attributes also allow for quantification of canopy architectural properties. Despite differences in measurement scale, the canopy roughness of the land cover types studied was found to appear similarly in the texture of the available spaceborne and short wavelength airborne radar images.

Keywords: remote sensing, radar, tropical rain forest, forest resource assessment, forest resource monitoring, sustainable forest management.

## Preface

Research into the use of radar remote sensing for application to forestry first started for me in 1984 as a three months project during my M.Sc. studies at the Wageningen Agricultural University (WAU). It has, with a number of diversions, now resulted in this doctoral thesis. From the beginning, my enthusiastic and knowledgeable guide has been dr.ir. Dirk H. Hoekman. As well as guiding me through the somewhat treacherous field of radar remote sensing, he introduced me to the art of external fund acquisition. Together we succeeded in obtaining the funds on the basis of which I was employed by the WAU for a period of over eight years. To Dirk Hoekman, my co-promotor, I want to direct my first and special acknowledgements. My promotors Prof.dr.ir. R.A. Feddes and Prof.dr.ir. R.A.A. Oldeman are also much appreciated for the supervision of my work and their constructive criticism during the realisation of this text.

The investigations described were carried out within the framework of the Dutch National Remote Sensing Programme (NRSP) under the responsibility of the Netherlands Remote Sensing Board (BCRS). I wish to express my gratitude to the BCRS for the financial support given and the confidence trusted in me. The Tropenbos Foundation, the Tropenbos-Colombia team and Demerara Timbers Ltd. are acknowledged for their kind cooperation and logistical support during field visits. I am especially grateful to the members of the Tropenbos-Guyana team who provided me with transportation, accommodated me in their field camps and houses, guided me through Georgetown and the Mabura Hill study area, and taught me their knowledge of the forest. Moreover they shared with me their home-cooked diners, military rations, imported potato chips and local beer. The Tropenbos-Guyana Programme is acknowledged for publishing this thesis in its series.

The radar data studied were made available by the European Space Agency (ESA) and the National Aeronautics and Space Administration (NASA). I owe these organisations many thanks for initiating their respective South American radar campaigns and for including the areas of interest to this study in the flight plans. I also want to acknowledge the Colombian and Guyanese aviation authorities for providing the clearance for the various radar over flights. Without the cooperation of these space organisations and national authorities this study would not have succeeded.

Part of the work presented in this text was carried out during my six months stay as a visiting scientist with the Canada Centre for Remote Sensing (CCRS). Dr. Frank J. Ahern is much appreciated for giving me this opportunity. To him and other CCRS employees and visiting scientists I want to express my gratitude for sharing with me their ideas and knowledge. I especially want to thank my helpful roommate and PCI EASI/PACE instructor Ron Pietsch. The mentioned producer of image analysis software is acknowledged for providing me with the source code of the module for textural processing by means of a moving window.

I wish to acknowledge my colleagues, initially at the Department of Land Surveying and Remote Sensing and later at the Department of Water Resources of the WAU,

who provided me a productive and pleasant working environment. I am particularly grateful to ir. Martin A.M. Vissers for his assistance in collecting forest data in Guyana and his outstanding technical support at the Department of Water Resources. The help of students of the WAU was also appreciated. I want to thank ir. Gerard Sicco Smit and dr.ir. Wietske Bijker from the International Institute for Aerospace Survey and Earth Sciences (ITC) for their collaboration on the BCRS project in the framework of which the research presented was carried out. Gerard Sicco Smit is also thanked for his helpful comments on chapter 4 of this text. Laurel Hyatt and Heine de Vries are acknowledged for editing and correcting the English manuscript and the Dutch summary, respectively.

Finally, I would like to express my gratitude to my friends and family who encouraged me and at times provided the distraction needed to complete this thesis. Many of them deserved more attention than I was able to give them in recent years. During the final phase of the writing, ample distraction was given to me by my newborn son Jeffrey. I am especially grateful to my beloved wife Rosemary Gillott who supported me and showed great patience throughout my work. Rosemary is also acknowledged for her contribution to correcting the syntax and spelling of the English text.

# Contents

## List of abbreviations

| Abbreviation | Description |
|---|---|
| ATSR-1 | Along Track Scanning Radiometer-1 |
| AVHRR | Advanced Very-High-Resolution Radiometer |
| BCRS | The Netherlands Remote Sensing Board |
| CCRS | Canada Centre for Remote Sensing |
| CEC | Commission of the European Communities |
| ECE | Economic Commission for Europe |
| ENVISAT-1 | First Environmental Satellite |
| EOPP | Earth Observation Preparatory Programme |
| ERS-1/2 | First/Second European Remote Sensing Satellite |
| ESA | European Space Agency |
| FAO | Food and Agriculture Organisation of the United Nations |
| FRA90 | Forest Resources Assessment 1990 |
| GAC | Global Area Coverage |
| GLCO | Grey-level co-occurrence |
| HH | Horizontal transmit - Horizontal receive polarization |
| HRV | High-Resolution-Visible |
| HV | Vertical transmit - Horizontal receive polarization |
| IR | Infrared |
| ITC | International Institute for Aerospace Survey and Earth Sciences |
| ITTA | International Tropical Timber Agreement |
| ITTO | International Tropical Timber Organisation |
| JERS-1 | Japanese Earth Resources Satellite |
| JPL | Jet Propulsion Laboratory |
| LAC | Local Area Coverage |
| LIDAR | Light Detection And Ranging |
| LL | Left-hand circular transmit - Left-hand circular receive polarization |
| LR | Right-hand circular transmit - Left-hand circular receive polarization |
| MSS | Multi Spectral Scanner |
| NASA | National Aeronautics and Space Administration |
| NGO | Non Governemental Organisation |
| NOAA | National Oceanic and Atmospheric Administration |
| PAN | Panchromatic |
| PPD | Polarization Phase Difference of HH and VV |
| RADARSAT | (Canadian) Radar satellite |
| RR | Right-hand circular transmit - Right-hand circular receive polarization |

| | |
|---|---|
| SAR | Synthetic Aperture Radar |
| SAREX-92 | South American Radar Experiment 1992 |
| SAR.PRI | SAR Precision image |
| SAR.SLC | SAR Single Look Complex image |
| SIR-A/B/C | Shuttle Imaging Radar A/B/C |
| SLR | Side-looking radar |
| SPOT | Système Probatoire d'Observation de la Terre |
| TIR | Thermal Infrared |
| TM | Thematic Mapper |
| TP | Total backscattered power |
| TREES | TRopical Ecosystem Environment observation by Satellite |
| UN | United Nations |
| UNCED | United Nations Conference on Environment and Development |
| UNCTAD | United Nations Conference on Trade and Development |
| UNEP | United Nations Environment Programme |
| VH | Horizontal transmit - Vertical receive polarization |
| VIS | Visible |
| VV | Vertical transmit - Vertical receive polarization |
| WAU | Wageningen Agricultural University |
| WCMC | World Conservation Monitoring Centre |
| XS | Multispectral |

## List of symbols

| Symbol | Unit | Description |
|---|---|---|
| $A$ | V m$^{-1}$ | Amplitude of electric field intensity |
| $\boldsymbol{A}$ | W m$^{-2}$ sr$^{-1}$ | Normalized Stokes vector |
| $\boldsymbol{A}^r$ | W m$^{-2}$ sr$^{-1}$ | Normalized Stokes vector of received wave |
| $\boldsymbol{A}^t$ | W m$^{-2}$ sr$^{-1}$ | Normalized Stokes vector of scattered wave |
| $A_{res}$ | m$^2$ | Resolution cell area |
| $c$ | m s$^{-1}$ | Speed of light |
| $\boldsymbol{c}_i$ | – | Covariance matrix for class $i$ |
| $\boldsymbol{c}_i^{-1}$ | – | Inverse covariance matrix for class $i$ |
| $d$ | cm | Diameter at breast height or dbh |
| $\boldsymbol{d}$ | – | Displacement vector or "lag" |
| $D_{ij}$ | – | Pairwise divergence for class pair $(i, j)$ |
| $\boldsymbol{E}_h$ | N c$^{-1}$ | Horizontal polarized electrical field vector |
| $\boldsymbol{E}_v$ | N c$^{-1}$ | Vertical polarized electrical field vector |
| $f_d$ | – | Double bounce scatter contribution to VV backscatter |
| $f_s$ | – | Odd bounce (or surface) scatter contribution to VV backscatter |
| $f_v$ | – | Diffuse (or volume) scatter contribution to VV backscatter |
| $\boldsymbol{F}$ | W m$^{-2}$ sr$^{-1}$ | Stokes vector |
| $\boldsymbol{F}^i$ | W m$^{-2}$ sr$^{-1}$ | Stokes vector of incident wave |
| $\boldsymbol{F}^s$ | W m$^{-2}$ sr$^{-1}$ | Stokes vector of scattered wave |
| $H$ | m | Flight altitude |
| $\bar{I}^2$ | W | Mean backscattered power |
| $j$ | – | Unit of complex number along imaginary axis $(\sqrt{-1})$ |
| $k$ | – | Number of independent looks |
| $k_0$ | rad m$^{-1}$ | Wave number in free space, $2\pi/\lambda_0$ |
| $\boldsymbol{L}$ | – | Stokes or Mueller matrix |
| $\boldsymbol{m}_i$ | – | Mean vector for class $i$ |
| $\boldsymbol{M}$ | – | Stokes scattering operator |
| $M_{ij}$ | – | Element $i,j$ of the Stokes scattering operator |
| $\boldsymbol{p}$ | – | Polarization vector |
| $\boldsymbol{p}^i$ | – | Polarization vector of incident wave |
| $\boldsymbol{p}^r$ | – | Polarization vector of received wave |
| $\boldsymbol{p}^s$ | – | Polarization vector of scattered wave |
| $\boldsymbol{p}^t$ | – | Polarization vector of transmitted wave |
| $p(i, j)$ | – | Grey level co-occurrence matrix |
| | | Refer to Table 5.1 for symbols used in textural descriptors |

| | | |
|---|---|---|
| $r_R$ | m | Slant range resolution |
| $r_y$ | m | Ground range resolution |
| $R$ | m | Slant range distance |
| $\boldsymbol{R}$ | – | Matrix relating $\boldsymbol{M}$ to $\boldsymbol{L}$ |
| $R_g$ | m | Ground range distance |
| $s_i$ | – | Element $i$ of Stokes vector |
| $\boldsymbol{S}$ | – | Scattering matrix |
| $S_{ij}$ | – | Element $i,j$ of scattering matrix |
| $\boldsymbol{S}'$ | – | $\begin{pmatrix} 1 & 0 \\ 0 & -1 \end{pmatrix}\boldsymbol{S}$ |
| $S'_{ij}$ | – | Element $i,j$ of $\boldsymbol{S}'$ |
| $S^2_{tot}$ | – | Total image variance |
| $S^2_F$ | – | Image fading variance |
| $S^2_T$ | – | Image texture variance |
| $S^2_z$ | – | Variance of observations on property $Z$ |
| $TD_{ij}$ | – | Pairwise transformed divergence for class pair $(i, j)$ |
| $\gamma$ | $m^2\ m^{-2}$ | Radar cross section per unit projected area |
| $\hat{\gamma}(\boldsymbol{d})$ | – | Estimated average semi-variance at "lag" $\boldsymbol{d}$ |
| $\delta_p$ | m | Depth of vertical penetration |
| $\varepsilon_c$ | farad $m^{-1}$ | Complex dielectric constant |
| $\varepsilon_r$ | – | Relative complex dielectric constant |
| $\varepsilon'_r$, $\varepsilon''_r$ | – | Real, imaginary part of $\varepsilon_r$ |
| $\varepsilon_0$ | farad $m^{-1}$ | Dielectric constant of free space |
| $\lambda$ | m | Wavelength |
| $\lambda_0$ | m | Free-space wavelength |
| $\theta_{el}$ | rad | Elevation angle |
| $\theta_{gr}$ | rad | Grazing angle |
| $\theta_{inc}$ | rad | Incidence angle |
| $\hat{\rho}(\boldsymbol{d})$ | – | Estimated average autocorrelation coefficient at "lag" $\boldsymbol{d}$ |
| $\sigma$ | $m^2$ | Radar cross section |
| $\sigma_{ij}$ | $m^2$ | Radar cross section in case of $i$ receive and $j$ transmit polarization |
| $\sigma^\circ$ | $m^2\ m^{-2}$ | Differential radar cross section |
| $\tau$ | s | Pulse duration |
| $\phi$ | rad | Phase |
| $\phi_h$ | rad | Phase of horizontal polarized electrical field vector |
| $\phi_v$ | rad | Phase of vertical polarized electrical field vector |
| $\phi_{ij}$ | rad | Phase in case of $i$ receive and $j$ transmit polarization |

| | | |
|---|---|---|
| $\Delta\phi$ | rad | Phase difference between horizontal and vertical polarized electrical field components |
| $\chi$ | rad | Ellipticity angle |
| $\chi_r$ | rad | Ellipticity angle of received wave |
| $\chi_t$ | rad | Ellipticity angle of transmitted wave |
| $\psi$ | rad | Orientation angle |
| $\psi_r$ | rad | Orientation angle of received wave |
| $\psi_t$ | rad | Orientation angle of transmitted wave |

# 1 Introduction

## 1.1 Rationale and objective

Among scientists, politicians and the public at large there is a still growing concern about the future of our natural environment in general and tropical rain forests in particular. Issues contributing to the explicit concern for forest resources in the humid tropics include: the alarming rate of tropical rain forest depletion; the potentially disastrous effects of deforestation on soil, water, climate, genetic richness and the future supply of economic products; the notion that the forest land is mostly converted to unsustainable uses and the fact that deforestation is often accompanied by violation of the rights of indigenous forest-dwelling people (Jacobs et al., 1988; Poore et al., 1989). The widespread concern is strengthened by uncertainty resulting from a present lack of accurate and/or up to date information on the state, extent and rate of change of tropical rain forests. This lack of information also hinders the development of programmes in support of and procedures for sustainable forest management.

The world's political leaders acknowledged the concern about tropical rain forest resources in, among others, the agreements negotiated during the 1992 United Nations Conference on Environment and Development (UNCED) in Rio de Janeiro, Brazil. The *need for more and better information on tropical rain forests* in particular is expressed strongly in the recommendations of an agreement commonly referred to as 'Agenda 21' (UNCED, 1992; Lanly, 1992). In general, the collection of information on rain forests is complicated by their enormous extent, poor accessibility, intricate constitution and dynamic nature. *Remote sensing systems* have the capability to image the Earth's surface in a systematic, synoptic and repetitive manner. Hence, these systems *make potentially outstanding tools for collecting up to date information to support the management of extensive natural resources of difficult access, such as tropical rain forests.*

The potential of remote sensing for application to the management of tropical forests and other land resources is acknowledged in the recommendations 7.33 and 11.36 of Agenda 21. These recommendations read as follows:

"7.33. All countries, particularly developing countries, alone or in regional or sub regional groupings, should be given access to modern techniques of land-resource management such as geographical information systems, satellite photography / imagery and other remote sensing technologies."

"11.36. Assessment and systematic observation activities involve major research efforts, statistical modelling and technological innovation. These have been internalised into the management-related activities. The activities in turn will improve the technological and scientific content of assessment and periodical evaluations.

Some of the specific scientific and technological components included under these activities are:

a) Developing technical, ecological and economic methods and models related to periodical evaluations;
b) Developing data systems, data processing and statistical modelling;
c) Remote sensing and ground surveys;
d) Developing geographical information systems;
e) Assessing and improving technology."

*The present study* addresses components c and e of the recommendation 11.36. It *aims to assess the potential of radar or microwave remote sensing for application to the management of tropical rain forests. To this end, the information content of images acquired by differing radar systems is evaluated and compared to the information requirements of parties involved in tropical forest management.* Development of new techniques for extracting information on tropical forests from radar images is not an objective of the present study. Instead the aim is to evaluate existing techniques for radar image analysis and to investigate how these techniques can be optimised for the application studied. Since tropical rain forests typically occur in poorly surveyed regions, the study does not apply image analysis techniques that require geographically-referenced ancillary data on, for example, terrain physiography, infrastructure, soil type and vegetation type.

The study distinguishes between the application of radar remote sensing to forest resource assessment and forest resource monitoring. Forest resource assessment is defined as the procedure for collecting, processing and presenting forest data. It usually results in a description of the location, extent and/or constitution of a certain forest area at a particular point in time. Forest resource monitoring, on the other hand, is defined as the process of continuously knowing the state of the forest environment and the changes that have and are taking place. Hence, it requires collecting, processing and presenting successive data on the location, extent and nature of changes. In order to plan and guide changes it is also important to gather information on the cause and rate of change. Forest resource assessment and monitoring are linked processes. Reliable monitoring of forest resources is feasible only if the starting point is well described by means of forest resource assessment. The processes of forest resource assessment and monitoring are essential parts of procedures for sustainable forest management.

## 1.2 Outline of the present text

Following the present introduction, the text continues with Chapter 2 which describes the individuals and organisations involved in tropical forest management, the spatial level at which they operate and their information requirements. All differing parties with a need for information on tropical forest resources are in fact potential users of the radar remote sensing data and analysis techniques studied. Chapter 2 also reviews selected publications on the potential of optical and radar remote sensing systems as tools for collecting information on tropical rain forests.

Chapter 3 introduces the reader to the principles of radar remote sensing and the terminology used in the present text. The chapter starts with an introduction to the basic concept of radar, the operating principles of radar systems used in remote sensing, the characteristics of radar signals, the specific properties of radar images and the concepts of radar polarimetry. This is followed by a discussion on the manner in which radar waves or microwaves interact with forests and on how this interaction is affected by microwave characteristics and forest properties.

The study areas selected and the available radar remote sensing data are the subjects of Chapter 4. A general description of the principal study area near Mabura Hill, Guyana and the additional study area near San José del Guaviare, Colombia is followed by an outline of the procedure adopted to collect ground reference data and detailed descriptions of the forest types studied. Data compiled on the structure of primary forest types present in Mabura Hill are summarised in Appendix III. The last section of Chapter 4 reports on the radar campaigns that provided the data analysed in the present study and lists the specifications of sensor systems deployed.

Chapter 5 discusses the methods and techniques used to extract information from the radar data sets studied and to appraise the value of this information for the identification of forest types and other land cover types, in particular. The available radar data sets are analysed according to two complementary approaches, i.e. analysis by means of image regions and pixel-per-pixel image processing techniques. Analysis of image texture by means of a technique based on grey level co-occurrence proved to be of great importance to the present study and is therefore described in detail.

The results and conclusions of the analysis of the potential of the available X-, C-, L- and P-band radar data to support forest resource assessment are presented in Chapter 6. Three fundamentally different information sources from the radar return signal are investigated: its strength (backscatter), polarization and phase, and spatial variability. Spatial variations of the radar return signal are conceived as image texture. The emphasis is on analysis in view of the application of radar to land cover type classification because this usually makes up the first step in forest resource assessment procedures. Chapter 6 also discusses the potential value of the available radar data for estimating biomass parameters and forest architectural parameters. Texture is an important source of information, especially in high resolution X- and C-band radar images. Details concerning the automated analysis of texture in radar images according to the grey level co-occurrence approach are presented in Appendix I.

Results and conclusions of investigations into the potential of radar images acquired by the first European remote sensing satellite ERS-1 to support forest resource monitoring are reported in Chapter 7. The chapter first discusses the temporal change in ERS-1 backscatter measurements for stretches of forest that are free of natural disturbance and human impact. This is followed by a discussion on the capabilities of ERS-1 to detect forest cover change resulting from industrial selective logging, in particular. Chapter 7 also reports on techniques for automated detection of change in radar images.

Considering the user requirements discussed in Chapter 2 and the analysis results given in Chapters 6 and 7, the last chapter of this text elaborates on the potential of radar remote sensing to support the management of tropical rain forests. After an assessment of the applicability of radar to forest management at global, national and local spatial levels, Chapter 8 continues with a discussion on radar data acquisition and analysis strategies or, in other words, on the implementation of radar remote sensing as a tool in tropical forest management.

# 2 User requirements and the potential of remote sensing

## 2.1 Users and their information requirements

In times past the management of tropical rain forests was primarily a topic of local and national concern. However, the ongoing world-wide depletion of this resource has made its management a point of significant global interest. *Today, individuals and organisations with a need for information on tropical forests, i.e. potential users of radar remote sensing data, operate roughly at three spatial levels: the global (or international) level, the national level and the local (or forest management unit) level.* The level of operation and the objectives of the user determine the spatial extent, the detail and the type of information required. Descending from the global to the local level the following trends in the information needs may be observed. First, the area for which information is needed decreases. Second, the information required is of an increasingly fine spatial detail. Third, the information needs diversify and become more specific.

The Food and Agriculture Organisation of the United Nations (FAO) and the World Conservation Monitoring Centre (WCMC) are examples of organisations that operate at the global level. These organisations typically require information on items such as the global extent of tropical rain forests and the world-wide rates of deforestation and forest degradation. Examples of users mostly interested in information at the national level are governmental organisations such as ministries, forest services and planning agencies. At this level needs for information concern, for instance, the location, extent and state of forest concession areas leased by logging companies. Forest concessionaires and forest plantation owners are examples of users at the local level. To plan their operations these users may require information on the location of areas with unfavourable conditions (steep slopes, poor drainage etc.) or the distribution of forest types with a high proportion of commercially valuable species.

The users identified so far are managers, policy makers, planners and/or controllers. An additional group of users is found in the scientific community. Scientists with an interest in tropical rain forests are active on all spatial levels and have a wide range of often very specific objectives. Hence, their information requirements vary widely and are difficult to pinpoint. The present text acknowledges but does not elaborate on the needs of scientific users. However, the information needs of scientists and other users overlap considerably. After all, many requirements of non-scientific users will be inspired by results of scientific research and, the other way around, research often addresses practical problems. The information needs of non-scientific users who operate at the global level are discussed in detail in section 2.1.1. Similarly, sections 2.1.2 and 2.1.3 elaborate on the needs of non-scientific users at the national and local level, respectively. Sections 2.1.1 through 2.1.3 discuss the *essential* users and information requirements. The overview presented is by no means exhaustive or exclusive. Experience shows that especially the inventory of user requirements is an invariably recurring and permanently difficult task.

### 2.1.1 Requirements at the global level

The FAO may be considered the most important user at the global level since it has the United Nations (UN) mandate for the world-wide inventory and monitoring of tropical and other forest resources. *The global information needs are discussed in international expert panels and dictated by major environmental issues*, i.e. (changes in) biodiversity, the carbon cycle, the hydrological cycle, forest condition and land cover / land use. The information requested serves as a basis for policy making and control of parties operating at the national level. Table 2.1 presents a series of parameters that are needed to assess the mentioned global environmental issues. The parameters listed were discussed during the UNEP/FAO Expert Consultation on Environmental Parameters in Future Global Forest Assessments and the FAO/ECE Meeting of Experts on Global Forest Resources Assessment (UNEP/FAO, 1993; Nyyssönen, 1993). It is desirable that the information on these parameters is georeferenced. The preferred scale for the mapping of locational information ranges from $1{:}10^6$ to $1{:}10^7$. Traditionally, FAO collected information on the world's forest resources over five year intervals. In recent years, however, the observation frequency has been lower. The reference year for the most recent assessment was 1990, whereas the preceding assessment describes the situation in 1981.

Table 2.1 shows that the parameters relating to forest cover and forest categories are most important. Hence, these parameters may be considered primary indicators of the state of the world's forest resources. The remaining parameters, with exception of those that relate to socio-economic factors, are shown to be of secondary importance. Unlike most of the parameters listed, socio-economic parameters do not relate to the state of the forest ecosystem but rather to the social system interacting with the forest. Nevertheless, socio-economic parameters are of vital importance as changes in these parameters may cause considerable depletion of forest resources. Examples of socio-economic changes that are known to result in the destruction of forest are: increasing population densities, introduction of programmes to support settlement and sudden drops in international prices for forest products such as natural rubber (e.g. Etter and Andrade, 1987; Unni, 1994; van Dijk et al, 1994; Richards, 1996). Due to the strong influence of environmental problems, *the emphasis is on information to be used in support of forest resource monitoring.* Monitoring, however, must be preceded by forest resource assessment in order to establish a reliable starting point.

**Table 2.1** Parameters required to assess major **global environmental issues**. The relative importance of each parameter is marked as follows: '+++' essential, '++' desirable, '+' optional. (After UNEP/FAO, 1993).

| | Global environmental issue | | | | |
|---|---|---|---|---|---|
| Parameter | Bio-diversity | Carbon cycle | Hydrolo-gical cycle | Forest condition | Land cover / land use |
| Ecofloristic zones | ++ | | | | + |
| Forest cover: | | | | | |
| - Forest / non-forest | +++ | +++ | +++ | +++ | +++ |
| - Burned areas | +++ | +++ | +++ | +++ | +++ |
| - Logged areas | | +++ | +++ | | |
| - Regeneration | ++ | +++ | +++ | | |
| - Biomass degraded areas | | +++ | +++ | | |
| - Deforested | +++ | +++ | +++ | +++ | +++ |
| Forest categories: | | | | | |
| - Potential forest vegetation type | +++ | | | | |
| - Actual forest vegetation type | +++ | +++ | +++ | | ++ |
| - Administrative / legal status (e.g. ownership) | +++ | | | | |
| - Management type (e.g. production forest) | ++ | ++ | | | |
| - Plantation / natural | +++ | +++ | | | +++ |
| Fires (numbers, distribution) | ++ | | | | |
| Percentage of vegetation cover | | | | | +++ |
| Crown cover / leaf index | + | +++ | +++ | | ++ |
| Tree species composition | ++ | | ++ | | |
| Diameter distribution | | +++ | | | |
| Stand height | | + | + | | |
| Stand architecture | ++ | | + | ++ | + |
| Soil characteristics / topography: | | | | | |
| - soil organic matter | ++ | +++ | + | ++ | |
| - texture and slope | | | +++ | | |
| Socio-economic factors (e.g. population density, infrastructure) | +++ | +++ | +++ | +++ | +++ |

### 2.1.2 Requirements at the national level

Westinga et al. (1993) listed the needs for information on tropical forest resources at the national level. At this level the requested information is mainly used in support of policy making, planning and control of parties operating at the local level. In many countries the collection of data on forest resources has a long tradition in National Forest Inventories. Yet the scope of the National Forest Inventory has widened in time. The survey by Westinga et al. shows that at present there is a *need for locational data on: forest cover, forest category, tree species composition, timber volume, ecological and socio-economic parameters.*

Information on parameters related to forest cover and forest category, i.e. on primary indicators of the state of the forest, is important for both forest resource assessment and forest resource monitoring. In countries where National Forest Inventories have been carried out, there is not usually an urgent need to assess forest cover and category parameters over extensive areas. Whenever there is need to do so, the common scale for mapping is 1:50,000. The information used in forest resource assessment is usually required to be updated once every five to 10 years. This frequency of observation agrees with that of traditional forest inventories. To enable forest resource monitoring the information on the primary indicators needs to be collected more frequently. The preferred observation frequency depends on the dynamics of the change processes and the size of the area of interest. However, under most circumstances it suffices to collect the required information once every two years. The minimum scale for maps to be used in forest resource monitoring at the national level is 1:250,000.

Parameters relating to tree species composition and timber volume are usually collected in forest inventories. Yet none of these parameters classify as primary indicators of the forest's state. Information on species and timber volume is mostly of importance in forest assessments that aim to prepare for logging. Such assessments, however, are typically carried out at the local spatial level. At the national level species and timber volume parameters are of secondary importance because of links with environmental issues, i.e. biodiversity and carbon cycle. Traditionally, these parameters are collected by means of sampling and for restricted areas only. Reliable monitoring of tree species composition and timber volume over extended areas is difficult since these parameters are difficult to estimate and highly dependent on both the forest type and the forest's development level (see Oldeman, 1990).

*Requests for data on ecological parameters, i.e. indicators of biodiversity, have gained considerable importance in recent years.* Ecological parameters represent the variety of life at the ecosystem, species community and genotype population levels. The increased need for information on these parameters can be explained from the growing concern with regard to the continuing depletion and degradation of forest resources. To date there is lack of parameters that give a good representation of (change in) biodiversity and yet are easy to estimate. The discussion as to which parameters are most suited and how these should be estimated is ongoing (Nyyssönen, 1993). FAO's assessment of loss in biodiversity at the global level is

**Table 2.2** Summary of parameters on which parties involved in the management of tropical forests at the **national spatial level** require information.

| Parameter |
| --- |
| Forest cover:<br>- Forest / non-forest<br>- Logged-over forest<br>- Secondary forest<br>- Primary forest types |
| Forest categories:<br>- Administrative / legal status<br>(e.g. ownership)<br>- Management type<br>(e.g. production forest, protection forest, conservation forest, conversion forest)<br>- Plantation / natural |
| Tree species composition |
| Timber volume / woody biomass |
| Biodiversity indicators<br>(e.g. canopy roughness, terrain physiography, cover fragmentation, road density, net primary production, actual evapotranspiration, leaf chemistry, leaf biomass, leaf area index) |
| Socio-economic factors<br>(e.g. population density, infrastructure, development programs, commodity agreements) |

based on an estimation of the loss in tree species which in turn is estimated from loss in forest cover by means of species-area relationships (see FAO, 1993). A similar indirect way of assessing biodiversity could be applied at the national (or local) level. However, at these lower spatial levels a more direct indicator of biodiversity would be preferable. Canopy roughness which is shown to be related to species diversity by Oldeman (1983a), Brünig and Huang (1989) and Brünig and Mohren (1989) could be that kind of indicator. Moreover, canopy roughness is a parameter such a could possibly be estimated with the use of remote sensing. Stoms and Estes (1993) list additional indicators of biodiversity that may in potential be assessed from remote sensing images, namely: terrain physiography, cover fragmentation, road density, net primary production, actual evapotranspiration, leaf chemistry, biomass and leaf area index.

Like at the global level, there is a need for information on socio-economic parameters at the national level. The importance of these parameters was discussed in section 2.1.1. Socio-economic parameters should indicate whether or not the existing social system offers sufficient protection against unwanted degradation and decline of forest resources. In fact, these parameters point out the necessity for appropriate action by policy makers and planners. The information requirements of the parties involved in tropical forest management at the national spatial level are summarised in Table 2.2.

### 2.1.3 Requirements at the local level

The users at the local level, both in the literal and figurative sense, stand the closest to the forest. Policy makers who decide at the higher spatial levels have mostly been replaced by decision-makers who truly interact with the forest. Generally speaking, *users at the local level have a need for specific and detailed information on relatively small areas*. Typical examples of local users are parties involved in the forestry industry (e.g. concessionaires, plantation owners) and the conservation of nature and natural resources.

The main objective of users working in the forestry industry is the production of timber. At best production is meant to be sustainable, at worst short term profit is the only concern. The information needs of foresters have since long been covered by conventional forest inventories. Foresters were also among the first to make use of remote sensing images, i.e. aerial photographs. Radar remote sensing will be of value to foresters only if it can deliver important new information or improve, simplify and/or speed up the traditional inventory process.

A regular forest inventory process to serve as a basis for sustainable forest management comprises four phases, namely: reconnaissance inventory, management inventory, operational inventory and post-harvest inventory (Husch, 1971). The reconnaissance inventory is intended to provide information for establishing new forest concessions or plantations. It is designed to collect data on the location and the extent of important forest types at the lowest possible costs. Aerial photographs are commonly used but ground examination is minimal. The management inventory (also working plan inventory) is aimed at collecting detailed data on the state of the terrain and the forest. These data provide the basis for the management of the forest. To simplify both inventory and management, the forest is usually subdivided in smaller units e.g. man-made compartments or stands. Terrain characteristics that need to be assessed include topography, drainage and the location of watercourses, buffer zones, protected areas, roads, landings etc. The state of the forest is commonly described in terms of parameters that express species composition, size class distribution, volume by species, growth rates etc. The preferred scale for the mapping of locational data is of the order of 1:1,000 to 1:10,000. In many management inventories the concept of "site classes" is introduced in order to label areas with comparable terrain and forest properties. The operational inventory (also logging plan inventory) is carried out in preparation for felling and extraction. At this stage there is a need for information on harvestable volume (by species, size and quality), positions of trees that are to be felled, the need to cut lianas and preferred routes for extraction. Following logging there ought to be a post-harvest inventory in order to assess logging damage, natural regeneration and the necessity of silvicultural interventions (e.g. replanting, weed and pest control).

In combination the described inventories do make up a ground-based procedure for the monitoring of forestry operations. *Monitoring is essential to ensure sustainable forest management as sustainability implies a time scale.* Sustainability means that the forest should be able to fulfil its functions now and in the future (Lammerts van

**Table 2.3** Summary of parameters on which parties involved in the management of tropical forests at the **local spatial level** require information.

| Parameter |
| --- |
| Terrain characteristics:<br>- Topography<br>- Water courses and drainage patterns<br>- Infrastructure<br>(e.g. roads, bridges, skidding trails, log-markets, logging camps) |
| Forest cover:<br>- Primary forest types<br>- Logged-over forest<br>- Clear-cuts<br>- (Natural) regeneration<br>- Burned areas |
| Forest categories:<br>- Management type<br>(e.g. production forest, protection forest, conservation forest, conversion forest)<br>- Plantation / natural |
| Forest composition and structure:<br>- Tree species composition<br>- Diameter distribution (size class distribution)<br>- Standing volume (by species)<br>- Growth rates<br>- Harvestable volume (by species, size, quality)<br>- Positions of harvestable trees |
| Site class |
| Sustainable management indicators<br>(see Table 2.4) |

Bueren and Blom, 1997). Unfortunately, sustainability is not yet the objective of all of those who are involved in the forestry industry. However, in the near future timber producers around the world may have to prove that they manage the forest in a sustainable manner. As consumers become increasingly reluctant to purchase wood originating from forests managed as mines, the call for timber certification grows louder. Under pressure of consumers, environmental and social groups, the 1985 International Tropical Timber Agreement (ITTA) has come to take the form of an agreement for sustainable development of tropical forest resources rather than of a pure commodity agreement (Bass et al., 1992). This agreement was negotiated by producer and consumer countries participating in the United Nations Conference on Trade and Development (UNCTAD). The organisation largely responsible for achieving the objectives of ITTA is the International Tropical Timber Organisation (ITTO). This organisation aims to accomplish its assignment by the year 2000.

ITTO, in cooperation with timber trade and environmental organisations formulated a standard for the sustainable management of natural tropical forests and plantations (Marjuni, 1990; ITTO, 1991; ITTO, 1992). Guidelines and criteria formulated in this standard are dictated by the following definition: *sustainable forest management is*

*the process of managing permanent forest land to achieve one or more clearly specified objectives of management with regard to the production of a continuous flow of desired forest products and services without undue reduction of its inherent values and future productivity and without undue undesirable effects on the physical and social environment.* The standard is intended to be of use to forest managers and administrators in all three tropical regions. Per region, the forest conditions and management procedures vary considerably. Hence, the ITTO guidelines and criteria are of a general nature. Managers at the national and/or local level will have to shape them into more specific guidelines and criteria. Following ITTO, various other entities have developed standards for sustainable (tropical) forest management. Lammerts van Bueren and Blom (1997) evaluated no less than 11 different standards with the object of setting up a hierarchical framework for the formulation of standards for sustainable forest management. This framework is designed in an attempt to help solve problems that result from inconsistencies in and a lack of coherence between existing 'standards'.

The framework proposed by Lammerts van Bueren and Blom (1997) consists of four hierarchical levels, namely: principles, criteria, indicators and verifiers. The principles and criteria describe what should be accomplished to ensure sustainable forest management. Indicators are parameters which allow to assess whether, and if so to what extent, the principles are followed and the criteria are realised. The indicators relate to either the forest ecosystem or the surrounding social system. Finally, verifiers are sources of information for the indicator or for the reference value for the indicator. For the purpose of the present study the indicators are of most importance. Especially, indicators of a spatial nature since these can presumably be assessed using the verifier "radar remote sensing data". The actual assessment of management performance should be based on a comparison between the actual value of the indicator and its reference value or norm. Unfortunately, the norms are the least developed elements in the existing standards. This is due to the fact that the formulation of norms requires much scientific knowledge and practical experience of the respective forest area or of similar forest areas. Because of the temporal dimension of sustainability, the indicators need to be assessed repeatedly over time so as to enable the manager to correct deviation. In other words, they need to be monitored. By monitoring protected forest areas, one can obtain information on the natural forest dynamics. This information can greatly facilitate the formulation of norms for sustainable forest management.

Standards for sustainable forest management support the activities of both forest managers and organisations involved in the control of forestry operations and/or the certification of forest products. To increase the chances of achieving sustainable forestry, control and certification organisations should be able to obtain critical data without the involvement of concessionaires or plantation owners. Radar and other types of remotely sensed images are typical examples of data that can be acquired independently. Hence, *remote sensing data have the potential to support control and certification organisations in their assignment. Similarly, remote sensing data may assist forest managers in their efforts to prove compliance with regulations for sustainable management.*

**Table 2.4** Examples of indicators proposed in existing standards for **sustainable forest management** (see Lammerts van Bueren and Blom, 1997). The selected indicators are of a spatial nature and hence can possibly be assessed and/or monitored with the help of remotely sensed images. The indicators are categorised on the basis of related sustainability principles.

---

The forest resource shall be sustained.

- Area and percentage of forest; classified by e.g. forest and vegetation type, administrative / legal status, age structure, origin of forest.
- Area and percentage of forest land negatively affected by air pollutants (e.g. sulphate, nitrate, ozone) or ultraviolet B.
- Area and percentage of forest affected by processes or agents beyond the range of historic variation, e.g. by insects, disease, fire, storm, flooding, salinisation.
- Extent of illegal exploitation and encroachment.
- Rate of conversion of forest cover to other uses (e.g. mining, ranching, energy, infrastructure).

The protection function of the forest shall be sustained.

- Percentage of crown cover.
- Area and percentage of forest soils affected by significant alterations in physical-chemical properties and erosion.
- Infrastructure (primary and secondary roads, timber yards, skidding tracks) is located on natural benches, ridges and flatter slopes.
- Sizes of infrastructure are reduced to the barest minimum possible.
- Infrastructure does not disturb the flow of water in the network of rivers, streams etc.
- Presence of infrastructure or logging gaps in buffer zones around watercourses or areas of protected forest.

Yields of forest products (timber and non-timber) shall be sustained.

- Annual number of trees and/or volume of timber per hectare harvested.
- Changes in total volume of the growing stock.
- Felled trees correspond to those identified for felling prior to harvest.
- Number of large trees retained as seed producers (mother trees) per ha and species.
- Natural or artificial regeneration of deforested areas is implemented successfully.

The biodiversity of the forest shall be sustained.

- Extent of forest disturbance due to logging (e.g. gap size and frequency).
- Presence of representative protected areas.
- Presence of ecological infrastructure (e.g. corridors of unlogged forest).
- Presence of light demanding (pioneer) species over extensive areas.

The long-term social and economic well-being of local communities shall be sustained.

- Sites of special cultural, ecological, economic or religious significance to indigenous peoples are excluded from forestry operations.

---

The current and future information requirements of the parties involved in tropical forest management at the local spatial level are summarised in Table 2.3. Table 2.4 specifies some of the indicators that are proposed in existing standards for sustainable forest management. The indicators are grouped according to related sustainability principles. All of the indicators shown are of a spatial nature and hence can in principle be assessed or monitored with the help of remote sensing data. Some of the listed indicators can be assessed solely on the basis of remote sensing data, whereas the assessment of others will require ancillary information (e.g. on location of ecological reserves, buffer zones, sites of importance to indigenous people etc.). At the local spatial level, forest resource monitoring can be expected to become an annually recurring procedure. The time-interval between forest resource assessments will be of the order of five years. Most likely, however, different parts of the management unit will need to be assessed in different years. Compatible scales for the mapping of locational data are large since the information needed is of a high spatial detail. The minimum scale for maps to be used in support of forest resource assessment is of the order of 1:10,000. Maps for use in forest resource monitoring are required to have a minimum scale of approximately 1:25,000.

## 2.2 Potential of remote sensing to meet user requirements

In history foresters were among the first ones to make use of remote sensing techniques. The earliest known application of remote sensing to forestry dates back to 1887 when aerial photographs were taken purposely from a balloon near Berlin in order to study beech, spruce and pine stands. Around 1919 aerial photography became much more operational due to the introduction of aeroplanes. Aeroplanes facilitated the use of aerial photography in large scale forest inventories as they provided a capacity for the acquisition of photographs in continuous strips along flight lines. The value of aerial photography for application to large scale forest inventory was first illustrated in Quebec. In this Canadian province, more than 200,000 hectares of boreal forest were successfully surveyed on the basis of aerial photographs. This survey took place as early as 1920. From here onwards the use of aerial photographs in forest inventory spread rapidly throughout the world (Howard, 1991).

Since the beginning of the 20th century a large number of remote sensing techniques, other than aerial photography, has been developed. The systems presently available offer a wide range of capabilities and operate from a variety of platforms. However, *the development of operational procedures for the use of remote sensing data and the development of remote sensing systems have not kept pace*. It has been argued that this is due to the development of systems having been driven by a push from remote sensing technologists rather than by a pull from users of remote sensing data. Certainly this development gap will continue to exist as long as users and technologists do not improve their communication. Poor communication is the cause of considerable misunderstanding, misconception, confusion and ignorance among both groups (see Shelton and Estes, 1981; Estes, 1982; Green et al., 1988).

Evidently, there is strong need for procedures that implement the operational use of remotely sensed data in different fields. The potential of remote sensing for it to be applied in many fields cannot be denied. In some fields of application remote sensing images have already become an indispensable source of information (e.g. meteorology, sea ice monitoring). *Remote sensing systems offer some distinct advantages. First, they are capable of acquiring data in a synoptic, systematic and repetitive manner. Second, remote sensing data can be georeferenced.* This implies that it is possible to retrieve the geographical location for each object observed. People or organisations with a need for information on extensive areas often of difficult access are likely to benefit most from the use of remote sensing because alternative methods for collecting information are limited.

Tropical rain forests cover extensive areas, are difficult to access and have a highly complex nature. Due to these characteristics, *rain forests are a resource for which information is scarcely available and difficult to obtain.* The availability of appropriate, reliable and up-to-date information is critical to any management process. Hence, *remote sensing as a tool for collecting information on tropical rain forests has the potential to facilitate the management of these forests.* However, at present there is little experience with the use of remote sensing for this field of application. The capabilities of different remote sensing systems and the information contents of different types of remote sensing data are still under investigation. Section 2.2.1 discusses characteristics of remote sensing systems that are of importance in view of the application of these systems to tropical forest management. Sections 2.2.2 and 2.2.3 review selected publications on the use of, respectively, optical and radar remote sensing in the tropical rain forest environment. The aim of these sections is to illustrate what types of information can be derived successfully from remote sensing data. Literature reviews can also be found in: Baltaxe (1980 and 1987), Joyce and Sader (1986), Ahern et al. (1990), Sader et al. (1990), van der Sanden (1990), Tittley (1992) and Hoffer et al. (1995).

### 2.2.1 Relevant characteristics of remote sensing systems

The applicability of a remote sensing system to forest management or any other field depends on both the specifications of the sensor and the supporting platform. *Most important are the specifications that control the coverage, the repeat cycle and the image information content.* Due to technical and operational limitations, the capabilities of sensor and platform are interrelated. This means that, for example, large areas can only be observed at the cost of spatial resolution.

The coverage, i.e. the area that is observed routinely, depends primarily on the specifications of the platform. Spaceborne systems such as satellites are better suited to acquire data over extended areas than airborne systems. Geostationary satellites orbit at very high altitudes (ca. 36,000 km) which enables them to instantaneously image half of the Earth's surface. Polar orbiting satellites, on the other hand, systematically image a strip of land/sea and make use of the Earth's rotation to provide global coverage. The coverage as provided customarily by satellite systems cannot be provided by airborne systems other than at great expense. It

follows, that for the assessment and/or monitoring of forest resources at national spatial level and, in particular, at the global spatial level, satellite systems are preferred over airborne systems.

Like the coverage, the repeat cycle or time interval between repetitive coverage is mostly dependent on platform specifications. *Due to their orbiting behaviour, spaceborne sensor systems routinely image every part of the Earth's surface at fixed time intervals, i.e. during each overpass.* For existing polar orbiting satellites this interval varies from 12 hours to roughly one month. Geostationary satellites orbit synchronously with the Earth's rotation and can therefore provide continuous coverage. Once again, *it will be more costly for airborne systems to provide a similar frequency of observation over extended areas.* Airborne systems, however, are under direct control and hence offer much greater flexibility with regard to the time of data acquisition.

In section 2.1 it was discussed that, depending on the spatial level, forest resource assessments are carried out with a frequency of once every five to 10 years. Likewise, procedures for forest resource monitoring were reported to be carried out annually or biennially. In theory, the data requirements associated with forest resources assessment and monitoring can be met by all of the currently available remote sensing systems. In practice, however, many remote sensing systems prove incapable to do so. Often this is due to adverse atmospheric conditions, i.e. the *presence of a large amount of moisture, clouds and/or smoke.* Such conditions which are known to be especially common in tropical regions, seriously hamper the imaging capability of optical remote sensing systems. *Whenever such conditions prevail, only radar remote sensing systems can offer a guaranteed imaging capability.*

The *image information content is primarily governed by sensor specifications, such as: number of channels, wavelength(s), polarization(s), spatial resolution(s) and stereoscopic capacity.* However, in practice the specifications of the sensor are linked to those of the platform. For example, airborne sensor systems generally acquire data of a higher spatial resolution than spaceborne sensor systems. The spatial resolutions of airborne systems are of the order of 1 to 10 m, whereas the spatial resolutions of spaceborne systems range from 10 m to 5 km. Local users will generally require data of a finer spatial detail than users at the national or global spatial level. Similarly, forest resource assessment will usually require data of a finer spatial detail than forest resource monitoring. Generally speaking, the use of data of an unnecessarily high spatial resolution is not recommended as it will result in needless expense for both data acquisition and data processing per unit area. The information content of different types of remotely sensed data from tropical rain forests is discussed in more detail in sections 2.2.2 and 2.2.3.

### 2.2.2 Information content of optical remote sensing data

Literature on the use of remote sensing in support of tropical forest assessment and monitoring shows that most of the applied optical remote sensing systems are satellite systems. Table 2.5 lists some relevant characteristics of the most frequently

**Table 2.5** Relevant specifications of **optical satellite systems** that are applied frequently to tropical forest resource assessment and monitoring procedures. For a description of the abbreviations please refer to the included List of abbreviations.

| | Remote sensing system | | | |
|---|---|---|---|---|
| Characteristic | NOAA AVHRR | Landsat MSS | Landsat TM | SPOT HRV |
| Spatial resolution | 1.1 km (LAC)<br>4 km (GAC) | 80 m | 30 m (VIS & IR)<br>120 m (TIR) | 10 m (PAN)<br>20 m (XS) |
| Spectral channels | 1 Visible<br>1 Near-IR<br>1 Mid-IR<br>2 Thermal-IR | 2 Visible<br>2 Near-IR | 3 Visible<br>1 Near-IR<br>2 Mid-IR<br>1 Thermal-IR | 1 Panchromatic<br>2 Visible<br>1 Near-IR |
| Area covered by single image | 4 million $km^2$ (central part) | 34,000 $km^2$ | 34,000 $km^2$ | 3,600 $km^2$ |
| Repeat cycle | 12 hours | 16 days | 16 days | 26 days (2-5 days in off-nadir view) |
| Compatible image map scales [1)] | ≤ 1:1.5 million (LAC)<br>≤ 1:6.5 million (GAC) | ≤ 1:150,000 | ≤ 1:50,000 (VIS & IR)<br>≤ 1:200,000 (TIR) | ≤ 1:20,000 (PAN)<br>≤ 1:40,000 (XS) |

1) According to Forster (1993).

used satellites. High resolution airborne optical sensors, other than cameras for aerial photography, have rarely been used. This can be explained by the prevalent poor atmospheric conditions and the fact that most of these systems are flown experimentally rather than operationally.

The present discussion with regard to the information content of optical remote sensing data will be structured on the basis of application fields which are inspired by the user requirements as discussed in section 2.1.

**Forest / non-forest mapping**

*Data from existing optical remote sensing systems are suitable for discriminating tropical forests from non-forest cover types (including large scale deforestations).* The best evidence of this is found in FAO (1993). This report discusses FAO's Forest Resources Assessment 1990 (FRA90), a project in the practice of forest resources assessment and monitoring. FRA90 aimed to assess the extent and location of the global tropical forest cover in 1990 as well as to estimate the change in forest cover relative to 1980. Low resolution NOAA AVHRR LAC and high resolution Landsat MSS/TM data were used in a multi-stage sampling approach.

The FRA90 results indicate that AVHRR LAC, MSS and TM data provide a suitable basis for distinguishing between forest and non-forest. However, it proved difficult to obtain a multi-temporal global coverage of cloud-free Landsat MSS or Landsat TM data. Cloudiness and atmospheric moisture are well known problems for the use of optical remote sensing in the humid tropics (Nelson and Holben, 1986; Päivinen and Witt, 1988; Cross, 1990; Garcia and Alvarez, 1994; etc.). Smoke has been reported

to create similar problems (e.g. Malingreau and Laporte, 1988; Malingreau and Tucker, 1990). An advantage of NOAA AVHRR is that the chance of obtaining clear data is relatively high. This is due to the high observation frequency. As a rule, there are two NOAA satellites in orbit, jointly these can image every spot on the globe twice a day.

Another advantage of NOAA AVHRR data is the relatively low cost. However, NOAA data are of a much lower spatial resolution than Landsat data (see Table 2.5). This limits their applicability to forest resource assessment and/or monitoring at the global level. Assessment and/or monitoring of forests at the national and, in particular, the local level requires images of a higher spatial resolution, e.g. images from Landsat MSS or Landsat TM. The capabilities of the NOAA satellites for forest/non-forest mapping and other environmental applications have been reported in various articles. A review of these can be found in Ehrlich et al. (1994). According to these authors there is at present a lack of standards for data analysis and accuracy verification. This may give rise to inconsistencies in global data sets and as such complicate global change detection.

Studies to improve the precision of NOAA AVHRR based forest cover estimates concentrate on techniques for decomposing pixels (e.g. Cross et al., 1991; Foody, 1994; Shimabukuro et al., 1994). Eva et al. (1995) investigated the capabilities of the ATSR-1 thermal infrared radiometer. This sensor, which is flown onboard the ERS-1, offers a spatial resolution comparable to that of the NOAA AVHRR LAC data. The forest/non-forest contrast in ATSR-1 data proves to be higher than in NOAA AVHRR data. Hence it is concluded that the ATSR-1 data are potentially more useful for global forest/non-forest mapping.

Kummer (1992) reports on the use of Landsat MSS and SPOT data to assess national forest cover and rates of forest cover change in the Philippines. In this country, a total of five forest surveys using remotely sensed data was conducted in the period from 1973 through 1987. Involvement of Filipino experts proved crucial to obtain sufficiently accurate results. Like Ehrlich et al. (1994), Kummer stresses the need for standardisation (both in technologies and sensor systems) in order to allow for effective change detection. Data from satellites in the Landsat and SPOT series have also been widely applied for forest cover mapping in Brazil (e.g. Nelson et al., 1987; Fearnside et al., 1990; de Oliveira, 1990).

**Deforestation and forest regeneration mapping**

The types of deforestation considered here are small in scale and result from human activities such as shifting cultivation, (selective) logging, mining etc. Forest regeneration is assumed to include both reforestation and the natural regrowth of forests.

Eden (1986) in Guyana, Singh (1986) in India and Gilruth et al. (1990) in Guinea investigated the value of Landsat MSS for detecting deforestation due to shifting cultivation. The authors report different results. According to Eden and Gilruth et al., the MSS images largely fail to show the effects of shifting cultivation, whereas Singh states that the deforestation resulting from shifting cultivation is detected with an accuracy of 74%. The inconsistency in these results is most likely due to differences

in the local shifting cultivation techniques, determining the dimensions of the shifting cultivation plots. *Sensor systems with spatial resolutions smaller than or equal to that of Landsat MSS appear unreliable tools for detecting shifting cultivation or other small scale human interference that may result in forest degradation.* According to Booth (1989), this type of forest degradation - and not large scale forest clearance - is the main cause of deforestation in West Africa. Thanks to the relatively high spatial resolution, Landsat TM and SPOT are expected to be better suited for detecting small scale forest disturbance. A study by King (1994) in Belize in fact shows that both TM and SPOT are able to detect shifting cultivation with an overall accuracy of ca. 90%. Wilkie (1990) successfully applied TM data to map the settlements of shifting cultivators and gold miners in Zaire. Kamaruzaman and Manaf (1995) report that TM images show logged-over forest.

*Naturally regenerating or secondary forests are often among the cover types that are most difficult to identify.* Depending on their development phase these forests are easily confused with either crops/grassland or primary forests. Investigators that used NOAA AVHRR or MSS data (e.g. Nelson and Holben, 1986; Singh, 1987; Cross, 1990) usually relate poorer results than those that applied the spectrally (and spatially) improved Landsat TM data (e.g. Garcia and Alvarez, 1994; Kamaruzaman and Manaf, 1995).

**Forest type and species mapping**

*Mapping of forest types or species requires data of a relatively fine spatial detail.* Still, in most studies dealing with Landsat or SPOT data, tropical rain forests are considered as one vegetation type or divided into a few clearly distinct types (e.g. Roy et al., 1985; Unni et al., 1985; Singh, 1987; Forstreuter, 1988; Roy et al., 1991; Garcia and Alvarez, 1994; Paradella et al., 1994). This implies that the required level of classification detail is rather low and explains why the reported classification accuracy is generally high. Results of low level classifications may well satisfy the information needs of users that operate at the global and national spatial level. Likewise, these results may meet the requirements for reconnaissance inventory at the local level. However, at this level there also is a need for more detailed information, e.g. at the level of primary forest types or species.

Tuomisto et al. (1994) evaluate the applicability of Landsat MSS and TM images for the detection of primary forest types in Peruvian Amazonia. The results indicate that both image types suit the purpose well. Landsat TM images offer the best capabilities due to better spatial and spectral resolutions. Visual interpretation of enhanced image products rather than pixel-by-pixel digital classification proves to yield the best results. This can be explained by the complex and heterogeneous (spectral) nature of primary forest types and the fact that most forest type transitions are not abrupt but gradual (cf. Vester, 1997). These characteristics of primary forests are the cause of an unacceptably high proportion of misclassified pixels in pixel-by-pixel digital classifications. A commonly expressed drawback of visual image interpretation is that it does not provide the technology for *operational* forest resource assessment or monitoring (e.g. Roy et al., 1985). This may hold true for assessment and monitoring at the global and national spatial level, but it probably is not so at the local spatial level.

Most tropical forest types comprise a large number of species. This seriously complicates the identification of species by the use of remotely sensed images. *Data from orbital remote sensing systems like Landsat MSS/TM or SPOT do not usually allow for species detection other than in forest types with a strong dominance of a particular species or in single-species forest plantations* (e.g. Roy et al., 1985; Unni et al., 1985; Singh et al., 1986; Garcia and Alvarez, 1994). Swellengrebel (1959) reports on the value of large scale aerial photographs (scale 1:10,000) for the identification of species in the Guyana rain forest. The author concludes that individual trees cannot be identified as to species. This is mainly due to the great variation in which the crowns of any one tree species appear on the photographs. Some species, occurring in groups, could be recognised on the photographs. However, this was attributed to the general appearance of the group rather than the features of individual trees within the group. According to Loetsch et al. (1973) the findings by Swellengrebel agree with those of other researchers that studied forests in different parts of the humid tropics.

**Forest fire detection**

Virtually all conversion of tropical moist forest to non-forest takes place through the use of fire. Hence, active fires, smoke plumes and fire scars are indicators of recently deforested land. Both *low resolution NOAA AVHRR data* (e.g. Malingreau et al., 1985; Matson and Holben, 1987; Pereira and Setzer, 1993a; Balladares et al., 1997) *and high resolution Landsat MSS/TM data* (e.g. Tanaka et al., 1983; Pereira and Setzer, 1993b) *have been applied successfully in the detection of forest fires.* Nezry et al. (1993) report the clear visibility of smoke plumes in SPOT images. Helfert and Lulla (1990) discuss the use of Space Shuttle photography for the mapping of smoke palls over the Amazon Basin.

**Biomass mapping**

*Investigators who aimed to map the biomass of tropical rain forests with the help of optical remote sensing data have met with little success.* The parameter most closely related to biomass is the Normalized Difference Vegetation Index or NDVI. This parameter is calculated from the reflectance in the near-infrared and visible red wavebands (see Lillesand and Kiefer, 1994). The NDVI is sensitive to variations in green leaf biomass rather than to variations in total biomass above the ground.

Box et al. (1989) compute annually integrated NDVI values from NOAA AVHRR data and evaluate the relationships with, among others, total aboveground biomass, leaf area index, net primary production and net biospheric $CO_2$ flux. The analysis is carried out at the global spatial level, across all major vegetation types, including tropical rain forests. The results show weak global relationships between NDVI and total aboveground biomass, leaf area index or net biospheric $CO_2$ flux. Across the full range of vegetation types, the NDVI proves to be closely related to the net primary production. However, for tropical rain forests alone the relationship between NDVI and net primary production is poor.

Sader et al. (1989) evaluated the capability of Landsat TM derived NDVI values in assessing the total aboveground biomass and age of secondary tropical forests in Puerto Rico and Costa Rica. Both the NDVI-biomass and NDVI-age relationship was found to be poor. The NDVI values for the study area in Puerto Rico were influenced

significantly by local topographic effects, i.e. slope and aspect. Results concerning the NDVI relationship to green leaf biomass were inconclusive. A well known problem associated with the use of NDVI for estimating green leaf biomass is the effect of saturation at higher leaf densities (e.g. Tucker et al., 1985). According to Sader et al. (1989), NDVI may be a good predictor of total aboveground biomass in low biomass, even age plantation forest on flat terrain. Lucas et al. (1993) adopted another approach to assessing the age of secondary forests. Rather than analysing single-date Landsat TM images, these authors analysed a time-series of TM images. The approximate age of secondary forests was estimated by comparison of classification results for images acquired at different points in time.

**Estimation of structural parameters**

No investigators other than those that had large scale aerial photographs available have attempted to estimate structural parameters for primary tropical forests. The capacity to obtain reliable estimates of forest/tree structural parameters from remotely sensed images can facilitate the process of forest inventory greatly. Although some parameters such as crown diameter, tree height, tree number and crown closure can in potential be directly assessed on (stereoscopic) images, others such as bole diameter and volume can only be estimated with the help of allometric equations.

Swellengrebel (1959) in Guyana investigated the possibilities for estimating the volume of tropical forests through the measurement of crown diameters on aerial photographs on a scale of 1:10,000. The author concludes that *volume estimation by crown diameter measurement is severely restricted by the impossibility of recognising tree species and the limited visibility of smaller trees on the photographs.* The inability to identify species implies that volume figures can only be given per forest type. Volume per forest type can be divided into volumes per (commercial) tree species only by extensive field work, thereby diminishing the value of photo volume estimation considerably. The chances of observing a particular tree on an image will decrease as the architecture of the forest canopy becomes more complex. Swellengrebel determines that chance of observing a tree with a bole diameter of ca. 50 cm in mixed forest in Guyana is approximately 70%.

Oza et al. (1989, 1992) developed regression equations which enabled them to estimate the mean crown diameter in managed even-aged teak (*Tectona grandis* L.) plantations from Landsat MSS data. This opens the way to the combined use of Landsat MSS data and allometric equations for assessing the timber volumes in teak plantations. The use of optical remote sensing data for estimating structural parameters of plantation forests in the tropics has not been studied widely. Other studies dealing with this field of application usually relate to temperate regions (e.g. Peterson et al., 1986; Ahern et al., 1991; Ardö, 1992; Brockhaus and Khorram, 1992).

### 2.2.3 Information content of radar remote sensing data

Compared to remote sensing with optical satellite systems, remote sensing with radar or microwave satellite systems is a new development. The European remote sensing satellite ERS-1, which was launched in 1991, became the first system to routinely acquire radar data on a global scale, over an extended period of time. Long before the launch of ERS-1, however, airborne surveys and experiments with spaceborne systems had shown the potential of radar for application in the humid tropics. Like in the previous section, the literature review presented here is structured on the basis of application fields which are inspired by the user requirements as discussed in section 2.1.

Publications from the 1970s and 1980s discuss results from over flights with different airborne radar systems and the spaceborne Shuttle Imaging Radars (SIR-A, SIR-B). Prior to the launch of ERS-1, multi-temporal data sets were scarce and therefore most of the results published concern forest resource assessment rather than forest resource monitoring. Results of studies that apply data from ERS-1 or its successor ERS-2 are gradually being published. So are results of studies that use data as acquired by SIR-C and the experimental multi-frequency, polarimetric radar system from NASA/JPL. To date, there are few publications on the capabilities of the Japanese radar satellite JERS-1 and the recently launched Canadian radar satellite RADARSAT. The most relevant characteristics of the currently operating radar satellite systems are listed in Table 2.6. For reasons of comparison the table also lists the characteristics of the airborne radar system from NASA/JPL (AIRSAR). The reader is referred to section 3.1 for a comprehensive discussion on the operating principles of radar systems.

**Forest / non-forest mapping**

*Radar remote sensing data can be used to discriminate between tropical forest and non-forest cover types (including large scale deforestations).* The first evidence of this is found in the results of a radar mapping project that was executed as early as 1965 in the Darien province of Panama (Viskne et al., 1970). Subsequent to the Panamanian project, a large number of regional and nation-wide radar mapping programs was carried out successfully in Southeast Asia and Africa, as well as Central and South America. The airborne radar systems deployed acquired high resolution data in short wavelength bands, i.e. $K_a$- or X-band. Most data were processed on image film and made available to users as radar mosaics at scales ranging from 1:25,000 to 1:250,000. The mosaics served a variety of purposes including thematic mapping for forestry, land-use, geology, geomorphology and soil survey (e.g. Parry and Trevett, 1979; Furley, 1986; Dams et al., 1987; Sicco Smit, 1988; Thompson and Dams, 1990).

Experiments with the AIRSAR system from NASA/JPL show that the backscatter *contrast between forest and non-forest increases with an increase in radar wavelength.* Hence, radar systems that operate with long wavelengths (e.g. L- or P-band) have more potential to discriminate between forest and non-forest than systems that operate with short wavelengths (e.g. X- or C-band) (Zebker et al., 1991; Hoekman et al., 1996). Single date AIRSAR images have been reported to show

**Table 2.6** Relevant specifications of currently operating **radar satellite systems**. The specifications of the airborne NASA/JPL AIRSAR system are included for reasons of comparison. For a description of the abbreviations please refer to the included List of abbreviations.

| | Remote sensing system | | | |
|---|---|---|---|---|
| Characteristic | ERS-1/2 | JERS-1 | RADARSAT | AIRSAR |
| Spatial resolution | 25 x 25 m | 18 x 18 m | 10 x 10 m (Fine beam)<br>30 x 30 m (Standard beam)<br>100 x 100 m (ScanSAR wide) | 7 x 12 m |
| Radiometric resolution (no. of looks) | 3 | 3 | 1 (Fine beam)<br>4 (Standard beam)<br>8 (ScanSAR wide) | 16 |
| Frequency and polarization | C-band VV | L-band HH | C-band HH | C-, L-, P-band polarimetric |
| Area covered by single image | 10,000 $km^2$ | 5,625 $km^2$ | 2,500 $km^2$ (Fine beam)<br>10,000 $km^2$ (Standard beam)<br>250,000 $km^2$ (ScanSAR wide) | 72 $km^2$ |
| Repeat cycle | 35 days | 44 days | ≤ 24 days | not applicable |
| Compatible image map scales | ≤ 1:200,000 | ≤ 1:200,000 | ≤ 1:100,000 (Fine beam)<br>≤ 1:200,000 (Standard beam)<br>≤ 1:500,000 (ScanSAR wide) | ≤ 1:50,000 |

recently cleared areas in addition to forest and non-forest areas. The clearance of tropical forests usually involves cutting and burning but is rarely complete in the sense that large dead trees often remain standing. It is assumed that these trees with their dry (charred) surfaces and wet cores are responsible for the very distinct backscatter signature of recently cleared forest areas (Hoekman et al., 1996).

Various authors have illustrated the relatively good forest/non-forest mapping capabilities of the spaceborne L-band radar systems as flown during the SIR-A and SIR-B experiments (e.g. Ford and Casey, 1988; Stone and Woodwell, 1988; Werle, 1989; Nezry et al., 1993). Results of the 1994 SIR-C experiment show that multi-polarization L-band data offer enhanced capabilities to discriminate between forest and non-forest (Rignot et al., 1997). The mapping potential of the C-band ERS-1 satellite was investigated by, among others, Conway et al. (1994), Keil et al. (1994), Leysen et al. (1994), van Dijk et al. (1994), Bijker and Hoekman (1996) and Le Toan et al. (1996). *Attempts to map forest and non-forest using single date ERS-1 images may meet with difficulties mostly due to confusion between forest and regenerating natural vegetation in early development phases.* The possibilities to discriminate

between forest and non-forest are enhanced considerably whenever a time series of ERS-1 images is available. Kux et al. (1995) use single date airborne radar images to simulate the forest/non-forest discriminating capabilities of RADARSAT (Standard beam). Their results are comparable to those of investigators that apply ERS-1 data.

Unlike optical sensor systems, radar systems are capable of acquiring usable data independent of daylight and atmospheric conditions. This a distinct advantage, in particular for applications that require timely information. *The most commonly noted disadvantage of both airborne and spaceborne radar sensors is their sensitivity to topography* (e.g. Sicco Smit, 1975; Dams et al., 1987; Leysen et al., 1994, Keil et al., 1994). Topographic variations affect the strength of the radar backscatter and as such create tonal differences in radar images. Topography induced differences in image tone may be easily confused with tonal differences resulting from other causes (e.g. cover type transitions) and hence complicate the visual and/or computerised analysis of radar images. Image analysis techniques that compensate for topographic effects are in development (e.g. Bayer and Winter, 1990; Wu, 1990; Meier et al., 1992; Ulander, 1996).

**Deforestation and forest regeneration mapping**

Like in section 2.2.2 the type of deforestation considered here is of a small scale. Forest regeneration is assumed to include both reforestation and natural forest regrowth.

*Depending on their spatial resolution radar systems may or may not be capable of detecting deforestation resulting from shifting agriculture or selective logging.* Evidently, image scale is of importance in those cases where analysis is based on visual interpretation of photographic image products. According to Sicco Smit (1975), the effects of shifting agriculture and selective logging show poorly in the 1:200,000 airborne images (X-band) that were produced in the framework of the Colombian Proradam project. Thompson and Dams (1990) discuss the results of the deployment of a high resolution (6 × 6 m) X-band radar system at a number of tropical forest locations in Asia, South and Central America. Based on visual interpretation of *stereoscopic* radar image strips at scales up to 1:25,000, the authors identified shifting cultivation clearings as small as 0.25 ha and three levels of selective logging disturbance (undisturbed, first cycle logging, second cycle logging). Areas of shifting cultivation were also observed in airborne, X- and C-band radar images for Araracuara, Colombia (Jorritsma, 1993; Hoekman et al., 1994).

*The limited spatial resolution and low incidence angle of the ERS-1 radar cause its data to be of little value for the detection of shifting cultivation areas* (van Dijk et al., 1994; Hoekman, 1996). *Still, Kuntz and Siegert (1994) report identifying the effects of selective logging in ERS-1 images for Borneo, Indonesia.* The interpretation of the images, however, is noted to require skilled personnel, i.e. personnel capable of integrating a-priori expert knowledge of land-use activities into the interpretation process. Using a combination of C- and L-band SIR-C data for the Rondonia State in Brazil, Saatchi et al. (1997) report detecting forest disturbance due to the clearing of vines and undergrowth with an overall accuracy of 77%. The key radar channel for distinguishing this type of forest disturbance is L-band HH.

Like in the case of optical remote sensing, naturally regenerating or secondary forests are often among the cover types that are most difficult to discriminate. Depending on the development phase, regenerating forests may be confused with either crops/grassland or primary forests. Detection of secondary forests in short wavelength airborne radar images proves feasible if the images provide stereoscopic coverage (e.g. Dams, 1987). Studies by Freeman et al. (1992) and Hoekman et al. (1996) illustrate that the *multi-frequency, multi-polarization data from the NASA/JPL AIRSAR system provide a good basis for the mapping of secondary forest. The routinely acquired C-band ERS-1 data prove to be of limited value for this purpose.* In single date ERS-1 images, regenerating and mature forests are easily confused (e.g. Conway et al. 1994; Keil et al., 1994; Bijker and Hoekman, 1996; Luckman et al., 1997). Knowledge-based analysis of multi-temporal ERS-1 data offers improved possibilities for secondary forest mapping (e.g. Bijker, 1997). Spaceborne radar systems that operate in L-band are more capable of identifying secondary forests than those that operate in C-band (i.e. ERS-1, RADARSAT). Studies that apply JERS-1 and/or SIR-C data show that L-band radar systems may be used to map and monitor forest regeneration up to a certain age (Luckman et al., 1997; Yanasse et al., 1997). The maximum age is a function of the rate of regrowth which strongly depends on the history of the site.

Hoekman et al. (1996) noted that secondary forests dominated by *Cecropia* species display higher L- and P-band backscatter values than other forests of a similar biomass. This deviating backscatter behaviour of *Cecropia* dominated forests is also observed by Bijker (1997) in ERS-1 images and Foody et al. (1997) in SIR-C images. The presence of *Cecropia* species indicates that the land had been used relatively lightly prior to abandonment.

**Forest type and species mapping**

The distribution of forest types is controlled by site conditions. These conditions are strongly influenced by physiographic terrain characteristics such as topography and drainage. Radar images represent these characteristics clearly and hence enable identification of forest types. *The method of identifying forest types based on physiographic terrain features was successfully applied in many of the earlier radar mapping programmes* (e.g. Viskne et al., 1970; Sicco Smit, 1975, 1978, 1988; Furley, 1986; Trevett, 1986). Although this method has never lost its value, the introduction of radar systems with *higher spatial resolutions enabled discrimination of forest types based on differences in canopy architecture.* In high resolution, short wavelength radar images canopy architecture can be observed as texture, i.e. the pattern of image tone. Forest type classification according to image texture has played a major role in the mapping projects as discussed by Thompson and Dams (1990). Results of experiments with the advanced airborne radar system from NASA/JPL show that this type of radars has great potential for application to tropical forest type mapping (Freeman et al., 1992; Pope et al., 1994; Hoekman et al., 1996).

*Attempts to map tropical forest types based on data from spaceborne radar systems have met with limited success.* Several researchers have demonstrated the capability of orbiting L-band radars to discriminate between flooded and non-flooded forest types. A review of their investigations is presented in a publication by Hess et al.

(1990). To date, there are few publications on the use of spaceborne radar data in more detailed tropical forest type classifications. Those that have appeared show variable results. Stone et al. (1989) report observing different primary forest types in L-band SIR-A data for the Brazilian state of Pará. Using L-band SIR-B images, Ford and Casey (1988) in Borneo, Indonesia distinguished among three different forest types in the coastal lowlands. However, the researchers failed to identify forest types in level (and mountainous) parts of the interior uplands. Nezry et al. (1993) do not seem to be capable of differentiating between primary forest types in L-band SIR-B data for central Sumatra as they do not mention so. Likewise, there are few investigators who report observing different primary forest types in ERS-1 images. The findings of an ERS-1 study by Hoekman (1996) in Araracuara, Colombia are positive but modest. Van Dijk et al. (1994) report negative results for the Bolivian Amazon.

Radar remote sensing data, like optical remote sensing data, may enable the detection of species in forests that are strongly dominated by certain species or in single-species forest plantations. Most tropical forests, however, have a very high species diversity and hence radar mapping is usually restricted to the forest type level. Thompson and Dams (1990) and Nezry et al. (1993) report identifying rubber plantations in airborne and spaceborne radar images, respectively.

**Estimation of biomass and other structural parameters**

Signals from radars that operate with long wavelengths (e.g. L- or P-band) have the potential to penetrate the surface of the forest canopy and hence to interact with underlying components (branches, trunks, undergrowth etc.). Thanks to this penetrating capacity, *radar remote sensing systems can offer better capabilities for estimating forest biomass and other structural parameters than optical remote sensing systems.*

Several researchers have studied the relationships between the radar backscatter and the structural characteristics of temperate forests in general and of coniferous forest plantations in particular. Their results show that the backscatter in L- and/or P-band is strongly correlated to structural parameters such as aboveground biomass, basal area, mean height and mean trunk diameter. Similar correlations have been found between L- and/or P-band backscatter and plantation age (e.g. Sader, 1987; Wu, 1987; Wu and Sader, 1987; Hussin et al., 1991; Moghaddam et al., 1994). The L-band backscatter has been shown to increase with increasing biomass until it saturates at a *dry* biomass level of ca. 100 t $ha^{-1}$. The backscatter in P-band appears to saturate at a *dry* biomass level of the order of 200 t $ha^{-1}$ (Dobson et al., 1992; Le Toan 1992).

To date, *few results have been published of studies on backscatter-structure relationships in uneven age, mixed tropical forests.* L-band multi-polarization backscatter measurements for closed primary forests in Costa Rica were shown to be poorly correlated to aboveground biomass and other structural parameters (Wu, 1990). Freeman et al. (1992) in Belize found evidence of backscatter-biomass relationships comparable to those as reported for forests in temperate regions. Similar qualitative evidence of correlations between P-band backscatter and aboveground biomass is presented for a riparian forest in Peru by Rignot et al. (1995). The studies by Freeman et al. and Rignot et al. illustrate a common problem

for investigations into relationships between remote sensing measurements and tropical forest structure, namely the difficulty of obtaining the required set of ground reference data.

Hoekman et al. (1996) in San José del Guaviare, Colombia quantitatively compared airborne multi-polarization C-, L- and P-band backscatter measurements with on site biomass measurements. They found good correlations between the backscatter in L- and P-band and the aboveground *fresh* biomass up to a level of approximately 200 t $ha^{-1}$. However, the authors demonstrate that *biomass is not always the parameter that governs the radar return signal in L- and P-band. Soil moisture* is shown to dominate the backscatter if biomass levels are below ca. 10 t $ha^{-1}$ (*fresh* weight). Likewise, *forest architecture* is shown to affect the backscatter in those cases where the biomass is over approximately 200 t $ha^{-1}$ (*fresh* weight). Procedures to estimate biomass from radar observations over hilly terrain should also account for the effect of topography on backscatter level and microwave interaction (van Zyl, 1993).

Luckman et al. (1997) in Tapajós, Brazil discuss the biomass mapping potential of the radars onboard SIR-C (C-, L-band), ERS-1 and JERS-1. Their results confirm the findings of other studies that C-band data are of little value for estimating biomass and that L-band data may be used to assess biomass up to a certain threshold level. The biomass level at which the backscatter in L-band was found to saturate is approximately 60 t $ha^{-1}$ (*dry* weight). The authors note that this saturation point is well below that quoted for forests in temperate regions. Saatchi et al. (1997) observed the same phenomenon in a study on the backscatter behaviour of secondary forests in Rondonia, Brazil. They explained it by the relatively high water content of the vegetation in young secondary forests and the strengthening effect of water on the height of the radar return signal. Foody et al. (1997) studied SIR-C data for an area with regenerating forests in the vicinity of Manaus. The aboveground *dry* biomass of these forests ranged from 64 to 141 t $ha^{-1}$. In this study no significant relationships between radar measurements in a single wavelength/polarization bands and biomass were found. Correlations between backscatter ratios and biomass were shown to be stronger. A higher sensitivity to biomass of polarization and/or frequency ratios and combinations has also been found in other studies (e.g. Sader, 1987; Wu, 1987; Ranson and Sun, 1994; Rignot et al., 1995).

# 3 An introduction to radar remote sensing of forests

## 3.1 Radar remote sensing principles

### 3.1.1 Radar system operation

The word radar is an acronym for RAdio Detection And Ranging. Written out in full, the name reveals that the system makes use of radio (electromagnetic) waves to detect the presence of objects and to determine their position. *A radar system transmits an electromagnetic wave signal, in a narrow beam, in the direction of interest.* Objects that are present within the radar beam will cause this signal to be reflected in various directions. Reflections in the direction of the system, that are above the threshold power level, will be detected by a detector and registered by a recorder. *The reflections that are observed by the radar are denoted as radar return signal or radar backscatter.* Radar systems provide their own radiation and are therefore referred to as active systems. Both the transmission and the reception of the electromagnetic waves is controlled by an antenna. The position of an object is determined by a combination of direction and distance (range). Direction is determined by the fact that the object is located within the radar beam, distance is derived from the speed at which the waves travel (speed of light) and the time elapsed between the transmission and reception of the signal.

Originally radar systems were developed for the detection of isolated objects such as ships or aircraft. Radar, in order to be used as a tool for remote sensing, was redesigned. The capability to detect and measure the backscatter contributions from

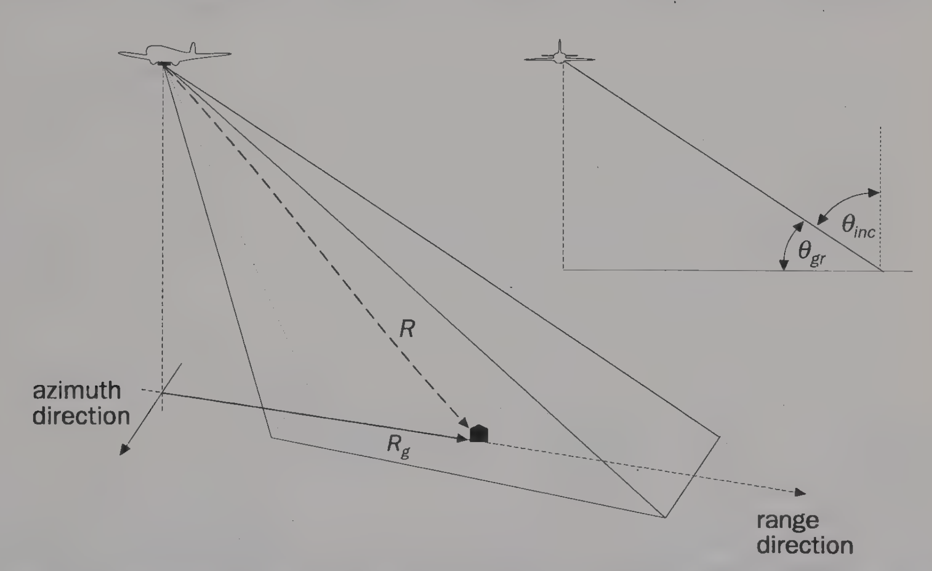



**Figure 3.1** Side-looking radar measurement geometry. Relationship between slant range distance $R$ and ground range distance $R_g$ as well as between incidence angle $\theta_{inc}$ and grazing angle $\theta_{gr}$. (Adapted from Hoekman, 1990.)

a variety of objects at the Earth's surface was added. Changes in system design resulted in a type of radar that is known as an imaging radar system. This system has additional imaging capacity but operates according to the same basic detection and ranging concepts as the original radar. The measurement geometry for an imaging radar system is illustrated in Figure 3.1. It can be seen that *the radar beam is pointing to the side, in a direction perpendicular to the direction of flight.* Because of this imaging radar systems are also known as side-looking radar (SLR) systems. The figure also introduces a number of commonly used terms: azimuth direction (direction of flight), range direction (direction perpendicular to the line of flight), slant range distance $R$ (direct sensor-to-object distance), ground range distance $R_g$ (distance from sensor-to-object projected on the ground), incidence angle $\theta_{inc}$ (angle

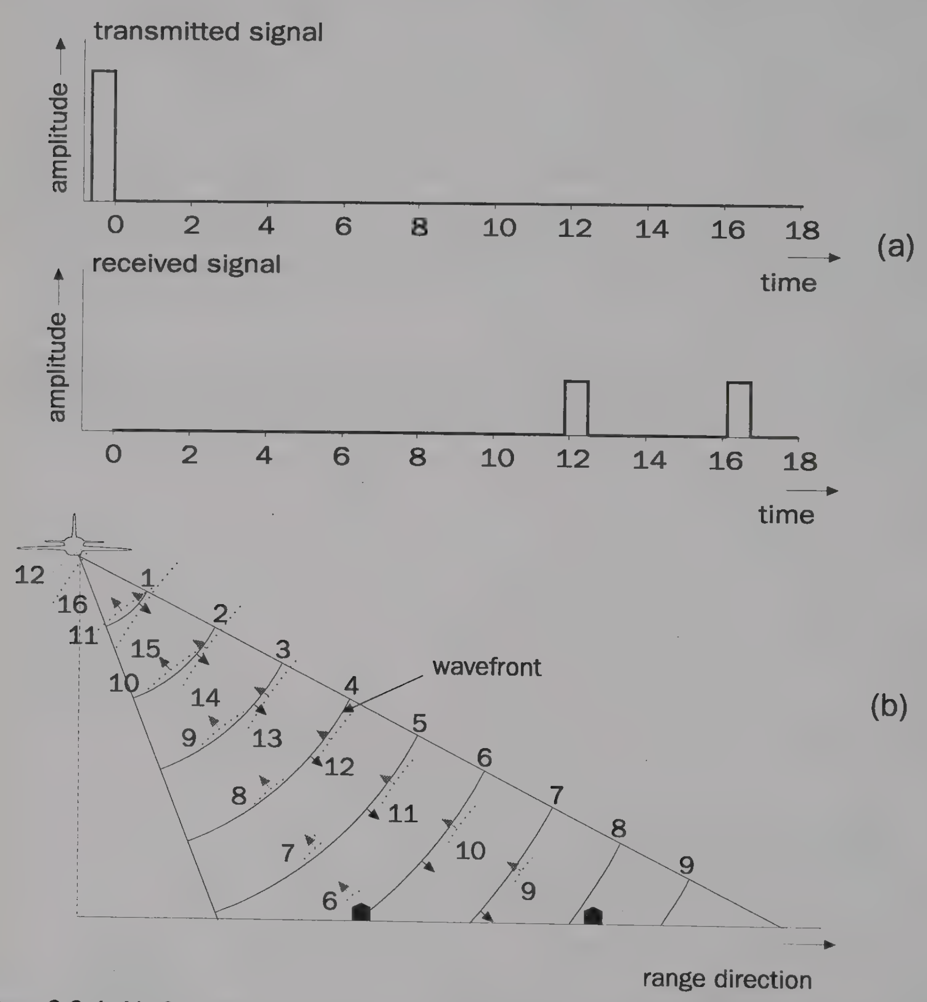



**Figure 3.2 (a-b)** Operating principle of side-looking radar with amplitude modulation. (**a**) Transmitted and received signal as a function of time. (**b**) Propagation of the wavefront from the transmitted and reflected signal in time and space. (Adapted from Lillesand and Kiefer, 1994.)

of viewing relative to the vertical at the point of the object observed) and grazing angle $\theta_{gr}$ (angle of viewing relative to the horizontal at the point of the object observed) (Skolnik, 1980; Colwell, 1983; Buiten and Clevers, 1993).

The capacity of radar remote sensing systems to detect and measure multiple objects in the range direction is based on the frequency and/or amplitude modulation of the transmitted radio wave. Modification, in time, of wave frequency and/or amplitude results in a 'time-coded' signal. *Due to this 'time-coding' the sensor is capable of discerning the backscatter contributions of objects (in range direction) that are separated in time, or in other words, of objects that are located at particular distances from the sensor.* The operating principle of a radar system that makes use of amplitude modulation is shown in Figure 3.2. This type of system is often referred to as a pulse radar since the amplitude modulation causes the waves to be transmitted in shorts bursts, or pulses. Figure 3.2a shows the transmitted and received electromagnetic signal as a function of time. Figure 3.2b illustrates the propagation of the front of one single radar pulse in space/time. The time lag between two consecutive pulses allows for the reception and recording of all reflections resulting from the first pulse prior to the transmission of the second pulse. In this manner a mix up of reflections resulting from different pulses can be avoided, and thus the erroneous localisation of objects within the field of view.

Two objects can be successfully discriminated in the range direction if the slant distance between them is sufficient. The minimum slant distance required is a measure of the spatial resolution of the radar in the slant range direction. This resolution is determined by the system's pulse length $c\tau$ (where $c$ is the speed of light and $\tau$ is the pulse duration). The relationship is illustrated in Figure 3.3. The

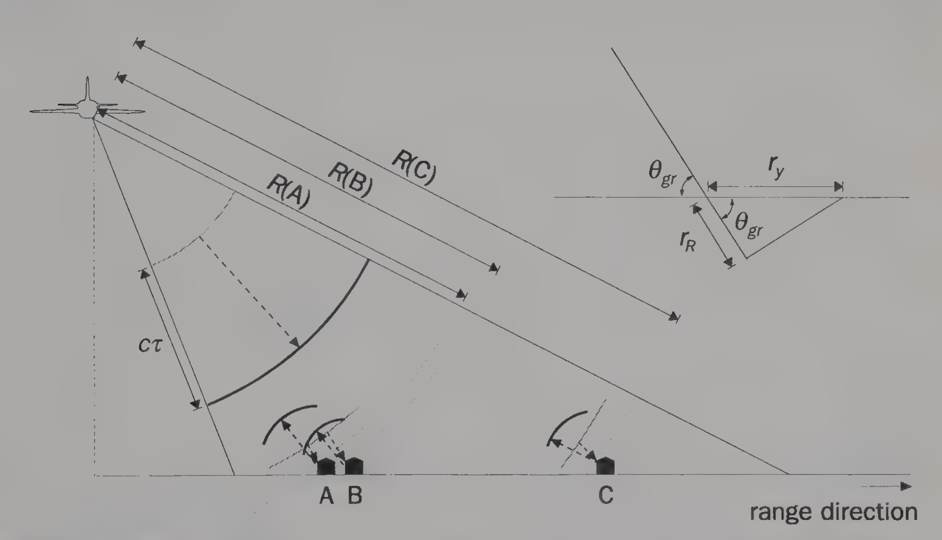



**Figure 3.3** Spatial resolution, in the range direction, of side-looking radar systems. Dependence of the slant range resolution $r_R$ on the pulse length $c\tau$ and on the relationship between slant range resolution, ground range resolution $r_y$ and grazing angle $\theta_{gr}$. Objects A and B, unlike C and A or B, cannot be discriminated since the offset in their slant range distances $(R(B) - R(A))$ is $< c\tau/2$. (Adapted from Lillesand and Kiefer, 1994.)

radar return signals (echoes) for objects A and B can be seen to overlap in space. The echoes of A and B will, therefore, not be separated in time when they arrive at the sensor. Consequently, the radar will not be capable of distinguishing these two objects. The "slant size" of return signals will be equal to the "slant size" of the incident signal (pulse length) as the objects will continue to generate backscatter for as long as they are illuminated. When one accounts for the two-way propagation of the signals (towards and away from the object), it can be seen that two objects will only generate separable echoes when their slant distance is equal to at least half of the echo "slant size", i.e. when the slant distance is $\geq c\tau/2$. In Figure 3.3 the slant distance between A and B ($R(\mathrm{B})-R(\mathrm{A})$) is $< c\tau/2$, while $R(\mathrm{C})-R(\mathrm{A})$ and $R(\mathrm{C})-R(\mathrm{B})$ are both $> c\tau/2$. The slant distances show that A and B can be discriminated from C and confirm the inseparability of A and B. It follows that the slant range resolution $r_R$ of a side-looking radar system is equal to $c\tau/2$. Figure 3.3, in addition, illustrates the relationship between the ground range resolution $r_y$ and the slant range resolution. The relationship between them is:

$$r_y = \frac{r_R}{\cos(\theta_{gr})} \quad [\mathrm{m}] \tag{3.1}$$

The spatial resolution on the ground improves in the range direction since it is inversely proportional to the cosine of the grazing angle and $r_R$ has a set value. Equation 3.1 is based on the assumption that the observed surface area is flat.

The data used for the purpose of this study were acquired by a type of radar that is known as a synthetic aperture radar (SAR). SAR systems make use of special data recording and processing techniques which enable them to provide images with high

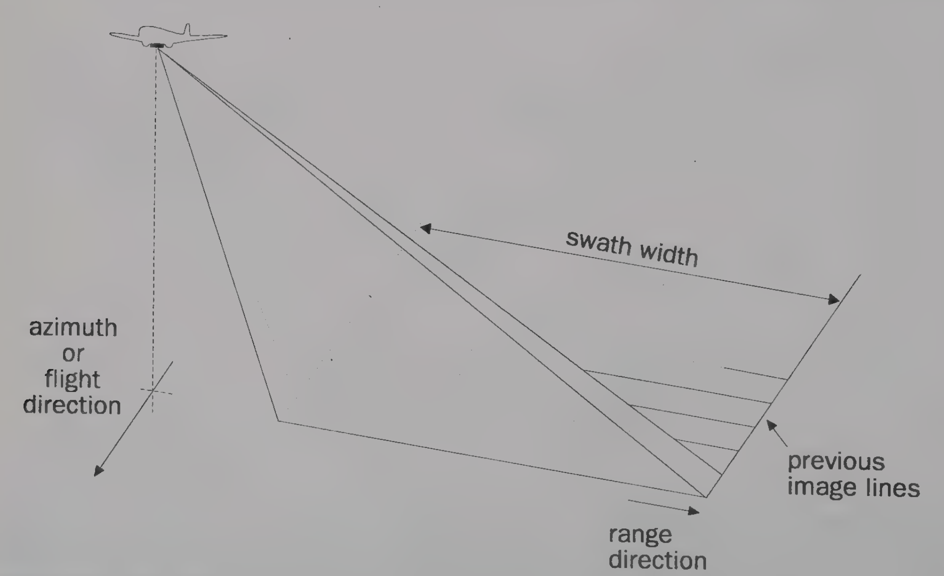



**Figure 3.4** Side-looking radar image formation in the azimuth or flight direction. The imaging capability in the flight direction is provided by aircraft motion. (Adapted from Curran, 1985.)

and constant spatial resolution in the azimuth direction. The azimuth resolution of a SAR system is equal to half of the antenna length and is thus independent of the distance between the sensor and the observed object (e.g. Curlander and McDonough, 1991). *Radar remote sensing systems are equipped with fixed antennas. The capability to localise objects in the direction of flight is therefore dependent on aircraft or satellite motion* (see Figure 3.4).

The radar systems described above, belong to a category of imaging radar systems that are capable of providing radar measurements for objects located within a strip of land (swath) at the Earth's surface. In addition to these imaging systems a category of non-imaging radar remote sensing systems can be distinguished. The ERASME scatterometer system that was flown for this study (see section 4.4.4) is an example of the latter category. Scatterometer systems, unlike imaging radar systems, have a very narrow beam width in the range direction. For this reason they only provide a single (narrow) line of backscatter measurements. The measurement geometry of a scatterometer system is illustrated in Figure 3.5. In this figure, a side-looking antenna is shown to allow for comparison with Figure 3.1. Scatterometers, however, may be operated in a number of different configurations, e.g. with a forward- or nadir-looking antenna. The ERASME data, for example, were acquired in a nadir-looking mode meaning that the antenna was pointed in a direction immediately below the aircraft, i.e. perpendicular to the Earth's surface.

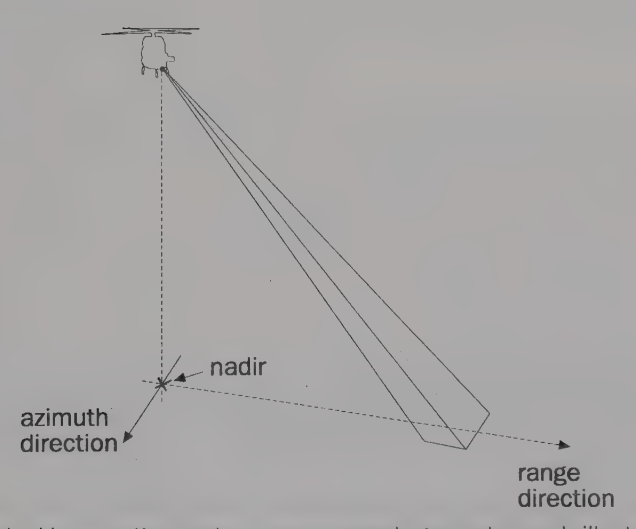



**Figure 3.5** Side-looking scatterometer measurement geometry and illustration of nadir. Scatterometers have a narrow beam width in the range direction and can only provide a single line of backscatter measurements. (Adapted from Hoekman, 1990.)

### 3.1.2 Characteristics of radar signals

Important characteristics of radar signals are: wavelength, polarization, amplitude and phase. The meaning of these parameters is illustrated in Figure 3.6. It should noted that this figure only shows part of the total electromagnetic wave, i.e. the electrical field. The magnetic field (not shown) is located in a plane that is at right angles to the electrical field plane. Both components of the electromagnetic wave behave in a similar fashion. Wavelength $\lambda$ is equal to the distance between two, successive, apices of the sine curve. The maximum deviation of the curve, the amplitude $A$, is an indication of the strength of a wave. Polarization is determined by the plane of vibration of the electrical field, e.g. vertical (V) for Figure 3.6a and horizontal (H) for Figure 3.6b. Another property of a vibrating point on the curve is its phase (angle) $\phi$. This parameter represents the point's deviation and direction of motion. Two points on the same curve have the same phase when their distance is equal to $n \cdot \lambda$ (where $n = 1,2,3,...$). Two waves are said to be "in phase" when they have the same frequency as well as the same phase angle at any point in time. The values of the phase angle may vary over a range from 0 to $2\pi$. Figure 3.6 also shows that the position of a specific point on the curve can be indicated with the help of a vector representation of the vertical (horizontal) electrical field vector $E_v$ ($E_h$).

*The technical specifications of the radar system determine the wavelength, polarization, amplitude and phase of the transmitted radio wave. Reflected waves may have a different polarization, amplitude and/or phase because these are subject to changes resulting from the interaction of the waves with the observed objects. The changes in polarization, amplitude and phase may be object specific and are therefore an important source of information for the discrimination of objects in radar images.* The majority of current radar systems, however, only record a small portion of the information available. For most systems the recording capacity is limited to the amplitude of either H- or V-polarized waves. A more advanced system is required, i.e. a polarimetric radar, to record all of the information in both polarization and phase. This type of radar system will be discussed in more detail in section 3.1.6.

Wavelength is an important characteristic of radar signals. It determines the extent to which specific objects, or object components, may act as reflectors and affects the propagation of both the transmitted and reflected waves through the atmosphere. Radar waves, independent of wavelength or other characteristics, will be attenuated by any object that is in the direction of propagation. Reflection, however, depends on the relative size of the object(s) encountered, i.e. the size of the object(s) compared to the wavelength. The effects of wavelength on the interaction of microwaves with forest are discussed in detail in section 3.2.2. Wavelength is important for the propagation of microwaves through the atmosphere because longer wavelengths are less susceptible to atmospheric attenuation and/or dispersion than shorter ones. However, serious atmospheric effects are usually restricted to operating wavelengths less than 3 cm and do not occur under conditions other than those of heavy rain storms. The wavelengths of the majority of radar remote sensing systems range from 0.8 to 100 cm. Specific wavelength bands are often referred to with a special, but arbitrarily chosen, letter code. The commonly accepted nomenclature for radar bands used in remote sensing and the corresponding wavelength range is shown in Table

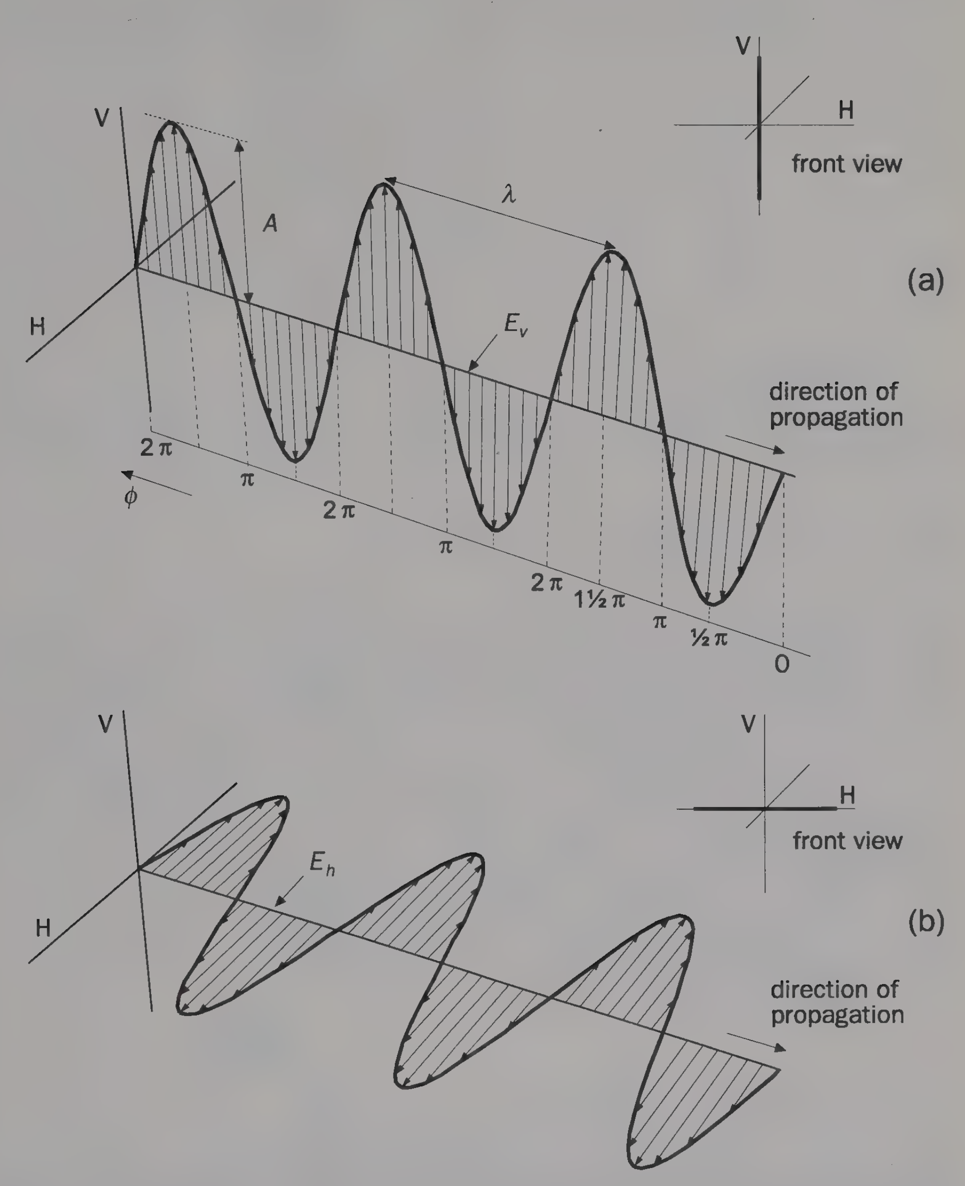



**Figure 3.6 (a-b)** Side and front view of the electrical field for an electromagnetic wave. (**a**) Wave with vertical (V) polarization. (**b**) Wave with horizontal (H) polarization. Illustration of wavelength $\lambda$, amplitude $A$, phase $\phi$, vertical electrical field $E_v$ and horizontal electrical field $E_h$. $\phi$ ranges from 0 to $2\pi$.

**Table 3.1** Nomenclature of radar bands for Earth observation and corresponding wavelengths.

| Band designation | Wavelength (cm) |
|---|---|
| $K_a$ | 0.84 - 0.85 |
| K | 1.24 - 1.25 |
| $K_u$ | 1.73 - 1.74 |
| $K_u$ | 2.14 - 2.24 |
| X | 3.06 - 3.16 |
| X | 3.47 - 3.51 |
| C | 5.61 - 5.71 |
| S | 9.09 - 9.68 |
| L | 23.08 - 24.69 |
| P | 30 - 100 [1)] |

1) Nominal wavelength range; at present there are no allocations for Earth observation within this range.

3.1. X-, C-, L- and P-band are of special interest since these were used to acquire the data sets for the present study.

Radar waves, regardless of wavelength, can be transmitted and received in different modes of polarization. Conventional radar systems, i.e. non-polarimetric systems, transmit and receive either horizontally (H) or vertically (V) polarized waves. However, the transmitted and received waves are not necessarily of the same polarization. Consequently, the radar signal may have four different polarization modes: HH (H receive, H transmit), VV (V receive, V transmit), HV (H receive, V transmit) and VH (V receive, H transmit). Polarization of radar signals is achieved through filtering of the outgoing and incoming electromagnetic waves. In practice, the HH and VV polarization modes are often referred to as like-polarizations, the HV and VH modes are known as cross-polarizations. As previously noted, the polarization of radar signals is an important source of information for the discrimination of objects in radar images. For further discussion of the information content of polarization as it applies to forests, please refer to section 3.2.3.

### 3.1.3 Characteristics of radar images

Radar images have special properties that differentiate them from other types of remote sensing images. The most striking image characteristics relate to the image geometry. These characteristics result from the side-looking configuration and the operation through ranging (see section 3.1.1). An important geometrical property of radar images is illustrated in Figure 3.7. It shows that radar systems measure the slant range distance of objects. *Radar systems, therefore, image objects on the ground in a slant range format. The image space, in contradiction to the ground space, does not have a constant scale.* For radar images the slant range scale increases with an increasing slant range (and ground range) distance. This results in

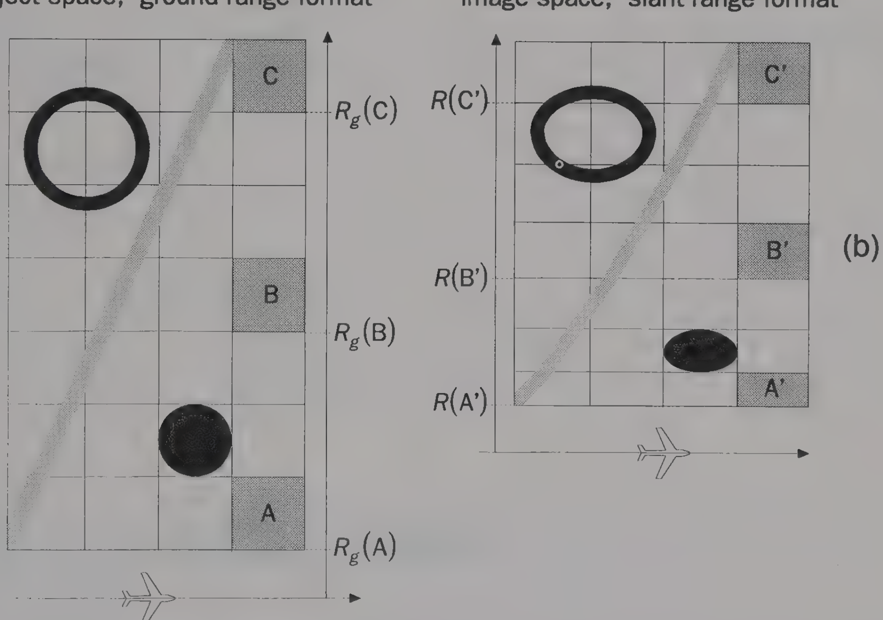



**Figure 3.7 (a-b)** Slant range versus ground range format. (**a**) Side-looking radar systems measure slant range $R$ rather than ground range distances $R_g$. $R_g$ can be derived from $R$ with the use of flight altitude $H$ information. (**b**) The side-looking configuration and the operation through ranging result in images with a distorted scale in range direction. (Adapted from Lillesand and Kiefer, 1994 and Lo, 1986.)

distorted images of the features on the ground. The slant range scale distortions may be a problem for applications that require images with correct geometry, i.e. images in a ground range format. However, with the use of image processing techniques this problem can be easily overcome. If the observed Earth surface is assumed to be flat, then the ground range distance $R_g$ is computed from the slant range distance $R$ and the flight altitude $H$ according to:

$$R_g = \sqrt{R^2 - H^2} \tag{3.2}$$

Figure 3.8 illustrates the geometrical effects that occur in radar images of terrain with varying relief. *Radar images of such terrain look distinctively "side-lighted" due to enhanced radar returns from slopes that face the sensor (front slopes) and reduced returns from those that face away from the sensor (back slopes).* The return signals from slopes are affected by the slope's aspect and by its displacement towards the line of flight. For front slopes the aspect causes strong reflection of microwaves in the direction of the sensor, while their displacement leads to the reflected power being confined to a small image region. For back slopes the aspect and displacement have the opposite effects, i.e. the reflections towards the sensor are weaker and spread over a large image region. The image of front slopes is comparatively small because these slopes will always appear shorter in the image than they would in an

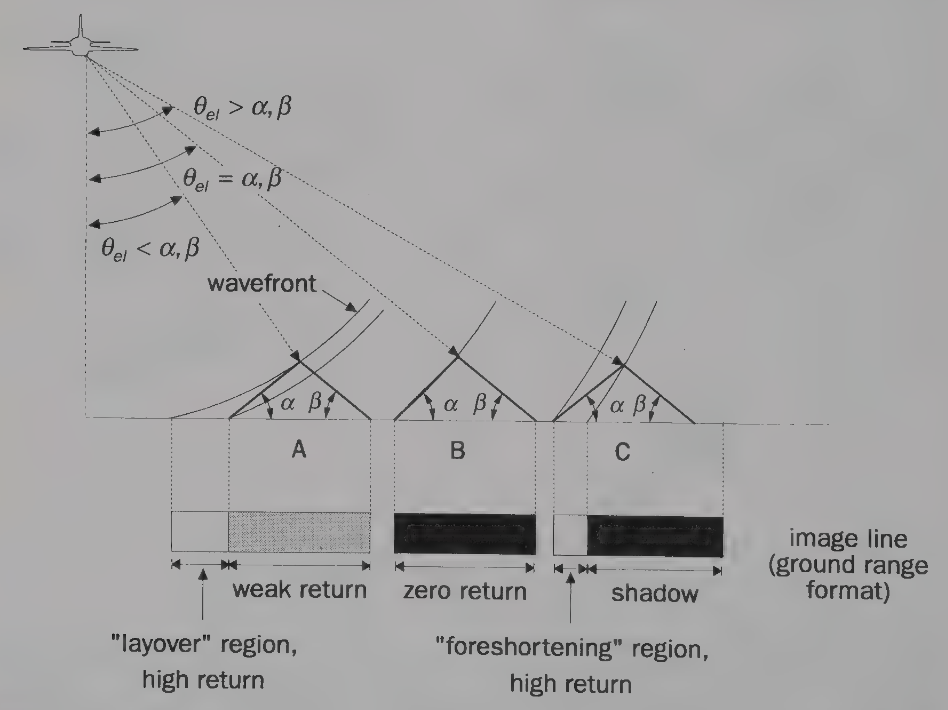



**Figure 3.8** Geometrical effects in SAR images of varying relief terrain. The appearance of front (back) slopes depends on the angle $\alpha$ ($\beta$) in relation to the elevation angle $\theta_{el}$. Regions of "layover" contain a double image, i.e. from the front slope and from the upper part of the back slope. (Adapted from Leberl, 1990.)

orthogonal map projection. Likewise, the image of back slopes is comparatively large because they will always appear longer. The appearance of front or back slopes in radar images depends on, respectively, the front slope angle $\alpha$ or the back slope angle $\beta$ in relation to the elevation angle $\theta_{el}$. Front slopes appear "foreshortened" when $\theta_{el} > \alpha$ (case C in Figure 3.8), "laid over" when $\theta_{el} < \alpha$ (case A), or as a line when $\theta_{el} = \alpha$ (case B). Back slopes may also be imaged in three different manners. First, when $\theta_{el} < \beta$ (case A) the slope is fully imaged because radar waves are incident on the entire slope surface; second, when $\theta_{el} = \beta$ (case B) the slope is imaged as a region of zero return because the radar waves travel parallel to the slope surface and are not incident, and finally, when $\theta_{el} > \beta$ (case C) the slope is not imaged because its surface is hidden in radar shadow. In case A the range distances for the upper parts of the back slope can be seen to be equal to those for the front slope. Regions of "layover" will, therefore, contain the signal from the front slope as well as the signal from upper back slope. The latter, of course, is an additional reason for the relatively high backscatter levels in "layover" regions. In the context of this text it is important to note that the *geometrical effects discussed above can also be found in short wavelength radar images of irregular forest canopies. In images of forests and other natural surfaces the local variation in backscatter is commonly referred to as image texture.* Image texture is discussed in detail in Chapter 5 as it proves to be an important information source in the discrimination of tropical forest types.

SAR data recording and processing techniques require the transmission of electromagnetic waves that have the same frequency and phase. The use of this so-called coherent illumination results in the formation of image speckle. *Speckle gives SAR images their well known "grainy" appearance* and can be seen best in homogeneous regions. *Speckle is caused by interference among the backscattered waves of the individual scattering elements (scatterers) that are present within one resolution cell.* In practice, a resolution cell (the smallest possible ground area to be observed by a sensor under the conditions in force) has a size of several square meters and will therefore contain numerous scatterers of varying sizes. Each of these scatterers, when illuminated by a radar wave, will produce an echo with a certain phase and amplitude or power (power is proportional to amplitude squared). The sum of these echoes, however, may vary as it depends on interference that occurs between echoes of individual scatterers. These interferences can either be constructive or destructive and therefore result in either a higher or lower overall backscatter.

The interference of radar echoes that originate from two scattering elements is illustrated in Figure 3.9. The example shown is simplified, there are only two echoes involved and these echoes are assumed to have the same amplitude and polarization. The echoes only differ in the sense that they have different phases. Phase differences result from dissimilarities in slant range distance that the transmitted, coherent waves travel before being reflected by a specific scatterer. Figure 3.9 shows that these phase differences are of great importance in determining the amplitude of the resulting radar echo. In situation A, where the phase difference is zero, the interference is shown to be constructive. The amplitude *A* of the resulting wave is equal to the sum of the amplitudes of the constituent waves. Constructive

interference is also shown in situation B, but in this case the resulting wave has a lower amplitude than in situation A. In situation C the wave interference leads to the total extinction of the resulting wave. Situation C, is a clear example of the destructive interference of radar echoes. For distributed objects the amplitude of a backscattered wave will generally change continuously. The echo from one specific resolution cell will change over time due to wind induced changes in the (relative) location of individual scatterers. The echoes from spatially adjoining resolution cells are subject to an additional source of variation, i.e. the natural spatial variation in size and location of scatterers.

The interference of radar echoes clearly obstructs consistent backscatter measurements from single resolution cells. However, the backscatter fluctuations have a stochastic nature, i.e. behave according to a certain probability distribution. For a wide range of distributed land targets, including forests, the backscatter *amplitude* fluctuations may be described with a theoretical probability distribution that is commonly referred to as the "Rayleigh-distribution". The backscattered *power* can be shown to have an exponential distribution (Hoekman, 1990). Both distributions are single parameter distributions. The Rayleigh distribution follows directly from the mean amplitude, the exponential distribution from the mean backscattered power. In order to characterise objects with the use of radar remote sensing it is therefore important that the radar measurements are accurate estimates of either mean amplitude or mean power.

In practice, the accuracy of radar measurements is often improved through linear averaging of measurements from resolution cells that adjoin in the azimuth direction. *A measurement from a single resolution cell is often denoted as a look*. This explains why the image resulting from the averaging process described is often referred to as a multiple look image. Multiple look images, when compared to single look images, show fewer fluctuations in backscatter, or in other words, are less "grainy". Relevant averaging, however, requires that the looks are statistically independent. This, in

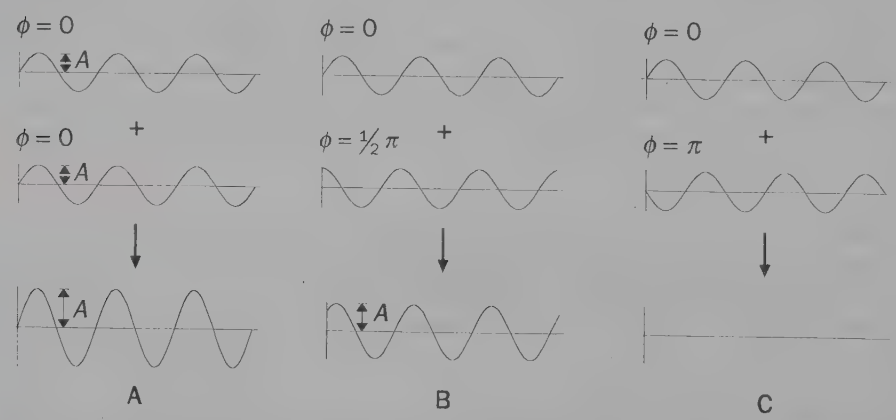



**Figure 3.9** Interference of radar echoes in relation to phase difference. Phase difference governs the amplitude *A* of the resulting wave. Case A and B show constructive interference, i.e. the amplitude of the resulting echo is larger than that of the interacting echoes. Case C shows destructive interference, i.e. total extinction of the resulting wave. Interference of radar echoes is the cause of image speckle.

general, will be true since the properties of the scatterers (size and relative location) and thus their backscatter will vary both in time and in space. The accuracy of mean amplitude or power estimations will increase with an increase in the number of averaged looks. The number of looks that are involved in the averaging process also affects the shape of the amplitude or power distribution. Figure 3.10 illustrates the distribution of backscattered power for 1, 3, 7 and 16 look radar data. The multiple look power distributions shown correspond to those found in the radar data used in this study. The 3 look distribution relates to the ERS-1 data, the 7 look distribution to the CCRS SAR data and the 16 look distribution to the NASA/JPL AIRSAR data (see section 4.4). In Figure 3.10 it can be seen that the distributions become higher and narrower as the number of looks increases. This implies that the fluctuations in the measurements of backscattered power are reduced as a result of look averaging. Look averaging improves the radiometric properties, i.e. the radiometric resolution, of radar images. However, look averaging may also cause deterioration of the geometrical properties of radar images as a reduced spatial resolution in azimuth direction may result.

### 3.1.4 Radar backscatter

The capacity of isolated objects to reflect radar waves is usually expressed by a parameter known as the "radar cross-section". Radar cross-section $\sigma$ (sigma) is a function of radar wavelength as well as of object characteristics (size, shape, orientation and composition). The radar cross-section can be defined by the "radar equation", which, in its simplest form, is equal to:

$$\sigma = 4\pi \cdot \frac{\text{power reflected back per unit solid angle}}{\text{incident power density}} \quad [m^2] \qquad (3.3)$$

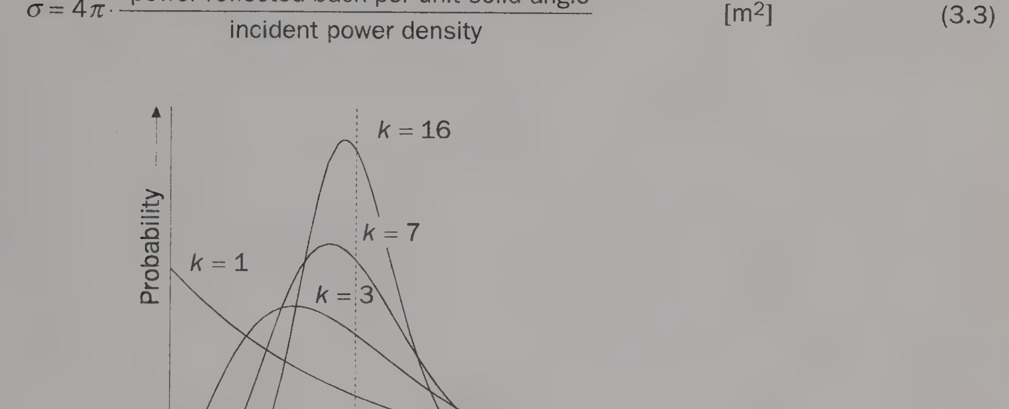



**Figure 3.10** Distributions of averaged power samples for 1, 3, 7 and 16 look radar images. A larger number of looks can be seen to reduce the fluctuation in the radar measurements, i.e. to improve radiometric resolution. The 3, 7 and 16 look distributions relate to the data from, respectively, ERS-1, CCRS SAR and NASA/JPL AIRSAR. Data from these SAR systems were used for the purpose of the study.

For a more extensive discussion of the basic radar equation please refer to e.g. Skolnik (1980) or Ulaby et al. (1981, 1982, 1986b).

For objects of interest to remote sensing, i.e. for distributed objects such as land surfaces, the $\sigma$ will depend on the size of the resolution cell. Larger resolution cells may have a larger backscattered power as they may contain more scatterers. *The parameter that describes the reflectivity of homogeneous land surface areas, unambiguously and independent of the area of the resolution cell $A_{res}$, is the "differential radar cross-section" $\sigma^\circ$* (sigma nought). This parameter is a dimensionless measure, that is defined as the expectation of the radar cross-section $\sigma$ per unit area:

$$\sigma^\circ = \frac{\langle \sigma \rangle}{A_{res}} \qquad [\mathrm{m^2\ m^{-2}}] \qquad (3.4)$$

Another commonly used backscatter measure for distributed objects is the "radar cross-section per unit projected area" $\gamma$ (gamma). Gamma is related to sigma nought by:

$$\gamma = \frac{\sigma^\circ}{\sin(\theta_{gr})} \qquad [\mathrm{m^2\ m^{-2}}] \qquad (3.5)$$

The relationship between resolution cell area and projected area $A_{proj}$ is illustrated in Figure 3.11. Both sigma nought and gamma are usually represented on a logarithmic, i.e. decibel (dB), scale. The conversion of $\sigma^\circ$ from the linear scale to the logarithmic dB scale is shown in Equation 3.6, the conversion for $\gamma$ is identical.

$$\sigma^\circ = 10 \cdot \log_{10}(\sigma^\circ) \qquad [\mathrm{dB}] \qquad (3.6)$$

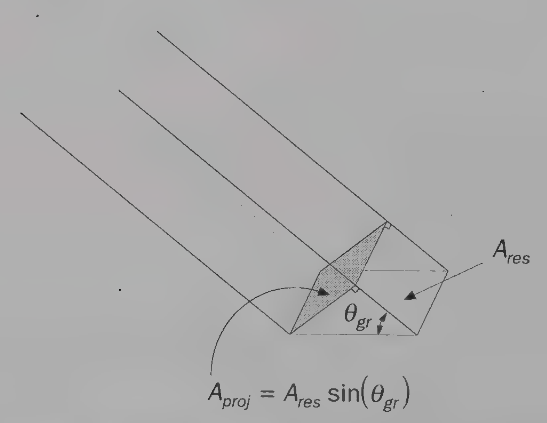



**Figure 3.11** The projected area $A_{proj}$ is related to the resolution cell area $A_{res}$ through the sine of the grazing angle $\theta_{gr}$. Sigma nought $\sigma^\circ$ is defined as the radar cross section per unit $A_{res}$, while gamma $\gamma$ is defined as the radar cross section per unit $A_{proj}$. (Adapted from Hoekman, 1990.)

### 3.1.5 Radiometric calibration

Radiometric calibration of SAR is defined by Curlander and McDonough (1991) as "the process of characterising the performance of the end-to-end SAR system, in terms of its ability to measure the amplitude (and phase) of the backscattered signal". The authors use the term 'end-to-end' to stress that all the elements that play a role in the process from data acquisition up to the data delivery must be taken into account. The need for calibration depends on the intended data analysis method which is usually determined by the application. *For quantitative analysis of SAR data calibration is required, but for qualitative analysis of SAR data calibration is not strictly necessary.* Applications with a quantitative analysis approach often aim to compare backscatter measurements. Comparisons may be made spatially across a single image frame, temporally from pass to pass in multiple image frames, across frequencies or polarization channels or ultimately across data acquired by different radar systems. Applications with a qualitative analysis approach frequently aim to extract spatial information from SAR images for mapping purposes.

The process of calibration can be separated into a lower level process (relative calibration) and a higher level process (absolute calibration). Relative calibration provides a common basis for all image pixels such that a given pixel intensity value represents a unique value of backscattered power. A good relative calibration will permit repeatable (precise) backscatter measurements both in space and in time.

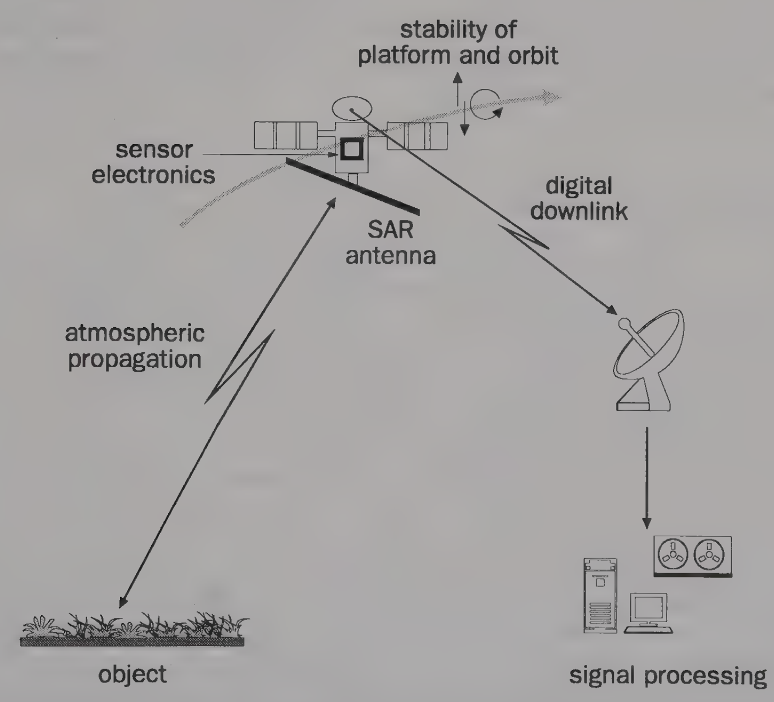



**Figure 3.12** Diagram of the error sources that need to be taken into account in the radiometric calibration of the "end-to-end" SAR system. (Adapted from Curlander and McDonough, 1991.)

Data from a system that has been relatively calibrated may contain a bias error in the backscatter values. However, this error does not hamper the use of the data in comparative studies as it will be the same at all times and for all spatial locations. A good absolute calibration will result in backscatter measurements that are both repeatable and absolute (accurate). Data from an absolutely calibrated radar system should not contain any bias error. This type of data are essential for applications that involve the comparison of backscatter across channels and/or systems as well as for studies that aim to validate backscatter measurements with the use of scattering models.

Figure 3.12 shows the error sources that must be considered in the radiometric calibration of space borne SAR systems. In the calibration of most airborne SAR systems the digital down link does not need to be accounted for since this subsystem is generally lacking. The calibration process usually consists of an internal calibration and an external calibration. Internal calibration involves the characterisation of the radar system's performance with the use of calibration signals that are injected into the radar data stream by built-in devices. This process compensates for errors that arise in the: sensor electronics, digital down link and signal processing. External calibration is required to compensate for errors that have their origin in the atmospheric state, the SAR antenna or the unstability of the platform/orbit. In external calibration the system's performance is characterised with the use of calibration signals that are transmitted or backscattered by ground targets. Suitable targets for external calibration are point targets with a known radar cross-section $\sigma$ (e.g. corner reflectors, transponders) or distributed targets with a known differential radar cross-section $\sigma^\circ$. The reader is referred to radar handbooks such as those by Ulaby et al. (1982) or Curlander and McDonough (1991) for a more elaborate discussion on SAR calibration.

### 3.1.6 Imaging radar polarimetry

In section 3.1.2 it was noted that the information contained in the polarization of a backscattered radar wave is related to the characteristics of the observed object. As such, polarization can be used to identify objects at the Earth's surface. Hence, it must be considered an important information source in radar remote sensing.

Thus far, the radar waves that have been discussed in this chapter were assumed to have either a horizontal (H) or a vertical (V) polarization (see Figure 3.6). However, as illustrated in Figure 3.13, the polarization of radar waves is often more complicated. *The electrical field of this wave can be seen to be equal to the vector sum of an H- and a V-polarized electrical field component. The resulting polarization, however, depends strongly on the phase difference between these two components.* In Figure 3.13 the difference in phase between the H- and V-component was chosen to be equal to $\frac{1}{4}\pi$. This results in a wave with an elliptical shape from the front view (seen from the direction of propagation). Based on its shape the wave in Figure 3.13 is said to have an elliptical polarization. The effects of the H-V phase difference on polarization are also illustrated in Figure 3.14. Depending on phase difference the resulting wave can be seen to have a linear, an elliptical, or a circular shape and thus

polarization. In addition it is shown (by means of an arrow) that elliptical or circular polarized waves can be either right- or left-handed. The handedness of a wave represents the sense of rotation of the tip of the electrical field in a fixed plane perpendicular to the direction of propagation. It is defined to be right-handed (left-handed) if the direction of rotation in this plane appears clockwise (counter clockwise) to an observer looking from the front of the wave in the direction of propagation (IEEE, 1983). This view will henceforth be referred to as the 'front view'. A wave that propagates in space as a left-handed (right-handed) screw will, when seen from the front view, create a right-handed (left-handed) sense of rotation in the plane of definition (see also Figure 3.13).

Figure 3.14 illustrates a limited selection of polarizations. In reality the number of polarizations is unlimited, since the H-V phase difference may have any value in the range from 0 to $2\pi$, the amplitudes of the H- and V-component may vary widely and because waves do not necessarily have both an H- and V-polarized component. All possible polarizations, however, may be described with the use of just two parameters from the so-called polarization ellipse (see Figure 3.15). The two relevant

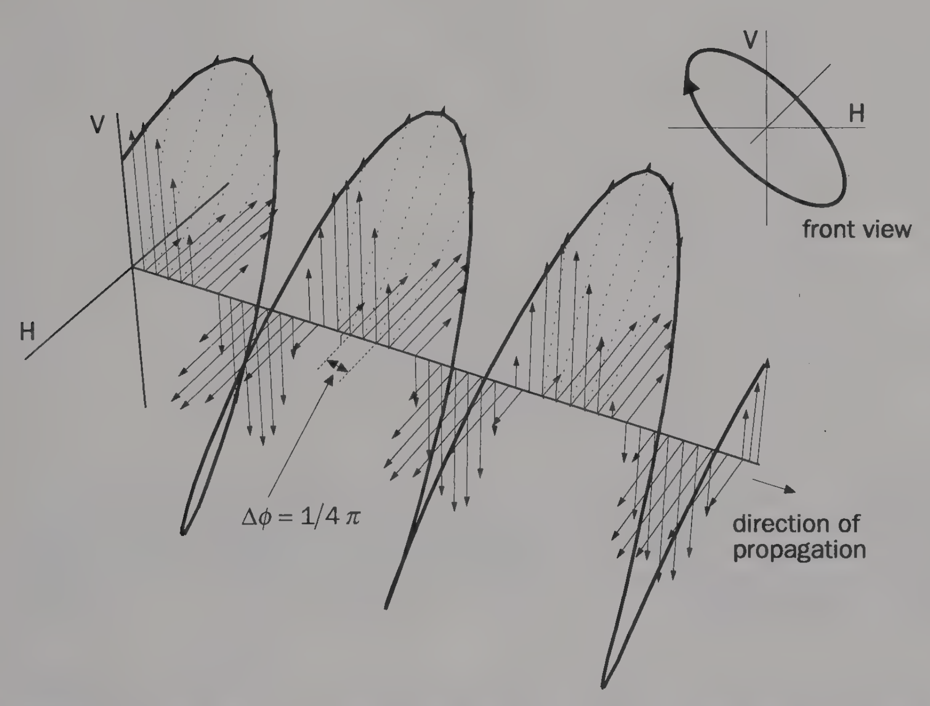



**Figure 3.13** Side and front view of the electrical field of a wave with H- as well as V-polarized electrical field components. The electrical field of the composite wave is equal to the vector sum of the H- and V-polarized components. The polarization of the composite wave is governed by the phase difference of the two components. A $\Delta\phi$ of $1/4\,\pi$ is shown to result in a wave with an elliptical front view, i.e. in a wave with an elliptical polarization. The wave propagates in space as a left-handed screw but is denoted to be right-handed as its tip (when observed from the front of the wave in the direction of propagation, i.e. in 'front view') rotates clockwise in the plane perpendicular to the direction of propagation.

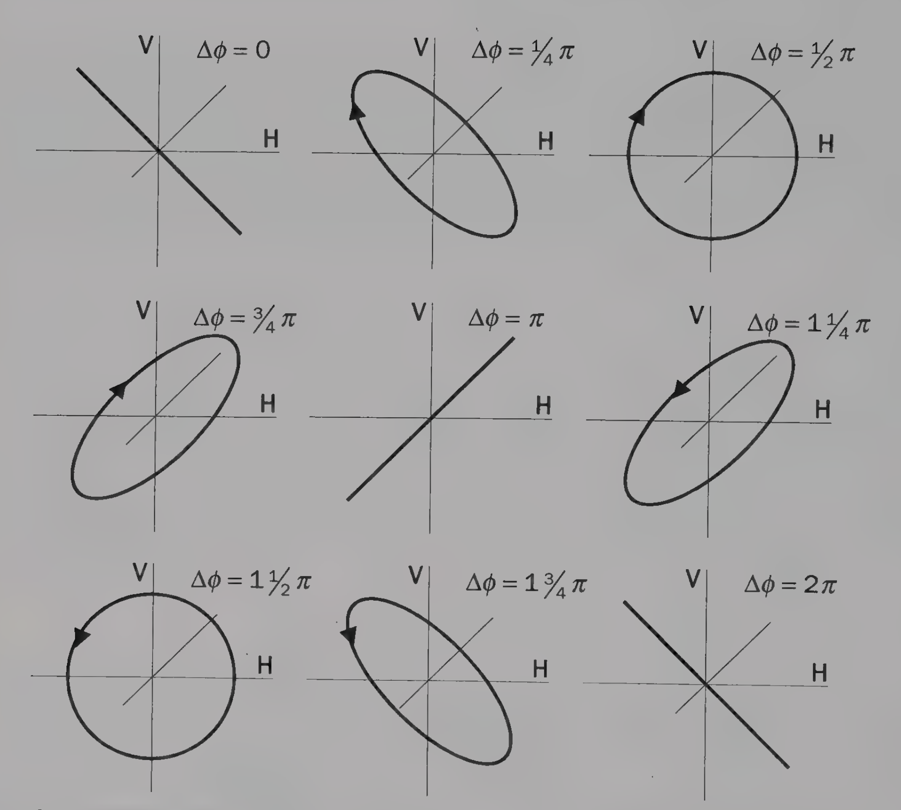



**Figure 3.14** Effect of the H-V phase difference on the polarization of composite waves. A limited selection of waves with linear, elliptical and circular polarizations is shown. Elliptical or circular polarized waves can be either right- or left-handed. Handedness is indicated by means of an arrow, an arrow pointing in a clockwise (counter clockwise) direction indicates a right-handed (left-handed) wave.

parameters from this ellipse are the ellipticity angle $\chi$ and the orientation angle $\psi$. Figure 3.15 shows that $\chi$ is related to the ratio of the major axis $a$ and the minor $b$ of the polarization ellipse, while $\psi$ corresponds to the angle between $a$ and reference direction H. *Any physical polarization may be represented by values of $\chi$ and $\psi$ that range from, respectively, -45° to 45° and 0° to 180°.* The sign of the ellipticity angle is indicative of handedness, with negative (positive) ellipticity angles corresponding to waves with a right-handed (left-handed) polarization. For linearly polarized waves the ellipticity angle is equal to 0° (axes ratio equal to 0). The orientation angle is 0° or 180° in case of H-polarization and 90° for V-polarization. Circularly polarized waves have ellipticity angles of plus or minus 45° (ellipse axes ratio equal to 1) while their orientation angles cannot be determined. The amplitude of the represented wave is proportional to the size of the polarization ellipse, i.e. to the square root of the sum of $a^2$ and $b^2$ (Evans et al., 1988).

The above characterisation of wave polarization using the geometrical parameters $\chi$ and $\psi$ is very suitable for a graphical representation of polarization but often not practical for use in computations. For computational purposes it is usually more

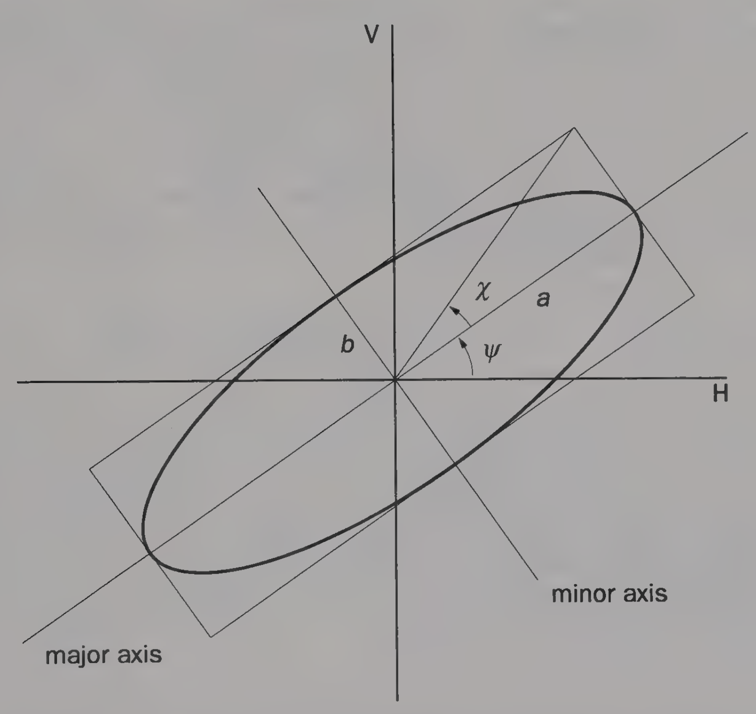



**Figure 3.15** All possible polarizations may be described with the use of just two parameters from the polarization ellipse, i.e. with ellipticity angle $\chi$ and orientation angle $\psi$. The values for $\chi$ may range from -45° to 45° and represent the ratio of the major $a$ and minor $b$ ellipse axes. The sign of $\chi$ is indicative of wave handedness. The values for $\psi$ may range from 0° to 180° and correspond to the angle between $a$ and the reference direction H. Wave amplitude is proportional to $\sqrt{a^2+b^2}$.

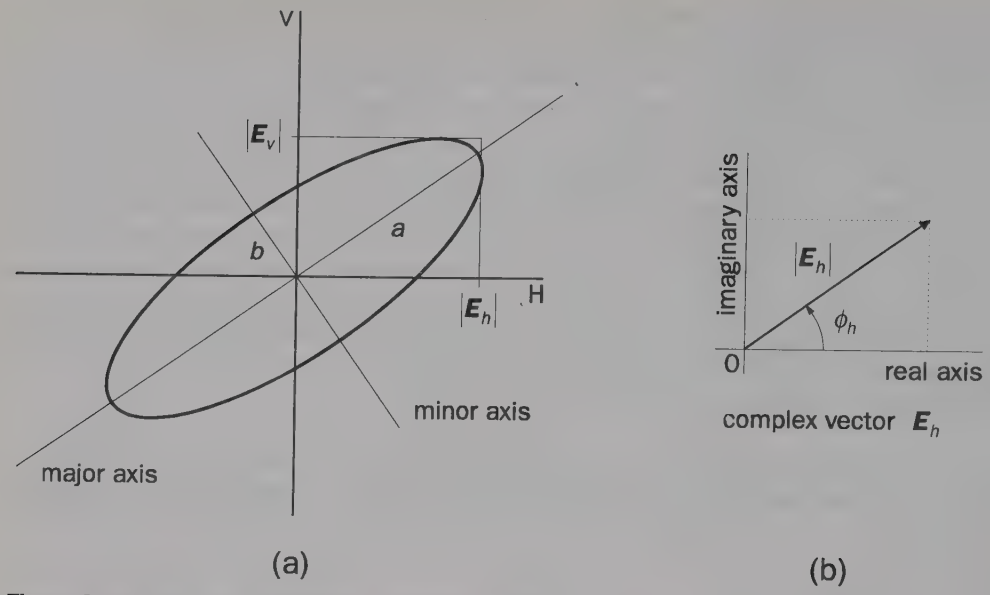



**Figure 3.16 (a-b)** (**a**) Relationship between polarization vector $\boldsymbol{p}$ and polarization ellipse. The shape of the ellipse agrees with the vector sum of the H- and V-polarized components of $\boldsymbol{p}$ as a function of time. (**b**) Vector representation of the H-polarized electrical field component $E_h$ in the complex plane. The vector length is indicative of amplitude $|E_h|$, while the angle between the vector and the real axis represents the phase $\phi_h$.

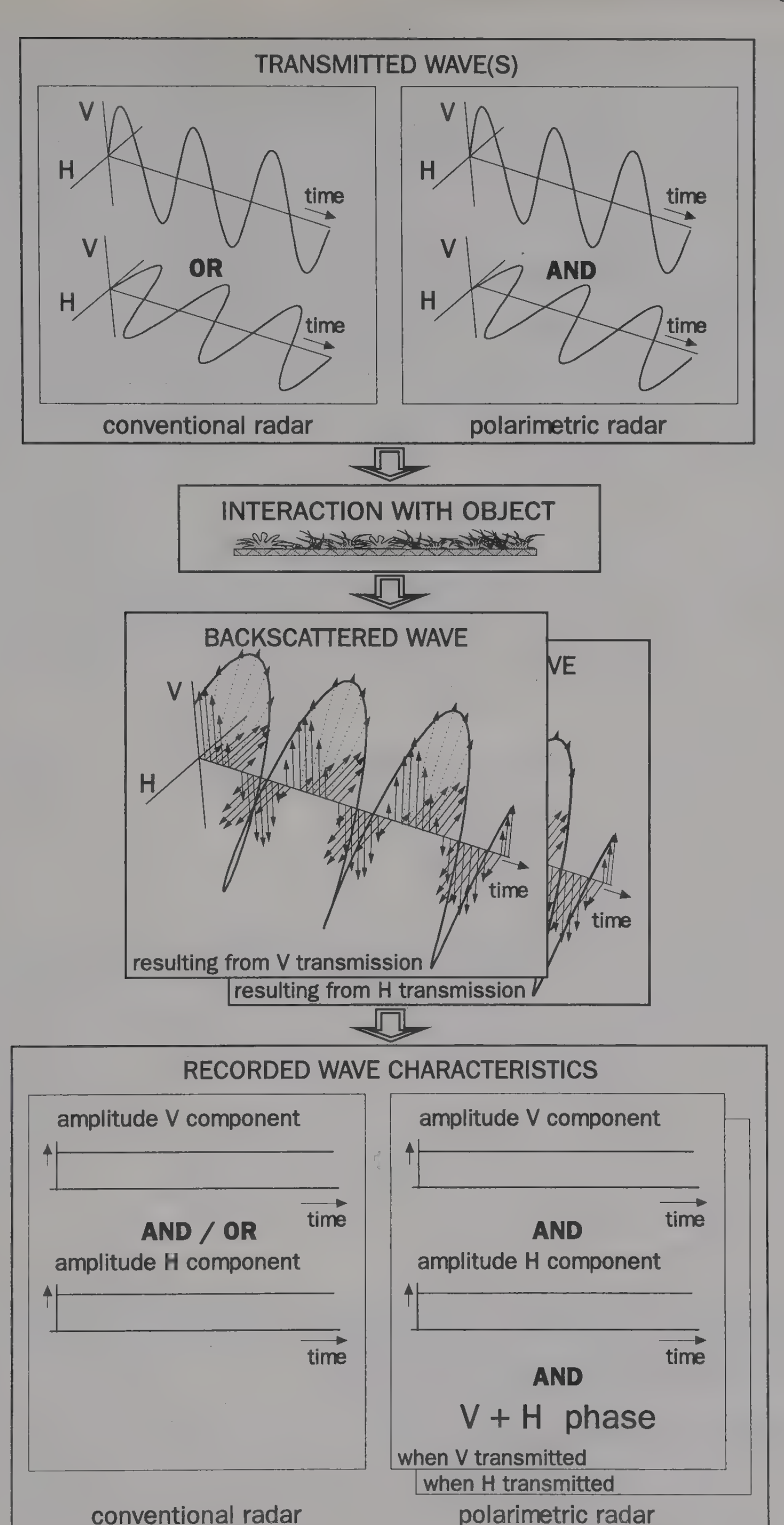
convenient to describe the polarization of a wave by means of a two-dimensional complex polarization vector $\boldsymbol{p}$. This vector can be written as (e.g. Kong, 1990; Ulaby and Elachi, 1990; Groot, 1991):

$$\boldsymbol{p} = \begin{pmatrix} E_h \\ E_v \end{pmatrix} = \begin{pmatrix} |E_h| e^{j\phi_h} \\ |E_v| e^{j\phi_v} \end{pmatrix} \tag{3.7}$$

where $E_h$ and $E_v$ represent the H- and V-polarized components of the electrical field, $|E_h|$ and $|E_v|$ the matching amplitudes and $\phi_h$ and $\phi_v$ the corresponding phases ($|\ |$ indicates modulus of complex number). The number $j$ in Equation 3.7 is equal to $\sqrt{-1}$. A graphical representation of the complex H-polarized electrical field component is shown in Figure 3.16. This figure, in addition, illustrates the relationship between the two alternative ways of describing wave polarization, i.e. the polarization ellipse and the polarization vector.

**Figure 3.17** Diagram of the operating principles of conventional and polarimetric radar systems. Conventional radars transmit either H- or V-polarized waves and record the amplitude of the received H- and/or V-polarized wave component. Polarimetric radars transmit both H- and V-polarized waves and record the amplitude as well as the phase of the received H- and V-polarized wave component.

→


TRANSMITTED WAVE(S)
V
H
time
V
OR
H
time
V
H
time
V
AND
H
time
conventional radar
polarimetric radar
INTERACTION WITH OBJECT
BACKSCATTERED WAVE
VE
V
H
time
time
resulting from V transmission
resulting from H transmission
RECORDED WAVE CHARACTERISTICS
amplitude V component
time
AND / OR
amplitude H component
time
amplitude V component
time
AND
amplitude H component
time
AND
V + H phase
when V transmitted
when H transmitted
conventional radar
polarimetric radar

To date, the information content of backscattered radar waves has not always been fully exploited in the practice of radar remote sensing. *Conventional radar systems are not capable of fully measuring the polarization properties of the radar return signal. Complete measurement of polarization properties requires the use of a more recently developed and more advanced type of radar, i.e. the imaging radar polarimeter or polarimetric radar system.* The operating principles of both conventional and polarimetric radar systems are illustrated in Figure 3.17. It can be seen that the two systems operate differently in both the transmission and the recording of the radar waves. Conventional radar systems transmit either an H- or V-polarized wave, while polarimetric radars transmit both H- and V-polarized waves. Following the interaction of the transmitted wave(s) with the observed object there will thus be one or two backscattered waves. These waves, when received by the radar antenna, will be recorded. A conventional radar system will record the amplitude of the received H- and/or V-component; a polarimetric system will record both the amplitude and the phase of the H- as well as the V-component. From Equation 3.7 it can be seen that only polarimetric systems can provide all of the measurements required to make up the polarization vector for a wave and therefore it is only these systems that can fully describe the polarization properties of both signals received. Polarimetric radar systems operate with two antennas. One of these controls the transmission and reception of waves/wave components with an H-polarization, the other of waves/wave components with a V-polarization (Ulaby and Elachi, 1990).

The combined measurements of a polarimetric radar system make up matrix $\boldsymbol{S}'$:

$$\boldsymbol{S}' = \begin{pmatrix} S'_{hh} & S'_{hv} \\ S'_{vh} & S'_{vv} \end{pmatrix} = \begin{pmatrix} \sqrt{\sigma_{hh}}e^{j\phi_{hh}} & \sqrt{\sigma_{hv}}e^{j\phi_{hv}} \\ \sqrt{\sigma_{vh}}e^{j\phi_{vh}} & \sqrt{\sigma_{vv}}e^{j\phi_{vv}} \end{pmatrix} \tag{3.8}$$

where $\sqrt{\sigma_{ij}}$ is the measured amplitude in case of $i$ receive and $j$ transmit and $\phi_{ij}$ the corresponding absolute phase. Using $\boldsymbol{S}'$ one can calculate the radar backscatter cross-section $\sigma_{rt}$ for any possible combination of transmitted $\boldsymbol{p}^t$ and received $\boldsymbol{p}^r$ radar waves according to:

$$\sigma_{rt}(\psi_r, \chi_r, \psi_t, \chi_t) = 4\pi\left|\boldsymbol{p}^r\boldsymbol{S}'\boldsymbol{p}^t\right|^2 \tag{3.9}$$

Matrix $\boldsymbol{S}'$ is related to the widely used scattering matrix $\boldsymbol{S}$ by:

$$\boldsymbol{S}' = \begin{pmatrix} 1 & 0 \\ 0 & -1 \end{pmatrix}\boldsymbol{S} = \begin{pmatrix} 1 & 0 \\ 0 & -1 \end{pmatrix}\begin{pmatrix} S_{hh} & S_{hv} \\ S_{vh} & S_{vv} \end{pmatrix} \tag{3.10}$$

Scattering matrix $\boldsymbol{S}$ describes the polarization transformation properties of the observed object, it relates the polarization of the scattered waves $\boldsymbol{p}^s$ to the polarization of the incident waves $\boldsymbol{p}^i$ according to:

$$\boldsymbol{p}^s = \frac{e^{jk_0R}}{R}\boldsymbol{S}\boldsymbol{p}^i \tag{3.11}$$

Here, $R$ is the slant range distance and $k_0$ the wave number of the illuminating wave in free space ($2\pi/\lambda_0$; where $\lambda_0$ is the free space wavelength). The discrepancy in the matrices $\boldsymbol{S}$ and $\boldsymbol{S}'$ results from differences in the description of polarization for scattered and received waves. These dissimilarities, in part, are due to different conventions for the definition of polarization for waves and antennas (e.g. Ulaby and Elachi, 1990).

The matrices and polarization vectors introduced apply to completely polarized waves, i.e. to waves with a time-independent polarization. However, in the practice of radar remote sensing the polarization of the received waves will usually vary in time and therefore the descriptors presented cannot be used. Application of radar polarimetry for earth observation requires the use of scattering descriptors as first set up by Stokes (1852). The Stokes equivalent for the polarization vector, i.e. the Stokes vector $\boldsymbol{F}$, can be written as:

$$\boldsymbol{F} = \begin{pmatrix} s_0 \\ s_1 \\ s_2 \\ s_3 \end{pmatrix} = \begin{pmatrix} |E_h|^2 + |E_v|^2 \\ |E_h|^2 - |E_v|^2 \\ 2|E_h||E_v|\cos(\phi_h - \phi_v) \\ 2|E_h||E_v|\sin(\phi_h - \phi_v) \end{pmatrix} = s_0 \begin{pmatrix} 1 \\ \cos(2\psi)\cos(2\chi) \\ \sin(2\psi)\cos(2\chi) \\ \sin(2\chi) \end{pmatrix} = s_0 \boldsymbol{A} \tag{3.12}$$

with $s_0 = |E_h|^2 + |E_v|^2$ and $\boldsymbol{A}$ being the normalized Stokes vector.

Stokes vectors of a scattered $\boldsymbol{F}^s$ and incident $\boldsymbol{F}^i$ wave are related through a $4 \times 4$ Stokes (or Mueller) matrix $\boldsymbol{L}$:

$$\boldsymbol{F}^s = \frac{1}{R^2} \boldsymbol{L} \boldsymbol{F}^i \tag{3.13}$$

Matrix $\boldsymbol{L}$ can be seen to correspond to the scattering matrix $\boldsymbol{S}$ (Equation 3.11). $\boldsymbol{L}$, like $\boldsymbol{S}$, relates the polarization properties of incident and scattered waves and not of transmitted and received waves. Consequently, $\boldsymbol{L}$ cannot be directly derived from radar system measurements. The matrix derived from these measurements, the $\boldsymbol{S}'$ equivalent, is denoted as the Stokes scattering operator $\boldsymbol{M}$ and related to $\boldsymbol{L}$ according to:

$$\boldsymbol{M} = \left[\boldsymbol{R}^{\mathrm{T}}\right]^{-1} \boldsymbol{R}^{-1} \boldsymbol{L} \tag{3.14}$$

with

$$\boldsymbol{R} = \begin{pmatrix} 1 & 1 & 0 & 0 \\ 1 & -1 & 0 & 0 \\ 0 & 0 & 1 & 1 \\ 0 & 0 & -j & j \end{pmatrix} \tag{3.15}$$

and with: T and -1 indicating, respectively, the transposed and the inversed matrix.

The elements of the Stokes scattering operator relate to the elements of matrix ***S'*** by:

$$M_{11} = \frac{1}{4}\left(|S'_{hh}|^2 + |S'_{vv}|^2 + 2|S'_{hv}|^2\right) \tag{3.16}$$

$$M_{12} = \frac{1}{4}\left(|S'_{hh}|^2 - |S'_{vv}|^2\right) \tag{3.17}$$

$$M_{13} = \frac{1}{2}\mathrm{Re}\left(S'^{*}_{hh}S'_{hv} + S'^{*}_{vv}S'_{hv}\right) \tag{3.18}$$

$$M_{14} = \frac{1}{2}\mathrm{Im}\left(S'^{*}_{hh}S'_{hv} - S'^{*}_{vv}S'_{hv}\right) \tag{3.19}$$

$$M_{22} = \frac{1}{4}\left(|S'_{hh}|^2 + |S'_{vv}|^2 - 2|S'_{hv}|^2\right) \tag{3.20}$$

$$M_{23} = \frac{1}{2}\mathrm{Re}\left(S'^{*}_{hh}S'_{hv} - S'^{*}_{vv}S'_{hv}\right) \tag{3.21}$$

$$M_{24} = \frac{1}{2}\mathrm{Im}\left(S'^{*}_{hh}S'_{hv} + S'^{*}_{vv}S'_{hv}\right) \tag{3.22}$$

$$M_{33} = \frac{1}{2}|S'_{hv}|^2 + \frac{1}{2}\mathrm{Re}\left(S'^{*}_{hh}S'_{vv}\right) \tag{3.23}$$

$$M_{34} = \frac{1}{2}\mathrm{Im}\left(S'^{*}_{hh}S'_{vv}\right) \tag{3.24}$$

$$M_{44} = \frac{1}{2}|S'_{hv}|^2 - \frac{1}{2}\mathrm{Re}\left(S'^{*}_{hh}S'_{vv}\right) \tag{3.25}$$

where the asterisk denotes the complex conjugate.

For most land surface areas it can be shown that $S'_{hv}$ and $S'_{vh}$ are identical. The latter causes ***M*** to be symmetrical and makes this $4 \times 4$ matrix fully describable with just 10 elements, i.e. the elements as defined in Equations 3.16 through 3.25. The equality of $S'_{hv}$ and $S'_{vh}$ for land surfaces follows from the reciprocity principle. This principle implies interchangeability of polarization states of radar signals. It may be described as follows: when a wave with polarization 'a' is incident and a scattered wave with polarization 'b' results, then a wave with polarization 'a' will result when a wave with polarization 'b' is incident and the propagation directions are reversed (Hoekman, 1997).

With the help of the Stokes scattering operator it is possible to calculate the radar cross-section, and thus sigma nought or gamma, for *any* combination of receive and transmit polarizations. The process for doing this is called wave synthesis (van Zyl et al., 1987) and can be written as follows:

$$\sigma_{re}(\psi_r, \chi_r, \psi_t, \chi_t) = 4\pi \boldsymbol{A}^r \boldsymbol{M} \boldsymbol{A}^t \tag{3.26}$$

The processing of polarimetric SAR images, like that of conventional SAR images, involves look averaging (see section 3.1.3). Therefore, in radar polarimetry, in practice, matrix $\boldsymbol{M}$ will always represent the spatial average of a series of $\boldsymbol{S}'$ matrices. In view of the analysis of polarimetric radar images it is useful to note that $\boldsymbol{M}$ matrices for neighbouring pixels may be averaged linearly.

## 3.2 Interaction of microwaves with forests

### 3.2.1 Microwave interaction principles

In order to describe the interaction of microwaves with the forest it is convenient to view the forest as a combination of three media, i.e. soil, vegetation and air. The surface of the forest soil makes a distinct boundary between the soil and air and/or the soil and vegetation media. The boundary between vegetation and air is less well defined since air can be found above as well as within vegetation. Both vegetation and soil consist of various particles that in part may be built up out of a multitude of materials. When compared to air, vegetation and soil are heterogeneous media. In fact, they constitute a mixture of several (sub-)media. Examples of vegetation and soil (sub-)media are the constituent materials to leaves, branches, trunks, litter and rocks.

*The processes that govern the interaction of microwaves with forests (or any other object) are: transmission, reflection (or scattering) and absorption.* Microwave transmission and reflection can occur at the boundaries of two adjoining media while microwave absorption takes place within a specific medium. Perfect (i.e. 100%) transmission is restricted to boundaries of media with identical electrical properties.

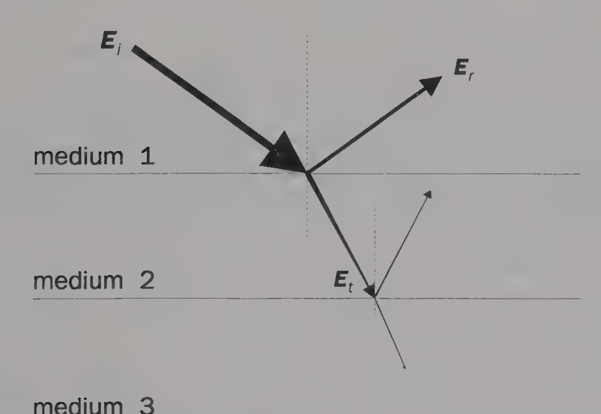



**Figure 3.18** Microwave interaction in adjoining homogeneous media with different electrical properties. The incident microwave $\boldsymbol{E}_i$ is both reflected $\boldsymbol{E}_r$ and transmitted $\boldsymbol{E}_t$ at the boundary of medium 1 and 2. The absorption of microwave energy by medium 2 causes the transmitted wave to loose power. At the interface of media 2 and 3 $\boldsymbol{E}_t$ is reflected and transmitted once again.

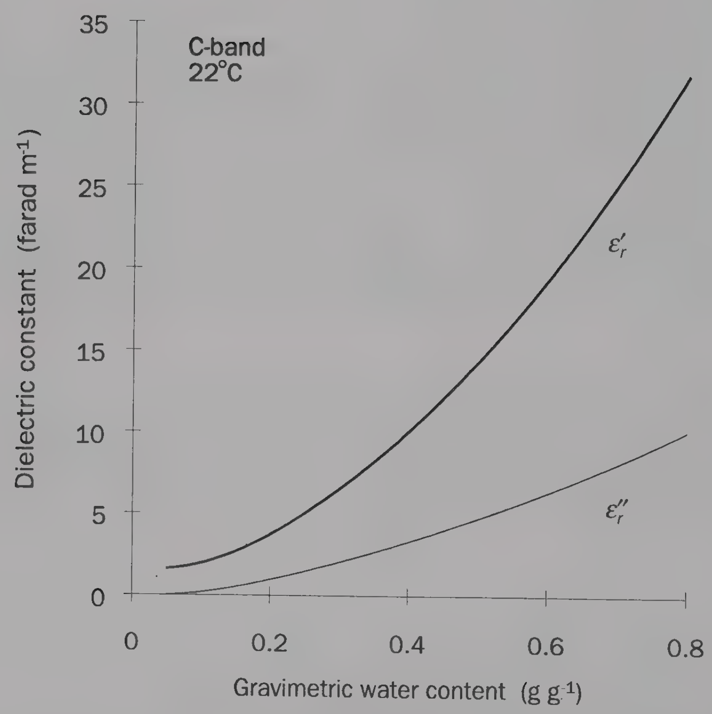



**Figure 3.19** Dielectric constant as a function of gravimetric water content for corn leaves in C-band at 22°C. $\varepsilon_r'$ and $\varepsilon_r''$ are the real and imaginary parts of the complex dielectric constant, respectively. Other vegetation materials display a similar trend in the variation of $\varepsilon_r'$ and $\varepsilon_r''$ with respect to water content. (Based on model by Ulaby and El-Rayes, 1987.)

Perfect reflection occurs only if the electrical properties of the medium encountered are like those of a theoretical object known as a perfect conductor. At boundaries between forest media perfect transmission or reflection does not generally occur. Usually, the incident microwaves are in part transmitted, while the rest are reflected (see Figure 3.18). Transmission and reflection of microwaves is a repetitive but finite process. Microwaves transmitted at one point in time may be reflected and/or transmitted once again when they encounter another boundary. The process, however, is finite since there is a loss of power in the direction of propagation due to both reflection and absorption. This *loss of power is known as the extinction or the attenuation of microwaves.* Extinction or attenuation is a two-way process because it occurs to microwaves travelling *into* as well as *out of* the object observed.

*The amount of power that is transmitted, reflected and/or absorbed is strongly influenced by the electrical properties of the media concerned.* The parameter that quantifies these electrical properties is known as the *relative dielectric constant* $\varepsilon_r$. $\varepsilon_r$ is complex and can be written as:

$$\varepsilon_r = \frac{\varepsilon_c}{\varepsilon_0} = \varepsilon_r' - j\varepsilon_r'' \tag{3.27}$$

where $\varepsilon_c$ is the dielectric constant of the material and $\varepsilon_0$ is the dielectric constant of free space. In practice the real part $\varepsilon_r'$ governs the ratio of transmitted and reflected power. In combination with $\varepsilon_r'$ the imaginary part $\varepsilon_r''$ determines the amount of absorbed power (de Hoop, 1975). Clearly, the designation relative relates to the fact that the dielectric constant of a medium is normalised to the dielectric constant of free space. Free space is a lossless medium, i.e. a medium with 100% transmission and no reflection or absorption. For media other than free space it holds that $\varepsilon_r' > 1$ and $\varepsilon_r'' > 0$. The values for $\varepsilon_r'$ and $\varepsilon_r''$ depend on intrinsic characteristics of the medium, i.e. type and proportion of constituent materials, as well as on external variables such as microwave frequency and temperature.

Natural media such as soil and vegetation can be seen as mixtures of bulk material, air and water. The *relative complex dielectric constant* (from here on referred to as the dielectric constant) for such media *tends to be strongly influenced by their water content.* Figure 3.19 illustrates the relationship between the water content and the dielectric constant for corn leaves in C-band at 22° C (Ulaby and El-Rayes, 1987). For vegetation material with a dry weight per unit volume other than that of corn leaves (i.e. 0.33 g $cm^{-3}$) the relationship will differ. However, the trend in the relationship will be the same, i.e. an increase in $\varepsilon_r'$ and $\varepsilon_r''$ with an increase in water content. In Figure 3.19 the moisture status of the vegetation is expressed in terms of the gravimetric water content. The gravimetric water content *for vegetation* is defined as the mass ratio of water to bulk material, i.e. gram water per gram *wet*-weighted vegetation material. In contrast, the gravimetric water content *for soil* is defined as the mass ratio of water to solid phase, i.e. gram water per gram *dry*-weighted soil material (Koorevaar et al., 1983). The dominating effect of water on the dielectric properties of vegetation and soil implies that this element strongly affects the transmission and extinction of microwaves in forests. An increase in water content

will generally result in decreased transmission and increased extinction (reflection plus absorption).

Figure 3.20 illustrates the changes in the radar cross section $\sigma_{leaf}$ and the extinction cross section $\sigma_{ext,\ leaf}$ as a function of gravimetric water content for a *single* tree-leaf in C-band. The two cross sections are normalised to those of a metal leaf (perfect conductor) of the same size. In practice the gravimetric water content of tree-leaves ranges from 0.4 to 0.8 g $g^{-1}$. An increase in gravimetric water content is shown to result in an increase in both the leaf's radar and extinction cross section. As the radar cross section of the leaf increases it will reflect more power, i.e. generate more backscatter. Similarly, as the extinction cross section of the leaf increases it will attenuate more power, i.e. generate less backscatter. *The backscatter of the ensemble of leaves in a forest canopy is governed by the radar cross section and the extinction cross section of the average leaf.* According to the Cloud model by Attema and Ulaby (1978) the radar cross-section per unit projected area $\gamma$ for an "opaque" forest canopy is given by:

$$\gamma = \frac{\sigma_{leaf}}{2\sigma_{ext,leaf}} \qquad [m^2\ m^{-2}] \qquad (3.28)$$

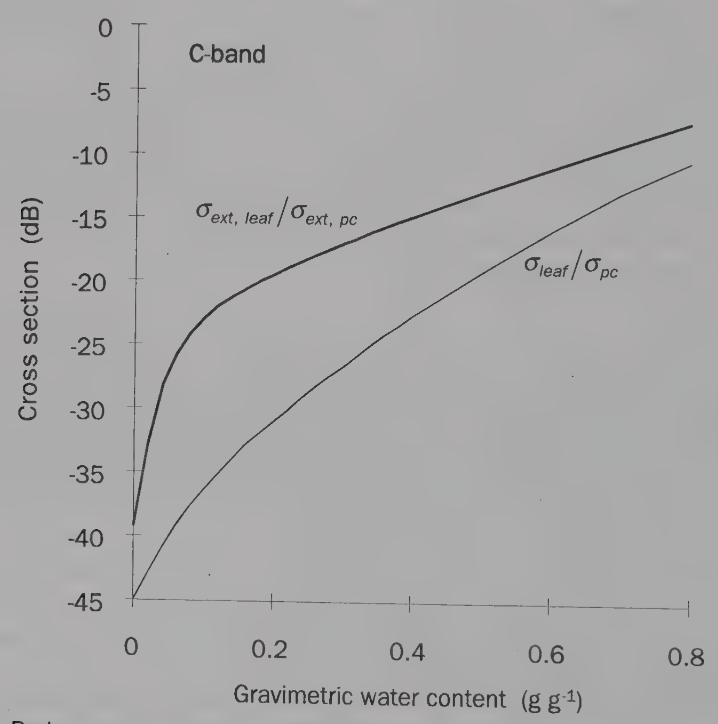



**Figure 3.20** Radar cross section $\sigma_{leaf}$ and extinction cross section $\sigma_{ext,\ leaf}$ as a function of gravimetric water content for a single tree-leaf at C-band. The values for $\sigma_{leaf}$ and $\sigma_{ext,\ leaf}$ have been normalized to those of a perfect conducting metal leaf of the same dimensions, i.e. $\sigma_{pc}$ and $\sigma_{ext,\ pc}$. (Adapted from Ulaby, 1992.)

At the logarithmic dB scale this translates into:

$$\gamma = \sigma_{leaf} - \sigma_{ext,leaf} - c \qquad \text{[dB]} \qquad (3.29)$$

where $c$ is a constant. The designation "opaque" implies that all incident microwaves are scattered by the canopy, i.e. that there is no transmission of microwaves and thus no backscatter from the forest soil. It follows from this equation that the $\gamma$ for an opaque forest canopy comprising leaves similar to the one used to derive the backscatter and extinction cross section curves shown in Figure 3.20 is reflected in the vertical distance between those curves. Figure 3.20 illustrates that an increase in gravimetric water content from 0.4 to 0.8 g $g^{-1}$ results in a smaller vertical distance between the curves. This implies that $\gamma$ becomes a smaller *negative* number, i.e. that the *radar backscatter increases as a function of water content.*

With regard to the reflection or scattering of microwaves one usually distinguishes between surface scattering and volume scattering. The designation surface scattering is used for reflections at boundaries between 'primary' media, e.g. the vegetation-soil interface. Volume scattering refers to reflections that originate from within the (heterogeneous) 'primary' media, e.g. from within the vegetation or the soil layer. The reflection of microwaves in the direction of the sensor, i.e. *back*scattering, provides the basis for radar system operation (see section 3.1.1). The backscattering process is therefore of utmost importance in radar remote sensing. *The radar backscatter from closed forests is generally dominated by return signals originating from volume scattering in the interior of the vegetation layer and surface scattering at the underlying forest soil.* Surface scattering at the air-vegetation interface usually is negligible since the average dielectric properties of the canopy are close to those of air. Exceptions occur in those situations where the scattering elements are of a size greater then or equal to ca. 10 times the incident wavelength. Under such circumstances, the scattering is governed by the dielectric properties of the individual scatterers and not by the average dielectric properties of the canopy at large. Generally speaking, the amount of backscatter resulting from soil volume scattering is small in comparison to that resulting from scattering at the forest soil surface. Hence, soil volume scattering is an insignificant interaction process in closed forests.

Volume scattering in the vegetation layer encompasses single scattering at individual vegetation particles (e.g. leaves, twigs, branches, trunks) and multiple scattering at a series of vegetation particles. Soil surface scattering may occur when the radar waves either directly or indirectly reach the soil surface under the forest. Direct soil surface scattering occurs when gaps are present or when the waves are able to penetrate through the vegetation layer. Indirect soil surface scattering results from multiple scattering between the vegetation particles and the soil. Generally speaking, *the amount of scattered, and thus backscattered energy will depend on both the wave parameters and the scattering properties of the object observed. Relevant wave parameters include:*

- frequency (or wavelength)
- polarization of transmitted and received waves
- observation incidence angle
- viewing geometry (i.e. relative orientation of sensor and observed object).

If the wave parameters are fixed by the system design and the flight plan, then the average backscattered energy will only vary with the scattering properties of the objects observed. At present the interaction of microwaves with complex objects such as forests is still not fully understood. Nevertheless, it is possible to list variables that have been found to govern the forest's (back)scattering behaviour. *The scattering properties of the forest soil are known to depend on the:*

- random surface roughness
- periodic surface patterns
- dielectric properties (mainly determined by water content)

*The scattering behaviour of the forest vegetation is influenced by the:*

- thickness of the volume
- density of the component particles (or scatterers)
- size distribution of the component particles
- shape distribution of the component particles
- orientation distribution of the component particles
- dielectric properties of the component particles.

The listed variables relate to structural, architectural and material forest properties. Surface roughness and surface patterns are structural properties of the forest soil. The distributions of the size, shape and orientation of the component vegetation particles reflect the forest's architecture. Soil and vegetation dielectric characteristics, vegetation volume thickness and particle density are qualified best as material properties.

Structural and architectural properties affect scattering behaviour because they govern the spatial distribution of the scattered power, i.e. the proportion of microwave energy scattered in the backscatter as well as in other directions. The effect of these properties, however, depends strongly on the incident wavelength. For a more detailed discussion on this topic the reader is referred to section 3.2.2. Material properties influence the magnitude of the scattered power in all directions. Their effect depends primarily on the soil and/or vegetation water content.

The relative importance of the soil and vegetation variables listed is strongly dependent on the wave parameters. The role of these parameters in the interaction of microwaves with forests is discussed in sections 3.2.2 through 3.2.5. For more information on the principles of microwave interaction with forests and other objects the reader is referred to handbooks such as Ulaby et al. (1981, 1982, 1986b) and Colwell et al. (1983).

### 3.2.2 Effects of wavelength

Wavelength $\lambda$ is of primary importance in the interaction of microwaves with forests as it affects the penetrating capacity of the microwaves and the spatial distribution of the scattered power.

The extent to which microwaves are able to vertically penetrate an object is denoted here as the depth of vertical penetration $\delta_p$. Depth of vertical penetration is defined as the vertical distance below the surface at which the power of the incident wave will have decreased to a level equal to $e^{-1}$ times the level at the surface. For most natural materials, with the exception of water, the depth of vertical penetration is approximated by:

$$\delta_p \cong \frac{\lambda\sqrt{\varepsilon_r'}\cos(\theta_{inc})}{2\pi\varepsilon_r''} \quad [\mathrm{m}] \qquad (3.30)$$

Equation 3.30 is simple, nevertheless it is problematic to reliably estimate $\delta_p$ for forests (and other vegetation types). This is due to difficulties in establishing the effective dielectric constant of the heterogeneous forest vegetation. However, the equation shows that *a microwave with a long wavelength $\lambda$ penetrates a forest with given dielectric properties to a greater depth than a microwave with a short wavelength.* Furthermore, the equation shows that $\delta_p$ decreases with an increase in incidence angle $\theta_{inc}$. Some indication of the penetration of microwaves in tropical forests is found in studies by Imhoff et al. (1986) and Aiba et al. (1988). Both studies analyse the penetration of L-band microwaves with incidence angles ranging from 35° to 55° in mangrove forest. The results, however, differ considerably. Imhoff et al. report that the $\delta_p$ may be as much 12.5 m, while Aiba et al. report a $\delta_p$ of ca. 6 m. Differences in $\delta_p$ affect the interaction of the microwaves with the forest because the processes of transmission, scattering and absorption take place in different parts of the volume and/or at different surfaces.

In section 3.2.1 the spatial distribution of the power scattered by forest components was said to depend on their structural and architectural properties. More indirectly however, the power distribution or scattering pattern is also dependent on the wavelength of the incident microwaves. *In the context of microwave interaction, the scale of soil surface roughness and soil surface pattern and the size of vegetation particles must be seen relative to the incident wavelength.* Wavelength defines the effective scale of soil roughness and pattern as well as the effective size of vegetation particles. The scattering patterns of forest components are governed by their effective rather than actual scales and sizes. It therefore follows that *wavelength affects scattering patterns.*

For a given wavelength the influence of effective roughness on the scattering pattern of a non-periodic soil surface is illustrated in Figure 3.21. A perfectly plane surface (Figure 3.21a) is shown not to generate backscatter since it reflects all of the incident microwaves in a narrow beam away from the sensor. This scattering pattern is commonly referred to as specular reflection while the direction in which the

scattering occurs is denoted as the forward direction. The other limiting case, i.e. the random rough surface (Figure 3.21c), reflects the incident power uniformly in all possible directions above the surface. It displays a so-called diffuse scattering pattern which results in a relatively strong radar backscatter. The scattering pattern of the surface with intermediate roughness (Figure 3.21b) comprises both a specularly reflected and diffusely scattered component. The magnitude of the specularly reflected component is smaller than that for the plane surface. Likewise, the magnitude of the diffusely scattered component, and thus of the backscatter, is smaller than that for the random rough surface.

In practice, the scale of the surface roughness may be approximated by the vertical relief, or the average height of the surface irregularities $h$. As a rule of thumb, $h$ is computed from observations with a horizontal spacing $\leq 0.1\lambda$ (Ulaby et al., 1982). According to Sabins (1987) the following criteria may be used in the definition of three *effective roughness* classes:

- smooth ; $$h < \frac{\lambda}{25\cos(\theta_{inc})} \tag{3.31}$$

- rough ; $$h > \frac{\lambda}{4.4\cos(\theta_{inc})} \tag{3.32}$$

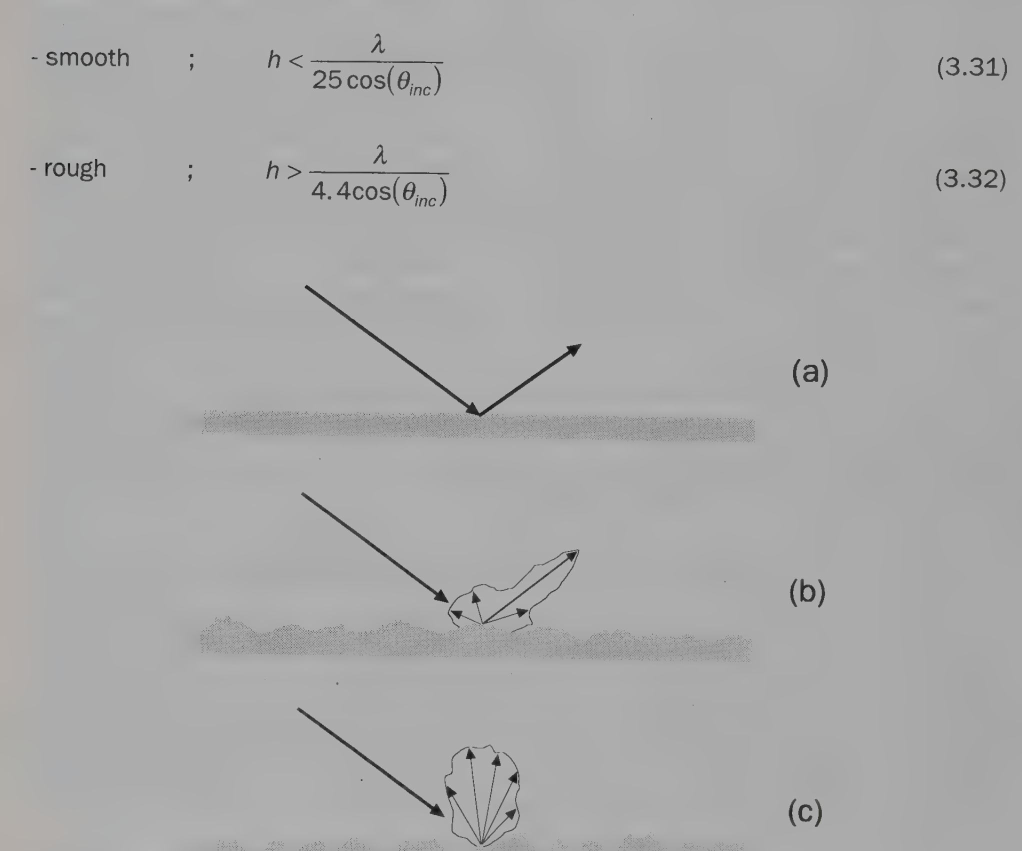



**Figure 3.21 (a-c)** Effect of surface roughness on scattering pattern. (**a**) Perfectly plane surface; no backscatter, all incident power is specularly reflected in the forward direction (away from sensor). (**b**) Intermediate surface; moderate backscatter, incident power is specularly reflected in the forward direction and diffusely scattered in all other directions above the surface. (**c**) Rough surface; strong backscatter, incident power is diffusely scattered in all possible directions above the surface. (Adapted from Schanda, 1986.)

- intermediate; $$\frac{\lambda}{4.4\cos(\theta_{inc})} < h < \frac{\lambda}{25\cos(\theta_{inc})} \quad (3.33)$$

where both $h$ and $\lambda$ are in m. Sabins' criterion for a smooth surface deviates slightly from the Fraunhofer criterion as proposed by Ulaby et al. (1982). In this criterion the multiplier in the denominator of Equation 3.31 equals 32 rather than 25. Ulaby et al. distinguish between smooth and rough surfaces only. The Equations 3.31 through 3.33 and Figure 3.21 show that the effective roughness of a scattering (forest soil) surface is assessed easily and that the relationship between wavelength and scattering pattern of a surface is well understood. The Equations 3.31 through 3.33 show that the effective roughness of a soil surface varies as a function of the incidence angle. For a more detailed discussion on the effects of incidence angle on the interaction of microwaves with forests the reader is referred to section 3.2.4.

The scattering pattern of the scatterers in the forest vegetation volume (e.g. leaves, branches and trunks) depends strongly on their *effective size*. According to Knott et al. (1985) the behaviour of scatterers with size $l$ may be classified as:

- low-frequency (or Rayleigh) scattering ; $l \leq 0.4\lambda$ (3.34)
- high-frequency (or geometric) scattering ; $l > 10\lambda$ (3.35)
- resonant scattering ; $0.4\lambda < l \leq 10\lambda$ (3.36)

Low-frequency scatterers act as a single scatterer, i.e. the entire object participates in a single scattering process. High-frequency and resonant scattering objects, on the other hand, may be said to comprise a collection of scatterers, as parts of the object create different scattering processes. In a resonant scattering process there is interaction between the waves reflected by the component scatters. In a high-frequency scattering process this is not the case. The patterns resulting from resonant scattering are more difficult to predict than those resulting from low- and high-frequency scattering. This is due to the fact that the resonant scattering process is more sensitive to the sizes, shapes and orientations of scatterers. For similar reasons, the radar cross sections for resonant scattering objects cannot be predicted as easily as those for low- or high-frequency scattering objects.

Scattering at the forest soil surface is a typical example of high-frequency scattering. However, high-frequency scattering may also occur at relatively large forest vegetation components, e.g. at tree trunks in X- or C-band. In practice, a radar system does not usually observe a single low-frequency scatterer but rather a collection of such scatterers. The scattering behaviour of a composite low-frequency scattering object is governed by the volume of the component scatterers. A volume of low-frequency scatterers does not usually generate much backscatter. The effect of such a volume on the overall backscatter level primarily results from its capability to attenuate microwave energy. A typical example of a low-frequency scattering volume is the collection of leaves, twigs and small branches in P-band. The presence of these forest components does in fact decrease the amount of microwave energy received by a P-band radar system.

**Table 3.2** Summary of the *general* [1] relationship between wavelength and the scattering behaviour of the components in a closed forest. The marking is as follows: '++' main backscattering source, '+' secondary backscattering source and '-' attenuating source.

| | Forest component | | | | | |
|---|---|---|---|---|---|---|
| Wavelength | Leaves | Twigs | Secondary branches | Primary branches | Trunks | Soil |
| X-band | ++ | ++ | ++ | | | |
| C-band | ++ | + | ++ | | | |
| L-band | - | - | ++ | ++ | ++ | + |
| P-band | - | - | - | ++ | ++ | ++ |

1) Depending on their effective size, components may have a scattering behaviour that deviates from the one listed.

*The effective size of forest vegetation particles depends on their physical dimensions but also on their shape and orientation.* Generally speaking, many of these particles act as resonant scattering objects since their size is neither small nor large in comparison to the incident wavelength (see Equations 3.34 through 3.36). The backscatter from such objects was said to be highly sensitive to variations in effective size and hence difficult to predict. In the practice of radar remote sensing, however, one does not observe the individual scattering particles but rather a collection of scatterers with a wide variation in both architectural and material properties. Therefore, *radar backscatter measurements of forests rarely expose the specific, and possibly extreme, backscattering behaviour of individual particles.*

The effect of wavelength on the backscattering behaviour of the components in a closed forest is summarised, in a generalised manner, in Table 3.2. Depending on their effective size, components may have a scattering behaviour that differs from the one listed. The information in this table is mainly based on results from analysis of radar data for forests in temperate regions. At present, results relating to tropical forests (notably in P-band) are scarce. The table shows clearly that microwaves with different wavelengths interact with different forest parts. It may thus be concluded that *microwaves with different wavelengths make up complementary information sources on forests.* This also implies that particular wavelengths are more suited for some applications than for others. L- and P-band, for example, are much better suited for estimating trunk biomass parameters than X- and C-band.

### 3.2.3 Effects of polarization

The polarization of incident microwaves affects their interaction with forests because it defines the plane in which the microwave interaction will take place. In the present text this plane will be referred to as the polarization plane. The polarization plane is built up by the vector defining the electrical field, i.e. the vector representing polarization, and the propagation vector (see section 3.1.2). For linear waves the orientation of the electrical field does not vary in time and as such the orientation of the polarization plane is constant. For non-linear waves, however, the orientation of

the electrical field and polarization plane will vary as a function of time over a $2\pi$ range.

*The polarization plane restricts the microwave interaction to object parts located in this plane.* Waves with a horizontal (vertical) polarization, for example, will only interact with object parts in the horizontal (vertical) plane. To describe the interaction between objects and microwaves with different polarizations the effective size concept as introduced in section 3.2.2 needs to be accentuated. *The effective size of an object must express its size in the polarization plane.* For all but spherical objects the effective size will thus depend on the polarization of the incident wave. The (back)scatter behaviour of non-spherical objects will therefore be polarization dependent.

The effect of polarization on microwave interaction may be illustrated with a very much simplified forest model. Consider a forest consisting of a collection of, rough, vertical cylinders over a smooth surface. The cylinder length (size in vertical direction) is $>0.4\lambda$ and much larger than the cylinder radius (size in horizontal direction). The forest is assumed to be observed under non-extreme incidence angles, e.g. in the range of 20° to 70°. Due to the orientation of the polarization plane vertically polarized waves will interact with a larger portion of the cylinders than horizontally polarized waves. The cylinders, in other words, act as resonant or high-frequency scatterers for vertically polarized waves and as low-frequency scatterers for horizontally polarized waves. Hence, for vertically polarized waves the cylinders act as (back)scattering objects, while for horizontally polarized waves they act as attenuating objects (see section 3.2.2). Consequently, vertically transmitted waves will be scattered back to a higher degree than horizontally transmitted waves. In both polarizations the backscatter originating from direct interaction of microwaves with the underlying surface is negligible since this surface is smooth. Backscatter contributions resulting from multiple interactions between the cylinders and the underlying surface are left aside. The example also shows why horizontally polarized waves may penetrate deeper into a forest than vertically polarized waves. On their way into the forest both the horizontally and vertically polarized waves will be attenuated by the cylinders. However, due to (back)scattering the loss of power for vertically polarized waves will be considerably higher than for horizontally polarized waves. Therefore, waves with a horizontal polarization will penetrate deeper than waves with a vertical polarization.

As noted in section 3.2.2 radar systems observe a collection of forest vegetation particles. *The effect of polarization on the interaction of microwaves with these particles diminishes as the particles' orientations and other architectural properties become more diverse.* In a forest the majority of the scatterers are distributed widely in orientation, architecture and space. Consequently, the interaction of microwaves with these scatterers will show little dependence on polarization. Tree trunks make exceptional scatterers because of a predominantly vertical orientation. Hence, the interaction of microwaves with tree trunks is noticeably polarization dependent (see example above).

The interaction of microwaves with an object may result in polarization changes. First, *microwave interaction may cause the polarization plane of the scattered wave to be different from that of the incident wave,* e.g. a transformation from horizontal to vertical. Second, *microwave interaction may result in depolarization.* Due to depolarization the scattered waves become partially polarized. Partially polarized waves have an unpolarized component. Waves transmitted by radar systems lack an unpolarized component and are therefore denoted as completely polarized. Partially polarized waves stand midway between completely polarized and completely unpolarized waves. Whereas the polarization of completely polarized waves is fixed both in time and in space, the polarization of completely unpolarized waves changes randomly. Microwaves transmitted by radar systems were given as examples of completely polarized waves. Waves emitted by the sun may be referred to as examples of completely unpolarized waves. Changes in the polarization of radar waves are often object specific and, therefore, an important source of information for discriminating objects in radar images.

Microwaves that interact with forests and other types of vegetation are known to become depolarized to a high degree. Depolarization in vegetation volumes is caused by the multiple reflection of waves at resonant scatterers, e.g. leaves, twigs and branches. Strong depolarization implies that the scattered waves will have a large unpolarized component. This large unpolarized component, in turn, gives rise to a substantial amount of cross-polarized backscatter which is characteristic for vegetation. Because of its dispersing effect on polarization the multiple reflection interaction process in vegetation volumes is often referred to as diffuse scattering. However, diffuse scattering in vegetation volumes is not to be confused with diffuse scattering at surfaces (see Figure 3.21c). *Diffuse volume scattering involves diffusion of polarization, whereas diffuse surface scattering involves diffusion of incident power.*

### 3.2.4 Effects of incidence angle

The effects of the incidence angle on the microwave-forest interaction are primarily due to its influence on the microwave penetration depth. *By affecting the depth of vertical penetration the incidence angle determines the extent to which microwaves interact with their main backscatter sources.* For microwaves with short wavelengths, the most important sources of backscatter are concentrated in the upper parts of the forest (e.g. leaves, twigs, secondary branches). For long wavelengths, the most important backscatter sources are found in the lower forest parts (e.g. primary branches, trunks, forest soil). According to Equation 3.30 the depth of vertical penetration $\delta_p$ will decrease with an increase in incidence angle $\theta_{inc}$. An increase in incidence angle will thus result in a reduced capability for long wavelengths to interact with their principal scatterers. Hence, radar systems that operate with long wavelengths will generally measure relative high (low) backscatter levels at small (large) incidence angles. The interaction process for waves with short wavelengths is not as sensitive to incidence angle variations because there are an abundance of scatterers in the upper parts of the forest. Generally speaking, measurements from systems with short wavelengths will show little dependence on incidence angle.

The importance of incidence angle in relation to microwave interaction is illustrated, in another way, in Equations 3.31 through 3.33 (see section 3.2.2). These equations are valid for high-frequency, surface scattering objects. They show that the effective roughness of such an object is inversely proportional to the cosine of the incidence angle. Consequently, an increase in incidence angle will result in a larger effective roughness. Changes in effective roughness as a function of incidence angle will affect the (back)scattering pattern of the object observed (see Figure 3.21). The most likely affected (back)scattering pattern in forests is that of the forest soil. In many circumstances, however, the microwaves will not be able to interact with the soil as their wavelength is too short to penetrate the overlying vegetation. Alternatively, in those cases where microwaves with long wavelengths are used, the soil may be effectively smooth throughout the entire incidence angle range. Hence, it may be concluded that *for the interaction of microwaves with forests the effect of the incidence angle on the effective surface roughness is of little importance.*

### 3.2.5 Effects of viewing geometry

The term viewing geometry describes the relative orientation of the sensor to the observed object. Its effect on the appearance of objects in radar images is a direct result of the radar operating principles, i.e. the side-looking configuration and the measurement through ranging. *Variations in viewing geometry can affect the appearance of objects with specific spatial features, i.e. non-randomly oriented scatterers and/or distinct spatial patterns.*

The effect of the viewing geometry on the image of objects that hold (non-spherical) scatterers with specific orientations relates to the effective size of the scatterers and results in varying backscatter levels. This size is dependent on the orientation of the scatterer relative to the direction of propagation of the incident wave and thus on viewing geometry. Leaves, for example, will exhibit their largest effective size when they are located in a plane perpendicular to the direction of propagation of the incident waves. Therefore, if a certain forest consists of trees with a specific leaf orientation then its backscatter (at short wavelengths) can be expected to reach a maximum when the viewing geometry is such that the microwaves travel in a direction perpendicular to the plane through the leaf surfaces.

The effects of viewing geometry in relation to the imaging of objects with specific spatial patterns, e.g. linear objects such as roads or row plantations, can be seen in the backscatter level as well as the image geometry. These objects, depending on their orientation relative to the sensor, may induce foreshortening, layover and shadowing effects (see section 3.1.3). Such effects greatly enhance their visibility in an image but occur only when their orientation is deviant from the radar range direction. If this is not the case then the radar may detect, for example, a road but no road-forest transitions. Consequently, there will be no distinct height differences in the range direction and thus no foreshortening, layover and shadowing effects.

### 3.2.6 Forest backscatter modelling

Forest backscatter models may be used in either a forward or an inverse modelling approach. In a forward modelling approach they serve to estimate the radar return signal as a function of wave parameters (i.e. frequency, polarization, incidence angle) and/or architectural and material forest properties. Forward modelling facilitates radar data analysis and image interpretation as it allows simulation of the effects of changing wave parameters and forest properties. In an inverse modelling approach the models are applied to estimate the forest's architectural and material properties from a given set of radar data.

Existing forest backscatter models may be grouped into three main categories: empirical models, physical models and semi-empirical models. Empirical models are developed by fitting mathematical expressions to experimental data sets (regression analysis). Physical models are developed on the basis of electromagnetic theory and knowledge of the (back)scattering behaviour of certain, simplified, media and/or objects. Semi-empirical models are based on a combination of physics and empirically derived expressions which allows them to utilise the best features of both approaches. Due to the physical basis semi-empirical models are more widely applicable than empirical models. The incorporation of empirical expressions, on the other hand, leads to a simplified and thus computationally less involved representation of the forest's (back)scattering characteristics.

The modelling of radar backscatter from forests is of much interest but still a topic of considerable research. Existing models are applied with varying rates of success. Inverse modelling approaches are substantially more difficult than forward modelling approaches. This is due to the highly simplified representation of the forest and

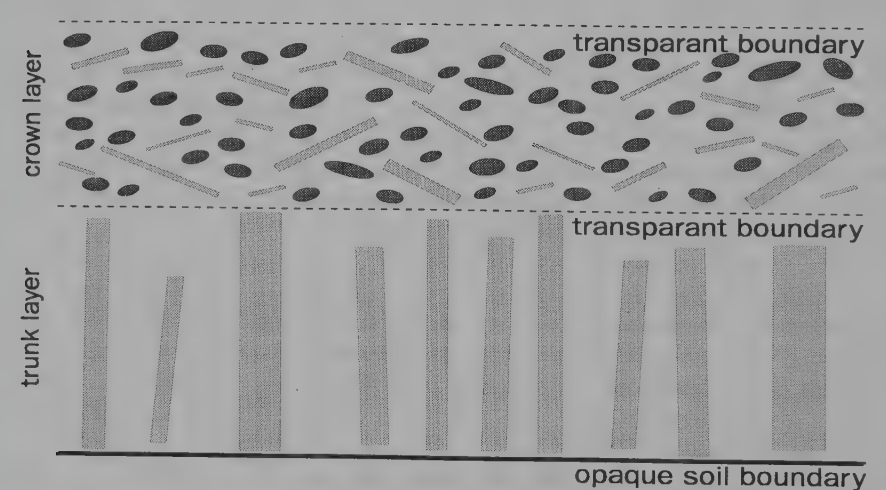



**Figure 3.22** A forest as represented in a radiative transfer backscatter model consists of a soil surface covered by two vegetation layers, i.e. a crown layer and a trunk layer. At the assumed transparent upper crown and crown-trunk boundary there is 100% transmission, and thus no reflection, of microwaves. At the assumed opaque soil-trunk interface there is 100% reflection, and thus no transmission, of microwaves. (Adapted from Ulaby et al. 1990.)

limitations of current model inversion techniques. An extensive discussion on existing forest backscatter models, on their principles and capabilities is beyond the scope of this text. For a review of the existing forest backscatter models the reader is referred to Simonett et al. (1987) and Richards (1990). Extensive discussions on the fundamentals of backscatter modelling can be found in Ulaby et al. (1982) and Fung (1994). Numerous publications address the capabilities of forest backscatter modelling , e.g. Hoekman (1987), McDonald et al. (1991), Beaudoin et al. (1992), Le Toan et al. (1992), Pulliainen (1994), Rignot et al. (1994) and Wang et al. (1994). The discussion in this text will focus on the representation of the forest and the forest-microwave interaction processes in the frequently used radiative transfer models.

The majority of the available radiative transfer models are of a semi-empirical nature. One widely applied model belonging to this category is the Michigan Microwave Canopy Scattering model (MIMICS) (Ulaby et al., 1990). *Radiative transfer models typically represent the forest as a soil surface covered by two layers of vegetation, i.e. a crown layer and a trunk layer. Both vegetation layers are treated as the sum of the constituent elements, such as leaves, branches and trunks. These elements are modelled as spatially isolated dielectric objects with smooth surfaces and of a simple geometry.* Leaves are usually represented as elliptical discs, branches and trunks as cylinders. The numbers, orientations, dimensions and dielectric properties of the modelled vegetation elements are defined on the basis of field measurements. Their spatial distribution within the vegetation layers is assumed to be random, while the height of these layers is specified based on field observations. In most models the vegetation layer is assumed to be continuous which implies that they cannot deal with the presence of canopy gaps. The characteristics of the vegetation constituents, with the exception of the dielectric properties, are usually expressed in terms of probability density functions. The way in which a radiative transfer backscatter model represents a forest is illustrated in Figure 3.22.

*The overall scattering behaviour of the forest is decomposed into a series of models representing the most important microwave interaction processes.* The processes that are commonly accounted for are illustrated in Figure 3.23 and listed below:

| | | |
|---|---|---|
| 1 | - | crown volume scattering |
| 2 | - | scattering from tree trunks |
| 3 | - | surface scattering from forest soil (specular or diffuse) |
| 4a | - | scattering from trunks followed by soil surface scattering |
| 4b | - | soil surface scattering followed by scattering from tree trunks |
| 5a | - | scattering from leaves or branches followed by soil surface scattering |
| 5b | - | soil surface scattering followed by scattering from leaves or branches. |

Process 1 involves both single (bounce) and multiple scattering. The processes 2 and 3 involve single (bounce) scattering, the processes 4a, 4b, 5a and 5b double (bounce) scattering. An alternative designation for single bounce scattering is odd bounce scattering. Likewise, multiple scattering is often referred to as diffuse scattering. The models assume that the vegetation-air and crown-trunk interfaces are transparent, i.e. that the microwaves incident on these interfaces are fully transmitted and not scattered. The vegetation-soil boundary, on the other hand, is

assumed to be opaque. This implies that the incident microwaves are fully scattered and not transmitted. Process 2 accounts for direct backscatter contributions from tree trunks. However, at incidence angles not close to 90° these contributions are small. At such angles trunks will scatter in the forward (towards the soil) and not in the backward (towards the sensor) direction. This is due to their near-vertical orientation, supposedly smooth surface and large dimensions. It follows that tree trunks primarily contribute to the overall backscatter through the trunk-ground interaction processes 4a and 4b.

The computation of the overall forest backscatter involves summation of the backscatter contributions from each of the processes listed. A key factor in computing the backscatter from processes 1, 2, 4 and 5 is the calculation of the scattering matrices $\boldsymbol{S}$ for all vegetation constituents within a certain volume (see section 3.1.6). These matrices are subsequently used to compute the backscatter and attenuation characteristics of the vegetation volume. To enable the computation of scattering matrices it is necessary to model the vegetation elements as objects of a simple geometry (i.e. discs and cylinders). The model for each process must account for the (back)scattering and attenuation properties of the vegetation. In addition, the models for processes 3, 4 and 5 must consider the (back)scattering properties of the forest soil. The soil's (back)scatter properties may be modelled in different manners. A number of frequently used soil models are described in Ulaby and Elachi (1990). In the soil backscattering process (process 3) the vegetation functions as an attenuating layer.

The decompositional backscatter models described may be used to identify the components that govern the backscatter behaviour of a specific forest at a particular frequency, polarization and/or incidence angle. Process 1, for example, will dominate the overall backscatter when the microwaves observe the crown layer (e.g. in X- or

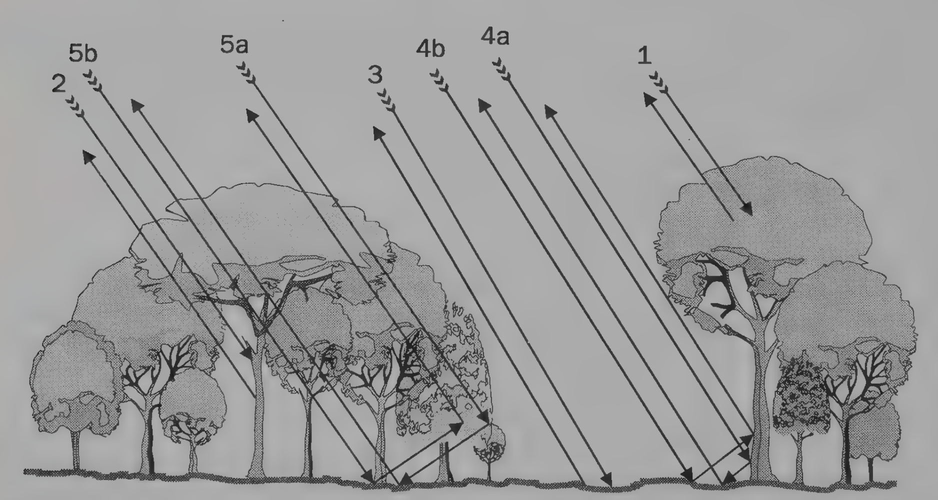



**Figure 3.23** Dominant backscattering sources in forests: (1) crown volume scattering, (2) direct scattering from tree trunks, (3) direct scattering from the soil surface, (4a) trunk - ground scattering, (4b) ground - trunk scattering, (5a) crown - ground scattering, (5b) ground - crown scattering.

C-band). Similarly, process 4 will be the most important contributor to the backscatter when the waves observe the trunk-soil combination (e.g. in P-band). Hence, the models lead to a better understanding of what the microwaves are observing or, in other words, of the microwave-forest interaction process. A better understanding of this process may greatly facilitate the interpretation and analysis of radar data sets. However, in practice the value of the model strongly depends upon the ability of the user to provide it with a good representation of the forest. Representing the vegetation layers in terms of dielectric cylinders and discs may prove to be a particularly difficult task. This especially holds true for very complex forests such as tropical rain forests.

Polarimetric radar images offer an additional opportunity to obtain a better understanding of the microwave-forest interaction processes. Each of the pixels in such an image represents a matrix denoted as a Stokes scattering operator $\boldsymbol{M}$. This matrix describes the depolarizing effects of the object observed (see section 3.1.6). These effects vary in a specific and known fashion as a function of the microwave interaction process. Hence, it is possible to identify the apparent interaction process(es) based on the information contained in $\boldsymbol{M}$. The *knowledge of the microwave interaction process may then be used to identify the forest constituents that dominate the radar backscatter, i.e. the forest constituents being observed by the radar.*

Based on the information contained in polarimetric radar images van Zyl (1989) developed a procedure for classifying the dominant microwave interaction process. This procedure compares the depolarizing effect of observed objects with that of three standard objects, i.e. a slightly rough dielectric surface, a dihedral corner reflector and a multiple scattering volume. These standard objects are known to act as, respectively, a single (or odd) bounce, double bounce and multiple (or diffuse) scatterers. The scattering process of each pixel (object) is classified as being primarily single bounce, double bounce or diffuse through comparison of the pixel's depolarizing effect with that of the three standard objects. A pixel with an incompatible scattering behaviour is labelled as 'unclassified'. Freeman and Durden (1992) developed a procedure that exploits the scattering information in polarimetric radar images to classify land cover. The basis of this procedure is a decomposition of the total backscattered power into backscatter contributions that may be ascribed to single bounce, double bounce and multiple scattering. This decomposition is done in C-, L- and P-band. Based on the resulting information the image pixels are empirically categorised by land cover type (i.e. bare soil or water, urban, low vegetation, low vegetation with double bounce dominance, medium high vegetation, medium high vegetation with double bounce dominance, forest and forest with double bounce dominance).

# 4 Description of study sites and radar data

## 4.1 General study site characteristics

### 4.1.1 Mabura Hill, Guyana

The study focuses on an area of tropical rain forest near the township of Mabura Hill in the Republic of Guyana. Guyana is situated in the northern part of South America between latitudes 1°10' and 8°35' North and longitudes 56°20' and 61°63' West. It borders the Atlantic Ocean, Venezuela, Brazil and Surinam and has a size comparable to that of the United Kingdom (ca. 215,000 km$^2$). The northern boundary of the study area is near Mabura Hill, approximately 235 km south of the capital Georgetown (see Figure 4.1). The study area covers roughly 235,000 ha and is part of a logging concession. An area of some 900 ha, however, is excluded from logging and set aside as an ecological reserve and study site for use by researchers from the Dutch Tropenbos Foundation (Tropenbos, 1991a; ter Steege et al., 1996).

Guyana has a tropical climate characterised by high temperatures, high rainfall and high humidity. North-south movements of the Intertropical Convergence Zone result in wet and dry seasons. There is a long wet season from May to August and a shorter one from December to February. The remaining periods are drier, with October being the driest month. On average, however, no month has less than 100 mm of rain. The

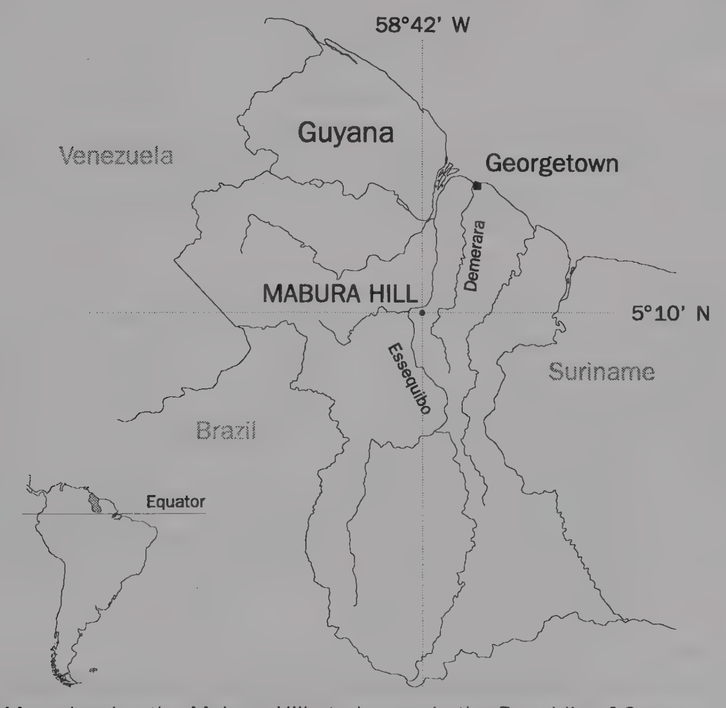



**Figure 4.1** Map showing the Mabura Hill study area in the Republic of Guyana.

annual rainfall is highest in the mountainous areas in the west of the country (ca. 4400 mm) and decreases towards the east and south-west (ca. 1700 mm). In Mabura Hill the average annual rainfall is 2700 mm. According to Jetten (1994) most rain falls in the late afternoon and the early evening. The author also notes that rainshowers rarely cover areas larger than 2 to 3 $km^2$ and that, therefore, the spatial variation in rainfall is large. Measurements at the Tropenbos meteorological station show that the mean annual temperature in Mabura Hill is 26°C. The changes in the mean monthly temperature are approximatley 2°C, while the daily temperature fluctuations are close to 6°C. September and October are warmer than average, January and February are cooler than average.

The study site is located in a lowland region where two main landscape types overlap, namely the White Sands Area and the Pre-Cambrian Plateau. These landscapes have their origin in the geological history of the area and have specific topographic, soil and vegetation characteristics. The White Sands formation has a uniform and gently undulating relief and constitutes the upper layer. In some places, however, the sands are penetrated by laterite-covered ridges from the underlying Pre-Cambrian Plateau. In the south-central and western parts of the study area such ridges are visible as low mountain ranges. The drainage of the study area is controlled by the Essequibo River in the east, the Demerara River in the west and many small creeks. In spite of their size, these creeks often form wide valleys due to the coarseness of the quartz-rich sand. At places where the White Sands formation is thin, streams have cut through the sandy layer into soil types associated with the Pre-Cambrian Plateau, i.e. Brown Loamy Sands and Sandy Loams. In the study area this water erosion process has resulted in a mixture of soil types. For more information on the geology, geomorphology and soils of Guyana and the Mabura Hill region the reader is referred to FAO (1966), Khan et al. (1980), Jetten (1994), van Kekem et al. (1996).

Forests cover about 80% of Guyana's land surface area. *According to the "life zone classification system" by Holdridge et al. (1971) Guyana's forests are 'Tropical Moist Forests'.* This classification is entirely based on the following environmental variables: mean annual precipitation, mean annual biotemperature [1)] and altitude above sea level. The system developed by Holdridge et al. provides classification at a continental scale but with a low level of detail. Guyana's forests may be categorised in greater detail by using Fanshawe's classification system (Fanshawe, 1952). This system is based on intrinsic forest properties such as habitat, physiognomy and floristic composition. It provides a basis to distinguish many different forest types but can only be applied at a regional scale, i.e. within Guyana. Fanshawe's classification system consists of three levels that are denoted as formation-series, formations and associations. Formation-series group forests with corresponding habitats. Forests within a single formation-series are subdivided into formations on the basis of their physiognomy (outward appearance). Formations, in turn, are further subdivided into associations that represent forests of a comparable floristic composition. In this study, Fanshawe's formations are used. The subdivision into associations was not

1) Mean annual biotemperature is defined as the mean of unit-period temperatures with the substitution of zero for all unit-period values below 0°C and above 30°C (Holdridge et al., 1971).

made as classification at this level requires information that cannot be obtained from the available radar remote sensing measurements.

According to Fanshawe the forests of Guyana, Venezuela (State of Guyana), Trinidad (once geologically joined to Venezuela), Surinam, French Guiana and Brazil (States of Para and Amazonas) comprise closely allied associations. For this reason these territories are commonly referred to as the "Guiana hylaea" (phytogeographic region). Given that *the forest types studied correspond to* a higher aggregation level, i.e. to *physiognomic classes (formations) rather than floristic classes (associations)*, they may be hypothesised to resemble forests beyond the "Guiana hylaea". This hypothesis is supported by the fact that Oldeman (1974) found similar forest architecture in rain forests in the Guianas and Africa. Forest physiognomy and forest architecture are not identical but the former may be seen as a derivative of the latter. While forest physiognomy is assessed from the overall appearance of sketched forest profile diagrams, forest architecture is analysed by using scale-drawings of forest transects on which precise criteria are coded. Architecture is an explanatory property of forests. Hallé et al. (1978) defined it as follows: "the visible, morphological, expression of the genetic blueprint of organic growth and development". Forest architecture is independent of species composition. An architecturally defined, similar niche in Asia, Africa or tropical America generally is occupied by taxonomically dissimilar species (Oldeman, 1996).

The forests of Guyana have been observed to deviate from others in being frequently dominated by one or a few tree species (Davis and Richards, 1933, 1934; Fanshawe, 1952; Richards, 1952; ter Steege, 1993). A low diversity in tree species causes the architecture and physiognomy of a forest to be more clearly defined, because individuals of taxonomically and ecologically similar species are more alike in architecture than individuals of taxonomically different species. Species dominance thus facilitates the recognition of forest types on the ground, from the air and hence on remotely sensed images (Swellengrebel, 1959; ter Welle et al., 1988; ter Steege et al., 1996). At times, the identification of forest types is further simplified due to the presence of well defined forest type boundaries. Such boundaries generally occur at locations were the soil type changes abruptly (Fanshawe, 1952; ter Steege, 1993).

Table 4.1 shows the land cover classification system that is used in the present study. The first level consists of two classes, i.e. Forest and Non-forest. At the second level the Forest class is subdivided into Primary forest, Logged-over forest and Secondary forest. The primary forest is subdivided once again at the third level and consists of: Mixed forest, Wallaba forest, Xeric mixed forest, Low swamp forest and Mora forest. These third level classes correspond to Fanshawe's formations and are representative of three of his formation-series, i.e. Rain forest, Dry Evergreen forest and Swamp forest (Fanshawe, 1952). *The study focusses on a total of eight classes at three different levels (classes 1 through 8 in Table 4.1). Mabura Hill only comprises six of these classes, namely, the five primary forest classes and the Logged-over forest class.* None of the primary forest classes have been exposed to human impact. In contrast, the Logged-over forest class represents forests that have been subject to industrial *selective* logging, not clear-cut. The data for the classes that are not represented in Mabura Hill, i.e. Secondary forest and Non-forest, were

**Table 4.1** Classification of land cover types considered in this study.

| Level | | | Formation-series according to Fanshawe |
|---|---|---|---|
| I | II | III | |
| Forest | Primary forest | Mixed (1) | Rain forest |
| | | Wallaba (2) | Dry evergreen forest |
| | | Xeric mixed (3) | Dry evergreen forest |
| | | Low swamp (4) | Swamp forest |
| | | Mora (5) | Swamp forest |
| | Logged-over forest (6)[1)] | | |
| | Secondary forest (7) | | |
| Non-forest (8) | | | |

1) Logged-over forest is primary forest that has been subject to industrial *selective* logging.

obtained from radar images of the San José del Guaviare area in Colombia (see section 4.1.2). The land cover classes studied, with the exception of the Non-forest class, are described in detail in section 4.3.

### 4.1.2 San José del Guaviare, Colombia

An area near the Colombian city of *San José del Guaviare* was selected as an additional study site. Unlike Mabura Hill, this site *represents the earlier identified Secondary forest and Non-forest classes* (Table 4.1). The combined use of the San José del Guaviare area and the Mabura Hill area was possible because a near-identical radar data set was available for both sites. This section gives a brief description of the San José del Guaviare area, for additional information the reader is referred to Bijker (1997).

The study site is situated in the Colombian department of Guaviare, some 275 km south-east of the capital Bogota and south of San José del Guaviare (see Figure 4.2). To the north the site is bounded by the Guaviare river. This river marks the boundary between the Amazonian forests of south-eastern Colombia (Orinoco-Apaporis region) and the natural grass savannahs with gallery forests in the east of the country (eastern plains). The study area is part of the transitional zone and consists of both forests and savannahs. The general topography is gently undulating but also comprises a number of rocky outcrops and a sandstone plateau. This plateau is the natural habitat for the savannahs (Tropenbos, 1991b). *The area's forests, according to the "life zone classification system" by Holdridge et al. (1971), are 'Tropical Moist transitional to Subtropical Wet Forests'.*

San José del Guaviare has a tropical seasonal climate. The mean annual rainfall is 2600 mm while the mean annual temperature is 26°C. These figures are comparable to those of Mabura Hill. The climate of San José del Guaviare, however, is characterised by a distinct dry season during which water deficits often develop. This

dry season lasts from December to March, with January and February being the warmest and driest months. In January and February the fluctuations in the daily temperature may be as much as 15°C. There is no clear wet season but most rain falls during the months of May, June and July (Andrade and Etter, 1987).

San José del Guaviare was first selected as a study site in 1990 by researchers from the Tropenbos Foundation (Tropenbos, 1991b). The main area of interest covers roughly 123,000 ha. In the past most of the area was covered with forests. Settlement by people from other parts of Colombia, however, has resulted in extensive conversion of natural forests into cropland, pasture and secondary forest. Remaining forests are not usually free of human disturbance as the most valuable trees have been extracted. The settlement of the region follows a specific land use sequence. It begins with the slash-and-burn of natural forests and ends with the establishment of 'permanent' pastures. The sequence includes periods of fallow during which secondary forests are left to develop. These *secondary forests do not usually grow older than 15 years as the soils are not left fallow for more than this period of time* (Andrade and Etter, 1987). They constitute one of the land cover classes studied in this text and are described in more detail in section 4.3.2. *The Non-forest class studied is of a heterogeneous nature as it represents a wide variety of land cover types, i.e. grass savannahs, (degraded) pastures, agricultural crops, burned areas and bare soils.* This class will not be discussed in more detail as the description given is sufficient for the aims of the study.




**Figure 4.2** Map showing the San José del Guaviare study area in Colombia.

## 4.2 Ground data collection

### 4.2.1 Sampling in a highly complex forest context

For the assessment of the information content of any type of remotely sensed data it is necessary to have an appropriate set of ground reference data. The denotation "appropriate" indicates that the ground data must correspond to the scale and variables measured by the sensor system applied. *In radar remote sensing they must therefore relate to object properties that affect backscatter, i.e. to dielectrical and structural properties.* Ground data collection for forests must account for the properties of both soil and vegetation. The dielectrical properties of soil and vegetation are governed by their water status and may be characterised by their gravimetric water content (see section 3.2.1). The most important structural property of forest soil is the soil surface roughness. This property may be described by the variation in surface height over a wavelength dependent horizontal distance (see section 3.2.2). Finally, there is a need for data on the structural or, in terms of Oldeman (1974), architectural forest properties. These data must describe the forest's architecture in terms of vegetation volume thickness and densities, sizes, shapes and orientations of architectural subsystems such as trunks, branches and leaves (see section 3.2.1).

The above list of forest properties with relevance to radar remote sensing covers a tremendous number of variables to be recorded on the ground. Their relative importance, however, is strongly dependent on radar data acquisition parameters such as frequency, polarization and incidence angle. Hence, these parameters can often be used to set the bounds of the ground data collection. For example, in those cases where an X- or C-band radar system is operated over a closed forest, data on soil water content are not needed as the soil is not likely to contribute to the backscatter. In the present study, however, it was not possible to limit ground data collection on the basis of data acquisition parameters. This is due to the fact that the backscatter measurements from the NASA/JPL multiband polarimetric SAR system deployed (see section 4.4.2) may be affected by the structural/architectural and dielectrical properties of every single forest component.

*To conform with the main objectives of the present study (see section 1.1) ground data collection focused on the most important variables in view of the application of the radar data.* These variables typically relate to the architecture of the forest and are among the ones that are traditionally recorded by foresters and forest ecologists. In addition, a restricted set of data relating to the forest's dielectrical properties was compiled. The ground data were collected at a scale in accordance with that of the radar data analysis (see section 4.1.1), namely at the forest type scale. An initial set of data was compiled in 1992 in conjunction with the first airborne radar campaign. Additional data were collected when the analysis of a radar data set indicated the need to do so. An overview of the forest dielectrical and architectural data is given in section 4.2.2 and 4.2.3, respectively. These sections, in addition, hold a detailed description of the ground data collection methods that were used.

**Table 4.2** Rainfall data in conjunction with radar data acquisition in **Mabura Hill**. Numbers in ⟨ ⟩ are estimates based on average monthly rainfall.

| Date | Overflight | Rainfall (mm) | |
|---|---|---|---|
| | | During week prior to date | On that date |
| 8 April 1992 | SAREX-92 | 17 | 0 |
| 11 June 1993 | AIRSAR | 81 | 8 |
| 29 April 1992 | ERS-1 | 133 | 0 |
| 3 June 1992 | ERS-1 | 107 | 0 |
| 30 December 1992 | ERS-1 | ⟨45⟩ | n.a. |
| 6 October 1993 | ERS-1 | 15 | 0 |
| 27 May 1994 | ERS-1 | 266 | 20 |
| 9 August 1994 | ERS-1 | 66 | 0 |

Within the framework of this study it was not feasible to collect detailed ground reference data for both Mabura Hill and San José del Guaviare. The fieldwork was concentrated in Mabura Hill since this was the main study area. The ground data for the Colombian site were borrowed from Quiñones (1995) and Bijker (1997). For the purposes of the study no detailed data were needed on the Non-forest class. All information required was confined to a simple "Non-forest" label.

### 4.2.2 Collection of data on dielectrical properties

Dielectrical properties reflect water status. Assessment is complicated by the fact that they are not constant but fluctutate with environmental conditions such as rainfall. Consequently, water status data are only of real value when collected at or close to the time of radar data acquisition. Near-simultaneous collection of soil/vegetation water content data and radar data would have required means out of proportion with this study. Hence, the ground data collection procedure adopted did not include the systematic assessment of soil or vegetation water status. *To obtain a rough-and-ready parameter, fully grown leaves of a number of recently felled or windblown trees were collected and their gravimetric water content was determined.* Using this method it was possible to get an approximate measurement of the leaf water status of trees in a tropical rain forest environment. The values of this parameter are given in section 4.3.3.

Rainfall data are indicative of the water status of a forest and as such are useful for the interpretation of radar images. Tables 4.2 and 4.3 therefore list rainfall data for Mabura Hill and San José del Guaviare. Two figures are shown in conjunction with each radar data take, i.e. one for the amount of rain that fell during the week prior to the system's overflight and one for the rainfall on the day of overflight. The 1992 and

**Table 4.3** Rainfall data in conjunction with radar data acquisition in **San José del Guaviare**. Numbers in ⟨ ⟩ are estimates based on average monthly rainfall.

| | | Rainfall (mm) | |
|---|---|---|---|
| Date | Overflight | During week prior to date | On that date |
| 29 April 1992 | SAREX-92 | 102 [1)] | 0 |
| 31 May 1993 | AIRSAR | 164 | 1 |
| 26 May 1992 | ERS-1 | ⟨79⟩ | n.a. |
| 4 August 1992 | ERS-1 | ⟨78⟩ | n.a. |
| 17 November 1992 | ERS-1 | ⟨62⟩ | n.a. |
| 22 December 1992 | ERS-1 | ⟨27⟩ | n.a. |
| 20 July 1993 | ERS-1 | ⟨95⟩ | n.a. |
| 28 September 1993 | ERS-1 | ⟨60⟩ | n.a. |

1) sum of rainfall for 4 days prior to overflight only.

1993 figures for Mabura Hill originate from the meteorological station in the Tropenbos ecological reserve while those for 1994 were obtained from a nearby station in Great Falls. The figures for San José del Guaviare represent means based on observations by two nearby meteorological stations. In the cases where observations were missing, the rainfall during the week prior to the overflight was assumed to be equal to ¼ of the average monthly rainfall.

### 4.2.3 Collection of data on architectural properties

Ground data on architectural forest properties, unlike those on dielectrical forest properties, were collected in a systematic manner according to a predefined sampling methodology. Since the data were not intended for statistical analysis, no randomness of sample areas was required. Sample areas could thus be chosen at characteristic locations and because of this it was possible to obtain a good representation of the studied forest types with relatively few sample areas. The use of a random sampling method could have resulted in data of a comparable quality but in this case the number of sample areas would have had to have been much larger. A random sampling method therefore would have been much more time consuming (Randall, 1978).

The initial set of forest architectural data was collected in the Tropenbos ecological reserve. This reserve was chosen intentionally to be well representative of the entire study area and comprises all of the studied *primary* forest types with exception of Low swamp forest. The latter type of primary forest hence remained unsampled as did Logged-over forest. This 'forest type' arises for the most part from Mixed forest. Its architecture, when compared to that of Mixed forest, is only locally different. The

**Table 4.4** Number of sampling locations per forest type.

| Primary forest type | Number of sampling locations |
|---|---|
| Mixed forest | 12 [1)] |
| Wallaba forest | 6 |
| Xeric mixed forest | 4 |
| Low swamp forest | - |
| Mora forest | 6 |

1) including seven with dominance of Greenheart.

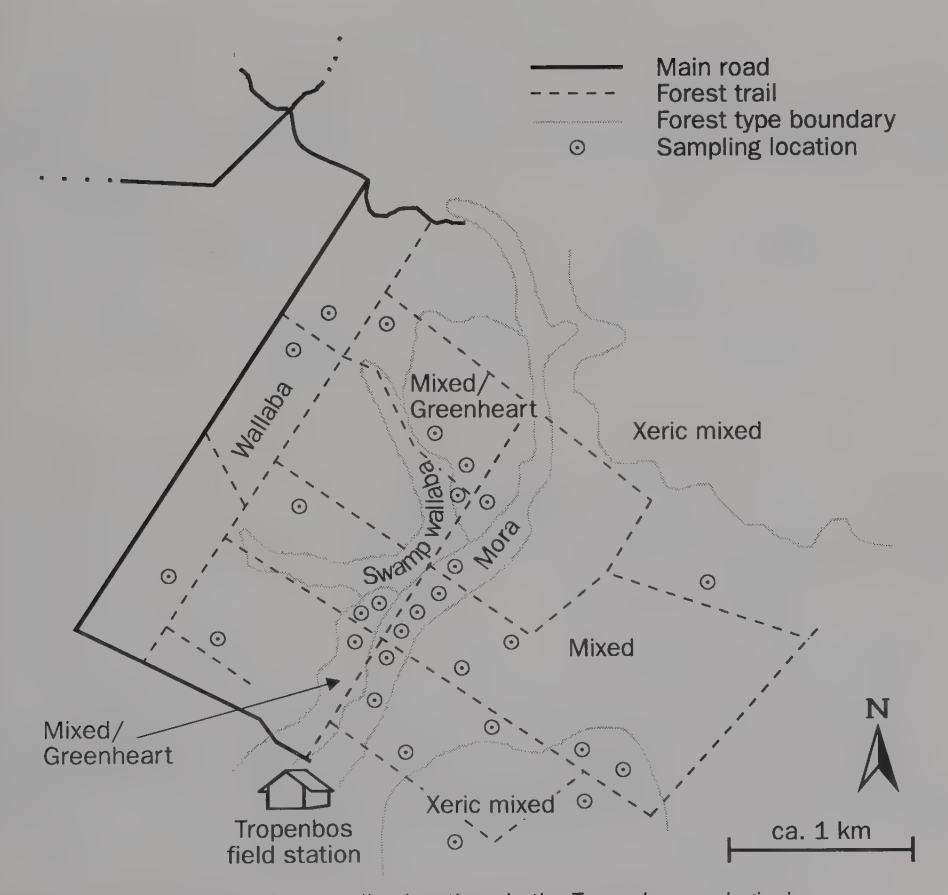



**Figure 4.3** Map showing the sampling locations in the Tropenbos ecological reserve.

required information regarding the effects of logging on the architecture of the remaining forest was borrowed from other studies (see section 4.3.2).

The segmentation basis for the collection of the ground data within the Tropenbos ecological reserve was provided by an existing forest type map. This map, shown in Figure 4.3, is a small but improved subset of a forest type map produced by the Guyana Forest Department (1970). The improvements were made by Tropenbos researchers. Within the boundaries of the primary forest types studied a minimum of four representative sampling locations were selected (see Figure 4.3, Table 4.4). *At each location two concentric circular sample plots as well as a line transect were laid out (see Figure 4.4). The sample plots were used to collect the usual forest density and composition parameters, e.g. number of trees ha$^{-1}$, basal area ha$^{-1}$, proportion of trees in specific diameter classes. The line transect served to collect data on the architecture of the forest and form parameters of individual trees, e.g. total tree height, crown depth, crown diameter.* Experience showed that a well trained team consisting of 3 members on average needed 1½ days to complete the work at a single sampling location. This included transportation by car between the Mabura Hill township and the Tropenbos ecological reserve (ca. 1 hour per day) and the time needed to hike into the sampling locations.

The activities within the sample plots involved the enumeration of (palm) trees, lianas and stemless palms as well as the measurement of the diameter at breast height [1)] (dbh; *d*) for all but the stemless palms. The dbh measurements were rounded off to the nearest cm. In this study circular sample plots were preferred over other plot forms because of their high ratio of area to perimeter (thus less borderline trees or error sources) and their ease of lay out. The motive for using concentric sample plots was to compensate for a decreasing numerical density with an increasing diameter/height of the trees (Loetsch et al., 1973; de Vries, 1986). Within the inner circle only (palm) trees and lianas with $d \geq 2$ cm or stemless palms with a height $\geq 2$ m were considered, while the criteria for these two groups in the outer sample plot were $\geq 10$ cm and $\geq 5$ m, respectively. The adopted dbh and height criteria were borrowed from Gelens (1983).

The inner and outer sample plots had areas of 100 and 1000 m$^2$, respectively. Selecting the best size for sample plots is a complex problem. For the inventory of relatively homogeneous forests (e.g. Wallaba and Xeric mixed forests), according to a random sampling approach, plot sizes of ca. 0.08 ha have been suggested (Alder, 1980). For more heterogeneous forests (e.g. Mixed forests) FAO (1981) recommends the use of plot sizes of ca. 0.4 ha. The larger plot size for more heterogeneous forests is suggested in order to ensure that the samples are sufficiently representative. The sample plot size proposed by FAO may be noted to exceed that of the nested plot in this study. Nevertheless, the plot size adopted is expected to yield reliable data for the characterisation of all forest types studied since the plots were not chosen at random but at representative locations. An area of 1000 m$^2$ has been recommended as the maximum size of circular sample plots by both Loetsch et al. (1973) and Alder (1980).

---

1) dbh is measured at 1.30 m above the ground or 0.30 m above the buttress.

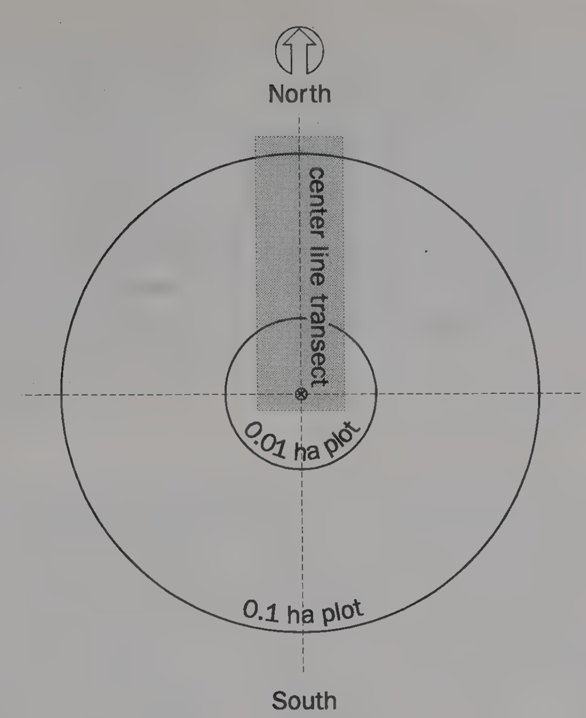



**Figure 4.4** Plan of sampling location for collection of ground data on architectural forest properties. At each location two concentric circular sample plots as well as a line transect were laid out.

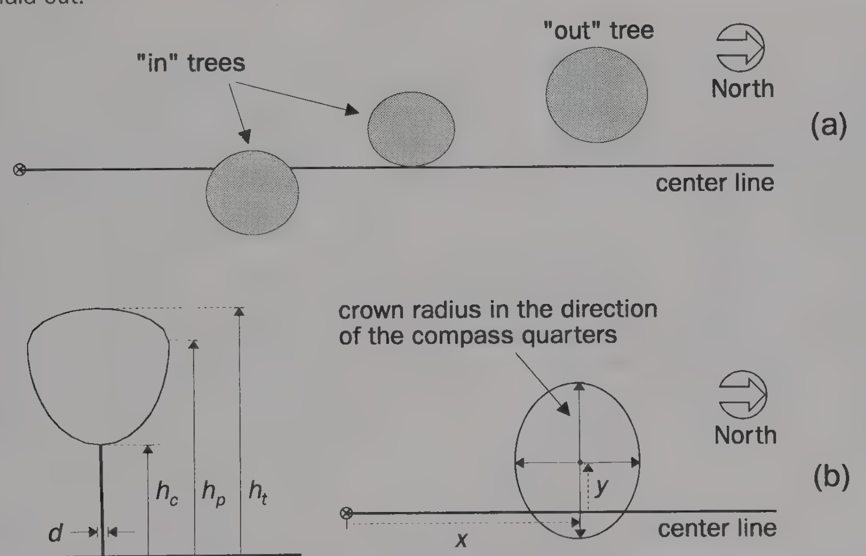



**Figure 4.5 (a-b)** (**a**) Selection of trees for incorporation in line transect measurements. In order for a tree to be measured it had to be an "in" tree, i.e. its projection had to either intersect or touch the center line of the transect. (**b**) Overview of measurements of "in" trees: $(x, y)$ co-ordinates, diameter at breast height $d$, crown radii, height of the crown base $h_c$, height of the greatest width of the crown periphery $h_p$, total height $h_t$. (After Koop, 1989).

The radius of the outer sample plot was used as the center for the line transect. Its direction was chosen to be perpendicular to a distinct physiographic gradient (e.g. slope) or in the north-south direction where such a gradient was absent. The measurements in the line transect were restricted to (palm) trees and lianas with $d \geq 2$ cm or stemless palms with a height ≥ 2 m. In order for a tree, liana or palm to be incorporated in the transect measurements its projection had to either intersect or touch the center line of the transect. Specimens that met the measurement criterium were considered to be "in" trees, those that did not were considered to be "out" trees (see Figure 4.5a). Line transects provide a relatively quick method for the mapping of the forest's architecture. They compensate for the decreasing numerical density of larger specimens since these will have a higher chance of being "in" trees. Line transects as such include a fair proportion of all size classes present and yet remain easy to read (Oldeman, 1983b).

All "in" trees were measured according to a method developed by Koop (1989). The measurements performed are illustrated in Figure 4.5b. They relate to the $x, y$-position of the tree/palm/liana, the dbh $d$, the crown radii, the height of the crown base $h_c$, the height at the greatest width of the crown periphery $h_p$ and the total height $h_t$. The dbh measurements were rounded off to the nearest cm, while the tree and crown position measurements were rounded off to the nearest 5 cm. Tree heights were measured with a Suunto clinometer. Measurements for trees with heights < 5 m, 5 to 10 m and > 10 m were rounded off to the nearest dm, 0.5 m and m, respectively (Cailliez, 1980). Comments on special stem characteristics (e.g. leaning, buttressed) were recorded in addition.

Sample plot and line transect *measurements were complemented with observations on: terrain condition (soil type, slope angle and direction, drainage), undergrowth and litter depth. In addition, some comments on the crown architecture, leaf types and leaf dimensions of dominant tree species were recorded.* In this context the denotation "dominant" refers to canopy cover. It should be noted, furthermore, that only adult trees and fully grown leaves were considered. Leaf types were classified according to Roth (1984) as: hygromorph, mesomorph and xeromorph. These classes relate to the degree of coriaceousness and indicate how a leaf reacts to alterations in water supply. Xeromorphic leaves are the most coriaceous (leathery) and as such are best designed to survive periods of water shortage. Typical and well known examples of hygromorphic, mesomorphic and xeromorphic leaves are those of lettuce, oak and holly, respectively. Leaf dimensions were classified according to criteria adapted from Raunkiaer (1934) as: nanophyll, microphyll, notophyll, mesophyll, macrophyll and megaphyll. The respective surface areas of these elliptical leaf classes were: ≤ 2.25, ≤ 20.25, ≤ 45.00, ≤ 182.25, ≤ 1640.25 and > 1640.25 $cm^2$ (Webb, 1968; Givnish, 1984). During field visits in 1993 and 1994 the length, width, surface area and thickness of a series of leaves from a number of canopy trees were measured. These measurements were done concurrently with the leaf water content measurements as described in section 4.2.2. The field measurements and observations were concluded with photographs of canopy cover and forest condition. The canopy photographs were taken with the use of a standard 50 mm lens at five locations along the diameter of the outer sample plot and in the direction of the line transect.

The majority of the ground data were collected in 1992. Two additional field work periods in 1993 and 1994 were mainly used to confirm findings from radar data analysis with field information. *With the help of the ground data collected and information from literature it was possible to roughly estimate the total dry biomass above the ground for the forest types studied.* The starting points for these estimations were the $d$ and $h_c$ transect measurements. They were used in a non-linear least squares regression procedure to establish the $d$-$h_c$ relationship for each forest type. These relationships were then used to estimate the bole volume (volume of trunk in between stump and crown base). Bole volume $V_b(d)$ for trees with dbh $d$ and crown base height $h_c(d)$ was calculated according to:

$$V_b(d) = 0.7 \cdot \frac{\pi}{4} d^2 \cdot h_c(d) \qquad [\mathrm{m}^3] \qquad (4.1)$$

where 0.7 represents the "form factor", i.e. a factor that compensates for the deviation of the conical tree trunks from a cylinder. This form factor was borrowed from Heinsdijk and de Miranda Bastos (1963, 1965). They calculated it on the basis of bole volume measurements for over 1500 sample trees in the Brazilian Amazon region. The factor was found to be appropriate for all species, dbh classes and bole heights. For each forest type the number of stems per hectare in each diameter class $N_d$ could be derived from the sample plot dbh data. It follows that the estimated bole volume per hectare $V_b$ for a forest type is given by:

$$V_b = \sum_{d=1}^{d_{max}} V_b(d) \cdot N_d \qquad [\mathrm{m}^3\ \mathrm{ha}^{-1}] \qquad (4.2)$$

where $d_{max}$ is the maximum dbh. The average dry density of the wood was estimated to be 0.75 t $m^{-3}$ (PRORADAM, 1979). Using this value it was possible to convert from trunk volume in $m^3$ $ha^{-1}$ to trunk dry biomass in t $ha^{-1}$. Biomass measurements in mixed forests in French Guiana (Lescure et al, 1983) and Surinam (Ohler, 1980; Busink, 1981) show that the contributions of trunks, branches and leaves to the total amount of dry biomass above the ground are of the order of 69%, 30% and 1%, respectively. The forest types in Mabura Hill were assumed to have a comparable biomass distribution and hence it was possible to estimate their total dry biomass above the ground. According to Busink (1981) the water content of the trunk, branches and leaves is of the order of 0.4, 0.4 and 0.55 g $g^{-1}$, respectively. The figure on leaf water content agrees well with the findings of the present study (see section 4.3.3).

## 4.3 Description of studied forest types

The following descriptions of the forest types are based on information obtained from both literature research and ground data collection. Fanshawe's publication of 'The Vegetation of British Guiana' (Fanshawe, 1952) was the main literature source. Additional sources were Davis and Richards (1933, 1934), Richards (1952), Mennega et al. (1988), ter Welle et al. (1988), ter Steege (1990), Polak (1992) and ter Steege et al. (1996). The ground data collection procedures and the resulting data set were discussed in section 4.2.

### 4.3.1 Primary forest types

Figure 4.6a-c illustrates the variability in most of the primary forest types in terms of stem number, basal area and total dry biomass above the ground. Additional characteristics of the primary forest types are discussed below.

**Mixed forest**

The Mixed forest formation is part of Fanshawe's (1952) Rain Forest formation-series. It is found on well drained sites from flat plains to broken country. Characteristic soil types are those that are associated with the Pre-Cambrian Plateau, i.e. Brown Loamy Sands, Sandy Loams and soils with a lateritic component. *Mixed forests by definition comprise numerous tree species.* Locally, however, they may be dominated by Greenheart [1] and/or Morabukea. The dominance of these species is thought to be related to soil properties such as drainage and nutrient content. Forest patches dominated by Greenheart and/or Morabukea are commonly referred to as "reefs" and may be considered as sub-classes, i.e. associations of the Mixed forest formation. Mixed forest dominated by Greenheart was considered as a separate class in the ground data collection because this particular forest type is the focus of the selective logging activities (see section 4.3.2).

*Mixed forests have an irregular upper canopy due to the clumped occurrence of dominant canopy trees and the presence of emergent trees.* In Fanshawe's (1952) view they are comprised of three to four storeys [2]. The main storey ranges from 20 to 40 meters but emergent trees may reach as high as 50 m. Additional storeys range from 10 to 20 m and 3 to 10 m. The understorey (3 to 10 m) is usually fairly well marked. The shrub layer is most often composed of seedlings and saplings of dominant trees and small or stemless palms. Ground cover is sparse to very sparse (< 10%). There are about 70 to 90 woody species, over 5 m tall, per hectare and the maximum dbh is 80 to 120 cm. Predominating species are Greenheart, Morabukea, Wamara, Aromata and Kakaralli, while Crabwood and Clump wallaba can be locally

---

1) In this text species are referred to by their vernacular names. The corresponding scientific names and family names are listed in Appendix II.

2) The description of forests as having several well recognizable storeys or strata has become almost obsolete since the time of Fanshawe (see Oldeman 1990 for a critical examination). They are given here for the sake of citing him completely.

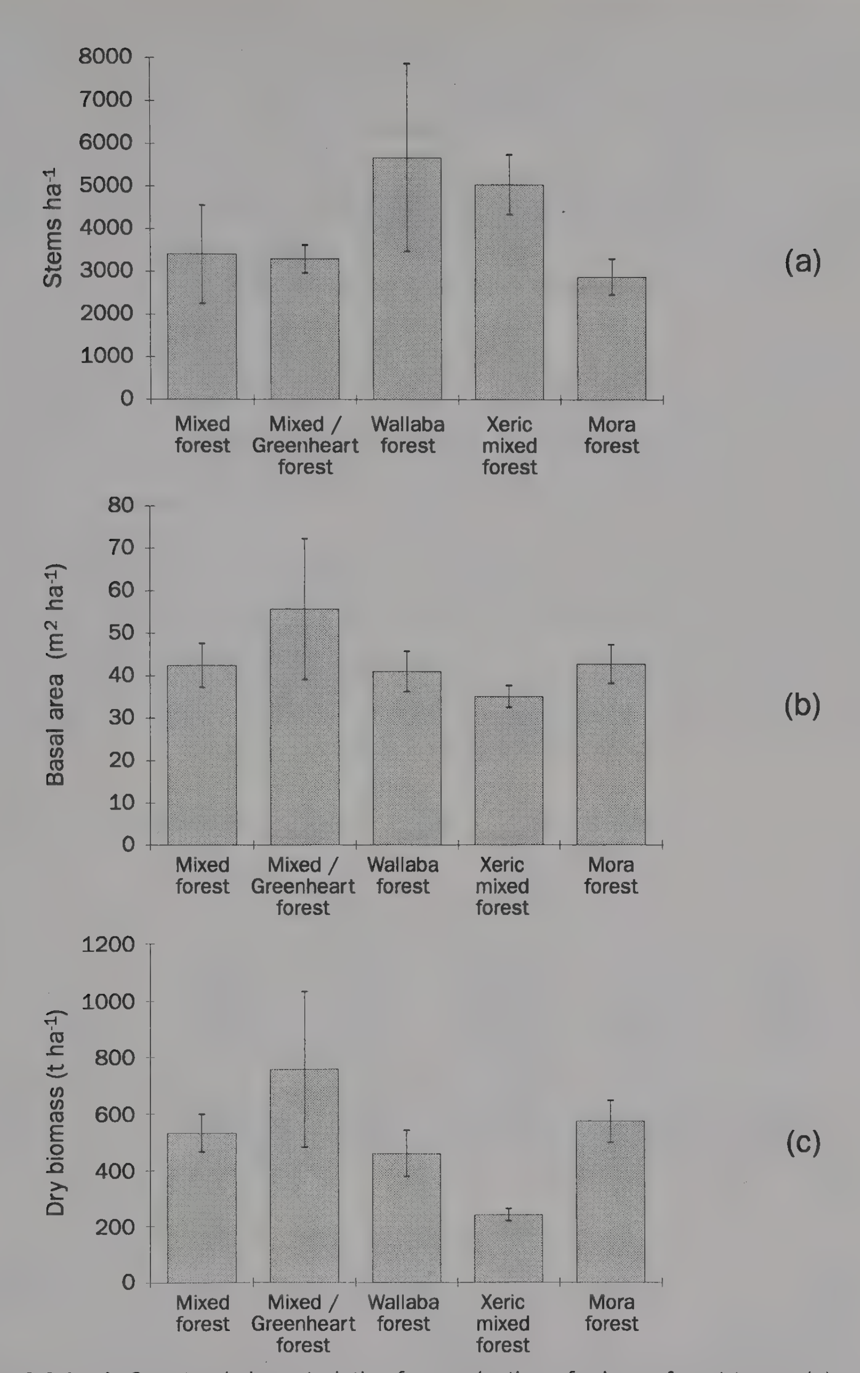


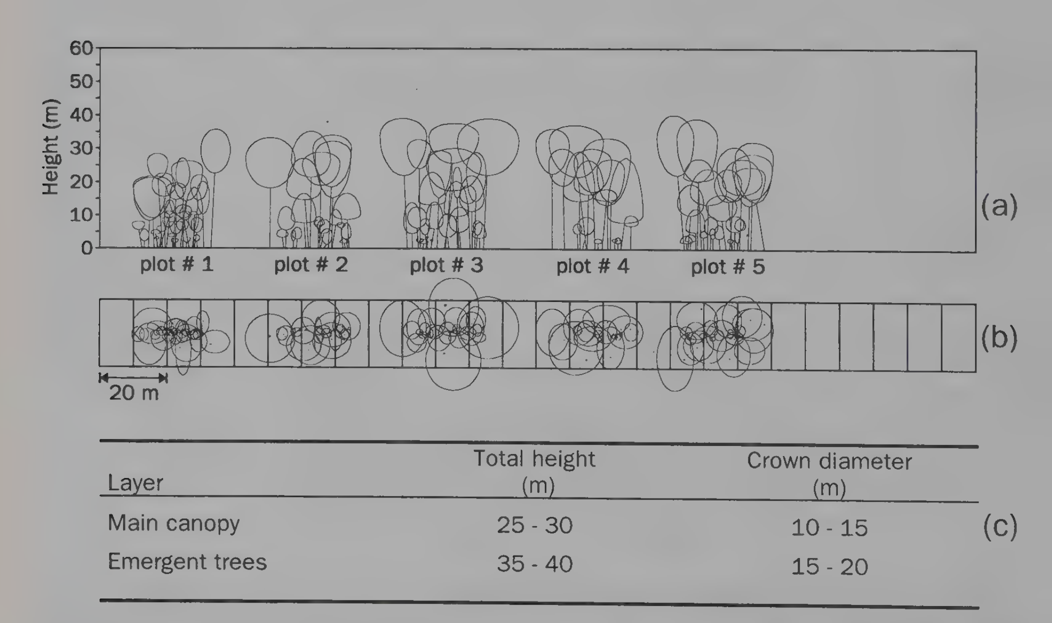

**Figure 4.6 (a-c)** Structural characteristics for a selection of primary forest types: (**a**) number of stems (**b**) stem basal area (**c**) total dry biomass above the ground. Representation of mean value ± standard deviation.

common. Morabukea is one of the few buttressed species. Buttresses are therefore not a marked feature of the Mixed forest in central Guyana. Lianas are occasional to common while epiphytes are scarce to fairly frequent. Palms are few and restricted to shrub layers or to the undergrowth (Fanshawe, 1952). Of all the primary forest types studied, Mixed forests have the most variable composition.

Figures 4.7 and 4.8 give generalised drawings of the architecture of Mixed forest and Greenheart dominated Mixed forest, respectively. The profiles and crown projection plans shown were calculated and plotted with the ARBOPLOT program (Koop, 1989). Additional ground reference data can be found in Appendix III.

**Wallaba forest**

The Wallaba forest formation belongs to Fanshawe's Dry Evergreen Forest formation-series. Forests of this series generally occur on sites with a consistent soil water deficit due to excessive drainage or excessive evapotranspiration. Wallaba forests are found on White Sands. This Guyanese soil type not only has a very poor water retention capacity but is also short in nutrients. Wallaba forests, when compared to Mixed forests, have a slightly xeromorphic character. This is expressed in the coriaceousness of the foliage and the fairly high proportion (33% of individuals with dbh > 10 cm) of semi-deciduous species. *Wallaba forests are dominated by relatively few species most of which belong to the Leguminosae family.* The most important species are Soft wallaba and Ituri wallaba. There are a large number of trees per hectare but their diameters are small. The maximum dbh is of the order of 70 cm. Fanshawe distinguishes three storeys: a continuous upper canopy that ranges from 25 to 35 m, a discontinuous understorey ranging from 10 to 25 m and a dense but




| Layer | Total height (m) | Crown diameter (m) |
|---|---|---|
| Main canopy | 25 - 30 | 10 - 15 |
| Emergent trees | 35 - 40 | 15 - 20 |

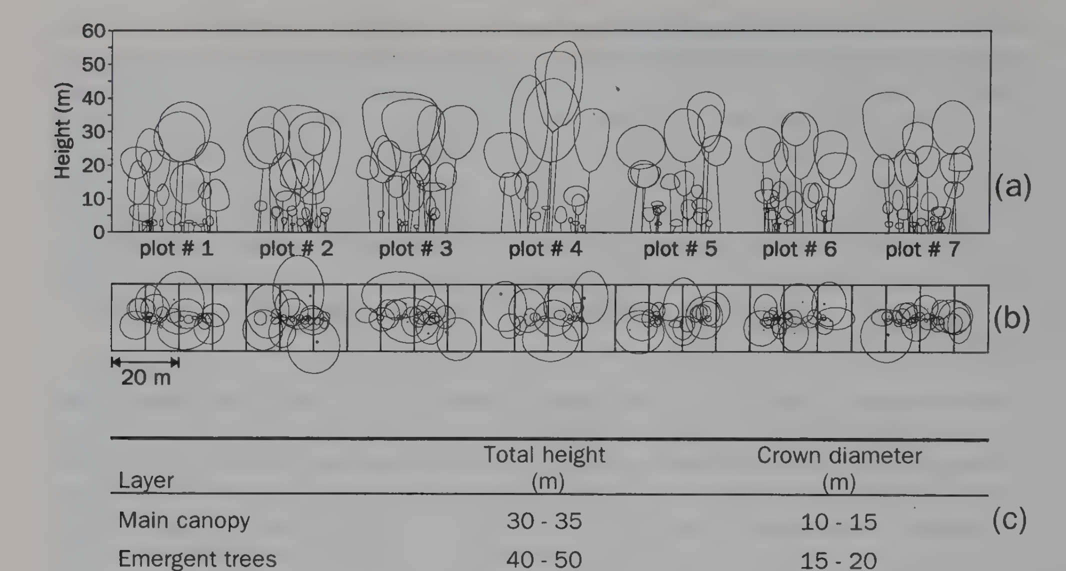
**Figure 4.7 (a-c)** (**a**) Generalised profiles and (**b**) crown projection plans for **Mixed forest** plots according to Koop's method (1989). (**c**) Summary of data on total tree height and crown diameter for emergent trees and trees of the main canopy.

ill-defined storey with undergrowth from 5 to 10 m. *The upper canopy is even, as emergent trees are absent.* This evenness is hypothesised to be an aerodynamic adaptation of the forest to water deficiency (Whitmore, 1990). Trees with heavy buttresses are scarce, lianas are few and small epiphytes are plentiful. The shrub layer is dominated by seedlings and saplings of the dominant trees and immature stemless palms. Additional information on the architecture and composition of the Wallaba forest can be found in ter Steege (1990), Loubry (1994) and ter Steege et al. (1996). Some of the ground data collected are represented in Figure 4.9 and Appendix III.

**Xeric mixed forest**
Xeric mixed forests, like Wallaba forests, belong to the Dry Evergreen Forest formation-series. They occur on ridges covered with sheets or boulders of concretionary laterite (ironstone). The soil layer available for rooting is usually very shallow (≈ 25 cm), while the soil gravel content is markedly high (≈ 80%). Xeric mixed forest is characterised by a *low stature and a high stocking of trees with small diameters.* Fanshawe distinguishes two storeys, i.e. a densely packed main canopy that ranges from 6 to 20 m and a discontinuous layer of 'small' emergent trees that may reach up to 30 m. The maximum dbh is ca. 50 cm but the majority of the trees in the main canopy have much smaller diameters (15 to 20 cm). Shrubs are very rare and ground cover is sparse (< 20%). *Wild guava is often dominant or at least common.* Other frequently found species are: Guava skin, *Micrandra elata* and Uriridan. For a representation of the ground reference data see Figure 4.10 and Appendix III. Additional information on Xeric mixed forest can be found in ter Steege et al. (1996).

**Low swamp forest**
Low swamp forests are part of the Swamp Forest formation-series. The forests of this series all occur on permanently inundated or water-logged soils. Their architecture and species composition depend on inundation characteristics (i.e. duration, seasonal moment, water level). Extended periods of flooding generally result in poor forests, i.e. in forests with a low stature, a single open storey and relatively few species. *The Low swamp forest occupies sites that are inundated during most of the year,* i.e. riparian fringes and depressions behind river levees. *It has a single open canopy layer that varies in height* from 25 m in more elevated sites to 12 m in low-lying sites. On higher sites, a larger number of tree species and trees with larger diameters (up to 60 cm) can be found, lower down trees tend to become more shrublike. Itikiboro, one of the dominant canopy species, has striking buttresses. Palms of the genus *Euterpe* and lianas are common while epiphytes are rare (Fanshawe, 1952).

**Mora forest**
Mora forests, like Low swamp forests, belong to the Swamp Forest formation-series. They are found along creeks on soils with high year round water tables. During the wet season, the Mora forest is usually flooded. Its architecture resembles that of Mixed forests rather than that of Low swamp forests. *The main canopy ranges from 20 to 35 m but emergent trees may be as high as 60 m.* Fanshawe (1952) notes a




| Layer | Total height (m) | Crown diameter (m) |
|---|---|---|
| Main canopy | 30 - 35 | 10 - 15 |
| Emergent trees | 40 - 50 | 15 - 20 |

(c)

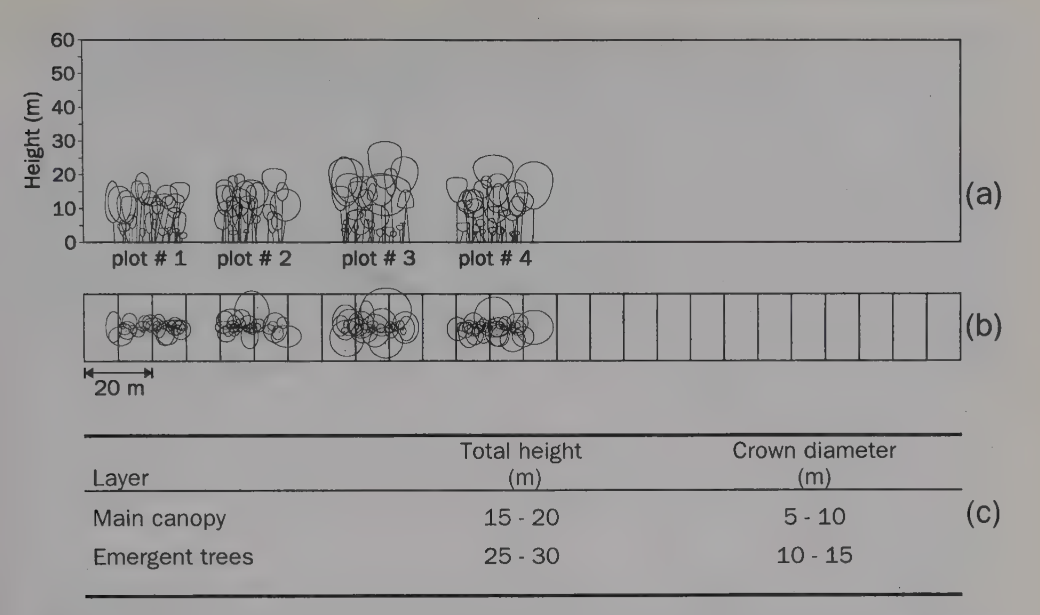
**Figure 4.8 (a-c)** (**a**) Generalised profiles and (**b**) crown projection plans for **Greenheart dominated Mixed forest** plots according to Koop's method (1989). (**c**) Summary of data on total tree height and crown diameter for emergent trees and trees of the main canopy.

Height (m)
60
50
40
30
20
10
0
plot # 1
plot # 2
plot # 3
plot # 4
plot # 5
plot # 6
(a)
(b)
20 m

| Layer | Total height (m) | Crown diameter (m) |
|---|---|---|
| Main canopy | 25 - 30 | 10 - 15 |
| Emergent trees | – | – |

(c)

**Figure 4.9 (a-b)** (**a**) Generalised profiles and (**b**) crown projection plans for **Wallaba forest** plots according to Koop's method (1989). (**c**) Summary of data on total tree height and crown diameter for emergent trees and trees of the main canopy.




| Layer | Total height (m) | Crown diameter (m) |
|---|---|---|
| Main canopy | 15 - 20 | 5 - 10 |
| Emergent trees | 25 - 30 | 10 - 15 |

(c)

**Figure 4.10 (a-c)** (**a**) Generalised profiles and (**b**) crown projection plans for **Xeric mixed forest** plots according to Koop's method (1989). (**c**) Summary of data on total tree height and crown diameter for emergent trees and trees of the main canopy.

| Layer | Total height (m) | Crown diameter (m) |
|---|---|---|
| Main canopy | 30 - 40 | 10 - 15 |
| Emergent trees | 40 - 60 | 20 - 30 |

(c)

**Figure 4.11 (a-c)** (**a**) Generalised profiles and (**b**) crown projection plans for **Mora forest** plots according to Koop's method (1989). (**c**) Summary of data on total tree height and crown diameter for emergent trees and trees of the main canopy.

lower canopy between 15 and 25 m, and an undergrowth stratum ranging from 5 to 15 m. The shrub layer typically consists of a dense layer of saplings of the markedly dominant Mora trees. Mora is a strongly buttressed species and *buttressing is therefore an outstanding feature of this forest type.* The number of trees per hectare is smaller than in Mixed forests but the trees, on average, have larger diameters. Emergent Mora trees usually have fairly open crowns that consist of heavy branches with relatively few leaves. The latter contributes to the fact that Mora forests, as compared to Mixed forests, have a rather open canopy. Epiphytes profit from the rather high light conditions and are abundant, while lianas are only moderately abundant. For a representation of the ground reference data see Figure 4.11 and Appendix III. More information on the Mora forest can be found in ter Steege (1990) and ter Steege et al. (1996).

### 4.3.2 Logged-over and secondary forest

**Logged-over forest**

*Large parts of Mabura Hill's forests are subject to industrial logging. Selective logging is used, not clear-cutting.* It involves the felling and extraction of a relatively small number of commercially valuable trees per hectare. According to the management plan felling is restricted to trees with a dbh ≥ 38 cm and carried out with an intensity of ca. 20 $m^3 ha^{-1}$ (≈ 8 trees, ≈ 22 t $ha^{-1}$ total dry biomass above the ground). The intention is to log 12,000 ha per year and the specified logging cycle is 20 years. The planned system is in accordance with the Celos Silvicultural System (De Graaf, 1986). In Mabura Hill logging is concentrated in Mixed forests, particularly those dominated by Greenheart. This preference for Greenheart is typical of most logging activities in Guyana. The high commercial value of the species is clearly reflected in Guyana's timber statistics. Greenheart accounts for some 45% of the harvested timber whereas it constitutes a mere 0.5 to 1.5% of the total volume of standing timber (Tropenbos, 1991a; ter Steege et al., 1996).

Logging affects the process by which forest architecture is built. Hallé et al. (1978) and Oldeman (1983a) refer to this process as "silvigenesis" (forest-making). The process is cyclic and may be divided into four development phases, namely the: innovation phase, aggradation phase, biostatic phase and degradation phase. For a detailed discussion of these phases and their architectural characteristics please refer to Oldeman (1990). In short, the innovation phase is characterised by the development of herbs, weedy climbers and tree seedlings. It starts immediately after the destruction of the original forest cover. The innovation phase is followed by the aggradation phase which commences when woody plants close the canopy. The result of the aggradation phase is a "fully developed"/"matured" forest, i.e. a forest in the biostatic phase. Ultimately, the forest will enter the degradation phase. This phase is characterised by the death and decay of trees and eventually enables the forest to re-enter the innovation phase. Forest degradation may result from senescence of trees or accidents caused by natural factors such as wind, water and lightning. The surface on which at a particular moment in time one process of silvigenesis has begun is defined by Oldeman (1990) as an "eco-unit". Intact tropical forests may be conceived as a small-scale mosaic of uneven-aged eco-units because

they regenerate tree-wise or by small groups of even-aged trees. Occasionally, they may comprise larger eco-units due to large scale natural disturbances such as hurricanes, landslides, earthquakes or fire. In Guyana such disturbances are probably rare (Hammond and Brown, 1995).

The impact of logging on silvigenesis varies with its intensity, frequency and spatial extent (e.g. Jonkers, 1987; Hendrison, 1990; Waide and Lugo, 1992). Non-industrial selective logging causes disturbances similar to those resulting from small-scale natural accidents and consequently has a low impact. The impact of clear-cutting or industrial selective logging is, at best, comparable to that of large scale natural accidents. Mechanised extraction of logs poses a greater threat to sylvigenesis than felling. Careless extraction may seriously damage the soil and under storey and as such obstruct the forest's regeneration (e.g. Jonkers, 1987; Hendrison, 1990; ter Steege et al., 1996). The direct result of felling is a canopy opening or, more popularly, a gap. The gap size determines the response of the remaining forest. Large gaps cause the forest to re-enter the innovation phase. They provide space for the establishment of one or more new eco-units (regeneration units). Small gaps do not induce such a development shift but are mostly 'repaired' by lateral crown growth of neighbouring trees (Oldeman, 1990). *Logged-over forests, when compared to intact forests, are characterised by a reduced total aboveground biomass and a reduced number of stems (of particular species) in specific diameter classes. Moreover, logged-over forests have an ecologically disorganised architecture.* The mosaic of recently logged forest comprises more regeneration units, a higher proportion of large regeneration units and regeneration units with an artificial architecture (e.g. due to destruction of under storeys). The most marked symptom of logging in the available radar images is the presence of an 'unnaturally' high density of gaps and/or of gaps with 'unnatural' sizes. However, if a gap is to be observed, it must be of a size larger than or equal to the spatial resolution of the radar system. Information on gap size and gap density in logged-over as well as intact forest was therefore of great importance to this study. In addition, there was a need for data on the closure rate of (un)natural gaps as this is relevant to the temporal resolution of radar observations. The information on these topics available from studies in Guyana (Mabura Hill), French Guiana and Surinam will be summarised in the following paragraphs.

In Mabura Hill the gap characteristics of logged-over forest and Mixed forest were studied by Hammond and Brown (1992). Logged-over forest was found to have over 50% more gaps than intact forest. Logging increased the total gap area by over 400%, as the size of artificial gaps was considerably larger than the size of natural gaps. Gaps accounted for 12.6% of the area in logged-over forest compared to 2.7% in intact forest. The size of artificial and natural gaps was found to be ca. 800 ± 200 $m^2$ and 100 ± 20 $m^2$, respectively. Gap size was noted to be largely influenced by the size and the number of trees contributing to the opening. In Mabura Hill gaps are often created by the felling of more than one tree, since the preferred species (Greenheart) usually grows in groups (Zagt, 1995).

Hammond and Brown's findings regarding the gap characteristics of intact Mixed forest in Mabura Hill are comparable to those reported for similar forest in French

Guiana by Hallé et al. (1978) and van der Meer (1995). These authors both come to the conclusion that recent gaps account for some 5% of the area of natural forest in regions not subjected to large scale natural disturbances. Annually, ca. 1% of the forest canopy can be expected to be opened up due to natural disturbances. Depending on their size, these disturbances remain visible as canopy gaps for five to 10 years. Measurements by van der Meer reveal an average gap size of 120 $m^2$. Individual gaps, however, may range in size from as little as 4 $m^2$ (caused by branch fall) to as much as 500 $m^2$. It should be noted that gap sizes reported in literature vary widely due to the use of different definitions and measurement techniques. In fact, the 'borders' of gaps (notably of natural gaps) are merely transitions.

Additional information on gap-formation due to logging may be derived from the experiments by Hendrison (1990) in Mapane (Surinam) and van der Hout (1996) in Mabura Hill. Hendrison compared the disturbances caused by directional felling to those resulting from conventional felling. Unlike conventional felling, directional felling aims to both position the felled trees in a direction favourable for extraction and to minimise the damage to the remaining forest. The felling intensity in both experiments was fixed at 8 to 10 trees $ha^{-1}$ (ca. 20 $m^3$ $ha^{-1}$). Application of directional felling techniques was found to result in a reduction of ca. 50% in both gap size and total gap area. The average size of the gaps resulting from directional and conventional felling was 120 $m^2$ and 250 $m^2$, respectively. In directionally felled forest compartments the gaps accounted for ca. 7% of the total area. In conventionally felled forest compartments it was 14% of the total area. Hendrison, furthermore, reports that the conventional extraction of logs (skidding) creates an additional 5% loss in canopy cover. For controlled (pre-planned) skidding this extra loss is less than 2%. van der Hout's experiments were designed to compare the disturbances resulting from directional felling with different intensities. Intensities of 4, 8 and 16 trees $ha^{-1}$, or 10-15, 20-30 and 40-60 $m^3$ $ha^{-1}$, were shown to result in an average gap size of 150, 250 and 300 $m^2$, respectively. The size of the individual gaps varied widely, i.e. from 30-350 $m^2$ at the lowest felling intensity to 20-800 and 15-1800 $m^2$ at the highest intensities. The loss in canopy cover increased accordingly from 6 to 15 to 30% (Brils and Laan, 1995; van der Hout, 1996).

These findings illustrate that logging does in fact result in an 'unnatural' forest architecture. *For discrimination between logged-over forest and intact forest in remote sensing images either gap density or total gap area may be used. Gap size appears to be the least reliable discriminating characteristic since the size of artificial gaps and natural gaps may be comparable.*

**Secondary forest**

Secondary forests consist of collections of eco-units in the innovation or early aggradation phases (regeneration units) (Oldeman, 1990). In San José del Guaviare they are part of a land use sequence that starts with the slash-and-burn of the natural forest and ends with the establishment of 'permanent' pastures. They develop in between periods of cultivation when the land is left fallow. Individual forest patches are usually 1 to 2 hectares in size. *Generally speaking, the secondary forests in San José del Guaviare do not exceed 15 years in age due to the fast reutilization of the land* (Andrade and Etter, 1987).

The architecture of the secondary forest is dependent on its age. Field measurements by Quiñones (1995) showed that a five year old forest was some 5 m high. Herbs, shrubs and tree seedlings constituted a dense vegetation that reached up to a level of ca. 2 to 3 m. A discontinuous growth consisting of slightly bigger trees and palms occupied the upper part of the forest. The number of trees per hectare with a dbh < 10 cm was approximately 11,000, the number of trees per hectare with a dbh ≥ 10 cm only 80. The basal area of the five year old forest was about 10 $m^2$ $ha^{-1}$, its total fresh biomass above the ground ca. 14 t $ha^{-1}$. In terms of dry biomass this will be equal to approximately 7 t $ha^{-1}$. As the forest grew older there was an increase in height, basal area, fresh biomass and the number of stems with dbh ≥ 10 cm. At the same time there was a reduction in the amount of herbaceous vegetation and the number of stems in the smaller diameter classes. Secondary forest of some 15 years in age was found to have a height of ca. 12 m, a basal area of 30 $m^2$ $ha^{-1}$ and a fresh biomass of 81 t $ha^{-1}$ (≈ 40 t $ha^{-1}$ dry weight). There were approximately 5,400 trees with dbh < 10 cm and 1,600 trees with dbh ≥ 10 cm per hectare (Quiñones, 1995).

The architecture and development of secondary forests was studied by Gräfe (1981) in western Venezuela and by Lescure (1978) in southern French Guiana. Gräfe, like Quiñones, studied secondary forests found in areas with permanent, 'large scale' human activity. Lescure, on the other hand, studied secondary forests that developed on small fields resulting from the temporary activities of Amerindian shifting cultivators. The secondary forests studied in Venezuela appear to develop more rapidly than those in San José del Guaviare. This was concluded from differences in height growth. For five year old secondary forests Gräfe and Quiñones reported heights of ca. 15 and 5 m, respectively. The 15 year old secondary forests in Venezuela were found to be ca. 20 m high, those in Guaviare, ca. 12 m.

The possible reasons for the height differences are not discussed in this study. The discrepancies in the development of the forests were pointed out to place the forests at the study site in San José del Guaviare in a wider framework. However, it is of interest to mention that *the re-establishment of a forest at a particular site is strongly dependant on the site's history.* Generally speaking, a forest will recover fully and swiftly as long as the upper soil horizons remain intact (Hallé et al., 1978). The presence of a fairly intact soil layer is probably the reason that the forests studied by Lescure (1978) developed more rapidly than either of those in Guaviare or Venezuela. four year old forests that developed on shifting cultivation sites were reported to be ca. 15 m high, 11 year old forests were found to be ca. 22 m high. The re-establishment of forests at such sites and in openings resulting from small-scale natural disturbances will be comparable.

### 4.3.3 Leaf properties

The fully grown leaves of most adult trees in Mabura Hill were observed to be xeromorphic or mesomorphic. Their leathery nature is reflected in the results of blade thickness measurements. A total of 500 fully developed leaves, derived from 10 canopy trees, were measured. Their thicknesses ranged from 0.2 to 0.4 mm and

were 0.3 mm on average. These findings agree well with those reported for a wide variety of species in the tropical rain forests of Venezualan Guiana (Roth, 1984; Rollet et al., 1990). Earlier measurements of leaves from temperate regions, i.e. oak and beech, showed an average blade thickness of circa 0.2 mm (Droesen et al., 1989). *The leaves of canopy trees in a tropical rain forest environment have long been known to be considerably thicker than those of trees in a temperate region* (Schimper, 1935, p.463). Leaf sizes were found to vary widely among trees and forest types. Based on visual observations the fully grown leaves of adult trees in the Xeric mixed forest were classified as notophyllous (20.25 to 45.00 $cm^2$) or microphyllous (2.25 to 20.25 $cm^2$), while those in the other forest types were categorised as mesophyllous (45.00 to 182.25 $cm^2$) or notophyllous (20.25 to 45.00 $cm^2$). These observations seem to contradict with those of Richards (1952, p.80) who denotes the dominance of the 'mesophyll' size-class of Raunkiaer as "a most striking feature" of tropical rain forests. However, this apparent discrepancy is due to the fact that Raunkiaer's classification, unlike the one adopted in this study, does not differentiate between the 'notophyll' and 'mesophyll' size-class. His classification includes all leaf sizes in the range from 20.25 to 182.25 $cm^2$ in the 'mesophyll' size-class. The surface areas of the 500 leaves that were measured in this study were all within the range of the visually observed size-classes.

In the field, no attempt was made to gather information on parameters representing the number of leaves, e.g. Leaf Area Index (LAI) or amount of leaf biomass. Some information on these parameters could be derived from literature (e.g. Cannell, 1982) but in many cases the reported figures were found to vary widely. In Cannell's "World forest biomass" review the LAI values for tropical rain forests range from 3.2 $m^2\ m^{-2}$ in Ivory Coast to 11 $m^2\ m^{-2}$ in Thailand. Likewise, the values for dry foliage biomass range from 2.3 $t\ ha^{-1}$ in Ivory Coast to 9.3 $t\ ha^{-1}$ in Brazil. The LAI and dry foliage biomass values quoted for a rain forest area in Guyana's neighbouring country of Venezuela, are 5.2 $m^2\ m^{-2}$ and 8.0 $t\ ha^{-1}$. However, the dry foliage biomass for a Mixed forest in French Guiana is estimated to be much lower, i.e. ca. 4.5 $t\ ha^{-1}$ (Lescure et al., 1983). According to Lescure et al. leaves account for 1 to 2% of the total dry biomass.

Measurements of fully grown leaves from adult trees in Mabura Hill revealed that the leaf gravimetric water content ranged from 0.4 to 0.5 $g\ g^{-1}$ in the dry season and from 0.5 to 0.6 $g\ g^{-1}$ in the wet season. Busink (1981) reports a comparable value, i.e. 0.55 $g\ g^{-1}$, for leaves from trees in a mixed forest at Kabo, Surinam. Droesen et al. (1989) and Vissers and van der Sanden (1993) found the gravimetric water content of leaves from trees in The Netherlands to range from 0.6 to 0.8 $g\ g^{-1}$. Apparently, *the water content of leaves from trees in temperate regions is higher than that of leaves from trees in tropical regions.* The relatively low gravimetric water content of leaves from tropical forest trees can be explained by their xeromorphic nature.

The leaves in the secondary forests of San José del Guaviare were observed to be mesomorphous and either mesophyllous (45.00 to 182.25 $cm^2$) or notophyllous (20.25 to 45.00 $cm^2$). The leaf area index for a five year old secondary forest was estimated to be 12 $m^2\ m^{-2}$, that for a 15 year old forest 4 $m^2\ m^{-2}$ (Quiñones, 1995). Data on blade thickness and leaf water content are not available.

## 4.4 Sensor and data acquisition characteristics

### 4.4.1 CCRS Airborne SAR

Data acquisition with the airborne SAR from the Canada Centre for Remote Sensing (CCRS) took place in the framework of the 1992 South American Radar EXperiment (SAREX-92). The aim of the experiment was to study the radar signature of tropical forests in support of ERS-1 data interpretation and to define mission requirements for future space borne radar systems. SAREX-92 was funded through the Earth Observation Preparatory Programme (EOPP) by the European Space Agency (ESA). The experiment provided a contribution to the ESA / CEC project TREES (TRopical Ecosystem Environment observation by Satellite) (Wooding et al., 1992).

Mabura Hill and San José del Guaviare constituted two of the 25 SAREX-92 test sites. The sites were located in six different countries in South and Central America: Venezuela, Guyana, French Guiana, Brazil, Colombia and Costa Rica. The data for Mabura Hill were acquired on April 8, while those for San José del Guaviare were taken on April 29. Additional information on the SAREX-92 data acquisition programme can be found in Bercha (1992). Technical specifications of the deployed CCRS Airborne SAR are given in Table 4.5. In Mabura Hill the aircraft made four successive runs along three different flight lines in order to obtain C- and X-band data in HH, VH, VV and HV polarization. Data acquisition in San José del Guaviare was restricted to C- and X-band, VV and HV polarization. These data were acquired in two runs along two different flight lines. All radar data were processed in real-time

**Table 4.5** Specifications of the **CCRS Airborne SAR**.

| | C-band system | X-band system |
|---|---|---|
| **Sensor characteristics** | | |
| Central frequency [1] | 5.30 GHz | 9.25 GHz |
| Wavelength | 5.66 cm | 3.24 cm |
| Polarization | HH, VH or VV, HV | |
| Spatial resolution in range | 4.8 m | |
| Spatial resolution in azimuth | 6.1 m | |
| **Image characteristics** | | |
| Number of looks | 7 | |
| Pixel size in range | 4.0 m | |
| Pixel size in azimuth | 4.31 m | 3.44 m |
| **Operational characteristics** | | |
| Platform | Convair-580 aircraft | |
| Mode | nadir swath | |
| Flight altitude | ca. 7000 m | |
| Incidence angle range (usable) | ca. 20° to 65° | |

1) 'time-coding' through frequency and pulse modulation (see section 3.1.1).

onboard the Convair-580 aircraft.

Prior to analysis the C-band data were radiometrically calibrated with the help of calibration parameters provided by the CCRS. The methodology for the computation of these parameters is described by Hawkins and Teany (1992). Only the C-band VV data are calibrated in the absolute sense (see section 3.1.5). The high calibration level for these data was obtained through intercomparison of CCRS SAR backscatter values for a specific rain forest area with those from the, absolutely calibrated, ERS-1 C-band VV scatterometer system. The C-band HH, VH and HV data were calibrated in the relative sense. This, according to Hawkins and Teany, should allow for the intercomparison of these data within the same image or from image to image within tolerances of approximately 1 dB. The X-band data could not be calibrated as the required calibration parameters were not made available. Comparison of backscatter levels for objects within those data, and notably for objects at different range distances or in different images, should therefore be undertaken with caution.

### 4.4.2 NASA/JPL Airborne SAR

Data acquisition with the airborne SAR (AIRSAR) from the Jet Propulsion Laboratory (JPL) of the National Aeronautics and Space Administration (NASA) took place in the framework of a campaign known as the "AIRSAR South American Deployment". The radar over flights were carried out in May and June 1993 at sites in: Mexico, Belize, Ecuador, Colombia, Peru, Bolivia, Argentina, French Guiana and Guyana. The nature of the sites varied widely, from volcanolic sites in Peru and Bolivia to rain forest sites in French Guiana, Guyana and Colombia. NASA/JPL funded and executed the campaign to facilitate fundamental research into the role of soils, vegetation and water in the global carbon cycle. In addition, the campaign was intended to familiarize researchers with polarimetric radar data and to prepare them for the analysis of data from SIR-C / X-SAR missions not yet carried out at that time. For more information on the campaign please refer to the plan of operations (NASA, 1993).

The AIRSAR data for San José del Guaviare and Mabura Hill were acquired on May 31 and June 11, respectively. In San José del Guaviare the system was operated in three runs along as many flight lines, while in Mabura Hill it was deployed in two runs along two flight lines. The flight lines were a selection of those that were flown during SAREX-92. Along each line of flight the system collected polarimetric radar data in P-, L- and C-band. The most important technical specifications of the NASA/JPL AIRSAR are listed in Table 4.6. A more detailed description of the system can be found in van Zyl et al. (1992). All data were processed on the JPL frame processor, which includes absolute radiometric calibration. However, the accuracy of the absolute calibration is questionable (see section 6.3.2 and Hoekman et al., 1996).

**Table 4.6** Specifications of the **NASA/JPL Airborne SAR**.

| | P-band system | L-band system | C-band system |
|---|---|---|---|
| **Sensor characteristics** | | | |
| Central frequency [1] | 0.44 GHz | 1.25 GHz | 5.26 GHz |
| Wavelength | 68 cm | 24 cm | 5.7 cm |
| Polarization | | polarimetric | |
| Spatial resolution in range | | 6.66 m | |
| Spatial resolution in azimuth | | 12.1 m | |
| **Image characteristics** | | | |
| Number of looks | | 16 | |
| Pixel size in range | | 6.66 m | |
| Pixel size in azimuth | | 8.20 m | |
| Processor version | | 3.56 | |
| **Operational characteristics** | | | |
| Platform | | DC-8 aircraft | |
| Flight altitude | | ca. 8100 m | |
| Incidence angle range | | ca. 20° to 65° | |

1) 'time-coding' through frequency + pulse modulation (see section 3.1.1).

### 4.4.3 First European remote sensing satellite ERS-1

The first European remote sensing satellite ERS-1 was launched by the European Space Agency (ESA) on 17 July 1991. ERS-1 carries various sensor systems that provide world-wide coverage of oceans, sea-ice and land surface areas. The data from ERS-1 are very suitable for monitoring purposes since they are acquired in a synoptic, systematic and repetitive manner. This study makes use of a time series of data acquired by the ERS-1 Synthetic Aperture Radar (SAR) system. The acquisition dates for these images are listed in Table 4.7. The images were made available by ESA in the framework of the SAREX-92 campaign and ERS-1 Anouncement of Opportunity (AO) projects.

**Table 4.7** Acquisition dates of ERS-1 SAR images.

| Mabura Hill, Guyana | San José del Guaviare, Colombia |
|---|---|
| 29 April 1992 | 26 May 1992 |
| 3 June 1992 | 4 August 1992 |
| 30 December 1992 | 17 November 1992 |
| 6 October 1993 | 22 December 1992 |
| 27 May 1994 | 20 July 1993 |
| 9 August 1994 | 28 September 1993 |

**Table 4.8** Specifications of the **ERS-1 satellite** system, the SAR sensor and the SAR image products.

| | C-band system |
|---|---|
| **Sensor characteristics** | |
| Central frequency [1] | 5.3 GHz |
| Wavelength | 5.6 cm |
| Polarization | VV |
| Spatial resolution in range | < 10 m |
| Spatial resolution in azimuth | < 10 m |
| **PRI image characteristics** | |
| Format | ground range |
| Number of looks | 3 |
| Spatial resolution in range | < 33 m |
| Spatial resolution in azimuth | < 30 m |
| Pixel size in range | 12.5 m |
| Pixel size in azimuth | 12.5 m |
| **SLC image characteristics** | |
| Format | slant range |
| Number of looks (nominal) | 1 |
| Spatial resolution in range | < 10 m |
| Spatial resolution in azimuth | < 10 m |
| Pixel size in range | 7.9 m |
| Pixel size in azimuth | 4.0 m |
| **Operational characteristics** | |
| Platform | satellite |
| Flight altitude (nominal) | 782 km |
| Incidence angle range | ca. 19.5° to 26.5° (23° mid swath) |
| Swath width | 100 km |
| Repeat cycle | 35, 168 |

1) 'time-coding' through frequency + pulse modulation (see section 3.1.1).

Table 4.8 lists characteristics of the satellite, the SAR sensor and the two ERS-1 SAR data products that were used in this study. For a more extensive description of the ERS-1 system and data products please refer to ESA (1992a, 1992b, 1993). When compared to SAR Single Look Complex (SLC) data, SAR Precision (PRI) data have lower spatial resolutions in both azimuth and range directions. The lower spatial resolution in azimuth and range result from, respectively, 3-look averaging and slant-to-ground range conversion (see section 3.1.3). In the production of PRI images, spatial resolution is sacrificed for the benefit of radiometric and geometric image properties. PRI images contain less speckle than SLC images and, unlike the latter, are free of slant range scale distortions. For these reasons they are the most widely

used ERS-1 SAR data product. The preference of most users for PRI images is strengthened by the fact that these images cover a larger ground surface area and yet constitute a smaller data volume.

The ERS-1 SAR data set for this study consisted of PRI images for San José del Guaviare and both PRI and SLC images for Mabura Hill. *SLC images were included because their better spatial resolution was hypothesised to result in a higher textural information content and as such in a better capacity for forest type classification.* The value of image texture for this purpose had become clear from the analysis of the SAREX-92 data (see section 6.1.1). The study made use of a radiometrically enhanced SLC image rather than a standard SLC image provided by ESA. This enhanced image was generated by averaging three standard SLC images from different acquistion dates. In this text the enhanced image will be referred to as the SLC-av image. Its radiometric properties are comparable to those of a PRI image, while its spatial resolution is equal to that of a SLC image. The images used in the production of the SLC-av were acquired on the 29 April 1992, 3 June 1992 and 6 October 1993. The SLC image from 30 December 1992 was not available. To study the effect of radiometric resolution on textural information content a radiometrically enhanced (9 looks) PRI product was created by averaging a series of three PRI images from Mabura Hill. In this text the enhanced PRI image will be referred to as the PRI-av image. The images used to produce the PRI-av image were acquired on the 29 April 1992, 3 June 1992 and 30 December 1992.

In order to create radiometrically enhanced images by look averaging in time, these looks must be statistically independent (uncorrelated). This will only be the case when the size and relative locations of the observed scatterers vary in time (see section 3.1.3). For forests and other types of vegetation this will almost always be the case due to growth and wind effects. In addition, decorrelation of looks in images from different acquisition dates results from small variations in the satellite's position.

The ERS-1 SAR data studied resulted from descending overpasses. They were acquired during the day, at approximately 10.30 a.m. local solar time. The data were received at the ERS-1 groundstation in Cuiaba, Brazil and processed at the ESA Processing and Archiving Facility in Germany (D-PAF). Prior to analysis the PRI images were absolutely calibrated according to the procedure described by Laur (1992) and Laur et al. (1993). For the SLC images accurate radiometric calibration was not strictly necessary. They were used to study local backscatter variations (image texture) rather than absolute backscatter levels or temporal backscatter changes.

### 4.4.4 ERASME scatterometer

The ERASME scatterometer is an example of a non-imaging radar remote sensing system (see section 3.1.1). In the framework of SAREX-92 the system was deployed over the Tropenbos ecological reserve in Mabura Hill on April 7, 1992. The system was mounted in a low flying helicopter and operated in a nadir as well as forward-looking mode to acquire C- and X-band, HH and VV polarised radar data (Dechambre

**Table 4.9** Specifications of the **ERASME scatterometer**.

| | X-band system |
|---|---|
| **Sensor characteristics** | |
| Central frequency [1)] | 9.65 GHz |
| Wavelength | 3.11 cm |
| Polarization | VV |
| Sample frequency | 150 MHz |
| Range resolution | 1.30 m |
| **Operational characteristics** | |
| Platform | Ecureuil helicopter |
| Looking mode | nadir-looking |
| Flight altitude | ca. 60 m |
| Antenna footprint | ca. 20 x 5 m |

1) 'time-coding' through frequency modulation (see section 3.1.1).

et al., 1993). Simultaneously black-and-white video data were acquired. The video images served as a tool for linking the radar measurements to the objects observed and as such facilitated the radar data analysis.

In this study only the nadir-looking X-band VV data are used. Unlike imaging radar systems, scatterometer systems have a "probing" capability. This implies that they can measure the backscatter from horizontal observation layers superimposed upon the forest. A single nadir-looking ERASME measurement, for example, represents the sum of the backscatter contributions from the scatterers within a 1.30 m high layer. In combination the *measurements at a particular location reflect the vertical architecture of the forest.* For an overview of the most relevant (operational) characteristics of the ERASME scatterometer please refer to Table 4.9.

# 5 Methods and techniques for radar data analysis

The present chapter describes the methods and techniques used to extract information from the available radar data sets and to appraise the value of this information for the identification of forest types and other land cover types, in particular. The results of radar data analysis for the purpose of forest resource assessment and monitoring are discussed in Chapters 6 and 7, respectively. The findings of experiments aimed at optimising procedures for automated analysis of texture in radar images by means of the grey level co-occurrence technique are discussed in Appendix I.

## 5.1 Textural analysis of radar images

### 5.1.1 Description of image texture and textural attributes

*Image texture is defined by Haralick and Bryant (1976) as "the pattern of spatial distributions of grey tone".* High frequency radar images are often rich in texture because of shadowing, layover and foreshortening at the surface of the observed object (see section 3.1.3). These effects, however, only occur when the object is comprised of structural elements with sizes greater than or equal to the size of the resolution cell. In other words, the object's intrinsic scale must match or exceed the measurement scale of the radar. *Texture in radar images of forests relates to canopy roughness which is a parameter of canopy architecture.* An effectively rough canopy results in a rougher image texture.

Over the years a large number of techniques to measure and quantify texture in digital images have been investigated. These investigations underline the importance and ubiquity of texture in image data but at the same time reflect that *a formal unambiguous definition of image texture is lacking.* Available textural analysis techniques fall into two main categories, i.e. statistical and structural ones. Statistical techniques describe texture in terms of parameters that characterise the statistical properties of the spatial distribution of grey levels. Examples of such techniques are those that make use of: autocorrelation functions, Fourier power spectra, Gaussian Markov random fields, grey level run lengths, textural edginess, textural spectra, fractals and grey level co-occurrence. Structural techniques conceive of texture as an arrangement of a set of spatial sub-patterns according to certain placement rules. They describe texture in terms of parameters that characterise the organisation and/or the spatial distribution of the sub-patterns. The parameters used are often statistical, but sometimes they are not. Examples of structural textural analysis techniques are those that tessellate images into cells of a certain structure (e.g. squares, hexagonals etc.) or those that attempt to match sub-patterns with predefined geometric figures. Reviews of techniques for analysis of image texture can be found in Weszka et al. (1976), Haralick (1979, 1986), Ahuja and Rosenfeld (1981) and Kilpelä and Heikkilä (1990).

*Textural analysis in the present study is based on a statistical technique that is known as the grey level co-occurrence technique.* This technique proved to be effective in many earlier studies (e.g. Weszka et al., 1976; Conners and Harlow, 1980; Hoekman, 1990; Kilpelä and Heikkilä, 1990; Marceau et al., 1990; Kushwaha et al., 1994). The grey level co-occurrence technique is *based on the spatial distribution and the mutual spatial dependence of the grey levels in an image.* Texture is quantified in terms of statistical parameters that are computed from the elements of a grey level co-occurrence (GLCO) matrix or a grey level difference (GLD) vector. In this text these parameters will be referred to as textural attributes. The elements of the GLCO matrix and GLD vector represent *grey level second-order statistics* of the pixel pairs contained in a certain image region or spatial window. The $i,j$-th entry in the GLCO matrix $p(i,j)$ is defined as the relative frequency of pixel pairs, for each possible pixel pair realisation in the area of interest, for which the "source" pixel with grey level $i$ is at position $(x,y)$ and the "target" pixel with grey level $j$ is at position $(x,y)+\boldsymbol{d}$. Vector $\boldsymbol{d}$ is denoted the "displacement vector". The $i$-th entry in the GLD vector $v(i)$ is defined as the relative frequency of pixel pairs, for each possible pixel pair realisation, for which the source pixel with grey level $k$ is at position $(x,y)$ and the target pixel with grey level $k+(i-1)$ or $k-(i-1)$ is at position $(x,y)+\boldsymbol{d}$ (Hoekman, 1990).

The results of the GLCO and GLD technique depend strongly on displacement length $|\boldsymbol{d}|$ and displacement direction $\alpha$. The dependence on $\alpha$, however, is not related to image texture. Instead of choosing another $\alpha$ the image might as well be rotated. Although a rotation does not change the image texture, it will generally result in a different GLCO matrix and GLD vector. Only rotations over 180°, i.e. displacements in opposite directions, yield identical GLD vectors and closely related GLCO matrices. The GLCO matrices that result from displacement in opposite directions are each other's transpose. They therefore are not substantially different. This notion is used in many studies, including the present one, to employ symmetrical GLCO matrices. These matrices allow for a speedier computation of textural attributes, while preserving the full textural information content. The lower computational load results from the fact that all relevant information is contained in just one matrix half. The

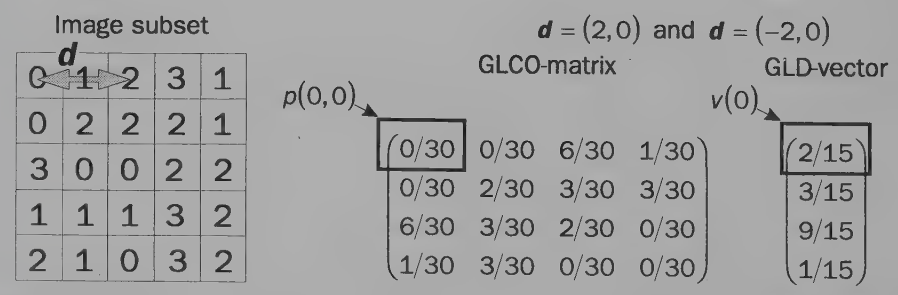



**Figure 5.1** Procedure to construct a grey level co-occurrence (GLCO) matrix and a grey level difference (GLD) vector for an image subset of $5\times5$ pixels. Successive displacements along the vectors $\boldsymbol{d}=(2,0)$ and $\boldsymbol{d}=(-2,0)$ are performed to attain that the GLCO matrix is symmetrical.

matrix entries represent the relative frequencies of pixel pairs with grey levels $p(i, j)$ for displacement in both the $\alpha$ and the $\alpha + 180^\circ$ direction. Due to the consecutive displacement in two opposite directions $p(i, j) = p(j, i)$. The procedure for constructing a symmetrical GLCO matrix and a GLD vector for a $5 \times 5$ image subset with $\boldsymbol{d} = (2, 0)$ and $\boldsymbol{d} = (-2, 0)$ is illustrated in Figure 5.1.

Both the GLCO matrix and GLD vector are intermediate components in the analysis of texture according to the grey level co-occurrence technique. They serve as input for computing one or more textural attributes (statistical parameters) that quantify image texture. The textural attributes used in this study are listed in Table 5.1. According to Baraldi and Parmiggiani (1995), Gerbrands (1986) and Zhan (1986), these attributes may be described as follows:

**GLCO-ASM (Angular Second Moment)**
Measures *textural uniformity;* high values occur when few $p(i, j)$ are large (close to 1) and others are small (close to 0). This is the case when the area of interest is either homogeneous or texturally uniform, i.e. when the grey level distribution is constant.
**GLCO-CONT (Contrast)**
Measures textural contrast, i.e. the *presence of sharp grey level transitions (edges).* Low values occur when edges are absent. In this case the matrix entries are concentrated around the principal diagonal.
**GLCO-COR (Correlation)**
Measures *linear-dependencies between the grey levels* of pixels pairs. High values (close to 1) imply a strong relationship between pixel pair grey levels. GLCO-COR is uncorrelated to GLCO-ASM as high GLCO-COR values can be measured either in low or high GLCO-ASM situations.
**GLCO-ENT (Entropy)**
Measures *the disorder in an image*, high values occur when many $p(i, j)$ have very small values. The parameter reaches its maximum when the pixels in the area of interest have completely random grey levels. GLCO-ENT is likely to be highly negatively correlated to GLCO-ASM. GLCO-ENT and GLCO-COR are uncorrelated.
**GLCO-IDM (Inverse Difference Moment)**
Measures *image homogeneity* as it assumes larger values when pixel pairs have smaller grey level differences. The parameter is highly negatively correlated to GLCO-CONT. When compared to GLCO-ASM the parameter is less sensitive to the differences in the grey levels of pixel pairs.
**GLCO-MAX PROB (Maximum Probability)**
Measures *textural uniformity;* high values occur when the area of interest is either homogeneous or texturally uniform, i.e. when the grey level distribution is constant. The parameter is positively correlated to GLCO-ASM and negatively correlated to GLCO-ENT.
**GLD-ASM (Angular Second Moment)**
Measures *uniformity in pixel pair grey level contrast;* high values occur when few $v(i)$ are large (close to 1) and others are small (close to 0). This is the case when the pixel pairs in the area of interest have set grey level differences, i.e. when the grey level distribution is constant, periodic or linear.

**Table 5.1** Overview of textural attributes that were computed from the GLCO matrix (1-6) and the GLD vector (7-9). $N_g$ represents the number of image grey levels and $m_x$, $m_y$, $s_x$ and $s_y$ represent, respectively, the mean values and standard deviations of the row and column positions of the counts in the GLCO matrix.

| | Attribute | Formula |
|---|---|---|
| (1) | Angular Second Moment : (GLCO-ASM) | $\sum_{i=1}^{Ng}\sum_{j=1}^{Ng} p^2(i,j)$ |
| (2) | Contrast : (GLCO-CONT) | $\sum_{i=1}^{Ng}\sum_{j=1}^{Ng} p(i,j)(i-j)^2$ |
| (3) | Correlation : (GLCO-COR) | $\sum_{i=1}^{Ng}\sum_{j=1}^{Ng} p(i,j)\frac{(i-m_x)(j-m_y)}{s_x s_y}$ |
| (4) | Entropy : (GLCO-ENT) | $-\sum_{i=1}^{Ng}\sum_{j=1}^{Ng} p(i,j)\log_e(p(i,j))$ |
| (5) | Inverse Difference Moment : (GLCO-IDM) | $\sum_{i=1}^{Ng}\sum_{j=1}^{Ng} p(i,j)\frac{1}{1+(i-j)^2}$ with $i \neq j$ |
| (6) | Maximum Probability : (GLCO-MAX PROB) | $\max_{i,j} p(i,j)$ |
| (7) | Angular Second Moment : (GLD-ASM) | $\sum_{i=1}^{Ng} v^2(i)$ |
| (8) | Entropy : (GLD-ENT) | $-\sum_{i=1}^{Ng} v(i)\log_e(v(i))$ |
| (9) | Mean : (GLD-MEAN) | $\sum_{i=1}^{Ng} (i-1)v(i)$ |

**GLD-ENT (Entropy)**
Measures *the disorder in pixel pair grey level contrast;* high values occur when many $v(i)$ have very small values. The parameter reaches its maximum when the pixels in the area of interest have completely random grey level differences. GLD-ENT is likely to be highly negatively correlated to GLD-ASM.
**GLD-MEAN (Mean)**
Measures *the magnitude of the contrast between pixel pairs,* i.e. the presence of sharp grey level transitions (edges). High values will occur in areas that are rich in contrast, i.e. where edges are present. GLD-MEAN is positively correlated to GLCO-CONT.

### 5.1.2 Textural analysis in the presence of speckle

Grey level co-occurrence and other statistical textural analysis techniques generate parameters that characterise the spatial variation of grey levels. *In radar images,* however, these *grey level variations do not only result from the spatial variability in the scattering properties of the object observed (texture) but also from the presence of speckle.* In homogeneous regions of radar *intensity* images from forests and other types of distributed land targets the total grey level variance, i.e. the total variance in backscattered *power* $S_{tot}^2$ is given by:

$$S_{tot}^2 = S_T^2 + S_F^2 + S_T^2 S_F^2 \tag{5.1}$$

Where $S_T^2$ is the texture variance, $S_F^2$ the speckle or fading variance and $S_T^2 S_F^2$ an interaction term equal to the product of the texture and fading variance (Ulaby et al, 1986a; Ulaby et al, 1986b, p. 1912). At the *linear scale* the fading variance is given by:

$$S_F^2 = \frac{\bar{I}^2}{k} \tag{5.2}$$

Where $\bar{I}^2$ is the mean backscattered power and $k$ is the number of independent looks (see section 3.1.3). From substitution of Equation 5.2 in 5.1 it follows that $S_{tot}^2$ *for a particular region of a linear scaled k-looks radar intensity image is dependent on the region's mean backscatter level.* Hence, two regions with an identical texture variance but with a different backscatter level will have a different total variance, i.e. a different grey level variation. The presence of speckle and its dependence on the amount of backscattered power thus complicates textural analysis of radar images.

Textural analysis only yields reliable results when the differences in image grey level variability can be attributed solely to differences in texture. This does not hold true for linearly scaled radar amplitude nor for linearly scaled radar intensity images and therefore this type of images is less suited for use in statistical textural analysis. Such images, however, may be made suitable by simply converting them to *logarithmically scaled* radar intensity images, i.e. to images in which the pixels represent backscattered power in dB. According to Hoekman (1990, 1991) the fading variance for this type of images is given by:

$$S_F^2 = a^2 \zeta(2,k) \tag{5.3}$$

with

$$a = \frac{10}{\log_e(10)} \tag{5.4}$$

and Riemann zeta function

$$\zeta(2,k) = \frac{\pi^2}{6} - \sum_{n=1}^{k-1} \frac{1}{n^2} \tag{5.5}$$

Unlike the $S_F^2$ for linearly scaled intensity images the $S_F^2$ for logarithmically scaled radar intensity images is independent of the backscattered power. For the latter type of images $S_F^2$ is dependent on the number of looks $k$ only. For logarithmically scaled radar intensity images the fading variance will be of a set value since $k$ is fixed. Substitution of Equation 5.3 in 5.1 shows that *the total variance for logarithmically scaled radar intensity images is a function of a predetermined fading variance and a variable texture variance and is thus in effect dependent on texture variance only.* Logarithmically scaled radar intensity images are therefore more fit for use in textural analysis than either linearly scaled radar amplitude or intensity images.

### 5.1.3 Textural analysis in this study

Grey level co-occurrence textural analysis techniques were only used in the handling of data from the CCRS SAR and ERS-1. *The study adopted two complementary approaches* which according to Hoekman (1985) may be denoted as *Gross Textural Analysis (GTA) and Moving Window Analysis (MWA).* GTA is intended to quantify the texture for predefined image regions while MWA is meant to do so for a relatively small spatial window around each image pixel. The textural attributes that result from GTA are computed on the basis of substantially more pixel pair realisations than those that result from MWA. GTA attributes therefore describe texture more accurately than MWA attributes. However, GTA requires a priori information on boundaries of regions of interest. In some situations this boundary information may be obtained from existing geographical data sets or through the use of image segmentation techniques. In many others, however, boundary information may be unobtainable. This applies in particular to tropical rain forests as these are environments poor in geographical information and as radar images of rain forest are difficult to segment. In such situations, the MWA is the only textural analysis method with potential for operational use.

In this study GTA was used as a precursor for MWA. GTA, among others, served to investigate whether or not the land cover types studied had different textural properties from a grey level co-occurrence point of view. This is in fact an assessment of the classification potential of MWA, since this approach will fail to discriminate land cover types with identical textural properties. GTA when compared to MWA is more economical as it requires considerably less computing time. This

makes GTA a useful tool for studies aimed at the development of optimised procedures for textural analysis according to the MWA approach.

*In this study GTA was used to investigate the textural information content of the available CCRS SAR and ERS-1 SAR images as a function of:*
- frequency and polarization (CCRS SAR)
- spatial resolution (ERS-1 PRI and PRI-av versus time averaged ERS-1 SLC images; see section 4.4.4)
- radiometric resolution (ERS-1 PRI versus PRI-av)
- number of grey levels (ranging from 256 to 8)
- textural attribute (see Table 5.1)
- displacement length (ranging from 1 to 10 pixels)
- displacement direction (range dir., azimuth dir., range and azimuth dir.)
- window size (ranging from $3 \times 3$ to $63 \times 63$ pixels).

The CCRS SAR and ERS-1 SLC images were analysed for texture (both GTA and MWA) in slant range format, the ERS-1 PRI and PRI-av images in ground range format. Slant to ground range conversions prior to textural analysis were avoided as this involves resampling of pixels and thus affects image texture. For ERS-1 PRI and PRI-av images the format could not be chosen freely since the PRI images are supplied by ESA in the resampled ground range format.

## 5.2 Approach for extraction and analysis of data for image regions

### 5.2.1 Extraction of radiometric attributes

The radiometric attribute for a particular part of a radar image quantifies the backscatter, i.e. the observed amount of backscattered energy. In this study backscatter will be expressed in terms of gamma ($\gamma$) (see section 3.1.4). The pixels in a radar image represent the smallest spatial elements for which the amount of backscatter is known. Radar backscatter analysis, however, is not usually based on backscatter values of individual pixels but on mean backscatter values for series of pixels, i.e. for image regions. The mean backscatter value for a region of interest is computed by averaging the values of all pixels within its boundaries. *Region averaged backscatter values are less susceptible to the effects of image speckle than backscatter values for pixels. Hence, these averaged values make more accurate radiometric attributes.*

The effect of speckle can be regulated by introducing a lower limit with respect to number of pixels that has to be averaged. In this study it was assumed that the speckle induced standard deviation of the mean backscatter values should be 0.2 dB or less. According to Hoekman (1990) this criterion can only be met through the averaging of 500 or more independent backscatter measurements (looks). The number of looks per pixel may vary from one image to another. Consequently, the lower limit for averaging in terms of pixels depends on the applied image data set. The studied CCRS SAR, NASA/JPL SAR and ERS-1 PRI images include, respectively,

**Table 5.2** Regions for which $\bar{\gamma}$ values were extracted; number per land cover class, for each of the radar data sets studied.

| | CCRS SAR | | NASA/JPL AIRSAR | ERS-1 | |
|---|---|---|---|---|---|
| Cover type | X HH, X VH C HH, C VH | X VV, X HV C VV, C HV | All bands 1) | C VV PRI, PRI-av | C VV SLC-av |
| Mixed forest | 10 | 10 | 16 | 10 | 3 |
| Wallaba forest | 14 | 11 | 12 | 10 | 3 |
| Xerix mixed forest | 6 | 4 | 6 | 8 | - |
| Low swamp forest | 5 | 5 | 6 | 7 | 3 |
| Mora forest | 10 | 10 | 16 | 10 | 3 |
| Logged-over forest | 11 | 11 | 12 | 10 | 3 |
| Secondary forest | - | 8 | 10 | 10 | - |
| Non-forest | - | 19 | 14 | 10 | - |

1) see Table 5.3.

7, 16 and 3 looks per pixel. In accordance with the 500 looks criterion it is thus required to average the backscatter values of ca. 75 CCRS SAR pixels, 35 NASA/JPL SAR pixels and 170 ERS-1 PRI pixels. However, there is evidence that the values of neighbouring ERS-1 PRI pixels are interrelated (see section 6.2.2). For the ERS-1 PRI images the lower limit for averaging is therefore estimated to be of the order of 500 pixels.

In this study the computation of the mean gamma values $\bar{\gamma}$ was restricted to image regions that represented the land cover classes studied. To define these regions their boundaries were digitised on the screen of an image processing system. The *required boundary information was obtained from ancillary data sets such as maps and black-and-white aerial photographs* (scale 1:40,000). The process of defining image regions was repeated for each of the available radar data sets, taking into account the appropriate lower limit for pixel averaging. A Landsat TM image from 19 September 1992 was used as an aid for defining regions of interest for the ERS-1 data sets. Table 5.2 lists the number of regions defined for each of the land cover classes and for each of the data sets studied. The Low swamp regions for the CCRS SAR data set were located in the 20° to 30° incidence angle range, the incidence angles for the other regions in this data set varied from 30° to 60°. The incidence angles for the AIRSAR image regions also ranged from 30° to 60°; those for the ERS-1 image regions from 20° to 25°. The relatively large incidence angle range for the regions in the CCRS SAR and AIRSAR data set was necessary to incorporate a fair number of regions in the analysis.

In handling the CCRS SAR data the definition of image regions had to be repeated several times since the images for the different frequency/polarization combinations did not co-register, i.e. did not cover the same area on the ground. This lack of co-registration between the bands in the CCRS SAR data set is due to the fact that this data set was acquired in multiple overpasses. The $\bar{\gamma}$ values for the different

**Table 5.3** Definition of studied polarization combinations in terms of $\psi$ and $\chi$; equations for computation of $\overline{\sigma}^\circ$ from the region averaged elements of Stokes scattering operator $\boldsymbol{M}$. The backscatter values for the shown polarization combinations were computed for C-, L- as well as P-band.

| Polarization combination | Polarization parameters: Receive wave $\psi$ | Receive wave $\chi$ | Transmit wave $\psi$ | Transmit wave $\chi$ | Computation of $\overline{\sigma}^\circ$ from $\boldsymbol{M}$ |
|---|---|---|---|---|---|
| HH | 0° | 0° | 0° | 0° | $M_{11} + 2 \cdot M_{12} + M_{22}$ |
| VH | 90° | 0° | 0° | 0° | $M_{11} - M_{22}$ |
| VV | 90° | 0° | 90° | 0° | $M_{11} + 2 \cdot M_{12} + M_{22}$ |
| RR | * | - 45° | * | - 45° | $M_{11} + 2 \cdot M_{12} + M_{22}$ |
| LR | * | 45° | * | - 45° | $M_{11} + 2 \cdot M_{12} + M_{22}$ |
| LL | * | 45° | * | 45° | $M_{11} + 2 \cdot M_{12} + M_{22}$ |
| TP | - | - | - | - | $M_{11} + 2 \cdot M_{12} + M_{22}$ |

* indicates 'not defined'
- indicates 'not applicable'

bands in the CCRS SAR data set therefore do not always correspond to exactly the same forest areas. The lacking co-registration also explains the differences in the number of image regions from one radar band to another. In San José del Guaviare the CCRS SAR did not acquire X HH, X VH, C HH or C VH data. Consequently, it was not possible to define secondary forest or non-forest regions for these radar bands. Similar co-registration problems did not occur in the handling of the AIRSAR and ERS-1 data sets. The AIRSAR system simultaneously acquires all of its data and therefore all radar bands are perfectly matched. The ERS-1 data set comprised images from different acquisition dates rather than from different frequencies and/or polarizations. Depending on the satellite's repeat cycle, these images represented a somewhat different ground surface area. For the analysis of the images this did not create problems since the selected image regions were confined to the area of overlap. Moreover, images from different dates could be easily co-registered through the use of simple linear transformations.

Whereas the pixels in the CCRS SAR and ERS-1 data sets represent backscatter values, the pixels in the NASA/JPL AIRSAR data set represent Stokes scattering operators $\boldsymbol{M}$. Hence, two steps were needed to compute the region averaged backscatter values from the AIRSAR data set. To begin with, the $\boldsymbol{M}$'s for all pixels within a specific region of interest were averaged linearly in order to obtain region averaged $\boldsymbol{M}$'s. Subsequently, region averaged backscatter values were computed through wave synthesis (see section 3.1.6). The wave synthesis process allows for the computation of the backscatter for *any* combination of receive and transmit polarizations. Selected combinations for this study include: horizontal - horizontal (HH), vertical - horizontal (VH), vertical - vertical (VV), right-hand circular - right-hand circular (RR), left-hand circular - right-hand circular (LR) and left-hand circular - left-hand circular (LL). The HV and RL polarization combinations were not included because it follows from the reciprocity relation (see section 3.1.6) that these are

identical to, respectively, VH and LR. The set of backscatter values for the described polarization combinations was complemented with the so-called total backscattered power TP. According to Zebker et al. (1991) $\sigma^{\circ}_{TP}$ may be defined as $\sigma^{\circ}_{TP} = \left(\sigma^{\circ}_{HH} + 2\sigma^{\circ}_{VH} + \sigma^{\circ}_{VV}\right)/4$. Table 5.3 shows the orientation angle $\psi$ and ellipticity angle $\chi$ for the polarization combinations studied as well as the equations for computing the corresponding $\overline{\sigma}^{\circ}$ values from the region averaged Stokes scattering operator elements. With the help of Equation 3.5 and information on the local grazing angle, the $\overline{\sigma}^{\circ}$ values could be easily converted to $\overline{\gamma}$ values.

For each region of interest in the NASA/JPL AIRSAR images a total of 21 (7 polarizations x 3 frequency bands) $\overline{\gamma}$ values was computed. *The data set for each image region was extended with a series of indices* that are denoted by Pope et al. (1994) as the: Canopy Structure Index CSI, Volume Scattering Index VSI and Biomass Index BMI. Like the $\overline{\gamma}$ values, these indices were computed for C-, L- as well as P-band. They are defined as follows:

$$\mathrm{CSI} = \frac{\overline{\gamma}_{VV}}{\overline{\gamma}_{VV} + \overline{\gamma}_{HH}} \tag{5.6}$$

$$\mathrm{VSI} = \frac{\overline{\gamma}_{HV}}{\overline{\gamma}_{HV} + \left(\dfrac{\overline{\gamma}_{VV} + \overline{\gamma}_{HH}}{2}\right)} \tag{5.7}$$

$$\mathrm{BMI} = \frac{\overline{\gamma}_{VV} + \overline{\gamma}_{HH}}{2} \tag{5.8}$$

As a result of differences in vertical penetration relative to wavelength, the C-, L- and P-band indices apply to different forest components. Generally speaking, C-band indices apply to characteristics of the upper canopy (e.g. leaves, twigs and secondary branches), L-band indices apply to primary and thicker secondary branches, and trunks. P-band indices apply to thick primary branches, trunks and the forest soil (see section 3.2.2). CSI is a parameter of the relative importance of vertical versus horizontal forest components and as such relates to architectural tree models (Oldeman, 1974; Hallé et al., 1978). VSI is a parameter of the depolarization of the linear-like polarized incident radar signal and therefore strongly related to the occurrence of volume scattering (see section 3.2.3). It reflects the density of the scatterers in the vegetation volume and the thickness of this volume. The most relevant biophysical parameter associated with BMI is biomass. However, the value of BMI is critically dependent on the size of the biomass constituents relative to the incident wavelength. The effective size of the biomass components determines whether they act as backscattering or attenuating sources. Depending on wavelength, an increase in biomass may therefore result in a higher or lower backscatter and likewise in a higher or lower BMI value. Both BMI and CSI may be affected by double bounce scattering since this interaction mechanism favours $\gamma_{HH}$ (Pope et al., 1994).

For each region of interest in the CCRS SAR and ERS-1 images, sd($\gamma$) *the standard deviation of gamma in dB was calculated in addition to* $\overline{\gamma}$. This attribute is an

expression of the variation in backscatter and *may therefore be used as a simple statistical descriptor for texture.* It relates to first-order statistical concepts as it describes the probability density function of the *individual* grey levels. Grey level co-occurrence attributes, on the other hand, relate to second-order statistical concepts as they describe the *joint* probability density function of grey level *pairs.* In this study the value of sd($\gamma$) and the grey level co-occurrence statistics for description of texture will be compared. This is done because sd($\gamma$) can be computed at a lower computational expense than the grey level co-occurrence statistics. For textural analysis in an operational environment sd($\gamma$) hence is preferred over grey level co-occurrence statistics. However, this preference only holds as long as its capability to discriminate between different image textures is either similar or better than that of grey level co-occurrence statistics.

### 5.2.2 Extraction of textural attributes

Extraction of textural attributes according to the Gross Textural Analysis approach (GTA) was restricted to regions of interest within the CCRS SAR, ERS-1 PRI, ERS-1 PRI-av and ERS-1 SLC-av images. The regions of interest for GTA were identical to the ones as defined for extracting radiometric attributes (see section 5.2.1; Table 5.2).

To begin with, GTA served to evaluate the capability of the textural attributes in Table 5.1 for discriminating the land cover classes studied. *The attributes were standard computed with consecutive displacements in both range and azimuth direction.* This implies that the GLCO matrices and GLD vectors from which the attributes were derived contained *summed* entries, i.e. entries from displacement in range direction and entries from displacement in azimuth direction. The applied displacement length $|\boldsymbol{d}|$ ranged from 1 to 10 pixels. In this text the combination of a textural attribute and a displacement length will be expressed as, e.g. GLCO-CONT[5]. The letter code represents the name of the GLCO attribute (see Table 5.1); the number between [ ] represents the displacement length. The denotation GLCO-CONT[5] thus refers to the GLCO Contrast attribute and a displacement length of 5 pixels. Textural analysis was preceded by a scaling procedure to convert the radar images from a 32 bit real to an 8 bit integer format. This scaling was done in such a way that the output images had 128 grey levels, i.e. had pixels with values ranging from 0 to 127. The backscatter input range for the CCRS SAR and ERS-1 images was fixed at, respectively, 51 and 18 dB. The grey level steps in the rescaled CCRS SAR images therefore represented backscatter steps of ca. 0.4 dB, while those in the rescaled ERS-1 images represented steps of ca. 0.15 dB. These were the standard scalings; in a later study phase different scalings were applied to investigate the relationship between the number of grey levels and textural information content.

The first step in the GTA of the CCRS SAR images was to establish which of the eight available radar bands contained the most textural information or, in other words, offered the most potential for textural classification of the land cover types studied. The most promising band was then used to evaluate the classification potential associated with the various textural attributes and displacement lengths. Next, the

preferred radar band was rescaled several times to obtain output images with 256, 128, 64, 32, 16 and 8 grey levels. These images were then used to investigate how image scaling affects the classification potential of textural attributes. Similarly, the preferred radar band was used to study the effect of displacement direction. To this end the classification potential of attributes computed with standard displacement and displacement in either range or azimuth direction was compared. Finally, GTA was used to investigate the classification potential of textural attribute/displacement length combinations as a function of window size. A single window of a size varying from $3 \times 3$ to $63 \times 63$ pixels was located within the boundaries of each region of interest in the best performing radar band. Next, the texture within these windows was quantified according to the usual GTA approach. By comparing the classification potential associated with the resulting textural descriptions, the effect of window size could be evaluated. The described *experiments with textural attributes, displacement lengths, scaling, displacement direction and window size were meant to support the development of optimised procedures for MWA textural analysis.*

In the case of ERS-1 the classification potential of the various textural attributes and displacement lengths was evaluated in connection with three images, i.e. the PRI image, the SLC-av image and the PRI-av image. The relationship between spatial resolution and textural information content was investigated by comparing the classification potential of PRI and SLC-av related textural attributes. Similarly, the effect of radiometric resolution was assessed by comparison of the classification potential of PRI and PRI-av associated textural attributes. The SLC-av image was rescaled to 256, 128, 64, 32, 16 and 8 grey levels to investigate the effect of image scaling on the classification potential of the textural attributes. In addition, this image was used to study the relationship between classification potential and displacement direction. This was done in a manner analogous to the one used in relation to the CCRS SAR images. Like the CCRS SAR GTA experiments, the ERS-1 GTA experiments were meant to support the development of optimised procedures for MWA textural analysis.

### 5.2.3 Extraction of polarimetric attributes

Polarimetric attributes relate to the polarization transformation properties of the observed object and can be computed from polarimetric radar data only. Hence, their extraction was restricted to regions of interest within the NASA/JPL AIRSAR images. The selected regions were identical to those used for calculating radiometric attributes (see section 5.2.1; Table 5.2). For each region of interest the C-, L- and P-band polarization phase difference of HH and VV (PPD) and the corresponding standard deviation sd(PPD) were computed. The PPD was computed from spatially averaged C-, L- and P-band Stokes scattering operators according to:

$$PPD = \tan^{-1}\left(\frac{-2M_{34}}{M_{33} - M_{44}}\right) \tag{5.9}$$

PPD standard deviations were computed from PPD processed images, i.e. images in which the pixels represent PPD values.

The PPD represents the difference in the phase angle for the HH and VV polarized signal. *HH-VV phase angle differences arise if the HH and VV signal are received separated in time or if the phase angle of the H and/or V wave has been transformed.* The former may happen in case the HH and VV backscatter sources are located at different range distances or in the event that the H and V waves travel through the object with different velocities. H and/or V phase angle transformations may result from specific mechanisms of scattering (Ulaby et al., 1987). *Every* single bounce scattering event causes the phase angle of the *scattered* H polarized wave (not V polarized wave!) to change by 180°. However, due to different conventions for defining the polarization of waves and antennas (see section 3.1.6) the phase angle of the *received* H wave shifts by 180° once again. Consequently, the resulting phase angle of the received H polarized wave is 360° (or 0°). This is equal to the phase angle of the received V polarized wave. The PPD for single bounce scattering therefore equals 0°. Similarly, it can be shown that double bounce scattering results in a PPD of 180°. Diffuse scattering usually results in PPD values that are considerably different from 0° or 180° (section 3.2.6; also see van Zyl, 1989).

It should be noted that region averaged PPD values will rarely equal exactly 0° or 180°. On the one hand, this results from the fact that scattering mechanisms are not exclusive within resolution cells and certainly not within image regions. On the other hand, specific scattering events are not the only possible cause of the HH-VV polarization phase difference. Generally speaking, however, high PPD values may be seen as indicators of double bounce scattering. Likewise, low PPD values are indicative of single bounce scattering and intermediate PPD values of diffuse scattering. Ulaby et al. (1987) show that objects such as crops and bare soils may have comparable region averaged PPD values but considerably different PPD distributions. The standard deviation of this distribution sd(PPD) therefore constitutes an additional information source. Low sd(PPD) values are indicative of objects with uniform scattering properties, i.e. of objects with a homogeneous structure. Similarly, high values are indicators of structural heterogenities. For tropical forests the sd(PPD), notably in C-band, is expected to reflect canopy closure and architecture. This makes sd(PPD), like the standard deviation of gamma (see section 5.2.1), a first-order textural descriptor. Evidence of the relationship between the PPD and canopy characteristics is found in Pope et al. (1994).

### 5.2.4 Evaluation of relative classification capacities of extracted attributes

The *potential of the extracted attributes for classifying the land cover types studied was evaluated on the basis of a class separability measure known as pairwise transformed divergence* (Swain and Davis, 1978). This measure represents the statistical distance between *class pairs* and is an *indirect* and *a priori* estimate of the probability of correct classification. The transformed divergence TD for class pair $(i, j)$ is given by:

$$TD_{ij} = 2000\left(1 - e^{\frac{-D_{ij}}{8}}\right) \tag{5.10}$$

with

$$D_{ij} = \frac{1}{2}\mathrm{tr}\left[\left(\boldsymbol{c}_i - \boldsymbol{c}_j\right)\left(\boldsymbol{c}_j^{-1} - \boldsymbol{c}_i^{-1}\right)\right] + \frac{1}{2}\mathrm{tr}\left[\left(\boldsymbol{c}_i^{-1} + \boldsymbol{c}_j^{-1}\right)\left(\boldsymbol{m}_i - \boldsymbol{m}_j\right)\left(\boldsymbol{m}_i - \boldsymbol{m}_j\right)^{T}\right] \tag{5.11}$$

where: $\boldsymbol{c}_i$ is the covariance matrix, $\boldsymbol{c}_i^{-1}$ the inverse covariance matrix and $\boldsymbol{m}_i$ the mean vector for class $i$. Similarly, $\boldsymbol{c}_j$, $\boldsymbol{c}_j^{-1}$ and $\boldsymbol{m}_j$ represent the statistics for class $j$. The trace of the matrix in question (sum of the diagonal elements) is indicated by tr, whereas T refers to the transposed matrix. Computation of $TD_{ij}$ is based on the assumption that the classes have Gaussian (normal) probability density functions.

The study aimed to rank the various attributes and/or attribute combinations according to their ability to discriminate between the land cover classes studied, i.e. according to their classification potential. Pairwise transformed divergence on its own was not suited for this purpose since the study deals with eight rather than two *classes*. Transformed divergence was used to assess for each attribute (combination) how many of the studied *class pairs* could be discriminated successfully. Subsequently, the number of discriminated class pairs was used for ranking the attributes. *It was assumed that two classes could be discriminated if their $TD_{ij}$ value was equal to or greater than 1900*. The adopted decision rule is on the safe side, other authors (e.g. Lillesand and Kiefer, 1994; Singh, 1987) have used a $TD_{ij}$ value of 1500 as a cut-off point between separable and unseparable class pairs.

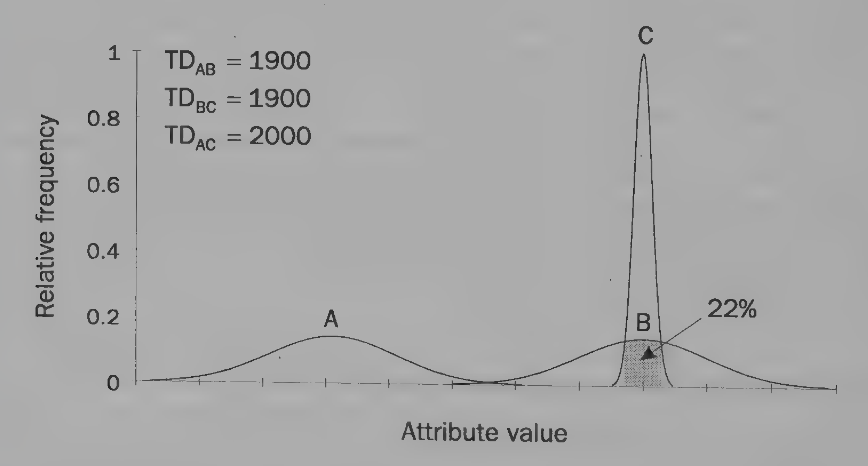



**Figure 5.2** Illustration of the relationship between pairwise transformed divergence and the likelihood of correct classification for a single variate case. Class pair (A,B) and (B,C) illustrate extreme cases for which $TD = 1900$. Class pair (B,C) have a relatively low likelihood of correct classification as a Gaussian maximum-likelihood classifier may erroneously contribute up to 22% of the observations for B to C. Class pair (A,B) and (A,C) have a high likelihood of correct classification.

A $TD_{ij}$ value of 1900 corresponds to a lower bound for the likelihood of correct classification of close to 78%. A maximum of 22% of one of the two classes may thus be misclassified. This maximum is reached only in exceptional cases, i.e. when two classes have identical mean values. The situation in which two classes have different means but identical variances may also be considered exceptional. In this case the likelihood of correct classification for $TD_{ij} = 1900$ will be close to 100%. Higher $TD_{ij}$ values imply higher probabilities for correct classification. The maximum value of 2000 is reached when the probability distributions of the two classes do not overlap, i.e. when the probability of correct classification is 1. The relationship between the adopted transformed divergence decision rule and the likelihood of correct classification for a single variate case is illustrated in Figure 5.2. Class pair (A,B) and (B,C) have a transformed divergence value of 1900 while $TD_{AC} = 2000$. Class A and B have different means but identical variances whereas class B and C have different variances but identical means. Both class pair (A,B) and (A,C) can be seen to have a high likelihood of correct classification. The likelihood of correct classification for class pair (B,C) is much lower, as in this case, the probability density functions overlap considerably. In a Gaussian maximum-likelihood classification up to 22% of the observations in class B may be contributed erroneously to class C.

*Following analysis based on pairwise transformed divergence, the data sets for highly ranked attributes and/or attribute combinations were used in a series of Gaussian maximum-likelihood classifications at a 95% confidence level.* Successive evaluation of classification results allowed for a *direct* and *a posteriori* but more time-consuming assessment of the classification capacity of the attributes in question. For a discussion of the Gaussian maximum-likelihood classification theory the reader is referred to one of the many available handbooks, e.g. Swain and Davis (1978), Jensen (1986), Lillesand and Kiefer (1994) and Richards (1993). In each of the classification/evaluation procedures in this study the same data set was used for both the design (training) of the classifier and the evaluation of the classification results. It is known that this may cause the classification results to be optimistic, i.e. that this may lead to an overestimation of the likelihood of correct classification. However, this does not pose a problem for the present study since it is intended to assess the *relative* rather than the *absolute* classification capacities of the studied attributes. Assessment of the absolute probability of correct classification requires substantially larger sets of both remote sensing and ground reference data.

The classification results were evaluated with the help of contingency tables and the $\hat{K}$ statistic. Contingency tables show the number of correctly and incorrectly classified data points. An example is given in Table 5.4. The columns represent the actual land cover type as verified in the field (ground reference) whereas the rows indicate the land cover type as assigned by the classifier. Contingency tables clearly present errors of omission (erroneous exclusion of points from a class) and errors of commission (erroneous inclusion of points in a class). Correctly classified data points are located on the major diagonal of the table. The ratio of the number of correctly classified data points and the total number of data points represents the actual agreement between the rows and columns of the table and may be used as a simple measure of the overall classification accuracy. However, in evaluating classification

**Table 5.4** Example of a contingency table. Contingency tables were used to evaluate the Gaussian maximum-likelihood classification results.

| Classification result | Ground reference | | | | | | | | Total | Percent commission error |
|---|---|---|---|---|---|---|---|---|---|---|
| | 1 | 2 | 3 | 4 | 5 | 6 | 7 | 8 | | |
| 1 Mixed | **6** | 0 | 0 | 0 | 0 | 2 | 0 | 0 | 8 | 25 |
| 2 Wallaba | 0 | **4** | 1 | 0 | 0 | 0 | 1 | 0 | 6 | 33 |
| 3 Xeric mixed | 1 | 5 | **2** | 0 | 0 | 0 | 0 | 0 | 8 | 75 |
| 4 Low swamp | 0 | 0 | 0 | **5** | 0 | 0 | 0 | 7 | 12 | 58 |
| 5 Mora | 0 | 0 | 0 | 0 | **10** | 3 | 0 | 0 | 13 | 23 |
| 6 Logged-over | 2 | 0 | 0 | 0 | 0 | **6** | 0 | 0 | 8 | 25 |
| 7 Secondary forest | 0 | 2 | 1 | 0 | 0 | 0 | **6** | 1 | 10 | 40 |
| 8 Non-forest | 0 | 0 | 0 | 0 | 0 | 0 | 1 | **10** | 11 | 9 |
| Unclassified | 1 | 0 | 0 | 0 | 0 | 0 | 0 | 1 | 2 | 100 |
| Total | 10 | 11 | 4 | 5 | 10 | 11 | 8 | 19 | 78 | |
| Percent correct | 60 | 36 | 50 | 100 | 100 | 55 | 75 | 53 | | |

| | | | |
|---|---|---|---|
| Total correct | 49 | Total percent correct | 63 |
| Total error | 29 | Total percent error | 37 |
| $\hat{K}$ | 0.5763 | $\hat{\sigma}^2_\infty[\hat{K}]$ | 0.0037 |

results it is important not only to note the proportion of correctly classified data points, but also to assess the nature of the errors of omission and commission on a class-by-class basis. When comparing classification results for different data sets, 'chance agreement' also has to be taken into account. Chance agreement in contingency tables results from the fact that any classifier will by chance assign data points to the correct class. It hinders direct comparison of classification results for different data sets as it is a function of the row and column totals (Congalton et al., 1983; Bishop et al., 1984).

*With the use of the* $\hat{K}$ *statistic it is possible to evaluate classification results in contingency tables while taking into account errors of omission and commission and compensating for the effects of chance agreement.* In remote sensing literature $\hat{K}$ is commonly referred to as either KHAT (e.g. Aronoff, 1982; Congalton et al., 1983) or Kappa (e.g. Benson and DeGloria, 1985). The statistic is calculated by:

$$\hat{K} = \frac{N\sum_{i=1}^{I} x_{ii} - \sum_{i=1}^{I} x_{i+} \cdot x_{+i}}{N^2 - \sum_{i=1}^{I} x_{i+} \cdot x_{+i}} \quad (5.12)$$

where $I$ is the number of rows (columns) in the table, $x_{ii}$ the number of data points in row $i$ and column $i$ (i.e. the $i$ th diagonal element), $x_{i+}$ the total of row $i$, $x_{+i}$ the total of column $i$ and $N$ the total number of data points. In this equation $\sum_{i=1}^{I} x_{ii}$ is proportional to the actual agreement and $\sum_{i=1}^{I} x_{i+} \cdot x_{+i}$ to the chance agreement. The maximum value for $\hat{K}$ is equal to 1. This maximum is reached when all data points are correctly classified. The approximate large sample variance of KHAT is:

$$\hat{\sigma}_{\infty}^{2}\left[\hat{K}\right] = \frac{1}{N}\left[\frac{o_1(1-o_1)}{(1-o_2)^2} + \frac{2(1-o_1)(2o_1o_2-o_3)}{(1-o_2)^3} + \frac{(1-o_1)^2\left(o_4-4o_2^2\right)}{(1-o_2)^4}\right] \tag{5.13}$$

where

$$o_1 = \sum_{i=1}^{I} \frac{x_{ii}}{N} \tag{5.14}$$

$$o_2 = \sum_{i=1}^{I} \frac{x_{i+} \cdot x_{+i}}{N^2} \tag{5.15}$$

$$o_3 = \sum_{i=1}^{I} \frac{x_{ii}\left(x_{i+} + x_{+i}\right)}{N^2} \tag{5.16}$$

$$o_4 = \sum_{i=1}^{I} \sum_{j=1}^{J} \frac{x_{ij}\left(x_{j+} + x_{+i}\right)^2}{N^3} \tag{5.17}$$

This variance may be used to compute confidence intervals for $\hat{K}$ and thus to construct a hypothesis test for significant difference between the $\hat{K}$'s for different contingency tables (Bishop et al., 1984). The test statistic for significant difference between two $\hat{K}$'s, i.e. for significant difference between two classification results, is given by:

$$\Delta\hat{K} = \frac{\left|\hat{K}_1 - \hat{K}_2\right|}{\sqrt{\hat{\sigma}_{\infty}^{2}\left[\hat{K}_1\right] + \hat{\sigma}_{\infty}^{2}\left[\hat{K}_2\right]}} \tag{5.18}$$

At the 95% confidence level two classification results may be considered significantly different when $\Delta\hat{K} > 1.96$ (Benson and DeGloria, 1985). *In this study all tests for significant difference between classification results were carried out at this 95% confidence level.*

*The adopted procedure for evaluating classification capacity assumes that the attribute values are Gaussian (normally) distributed.* Often this is tacitly assumed to be so, but careful thinking requires further consideration of this matter. In case the

actual distribution deviates from Gaussian, the classification results will be sub-optimal. Consequently, the classification capacity of the attribute in question will be *underestimated.* Probability density function's (pdf's) for radiometric attributes, unlike those for textural or polarimetric attributes, may be theoretically derived. Hoekman (1990) derives the pdf for linearly averaged power (backscatter) values at the logarithmic scale, e.g. $\bar{\gamma}$ in dB. The derivation holds for homogeneous forests and other types of distributed land targets. Figure 5.3 shows the theoretical distributions and the corresponding Gaussian approximations for logarithmically scaled $\bar{\gamma}$ values computed by linear averaging over 3, 7, 16 and 500 independent looks. According to specifications by ESA, linear averaging over 3 looks is part of the processing procedure for the ERS-1 PRI images (see Table 4.8). Similarly, the processing procedures for the CCRS SAR and NASA/JPL AIRSAR images include linear averaging over 7 and 16 looks, respectively (see Table 4.5 and 4.6). The shown '500-look-distribution' approximates that of the radiometric attributes studied since these were computed by regionally averaging over a minimum of 500 looks (see section 5.2.1). This distribution is clearly near-Gaussian.

Figure 5.4 shows the actual distributions and the corresponding Gaussian approximations of linearly averaged, logarithmically scaled $\bar{\gamma}$ samples for six land cover types found in the X-band HH CCRS SAR image. Individual samples were

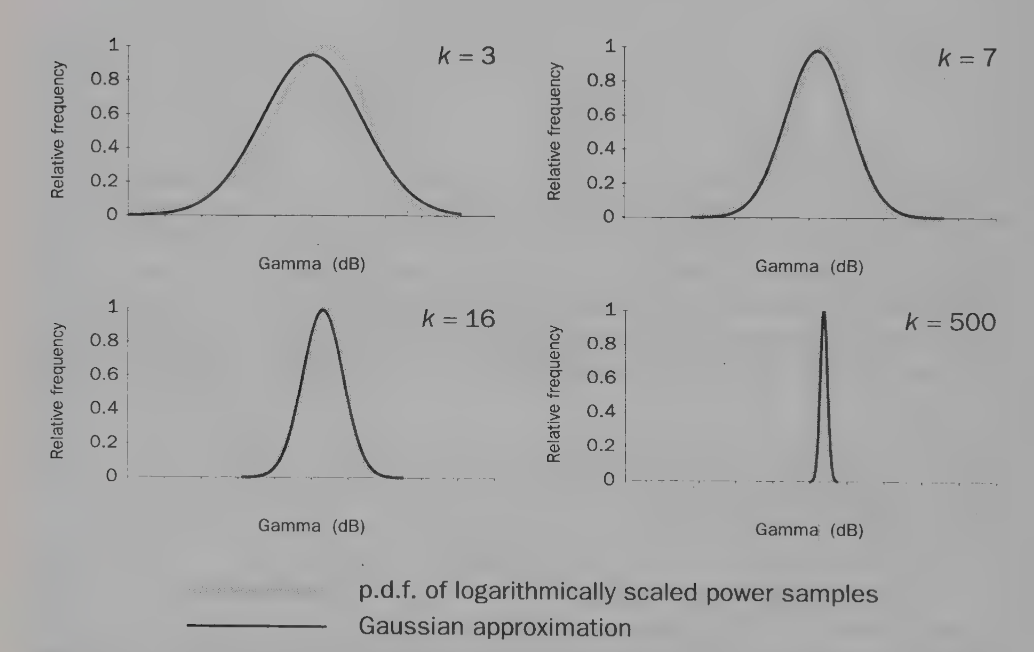



**Figure 5.3 Theoretical** probability density functions (pdf's) and corresponding Gaussian approximations for **logarithmically scaled $\bar{\gamma}$ values** computed by linear averaging over 3, 7, 16 and 500 independent looks. Linear averaging over 3, 7 and 16 looks is part of the processing procedure for the ERS-1 PRI, CCRS SAR and NASA/JPL AIRSAR images, respectively. The '500-look-distribution' approximates that of the radiometric attributes studied since these were computed by regionally averaging over a minimum of 500 looks (see section 5.2.1). This distribution is clearly near-Gaussian.

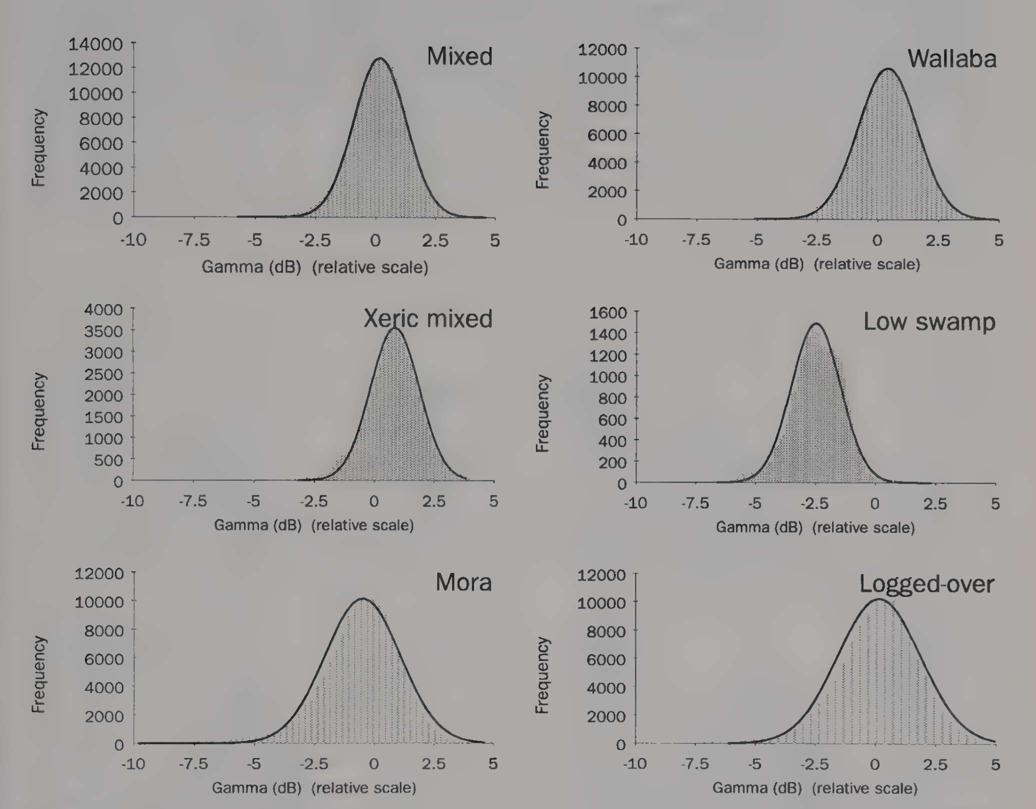



**Figure 5.4 Actual** distributions and Gaussian approximations of **linearly averaged, logarithmically scaled** $\bar{\gamma}$ **samples** for 6 land cover types found in the X-band HH CCRS SAR image. Individual samples were averaged over an image region of $9 \times 9$ pixels (567 looks). The distributions are in fact near-Gaussian.

averaged over an image region of 9×9 pixels or 567 looks. The pdf's in this figure confirm the theoretical expectations and are in fact near-Gaussian. Deviations from Gaussian may arise because the backscatter of the studied land cover types, unlike that of fully homogeneous vegetation layers, will vary locally. In other words, the images of the studied cover types are not free of texture.

Figure 5.5 and 5.6 show the distributions of the values for two textural attributes, namely GLCO-COR[1] and GLCO-CONT[5]. These values were computed from the X-band HH CCRS SAR data over image regions of 9×9 pixels. The distributions for GLCO-COR[1] are close to Gaussian but those for GLCO-CONT[5] clearly deviate from Gaussian. As a result the classification capacities of the latter attribute will be underestimated in this study. It cannot be precluded that apart from GLCO-CONT[5] there are no other textural attributes with non-Gaussian distributions. At present there is little knowledge on the distribution of the values of textural attributes. In addition, there is little understanding of the relationship between these distributions and, for example, object or system properties (e.g. spatial resolution, incidence angle).

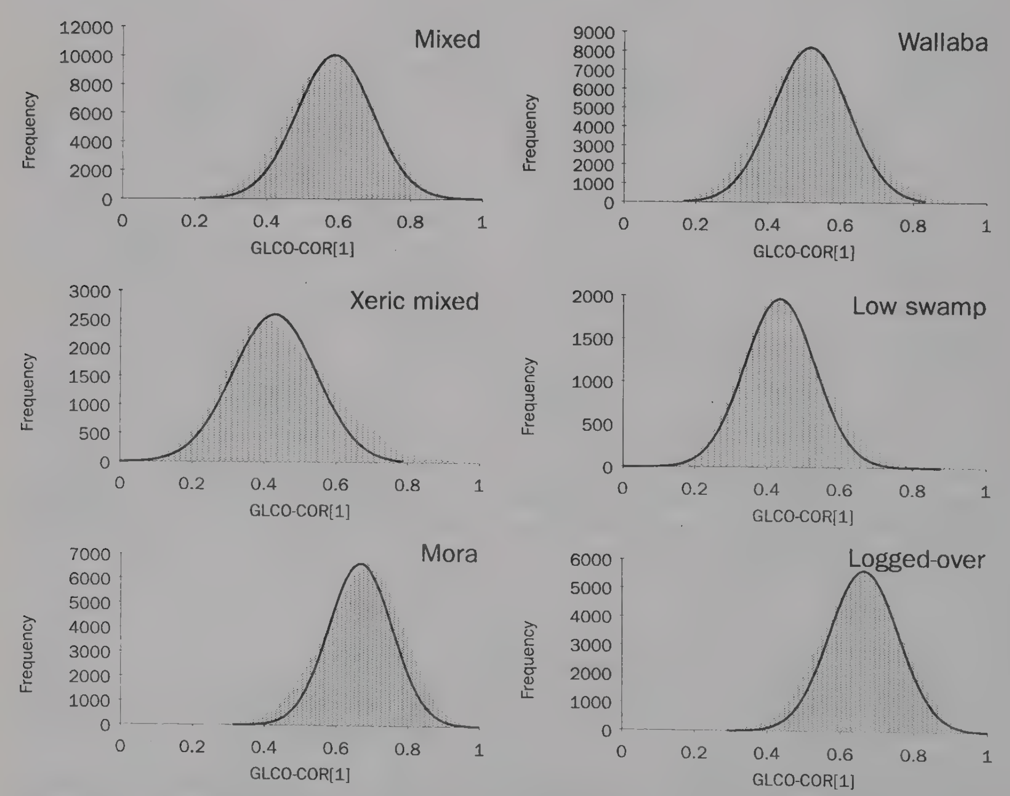



**Figure 5.5 Actual** distributions and Gaussian approximations of **GLCO-COR[1] values** for 6 land cover types found in the X-band HH CCRS SAR image. Individual values were computed over an image region of 9×9 pixels. The distributions are close to Gaussian.

Nevertheless, maximum likelihood or related classifiers that assume the variables to be Gaussian distributed are often used for classifying land cover based on GLCO textural variables (e.g. Hoekman, 1985; Ulaby et al., 1986a; Marceau et al., 1990). The motivation for this is that the Bayes decision rule which is found at the basis of these classifiers can be shown to yield the minimum number of erroneous classifications (Boekee and Boxma, 1976; Hoekman, 1990).

Figure 5.7 shows the distributions of the PPD values for the eight classes studied in the JPL/AIRSAR P-band data. The individual PPD values represent the average for a region of $5 \times 7$ pixels (560 looks). It can be seen that these distributions do not deviate much from Gaussian. The distributions of the PPD in C- and L-band (not shown) are comparable.

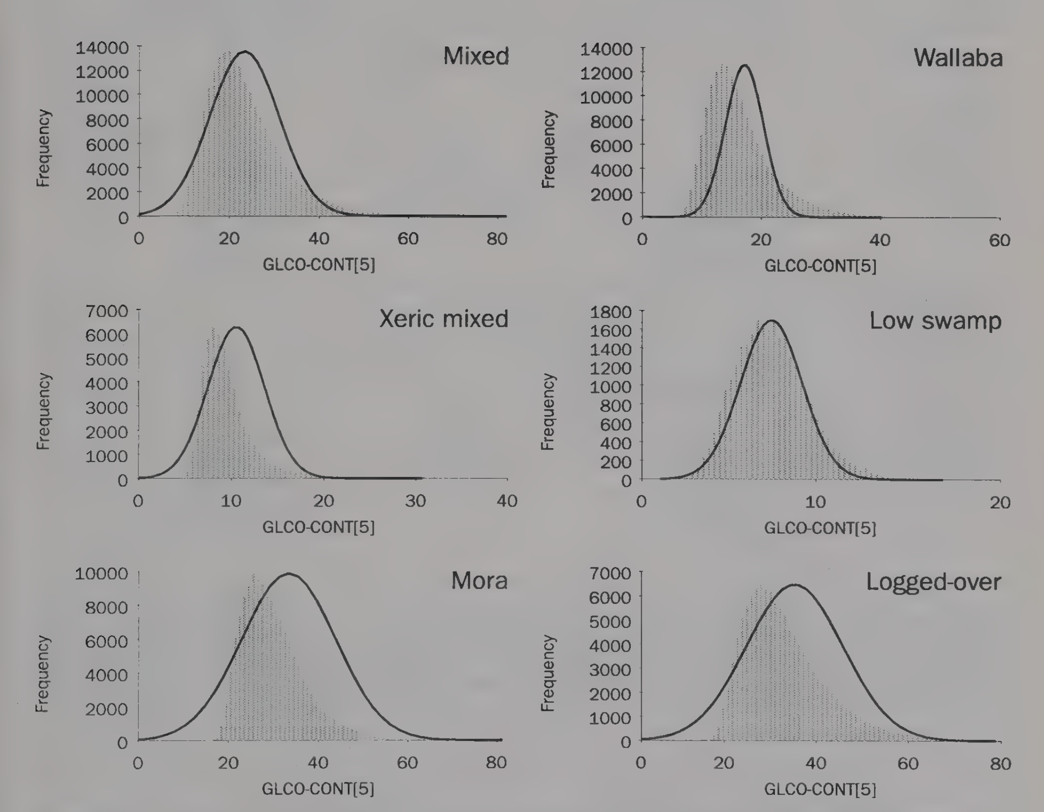



**Figure 5.6 Actual** distributions and Gaussian approximations of **GLCO-CONT[5] values** for 6 land cover types found in the X-band HH CCRS SAR image. Individual values were computed over an image region of $9 \times 9$ pixels. The distributions deviate from Gaussian.

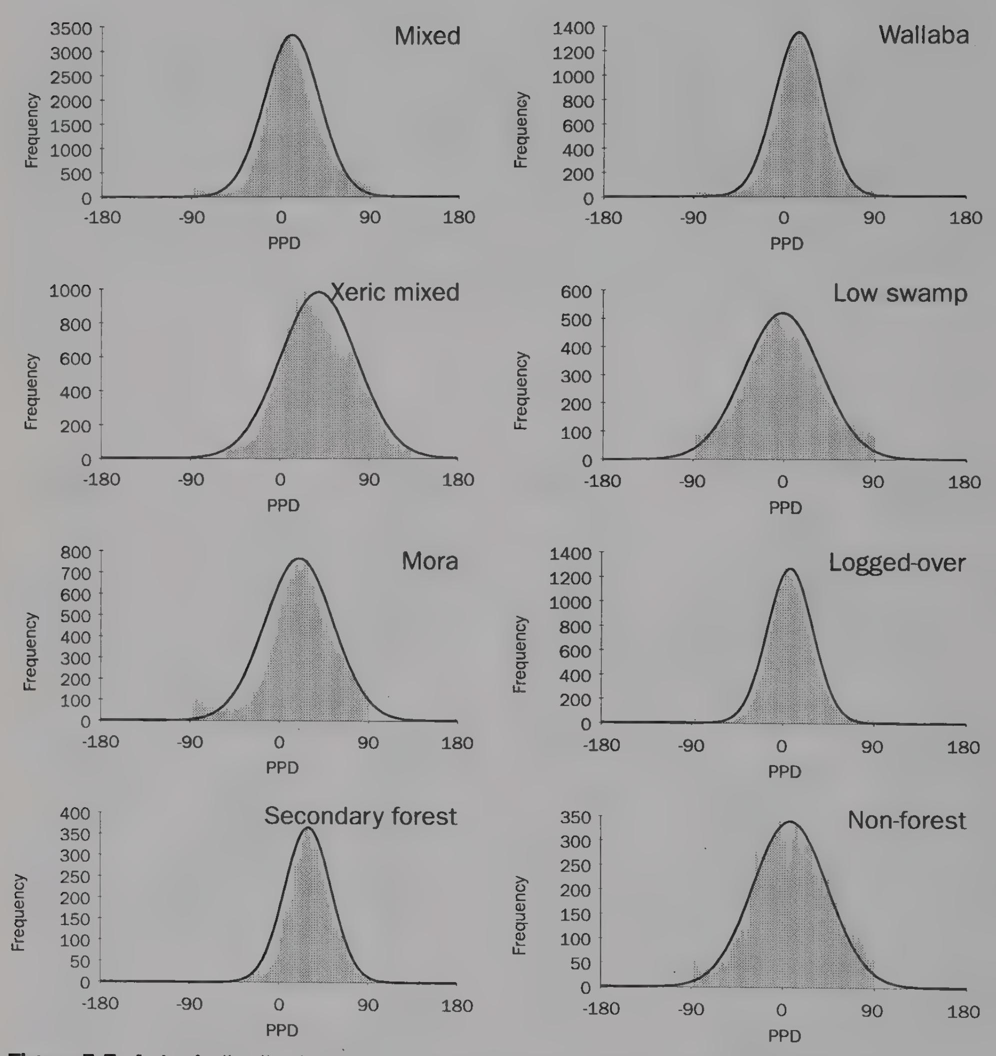



**Figure 5.7 Actual** distributions and Gaussian approximations of **PPD values** for 8 land cover types found in the P-band NASA/JPL AIRSAR image. Individual values represent the average for a region of 5 × 7 pixels (560 looks). The distributions are close to Gaussian.

## 5.3 Pixel-by-pixel image processing approaches

### 5.3.1 Textural analysis by means of a moving window

In Moving Window Analysis (MWA) a textural attribute is computed for a relatively small spatial window around each image pixel. *MWA results in a texturally transformed image, i.e. an image in which the pixel values are a measure of the local pattern of spatial distributions of grey tone or, in other words, texture.* Texturally transformed images show different forest types as far as these forest types have different textural properties. They can be visually interpreted or used as input for (un)supervised classification procedures. MWA was preceded by Gross Textural Analysis (GTA) to determine the effect of frequency, polarization, number of grey levels, GLCO textural attribute, displacement length, displacement direction and window size (see section 5.1.3 and Appendix I).

In the present study, various moving window analyses were performed. The current section describes the common methodology; the particulars of the different analyses are discussed together with the results in Chapter 6. In all cases MWA was preceded by a rescaling procedure to convert the logarithmically scaled radar intensity image from a 32 bit real to an 8 bit integer format. Rescaling was done in such a way that the resulting image had 128 grey levels, i.e. that its pixel values ranged from 0 to 127. The reason for using logarithmically scaled intensity images as input for textural analysis was discussed in section 5.1.2. Rescaling to 128 grey levels was adopted as the standard. Yet, the results of GTA rescaling experiments in section I.2 of Appendix I indicate that a lower number of grey levels would not have resulted in a loss of textural information. The lower the number of grey levels, the lower the computational load and hence the more economical the textural analysis.

*GLCO attributes were computed with consecutive displacements in range and azimuth direction.* Results of GTA experiments in section I.3 show that this method of computing yields a better textural description than a method with displacement in just one of these directions. The CCRS SAR and ERS-1 SLC images were analysed in the slant range format; the ERS-1 PRI images in the ground range format. Slant to ground range conversions prior to textural analysis were avoided as this involves resampling of pixels and thus deforms image texture. For the ERS-1 PRI images, however, the format could not be chosen freely since these were supplied by ESA in the ground range format.

The forest type information in the textural transforms resulting from MWA of the CCRS SAR images was assessed both numerically and visually; the forest type information in the MWA results for the ERS-1 SLC and PRI images was only evaluated visually. To numerically evaluate the results, the texturally transformed images were used as input for pixel-by-pixel supervised Gaussian maximum-likelihood classifications at a 95% confidence level. Subsequently, the outcome of the classifications was evaluated with the help of contingency tables and the $\hat{K}$ statistic. The pixels within half the number of the earlier defined regions of interest (see section 5.2.1) were used for designing the classifier; the pixels within the remaining regions of interest for evaluating the classification outcome. Thus, *the training data*

*sets were different from the evaluation data sets.* In this respect the classification/evaluation procedure associated with MWA differed from the one associated with GTA (see section 5.2.4).

Visual evaluation of the MWA results was done on the basis of texturally enhanced colour composite images. These images were produced by applying Red-Green-Blue (RGB) colour space transformations to SAR images in combination with their textural transforms and fixed grey channels. The digital values of the SAR images and the textural transforms ranged from 0 to 255, the digital values of the grey channels were set equal to 127. Prior to RGB transformations the CCRS and ERS-1 SLC SAR images and textural transforms were converted from the slant range format to the geometrically correct ground range format. An RGB transformation is in fact a reversed Intensity-Hue-Saturation (IHS) transformation (e.g. Lillesand and Kiefer, 1994). In the present study the SAR images were associated with intensity, the textural transformed images with hue and the grey channels with saturation. Hence, the brightness of the RGB transformed images relates to the backscatter level, the colour to the value of the textural attribute and the colour purity to the digital value of the grey channel. *RGB transformed colour composite images are seen as SAR images with colour coded textural overlays.* Their value for the purpose of forest type discrimination was assessed by visually comparing the spatial distribution of textural classes with the spatial distribution of forest types. The required ground information with regard to the spatial distribution of forest types was obtained from maps and by field visits.

### 5.3.2 Analysis of scattering behaviour by means of decomposition

Polarimetric radar images such as those acquired by the NASA/JPL AIRSAR system hold information on the way in which the microwaves transmitted by the radar interact with the forest observed (see section 3.1.6). This information facilitates radar image analysis because it indirectly discloses the forest components that contribute to the total backscattered power TP. Information on the nature of the microwave-forest interaction process may be extracted from polarimetric radar images with the help of scattering models.

The model applied in the present study was developed by Freeman and Durden (1992). It assumes that scattering from a vegetation layer is a combination of diffuse scattering from the vegetation volume, double (or even) bounce scattering from trunk-ground interaction and odd (or single) bounce scattering from a moderately rough surface. For diffuse scattering it is assumed that the backscatter is from randomly oriented, very thin cylinder-like scatterers. Trunk-ground interaction is modelled by scattering from a dihedral corner reflector and surface scattering is represented by the Bragg scattering model. It is assumed that linear like- and cross-polarized return signals are uncorrelated and that the HV and VH backscatter are identical. Likewise, the diffuse, double bounce and odd bounce scattering components are presumed uncorrelated.

The model of Freeman and Durden is comprised of four components:

$$\left\langle \left|S'_{hh}\right|^2 \right\rangle = \beta^2 f_s + \left|\alpha\right|^2 f_d + f_v \tag{5.19}$$

$$\left\langle \left|S'_{vv}\right|^2 \right\rangle = f_s + f_d + f_v \tag{5.20}$$

$$\left\langle \left|S'_{hv}\right|^2 \right\rangle = f_v/3 \tag{5.21}$$

$$\left\langle S'_{hh}S'^{*}_{vv} \right\rangle = \beta\, f_s - \alpha\, f_d + f_v/3 \tag{5.22}$$

where $S'_{hh}$, $S'_{vv}$ and $S'_{hv}$ are elements of matrix $\boldsymbol{S'}$ (see Equation 3.8); $f_s$, $f_d$ and $f_v$ are the odd bounce (or surface), double bounce and diffuse (or volume) scatter contributions to VV backscatter; $\beta$ is the HH/VV amplitude ratio for odd bounce scattering and $\alpha$ the HH/VV voltage ratio for double bounce scattering. $\left\langle \left|S'_{hh}\right|^2 \right\rangle$, $\left\langle \left|S'_{vv}\right|^2 \right\rangle$ and $\left\langle \left|S'_{hv}\right|^2 \right\rangle$ represent the expectation of the backscatter power in HH, VV and HV, respectively. For each pixel in a NASA/JPL AIRSAR image the information required for solving the model is contained in the corresponding Stokes scattering operator $\boldsymbol{M}$ (see Equations 3.16 through 3.25).

The four equations in the model can be seen to include five unknowns. According to Equation 5.21, $f_v$ can be estimated directly from the HV-polarized backscattered power since it is assumed that odd bounce and double bounce scattering do not contribute HV backscatter. Subtraction of the diffuse scattering contribution off the backscatter in HH, VV and the $\left\langle S'_{hh}S'^{*}_{vv} \right\rangle$ term leaves three equations with four unknowns. Based on the sign of the real part of the $\left\langle S'_{hh}S'^{*}_{vv} \right\rangle$ term or, in other words, the sign of the cosine of the HH-VV polarization phase difference PPD (see section 5.2.3), it is then decided whether odd bounce or double bounce scattering is the dominant source of backscatter. If odd bounce scattering dominates $(\cos(\text{PPD})$ is positive) $\alpha$ is set to 1. Likewise, if double bounce scattering dominates $(\cos(\text{PPD})$ is negative) $\beta$ is set to 1. In both cases this leaves 3 equations from which $f_s$, $f_d$ and either $\alpha$ or $\beta$ can be estimated. The expectation of the total backscattered power TP is given by:

$$\left\langle \sigma^{\circ}_{TP} \right\rangle = \frac{1}{4}\left( \left\langle \left|S'_{hh}\right|^2 \right\rangle + 2\left\langle \left|S'_{hv}\right|^2 \right\rangle + \left\langle \left|S'_{vv}\right|^2 \right\rangle \right) \tag{5.23}$$

The contributions of odd bounce, double bounce and diffuse scattering to TP can then be calculated by substituting the Equations 5.19, 5.20 and 5.21 in Equation 5.23.

### 5.3.3 Processing of ERS-1 SAR Precision images

The present section describes the *digital processing techniques applied to improve the visual interpretability of the available ERS-1 PRI images and to prepare these images for automated detection of change.* Processing of images to improve the visual interpretability by increasing the apparent distinction between the features in the scene is denoted image enhancement. Since visual interpretation is a qualitative analysis method, radiometric calibration is not a strictly necessary step in image enhancement procedures. In fact, the backscatter values of pixels in images used for visual interpretation are irrelevant. All that matters is that the differing features present can be clearly observed. Automated detection of change, on the other hand, is a quantitative analysis method. Hence, the procedure to prepare ERS-1 PRI images for change detection must include radiometric calibration (see section 3.1.5).

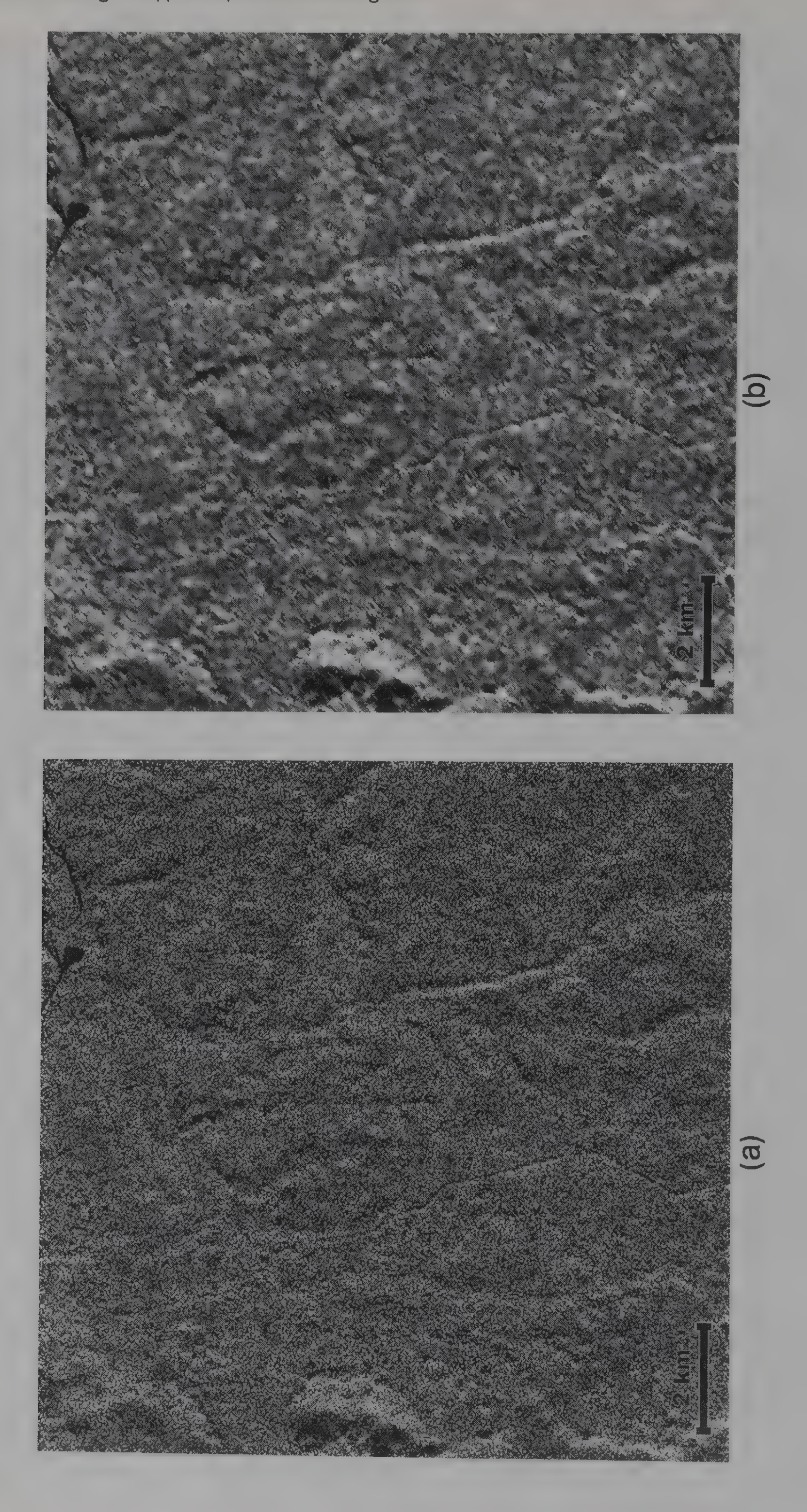
Results of processing techniques applied to improve the visual interpretability of ERS-1 PRI images are illustrated in Figure 5.8. The image subsets in this figure show the West Pibiri compartment in Mabura Hill, Guyana. Figure 5.8a depicts the 'unprocessed' ERS-1 SAR PRI image. The pixel values in this image represent the amplitude of the radar return signal (see section 3.1.2). This image was not enhanced other than by means of a linear stretch to optimise contrast. Figure 5.8b shows the contrast stretched result of a speckle filtering procedure applied to the 'unprocessed' image in Figure 5.8a. The filter used is known as the "refined Gamma-Gamma Maximum A Posteriori filter". Lopes and Nezry (1991) and Lopes et al. (1993) describe the working of this filter in detail. Unlike most speckle filters, the Gamma-Gamma MAP filter largely preserves strong scatterers and structural image features such as roads. Visual comparison of the images in the Figures 5.8a and 5.8b shows that filtering resulted in drastic speckle removal. Evaluation of the corresponding image statistics confirms this observation as it indicates that the speckle standard deviation of the amplitude is lowered by a factor three. For a discussion on the cause of speckle in radar images please refer to section 3.1.3.

Figure 5.8c illustrates the result of the next step in the enhancement procedure adopted. The image shown in essence represents the mean of the original amplitude image (Figure 5.8a) and the speckle filtered image (Figure 5.8b). Prior to averaging, the amplitude image and the filtered image were rescaled from 16 bits to 8 bits so that the pixel values ranged from 0 to 255. Subsequently, the contrast in the resulting image was optimised by means of a linear stretch. To those working in the radar remote sensing group of the department of Water Resources of the Wageningen Agricultural University, this averaging and scaling step is known as the 'Martin enhancement'. The resulting image shows less speckle than the amplitude image and more spatial detail than the speckle filtered image. Hence, it provides a better basis for visual interpretation than either of these images.

To obtain a further enhanced image, the described procedure was repeated three times using co-registered scenes from different acquisition dates. Next, the obtained images were averaged to further reduce the effects of speckle. The result of this final step in the enhancement procedure adopted is illustrated in Figure 5.8d. Like in Figures 5.8a through 5.8c, the contrast has been optimised. The ERS-1 PRI images

contributing to Figure 5.8d date from October 1993, May 1994 and August 1994. To emphasise the situation in August 1994 the images were weighted differently in the averaging process. The earliest image was weighted by a factor 1/6, the middle image by a factor 2/6 and the image from August 1994 by a factor 3/6. The information content of the image in Figure 5.8d is discussed in section 7.2.1. In this section the image is shown in the Figures 7.2b and 7.3.

Like in image enhancement, the initial step in the procedure aimed at preparing an ERS-1 PRI image for automated detection of change involved filtering of the 'unprocessed', amplitude image in order to reduce speckle. Subsequently, the filtered image was absolutely calibrated according to the procedure described by Laur (1992) and Laur et al. (1993). The pixel values in a calibrated image represent backscattered power in terms of $\sigma^{\circ}$ in dB (see section 3.1.4). Filtered and absolutely calibrated ERS-1 PRI images provide suitable bases for automated detection of temporal change in backscatter. In the present study, the two images which served as the basis for change detection resulted from further processing. Each of these images was in fact the weighted average from a series of three filtered and calibrated ERS-1 PRI images from differing dates. Temporal averaging of images was applied to reduce the level of speckle further and hence to enable detection of smaller changes in the forest's backscatter behaviour. The averaging step is described and motivated in more detail in section 7.2.2. This section also discusses the method used for automated detection of backscatter change.


(b)
2 km
(a)
2 km

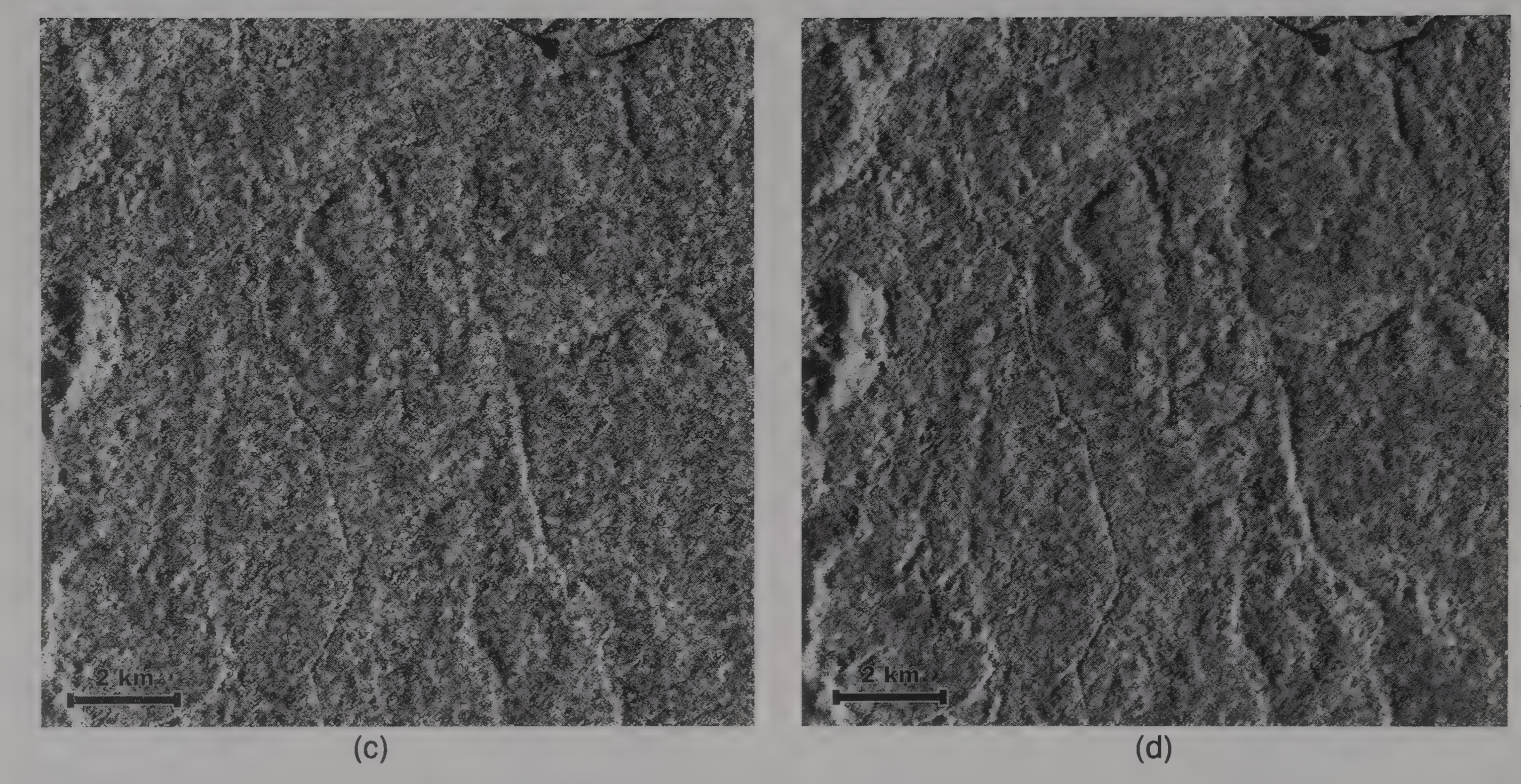



**Figure 5.8 (a-d)** ERS-1 SAR PRI image subsets illustrating the techniques applied to improve visual interpretability: (**a**) the original, 'unprocessed' amplitude image (**b**) image resulting from speckle filtering applied to image shown in **a** (**c**) enhanced image resulting from averaging of the images shown in **a** and **b** (**d**) image obtained by averaging of three enhanced images (including the one shown in **c**) from differing acquisition dates. The contrast of all images shown was optimised by means of a linear stretch.

# 6 Radar remote sensing to support forest resource assessment

*Forest resource assessment* was defined in section 1.1 as the procedure for collecting, processing and presenting forest data. It usually *results in a description of the location, extent and/or constitution of a certain forest area at a particular point in time.* Radar remote sensing may be used in such procedures for the collection of data. The value of this tool in forest resource assessment strongly depends on its capacity to provide the required information. This chapter reports on the information content of the radar data sets described in section 4.4.

The first step in a forest resource assessment is usually the stratification of the extant land/forest cover according to type. The present study, therefore, focused on the evaluation of radar data as a basis for the classification of the land cover types as defined in section 4.1.1 (see Table 4.1). The potential value of radar for estimating biomass parameters and forest architectural parameters was also studied. *To assess the information content of the radar data, the study used three fundamentally different information sources from the radar return signal: its strength (backscatter), polarization and phase, and spatial variability.* Spatial variations of the radar return signal are seen in images as texture. The methods and techniques used to obtain the results as presented in this chapter were discussed in Chapter 5.

## 6.1 Results of the analysis of the CCRS SAR data

The present section reports on the results of the analysis of the high resolution radar data as acquired by the CCRS airborne SAR system. The CCRS SAR operates in X- and C-band and in HH, VH, HV and VV polarization (see section 4.4.1). *The aim of the analysis was to assess the value of the available radar data sets for the classification of land cover and the study of canopy architecture.* The information content associated with the backscatter level is compared to that associated with the textural pattern. Particulars of the analysis of image texture according to the GLCO approach (see section 5.1.1) are discussed in Appendix I.

### 6.1.1 Classification of land cover per region using backscatter and texture

Table 6.1 illustrates the potential of $\bar{\gamma}$, sd($\gamma$) and the best as well as the worst performing GLCO attribute for the classification per region of the land cover types studied. $\bar{\gamma}$ quantifies radar backscatter while sd($\gamma$) and GLCO attributes quantify image texture (see section 5.2). The values given represent the number of class pairs that can be successfully discriminated, i.e. the number of class pairs for which $TD_{ij} \geq 1900$ (see section 5.2.4).

The textural attributes can be seen to have a higher classification potential than $\bar{\gamma}$ in all radar data sets. In addition, a considerable discrepancy is shown to exist in the

**Table 6.1** Potential of $\bar{\gamma}$, sd($\gamma$) and GLCO attributes for the classification per region of the land cover types studied. The values in this table represent the number of class pairs that can be successfully discriminated, i.e. the number of class pairs for which $TD_{ij} \geq 1900$.

| | | | GLCO attribute | |
|---|---|---|---|---|
| | $\bar{\gamma}$ | sd($\gamma$) | Best performing | Worst performing |
| **Exclusive of Secondary forest and Non-forest** (total number of class pairs is equal to 15) | | | | |
| X-band HH | 3 | 10 | 11 | 1 |
| X-band VH | 2 | 10 | 11 | 1 |
| X-band HV | 0 | 5 | 9 | 2 |
| X-band VV | 0 | 5 | 8 | 1 |
| C-band HH | 0 | 10 | 10 | 0 |
| C-band VH | 2 | 10 | 10 | 0 |
| C-band HV | 5 | 7 | 9 | 0 |
| C-band VV | 4 | 7 | 9 | 0 |
| **Inclusive of Secondary forest and Non-forest** (total number of class pairs is equal to 28) | | | | |
| X-band HV | 0 | 13 | 18 | 2 |
| X-band VV | 0 | 12 | 18 | 3 |
| C-band HV | 8 | 15 | 18 | 0 |
| C-band VV | 5 | 15 | 16 | 0 |

classification potential of the best and worst performing GLCO attribute. The performance of these attributes differs because they either represent different statistical parameters or are computed for different displacement lengths (see section 5.1.1). The relative performance of the GLCO attributes studied (90 for each radar data set) is discussed in section I.4 of Appendix I. Finally, Table 6.1 shows a variability in the performance of the textural attributes in the different radar data sets. Apparently, the land cover classes are texturally more distinct in some data sets than in others. To some extent the texture of the classes in different data sets will be affected by radar frequency and polarization. This is discussed in detail in section I.1 of Appendix I.

Apart from frequency and polarization there are other possible causes for the variation in the textural separability of the classes in different data sets. One of these is the difference in the size of the pixels in the X- and C-band data sets (see Table 4.5). This difference in pixel size, though small, may well affect the textural separability of the classes. Another possible cause relates to the manner in which the data sets were acquired. Data sets with HH and VH polarization were acquired along different flight lines than those with VV and HV polarization. Consequently, the associated radiometric and textural attributes do not necessarily cover the same

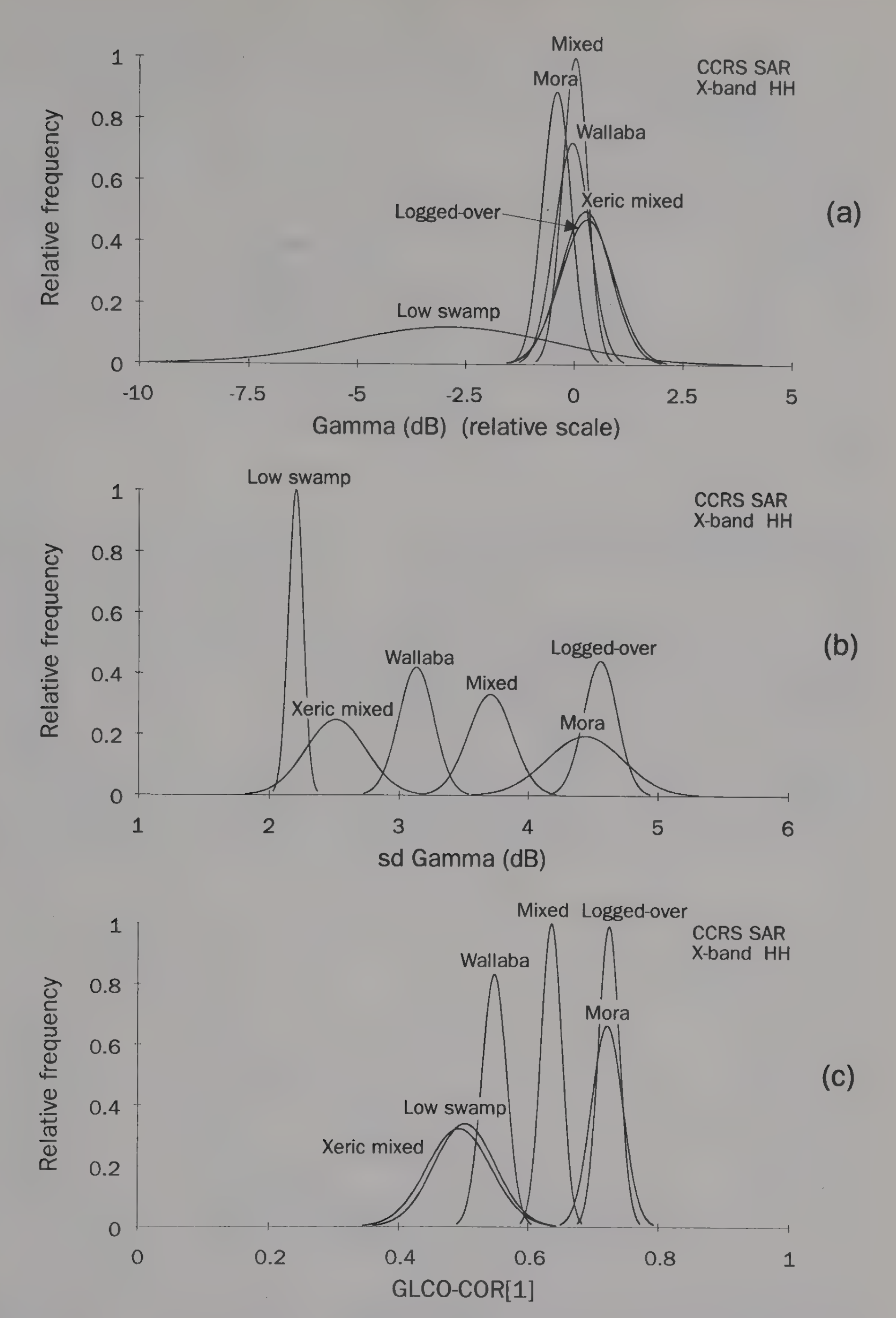



**Figure 6.1 (a-d)** Gaussian approximations of pdf's for region averaged radiometric and textural attributes associated with land cover types present in the **X-band HH CCRS SAR** image: (**a**) pdf's for $\overline{\gamma}$ (**b**) pdf's for sd($\gamma$) (**c**) pdf's for GLCO-COR[1] (**d**) pdf's for GLCO-CONT[5].

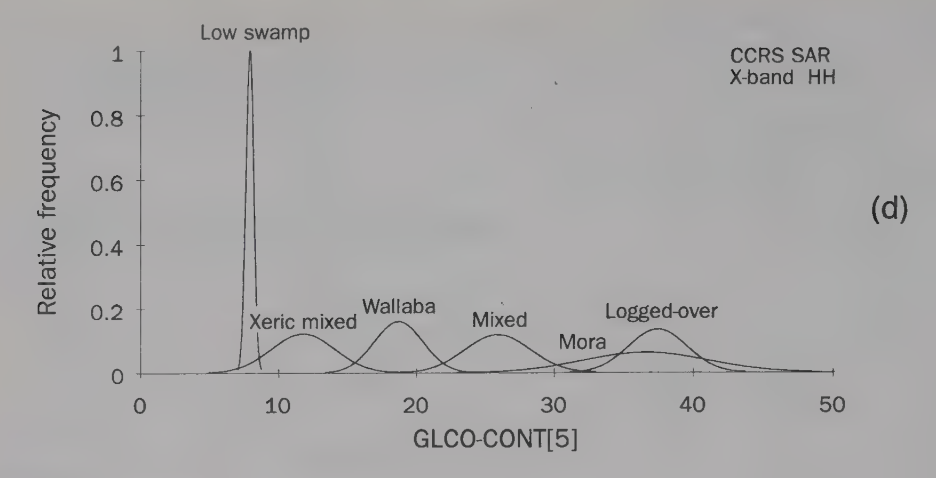



**Figure 6.1** Continued.

incidence angle range. Moreover, the attributes do not necessarily relate to exactly the same areas on the ground. A discrepancy in the incidence angle range for the Logged-over forest class is in fact the main cause of the deviating results for the VH and HV polarized channels of both X- and C-band. For more details please refer to section I.1 of Appendix I. The discrepancy in the results for the VH and HV channel contradicts the "reciprocity principle" which claims that the polarization states of radar signals are interchangeable (see section 3.1.6).

For X-band HH and C-band VV the differences in the discriminating capacities of radiometric and textural attributes are illustrated in Figure 6.1 and Figure 6.2, respectively. X-band HH was selected because this radar band was found to be among the most suitable for textural analysis (see section I.1, Appendix I). C-band VV

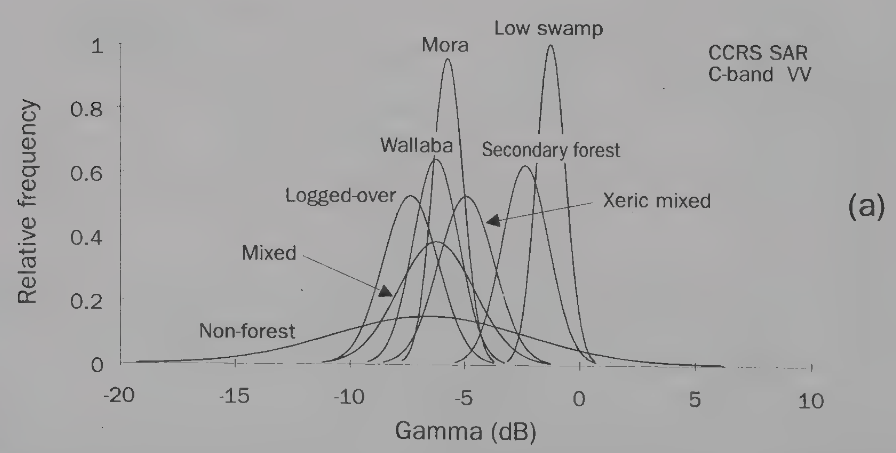



**Figure 6.2 (a-d)** Gaussian approximations of pdf's for region averaged radiometric and textural attributes associated with land cover types present in the **C-band VV CCRS SAR** image: (**a**) pdf's for $\overline{\gamma}$ (**b**) pdf's for sd($\gamma$) (**c**) pdf's for GLCO-COR[1] (**d**) pdf's for GLCO-CONT[5].

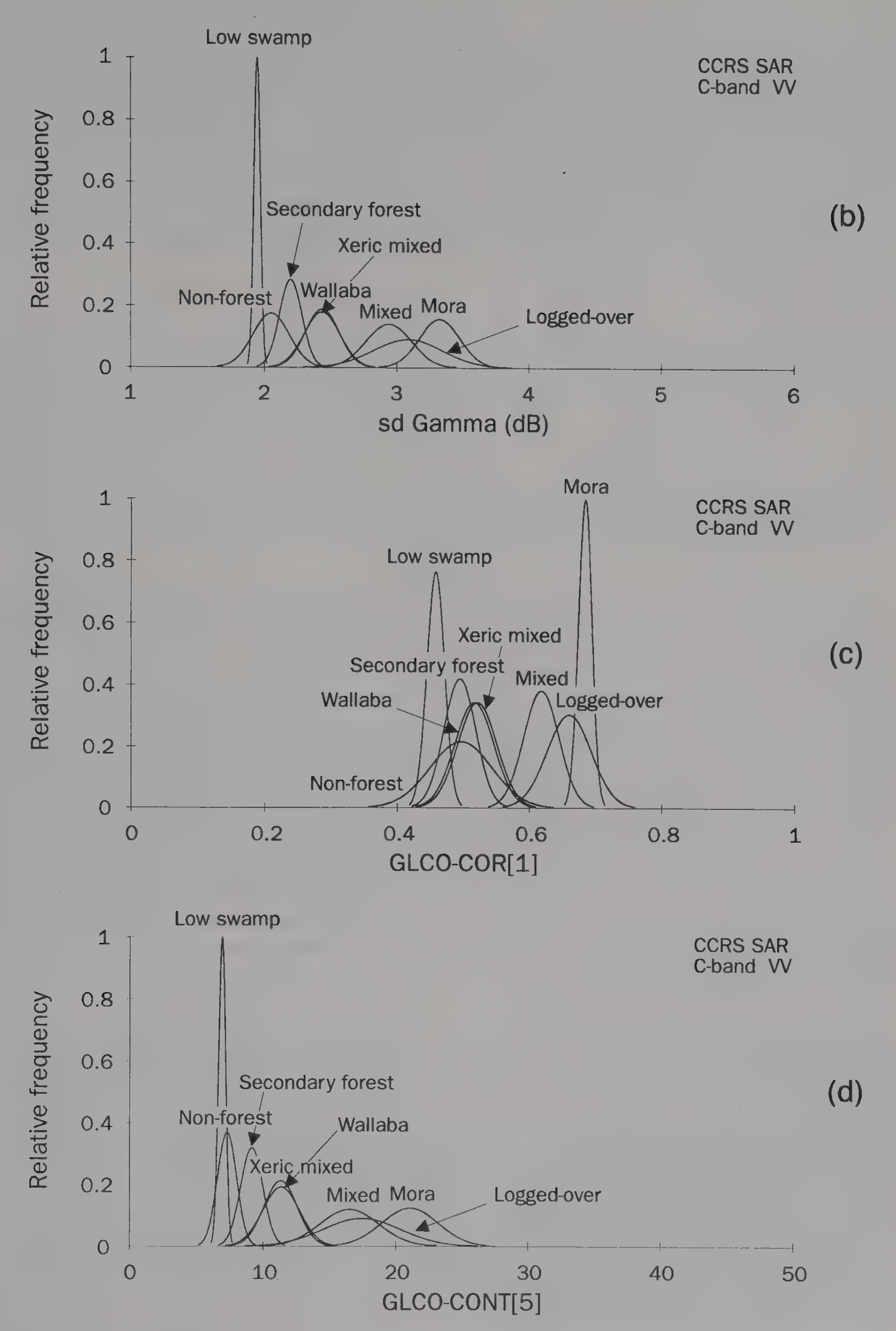



**Figure 6.2** Continued.

was chosen to allow for a comparison with the results of the textural analysis of the ERS-1 data (see section 6.2.1). GLCO-CONT[5] (GLCO-Contrast at displacement length 5) and GLCO-COR[1] (GLCO-Correlation at displacement length 1) were used to demonstrate the discriminating capacities of the GLCO attributes as these are among the best performing ones. According to the transformed divergence decision rule adopted (see section 5.2.4) the GLCO-CONT[5] attribute can discriminate the most class pairs, i.e. 11 out of 15. Both sd($\gamma$) and GLCO-COR[1] can discriminate between 10 out of 15 class pairs, while $\bar{\gamma}$ can only discriminate between three out of 10 class pairs. GLCO-CONT[5] fails to discriminate between Mora forest and Logged-over or Mixed forest. Neither can it distinguish Wallaba forest from Mixed or Xeric mixed forest.

In both Figure 6.1 and Figure 6.2, the *positions of the probability density functions (pdf's) for the textural attributes of the individual forest classes very well reflect the classes' canopy architecture.* Forests with a natural or, as in the case of Logged-over forest, artificial rough upper canopy can be found on the right hand side of the graphs. In contrast, forests with a smooth upper canopy are located on the left hand side (see Figures 4.7 through 4.11). Non-forest is positioned among the classes with a smooth upper canopy. The relation between GLCO textural attributes and canopy architecture is discussed in detail in section 6.1.2.

Comparison of the positions of the pdf's in Figure 6.1a with those in Figure 6.1b, 6.1c and 6.1d *shows that* sd($\gamma$) *as well as* GLCO-COR[1] *and* GLCO-CONT[5] *offer a much superior classification capacity than* $\bar{\gamma}$. In C-band VV (Figure 6.2) sd($\gamma$), GLCO-COR[1] and GLCO-CONT[5] also show the most classification potential. However, in this case the difference in the apparent classification capacity of textural attributes and $\bar{\gamma}$ is less pronounced. In X-band HH the classes are texturally more distinct than in C-band VV since their pdf's for sd($\gamma$), GLCO-COR[1] and GLCO-CONT[5] occupy a wider range and show considerably less overlap. A Gaussian maximum-likelihood classification on the textural attributes computed per region for X-band HH can therefore be expected to yield the best results. However, for reasons already mentioned above it may not be simply concluded that the difference in the apparent classification capacity of X-band HH and C-band VV results from differences in frequency and/or polarization.

The results in Table 6.2 confirm the observations made in relation to Figures 6.1 and 6.2 and quantify the classification capacities of radiometric and textural attributes in X-band HH and C-band VV. The table in addition contains some results from classifications based on attributes computed from the X-band HV data set in order to demonstrate the capacity of X-band for classifying Secondary forest and Non-forest. These two classes, unfortunately, are not represented in the X-band HH data set. Unlike the X-band HH data, the X-band HV data were acquired along the same flight lines as the C-band VV data. Therefore, possible differences in classification capacity for attributes associated with these data sets must result from differences in frequency, polarization and/or pixel size.

**Table 6.2** Gaussian maximum-likelihood classification results. Classification based on radiometric and textural attributes computed per region from **CCRS SAR** images.

| | $\hat{K}$ | $\hat{\sigma}^2_\infty[\hat{K}]$ | Percentage correct | | | | | | | | |
|---|---|---|---|---|---|---|---|---|---|---|---|
| | | | Total | Mixed | Wallaba | Xeric mixed | Low swamp | Mora | Logged-over forest | Secondary forest | Non-forest |
| **Exclusive of Secondary forest and Non-forest** | | | | | | | | | | | |
| X-band HH | | | | | | | | | | | |
| $\bar{\gamma}$ | 0.2702 | 0.0056 | 39 | 40 | 0 | 33 | 80 | 80 | 36 | - | - |
| sd($\gamma$) | 0.7802 | 0.0039 | 82 | 100 | 100 | 67 | 100 | 40 | 82 | - | - |
| GLCO-COR[1] | 0.5627 | 0.0056 | 64 | 100 | 79 | 0 | 60 | 40 | 73 | - | - |
| GLCO-CONT[5] | 0.8024 | 0.0036 | 84 | 100 | 93 | 83 | 100 | 40 | 91 | - | - |
| C-band VV | | | | | | | | | | | |
| $\bar{\gamma}$ | 0.3056 | 0.0071 | 43 | 0 | 27 | 50 | 100 | 50 | 64 | - | - |
| sd($\gamma$) | 0.5207 | 0.0062 | 61 | 80 | 73 | 25 | 100 | 90 | 0 | - | - |
| GLCO-COR[1] | 0.5039 | 0.0062 | 59 | 70 | 45 | 50 | 100 | 100 | 9 | - | - |
| GLCO-CONT[5] | 0.5444 | 0.0062 | 63 | 90 | 73 | 25 | 100 | 80 | 9 | - | - |
| **Inclusive of Secondary forest and Non-forest** | | | | | | | | | | | |
| X-band HV | | | | | | | | | | | |
| $\bar{\gamma}$ | 0.2047 | 0.0027 | 31 | 0 | 0 | 0 | 0 | 80 | 55 | 50 | 32 |
| sd($\gamma$) | 0.5626 | 0.0037 | 63 | 80 | 73 | 25 | 20 | 80 | 0 | 75 | 89 |
| GLCO-COR[1] | 0.5482 | 0.0037 | 62 | 80 | 55 | 25 | 0 | 90 | 18 | 63 | 89 |
| GLCO-CONT[5] | 0.5823 | 0.0037 | 64 | 80 | 64 | 25 | 100 | 70 | 0 | 75 | 84 |
| C-band VV | | | | | | | | | | | |
| $\bar{\gamma}$ | 0.2584 | 0.0034 | 35 | 0 | 27 | 25 | 80 | 50 | 64 | 50 | 16 |
| sd($\gamma$) | 0.4725 | 0.0037 | 54 | 80 | 73 | 0 | 100 | 90 | 0 | 75 | 32 |
| GLCO-COR[1] | 0.3568 | 0.0033 | 42 | 70 | 18 | 50 | 100 | 100 | 9 | 63 | 5 |
| GLCO-CONT[5] | 0.4465 | 0.0037 | 51 | 90 | 55 | 25 | 100 | 80 | 9 | 63 | 26 |

Using $\hat{K}$ and $\hat{\sigma}_{\infty}^{2}\left[\hat{K}\right]$ it can be computed whether or not there are significant differences between the overall classification results shown (see section 5.2.4). At the 95% confidence level the classification results for GLCO-CONT[5] prove to be significantly better than those for $\bar{\gamma}$ in all of the cases shown. The results for GLCO-COR[1] are significantly better than those for $\bar{\gamma}$ in X-band HH and X-band HV only. sd($\gamma$) yields significantly better classification results than $\bar{\gamma}$ in all but one case, namely the case of C-band VV when Secondary forest and Non-forest are being excluded. *The overall classification results obtained with the textural attributes may be said to be reasonable to good as some 50 to 85% of the data points is classified correctly.* Both GLCO-CONT[5] and sd($\gamma$) render significantly better results than GLCO-COR[1] in X-band HH. The difference in the overall classification results for sd($\gamma$) and GLCO-CONT[5] is not significant in any case. Since GLCO-CONT[5] is among the best performing GLCO attributes there is no reason to assume that any other of those attributes may yield results that are significantly better than those for sd($\gamma$). Taking into account the results shown in Table 6.1 there also is no reason to assume that this could be different in any other of the CCRS SAR data sets.

The GLCO-CONT[5] and sd($\gamma$) attributes associated with X-band HH yield significantly better classification results than any of the textural attributes derived from the C-band VV data (excluding Secondary forest and Non-forest). There are no significant differences in the performance of C-band VV textural attributes and the X-band HH GLCO-COR[1] attribute. Comparison of the overall classification results for the textural attributes associated with X-band HV and C-band VV (inclusive of Secondary forest and Non-forest) shows that the C-band VV GLCO-COR[1] attribute yields significantly poorer discrimination than any of the attributes associated with X-band HV. Otherwise, there are no significant differences in the overall results for the textural attributes in X-band HV and C-band VV.

Inclusion of data points for Secondary forest and Non-forest in the C-band VV data set does not yield significantly different classification results. This indicates that the textural characteristics of these classes in this data set are neither similar nor dissimilar to those of the other classes. In C-band VV there is in fact considerable confusion between Non-forest and Low swamp forest. This is not as much a problem in X-band HV. Taking into account the results for all data sets studied, the *GLCO attributes fail to uniquely describe the texture of Logged-over forest, in particular.* In the classifications Logged-over forest is confused repeatedly with Mora forest and, to a lesser extent, with Mixed forest, i.e. the forest type being logged. Other frequently confused classes are Non-forest and Secondary forest, as well as Xeric mixed forest and Wallaba forest. Although Logged-over forest and Mora forest represent similar textural patterns in radar images, the architecture of their canopies is different. For a more detailed discussion on the relationship between canopy architecture and GLCO textural attributes, please refer to section 6.1.2.

The results show that sd($\gamma$) *and selected GLCO attributes are equally suitable for classification per region of the land cover types studied.* In practice, the use of both sd($\gamma$) and GLCO attributes has certain advantages as well as disadvantages. One advantage associated with the use of sd($\gamma$) is that its calculation requires a relatively small amount of computer time. It follows that sd($\gamma$) can be computed at a lower

**Table 6.3** Gaussian maximum-likelihood classification results. Classification based on combinations of two textural attributes computed from **CCRS SAR** images (data sets include Secondary forest and Non-forest).

| | | | Percentage correct | | | | | | | | |
|---|---|---|---|---|---|---|---|---|---|---|---|
| | $\hat{K}$ | $\hat{\sigma}_{\infty}^{2}[\hat{K}]$ | Total | Mixed | Wallaba | Xeric mixed | Low swamp | Mora | Logged-over forest | Secondary forest | Non-forest |
| X-band HV | | | | | | | | | | | |
| GLCO-CONT[5] + GLCO-COR[1] | 0.6728 | 0.0033 | 72 | 70 | 55 | 100 | 100 | 90 | 36 | 63 | 84 |
| GLCO-CONT[5] + GLCO-CONT[10] | 0.7778 | 0.0026 | 81 | 90 | 73 | 100 | 100 | 90 | 64 | 75 | 79 |
| GLCO-CONT[5] + GLCO-MPROB[4] | 0.8196 | 0.0022 | 85 | 90 | 100 | 100 | 100 | 80 | 36 | 75 | 100 |
| C-band VV | | | | | | | | | | | |
| GLCO-CONT[5] + GLCO-COR[1] | 0.5763 | 0.0037 | 63 | 60 | 36 | 50 | 100 | 100 | 55 | 75 | 53 |
| GLCO-CONT[5] + GLCO-CONT[9] | 0.5908 | 0.0036 | 64 | 80 | 36 | 50 | 100 | 80 | 55 | 100 | 47 |
| GLCO-CONT[5] + GLCO-IDM[3] | 0.6187 | 0.0036 | 67 | 80 | 55 | 100 | 100 | 80 | 36 | 88 | 53 |

expense than the GLCO attributes. This is only of moderate importance in the GTA approach followed thus far but may be considered an important benefit if complete images need to be processed (MWA approach). Another advantage of using sd($\gamma$) is that one can avoid the often difficult choices required in GLCO textural analysis, namely choices concerning the preferred statistical parameter, displacement length and displacement direction. The significance of these choices is reflected in the deviating classification potential of the best and worst performing GLCO attribute (see Table 6.1). Nevertheless, precisely these options cause GLCO attributes to be the more powerful descriptors of textural patterns. By selecting a specific statistical parameter, displacement length and/or displacement direction, one can in fact construct a textural attribute that is optimal for describing the textural pattern of interest. This cannot be done if one uses a simple textural descriptor like sd($\gamma$), which is not at all sensitive to the spatial organisation of the pixels, i.e. pattern. It merely describes the average difference in grey level between pixels and their mean.

It will be clear that sd($\gamma$) is a less potent textural descriptor than the more complex and more flexible GLCO attributes. Yet, as pointed out before it is not always very simple to select the optimal settings for GLCO textural analysis. On the one hand, this is due to the fact that it is often difficult to conceive how GLCO attributes and textural patterns associate (see section 6.1.2). On the other hand, there will always be the problem that no single GLCO analysis setting is optimal for discriminating all

patterns present. Usually, the 'optimal' setting can only be established empirically. The choices associated with the GLCO textural analysis in this study are discussed in detail in Appendix I.

*Combined use of GLCO attributes may enhance the possibilities for discriminating different textural patterns.* The effects of using GLCO-CONT[5] in combination with some other GLCO attributes are illustrated in Table 6.3. For all combinations shown, the resulting classifications prove to be better than those for just GLCO-CONT[5] (see Table 6.2). At the 95% confidence level, however, the difference between GLCO-CONT[5] and the combination of GLCO-CONT[5] and GLCO-COR[1] in X-band HV is not significant. Likewise, there is no significant difference in the results for GLCO-CONT[5] and for combinations of this attribute with GLCO-COR[1] or GLCO-CONT[9] in C-band VV. The incorporation of a second GLCO attribute in the classification procedure does especially improve the identification of Xeric mixed forest and the Logged-over forest. Apparently, GLCO-CONT[5] alone cannot uniquely describe the patterns of these cover types.

### 6.1.2 Analysis of canopy architecture using GLCO textural attributes

Texture in radar images results primarily from radar "layover", "shadowing" and "foreshortening" effects (see section 3.1.3). In high frequency and high resolution radar images of forested areas (on flat terrain) these effects relate to canopy roughness which is a parameter of canopy architecture. The architecture of a forest canopy is an expression of the development phase, size and recurrence of the eco-units building the forest mosaic (Oldeman, 1990). *Forests with different canopy architectures give rise to different textural patterns and thus to different values for textural descriptors.* The relationship between GLCO textural attributes and canopy architecture can best be seen in plots that show the variation in their values as a function of displacement length. Figure 6.3 shows such plots for three GLCO statistics associated with the X-band HH data set, i.e. GLCO-COR, GLCO-CONT and GLCO-ENT. Unlike in the 'standard' GTA approach (see section 5.2.2), these statistics were computed with displacement in range direction only. In this direction the relationship between texture and canopy architecture is usually most pronounced because of the side-looking measurement geometry of imaging radar systems (see section 3.1.1). The plots in Figure 6.3 exemplify the behaviour of all GLCO statistics studied. The GLCO-CONT plots are similar to those for GLD-MEAN, whereas those for GLCO-ENT compare to the ones for GLCO-ASM, GLCO-IDM, GLCO-MAX PROB, GLD-ASM and GLD-ENT.

The values of each textural attribute can be seen to be related to the canopy roughness of the forest type in question. Depending on the nature of the attribute this relationship can either be negative or positive. For example, rougher forest canopies have higher GLCO-CONT values but lower GLCO-ENT values. In case of GLCO-COR the relationship is more complex. At short displacement lengths the values for 'rough' forests are higher than those for 'smooth' forests but at longer displacements the opposite holds true. It follows that *GLCO textural attributes may*

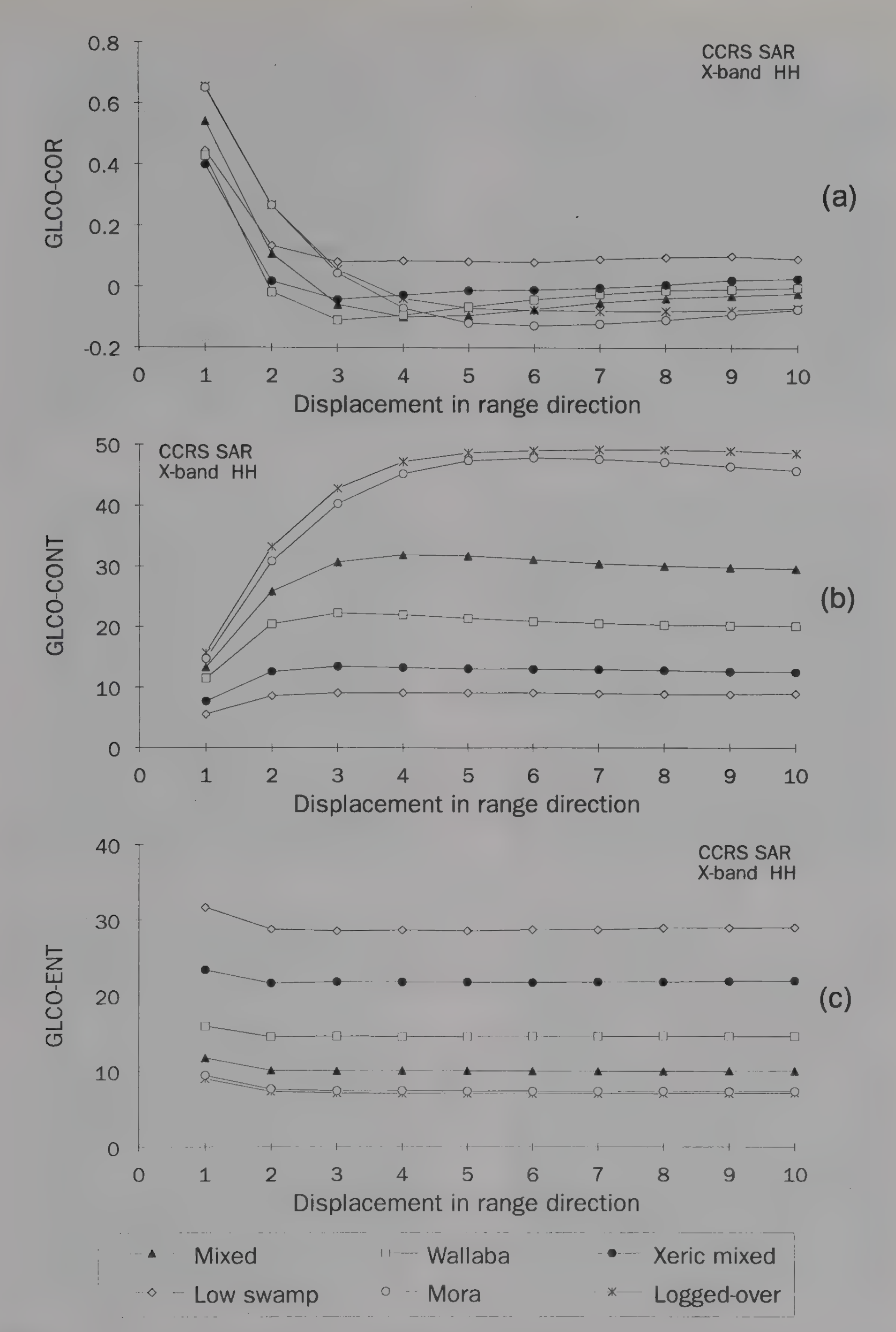



**Figure 6.3 (a-c)** Plots showing the relationship between the GLCO textural attributes for forest types present in the X-band HH **CCRS SAR** image and the displacement length in range direction: (**a**) plots for GLCO-COR (**b**) plots for GLCO-CONT (**c**) plots for GLCO-ENT. The plots mirror architectural characteristics of the observed forest canopies.

*be used to rank the forest types according to their degree of canopy roughness.* The studied forest types rank as follows, in order of increasing canopy roughness: Low swamp, Xeric mixed, Wallaba, Mixed, Mora and Logged-over forest. This sequence agrees with what one would expect based on the available set of ground reference data (see section 4.3).

The values for GLCO-ENT can be seen to only vary slightly as a function of displacement length. Also, the variations present do not appear to be specific per forest type. In this respect, the behaviour of GLCO-ENT differs from that of GLCO-COR and GLCO-CONT. The variation induced by displacement length in the values for these attributes is considerable and clearly specific for each forest type. For Low swamp, Wallaba and Xeric mixed forest the GLCO-COR statistic reaches a minimum at a displacement of 3 pixels. For Mixed forest the minimum is reached at a displacement of 4 pixels, while the minima for Mora forest and Logged-over forest are found at a displacement of 6 and 7 pixels, respectively. Whenever GLCO-COR reaches a minimum, the value for GLCO-CONT reaches a maximum. It follows from the definition of the GLCO-COR statistic (see section 5.1.1) that its value is minimal if the displacement length matches the distance over which on average the grey levels are the least correlated or the most negatively correlated. Likewise, the value for GLCO-CONT is maximal when the displacement length is equal to the distance over which on average the sharpest grey level transitions occur. These minimum and/or maximum values occur when the "source" and "target" pixel are frequently located in different textural sub-patterns, i.e. when the displacement length equals the cross-section of the most occurring (dominant) textural sub-pattern.

Textural sub-patterns are clusters of pixels with comparable grey levels. In combination they constitute the overall textural pattern. *To a certain extent, the textural sub-patterns in the high resolution CCRS SAR images are congruent with canopy elements such as individual tree crowns, tree crown clusters or canopy openings. However, super-imposed on these textural sub-patterns related to the canopy there are sub-patterns resulting from radar "layover", "shadowing" and "foreshortening" effects* (see section 3.1.3). For example, due to "foreshortening" the front (radar facing) side of a large tree crown may appear much brighter than the back side. Consequently, the two sides of this crown show up as two different textural sub-patterns.

Figure 6.4 illustrates textural (sub-)patterns that are typical for the primary and logged-over forest types studied. The image subsets shown were taken from the CCRS SAR X-band HH data and have a size of $64 \times 64$ pixels ($\approx 200 \times 200$ m). Logged-over, Mora and Mixed forest can be seen to have relatively large textural sub-patterns. Consequently, their textures are conceived as being 'coarse'. Wallaba, Xerix mixed and Low swamp forest have relatively small textural sub-patterns and are therefore conceived as being 'fine' textured. In addition, it can be seen that the grey levels of the textural sub-patterns for some forest types vary more widely than for others. Much variation in grey levels results in textures rich in contrast, e.g. Logged-over and Mora forest. Similarly, little variation in grey levels results in textures poor in contrast, e.g. Xeric mixed and Low swamp forest. Textures that are rich in contrast are characterised by high GLCO-CONT values, whereas textures that are poor in contrast have low GLCO-CONT values (see Figure 6.3b).

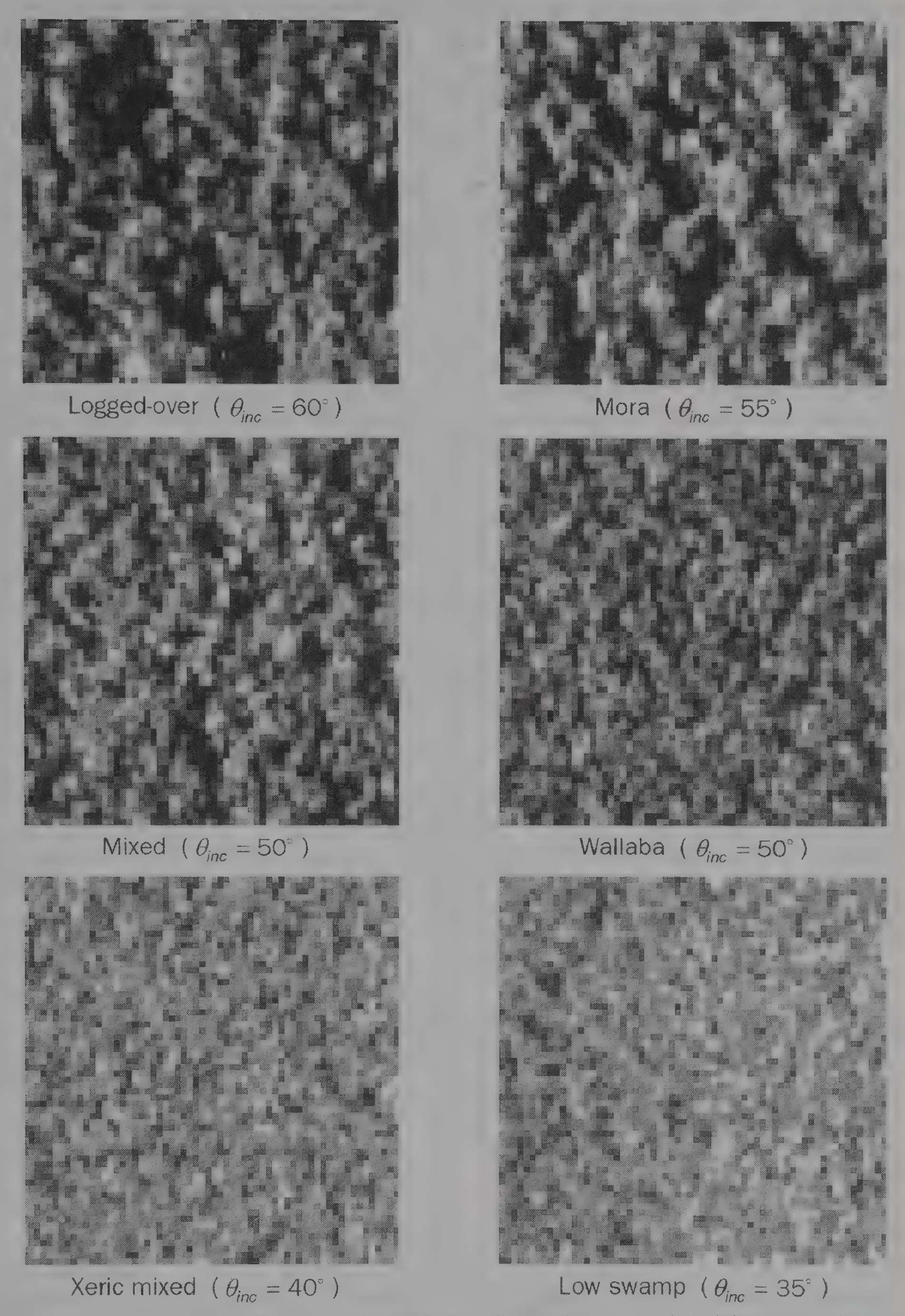



**Figure 6.4** CCRS SAR X-band HH image subsets illustrating textural (sub-)patterns that are typical for the primary and logged-over forest types studied.

The results in Figures 6.3a and 6.3b show that the dominant textural sub-patterns for Logged-over and Mixed forest have different cross-sections, i.e. are of a different nature. This textural difference reflects the presence of artificial canopy openings in the Logged-over forest. Artificial openings constitute the only essential difference in the canopy of the two forest types. After all, Logged-over forests originate from Mixed forests. Ground reference data indicate that natural and artificial canopy openings may be of a comparable size (see section 4.3.2). Yet, natural openings do not dominate the texture of Mixed forest regions because of their relatively low frequency. Also natural openings, in contrast to openings resulting from logging, do not usually occur in clusters. Due to logging the canopy architecture of Mixed forest becomes ecologically disorganised (see section 4.3.2).

Figures 6.3a and 6.3b indicate that the sub-patterns in the Logged-over forest have an average cross-section of 7 slant range pixels or $7 \times 4.0 = 28$ m. In the CCRS SAR X-band HH image most of the Logged-over forest areas are found at an incidence angle of ca. 60°. At this incidence angle a slant range cross-section of 28 m corresponds to a cross-section of $28/\sin(60) \approx 32$ m on the ground (see Figure 3.3 and Equation 3.1). Results of GTA with displacement in azimuth direction show that the azimuth cross-section of the artificial canopy openings, on average, is 9 pixels or $9 \times 3.44 \approx 31$ m. If the artificial openings in the Logged-over forest are assumed to be approximately circular and have a cross-section equal to the average of the cross-sections in range and azimuth direction, then the average size of these openings can be estimated to be equal to $\pi \times (31.5/2)^2 = 779$ m$^2$. Field measurements by Hammond and Brown (1992) show an average size of ca. $800 \pm 200$ m$^2$ (see section 4.3.2). The two results compare very well.

Figure 6.4 shows that the ecologically disorganised canopy of Logged-over forest and the canopy of Mora forest have a similar textural appearance. The textures of both forest types are dominated by dark textural sub-patterns. In the case of Mora forest, however, these sub-patterns are not primarily related to the presence of canopy openings since these are not frequent in the Mora forest canopy. The most important characteristic of the Mora forest canopy is the presence of many, large emergent trees (see section 4.3.1). These emergents induce radar "layover", "foreshortening" and "shadowing" effects, the latter of which may be assumed to be the principal cause of the observed dark textural sub-patterns. The dominant role of radar shadow areas in the Mora forest texture is also reflected in the high maximum GLCO-CONT value for this forest type in Figure 6.3b. It follows from this figure that the average cross-section of the radar shadow areas (in range direction) is equal to 6 pixels since a displacement length of 6 pixels yields the maximum GLCO-CONT value. This information may be used to compute the average height difference between the emergent trees and their surroundings. It should be remembered, however, that the results shown relate to multiple Mora forest areas with incidence angles ranging from ca. 50° to 60°. The observed average cross-section of the shadow areas can therefore not be associated to a particular incidence angle. Consequently, the average height difference between the emergents and their surroundings can be approximately assessed only. In the CCRS SAR image an average shadow length of 6 slant range pixels equals $6 \times 4.0 = 24$ m. At a 50° incidence angle this shadow

length corresponds to an average height difference of $24 \times \cos(50) \approx 15$ m. The same shadow length at an incidence angle of 60° corresponds to an average height difference of 12 m. The ground reference data agree quite well with these findings; they indicate that emergent trees may be up to ca. 20 m higher than the main canopy (see section 4.3.1). It follows that in the case of Mora forest the GLCO-COR, GLCO-CONT and GLD-MEAN textural attributes allow for a quantification of canopy roughness.

The results in Figures 6.3a and 6.3b also indicate the presence of dominant textural sub-patterns in Mixed, Wallaba, Xeric mixed and Low swamp forests. Unfortunately, it is difficult to identify the canopy elements that constitute the dominant textural sub-patterns for these forest types. Identification of these canopy elements analogous to the manner in which those that dominate the texture for Logged-over forest were identified, i.e. through comparison, fails due to the absence of 'reference' textures. Moreover, identification through visual interpretation of the sub-images in Figure 6.4 fails because the dominant sub-patterns cannot be conceived. The inability to link the dominant sub-patterns (and corresponding cross-sections) to particular canopy elements prevents quantification of architectural properties of Mixed, Wallaba, Xeric mixed and Low swamp forest canopies. In a more qualitative way the information resulting from the computation of GLCO-COR, GLCO-CONT or GLD-MEAN statistics may still be put to use. Generally speaking, bigger tree crowns will give rise to larger textural sub-patterns. As such, it may be assumed that the forest canopy with the largest textural sub-pattern comprises the biggest tree crowns. Based on this assumption, the four forest types rank in two groups, i.e. Mixed forest and Wallaba, Xeric mixed and Low swamp forest (in order of decreasing crown size). Mora forest ranks higher than either of these groups. The ordering of the primary forest types with the help of the available ground reference data would have resulted in a comparable sequence.

*Because of their ability to describe dimensions of textural sub-patterns GLCO-COR, GLCO-CONT and GLD-MEAN may be said to be more sensitive to canopy architecture than any of the other GLCO statistics. Plots that show the changes in these GLCO attributes as a function of displacement length reflect physical properties of the observed canopy.*

*In essence, GLCO-CONT is equal to a statistic known as semi-variance.* Traditionally, semi-variance is used by geostatisticians to describe spatial interrelations between observations. According to Webster and Oliver (1990) the estimate of the average semi-variance is defined as:

$$\hat{\gamma}(\boldsymbol{d}) = \frac{1}{2N_p} \sum_{i=1}^{N_p} \left( z(\boldsymbol{i}) - z(\boldsymbol{i} + \boldsymbol{d}) \right)^2 \tag{6.1}$$

where $z(\boldsymbol{i})$ and $z(\boldsymbol{i}+\boldsymbol{d})$ represent the observed values of property $Z$ at the one, two or three dimensional positions $\boldsymbol{i}$ and $\boldsymbol{i}+\boldsymbol{d}$, $\boldsymbol{d}$ is a vector embracing the distance and direction from one observation to the other (the "lag") and $N_p$ represents the number of observation pairs (e.g. Webster and Oliver,1990). In grey level co-occurrence terms

$z(\boldsymbol{i})$ and $z(\boldsymbol{i}+\boldsymbol{d})$ stand for the grey levels of source pixel $i$ and target pixel $j$, vector $\boldsymbol{d}$ is the displacement vector. $\frac{1}{N_p}$ normalises $\hat{\gamma}(\boldsymbol{d})$ for the number of observation pairs like $p(i,j)$ normalises the GLCO-CONT statistic (see the equation for GLCO-CONT in Table 5.1). $\hat{\gamma}(\boldsymbol{d})$ and $\text{GLCO-CONT}[\boldsymbol{d}]$ compare as 1:2 and are thus essentially the same. Plots that show the variation in $\hat{\gamma}(\boldsymbol{d})$ as a function of $\boldsymbol{d}$ are referred to in geostatistics as semi-variograms. It follows that plots showing the variation in GLCO-CONT as a function of $\boldsymbol{d}$ are in fact semi-variograms (see Figure 6.3b).

The theory of semi-variance and the use of semi-variograms in geostatistics is discussed in detail in e.g. Journel and Huijbregts (1978), Isaaks and Srivastava (1989), Webster and Oliver (1990). The application of semi-variograms to analyse the spatial dependence of pixel values in remotely sensed images is discussed by: Dubé et al. (1986), Woodcock et al. (1988a, 1988b), Cohen et al. (1990), Miranda et al. (1992) and St-Onge and Cavayas (1995). None of these authors notes the link between semi-variance and GLCO-CONT, whereas some present semi-variograms as a 'new' tool for image analysis. They all seem to have overlooked the capacities of the earlier available GLCO-CONT statistic (Haralick, 1973).

*GLCO-COR can be shown to be closely related to a statistic known as the autocorrelation coefficient.* This coefficient has its origin in the analysis of time series but has also been used in image analysis, i.e. to investigate interrelations between spatially separated observations (e.g. Box and Jenkins, 1970; Haralick, 1979 and 1986). According to Journel and Huijbregts (1978) the estimate of the average autocorrelation coefficient at lag $\boldsymbol{d}$ is:

$$\hat{\rho}(\boldsymbol{d}) = \frac{1}{N_p}\sum_{i=1}^{N_p}\frac{\left(z(\boldsymbol{i})-\bar{z}\right)\left(z(\boldsymbol{i}+\boldsymbol{d})-\bar{z}\right)}{S_z^2} \tag{6.2}$$

where $\bar{z}$ is the mean and $S_z^2$ is the variance of the complete set of observations. The definition for $\hat{\rho}(\boldsymbol{d})$ assumes second-order stationarity. This implies that $\bar{z}$ is constant, $S_z^2$ is finite and that both $\bar{z}$ and $S_z^2$ are independent on position $\boldsymbol{i}$. Plots showing the variation in $\hat{\rho}(\boldsymbol{d})$ as a function of $\boldsymbol{d}$ are denoted autocorrelation functions.

The definition for GLCO-COR (see Table 5.1) differs from the one for $\hat{\rho}(\boldsymbol{d})$ because it is based on the means and standard deviations of the source and target pixel sets rather than on the mean and variance of the complete pixel set. The use of symmetrical GLCO matrices causes the means and the standard deviations of the source and target pixel sets to become identical. Nevertheless, this mean and standard deviation remain different from the mean and standard deviation of the complete pixel set. This may be exemplified with the use of Figure 5.1 (see section 5.1.1). The mean of the source and target pixel set in this figure is equal to 1.40, the standard deviation is equal to 0.973. The mean grey level of the complete image subset equals 1.48, the corresponding standard deviation is 0.970. The differences result from the fact that the pixels in column 3 contribute to twice as many

source-target class pairs as those in the other columns. This, in turn, relates to the adopted displacement vector. For a particular $\boldsymbol{d}$ the difference between $\text{GLCO-COR}[\boldsymbol{d}]$ and $\hat{\rho}(\boldsymbol{d})$ will become smaller as the number of observed pixel values increases. Given a particular series of pixels, $\text{GLCO-COR}[\boldsymbol{d}]$ and $\hat{\rho}(\boldsymbol{d})$ will become more alike as the displacement length decreases. In other words, the expectation of $\text{GLCO-COR}[\boldsymbol{d}]$ is equal to the expectation of $\hat{\rho}(\boldsymbol{d})$:

$$\langle \text{GLCO} - \text{COR}[\boldsymbol{d}] \rangle = \langle \hat{\rho}(\boldsymbol{d}) \rangle \tag{6.3}$$

Journel and Huijbregts (1978) show that when the assumptions of second-order stationarity hold, semi-variance and autocorrelation relate as:

$$\hat{\gamma}(\boldsymbol{d}) = S_z^2 \left(1 - \hat{\rho}(\boldsymbol{d})\right) \tag{6.4}$$

It follows that semi-variance and autocorrelation are equivalent but complementary descriptors of spatial interrelations between observations. Nevertheless, semi-variance is regarded as generally more useful because it demands weaker assumptions. If the number of observed pixel values is large, then $\text{GLCO} - \text{COR}[\boldsymbol{d}] \approx \hat{\rho}(\boldsymbol{d})$ and Equation 6.4 may be rewritten as:

$$\text{GLCO-CONT}[\boldsymbol{d}] \approx 2S_z^2 \left(1 - \text{GLCO-COR}[\boldsymbol{d}]\right) \tag{6.5}$$

In section 5.1.2 the variance of the set of observations in a radar image, i.e. the set of pixel values, was shown to be equal to the total variance $S_{tot}^2$. Equation 6.5 can therefore also be written as:

$$\text{GLCO-CONT}[\boldsymbol{d}] \approx 2S_{tot}^2 \left(1 - \text{GLCO-COR}[\boldsymbol{d}]\right) \tag{6.6}$$

Comparison of the plots for GLCO-CONT in Figure 6.5 with those in Figure 6.3b gives empirical evidence for the correctness of this equation. The GLCO-CONT values plotted in Figure 6.5 were computed from values for GLCO-COR according to Equation 6.6, whereas those plotted in Figure 6.3b were calculated directly from the GLCO matrix. The plots in the two figures are in close agreement. The equation resolves why a maximum for GLCO-CONT was found to correspond to a minimum for GLCO-COR.

Generally speaking, the degree of correlation between two observed pixels decreases as the distance $|\boldsymbol{d}|$ between them increases. Therefore, when $|\boldsymbol{d}| \to \infty$, $\hat{\rho}(\boldsymbol{d}) \to 0$. It follows from Equation 6.3 that when $\hat{\rho}(\boldsymbol{d}) \to 0$, $\hat{\gamma}(\boldsymbol{d}) \to S_z^2$. Similarly, when $|\boldsymbol{d}| \to \infty$, $\text{GLCO-CONT}[\boldsymbol{d}]$ approaches its upper limit value of two times the total image variance ($\text{GLCO-CONT}[\boldsymbol{d}] \to 2S_{tot}^2$). The total variance $S_{tot}^2$ within a particular region of a radar image is equal to the sum of three terms, i.e. texture variance $S_T^2$, fading (speckle) variance $S_F^2$ and the product of texture and speckle variance $S_T^2 S_F^2$ (see Equation 5.1, section 5.1.2). In theory, $S_{tot}^2$ is always $\geq S_F^2$ since speckle is an

inherent feature of radar images. The theoretical lower limit for $\text{GLCO-CONT}[\boldsymbol{d}]$, when $|\boldsymbol{d}| \rightarrow \infty$ will thus be equal to $2S_F^2$. GLCO-CONT will attain its lower limit in homogeneous or textureless image regions. In Figure 6.5 the lower limit for the GLCO-CONT values is marked. The level indicated corresponds to a variance of 5.79 dB (two times the speckle variance in a logarithmically scaled 7 look radar image).

### 6.1.3 Textural analysis by means of a moving window

The common methodology for Moving Window textural Analysis (MWA) and the evaluation of the MWA results was described in section 5.3.1. The present section discusses the particulars and results of the MWA's carried out using the CCRS SAR X-band HH image. This specific CCRS SAR image was chosen because results of Gross Textural Analysis (GTA) show that it has a relatively high textural information content (see section I.1, Appendix I). The employed textural attributes were: GLCO-COR[1], GLCO-CONT[5] and sd($\gamma$). GLCO-COR[1] and GLCO-CONT[5] were selected since the GTA results in section 6.1.1 indicate that these are among the best performing GLCO attributes. Moreover, GLCO-COR and GLCO-CONT are, together with GLD-MEAN, the GLCO attributes most sensitive to canopy architecture (see section 6.1.2). Results in section I.4 of Appendix I show that the preferred displacement length is equal to one pixel for GLCO-COR and 5 pixels for GLCO-CONT. GTA with the help of the first-order statistic sd($\gamma$) also lead to good results. The advantage of sd($\gamma$) over the GLCO attributes is its relatively low computational load.

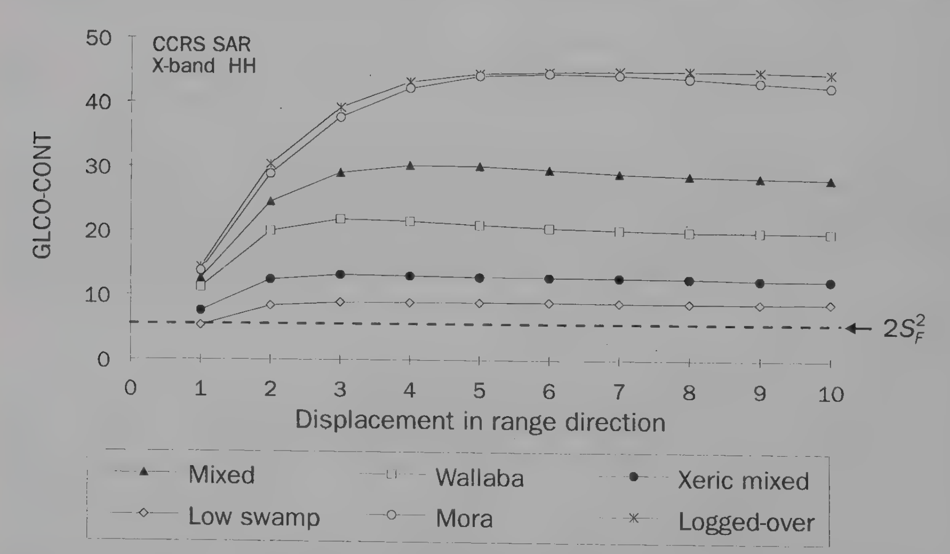



**Figure 6.5** Plots showing the relationship between the GLCO-CONT textural attribute for forest types present in the X-band HH **CCRS SAR** image and the displacement length in range direction. Unlike in Figure 6.3b *the values plotted in this figure were computed from values for GLCO-COR* according to Equation 6.3. The theoretical lower limit value for $\text{GLCO-CONT}[\boldsymbol{d}]$ is equal to $2S_F^2$, i.e. two times the fading (speckle) variance.

**Table 6.4** Gaussian maximum-likelihood classification results. Classification per pixel using $\gamma$ and textural attributes. Textural attributes were computed with the help of a moving spatial window. Input image **CCRS SAR** X-band HH.

| | $\hat{K}$ | $\hat{\sigma}^2_\infty[\hat{K}]$ | Percentage correct | | | | | | | | |
|---|---|---|---|---|---|---|---|---|---|---|---|
| | | | Total | Mixed | Wallaba | Xeric mixed | Low swamp | Mora | Logged-over forest | Secondary forest | Non-forest |
| **Exclusive of Secondary forest and Non-forest** | | | | | | | | | | | |
| $\gamma$ | 0.0102 | 0.0001 | 14 | 4 | 22 | 5 | 17 | 31 | 1 | - | - |
| <u>Window 11x11</u> | | | | | | | | | | | |
| sd($\gamma$) | 0.2381 | 0.0001 | 38 | 42 | 46 | 36 | 92 | 4 | 47 | - | - |
| GLCO-COR[1] | 0.2126 | 0.0001 | 36 | 36 | 44 | 0 | 83 | 0 | 65 | - | - |
| GLCO-CONT[5] | 0.1894 | 0.0001 | 33 | 35 | 40 | 33 | 94 | 8 | 35 | - | - |
| <u>Window 25x25</u> | | | | | | | | | | | |
| GLCO-CONT[5] | 0.3592 | 0.0001 | 48 | 60 | 58 | 26 | 100 | 24 | 43 | - | - |

All textural attributes were computed with a moving window $11 \times 11$ pixels in size. To illustrate the effect of window size, the computation of GLCO-CONT[5] was repeated using a window of $25 \times 25$ pixels. Based on the results of GTA (see section I.5, Appendix I) it is expected that a larger window size results in an improved quantification of textural patterns. However, a larger window will more often enclose image areas with different textures, i.e. image areas corresponding to different cover types. Consequently, the spatial extent of cover types will be defined less accurately when large windows are used. GTA results in section I.5 show that GLCO-CONT[5] yields better textural descriptions than most other GLCO attributes when small window sizes are used. The results of GTA also show that the performance of sd($\gamma$) as a function of window size is comparable to that of GLCO-CONT[5].

Table 6.4 allows a quantitative evaluation of the MWA results. It should be noted that the results of the classifications associated with MWA, in contrast to those associated with GTA, were evaluated using an independent data set, i.e. a data set different from the one used for designing the classifier (see section 5.3.1). The results of a classification per pixel using $\gamma$ are given for reasons of comparison. At the 95% confidence level the overall classification result for $\gamma$ is significantly poorer than that for the textural attributes. Given the window size of $11 \times 11$ pixels, the best overall classification result is obtained when sd($\gamma$) is applied. The performance of sd($\gamma$) is significantly better than that for GLCO-CONT[5] but there is not a significant difference in the performance of sd($\gamma$) and GLCO-COR[1]. Similarly, there is no significant difference in overall result for GLCO-COR[1] and GLCO-CONT[5]. The

increase in window size from $11 \times 11$ to $25 \times 25$ pixels improves the overall results for GLCO-CONT[5] significantly. Like in GTA, it is most difficult to discriminate between Mora and Logged-over forest. Two other classes frequently confused are Low swamp forest and Xeric mixed forest.

Comparison of the results in Table 6.4 with those in Table 6.2 shows that the MWA results are significantly poorer than the GTA results. This agrees with the findings in section I.5 which show that *textural descriptions improve with an increasing window size and are best if image regions are used.* In general, textural decriptions resulting from MWA are less accurate than those resulting from GTA because they are based on considerably less pixel pair realisations (see section 5.1.1). The limited number of pixel pair realisations also make that MWA descriptions are easily disturbed by variations in the architecture of the forest canopy. This can be clarified by taking the Wallaba forest as an example. For the most part, the Wallaba canopy is even, homogeneous and closed. This general appearance causes its overall texture to be different from that of Mixed forest, for example. However, locally the architecture of the Wallaba canopy deviates from 'normal' due to the presence of canopy openings. These canopy openings are sources of textural noise, i.e. they cause the texture to be locally different. The extent to which textural noise shows up in textural descriptions depends on the applied window/region size and attribute. Textural descriptions based on large spatial windows or image regions are less troubled by textural noise because this noise will be mostly averaged out. Similarly, the effects of textural noise will be less disturbing if the applied attribute is less susceptible to noise or, in other words, is more stable.

Texturally enhanced colour composite images provided the basis for a qualitative evaluation of the MWA results. The procedure for creating these images was described in section 5.3.1. Figures V.1 through V.3 in Appendix V illustrate this procedure for two subsets of the X-band HH CCRS SAR image. Image **a** covers the Tropenbos ecological reserve and its surroundings, image **b** covers a part of the logging concession known as West Pibiri. Figure V.1 shows the SAR image, Figure V.2 the texturally transformed image and Figure V.3 the final product, i.e. the RGB transformed colour composite image. All of the images are in ground range format. The texturally transformed image is the result of a MWA using GLCO-CONT[5] and a window size of $11 \times 11$ pixels. In Figure V.3 the areas marked by squares demonstrate the appearance of the forest types studied. Blue colours correspond to low GLCO-CONT[5] values, red colours to high GLCO-CONT[5] values and green/yellow colours to intermediate GLCO-CONT[5] values. The value for GLCO-CONT[5] increases with an increase in canopy roughness. Therefore, blue colours predominate in areas covered by forests with a relatively low degree of canopy roughness, e.g. in areas covered by Low swamp, Wallaba and Xeric mixed forest. For similar reasons, red colours prevail in areas of Logged-over and Mora forest, whereas green/yellow colours are preponderant in Mixed forest areas.

In the present study a number of texturally enhanced colour composite images was visually interpreted to assess their value for forest type mapping. The resulting interpretations were checked in the field and compared with existing maps. It was concluded that *texturally enhanced radar images provided a good basis for visual interpretation aimed at forest type mapping.* However, *Logged-over forest and Mora*

forest have very similar textures. These two forest types *cannot be discriminated other than with the use of contextual information.* Examples of features found in association with Logged-over forests are logging roads and log landings. Mora forests, on the other hand, occur in the vicinity of streams and rivers. By comparing image interpretations checked in the field with the available 1:50,000 forest type map (Guyana Forest Department, 1970) it was found that the map was incorrect at various locations. In fact, the forest type patterns found in the present study proved to agree better with the patterns of the landforms and soils map by van Kekem et al. (1996). Figure V.4 shows the landform/soil map segments for the Tropenbos ecological reserve and the West Pibiri compartment. The resemblance in the patterns on the colour composites in Figure V.3 and the maps in Figure V.4 can be explained from the classical, strong connection between forest type and soil type (see section 4.3.1).

Figures V.5 and V.6 show colour composite images produced from, respectively, a GLCO-COR[1] and a sd($\gamma$) textural transform. Like in the case of GLCO-CONT[5], the employed window size was $11 \times 11$ pixels. Comparison of Figure V.5 with Figure V.3 shows that the images in Figure V.5 have a much noisier appearance. This suggests that GLCO-COR[1] is more sensitive to canopy architecture than GLCO-CONT[5]. Due to this sensitivity, the overall textural differences in Figure V.5 are less pronounced than in Figure V.3. Comparison of Figure V.6 and Figure V.3 shows that sd($\gamma$) is less sensitive to local variations in canopy architecture than GLCO-CONT[5]. Unlike GLCO-CONT[5] and GLCO-COR[1], sd($\gamma$) is not sensitive to the spatial organisation of the pixels, i.e. pattern. The attribute merely describes the average difference in grey level between pixels and their mean. Nevertheless, sd($\gamma$) proves to be well capable of distinguishing between textures of the land cover types studied. It is assumed that this is partly due to the fact that the studied textures lack a directional pattern, i.e. are isotropic.

### 6.1.4 Conclusions

Analysis of the CCRS SAR data leads to the following conclusions.

➤ *Texture, not backscatter is the most important source of information for identifying tropical land cover types in high frequency and high resolution radar images.*

➤ *Using texture, high frequency and high resolution radar images make modest to good bases for region-based classification of tropical land cover types, including primary forest types.*

- In contrast to grey level co-occurrence (GLCO) attributes, the standard deviation of gamma in dB (sd($\gamma$)) is not sensitive to textural pattern. Nevertheless, textural descriptions in the form of individual GLCO attributes and sd($\gamma$) make equally suitable bases for classifying tropical land cover types in high frequency and high resolution radar images.

- Combined use of two or more GLCO attributes results in improved textural descriptions and hence enhances the chances of classifying tropical land cover types correctly.

- The classification potential associated with different GLCO attributes varies widely.

➤ *The combination of gross textural analysis and classification of tropical land cover per region yields better results than the combination of moving window textural analysis and classification per pixel.*

➤ *Texturally enhanced high frequency and high resolution radar images make a good basis for the mapping of tropical primary forest types by means of visual interpretation.*

- Computerised and visual identification of logged-over forest in mono-temporal high frequency and high resolution radar images of Mabura Hill is complicated by the fact that the textural pattern of logged-over forest is very similar to that of Mora forest. This problem may be overcome by using contextual information.

➤ *Both GLCO attributes and sd($\gamma$) can be used to rank cover types according to the degree of canopy roughness.*

- Plots of GLCO-Correlation, GLCO-Contrast and GLD-Mean as a function of displacement length hold information on the dimensions of dominant textural sub-patterns. This information enables the quantification of canopy architectural properties provided that the link between the dominating textural sub-pattern and the prevailing canopy element can be established.

➤ *GLCO-Contrast and semi-variance are essentially the same statistic.*

➤ *The expectation of GLCO-Correlation is equal to the expectation of the autocorrelation coefficient.*

- GLCO-Contrast and GLCO-Correlation, like semi-variance and autocorrelation, are equivalent but complementary descriptors of the spatial interrelations between the grey levels of pixels. GLCO-Contrast and GLCO-Correlation are related through the total variance of the observed set of grey levels.

➤ *The GLCO-Contrast value for homogeneous or textureless regions in radar images is equivalent to two times the fading variance.*

## 6.2 Results of the analysis of the ERS-1 SAR data

The present section reports on the results of the analysis of the SAR data as acquired by the ERS-1 satellite system. The ERS-1 SAR operates in a single frequency

**Table 6.5** Potential of $\bar{\gamma}$, sd($\gamma$) and GLCO attributes for the classification per region of the land cover types studied. The values given represent the number of class pairs that can be successfully discriminated, i.e. the number of class pairs for which $TD_{ij} \geq 1900$.

| | | | GLCO attribute | |
|---|---|---|---|---|
| | $\bar{\gamma}$ | sd($\gamma$) | Best performing | Worst performing |
| **Exclusive of Xeric mixed forest, Secondary forest and Non-forest** (total number of class pairs is equal to 10) | | | | |
| C-band VV, PRI | 0 | 0 | 2 | 0 |
| C-band VV, SLC-av | 0 | 0 | 6 | 0 |
| C-band VV, PRI-av | 0 | 1 | 3 | 0 |
| **Inclusive of Xeric mixed forest, Secondary forest and Non-forest** (total number of class pairs is equal to 28) | | | | |
| C-band VV, PRI | 5 | 0 | 5 | 0 |

and polarization, i.e. C-band VV. In addition to two single date SAR Precision images, a radiometrically enhanced SAR Single Look Complex image as well as a radiometrically enhanced SAR Precision image was studied. The Precision image used for Mabura Hill was acquired on 29 April 1992, that for San José del Guaviare on 26 May 1992. The radiometrically enhanced image products were generated by averaging images from three different acquisition dates (see section 4.4.3). *The aim of the analysis was to assess the value of the different ERS-1 data sets for the classification of land cover and the study of canopy architecture.* The information content associated with the backscatter level is compared to that associated with the textural pattern. Particulars of the analysis of image texture according to the GLCO approach (see section 5.1.1) are discussed in Appendix I.

### 6.2.1 Classification of land cover per region using backscatter and texture

Table 6.5 illustrates the potential of $\bar{\gamma}$, sd($\gamma$) and GLCO attributes for the classification per region of the land cover types studied. The results relate to three different data sets, namely: a single date ERS-1 SAR Precision image (PRI), a time-averaged SAR Single Look Complex image (SLC-av) and a time-averaged SAR Precision image (PRI-av) (see section 4.4.3). The values shown represent the number of class pairs that can be successfully discriminated, i.e. the number of class pairs for which $TD_{ij} \geq 1900$ (see section 5.2.4).

The SLC-av data set proves most suitable for use in a textural analysis. The best performing GLCO attribute derived from this image can both in the absolute and the relative sense discriminate the most class pairs (six out of 10). This finding confirms the hypothesis that the image with the highest spatial resolution contains most textural information and will thus be best suited for analysis of texture (see section 4.4.3). *The second-order GLCO statistics offer a better potential for classification*

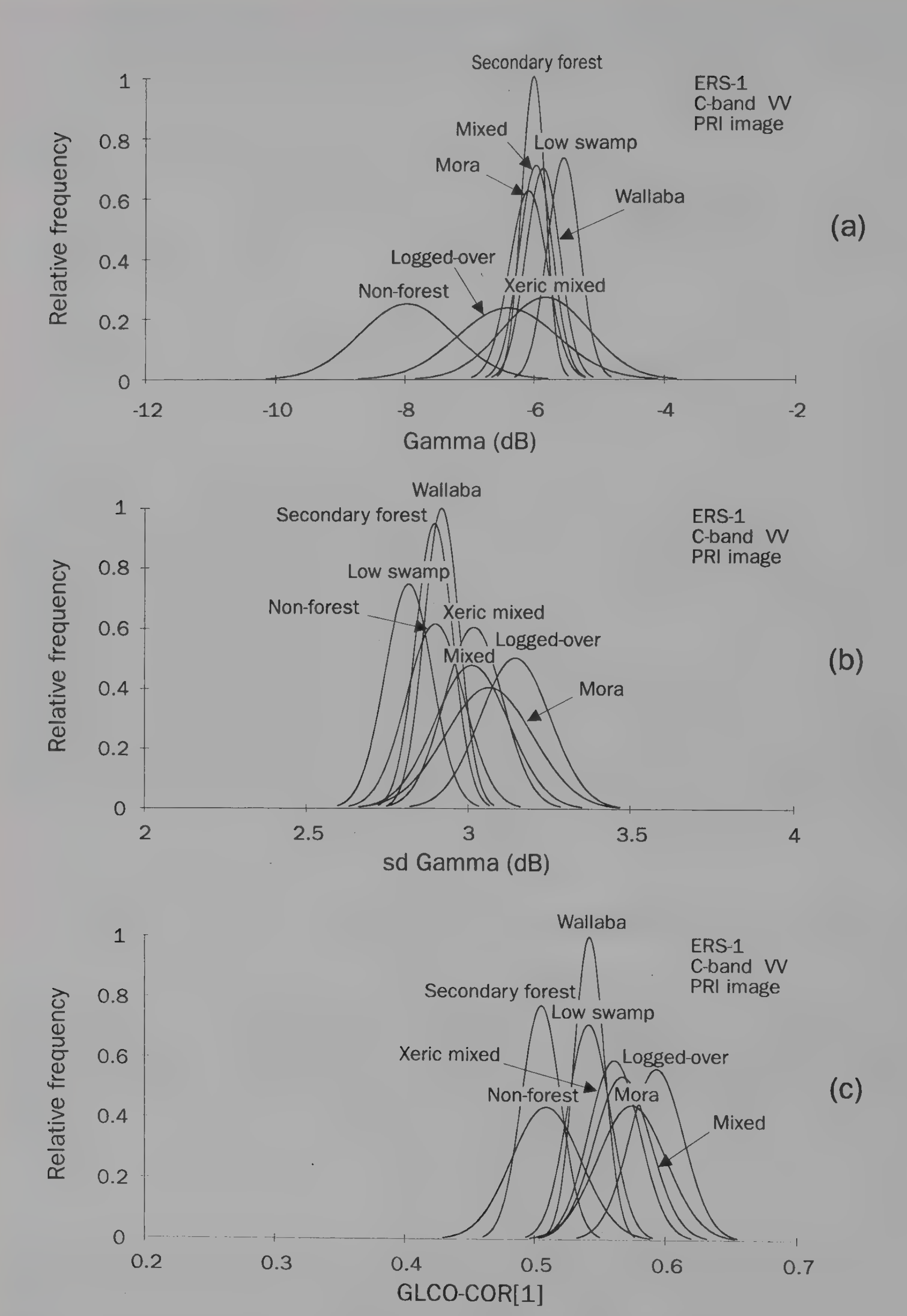



**Figure 6.6 (a-d)** Gaussian approximations of pdf's for region averaged radiometric and textural attributes associated with land cover types present in the **ERS-1 C-band VV PRI** image: (**a**) pdf's for $\bar{\gamma}$ (**b**) pdf's for sd($\gamma$) (**c**) pdf's for GLCO-COR[1] (**d**) pdf's for GLCO-CONT[5].

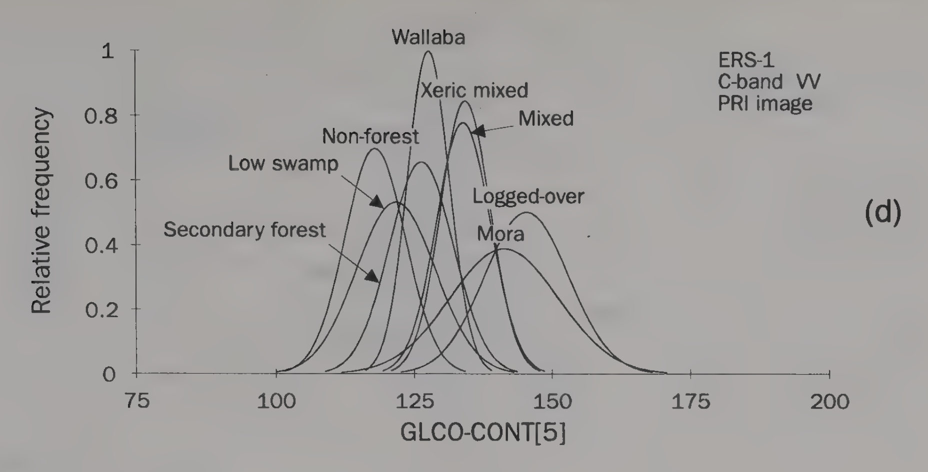



**Figure 6.6** Continued.

*than the first-order statistic* sd($\gamma$). A similar discrepancy in the performance of first- and second-order textural descriptors was not found in the analysis of the CCRS SAR data (see Table 6.1). Like in the case of the CCRS SAR data there is a distinct difference in the performance of the best and worst performing GLCO attribute.

The classification potential of $\bar{\gamma}$ appears to be low. However, in the case of the PRI image when data for all classes are included, its classification potential matches that of the best performing GLCO attribute. In this particular data set both $\bar{\gamma}$ and the best performing GLCO attribute can discriminate five out of 28 class pairs. In the CCRS SAR C-band VV data set $\bar{\gamma}$ could also distinguish between five out of 28 class pairs. However, in this case the performance of the best performing GLCO attribute was much better since it could discriminate 16 out of 28 class pairs (see Table 6.1). In the ERS-1 PRI images the textural differences between the land cover types studied are obviously much smaller than in the CCRS SAR images. Table 6.5 shows that *averaging of PRI images from different acquisition dates does not result in an image with a much higher textural information content.* The performance of the best GLCO attribute associated with the SLC-av data can be shown to be comparable to that of the best GLCO attribute associated with the C-band VV CCRS SAR data. In general, however, the performance of GLCO attributes derived from the SLC-av data is considerably poorer. On average, GLCO attributes derived from the SLC-av data can discriminate 1.7 out of 10 class pairs; those associated with the C-band VV CCRS SAR data can distinguish 4.2 out of 10 class pairs.

Figure 6.6 illustrates the discriminating capacities of four attributes associated with ERS-1 PRI image regions, namely $\bar{\gamma}$, sd($\gamma$), GLCO-COR[1] and GLCO-CONT[5]. Likewise, Figure 6.7 depicts the discriminating capacities of attributes computed from the ERS-1 SLC-av data. Figure 6.7 does not show pdf's for $\bar{\gamma}$, since these are similar to the ones shown in Figure 6.6. After all, the PRI and SLC-av image have comparable radiometric characteristics. These two images possess different spatial properties only (see section 4.4.3). The pdf's for attributes associated with the

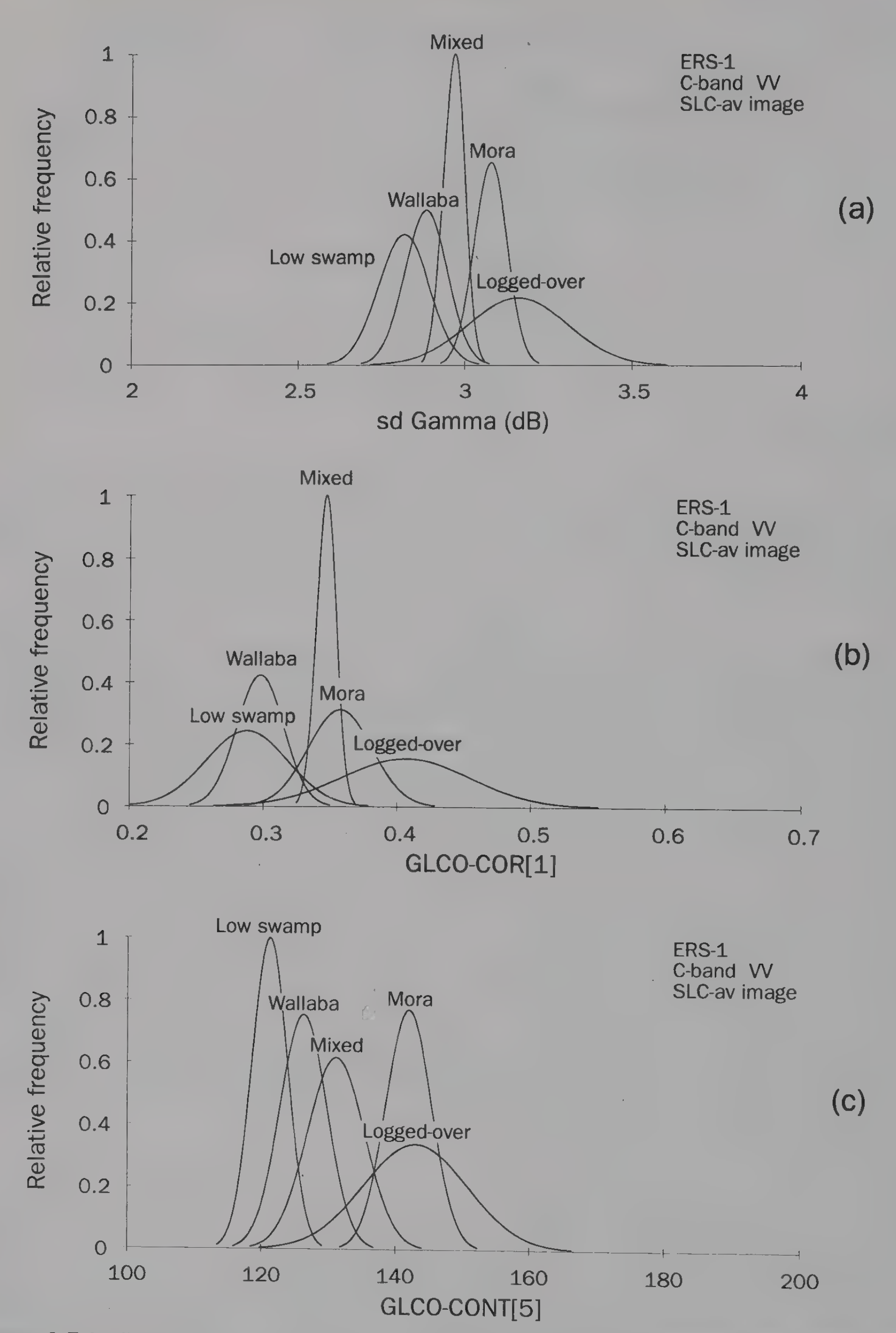



**Figure 6.7 (a-d)** Gaussian approximations of pdf's for region averaged radiometric and textural attributes associated with land cover types present in the **ERS-1 C-band VV SLC-av** image: (**a**) pdf's for sd($\gamma$) (**b**) pdf's for GLCO-COR[1] (**c**) pdf's for GLCO-CONT[5] (**d**) pdf's for GLD-ASM[9].

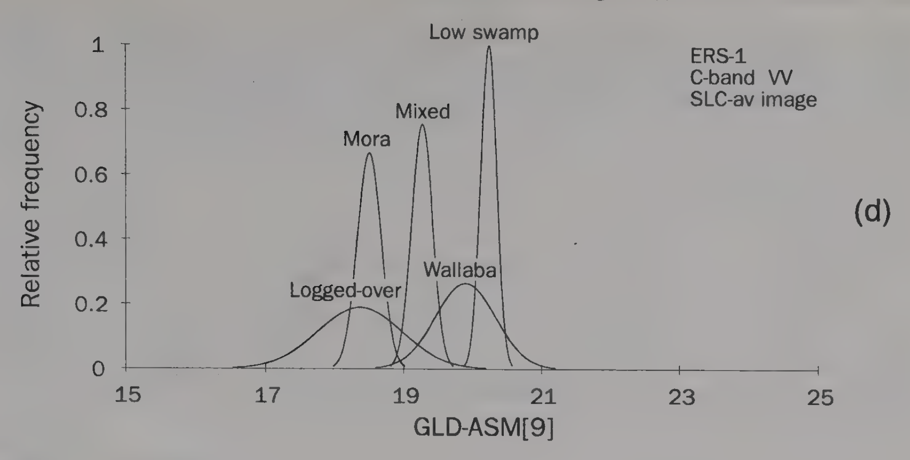



**Figure 6.7** Continued.

PRI-av image are not shown since their mutual positions are very much like those shown in Figure 6.6. It was chosen to present the pdf's for GLCO-COR[1] and GLCO-CONT[5] in order to allow for comparison with Figure 6.2. Figure 6.7 also shows the pdf's for GLD-ASM[9] since this attribute is best performing for the SLC-av image. GLCO-CONT[5], although not the best performing attribute associated with the PRI image does in fact represent the capacities of GLCO attributes for this data set very well. Just like 80 (out of 90) other attributes, it cannot discriminate any of the class pairs studied. The best performing attribute distinguishes between five out of 28 class pairs. Furthermore, there are nine GLCO attributes that can discriminate just one class pair. GLCO-COR[1] is among these, it can successfully discriminate between Secondary forest and Logged-over forest.

In Figure 6.6 the pdf's can be seen to have much overlap. This is indicative of the poor classification capabilities of the attributes in question. The pdf's for $\overline{\gamma}$ overlap the least; the pdf for Non-forest is well separated from those for most other classes. When compared to Figures 6.6b, 6.6c and 6.6d the pdf's shown in Figure 6.7 show less overlap. *The higher spatial resolution of the SLC-av image results in higher textural information content and causes the classes to be separated more easily with the help of textural attributes.* GLD-ASM[9] can more easily discriminate the various classes than either GLCO-COR[1] or GLCO-CONT[5]. Likewise, GLCO-COR[1] can more easily distinguish between classes than GLCO-CONT[5]. The pdf's in Figures 6.7a, 6.7b and 6.7c are confined to a narrower range and have more overlap than those associated with the CCRS SAR C-band VV image (see Figure 6.2). This fits the general perception that high resolution images are more suited for use in textural analysis than low resolution images.

Comparison of Figures 6.6a and 6.2a shows that the relative positions of the pdf's for Non-forest, Secondary forest and Mixed forest in the CCRS SAR data set differ from those in the ERS-1 PRI data set. In the CCRS SAR data set the $\overline{\gamma}$ for Non-forest matches the $\overline{\gamma}$ for Mixed forest, whereas the $\overline{\gamma}$ for Secondary forest exceeds the $\overline{\gamma}$ for Mixed forest by ca. 4 dB. In the ERS-1 PRI data set the $\overline{\gamma}$ for Non-forest is

**Table 6.6** Gaussian maximum-likelihood classification results. Classification based on radiometric and textural attributes computed per region from **ERS-1** images.

| | | | Percentage correct | | | | | | | | |
|---|---|---|---|---|---|---|---|---|---|---|---|
| | $\hat{K}$ | $\hat{\sigma}^2_\infty[\hat{K}]$ | Total | Mixed | Wallaba | Xeric mixed | Low swamp | Mora | Logged-over forest | Secondary forest | Non-forest |
| **Exclusive of Xeric mixed forest, Secondary forest and Non-forest** | | | | | | | | | | | |
| C-band VV, PRI | | | | | | | | | | | |
| $\bar{\gamma}$ | 0.3930 | 0.0078 | 51 | 60 | 40 | - | 86 | 30 | 50 | - | - |
| sd($\gamma$) | 0.3649 | 0.0071 | 49 | 30 | 70 | - | 86 | 0 | 70 | - | - |
| GLCO-COR[1] | 0.3316 | 0.0069 | 47 | 60 | 70 | - | 29 | 0 | 70 | - | - |
| GLCO-CONT[5] | 0.3580 | 0.0074 | 49 | 50 | 60 | - | 57 | 0 | 80 | - | - |
| GLD-ASM[9] | 0.3847 | 0.0073 | 51 | 30 | 80 | - | 57 | 10 | 80 | - | - |
| C-band VV, SLC-av | | | | | | | | | | | |
| sd($\gamma$) | 0.5833 | 0.0210 | 67 | 100 | 33 | - | 67 | 100 | 33 | - | - |
| GLCO-COR[1] | 0.5833 | 0.0221 | 67 | 100 | 67 | - | 67 | 33 | 67 | - | - |
| GLCO-CONT[5] | 0.5000 | 0.0238 | 60 | 67 | 33 | - | 67 | 100 | 33 | - | - |
| GLD-ASM[9] | 0.8333 | 0.0117 | 87 | 100 | 67 | - | 100 | 100 | 67 | - | - |
| C-band VV, PRI-av | | | | | | | | | | | |
| sd($\gamma$) | 0.4443 | 0.0080 | 55 | 40 | 60 | - | 86 | 60 | 40 | - | - |
| GLCO-COR[1] | 0.2627 | 0.0060 | 40 | 0 | 10 | - | 71 | 80 | 50 | - | - |
| GLCO-CONT[5] | 0.4698 | 0.0079 | 57 | 60 | 70 | - | 86 | 50 | 30 | - | - |
| GLD-ASM[9] | 0.5494 | 0.0075 | 64 | 70 | 70 | - | 86 | 50 | 50 | - | - |
| **Inclusive of Xeric mixed forest, Secondary forest and Non-forest** | | | | | | | | | | | |
| C-band VV, PRI | | | | | | | | | | | |
| $\bar{\gamma}$ | 0.3094 | 0.0036 | 39 | 0 | 40 | 0 | 86 | 10 | 30 | 60 | 91 |
| sd($\gamma$) | 0.2243 | 0.0031 | 32 | 0 | 60 | 50 | 86 | 0 | 50 | 30 | 0 |
| GLCO-COR[1] | 0.2805 | 0.0032 | 37 | 20 | 70 | 25 | 14 | 0 | 70 | 90 | 0 |
| GLCO-CONT[5] | 0.2924 | 0.0032 | 38 | 0 | 50 | 63 | 0 | 0 | 80 | 10 | 91 |
| GLD-ASM[9] | 0.2630 | 0.0033 | 36 | 30 | 70 | 0 | 57 | 10 | 80 | 40 | 0 |

**Table 6.7** Gaussian maximum-likelihood classification results. Classification based on radiometric and textural attributes computed per region from **CCRS SAR** images.

| | $\hat{K}$ | $\hat{\sigma}^2_\infty[\hat{K}]$ | Percentage correct: Total | Mixed | Wallaba | Xeric mixed | Low swamp | Mora | Logged-over forest | Secondary forest | Non-forest |
|---|---|---|---|---|---|---|---|---|---|---|---|
| **Exclusive of Xeric mixed forest, Secondary forest and Non-forest** | | | | | | | | | | | |
| C-band VV | | | | | | | | | | | |
| $\bar{\gamma}$ | 0.3787 | 0.0086 | 51 | 20 | 27 | - | 100 | 50 | 82 | - | - |
| sd($\gamma$) | 0.6244 | 0.0063 | 70 | 80 | 100 | - | 100 | 90 | 0 | - | - |
| GLCO-COR[1] | 0.6251 | 0.0064 | 70 | 70 | 91 | - | 100 | 100 | 9 | - | - |
| GLCO-CONT[5] | 0.6511 | 0.0062 | 72 | 90 | 100 | - | 100 | 80 | 9 | - | - |
| GLD-ASM[9] | 0.6509 | 0.0063 | 72 | 80 | 100 | - | 100 | 90 | 9 | - | - |
| **Inclusive of Xeric mixed forest, Secondary forest and Non-forest** | | | | | | | | | | | |
| C-band VV | | | | | | | | | | | |
| $\bar{\gamma}$ | 0.2584 | 0.0034 | 35 | 0 | 27 | 25 | 80 | 50 | 64 | 50 | 16 |
| sd($\gamma$) | 0.4725 | 0.0037 | 54 | 80 | 73 | 0 | 100 | 90 | 0 | 75 | 32 |
| GLCO-COR[1] | 0.3568 | 0.0033 | 42 | 70 | 18 | 50 | 100 | 100 | 9 | 63 | 5 |
| GLCO-CONT[5] | 0.4465 | 0.0037 | 51 | 90 | 55 | 25 | 100 | 80 | 9 | 63 | 26 |
| GLD-ASM[9] | 0.3846 | 0.0034 | 45 | 80 | 18 | 100 | 100 | 90 | 9 | 63 | 5 |

ca. 2 dB lower than the $\bar{\gamma}$ for Mixed forest, whereas the $\bar{\gamma}$'s for Secondary forest and Mixed forest match. The situation in the ERS-1 PRI data set is comparable to the one in the C-band VV NASA/JPL AIRSAR data set (see Figure 6.14c). Hence, it is concluded that in the CCRS SAR data set the backscatter levels for Non-forest and Secondary forest are exceptionally high. The generally acknowledged high radiometric accuracy of the ERS-1 data supports this conclusion (e.g. Laur et al., 1993).

Unlike the data for the primary forest types, the data for Non-forest and Secondary forest were not obtained from the images for Mabura Hill but from the images for San José del Guaviare (see sections 4.1.1, 4.1.2). The high CCRS SAR C-band VV backscatter values for Non-forest and Secondary forest with respect to Mixed forest suggest a discrepancy in the absolute calibration of the two image data sets. Rainfall data indicate that the conditions at the time of the CCRS SAR data acquisition were moister in San José del Guaviare than in Mabura Hill (see Table 4.2 and Table 4.3). This may have enhanced the backscatter levels for Non-forest and Secondary forest, but cannot explain an apparent increase in backscatter of the order of 2 to 4 dB.

Table 6.6 shows the classification results for a selection of radiometric and textural attributes derived from the three types of ERS-1 images. For reasons of comparison, Table 6.7 does the same for attributes derived from the CCRS SAR C-band VV image.

The results in Table 6.6 show that *at the 95% confidence level $\bar{\gamma}$ and the PRI derived textural attributes perform equally well.* Moreover, there is no significant difference in the performance of $\bar{\gamma}$ and that of the textural attributes associated with the PRI-av data set. From the textural attributes computed for the SLC-av data, only GLD-ASM[9] performs significantly better than $\bar{\gamma}$. This attribute also performs significantly better than any of the PRI and PRI-av derived textural attributes. However, at the 95% confidence level the difference in the classification results for GLD-ASM[9] and the other SLC-av associated textural attributes is not significant. This results primarily from the considerable variance of the KHAT statistic, which, in turn, is due to the limited number of data points in the SLC-av data set. Textural attributes computed for the PRI and PRI-av data sets perform equally well. It may thus be concluded that radiometric enhancement of PRI images does not significantly improve the possibilities for textural classification.

Comparison of Tables 6.6 and 6.7 shows that most of the PRI derived textural attributes have a significantly *poorer* classification capacity than the CCRS SAR derived textural attributes. The performance of most textural attributes computed for the SLC-av and PRI-av data is not significantly different from that of the C-band VV CCRS SAR associated textural attributes (exclusive of Xeric mixed forest, Secondary forest and Non-forest). The CCRS SAR derived $\bar{\gamma}$ values are shown to be considerably less suited for classifying Non-forest than ERS-1 PRI derived $\bar{\gamma}$ values. This difference in classification capacity can be explained from the earlier noted relatively high backscatter levels for Non-forest in the CCRS SAR data set. Moreover, the backscatter level for Non-forest is much more variable in the CCRS SAR data set than in the ERS-1 PRI data set. The backscatter levels for the other cover types vary accordingly. The high variability of the CCRS SAR derived backscatter values results from a more variable incidence angle. In the CCRS SAR data set the incidence angle ranges from 30° to 60°; in the ERS-1 data set from 20° to 25°.

Like the results for the CCRS SAR (see section 6.1.1), the results for ERS-1 indicate that Logged-over and Mora forest are among the classes most difficult to discriminate. The percentage of correctly classified Mora regions in the SLC-av data set often equals 100%, but a considerable proportion of the Logged-over class will be classified as Mora forest. Wallaba forest is frequently confused with Low swamp forest and Mixed forest because of its intermediary texture. Generally speaking, the inclusion of additional classes results in more confusion between classes and hence yields poorer classification results. In Table 6.6 this is illustrated by the classification of the ERS-1 PRI data set without and with inclusion of data points for Xeric mixed forest, Secondary forest and Non-forest. Inclusion of data points for these classes in the SLC-av data set can therefore also be expected to lead to poorer classifications. It follows that a reduction in the number of classes may have the opposite effect: it may enhance the classification results. Depending on the objective of the study, one may, for example, decide to group all primary forest data points into one class. This results in a data set that requires a lower level of classification. The effects of

**Table 6.8** Gaussian maximum-likelihood classification results. Classification based on radiometric and textural attributes computed per region from **ERS-1** images. Different primary forest types are not distinguished but grouped into one class.

| | $\hat{K}$ | $\hat{\sigma}^2_\infty[\hat{K}]$ | Percentage correct | | | | |
|---|---|---|---|---|---|---|---|
| | | | Total | Primary forest | Logged-over forest | Secondary forest | Non-forest |
| **C-band VV, PRI** | | | | | | | |
| $\bar{\gamma}$ | 0.2958 | 0.0056 | 49 | 38 | 30 | 70 | 91 |
| sd($\gamma$) | 0.1405 | 0.0034 | 32 | 16 | 70 | 80 | 18 |
| GLCO-COR[1] | 0.4807 | 0.0057 | 66 | 69 | 80 | 90 | 18 |
| GLCO-CONT[5] | 0.3510 | 0.0049 | 50 | 29 | 90 | 60 | 91 |
| GLD-ASM[9] | 0.1752 | 0.0037 | 34 | 18 | 80 | 70 | 27 |
| $\bar{\gamma}$ + sd($\gamma$) | 0.4584 | 0.0055 | 61 | 44 | 70 | 90 | 91 |
| $\bar{\gamma}$ + GLCO-COR[1] | 0.8144 | 0.0034 | 88 | 82 | 90 | 100 | 100 |

grouping on the classification results for data derived from the ERS-1 PRI image are shown in Table 6.8. Moreover, this table illustrates the results of two classifications that use a combination of $\bar{\gamma}$ and a textural attribute.

The grouping of the primary forest classes has resulted in better overall classification results for $\bar{\gamma}$, GLCO-COR[1] and GLCO-CONT[5]. In the case of $\bar{\gamma}$ the grouping has not improved the classification results for Logged-over forest and Non-forest. *Both the textural attributes and $\bar{\gamma}$ have difficulty in distinguishing between Logged-over and primary forest.* In classifications based on $\bar{\gamma}$ Logged-over forest is frequently classified as primary forest, whereas in classifications based on texture, primary forest is often classified as Logged-over forest. Similarly, $\bar{\gamma}$ and textural attributes other than GLCO-COR[1] have *difficulty to discriminate between primary forest and Secondary forest.* Primary forest data points are often contributed to the Secondary forest class.

Combined use of $\bar{\gamma}$ and sd($\gamma$) or GLCO-COR[1] yields improved classification results. The results associated with $\bar{\gamma}$ + sd($\gamma$) are significantly better than those for sd($\gamma$) and GLD-ASM[9]. $\bar{\gamma}$ in combination with GLCO-COR[1] performs significantly better than all other attributes, including $\bar{\gamma}$ + sd($\gamma$). In classifications based on $\bar{\gamma}$ + GLCO-COR[1] all Non-forest and Secondary forest data points are correctly classified. Moreover, primary forests are no longer confused with Secondary forests. However, there is still confusion between primary forest and Logged-over forest. The result associated with $\bar{\gamma}$ + GLCO-COR[1] is a good result but one should bear in mind that it is obtained by classifying data extracted from image regions. In the present study it was possible to define these regions with the help of ground reference data (see section 5.2.1). However, in many practical situations such data may not be available. Under such circumstances, a region-based approach is feasible only if one

is able to delimit regions of interest with the help of automated image segmentation techniques. In this case, the success of the applied segmentation technique will govern the success of the classification.

*Computerised definition of Logged-over forest regions will be problematic since these regions are far from homogeneous and do not usually have clear boundaries. Attempts to segment areas of primary forest into regions representing different forest types will meet similar problems.* Tropical rain forests do not generally consist of a collection of homogeneous, well-defined forest types with distinct boundaries. A high variability in species composition and architecture, the presence of transitional forest types as well as of transitions between forest types are more characteristic. This not only poses problems for mapping tropical rain forest types by means of remotely sensed images, but also for mapping methods based on data from forest inventories. These problems motivated van Rompaey (1993) to develop a technique to map the gradual changes (gradients) in the species composition of West African rain forests. The technique is based on data from forest inventories and provides an alternative to mapping by forest types.

### 6.2.2 Analysis of canopy architecture using GLCO textural attributes

In section 6.1.2, GLCO-CONT was shown to be among the GLCO attributes most sensitive to canopy architecture. The architectural properties of the observed canopy are reflected in plots that show the changes in GLCO-CONT as a function of displacement length. Figure 6.8 shows the GLCO-CONT plots for the cover types present in the ERS-1 PRI, PRI-av and SLC-av data sets. The plots for the ERS-1 PRI and PRI-av image result from computations with displacement in range direction. In association with the SLC-av image, two plots are shown, i.e. one for each displacement direction. The two SLC-av plots show the canopy architectural properties at different measurement scales since the pixel size in range direction is around two times the pixel size in azimuth direction (see Table 4.8). The PRI and PRI-av image consist of pixels with identical sizes. Consequently, the corresponding GLCO-CONT plots show the architectural characteristics at identical measurement scales. However, the measurement scales of these plots differ from those of the SLC-av plots. In each figure, the level of contrast or semi-variance resulting from the presence of image speckle $2S_F^2$ is indicated. This level is equivalent to 14.89 dB for the 3 look ERS-1 PRI and SLC-av images and 4.43 dB for the 9 look PRI-av data. The lower speckle level in the PRI-av data is reflected in the relatively low GLCO-CONT values; less speckle implies less variation in grey levels and thus less grey level contrast.

The plots in Figures 6.8a through 6.8d show that all of the GLCO-CONT[1] and some of the GLCO-CONT[2] values are lower than the theoretical lower limit of $2S_F^2$ (see section 6.1.2). *Apparently, the variation in the grey levels of neighbouring pixels is lower than the speckle variance. This suggests that these pixels do not represent independent radar measurements.* The relationship between the grey levels of adjoining pixels in ERS-1 images may be explained by the ERS-1 image

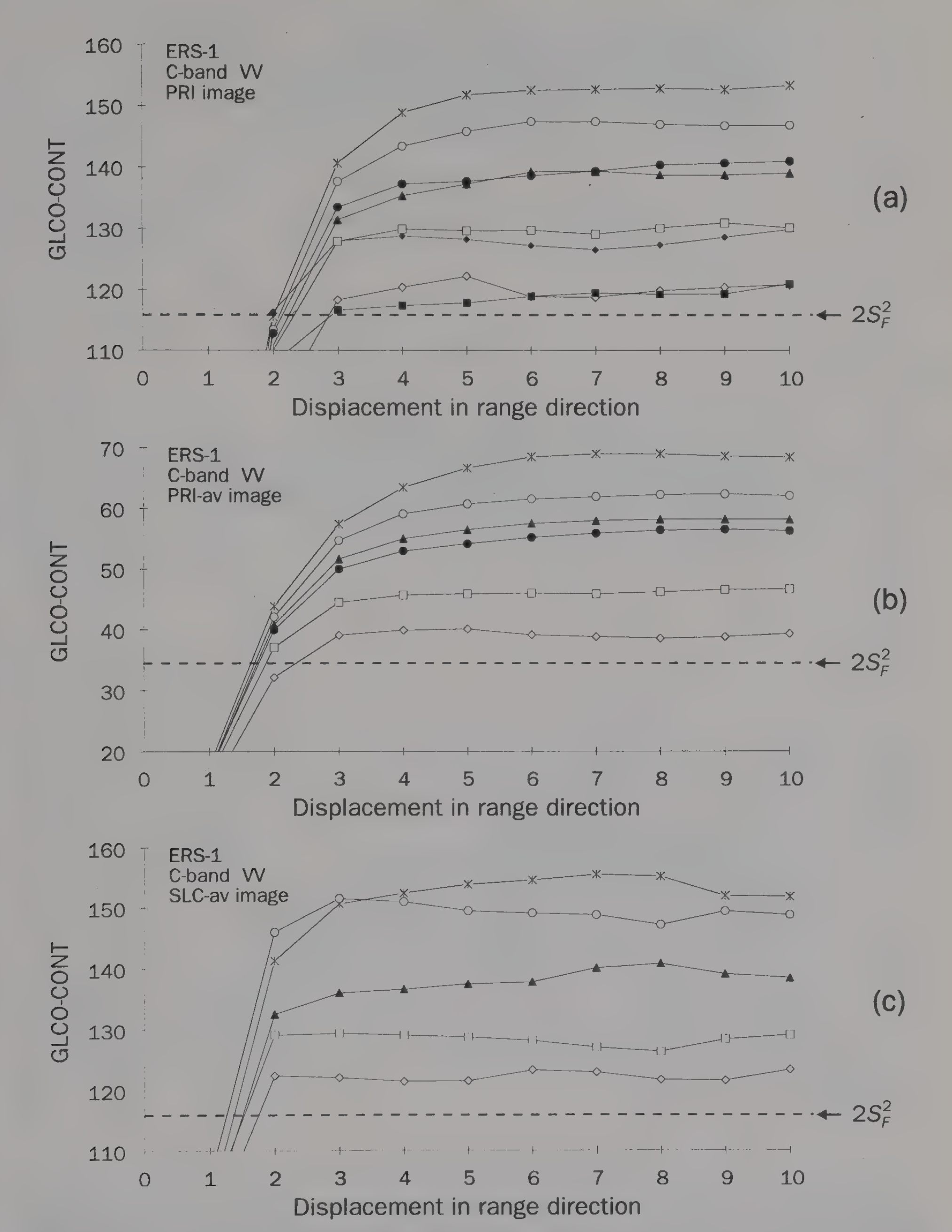



**Figure 6.8 (a-d)** Plots showing the relationship between the GLCO-CONT textural attribute for land cover types present in the **ERS-1 SAR** image data sets and the displacement length: (**a**) plots associated with PRI image (**b**) plots associated with PRI-av image (**c**) plots associated with SLC-av image, displacement is in range direction (**d**) plots associated with SLC-av image, displacement is in azimuth direction.

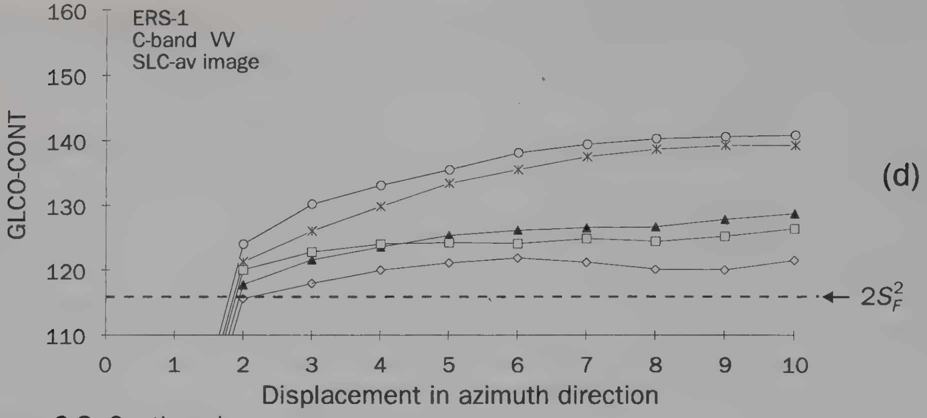



**Figure 6.8** Continued.

specifications in Table 4.8. According to this table the range resolution of a PRI image is ca. 33 m, however, the pixel size in range direction is only 12.5 m. This implies that the measurement of a single resolution cell contributes to the grey levels of ca. 2.6 adjoining pixels in range direction. As a result, all ERS-1 PRI pixels with an inter-pixel spacing less than 2.6 pixels will have related grey values. This agrees with the fact that the values for GLCO-CONT in Figure 6.8a do not exceed the $2S_F^2$ value, i.e. are not independent, if the displacement is less than 3 pixels.

The sizes of the pixels in the PRI-av image are identical to those of the pixels in the PRI image. However, the $2S_F^2$ line crosses the GLCO-CONT plots in Figure 6.8b at a shorter displacement length than those in Figure 6.8a. This suggests that the pixel values in the PRI-av are not as spatially correlated as those in the PRI image. The added variance between the pixels in the PRI-av image results from the fact that this image was created through the averaging of a series of three PRI images (see section 4.4.3). The sizes of the pixels in the SLC-av image differ from those in the PRI and PRI-av image. According to Table 4.8 the pixel size of a ERS-1 SLC image, and thus of the employed SLC-av image, is 7.9 m in range direction and 4.0 m in azimuth direction. The range and azimuth resolution are of the order of 10 m. Hence, the measurement of a single resolution cell contributes to the grey levels of ca. 1.3 pixels in range direction and of ca. 2.5 pixels in azimuth direction. Like in the case of the PRI-av image, the interrelationship of the pixels in the SLC-av image is affected by the averaging process involved in its production (see section 4.4.3). Nevertheless, Figures 6.8c and 6.8d show a difference in the spatial dependence of SLC-av pixels in range and azimuth direction.

In comparison to the GLCO-CONT plots as computed from the CCRS SAR data, those as computed from the ERS-1 data are less well defined. This is due to the high degree of variability in the GLCO-CONT values for particular cover types. The variability in the ERS-1 PRI and SLC-av associated GLCO-CONT values for Logged-over forest and Low swamp forest (two cover types with an extreme difference in canopy roughness) is illustrated in Figures 6.9a and 6.9b. The areas represent 95%

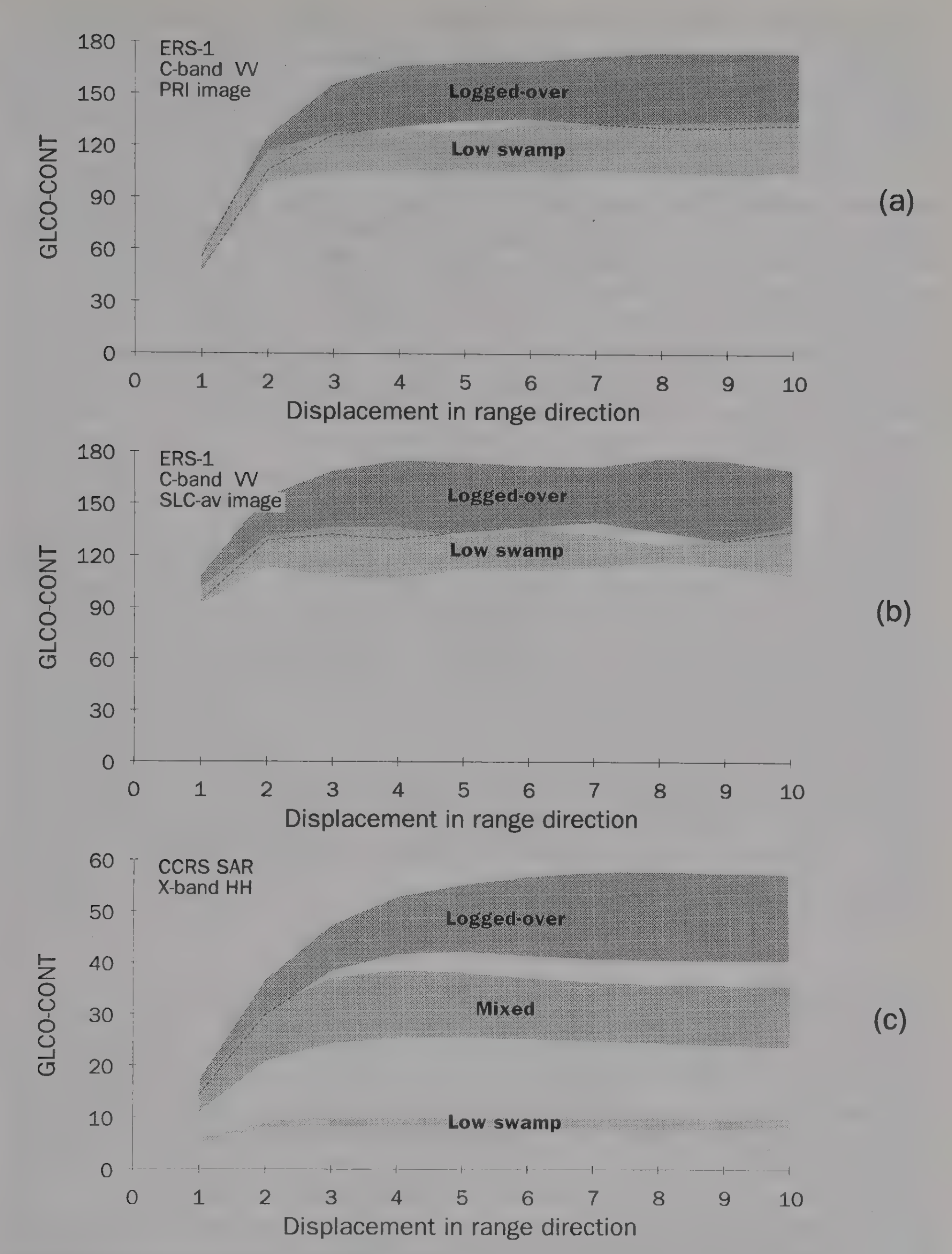



**Figure 6.9 (a-c)** Illustration of differences in the degree of within class and between class variability for GLCO-CONT values associated with (**a**) ERS-1 PRI image data (**b**) ERS-1 SLC-av image data and (**c**) X-band HH CCRS SAR image data. The areas shown represent 95% confidence intervals; the interrupted line marks the boundary of the confidence interval for Logged-over forest. In the case of the ERS-1 image data the confidence intervals overlap even for the two cover types with the most extreme difference in canopy roughness, i.e. Logged-over forest and Low swamp forest.

confidence intervals. For reasons of comparison, Figure 6.9c depicts the variability in the CCRS SAR derived GLCO-CONT values for Logged-over, Mixed and Low swamp forest. *The variability in the GLCO-CONT values associated with the ERS-1 images is so high that even the confidence intervals overlap for the two cover types with the most extreme difference in canopy roughness.* Clearly, the confidence intervals for the other cover types will also overlap. The CCRS SAR derived GLCO-CONT values are much less variable. The differences in the variability of the CCRS SAR and ERS-1 derived GLCO-CONT values are reflected in the classification results in section 6.1.1 and 6.2.1. The higher the variability within the cover types, the poorer the classification results.

The high variability in the ERS-1 derived GLCO-CONT values has to be kept in mind when interpreting the plots in Figure 6.8. Many of the plots in this figure do not reach a maximum value within the adopted range of displacement lengths (e.g. Logged-over, Mixed and Non-forest in PRI image; Mora, Mixed, Xeric mixed and Wallaba in PRI-av image; all plots in SLC-av image with azimuth displacement). This indicates the absence of a dominant textural sub-pattern. Other plots are essentially flat (e.g. Low swamp in PRI-av; Low swamp and Wallaba in SLC-av with range displacement), exhibiting a behaviour similar to the expectation for random data (see Woodcock et al., 1988). Based on the ERS-1 PRI GLCO-CONT plots, the cover types rank in the following order of increasing canopy roughness: Non-forest, Low swamp, Secondary forest, Wallaba, Xeric mixed/Mixed, Mora, Logged-over. A ranking based on the plots as derived from the PRI-av or SLC-av data leads to a comparable sequence. The arrangement also agrees with the one found in association with the CCRS SAR data (section 6.1.2) as well as with the available ground reference data (section 4.3). *Although the ERS-1 PRI(-av), ERS-1 SLC-av and CCRS SAR plots relate to different measurement scales, the canopy roughness appears to present itself in a similar fashion. Canopy roughness has been identified as an indicator of species diversity* by Oldeman (1983a), Brünig and Huang (1989) and Brünig and Mohren (1989).

### 6.2.3 Textural analysis by means of a moving window

The common methodology for Moving Window textural Analysis (MWA) and the evaluation of the MWA results was described in section 5.3.1. This section discusses the particulars and results of the MWA's carried out using the ERS-1 PRI and SLC-av images. The ERS-1 results were evaluated qualitatively, i.e. by means of visual interpretation of texturally enhanced colour composite images. Texture was computed using GLCO-CONT[5]. For the ERS-1 PRI image the window was 11x11 pixels in size, for the ERS-1 SLC-av image 11x33 pixels (11 in range, 33 in azimuth). The corresponding area on the ground is comparable since the azimuth pixel size of the SLC-av image is roughly 1/3 of the azimuth pixel size of the PRI image (see Table 4.8).

Figure V.7 in Appendix V shows two texturally enhanced colour composite images for the West Pibiri compartment. Figure V.7a was produced from the texturally transformed ERS-1 PRI image, Figure V.7b from the texturally transformed ERS-1

SLC-av image. The area shown overlaps with the area as shown in the images **b** of Figures V.1 through V.6. The marked Wallaba and Mora forest regions in Figure V.7 and Figures V.3b, V.5b, V.6b correspond approximately to the same area on the ground. The significance of the colours in Figure V.7 conforms to the colours in Figure V.3 (see section 6.1.3).

Compared to the images in Figure V.7a, those in Figure V.7b show better defined textural patterns. The higher textural information content of the ERS-1 SLC-av image is in agreement with the findings of GTA (see section 6.2.1). Yet, the textural information content of this image is not sufficient for forest type mapping. Patterns and/or forest types readily recognised in the texturally transformed CCRS SAR X-band HH image (Figures V.3b, V.5b and V.6b) can only be recognised with difficulty in Figure V.7b. *Texture in ERS-1 images should be interpreted with care as a large proportion of the coarse textures results from relief rather than from canopy architecture.*

### 6.2.4 Conclusions

Analysis of the ERS-1 SAR data leads to the following conclusions.

➤ *Texture and backscatter are equivalent sources of information for identifying tropical land cover types in single date and time-averaged ERS-1 SAR Precision (PRI) images.*

➤ *Single date and time-averaged ERS-1 SAR PRI images make modest bases for region-based classification of tropical land cover at the level of primary forest, logged-over forest, secondary forest and non-forest.*

➤ *Single date and time-averaged ERS-1 SAR PRI images make poor bases for region-based classification of tropical land cover at the level of primary forest types.*

- Compared to single date and time-averaged ERS-1 SAR PRI images, time-averaged ERS-1 SAR Single Look Complex (SLC) images have higher textural information contents.

- Using texture, time-averaged ERS-1 SAR SLC images make modest bases for region-based classification of tropical land cover at the level of primary forest types.

- Grey level co-occurrence (GLCO) attributes make better bases for classifying tropical land cover types in ERS-1 images than the standard deviation of gamma in dB (sd($\gamma$)).

- The classification potential associated with different GLCO attributes varies widely.

- ➤ *Texturally enhanced single date ERS-1 SAR PRI and time-averaged ERS-1 SAR SLC images make an inadequate basis for the mapping of tropical primary forest types by means of visual interpretation.*

- A large proportion of the coarse textures in ERS-1 SAR images results from relief rather than from canopy architecture.

- ➤ *Canopy roughness, which has been identified as an indicator of species diversity by Oldeman (1983a), Brünig and Huang (1989) and Brünig and Mohren (1989), presents itself in a similar fashion in the texture of high frequency radar images with differing measurement scales.*

## 6.3 Results of the analysis of the NASA/JPL AIRSAR data

The present section reports on the results of the analysis of the data as acquired by the NASA/JPL airborne SAR system. The NASA/JPL AIRSAR is an example of a polarimetric radar system and operates in three frequency bands, i.e. C-, L- and P-band (see section 4.4.2). *The aim of the analysis was to assess the value of the different frequency bands and polarizations for the classification of land cover and the estimation of biomass and architectural parameters. The study makes use of information contained in the strength, polarization and phase of the radar return signal.* The textural information content of the AIRSAR images was not studied in detail. However, visual comparison of C-, L- and P-band images showed that the textural information in L- and P-band is minimal. This can be explained by the fact that L- and P-band radar waves penetrate the forest canopy to a greater depth than C-band radar waves (see Equation 3.30). Consequently, the scattering of L- and P-band microwaves is not affected by the surface roughness of the forest canopy and hence L- and P-band images are free of canopy induced radar "layover", "shadowing" and "foreshortening" effects (see section 3.1.3). These geometrical effects are the most important cause of texture in C-band (and X-band) radar images.

### 6.3.1 Scattering behaviour of land cover types studied

Figures 6.10, 6.11 and 6.12 illustrate the scattering behaviour of the land cover types studied in C-, L- and P-band. The individual graphs depict the relative importance of the odd (or single) bounce, double (or even) bounce and diffuse scattering mechanisms by showing the frequency with which they contribute a specific fraction of the total backscattered power TP. The procedure at the basis of these graphs is the following. Firstly, for each pixel within an area of interest (see section 5.2.1) the fraction of the total backscattered power TP (in %) resulting from odd bounce, double bounce and diffuse scattering was computed. Secondly, the TP fractions computed for each of the scattering mechanisms were grouped into five classes, i.e. from 0 to 20%, 21 to 40%, 41 to 60%, 61 to 80% and 81 to 100%. In

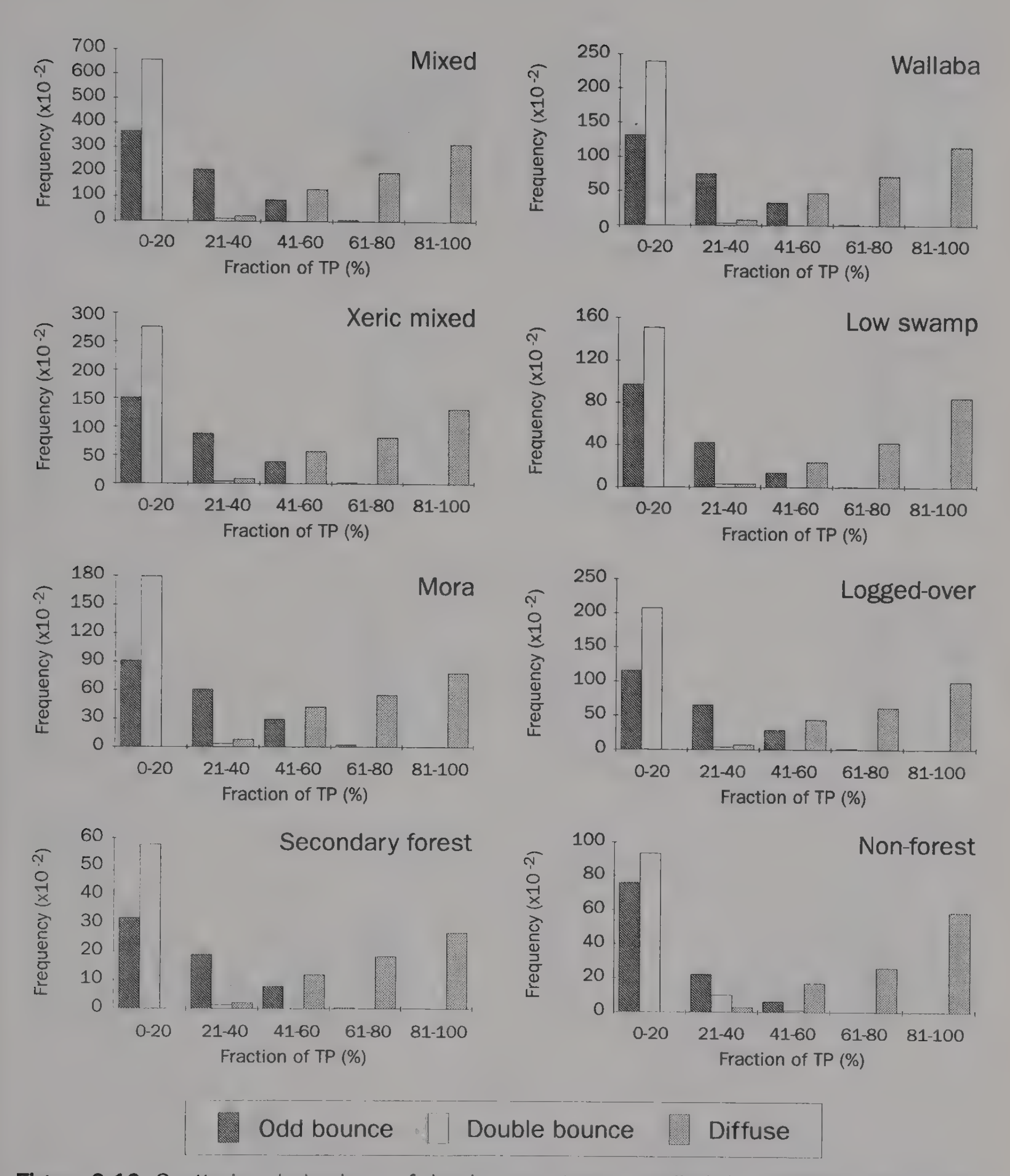



**Figure 6.10** Scattering behaviour of land cover types studied in **C-band**. The relative importance of the single bounce, double bounce and diffuse scattering mechanism is illustrated by showing the frequency with which these mechanisms contribute a specific fraction of the total backscattered power TP.

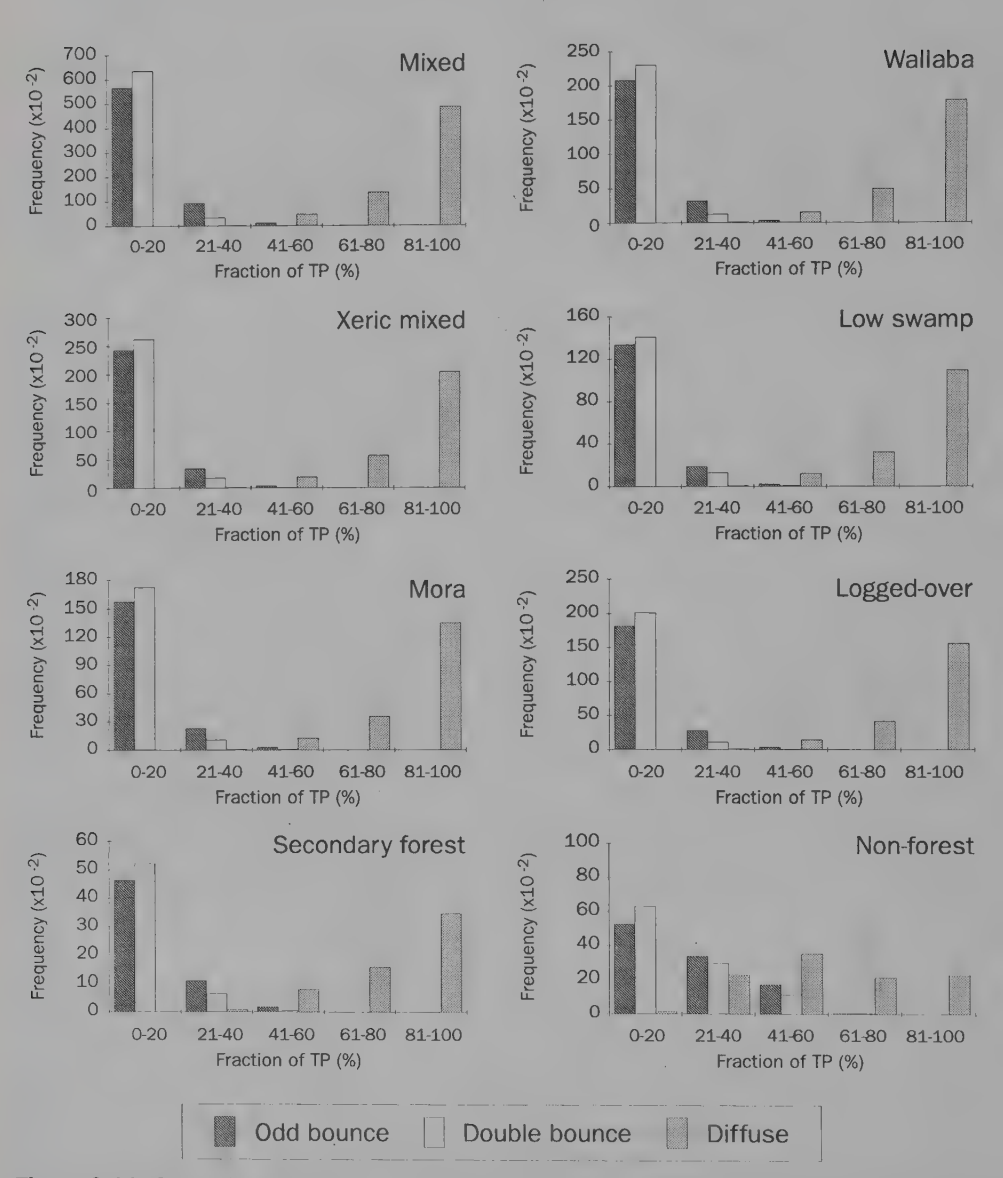



**Figure 6.11** Scattering behaviour of land cover types studied in **L-band**. The relative importance of the single bounce, double bounce and diffuse scattering mechanism is illustrated by showing the frequency with which these mechanisms contribute a specific fraction of the total backscattered power TP.

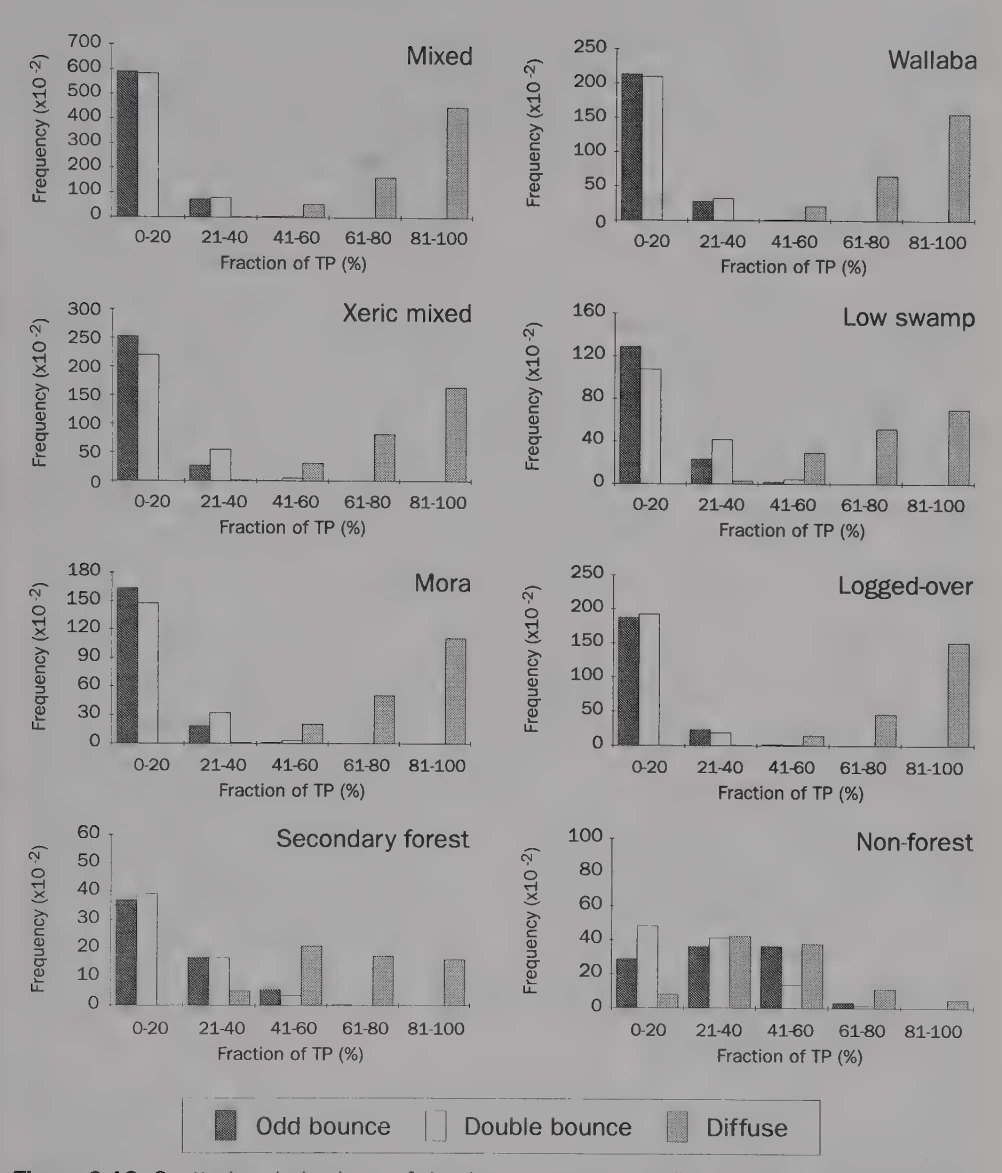



**Figure 6.12** Scattering behaviour of land cover types studied in **P-band**. The relative importance of the single bounce, double bounce and diffuse scattering mechanism is illustrated by showing the frequency with which these mechanisms contribute a specific fraction of the total backscattered power TP.

effect, this resulted in a total of 15 classes, i.e. three scattering classes consisting of five TP fraction classes each. Thirdly, the pixels associated with the land cover types studied were assigned to three out of the 15 classes, i.e. one odd bounce, one double bounce and one diffuse scattering class. Fourthly, the pixels in each of the 15 classes were enumerated. Finally, the number of pixels in each class was charted per land cover type in the manner as shown in Figures 6.10, 6.11 and 6.12. The decomposition of the total backscatter into the contributions of the three scattering mechanisms was achieved with the help of the MAPVEG program by Freeman et al. (1993). The three-component scattering model at the basis of this program was briefly explained in section 5.3.2. A more detailed description of this model can be found in Freeman and Durden (1992).

The results in Figure 6.10 show that *in C-band, for all of the land cover types studied, the diffuse scattering mechanism is the most important contributor to the TP.* For the majority of the pixels in each land cover type it is responsible for 61 to 100% of the TP. The odd bounce scattering mechanism usually contributes ≤ 40% of the TP. Contributions up to 60% of TP are less common and contributions up to 80% of TP are rare. The double bounce scattering mechanism does not generally contribute more than 20% of the TP. In C-band, the scattering behaviour of the primary forest types is comparable to that of Logged-over forest and Secondary forest. For Non-forest the contribution of odd bounce scattering to the TP is less important than for the forest types; the contribution of diffuse scattering is more important.

*In L-band* (see Figure 6.11), when compared to C-band, *the diffuse scattering mechanism has gained importance and the odd bounce scattering mechanism has lost importance for all but the Non-forest class.* For more than half of the pixels belonging to the different forest classes, diffuse scattering is responsible for ≥ 81% of the TP. Odd bounce scattering generally contributes ≤ 20% of the TP. Like in C-band the backscatter resulting from double bounce scattering is usually ≤ 20% of the TP. Nevertheless, this scattering mechanism has gained some importance since in L-band the number of pixels for which it contributes 21 to 40% of the TP is larger than in C-band. The scattering behaviour of the various forest classes in L-band is well comparable but different from that of Non-forest. Going from C- to L-band the number of Non-forest pixels for which diffuse scattering contributes ≥ 61% of the TP has decreased considerably. The lower contribution of diffuse scattering to TP is compensated by higher contributions from both the odd bounce and the double bounce scattering mechanism.

*Going from L- to P-band* (see Figure 6.12) *there is a decrease in the contribution of diffuse scattering to the TP.* For the primary forest classes as well as the Logged-over forest class the loss in backscattered power resulting from diffuse scattering is small. For these classes the lower diffuse scattering contribution is made up for by a higher contribution from double bounce scattering. However, double bounce scattering can be seen to rarely contribute ≥ 41% of the TP. The loss in power resulting from diffuse scattering and the gain in power resulting from double bounce scattering is the highest for the Low swamp forest. *For Secondary forest and Non-forest the loss in backscattered power resulting from diffuse scattering* is considerable. It *is compensated by a higher contribution from both odd bounce and*

*double bounce scattering.* Odd bounce and double bounce scattering make the most important contribution to TP in the Non-forest class. For close to half of the pixels in this class the diffuse scattering mechanism contributes ≤ 40% of the TP.

The above findings with regard to the role of odd bounce, double bounce and diffuse scattering in the scattering behaviour of tropical land cover types in C-, L- and P-band agree well with the results from an unsupervised classification of scattering behaviour according to van Zyl (1989). These results are reported in van der Sanden and Hoekman (1994, 1995).

It is interesting to note the discrepancy in the scattering behaviour of Secondary forest and Low swamp forest. In the case of Secondary forest the loss in power from diffuse scattering (when going from L- to P-band) is compensated by equivalent contributions from the odd and the double bounce scattering mechanism. However, in the case of Low swamp forest the reduction in power from diffuse scattering is primarily compensated by a contribution from the double bounce scattering mechanism. It is hypothesised that this difference in the backscatter behaviour of the two forest types is related to forest flooding. The AIRSAR data were acquired during the rainy season. Consequently, the Low swamp forest was more than likely to be inundated. Due to sheltered conditions underneath the forest canopy the water surface will have been smooth. This caused the water to reflect the incident power in the forward direction and not in the backscatter direction. Hence, odd bounce scattering did not generate backscatter. The only way the deeply penetrating P-band microwaves could be reflected towards the sensor was through double bounce interaction between the water surface and primary branches or tree trunks. Different authors have reported on the *relationship between forest flooding and double bounce scattering* (e.g. Hoffer et al., 1985; Imhoff et al., 1986; Richards et al., 1987; Freeman and Durden, 1992). The scattering behaviour of the Low swamp forest supports their findings. Mora forest, like Low swamp forest, is generally flooded in the rainy season. Yet, the scattering behaviour of this forest type shows little evidence of double bounce interaction. This is probably due to the forest's high aboveground biomass (see Figure 4.6). High biomass levels have a strong attenuating effect on the incident as well as the reflected waves and hence obstruct double bounce (back)scattering.

Figure 6.13 shows $\overline{\gamma}$ as a function of incidence angle in C-, L- and P-band, HH, VH and VV polarization, for a stretch of dense tropical rain forest on flat to gently undulating terrain. In C- and L-band, regardless of polarization, the effect of the incidence angle on $\overline{\gamma}$ is minimal. This suggests the dominance of diffuse scattering which agrees well with the results shown in Figures 6.10 and 6.11. In P-band $\overline{\gamma}$ can be seen to increase by 2 to 3 dB as the incidence angle increases from ca. 20° to 60°. This contradicts the earlier observation that most of the backscattered power for tropical forest in P-band results from diffuse scattering. However, the small difference in HH and VV backscatter supports this observation. The shown change in $\overline{\gamma}$ as a function of incidence angle also does not indicate the dominance of either odd bounce or double bounce scattering. If the backscatter resulted from odd bounce scattering, i.e. from scattering at the forest soil, one would expect a decrease in $\overline{\gamma}$

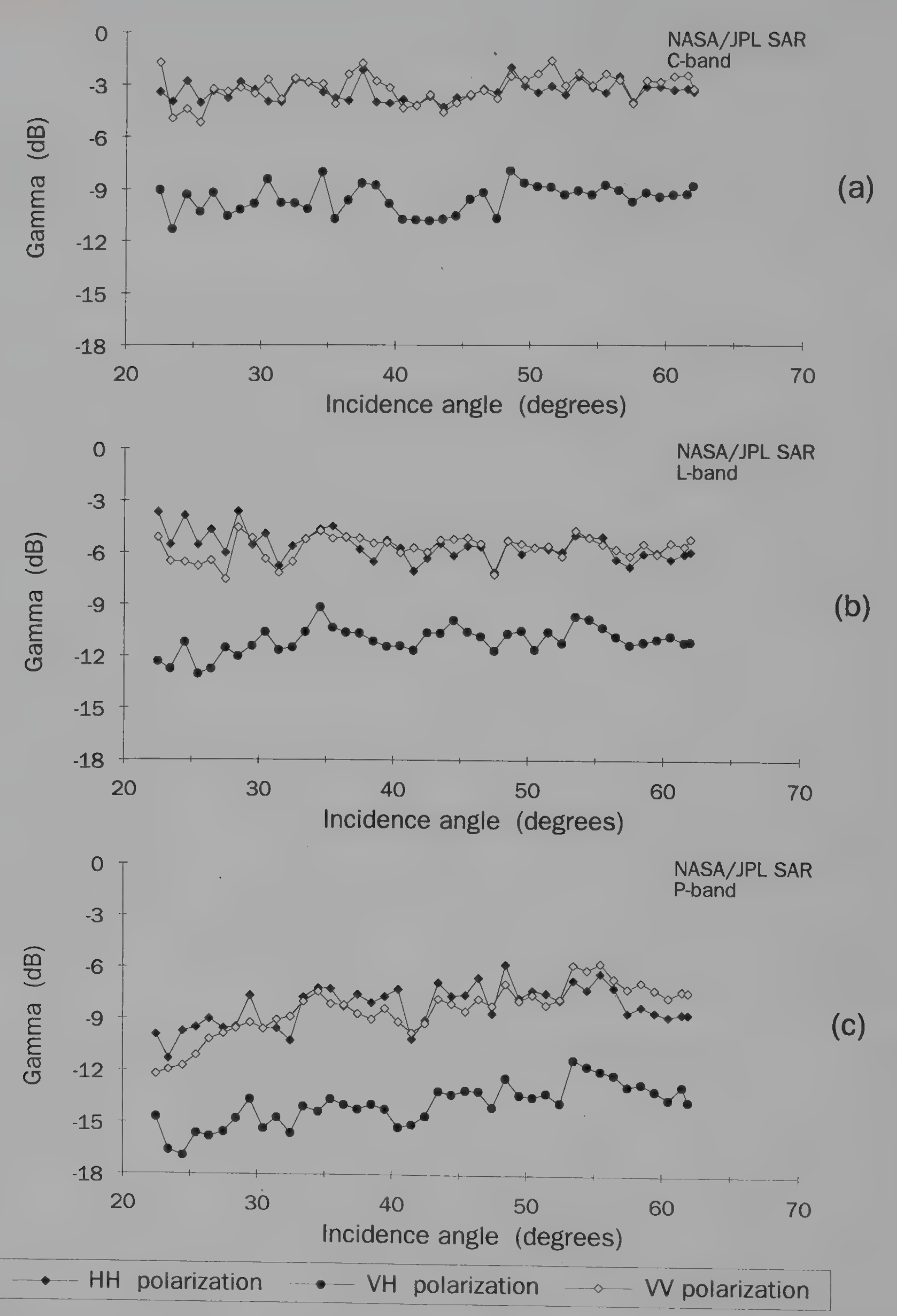



**Figure 6.13 (a-c)** Plots of $\overline{\gamma}$ as a function of the incidence angle for a stretch of dense tropical rain forest on flat to gently undulating terrain: (**a**) in C-band HH, VH and VV (**b**) in L-band HH, VH and VV (**c**) in P-band HH, VH and VV.

with an increase in incidence angle. This may be explained by the reduced depth of vertical penetration at larger incidence angles (see Equation 3.30, section 3.2.4). If, on the other hand, the backscatter resulted from double bounce scattering, i.e. trunk-ground interaction, one would generally find a maximum value for $\bar{\gamma}$ at around the 45° incidence angle and certainly no increase in $\bar{\gamma}$ beyond this angle of incidence. The apparent variation induced by the incidence angle in P-band HH, VV and VH backscatter cannot be explained by physics and is most likely a calibration artefact.

### 6.3.2 Classification of land cover per region using backscatter and PPD

**Results of classifications based on a single radiometric or polarimetric attribute**
Table 6.9 shows the results of Gaussian maximum-likelihood classifications using $\bar{\gamma}$, PPD and sd(PPD) values computed per region for a selection of polarizations in the C, L and P frequency band. The results are sorted, in descending order, according to the value of the $\hat{K}$ statistic (see section 5.2.4). Of the combinations listed, L VV yields the best and C PPD the poorest overall classification results. At the 95% confidence level the results for the highest ranking L VV combination are not significantly different from those for the series of combinations beginning with P HH and ending with P VH. In the table this is indicated by a vertical line at the left-hand side of the first column. Likewise, the line at the right-hand side of the last column marks the combinations for which the results are not significantly different from those for lowest ranked C PPD combination.

All C-band combinations are clustered in the lower half of the table. The results for these combinations do not differ significantly from those for the lowest ranked combination. It is evident that the *C-band combinations provide a poor basis for classifying the land cover types studied. L- and P-band combinations other than L PPD, L sd(PPD), P PPD and P sd(PPD) yield significantly better overall classification results. Among these L HH, P VV and P RL are the least discriminative.* Figure 6.14 illustrates the classification capacities for L VV, P RR and C VV. From C VV to L VV and from L VV to P RR the backscatter differences between the classes increase. However, in P RR the larger between class backscatter differences are accompanied by larger within-class variances. This contributes to the fact that the maximum-likelihood classification results for P RR and L VV are not significantly different.

Comparison of Figures 6.14c and 6.6a shows that the C-band VV backscatter values computed from the NASA/JPL AIRSAR data set are ca. 4 dB higher than the backscatter values derived from the ERS-1 SAR PRI data. ERS-1 SAR data are known to have a high radiometric accuracy (e.g. Laur et al., 1993). It is therefore plausible that the difference in the absolute backscatter level for the two data sets is due to a defect in the absolute calibration of the AIRSAR data. Multiple incidence angle backscatter measurements by the ERS-1 windscatterometer support this supposition (Wismann et al., 1996). The observed calibration defect does *not* modify the classification results discussed in this text as it affects the backscatter levels of all classes in a similar manner.

**Table 6.9** Gaussian maximum-likelihood classification results. Classification based on $\bar{\gamma}$, PPD and sd(PPD) values computed per region for selected polarizations in the C, L and P frequency band.

| Combination | $\hat{K}$ | $\hat{\sigma}^2_\infty[\hat{K}]$ | Percentage correct | | | | | | | | |
|---|---|---|---|---|---|---|---|---|---|---|---|
| | | | Total | Mixed | Wallaba | Xeric mixed | Low swamp | Mora | Logged-over forest | Secondary forest | Non-forest |
| L VV | 0.5322 | 0.0035 | 60 | 63 | 83 | 0 | 100 | 44 | 58 | 50 | 71 |
| P HH | 0.5228 | 0.0034 | 59 | 38 | 42 | 17 | 83 | 81 | 75 | 50 | 71 |
| P LL | 0.4853 | 0.0034 | 55 | 13 | 67 | 0 | 50 | 56 | 83 | 80 | 79 |
| L TP | 0.4579 | 0.0035 | 53 | 69 | 67 | 0 | 83 | 19 | 58 | 50 | 71 |
| L VH | 0.4575 | 0.0036 | 53 | 38 | 33 | 0 | 83 | 50 | 67 | 90 | 64 |
| P RR | 0.4473 | 0.0034 | 52 | 6 | 58 | 0 | 67 | 56 | 75 | 80 | 71 |
| P TP | 0.4222 | 0.0035 | 50 | 13 | 75 | 0 | 50 | 38 | 75 | 80 | 64 |
| L RL | 0.4209 | 0.0034 | 50 | 63 | 75 | 0 | 83 | 13 | 42 | 50 | 71 |
| L LL | 0.4078 | 0.0036 | 49 | 56 | 42 | 0 | 83 | 25 | 67 | 50 | 64 |
| L RR | 0.4051 | 0.0037 | 49 | 50 | 42 | 0 | 83 | 38 | 58 | 50 | 64 |
| P VH | 0.3925 | 0.0030 | 47 | 0 | 75 | 33 | 33 | 0 | 92 | 90 | 71 |
| L HH | 0.3436 | 0.0035 | 43 | 63 | 25 | 0 | 83 | 19 | 42 | 40 | 71 |
| P RL | 0.3272 | 0.0032 | 41 | 0 | 67 | 0 | 50 | 25 | 58 | 70 | 64 |
| P VV | 0.3140 | 0.0030 | 40 | 0 | 83 | 0 | 67 | 6 | 67 | 30 | 79 |
| L PPD | 0.2824 | 0.0033 | 38 | 25 | 0 | 0 | 100 | 56 | 50 | 60 | 29 |
| C sd(PPD) | 0.2714 | 0.0026 | 36 | 6 | 83 | 0 | 83 | 6 | 25 | 20 | 79 |
| P sd(PPD) | 0.2251 | 0.0026 | 32 | 19 | 0 | 83 | 67 | 38 | 58 | 40 | 0 |
| L sd(PPD) | 0.2130 | 0.0023 | 29 | 31 | 0 | 67 | 83 | 0 | 67 | 0 | 36 |
| C VH | 0.2114 | 0.0023 | 32 | 0 | 75 | 0 | 83 | 63 | 0 | 0 | 36 |
| C LL | 0.1974 | 0.0023 | 30 | 0 | 75 | 0 | 83 | 63 | 0 | 10 | 21 |
| P PPD | 0.1932 | 0.0027 | 30 | 19 | 17 | 0 | 50 | 31 | 92 | 40 | 0 |
| C VV | 0.1845 | 0.0023 | 28 | 0 | 42 | 0 | 67 | 56 | 8 | 0 | 50 |
| C TP | 0.1826 | 0.0021 | 28 | 13 | 8 | 0 | 83 | 69 | 0 | 0 | 50 |
| C RR | 0.1783 | 0.0020 | 28 | 0 | 67 | 0 | 83 | 63 | 0 | 0 | 21 |
| C RL | 0.1708 | 0.0021 | 27 | 6 | 8 | 0 | 67 | 63 | 8 | 0 | 57 |
| C HH | 0.1634 | 0.0024 | 28 | 44 | 0 | 0 | 50 | 63 | 8 | 0 | 36 |
| C PPD | 0.1484 | 0.0017 | 23 | 0 | 67 | 33 | 83 | 0 | 42 | 0 | 7 |

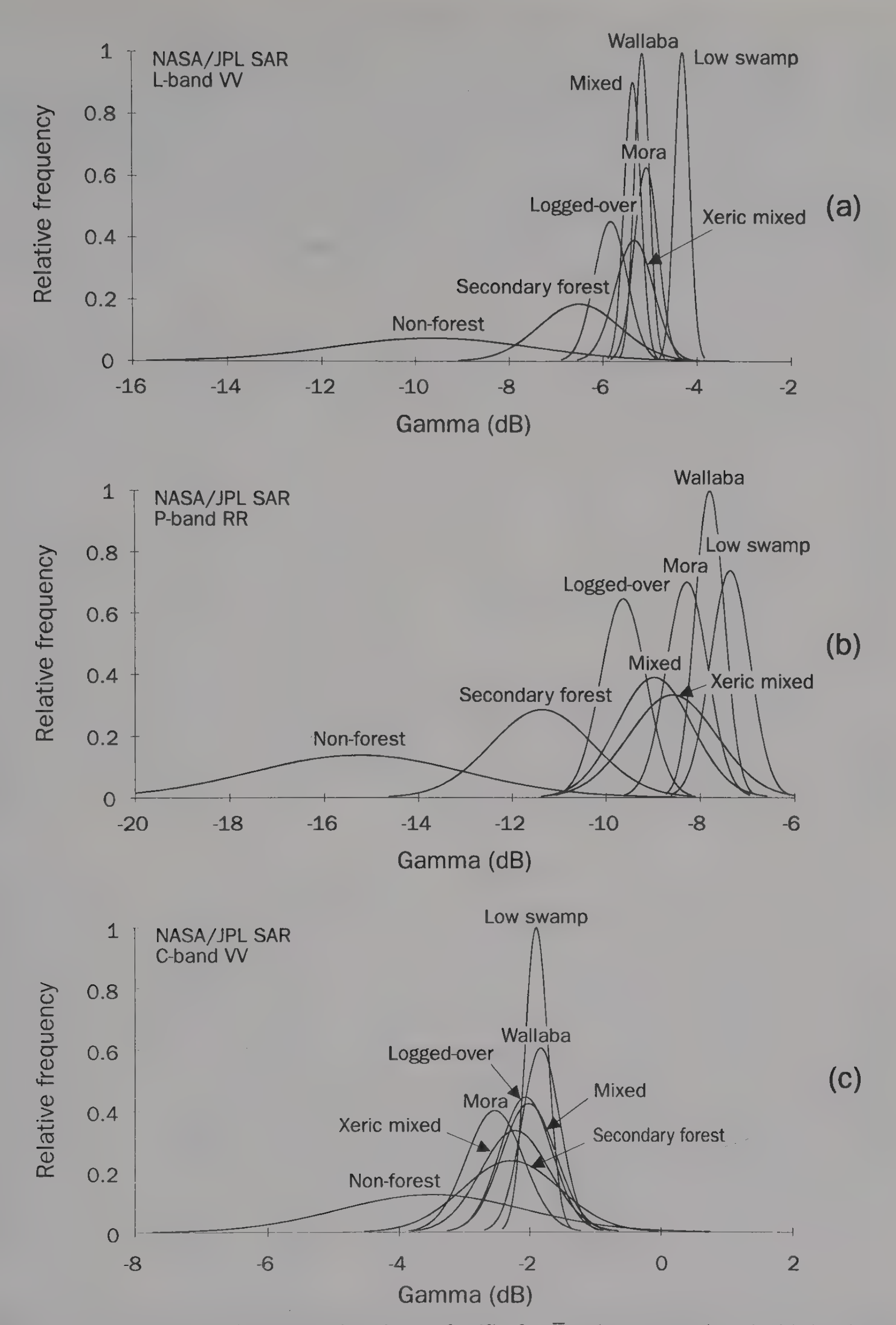



**Figure 6.14 (a-c)** Gaussian approximations of pdf's for $\overline{\gamma}$ values associated with land cover types present in the **NASA/JPL AIRSAR** data set: (**a**) pdf's for L-band VV (**b**) pdf's for P-band RR (**c**) pdf's for C-band VV.

Comparison of Figures 6.14c and 6.6a furthermore shows that the within-class variance in the AIRSAR data set is larger than in the ERS-1 data set. This is due to the fact that the two systems operate with a different incidence angle (range) (see Tables 4.6 and 4.8). An incidence angle range as wide as in the AIRSAR data causes backscatter variations which are not related to the object observed and therefore reduces the likelihood of correct classification. The question as to whether the small ERS-1 or large AIRSAR incidence angles are to be preferred cannot be answered adequately with the help of the data sets available. It is evident, however, that the answer will not be unequivocal since the 'optimal' incidence angle will strongly depend on the wavelength.

The advantage of microwaves with long wavelengths such as L- and P-band is their vertical penetrating capability. This capability is higher at small than at large incidence angles (see Equation 3.30). For most of the areas of interest in the AIRSAR data set the incidence angle ranges approximately from 40° to 60°. At these incidence angles the capability of L- and P-band microwaves to penetrate the dense tropical forest is limited. This follows from the generally small contributions of the odd bounce and double bounce scattering mechanisms to the total backscattered power (see section 6.3.1). Due to the limited vertical depth of penetration of the incident microwaves, the information present in the lower quarters of the forest is not observed. This restricts the possibilities to discriminate between different forest types and suggests that a smaller incidence angle (ca. 30°) could be advantageous. On the other hand, the importance of microwaves with short wavelengths relates to their ability to observe architectural properties of the forest canopy. Since these properties are best reflected in image texture (see sections 6.1.1 and 6.2.1) the 'optimal' incidence angle is the one at which the textural differences between cover types are most pronounced. From the results in section I.1 of Appendix I it follows that this is the case at large incidence angles.

Table 6.9 shows that *L- and P-band have comparable capabilities for discriminating between Non-forest and other cover types.* Based on a single L- or P-band combination, ca. 65 to 80% of the Non-forest data points are classified correctly. *Non-forest is not generally confused with any class other than Secondary forest.* P VH and L VH are able to classify Secondary forest with a 90% accuracy. Other L- and P-band combinations yield less accurate results; the results for P-band are generally better than those for L-band. P TP and the circular polarized P-band combinations yield more accurate results than P HH and P VV. Secondary forest is easily confused with Logged-over forest and, to a lesser extent, with Mixed forest and Xeric mixed forest. Generally speaking, Logged-over forest is classified more accurately by P-band combinations than by L-band combinations. P VH and P LL yield the best results (≥ 83% accuracy), P VV and P RL the poorest. *Logged-over forest is primarily confused with Mixed forest, i.e. the forest type being logged, Secondary forest and Mora forest.*

*On the average, the primary forest types are most difficult to classify.* Within a particular frequency band the results vary strongly as a function of polarization. L VV and P HH yield the best *overall* results. They correctly identify 59% and 54% of the primary forest data points. However, no single combination may be denoted as

**Table 6.10** Gaussian maximum-likelihood classification results after grouping all of the primary forest type data points into a single Primary forest class. Classification based on $\overline{\gamma}$, PPD and sd(PPD) values computed per region for selected polarizations in the C, L and P frequency band.

| | | | Percentage correct | | | | |
|---|---|---|---|---|---|---|---|
| Combination | $\hat{K}$ | $\hat{\sigma}^2_\infty[\hat{K}]$ | Total | Primary forest | Logged-over forest | Secondary forest | Non-forest |
| P LL | 0.6898 | 0.0040 | 80 | 80 | 83 | 80 | 79 |
| P RR | 0.6874 | 0.0039 | 80 | 82 | 83 | 80 | 71 |
| L VH | 0.6832 | 0.0040 | 80 | 84 | 75 | 90 | 64 |
| P HH | 0.6442 | 0.0043 | 78 | 84 | 83 | 50 | 71 |
| L TP | 0.6093 | 0.0041 | 75 | 79 | 83 | 50 | 71 |
| L RR | 0.6032 | 0.0042 | 75 | 80 | 83 | 50 | 64 |
| P TP | 0.6001 | 0.0043 | 74 | 73 | 83 | 80 | 64 |
| L HH | 0.5940 | 0.0047 | 75 | 80 | 83 | 40 | 71 |
| L LL | 0.5935 | 0.0041 | 74 | 79 | 83 | 50 | 64 |
| P VH | 0.5850 | 0.0043 | 72 | 64 | 92 | 90 | 71 |
| L VV | 0.5738 | 0.0044 | 73 | 77 | 75 | 50 | 71 |
| L RL | 0.5711 | 0.0044 | 73 | 79 | 67 | 50 | 71 |
| P VV | 0.4855 | 0.0043 | 65 | 64 | 83 | 30 | 79 |
| P RL | 0.4835 | 0.0046 | 65 | 64 | 67 | 70 | 64 |
| C sd(PPD) | 0.3426 | 0.0051 | 55 | 54 | 67 | 20 | 79 |
| P sd(PPD) | 0.3290 | 0.0042 | 57 | 68 | 67 | 40 | 14 |
| L sd(PPD) | 0.2469 | 0.0044 | 47 | 43 | 83 | 40 | 36 |
| C HH | 0.1768 | 0.0050 | 46 | 50 | 25 | 30 | 57 |
| P PPD | 0.1510 | 0.0018 | 27 | 4 | 100 | 70 | 29 |
| C RL | 0.1498 | 0.0058 | 47 | 55 | 25 | 10 | 57 |
| C RR | 0.1415 | 0.0051 | 48 | 63 | 25 | 20 | 29 |
| L PPD | 0.1404 | 0.0023 | 30 | 13 | 100 | 60 | 21 |
| C VH | 0.1086 | 0.0047 | 42 | 52 | 33 | 10 | 36 |
| C PPD | 0.1017 | 0.0048 | 42 | 50 | 58 | 20 | 14 |
| C TP | 0.0946 | 0.0051 | 45 | 57 | 17 | 0 | 50 |
| C VV | 0.0670 | 0.0024 | 25 | 14 | 67 | 0 | 50 |
| C LL | 0.0592 | 0.0031 | 29 | 27 | 50 | 30 | 21 |

'the best' for classifying all of the primary forest types studied. Mixed forest and Xeric mixed forest are especially difficult to classify. Mixed forest is easily confused with Mora, Wallaba and Logged-over forest. Xeric mixed forest is confused with every other class with the exception of Non-forest and Secondary forest. For the classification of Logged-over forest, Secondary forest and Non-forest, the L- and P-band combinations are clearly more suitable than the C-band combinations. A similar discrepancy in the classification results for L- or P- and C-band is not seen in connection with the primary forest types. The C-band results for Mora forest, for example, exceed those for most L- and P-band combinations. Since C-band radar waves are sensitive to *differences in canopy architecture* it may be concluded that such differences *are an important basis for discriminating primary forest types in radar images.*

Comparison of Table 6.9 and Table 6.2 shows that the overall classification results as associated with the L VV through L RL $\overline{\gamma}$ values and the X HV and/or C VV sd($\gamma$) and GLCO-CONT[5] values are *not significantly different*. Hence, *it is concluded that textural patterns in high resolution X- and C-band SAR images and backscatter levels in L- and P-band SAR images are equally suitable information sources for classifying the land cover types studied.*

Table 6.10 shows the results of a lower level classification, i.e. a classification in which all primary forest type data points are grouped into a single Primary forest class. This table has the same layout as Table 6.9. Thanks to the grouping of the most easily confused cover types, the overall classification results have become better. An overall classification accuracy of ca. 70% to 80% is judged good. At the 95% confidence level, however, the improvement in the classification results is not significant. The grouping of the primary forest types also resulted in higher classification accuracy for Logged-over forest and Secondary forest. The classification results for Non-forest generally did not improve since this cover type is not easily confused with primary forest types.

The grouping of the primary forest types has had little effect on the ranking of the various combinations. L HH is added to the series of combinations for which the results do not differ significantly from those of the best performing combination. C sd(PPD), L sd(PPD) and P sd(PPD) no longer belong to the series of worst performing combinations but this series is otherwise unchanged. Interesting to note are the high percentages of correctly classified Logged-over forest data points for L PPD and P PPD. A closer look at the data shows that this is due to the fact that data points for Logged-over forest are confined to a much narrower range than those for Primary forest, Secondary forest and Non-forest. Consequently, the pdf's for Logged-over forest are high and narrow while those for the other classes are low and wide. This results in good classification results for Logged-over forest despite the fact that the L PPD and P PPD values for this class and, in particular, Primary forest, are not substantially different. Unfortunately, the good results for Logged-over forest are accompanied by poor results for Primary forest since many of the data points belonging to this class are classified as Logged-over forest.

**Table 6.11** Differences in $\bar{\gamma}$ values for Mixed forest and Logged-over forest as well as for Primary forest and Logged-over forest, Secondary forest and Non-forest in frequency bands and polarizations studied.

| | Polarization | | | | | | |
|---|---|---|---|---|---|---|---|
| | HH | VH | VV | RR | RL | LL | TP |
| **$\bar{\gamma}$ Mixed forest minus $\bar{\gamma}$ Logged-over forest (dB)** | | | | | | | |
| C-band | 0.10 | 0.12 | 0.05 | 0.04 | 0.07 | 0.15 | 0.08 |
| L-band | 0.40 | 0.46 | 0.47 | 0.46 | 0.41 | 0.48 | 0.44 |
| P-band | 0.77 | 0.53 | 0.45 | 0.66 | 0.51 | 0.68 | 0.60 |
| **$\bar{\gamma}$ Primary forest minus $\bar{\gamma}$ Logged-over forest (dB)** | | | | | | | |
| C-band | -0.09 | -0.02 | -0.07 | -0.08 | -0.09 | 0.02 | -0.07 |
| L-band | 0.67 | 0.63 | 0.71 | 0.73 | 0.60 | 0.75 | 0.67 |
| P-band | 1.51 | 0.75 | 0.99 | 1.32 | 0.95 | 1.26 | 1.14 |
| **$\bar{\gamma}$ Primary forest minus $\bar{\gamma}$ Secondary forest (dB)** | | | | | | | |
| C-band | -0.08 | 0.16 | 0.15 | -0.03 | 0.08 | 0.11 | 0.06 |
| L-band | 0.90 | 1.92 | 1.38 | 1.37 | 1.22 | 1.43 | 1.31 |
| P-band | 1.83 | 3.96 | 2.90 | 3.06 | 2.20 | 2.93 | 2.62 |
| **$\bar{\gamma}$ Primary forest minus $\bar{\gamma}$ Non-forest (dB)** | | | | | | | |
| C-band | 0.47 | 0.57 | 1.36 | 0.12 | 1.47 | -0.07 | 0.82 |
| L-band | 3.87 | 6.38 | 4.51 | 4.86 | 4.42 | 4.67 | 4.59 |
| P-band | 5.42 | 8.69 | 6.07 | 6.96 | 5.53 | 6.73 | 6.20 |

The results in Table 6.10 show that many radar bands, notably those involving long wavelengths, can accurately discriminate between Primary forest, Logged-over forest, Secondary forest and Non-forest. Yet, *the difference in the mean backscatter level of these cover types is often small. In order to discriminate between them, a SAR system with a high radiometric resolution is needed.* Depending on the radar band and the cover types in question, the backscatter difference and hence the required radiometric resolution may vary. The differences in the $\bar{\gamma}$ values for Mixed forest (the forest type being logged) and Logged-over forest as well as for Primary forest and Logged-over forest, and Secondary forest and Non-forest are listed in Table 6.11. The incidence angle for most of the data points in these classes ranges from roughly 40° to 60°. In L- and P-band the backscatter differences are more distinct than in C-band. This largely explains the good results for classifications based on L- and P-band data.

**Table 6.12** Potential of the $\bar{\gamma}$ values for dual frequency and/or polarization combinations for the classification per region of the land cover types studied. The values given represent the number of class pairs that can be successfully discriminated, i.e. the number of class pairs out of a total of 28 for which $TD_{ij} \geq 1900$.

| | Combination | | | | | | | | | | | | | | | | | | | |
|---|---|---|---|---|---|---|---|---|---|---|---|---|---|---|---|---|---|---|---|---|
| | C HH | C VH | C VV | C RR | C RL | C LL | C TP | L HH | L VH | L VV | L RR | L RL | L LL | L TP | P HH | P VH | P VV | P RR | P RL | P LL |
| C VH | 7 | | | | | | | | | | | | | | | | | | | |
| C VV | 3 | 9 | | | | | | | | | | | | | | | | | | |
| C RR | 1 | 8 | 11 | | | | | | | | | | | | | | | | | |
| C RL | 6 | 12 | 5 | 7 | | | | | | | | | | | | | | | | |
| C LL | 5 | 9 | 10 | 4 | 11 | | | | | | | | | | | | | | | |
| C TP | 3 | 7 | 4 | 7 | 13 | 10 | | | | | | | | | | | | | | |
| L HH | 7 | 8 | 6 | 8 | 6 | 12 | 6 | | | | | | | | | | | | | |
| L VH | 14 | 14 | 12 | 15 | 13 | 16 | 13 | 12 | | | | | | | | | | | | |
| L VV | 16 | 15 | 15 | 15 | 15 | 15 | 15 | 15 | 15 | | | | | | | | | | | |
| L RR | 12 | 13 | 12 | 12 | 11 | 14 | 12 | 15 | 14 | 16 | | | | | | | | | | |
| L RL | 12 | 11 | 9 | 10 | 9 | 12 | 9 | 11 | 12 | 16 | 15 | | | | | | | | | |
| L LL | 11 | 12 | 10 | 11 | 10 | 13 | 10 | 15 | 15 | 15 | 11 | 11 | | | | | | | | |
| L TP | 12 | 12 | 10 | 11 | 11 | 13 | 10 | 15 | 14 | 16 | 15 | 12 | 10 | | | | | | | |
| P HH | 15 | **18** | 16 | **18** | 15 | **19** | 17 | 12 | 17 | 17 | 13 | 16 | 13 | 15 | | | | | | |
| P VH | 13 | 16 | 12 | 16 | 12 | 16 | 13 | 10 | 12 | 15 | 11 | 11 | 12 | 12 | 14 | | | | | |
| P VV | 12 | 15 | 14 | 15 | 11 | 16 | 12 | 10 | 12 | 14 | 10 | 13 | 11 | 11 | 14 | 13 | | | | |
| P RR | 15 | **18** | 14 | 17 | 12 | **21** | 14 | 12 | 13 | 15 | 12 | 11 | 11 | 11 | 14 | 16 | 12 | | | |
| P RL | 12 | 17 | 14 | 16 | 12 | 16 | 14 | 10 | 14 | 16 | 13 | 13 | 12 | 12 | 14 | 17 | 13 | 13 | | |
| P LL | 15 | **20** | 16 | **20** | 14 | **18** | 16 | 12 | 12 | 15 | 11 | 12 | 11 | 12 | 13 | 17 | 14 | 11 | **19** | |
| P TP | 15 | **20** | 15 | 17 | 12 | **20** | 15 | 12 | 12 | 15 | 12 | 12 | 11 | 11 | 14 | 15 | 13 | 12 | 15 | 17 |

**Results of classifications based on two and three radiometric attributes**
The relatively low accuracy in Table 6.9 for classifying primary forest types lead to an analysis of the classification capabilities of dual and triple frequency and/or polarization radar band combinations. The analysis concerned a total of 210 dual and 1330 triple frequency and/or polarization combinations. Combinations inclusive of the polarimetric PPD or sd(PPD) attributes were not considered.

Table 6.12 lists the overall classification potential of the $\overline{\gamma}$ values for dual frequency and/or polarization combinations. The entries of this table represent the number of class pairs that can be successfully discriminated, i.e. the number of class pairs out of a total of 28 for which $TD_{ij} \geq 1900$ (see section 5.2.4). Tables IV.1 through IV.4 in Appendix IV show the potential of the $\overline{\gamma}$ values for dual frequency and/or polarization combinations for classifying primary forest types, Logged-over forest, Secondary forest and Non-forest, respectively.

Table 6.12 shows that *the highest overall classification potential is generally offered by a combination of C- and P-band.* C VH, C RR and C LL are the best performing C-band channels, P HH, P RR, P LL and P TP the best performing P-band channels. Table IV.1 reveals that *even dual frequency and/or polarization radar band combinations have difficulty to distinguish between the primary forest types studied.* The maximum number of primary forest class pairs that can be successfully discriminated is six out of a total of 10. Combinations of C- and P-band offer the highest classification potential. C VH, C LL, P HH, P RR, P LL and P TP are among the best performing channels. The results in Table IV.2 show that the *availability of P-band HH data is important for classifying Logged-over forest.* Combinations consisting of two P-band channels, one of which is P HH, are performing the best. Such combinations successfully discriminate six out of seven class pairs. The one class pair causing problems comprises Logged-over forest and the forest type that is being logged, i.e. Mixed forest.

Table IV.3 shows that *combinations of either L VH or P VH with C-band (any polarization) offer the best possibilities for classifying Secondary forest.* These combinations are able to discriminate between all class pairs involving Secondary forest. Classification of Non-forest does not generally create problems. Any combination involving L- or P-band (with exception of C HH, P VV) can at least discriminate between six out of seven Non-forest class pairs (see Table IV.4). Combinations that include C LL or L VH perform better than others. In classifying Non-forest one does not usually gain much by using double frequency and/or double polarization combinations since all individual L- and P-band channels (with exception of P VV) are already capable of discriminating between six out of the seven Non-forest class pairs. In absence of L- and P-band, the combined use of C-band channels does enhance the Non-forest classification possibilities. The best performing C-band combinations are those that include a circular polarized channel.

Table 6.13 presents the Gaussian maximum-likelihood classification results for a limited selection of the dual frequency and/or polarization combinations studied. The selection includes the combinations offered by currently available radar satellite

**Table 6.13** Gaussian maximum-likelihood classification results for a selection of dual frequency and/or polarization combinations. Classification based on $\bar{\gamma}$ values computed per region.

| Combination | $\hat{K}$ | $\hat{\sigma}^2_\infty[\hat{K}]$ | Percentage correct | | | | | | | | |
|---|---|---|---|---|---|---|---|---|---|---|---|
| | | | Total | Mixed | Wallaba | Xeric mixed | Low swamp | Mora | Logged-over forest | Secondary forest | Non-forest |
| C RR, P LL | 0.6889 | 0.0028 | 73 | 38 | 67 | 83 | 100 | 56 | 92 | 90 | 93 |
| C VH, P LL | 0.6882 | 0.0028 | 73 | 31 | 75 | 67 | 100 | 63 | 92 | 90 | 93 |
| P HH, P VH | 0.6755 | 0.0028 | 72 | 56 | 42 | 67 | 83 | 75 | 100 | 90 | 71 |
| C LL, P RR | 0.6752 | 0.0029 | 72 | 25 | 67 | 83 | 100 | 75 | 83 | 90 | 86 |
| C LL, P TP | 0.6640 | 0.0029 | 71 | 19 | 83 | 83 | 100 | 75 | 75 | 90 | 79 |
| C VH, P TP | 0.6026 | 0.0031 | 65 | 19 | 67 | 67 | 100 | 63 | 83 | 80 | 79 |
| C VV, P RR | 0.5897 | 0.0031 | 64 | 13 | 58 | 50 | 67 | 69 | 92 | 90 | 86 |
| C HH, P RR | 0.5851 | 0.0034 | 64 | 44 | 67 | 33 | 83 | 56 | 75 | 80 | 79 |
| L HH, P RR | 0.5851 | 0.0034 | 64 | 44 | 67 | 33 | 83 | 56 | 75 | 80 | 79 |
| C HH, L VV | 0.5478 | 0.0035 | 61 | 69 | 33 | 50 | 100 | 44 | 92 | 60 | 57 |
| C VV, P VH | 0.5339 | 0.0031 | 59 | 0 | 50 | 67 | 83 | 44 | 75 | 100 | 93 |
| C VV, L VV | 0.5096 | 0.0036 | 58 | 25 | 83 | 33 | 100 | 56 | 58 | 60 | 64 |
| C HH, L HH | 0.4854 | 0.0035 | 55 | 69 | 42 | 17 | 83 | 50 | 58 | 50 | 64 |
| C VV, L HH | 0.4610 | 0.0035 | 53 | 19 | 67 | 17 | 83 | 69 | 50 | 40 | 79 |
| C HH, C VV | 0.3181 | 0.0031 | 40 | 19 | 75 | 17 | 83 | 44 | 17 | 20 | 57 |

systems, i.e. ERS-1/2 (C VV), RADARSAT (C HH) and JERS-1 (L HH). The layout of the table conforms to Table 6.9. C RR, P LL is the best performing combination: the associated overall classification accuracy is 73%. This is 45% and 18% higher than the overall accuracy for C RR and P LL, respectively. For individual classes the increase in classification accuracy may be much higher. For example, separately C RR and P LL cannot classify any of the Xeric mixed forest data points correctly. Yet, in combination they classify the data points for this forest type with an accuracy of 83%. Generally speaking, dual frequency and/or polarization combinations do not suffice for classifying Mixed forest. Various combinations yield good results for Logged-over forest, Secondary forest and Non-forest. At the 95% confidence level the overall classification accuracy for both C RR, P LL and C VH, P LL is significantly better than that for the best performing single frequency and/or polarization combination in Table 6.9, i.e. L VV. *The combinations consisting of radar bands similar to the ones available in current satellite systems are clustered in the lower part of the table.* The overall classification result for C HH, L HH and C VV, L HH is not significantly different

**Table 6.14** Gaussian maximum-likelihood classification results for a selection of triple frequency and/or polarization combinations. Classification based on $\overline{\gamma}$ values computed per region.

| | | | Percentage correct | | | | | | | | |
|---|---|---|---|---|---|---|---|---|---|---|---|
| Combination | $\hat{K}$ | $\hat{\sigma}^2_\infty[\hat{K}]$ | Total | Mixed | Wallaba | Xeric mixed | Low swamp | Mora | Logged-over forest | Secondary forest | Non-forest |
| C LL, P VH, P TP | 0.8616 | 0.0015 | 88 | 69 | 92 | 100 | 100 | 88 | 83 | 100 | 93 |
| C VH, P HH, P VH | 0.8367 | 0.0018 | 86 | 69 | 67 | 83 | 100 | 88 | 100 | 100 | 93 |
| P HH, P TP, P RL | 0.8123 | 0.0020 | 84 | 81 | 75 | 100 | 83 | 63 | 92 | 100 | 93 |
| C RR, P HH, P RR | 0.7993 | 0.0021 | 83 | 69 | 75 | 67 | 100 | 81 | 100 | 100 | 79 |
| C VH, P VH, P RR | 0.7870 | 0.0022 | 82 | 50 | 67 | 100 | 100 | 81 | 92 | 100 | 93 |
| C VH, LRL, P VV | 0.7381 | 0.0025 | 77 | 56 | 83 | 100 | 83 | 56 | 92 | 90 | 86 |
| C HH, L HH, P RR | 0.7246 | 0.0026 | 76 | 69 | 67 | 83 | 83 | 50 | 100 | 90 | 86 |
| L HH, L VH, L LL | 0.6499 | 0.0030 | 70 | 56 | 75 | 67 | 100 | 56 | 75 | 90 | 64 |
| C VV, L HH, P RR | 0.6398 | 0.0029 | 68 | 19 | 75 | 50 | 83 | 69 | 92 | 90 | 86 |
| C VV, C TP, C RR | 0.4778 | 0.0034 | 54 | 19 | 83 | 50 | 100 | 50 | 50 | 40 | 71 |

from the result for L HH. Likewise, the result for C HH, C VV does not differ significantly from the result for C VV.

Table 6.14 presents the Gaussian maximum-likelihood classification results for a selection of triple frequency and/or polarization combinations. The layout of the table conforms to Table 6.9. The combinations shown were selected following an evaluation of the potential classification capacity for all combinations possible (see section 5.2.4). The results of this analysis showed that the combination of C LL, P VH, P TP had the highest classification potential. This is confirmed by the maximum-likelihood classification results in Table 6.14. Both C LL, P VH, P TP and C VH, P HH, P VH perform significantly better than the best performing dual frequency and/or polarization combination, i.e. C RR, P LL. Scatter diagrams in Figure 6.15 illustrate the measurement space of the different cover types in the C LL, P VH, P TP combination. The centre of the ellipses coincides with the mean backscatter values. The eigenvectors and eigenvalues of the inverse covariance matrices define the direction and length of the ellipse axes. The ellipses include measurements within a distance of once the standard deviation from the mean values. It is evident from Figure 6.15 that P VH provides a good basis for discriminating Non-forest and Secondary forest from each other as well as from the other cover types. *The backscatter differences between the primary forest types and between those and Logged-over forest are small.* For these cover types the classification results are

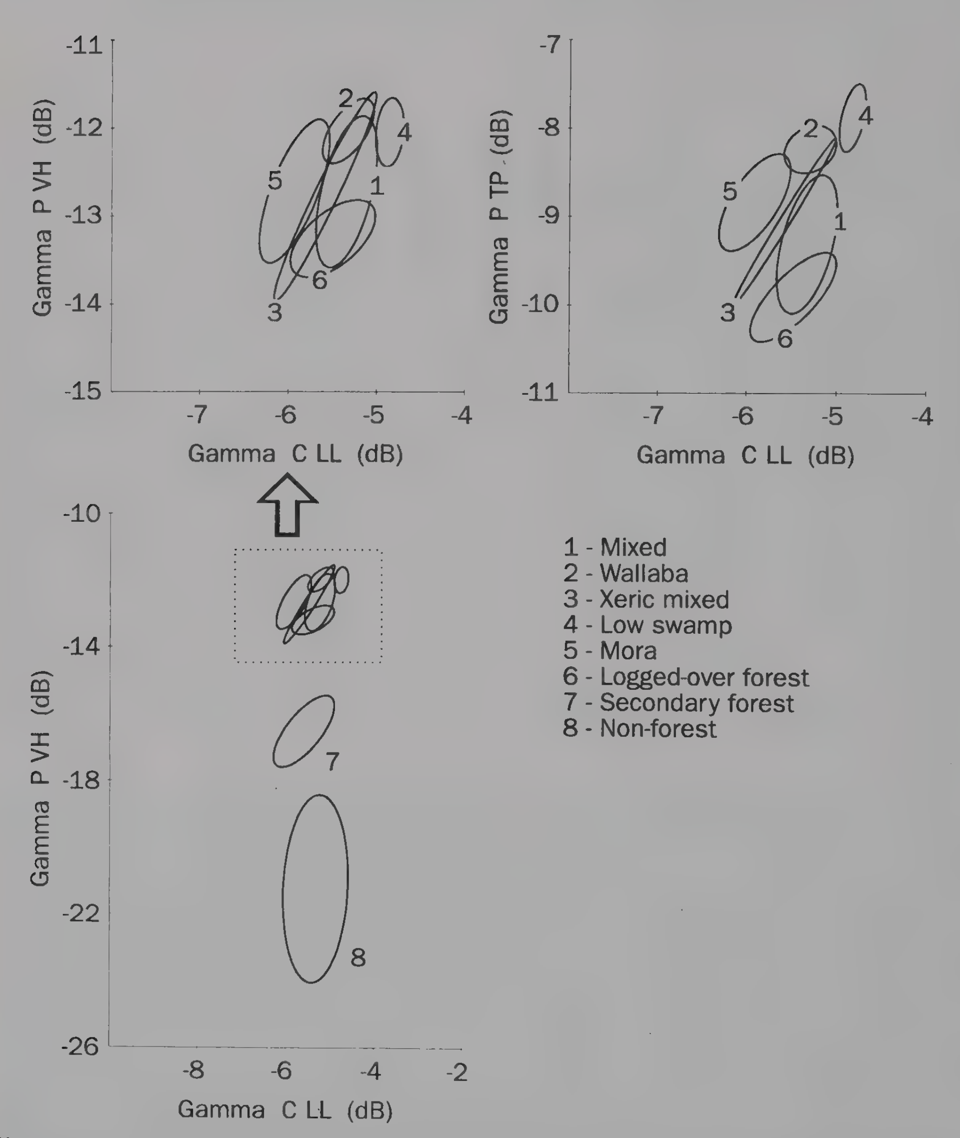



**Figure 6.15** Scatter diagrams illustrating the measurement space of the land cover classes studied in the C LL, P VH, P LL band combination. The ellipses include measurements within a distance of once the standard deviation from the mean values.

primarily governed by shape and orientation of their probability density functions. The ellipses in Figure 6.15 do in fact represent the contours of these probability density functions. The probability for a measurement in a particular class to be located within the boundaries of the corresponding ellipse is equal to 0.68.

*Triple frequency and/or polarization combinations in the first place yield better results for the primary forest types.* Generally speaking, the best performing combinations consist of the following frequency bands: C,P,P or C,C,P or C,L,P or P,P,P. Combinations including linear cross-polarized or circular like-polarized channels often yield better results than others. This suggests that canopy architecture is important for discriminating forest types in radar images since radar return signals with such polarizations typically result from diffuse scattering in the forest canopy.

**Recapitulation**

Figure 6.16 shows the percentage of primary forest, Logged-over forest, Secondary forest and Non-forest *class pairs* that is discriminated by the best performing single, dual and triple frequency and/or polarization combination(s). Assuming that a combination provides a successful classification basis if it can discriminate at least 80% of the class pairs, then it may be concluded that *successful classification of primary forest types requires a triple frequency and/or polarization combination, successful classification of Secondary forest and Logged-over forest requires a dual frequency and/or polarization combination, and successful classification of Non-forest requires a single frequency and/or polarization combination.*

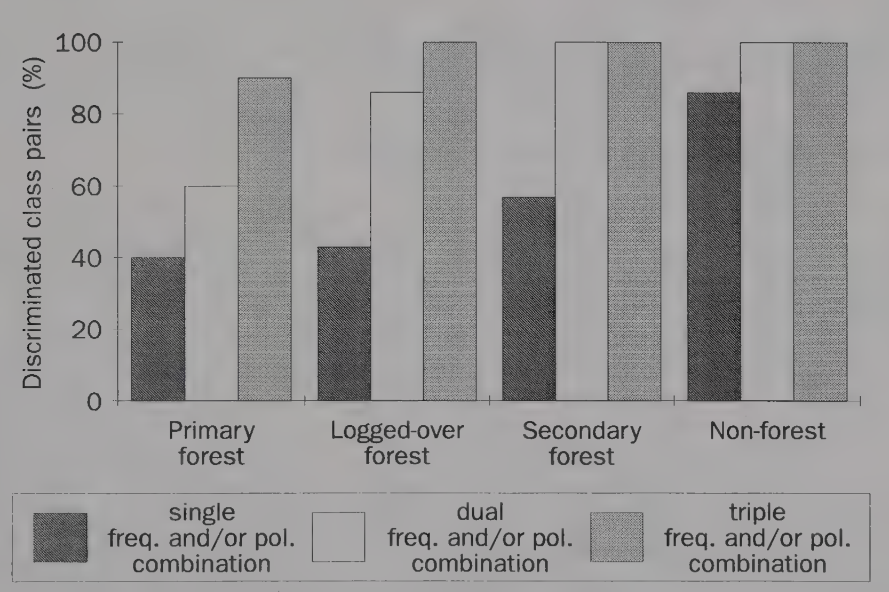



**Figure 6.16** Potential of single, dual and triple frequency and/or polarization combinations for the classification per region of primary forest, Logged-over forest, Secondary forest and Non-forest. The values on the ordinate represent the percentage of class pairs that can be successfully discriminated by the best performing combination(s), i.e. the percentage of class pairs for which $TD_{ij} \geq 1900$.

Combinations most suitable for classifying primary forest types comprise the following frequency bands: C,P,P or C,C,P or C,L,P or P,P,P. Combinations inclusive of linear cross-polarized or circular like-polarized channels are usually more suited than others. For the classification of Logged-over forest a dual combination consisting of P HH and one other P-band channel is most appropriate. However, other combinations such as P HH with C- or L-band (any polarization) or P RR with C VH or C LL also yield good results. Combinations of either L VH or P VH and C-band (any polarization) are most capable of classifying Secondary forest. Finally, Non-forest is classified best by L- or P-band (any polarization).

### 6.3.3 Backscatter as a function of aboveground biomass and architecture

Figure 6.17 shows the variation in the mean backscatter level of the cover types studied in C-, L-, P-band and in HH, VH, VV, RR, RL, LL and TP polarization. In this figure the cover types are ordered based on the total amount of dry biomass above the ground. Non-forest has the lowest aboveground biomass; Mixed forest the highest (see section 4.3). *In all frequency bands and polarizations the backscatter increases with an increase in biomass up to a point corresponding to the biomass level of Low swamp forest. Beyond this point the radar return signal essentially reaches a plateau and saturates.* The total aboveground dry biomass of Low swamp forest is in between that of Secondary forest and Xeric mixed forest, i.e. between 40 and 240 t $ha^{-1}$. A more accurate assessment cannot be made since Low swamp forest was not among the forest types for which ground data on structural forest properties were collected (see section 4.2.3). Other researchers have studied the relationship between the radar backscatter and the aboveground biomass of mostly coniferous forest plantations in temperate regions. They have shown that the backscatter in L- and P-band saturates at a dry biomass level of the order of 100 t $ha^{-1}$ and 200 t $ha^{-1}$, respectively (Dobson et al., 1992; Le Toan et al., 1992). These results agree with the findings in the present study.

*With a sensitivity to dry biomass up to 200 t $ha^{-1}$, P-band SAR systems will be capable of mapping the biomass of tropical forests in the innovation and early aggradation phase but not in the biostatic or mature phase* (see section 4.3.2). This statement is based on the assumption that the forest to be mapped is of a type similar to that of the forests present in Mabura Hill. However, various empirical and backscatter modelling studies show that the radar return signal not only depends on the quantity of biomass above the ground, but also on forest architecture, i.e. on the size, shape and orientation distributions of trunks, branches and foliage (e.g. Sader, 1987; Westman and Paris, 1987; McDonald et al., 1991; Imhoff, 1995; Hoekman, et al., 1996). The modelling study by Imhoff (1995) clearly illustrates that forest stands with equal biomass levels but differing architectures may generate very different radar return signals. This holds true for both stands with biomass levels below and above the threshold at which the backscatter saturates. It follows that *forest architectural differences complicate the development of universal formulations for estimating biomass from radar backscatter.* Yet these architectural differences provide a basis for discriminating forest types with biomass levels above the

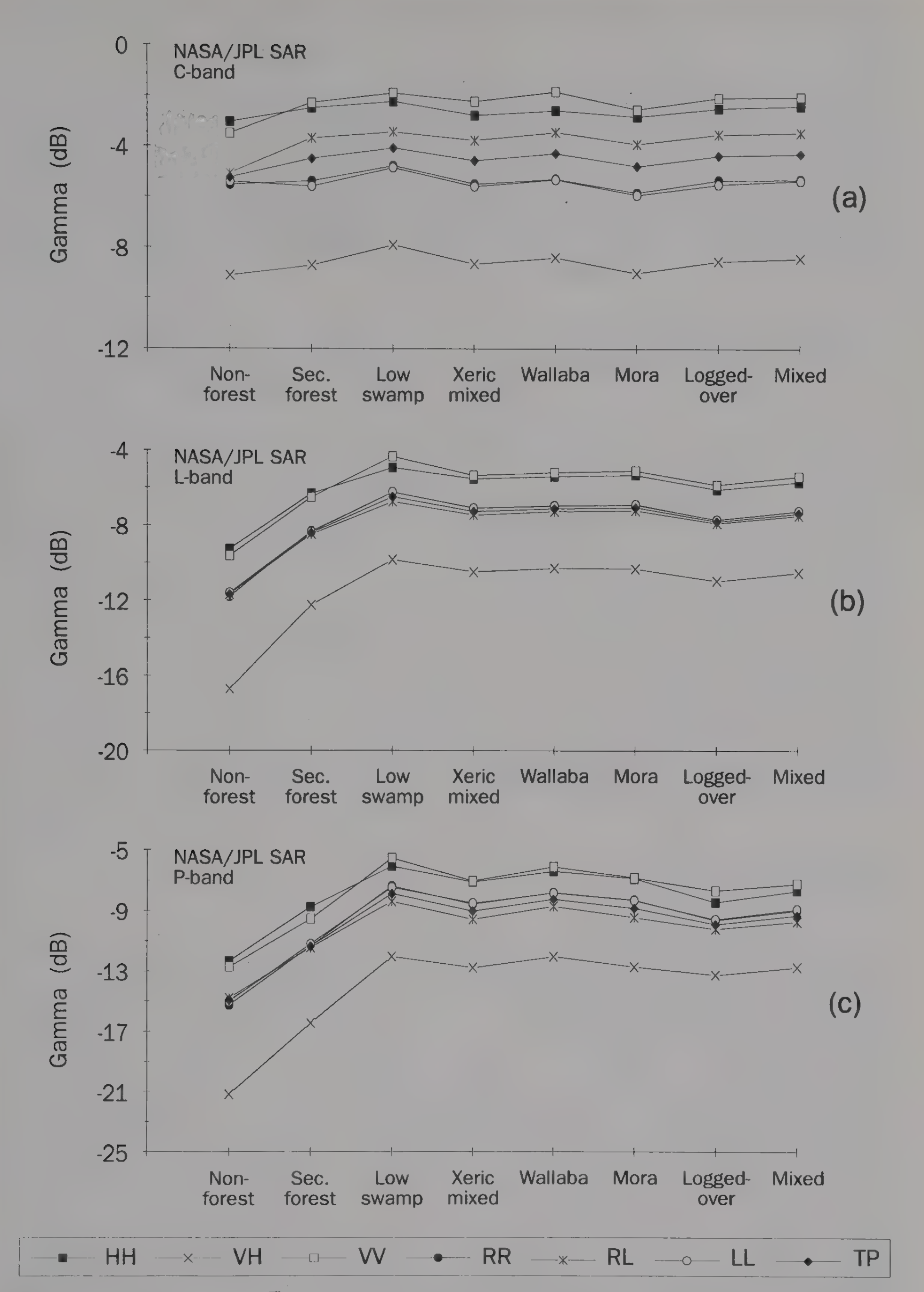



**Figure 6.17 (a-c)** Plots of $\bar{\gamma}$ as a function of total aboveground biomass: (**a**) in C-band HH, VH, VV, RR, RL, LL and TP polarization (**b**) ditto in L-band (**c**) ditto in P-band. The cover types studied are presented as a series from low to high total aboveground biomass.

threshold, i.e. for discriminating forest types such as the ones studied in the present text.

*Architectural differences are hypothesised to be the main cause of the backscatter variations present in the plateaux of the plots in Figure 6.17.* In C-band these variations primarily result from differences in the size, shape and/or orientation distributions of leaves, twigs and/or secondary branches. The backscatter variations in L-band are most likely due to architectural differences in secondary branches, primary branches and/or trunks, and in P-band to architectural differences in primary branches and/or trunks (see section 3.2.2).

With regard to the scattering behaviour of the primary forests and Logged-over forest in C-band, the following observations may be made. In comparison to the other forest types, Wallaba forest and to a lesser extent Xeric mixed forest show a noticeably larger difference in HH and VV backscatter. In both cases the VV backscatter is larger than the HH backscatter. This suggests that the scatterers in the canopies of these forest types are mostly oriented in the vertical plane, i.e. the presence of a special architecture. The scatterers in the other forest types have a more randomly distributed orientation. Generally speaking, the return signals for Xeric mixed and Mora forest are somewhat lower than those for the other forest types. In C-band the different forest types may be considered to constitute an "opaque" vegetation layer. This implies that the backscatter is only dependent on the ratio between the scatterers' radar cross section and extinction cross section (see Equation 3.28, section 3.2.1). The lower backscatter levels for Xeric mixed forest and Mora forest thus indicate either a smaller radar cross section or a larger extinction cross section. Ground observations show that many of the species in Xeric mixed forest have a relatively small leaf size (see section 4.3.3). A small leaf size implies a small radar cross section. The, on average, small leaf size for Xeric mixed forest fits in well with the noted low backscatter levels, since in C-band, the leaves are important scatterers. The available ground reference data do not explain the scattering behaviour of the Mora forest.

In L-band the backscatter signatures associated with the different polarizations show more similar trends than in C- and P-band. This suggests that the orientation of the L-band scatterers is randomly distributed. The backscatter levels for Low swamp forest are somewhat higher than those for the other forest types. According to the results discussed in section 6.3.1 double bounce scattering does not contribute much to the backscatter for Low swamp forest in L-band. It may be assumed, however, that the relatively high L-band backscatter levels for Low swamp result from an enhancement of double bounce scattering by forest flooding. After all the backscatter difference between Low swamp forest and the other primary forest types is small. Moreover, the assumption is supported by the fact that Low swamp forest displays a similar behaviour in P-band. In this frequency band the backscatter of Low swamp forest was found to include contributions resulting from double bounce interaction.

*The backscatter level for Logged-over forest, when compared to that of primary forest types other than Low swamp forest, is slightly lower.* Logged-over forest originates from Mixed forest. The backscatter difference between these forest types may thus

be attributed to logging. *Logging results in a reduced total biomass above the ground and affects forest architecture.* Felled and extracted trees represent a dry biomass of the order of 22 t $ha^{-1}$ (see section 4.3.2). The total reduction in aboveground biomass, however, is usually considerably larger due to logging inflicted damage to the remaining forest (e.g. Jonkers, 1987; Hendrison, 1990). Nevertheless the biomass decrease due to logging will usually be small in comparison to the biomass level of the Mixed forest (ca. 650 t $ha^{-1}$, see Figure 4.6). On average *per hectare*, the dry biomass level of Logged-over forest will be well above the threshold value of ca. 100 t $ha^{-1}$ at which the L-band backscatter saturates. However, the actual felling of trees is generally concentrated in relatively small areas. This especially holds true in Mabura Hill since the preferred species grows in groups (see section 4.3.2). At felling locations the biomass may well be reduced to a level below that of backscatter saturation. Hence, the corresponding regions in radar images may show considerably decreased backscatter levels.

The small difference in the L-band backscatter for Logged-over and Mixed forest can be explained by the fact that the backscatter values studied are mean values for image regions. The image regions for Logged-over forest are much more heterogeneous than those for the other forest types. They comprise a mixture of smaller areas where trees have been felled (artificial gaps) and larger areas where the forest is more or less intact. By computing the mean backscatter values for such regions the low backscatter values associated with locations of felling are largely averaged out. Consequently, the backscatter values for Logged-over forest are relatively high, i.e. not much lower than those for Mixed forest. In the analysis of radar data the averaging of backscatter values is necessary to limit backscatter variations due to speckle. The studied NASA/JPL AIRSAR backscatter values were computed by averaging over a region of at least 2500 $m^2$ in order to meet the 500 looks criterion adopted (see section 5.2.1). According to Hammond and Brown (1992) the average size of the felling gaps in Mabura Hill is 800 $m^2$.

Like in L-band, the backscatter values for Low swamp forest in P-band are higher than those for the other primary forest types. Results in section 6.3.1 show that the microwave interaction in P-band includes double bounce scattering. Double bounce scattering involves trunk-ground and/or crown-ground interaction and thus benefits from a highly reflective ground surface, i.e. from forest flooding. It is therefore hypothesised that *forest flooding contributes to the high P-band backscatter values for Low swamp forest.* Similar to in L-band, the backscatter values for Logged-over forest in P-band are lower than those for Mixed forest and the other primary forest types. The difference in backscatter between Logged-over forest and Mixed forest is the largest in HH polarization, i.e. 0.77 dB. An explanation for the relatively small difference in the backscatter for Logged-over forest and primary forest was given above.

The P-band backscatter levels for Wallaba forest are high in comparison to those for the other primary forest types (excluding Low swamp forest). This cannot be an effect related to the amount of biomass present, for more than one reason. First, the aboveground biomass of Wallaba forest is lower than that of Mora forest and Mixed forest. Second, the dry biomass level of all primary forest types exceeds 200 t $ha^{-1}$, i.e. the threshold at which the backscatter in P-band saturates. The relatively high

**Table 6.15** Available dynamic range for each of the radar bands studied. The values in this table represent the backscatter difference in dB between the cover types with the lowest and highest aboveground biomass, i.e. Non-forest and Mixed forest.

| | Polarization | | | | | | |
|---|---|---|---|---|---|---|---|
| | HH | VH | VV | RR | RL | LL | TP |
| C-band | 0.66 | 0.71 | 1.48 | 0.24 | 1.63 | 0.07 | 0.97 |
| L-band | 3.60 | 6.21 | 4.27 | 4.59 | 4.22 | 4.41 | 4.36 |
| P-band | 4.68 | 8.48 | 5.53 | 6.30 | 5.09 | 6.14 | 5.66 |

backscatter levels for Wallaba forest most likely result from specific architectural properties of the main backscattering sources, namely primary branches and trunks. In a study by Loubry (1994) on the architectural properties of Soft wallaba, i.e. one of the two most important species in Wallaba forest, it is in fact observed that the crowns of mature trees comprise big complexes of reiterated branches. Further evidence of a high concentration of branches and leaves in the upper quarters of the Wallaba forest is found in the ERASME scatterometer data (see section 6.4.1). The presence of a dense layer of primary branches could well be the cause of the relatively high backscatter levels for Wallaba forest in P-band. The absence of similar effects in L-band suggests that in this frequency band, like in C-band, the upper forest canopy is equivalent to an "opaque" layer (see section 3.2.1).

The backscatter difference between the cover type with the lowest and highest aboveground biomass, i.e. Non-forest and Mixed forest, reflects the sensitivity of a radar band to biomass. This backscatter difference is commonly referred to as the dynamic range. Table 6.15 lists the dynamic range for each of the radar bands studied. *The dynamic range and hence the sensitivity to biomass is shown to increase with an increase in wavelength.* This phenomenon is well known and may be explained by the relationship between wavelength and the scattering behaviour of the different forest components (see Table 3.2). *The C-, L- and P-band combinations most sensitive to biomass are C RL, L VH and P VH.* The high sensitivity of the L- and P-band linear cross-polarizations, relative to that of the linear like-polarizations, was also observed in studies based on data from temperate forest plantations by e.g. Wu and Sader (1987), Hussin et al. (1991), Dobson et al. (1992), Le Toan et al. (1992) and Moghaddam et al. (1994). According to these authors the dynamic range between clear-cuts and the highest biomass forest stands is 5 to 10 dB in L-band and 10 to 15 dB in P-band. The ranges shown in Table 6.15, in particular in P-band, are considerably smaller. This is probably due to the fact that the Non-forest class represents a mixture of non-forest cover types with varying degrees of aboveground biomass rather than clear-cuts. Results by Rignot et al. (1995) suggest that RR polarized P-band data are less suited for biomass mapping than linear polarized P-band data. P-band RR data are found to overpredict biomass in relatively open flooded and non-flooded forests where trunk-ground scattering is a strong contributor to total backscatter. The Low swamp forest studied exhibits equally enhanced P-band backscatter levels in all polarizations with the exception of VH (see Figure 6.17c). This does not seem to agree with the findings by Rignot et al. (1995). However, the

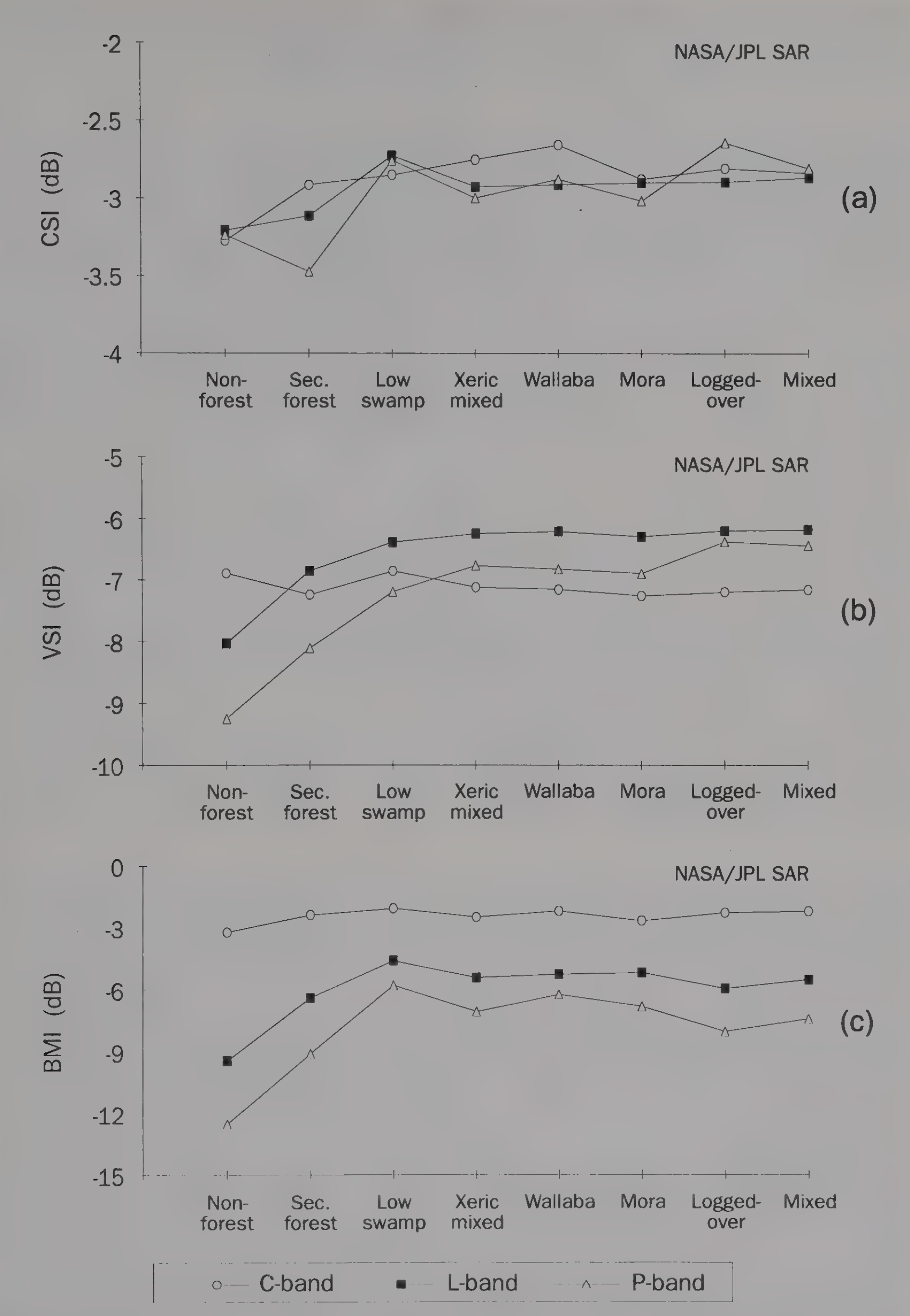



**Figure 6.18 (a-c)** Plots of indices according to Pope et al. (1994) as a function of total aboveground biomass in C-, L- and P-band: (**a**) 'Canopy Structure Index' CSI (**b**) 'Volume Scattering Index' VSI (**c**) 'Biomass Index' BMI. The cover types studied are presented as a series from low to high total aboveground biomass.

backscatter behaviour of the Low swamp forest may well be affected by the relatively large angle of incidence (ca. 60°). Large incidence angles result in a reduced depth of vertical penetration and hence hinder trunk-ground scattering.

Figure 6.18 shows the C-, L- and P-band Canopy Structure Index CSI, Volume Scattering Index VSI and Biomass Index BMI of the cover types studied (see section 5.2.1). Like in Figure 6.17, the cover types are presented as a series from low to high total aboveground biomass. The results as discussed in section 6.3.1 need to be taken into account in the interpretation of Figure 6.18 since the indices are meaningful only in the context of the scattering mechanism.

*The CSI for cover types dominated by diffuse scattering is a parameter of the proportion of vertical and horizontal scatterers.* Dominance of vertically oriented scatterers results in high CSI values, whereas dominance of horizontally oriented scatterers results in low CSI values. Trunk-ground double bounce scattering may give rise to reduced CSI values since this type of interaction in particular results in HH backscatter (e.g. Dobson et al., 1992; Pope et al., 1994). In C-band, Xeric mixed forest and Wallaba forest can be seen to have the highest CSI values. For all cover types studied, the C-band backscatter primarily results from diffuse scattering (see section 6.3.1). Hence, it appears that Xeric mixed forest and Wallaba forest have a relatively high proportion of vertically oriented scatterers, i.e. leaves, twigs and secondary branches. The low CSI value for Secondary forest in P-band is most likely due to the strengthening effect of trunk-ground scattering on the HH backscatter in particular. In P-band and to a lesser extent in L-band there is also evidence of trunk-ground scattering in the flooded Low swamp forest. Yet the P- and L-band CSI values for Low swamp forest are relatively high. This is may be explained by the large angle of incidence (ca. 60°) which causes diffuse scattering to be more important than trunk-ground scattering.

VSI is a parameter of the depolarization of the linear-like polarized incident radar signal. High VSI values occur when cross-polarized backscatter is large with respect to the like-polarized backscatter. *VSI is indicative of diffuse or volume scattering as this is the most important depolarizing interaction mechanism (see section 3.2.3). It reflects the density of scatterers in the vegetation volume and the vegetation volume thickness.* In C-band the different cover types are shown to have comparable VSI values. It follows that the different cover types have a comparable number density of C-band scatterers such as leaves, twigs and secondary branches. Since the Non-forest cover type is poor in twigs and branches it may be concluded that leaves are the most important source of cross-polarized C-band backscatter. In L-band the VSI values increase over the range from Non-forest to Xeric mixed forest and then become saturated. An increase in the L-band VSI values signifies an increase in the volume or the density of the most important sources of cross-polarized L-band backscatter, i.e. of secondary and primary branches. The point where the VSI value becomes saturated corresponds to the point where the scatterer volume becomes "opaque". In P-band the VSI values appear to become saturated at a point similar to in L-band but then rise again for Logged-over and Mixed forest. However, the relatively high VSI values for Logged-over and Mixed forest do not result from especially high $\gamma_{VH}$ values but rather from low $\gamma_{HH}$ values (see Figure 6.17). HH backscatter mostly

results from trunk-ground interaction. It appears that this interaction mechanism is even less common in Logged-over and Mixed forest than in Xeric mixed, Wallaba and Mora forest.

*The most relevant biophysical parameter associated with BMI is biomass.* However, the value of BMI depends strongly on the size of the biomass constituents relative to the incident wavelength. The effective size of the biomass components determines whether they act as backscattering or attenuating sources. Depending on wavelength, an increase in biomass may therefore result in a higher or lower backscatter and likewise in a higher or lower BMI value. The value of BMI may be elevated due to double bounce scattering since this interaction mechanism enhances $\gamma_{HH}$. Comparison of Figure 6.18c with Figures 6.17a-c shows that the BMI and backscatter plots are essentially the same. *The BMI plots do not contain new information* and therefore need no further discussion. BMI appears to be of little value to this study.

### 6.3.4 Conclusions

Analysis of the NASA/JPL AIRSAR data leads to the following conclusions.

➤ *The backscatter of primary and logged-over tropical forests in C-, L- and P-band results primarily from the diffuse scattering of microwaves in the forest canopy.*

- Double bounce or trunk-ground interaction of P-band microwaves in primary tropical forests, with the exception of flooded swamp forests, is uncommon.

➤ *Backscatter measurements in L- and P-band make considerably better bases for classifying tropical land cover types than backscatter measurements in C-band.*

➤ *Backscatter values computed from L- and P-band radar data and textural values computed from high resolution X- and C-band radar data are equally suitable bases for region-based classification of tropical land cover types, including primary forest types.*

- Regardless of the frequency band, the HH-VV phase difference PPD and the corresponding standard deviation sd(PPD) are poor bases for region-based classification of tropical land cover types.

➤ *Backscatter measurements in either a single L- or P-band channel make good bases for region-based classification of tropical land cover at the level of forest / non-forest.*

➤ *Backscatter measurements in a minimum of two radar channels make good bases for region-based classification of secondary and logged-over forest.*

- Reliable classification of secondary forest requires inclusion of at least one L- or P-band channel. Reliable classification of logged-over forest requires inclusion of at least one P-band channel. C-band is of little value for classification of secondary and logged-over forest.

➤ *Backscatter measurements in a minimum of three radar channels make good bases for region-based classification of primary tropical forest types.*

- Reliable classification of primary tropical forest types requires inclusion of at least one P-band channel. C-band is of value for classification of primary forest.

- Inclusion of linear cross-polarized or circular like-polarized channels enhances the chances of classifying primary forest types correctly.

- Architecture and not biomass governs the backscatter behaviour of primary tropical forests in C-, L- as well as P-band. Hence, architectural differences are the key to identifying primary tropical forest types in radar images.

➤ *The potential of L- and P-band radar systems to map biomass is limited to tropical forests in early developmental phases.*

- Regardless of the frequency band, the Canopy Structure Index (CSI), Volume Scattering Index (VSI) and Biomass Index (BMI) contribute little to the understanding of the backscatter behaviour of the land cover types studied.

## 6.4 Results of the analysis of the ERASME scatterometer data

In the present study the data acquired by the ERASME scatterometer system were not analysed in detail. The results presented in this section just serve to illustrate the information content and application potential of scatterometer data in a tropical forest environment. ERASME's technical specifications and operational characteristics are discussed in section 4.4.4. Other authors who report on the use of this system in a tropical forest environment are: Dechambre et al. (1993), Dechambre (1994), Riéra et al. (1994) and Dechambre and Bourdeau (1996).

### 6.4.1 Capabilities of ERASME: an illustration

ERASME's main feature is its "probing" capability. This enables the system to measure the backscatter from 1.30 m high horizontal observation layers superimposed upon the forest. *The combined measurements hold information on the vertical architecture of the forest and the changes in this architecture along the system's ground track.* Observed architectural characteristics are forest height and vertical distribution of backscatterers such as leaves and branches. Tree trunks did not act as backscattering sources since ERASME operated in the nadir-looking mode. The *measurements in addition reflect changes in the topography of the terrain.*

Figure V.8 in Appendix V illustrates the deployment of ERASME over the Tropenbos ecological reserve in Mabura Hill and shows the corresponding transect of radar measurements. The colour coding expresses the relative strength of the radar return signal. The first radar return signal at a particular location along the flight path flown corresponds to the upper boundary of the forest canopy. Successive return signals from the same location result from consecutive observation layers. The strength of these signals is a function of the forest's backscatter and extinction properties. Due to the nadir-looking operating mode of ERASME, the forest soil has the potential to create a relatively high radar return signal. However, the strength of this return signal depends strongly on the attenuating properties of the overlying vegetation. In the ERASME data from Mabura Hill, unmistakable high return signals from the forest soil are not always present. Whenever such a signal is lacking, forest height cannot be estimated accurately. The absence of a clear return signal from the soil indicates that the forests in Mabura Hill have a strong attenuating capacity, i.e. that the forests have a high leaf and branch biomass.

Figure V.8 illustrates how ERASME measurements show the changes in the topography of the terrain observed. The higher parts of the terrain are locations where Wallaba and Mixed forests are found. The system's ground track intersects twice with an area of low lying, swampy grounds. On these grounds a forest type known as Swamp wallaba is found. *The transect clearly shows the difference in the canopy roughness for Wallaba forest and Mixed forest.* The canopy of the latter forest type can be seen to be substantially rougher. This agrees with the findings based on the textural analysis of the CCRS SAR and ERS-1 data sets (see sections 6.1.2 and 6.2.2). Data from systems like ERASME appear very suitable for the assessment of quantitative canopy roughness parameters.

Data on the surface roughness of forests or other types of land cover are valuable information for land surface - atmosphere interaction studies. Surface roughness affects the exchange processes between the land and the atmosphere. These exchange processes in turn influence the dynamics of the entire atmosphere. Consequently, surface roughness is an important parameter in weather models and General Circulation Models (GCM's) (see Wood, 1991; van den Hurk, 1996). Oldeman (1983a), Brünig and Huang (1989) and Brünig and Mohren (1989) suggest that *canopy roughness is a good indicator of species diversity.* The reasoning behind this hypothesis is the following: a rough canopy is indicative of a high architectural diversity, of the presence of many environmental gradients and consequently of a high diversity in ecological niches and species. In this ecological context, the conclusion by Duivenvoorden and Lips (1995) that plant diversity is predictable by physiography and forest canopy height is also of interest. For some applications, a qualitative characterisation of the canopy roughness may suffice. Such a characterisation may be obtained from data from both imaging and non-imaging radar systems (see section 6.1.2 and 6.2.2). Weather and global circulation modelling, on the other hand, requires quantitative surface roughness information. In the microwave region of the electromagnetic spectrum this information can be derived from data acquired by non-imaging scatterometers such as ERASME or by high resolution imaging radar systems with interferometric capabilities.

The ERASME transect in Figure V.8 shows the vertical distribution of the scatterers, and thus of the leaf and branch biomass, in Wallaba and Mixed forests. In the higher quarters of the Wallaba forest there proves to be a high concentration of scatterers. This agrees with the findings by Loubry (1994) with respect to the architectural properties of one of the two most important Wallaba forest species, i.e. Soft wallaba. According to this author, the crowns of mature Soft wallaba trees are characterised by big complexes of reiterated branches. The scatterer density is increased further by the fact that the forest has a well-defined and continuous upper canopy (see Figure 4.9). In Mixed forest a similar dense layer of scatterers is absent; within the range from the canopy boundary to the forest floor the leaf and branch biomass of this forest type is more evenly distributed. *The opportunity of distinguishing between sources of scattering leads to a better notion of the forest's scattering behaviour and supports backscatter modelling studies* (see Hoekman, 1990). From the viewpoint of forest management, scatterometer data are useful because they reflect both the vertical and horizontal architecture of the forest. Scatterometer data can complement hand-measured profile diagrams like the ones in Figures 4.7 through 4.11. Hence, *these data support the analysis of forest architecture and forest dynamics and so can contribute to the development of forest management procedures.*

Figure 6.19 presents ERASME spectra (backscatter profiles) for Mixed, Wallaba and Mora forest. The forest height as derived from the ERASME data agrees well with the ground reference data in section 4.3.1. It is shown that ERASME is capable of discriminating between an emergent Mora tree and the Mora forest's main canopy. *The variability of the backscatter with the height is indicative of inhomogenities in the vertical distribution of the scatterers.* The high backscatter levels for Wallaba forest at a height somewhere between 20 and 30 m illustrate the high concentration of scatterers in this particular part of the forest. Descending from ca. 20 to 5 m, the scatterer density decreases rapidly. The vertical distribution of the backscatterers in Mixed forest and especially in Mora forest is much more uniform.

Unlike most Mixed and Mora forest backscatter profiles, the ones presented in Figure 6.19 show a radar return signal from the forest soil. This indicates that the forest patches corresponding to these profiles have a relatively low leaf and branch biomass. The total amount of power as received by ERASME for Mixed forest and Mora forest can be shown to be approximately -25 dB. For Wallaba forest, on the other hand, the total received power is of the order of -20 dB. It follows that the total power received for Wallaba forest is about three times higher than that for Mixed forest and Mora forest. *The total received power is a function of the scattering and extinction properties of the leaves and branches but cannot be directly related to leaf and/or branch biomass.* In other words, a high amount of total received power is not necessarily indicative of a high quantity of leaf and/or branch biomass.

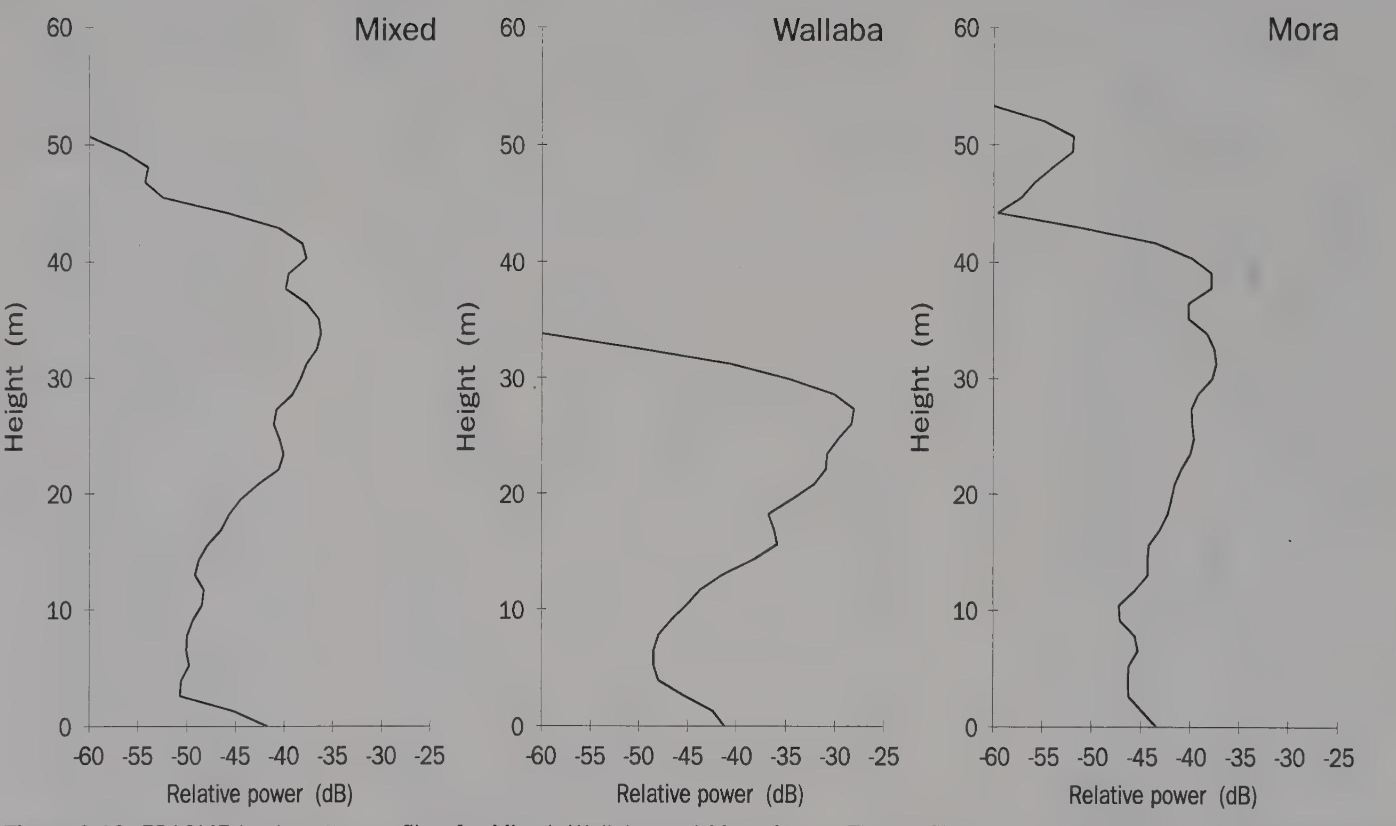



**Figure 6.19** ERASME backscatter profiles for Mixed, Wallaba and Mora forest. The profiles hold information on the vertical architecture of the forest, i.e. on the forest height and the vertical distribution of backscatterers such as leaves and branches. High backscatter levels are indicative of high concentrations of scatterers.

### 6.4.2 Conclusions

Analysis of the ERASME scatterometer data leads to the following conclusions.

➤ *Data from ERASME and comparable nadir-looking scatterometer systems enable the assessment of quantitative canopy roughness parameters.*

- The frequent absence of return signals from the forest soil illustrates the high leaf and branch biomass levels of the forests in Mabura Hill and complicates the assessment of forest heights.

- Scatterometer measurements, like hand-measured profile diagrams, support analysis of forest architecture and forest dynamics and hence contribute to the development of forest management procedures.

# 7 Radar remote sensing to support forest resource monitoring

*Forest resource monitoring* was defined in section 1.1 as *the process of continuously knowing the state of the forest environment and the changes that have and are taking place.* The starting point for a monitoring process is a description of the forest's state at time $t_0$. This description is obtained through forest resource assessment. The aim of forest resource monitoring is to check the state of the forest by collecting information on the location, extent and nature of changes. In order to plan and guide changes it is also important to gather information on the cause and rate of change. As in forest resource assessment, radar remote sensing may be used in forest resource monitoring as a tool for collecting data. However, in the case of forest monitoring there is a need for repetitive and systematic data coverage. Orbiting remote sensing satellite systems can fulfil these requirements at lower expense than airborne remote sensing systems (see section 2.2.1). Therefore, *provided that data can be acquired of the necessary type and spatial detail, satellite systems are the preferred platform for use in forest resource monitoring.*

The present chapter reports on the capability of the ERS-1 SAR to provide information in support of tropical forest monitoring. The emphasis is on the main study area in Mabura Hill, Guyana. ERS-1's capabilities to detect land cover change in the settlement area of San José del Guaviare, Colombia are discussed by Bijker (1997). Unlike San José del Guaviare, Mabura Hill is a relatively stable area. Forest cover changes result from either natural causes or relatively small scale human impacts. During the period of observation there were no large scale natural disturbances, such as those resulting from hurricanes, landslides, earthquakes or fire. Small scale natural disturbances due to e.g. tree senescence, windblow or lightning must have been abundant as these drive the process of silvigenesis (see section 4.3.2 and Oldeman, 1990). Disturbances of a human origin primarily result from industrial selective logging. Clear-cut or shifting cultivation are not practised. *The present study focuses on an assessment of ERS-1's capabilities to image change related to selective logging.* Results in section 6.2.1 indicate that ERS-1 backscatter measurements may be used for discriminating between forest and non-forest regions. Therefore, it may be assumed that ERS-1 offers a good potential for monitoring the large scale disturbance resulting from clear-cut or forest/non-forest conversion. This is confirmed by findings of other authors (e.g. Conway et al., 1994; Keil et al., 1994; Leysen et al., 1994; Le Toan et al., 1996 and Bijker, 1997).

Forest cover disturbances will appear in radar images as long as they are accompanied by changes in backscatter or texture. *Detection of forest cover disturbance is complicated by the fact that the backscatter of forest stretches free of natural disturbance or human impact may also vary.* Backscatter fluctuations in such forest patches may *result from phenological changes* (e.g. leaf-fall or -flush) or *changes in environmental conditions* (e.g. rainfall fluctuations). Often, this type of change is not of special interest to forest management. Nevertheless, there is a need to assess to what extent such changes affect radar backscatter. This information allows for better founded decisions with regard to the cause of observed backscatter changes and thus supports the application of radar images in monitoring

procedures. Moreover, information on the variation of the backscatter for tropical rain forests is of interest to engineers involved in the development and operation of radar satellite systems. The interest of this community is dictated by the idea that tropical rain forests have very steady backscatter levels and therefore make good calibration targets (e.g. Bernard and Vidal-Madjar, 1989; Kennett and Li, 1989; Laur, 1992; Shimada, 1993).

The present study on the value of ERS-1 data for tropical forest resource monitoring uses SAR Precision (PRI) products. A series of six images was analysed both for Mabura Hill and San José del Guaviare. The acquisition dates of these images were listed in Table 4.7, section 4.4.3. Temporal backscatter changes in intact forest and other cover types were assessed by extracting $\overline{\gamma}$ values for fixed regions of interest from images of different dates. The employed image regions were identical to those used for assessing the value of ERS-1 PRI images for land cover classification (see section 6.2.1). The method for extracting $\overline{\gamma}$ values for image regions was discussed in section 5.2.1. ERS-1's capabilities for detecting forest cover changes were evaluated by visual comparison of multi-date enhanced image products and application of an image ratioing technique. Texture was taken into account only in the visual analysis of the multi-date images. Computerised textural analysis of ERS-1 PRI images from successive dates was not implemented because the results in section 6.2.1 indicate that this would yield inadequate results.

## 7.1 Temporal change in ERS-1 SAR backscatter measurements

Figure 7.1 shows the variations in the $\overline{\gamma}$ values for the land cover classes studied as a function of time. The figure also presents the sum of the amounts of rain that fell in the week prior to data acquisition and on the day of data acquisition. In case measurements around the date of data acquisition were lacking, rainfall was estimated from average monthly rainfall figures (see section 4.2.2). Measured and estimated rainfall quantities are represented by columns with dark and light grey tones, respectively. The abscissas indicate the seasonal variation in rainfall. Months inside the dry season are shown as unfilled line-elements, whereas months inside the wet season are represented by solid line-elements. In the case of San José del Guaviare an additional class is introduced, i.e. a Primary forest class. The data for this class served to verify whether the backscatter signature for the Secondary forest class was governed by either forest type characteristics or environmental conditions. The resemblance in the signatures for the two forest types suggests dominance of environmental conditions.

Most striking in Figure 7.1 is the *difference in the backscatter behaviour of the forests in Mabura Hill and those in San José del Guaviare.* The backscatter of the forests in Mabura Hill varies considerably with time, whereas the backscatter of the forests in San José del Guaviare is much more stable. The large backscatter variability in Mabura Hill is shown to be accompanied by large fluctuations in rainfall. In San José del Guaviare the changes in both backscatter and rainfall are

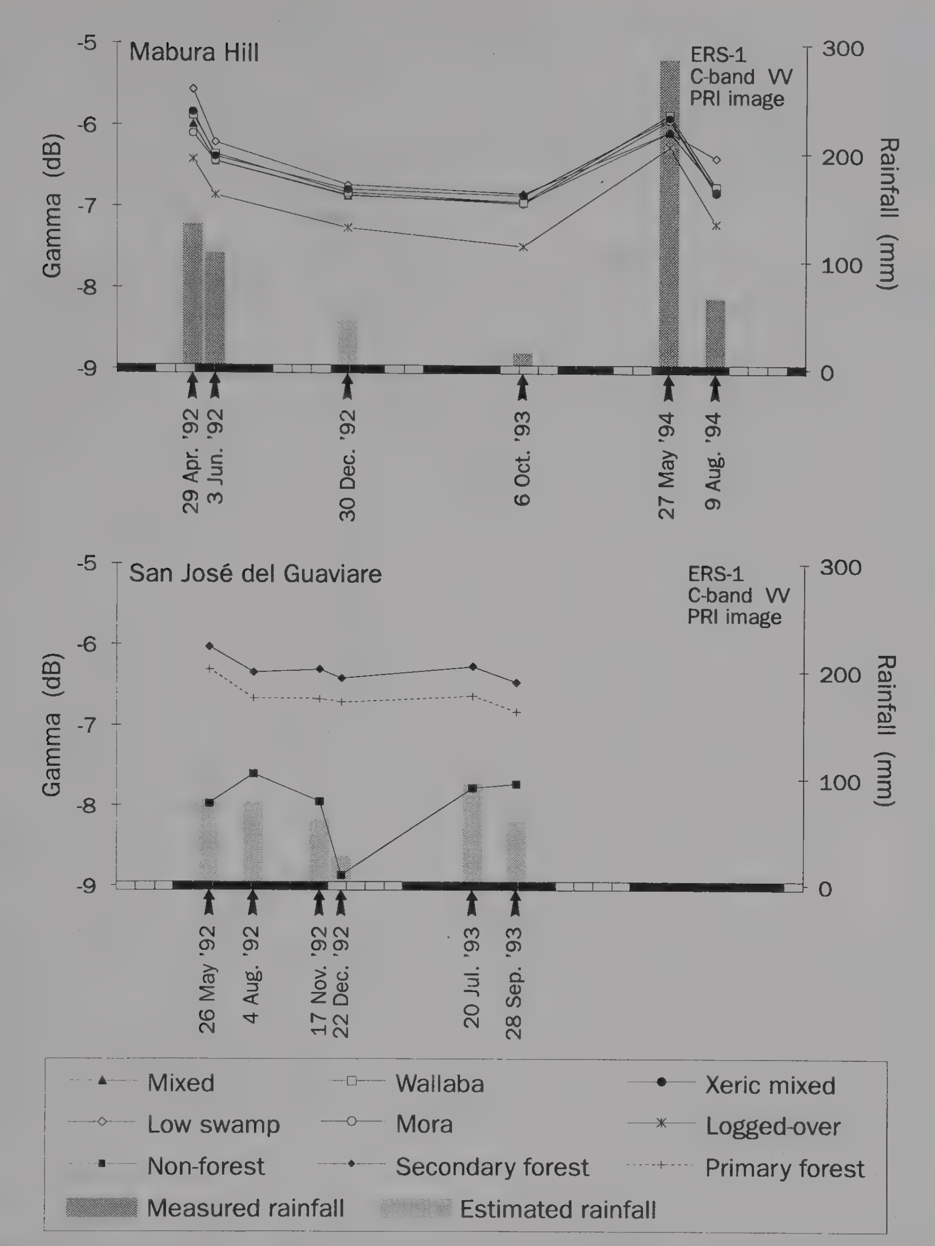



**Figure 7.1** Variation in $\overline{\gamma}$ values for land cover types studied and rainfall as a function of time. The rainfall columns represent the sum of the amounts of rain that fell in the week prior to data acquisition and on the day of data acquisition. The abscissas indicate the seasonal variation in rainfall. Dry months are represented by unfilled line-elements and wet months by solid line-elements.

considerably smaller. Backscatter level and rainfall quantity appear to be well correlated. High backscatter values are found in connection with high rainfall quantities, and the inverse. The Mabura Hill data show this correlation more clearly than the San José del Guaviare data. In the latter case, the relationship between backscatter and rainfall is probably obscured by the fact that rainfall was not measured at the time of data acquisition but estimated from average monthly rainfall figures. Altogether, *Figure 7.1 strongly suggests that rainfall governs the temporal backscatter behaviour of tropical rain forests.*

Leaves, twigs and secondary branches are the most important C-band backscattering sources in forests. Rainfall influences the scattering properties of these canopy elements in different ways. *The direct effect of rainfall is the wetting of the canopy due to interception.* According to Bernard et al. (1987) and Lichtenegger (1996) this effect may cause the backscatter in C-band to increase by about 0.6 dB. This effect is relatively short-lived. Following rainfall it diminishes and finally ceases to exist as a result of evaporation and through fall. It may have contributed to the high backscatter levels for the forests in Mabura Hill on March 27, 1995. On this particular date rainfall amounted to 20 mm (see Table 4.2, section 4.2.2). In contrast, the rain quantities as shown in connection with the other acquisition dates all fell during the week prior to these dates.

The more indirect effect of rainfall is of a seasonal nature. *Seasonal increases in rainfall and humidity are likely to result in higher proportions of water within tree components, i.e. in higher gravimetric water contents.* Evidence for this is found in the results of water content measurements on fully grown leaves in Mabura Hill. In the dry season the leaf gravimetric water content ranged from 0.4 to 0.5 g $g^{-1}$, whereas in the wet season it ranged from 0.5 to 0.6 g $g^{-1}$ (see section 4.3.3). Other investigators have reported seasonal (and diurnal) changes in the water status of trees in temperate regions (e.g. Gates, 1991; Mcdonald et al., 1991; Weber and Ustin, 1991; Salas et al., 1994). For radar observations in C-band a tropical forest canopy may be assumed to make up an "opaque" vegetation layer. Hence, its backscatter is governed by the average radar cross section and the average extinction cross section of the dominant vegetation component, i.e. the leaves. Figure 3.20 in section 3.2.1 illustrates that if the water content of the average leaf grows from 0.4 to 0.5 g $g^{-1}$ or from 0.5 to 0.6 g $g^{-1}$ the radar backscatter increases by ca. 1.5 dB. According to the Cloud model the radar return signal for the forest canopy at large will increase correspondingly (see Equation 3.29). This increase is of the same order of magnitude as the variability in the backscatter measurements for Mabura Hill.

The phenological processes of leaf-fall and leaf-flush are likely to affect the backscatter of forests in C-band. After all, leaves are the most important C-band scattering sources. In Mabura Hill and other tropical regions where water stress situations are uncommon, leaf-fall and -flush peak in the period of maximum solar irradiation (e.g. ter Steege, 1993; Loubry, 1994; Brouwer, 1996). In Mabura Hill this is the case from September through November, i.e. in the driest period (Jetten, 1994). Tropical rain forest trees do not drop their leaves collectively or for extended periods of time. Consequently, the rain forest does not lose its evergreen appearance. Loubry (1994) in French Guiana reports an average leaf-off period of

24.5 days. *The time series of backscatter measurements for the forests in Mabura Hill holds no clear evidence of leaf-fall and/or leaf-flush effects.* The influence of these phenomena on the backscatter of the forest at large is difficult to predict because different trees shed and flush at different points in time. Moreover, leaf-fall does not necessarily result in a reduced C-band backscatter, nor does leaf-flush always result in an enhanced C-band backscatter. Evidence for this can be found in studies that address the temporal change in the backscatter for deciduous trees in temperate regions (e.g. Cihlar et al., 1992; Hoekman et al., 1994).

The Non-forest and forest classes in San José del Guaviare display a different backscatter behaviour (see Figure 7.1). *Unlike the backscatter of the forest classes, the backscatter of the Non-forest class varies considerably in time.* Also, the trends in the backscatter for non-forest and forest are slightly different. For non-forest the relationship between rainfall and backscatter level appears somewhat poorer than for forest. However, it should be taken into account once again that the rainfall figures for Guaviare were estimated from long-term monthly figures. The difference in the backscatter behaviour of non-forest and forest is partly due to a difference in the size of the vegetation volume. Relative to forests, the cover types in the Non-forest class constitute small vegetation volumes. This results in a small storage capacity for water, an unstable water status and hence a variable backscattering behaviour. Moreover, the overall backscatter behaviour of non-forest cover types is likely to be affected by the backscattering properties of the underlying soil layer. Hence, the soil makes an additional source of backscatter variations. Finally, the backscatter variability for non-forest cover types such as crops and pastures may be enhanced as a result of farming practices or natural vegetation regeneration processes. Temporal backscatter variability has been used successfully as a parameter for discriminating between forest and non-forest classes (e.g. Le Toan et al., 1996). For the combined data sets of Mabura Hill and San José del Guaviare this method would not work since the backscatter variability of the forest cover classes in Mabura Hill is not much different from that of the Non-forest class in San José del Guaviare.

According to Figure 7.1 *the temporal change in the ERS-1 backscatter from the intact forests in Mabura Hill is of the order of 1 dB.* This is about two times as high as the temporal change in the backscatter values for the forests in San José del Guaviare. Yet it may not be concluded that the backscatter changes in Mabura Hill are exceptionally high. Le Toan et al. (1996) quote exactly the same figure for the temporal backscatter variation of forests in Sumatra. The temporal change in the backscatter for the Logged-over forest class is ca. 1.2 dB, which is slightly higher than for intact forest. Non-forest displays the largest temporal backscatter fluctuations, i.e. ca. 1.3 dB. In this context it is important to note that the radiometric stability value of the ERS-1 SAR system is 0.2 dB (Laur et al., 1993). This value corresponds to the smallest temporal backscatter difference that can be measured reliably.

Rainfall is shown to slightly enhance the backscatter contrasts between the primary forest types in Mabura Hill (e.g. compare backscatter levels for 29 April 1992 and 6 October 1993). On the other hand, the backscatter contrast between logged-over forest and primary forest is marginally higher in dry conditions. A similar phenomenon may be observed with regard to the contrast between non-forest and primary or

secondary forest. However, in this case the difference in the backscatter contrast for wet and dry periods is much more pronounced. Enhanced forest/non-forest backscatter contrasts during dry conditions were also observed by Conway et al. (1994) in the Ivory Coast and Keil et al. (1994), Luckman et al. (1997) in Brazil. The data in Figure 7.1 suggest that *different primary forest types can be discriminated best in ERS-1 images acquired during wet periods. Images acquired during dry spells seem to offer better possibilities for discriminating logged-over forest from primary forest and non-forest from primary or secondary forest.* Clearly, the chances of acquiring data during wet (dry) conditions will be the highest in the wet (dry) season.

By using images from wet and dry periods the possibilities for classifying the land cover types studied can be improved. The improvement, however, will be marginal since there is no point in time at which the primary forest types may be considered 'separable' from each other, from logged-over forest or from secondary forest. This follows from an evaluation of the separability of the different class pairs according to the method described in section 5.2.4. *Multi-temporal ERS-1 data do not substantially enhance the chances for discriminating between tropical forest types because these forests exhibit very similar temporal backscatter signatures.* Moreover, the temporal changes in backscatter are often small in comparison to the within-class backscatter variations. The variance within the Non-forest class appears to be higher in dry conditions than in wet conditions. This reduces the possibilities to discriminate between forest and non-forest when conditions are dry. It follows that the high non-forest variance counteracts the effect of earlier noted high forest/non-forest backscatter contrast.

## 7.2 Detection of change in forest cover

### 7.2.1 Capability of ERS-1 to image forest cover disturbance

Figure 7.2 shows two ERS-1 image products for Mabura Hill's West Pibiri compartment. The images in Figures 7.2a and 7.2b represent the situation in 1992 and 1994, respectively. During this period the compartment was the location of logging activities by the concessionaire and of directional felling experiments by van der Hout (van der Hout, 1996). Figure 7.2a is the weighted average of three enhanced PRI images from 29 April 1992, 3 June 1992 and 30 December 1992. The respective weights for the images were 3/6, 2/6, 1/6. Similarly, Figure 7.2b represents the weighted average of enhanced PRI images from 6 October 1993 (weight 1/6), 27 May 1994 (weight 2/6) and 9 August 1994 (weight 3/6). The method used to enhance the PRI images was described in section 5.3.3. Images from different acquisition dates were averaged to create a product with better qualities for visual interpretation. The applied weights are meant to suppress change within the first image series, to enhance change within the second image series and thus to emphasise changes that occurred over the period from April 1992 to August 1994.

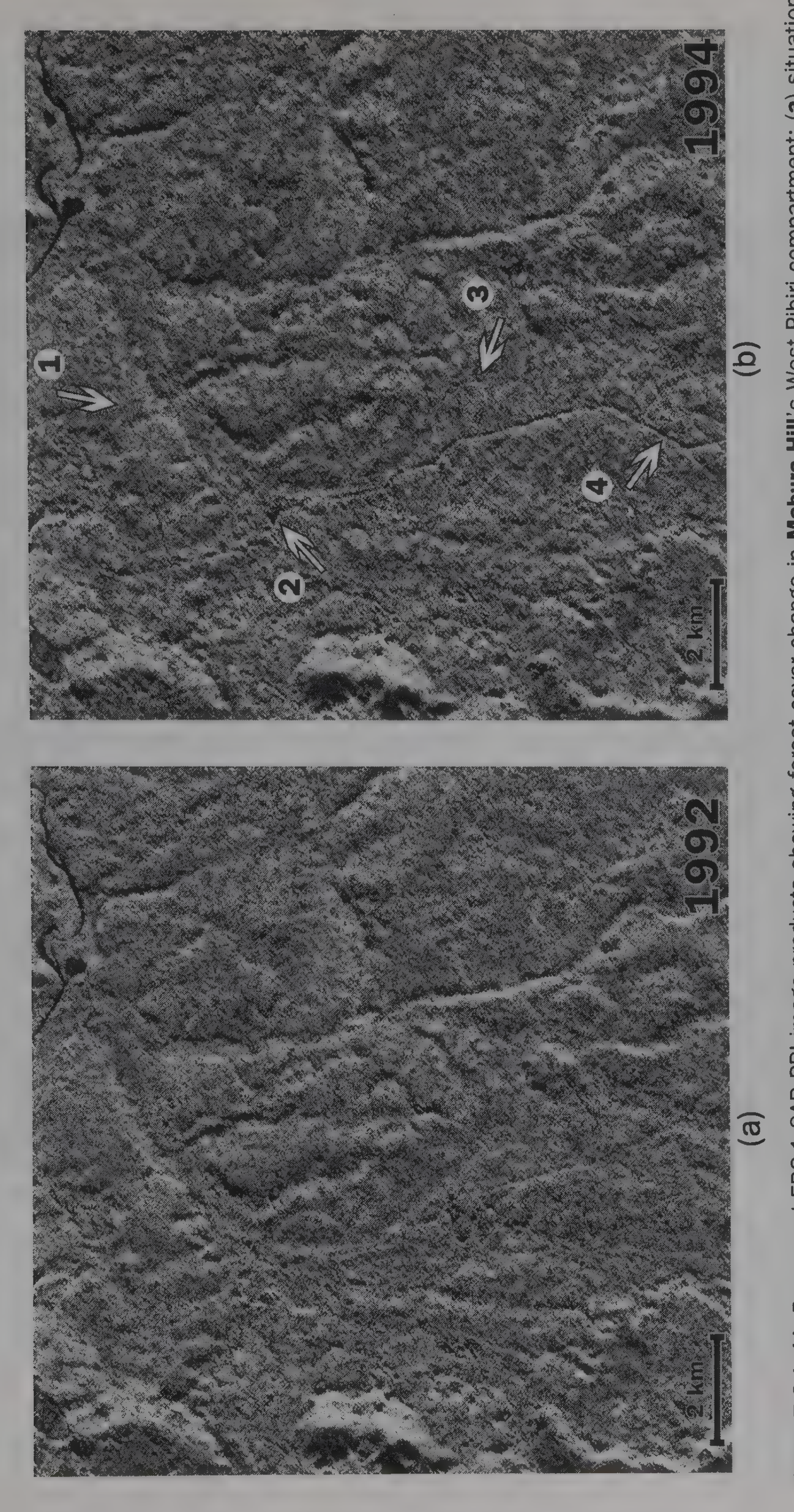



**Figure 7.2 (a-b)** Processed ERS-1 SAR PRI image products showing forest cover change in **Mabura Hill**'s West Pibiri compartment: (**a**) situation in 1992 (**b**) situation in 1994. The most prominent changes relate to the logging road network. Arrow 1 marks a new road, arrow 2 and 3 log-markets and arrow 4 the widened and extended main access road.

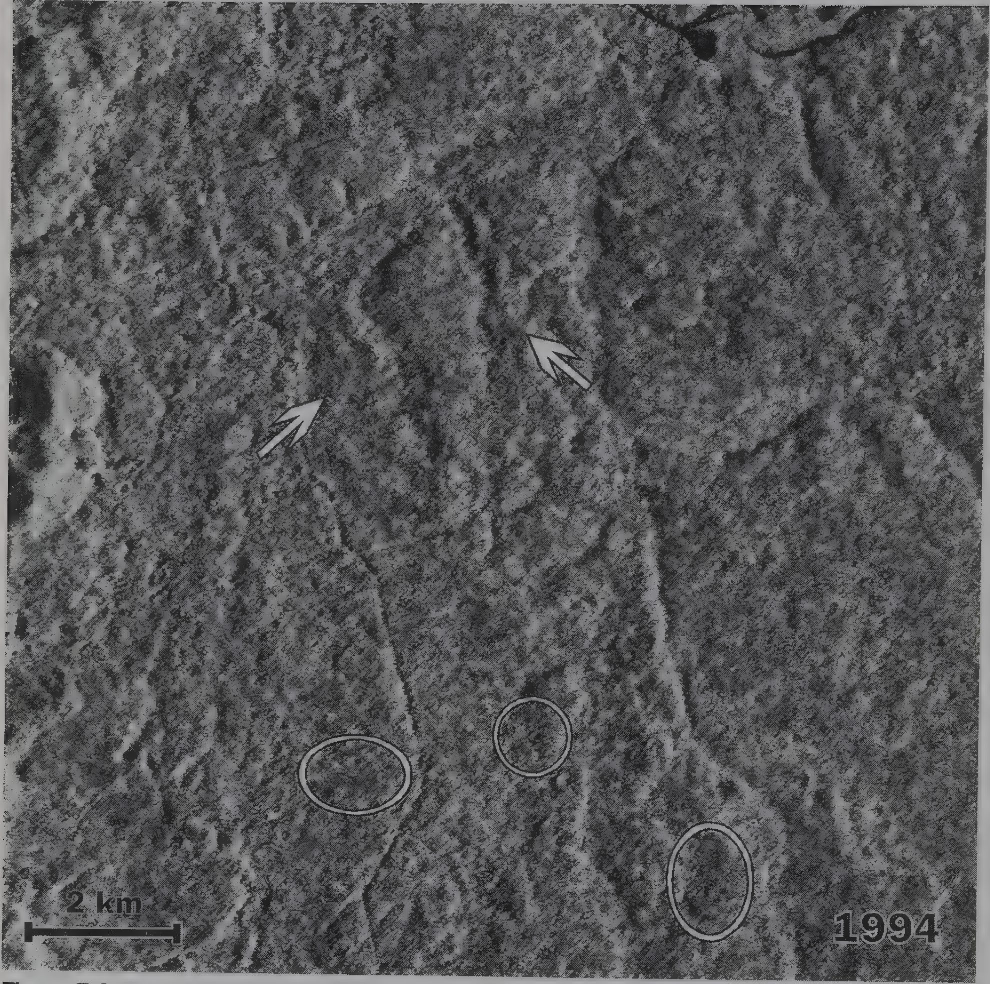



**Figure 7.3** Processed ERS-1 SAR PRI image showing **Mabura Hill**'s West Pibiri compartment in 1994. Some image parts that show canopy gaps resulting from selective logging have been encircled. The arrows mark locations where the directional felling experiments were carried out by van der Hout (1996). The gaps resulting from these experiments do not show clearly in the image.

The most prominent changes in Figure 7.2b relate to the road network. Some locations where changes took place are marked with arrows. Arrow 1 marks a location where a new logging road has been put in. Arrow 2 points to an enlarged log-market, i.e. a cleared area alongside a road where felled logs are assembled pending transportation to the sawmill. Arrow 3 indicates a small, newly constructed road and log-market. Finally, arrow 4 points to the widened and extended main access road. *The larger canopy gaps resulting from selective logging may be observed by trained interpreters with a priori knowledge of logging locations.* This is illustrated in Figure 7.3, which is an enlargement of the image in Figure 7.2b. A number of image parts showing logging gaps have been encircled, the two arrows mark locations where the directional felling experiments were carried out (van der Hout, 1996). The gaps that resulted from these experiments do not show clearly in the image. *Gaps resulting from selective logging and natural gaps often appear very similar and are therefore difficult to discriminate.* Observables indicative of logging are the clustered occurrence of gaps, the systematic occurrence of gaps and the occurrence of gaps in the vicinity of logging roads.

It may be concluded that *roads are by far the best observable indicators of selective logging in ERS-1 images.* Canopy gaps are difficult to recognise primarily because their size is too small with respect to the satellite's spatial resolution. According to Hammond and Brown (1992) the average logging gap size is ca. 800 $m^2$; this equals little more than 5 pixels in an ERS-1 PRI image. For comparison, a full ERS-1 PRI scene covers an area of 10,000 $km^2$ and comprises 64 million pixels. The visibility of logging roads in ERS-1 images depends on their orientation relative to the sensor (viewing geometry) and their geometrical properties. The relationship between viewing geometry and the visibility of linear features such as roads was discussed in section 3.2.5. The most important geometrical property of a road is its width. Road width obviously depends on the road's status within the road network. However, in Mabura Hill, road width is also a function of soil type. Roads on white sand soils are usually narrower than roads on loamy and lateritic soils. The motivation for building relatively narrow roads on white sands is to keep the road surface moist so it provides good traction. On the other hand, roads on loamy and lateritic soils tend to get wet and slippery. By making these roads wider they are more exposed to sunlight and thus stimulated to dry. Whenever accessibility requires a white sand road to be wide, the road is paved with loam or laterite. In Mabura Hill the width of the main access road, inclusive any shoulders, is of the order of 10 to 25 m (Hammond, 1997). Skidding trails with widths of ca. 4 m are found at the other end of the road spectrum. These trails are used to haul the logs from the tree stump to the nearest road and are usually completely overtopped by surrounding vegetation.

For reasons similar to the ones discussed, roads on white sand soils are often less crooked than roads on loamy and lateritic soils. White sands soils are well drained and therefore enable roads to be laid out in straight lines. Since loamy and lateritic soils are less well drained, the roads on these soils are preferably built along water divides on higher terrain parts. In particular, for road construction on less well drained soils, forest management may benefit from information on physiographic terrain characteristics such as topography and drainage. In fact some roads in the Mabura Hill concession were found to come to a dead end in swamps. Physiographic




**Figure 7.4** Processed ERS-1 SAR PRI image showing the Tropenbos ecological reserve in **Mabura Hill** and its surroundings. Note the representation of geomorphic features and drainage patterns. The arrow marks the location of the Tropenbos field station.

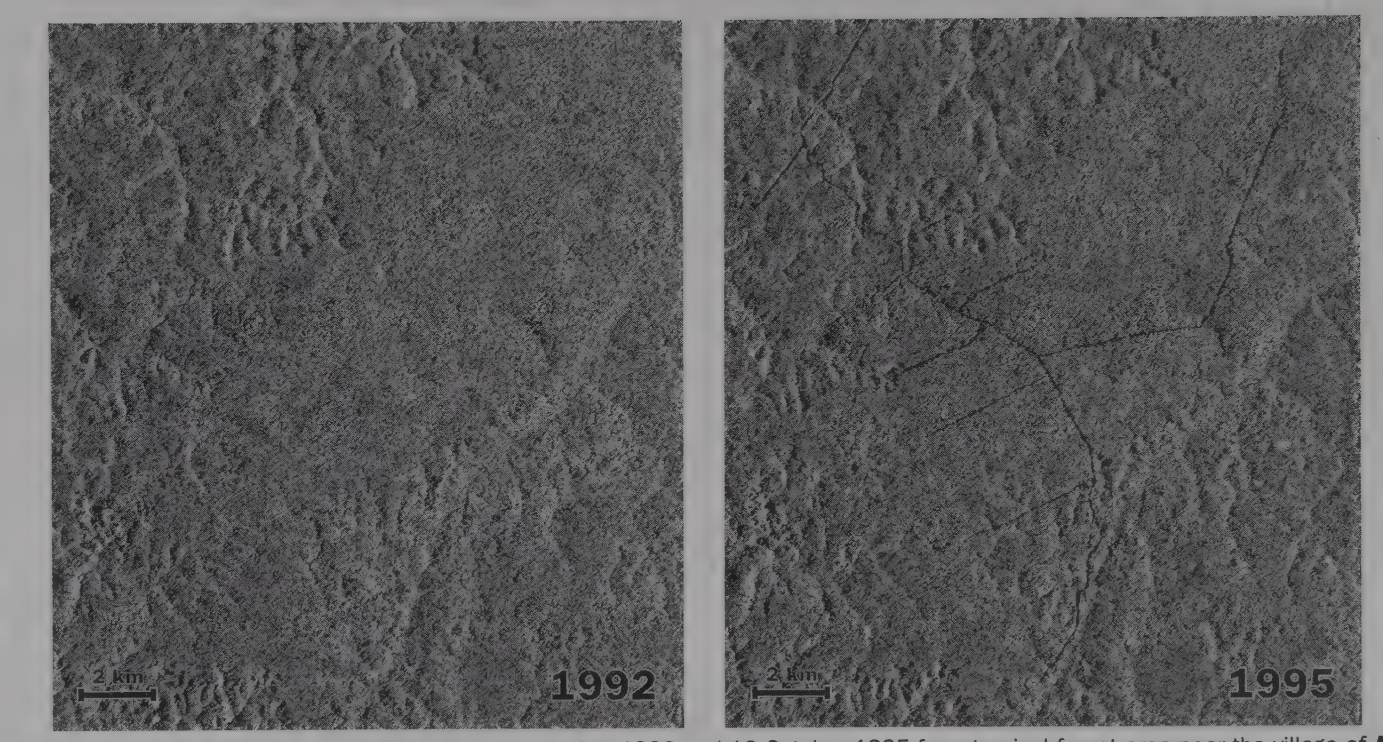



**Figure 7.5** Single date ERS-1 SAR PRI images from 8 December 1992 and 12 October 1995 for a tropical forest area near the village of **Apura** in **Surinam**. The clearly visible road network suggests large scale logging operations. However, it cannot be observed whether or not logging resulted in serious forest degradation.

features are clearly represented in radar images and hence such images can support road planning. Obviously, airborne radar images will show these terrain properties in more detail but the information in ERS-1 images may well suit the purpose. ERS-1's capabilities to image topography and drainage patterns is illustrated in Figure 7.4. This figure shows the Tropenbos ecological reserve and surrounding areas. The arrow marks the location of the Tropenbos field station. Like the images in Figures 7.2b and 7.3, the image in Figure 7.4 represents the weighted time average of PRI images from 6 October 1993, 27 May 1994 and 9 August 1994. It is interesting to compare the information content of the images in Figures 7.2 through 7.4 with that of the CCRS SAR images in Figure V.1 and the soil maps in Figure V.4 of Appendix V.

Certain parts of the road network in Mabura Hill were difficult to recognise in single date ERS-1 images. By averaging ERS-1 images from different dates this problem could be eased. At other sites the situation may be different. This depends on the local conditions and the scale of the logging operations. Evidence of this is shown in Figure 7.5. This figure shows *single date* ERS-1 PRI images from 8 December 1992 and 12 October 1995 for a tropical forest area near the village of Apura in Guyana's neighbouring country Surinam (ca. 5°10' North, 57°5' West). In 1994 the Apura region received considerable attention in Dutch newspapers. Environmentalists expressed their concern about the willingness of the newly established concessionaire to comply with regulations for sustainable management. The fact that the road network shows so clearly in the 1995 image suggests that large scale logging operations took place. However, it is not possible to tell from this image whether or not the operations resulted in serious forest degradation. All that may be observed with certainty is that the forest was not clear-cut.

### 7.2.2 Techniques for automated change detection

Because of large data volumes associated with forest resource monitoring, in particular at the global and national level, there is a need for automated change detection techniques. Change detection techniques bring about data reduction and as such assist human interpreters or subsequent computer algorithms in data analysis. The ideas behind different techniques may vary, e.g. from simple temporal comparison of pixel values to more complex temporal tracking of shape, size and/or location of specific image features. To ensure reliable results all techniques require accurate spatial registration of the multi-temporal data set (see Townshend et al., 1992). Detection of temporal differences in pixel values in addition requires the data to be radiometrically stable.

To date there has been considerably more experience with change detection in optical remote sensing data than with change detection in microwave remote sensing data. Singh (1986) gives an overview of techniques frequently used for detecting change in data from optical remote sensing systems. The author compares the performance of several techniques using Landsat MSS data for a tropical forest region in North-eastern India. Results indicate that sophisticated techniques such as image regression, principal component analysis and post-classification comparison do not perform better than simpler image differencing or ratioing techniques. All

techniques discussed by Singh are based on detecting temporal change in pixel values.

Rignot and van Zyl (1993) discuss the effectiveness of image differencing and image ratioing techniques in relation to microwave remote sensing data, i.e. ERS-1 SAR data. The authors conclude that *image ratioing is preferred to image differencing because it is better adapted to the statistics of SAR images.* When image ratioing is applied the detection of change is independent of the backscatter level of the pixels. In contrast, the image differencing technique will not detect change in the same fashion in regions of high backscatter compared to regions of low backscatter. Another advantage of the ratioing technique is that it eliminates systematic radiometric inaccuracies in repeat-pass images. Such inaccuracies may arise during SAR processing in those cases where the flat Earth assumption is violated. Since radar images are often logarithmically and not linearly scaled it is good to note that image ratioing at the linear scale is equal to image differencing at the logarithmic scale.

*Detection of temporal backscatter changes in SAR images is complicated by the presence of speckle.* Like change in object properties, speckle causes backscatter fluctuations. In change detection the two causes of backscatter change may easily be confused. Rignot and van Zyl (1993) derive the relationship between speckle level (expressed by number of looks), backscatter change and the level of confidence for detecting this change by means of image ratioing. This relationship is illustrated in Figure 7.6. The level of confidence for detecting change is shown to increase slowly with a decreasing speckle level, i.e. an increasing number of looks $k$. In practice the negative impact of speckle may be reduced by applying speckle filters and/or the averaging of independent backscatter measurements.

The effectiveness of the image ratioing technique was tested at the local spatial level for detecting forest cover change in Mabura Hill's West Pibiri compartment. Input image for time $t_0$ was the weighted average of the ERS-1 PRI images from 29 April 1992, 3 June 1992 and 30 December 1992. The weighted average of the images from 6 October 1993, 27 May 1994 and 9 August 1994 was used as the input image for time $t_1$. Applied weights were mentioned above (section 7.2.1). Prior to averaging individual images were speckle filtered and calibrated (see section 5.3.3). Speckle filtering in combination with temporal averaging reduced the backscatter fluctuations per pixel to a level equivalent to that in a 96 looks image.

Figure V.9a of Appendix V shows the ratioed image. This image was used to generate the change map which is shown in Figure V.9b in combination with the time averaged PRI image for 1994. The red colours in this change map indicate image regions for which the backscatter over the 1992-1994 time period decreased by > 1 dB. Similarly, green colours indicate image regions with a > 1 dB increase in backscatter. Results in section 7.1 suggest that backscatter differences up to ca. 1 dB may just as well result from changing environmental conditions as from forest cover disturbance. Hence, *a threshold value of 1 dB may be considered as the lower limit for detecting forest cover disturbance.* Given an equivalent number of looks of 96 the backscatter standard deviation resulting from speckle is of the order of 0.44 dB. This

is considerably less than the threshold value. Therefore the mapped changes are not likely to result from the presence of image speckle. Figure 7.6 shows that with 96 looks per pixel the ratioing technique is capable of detecting a backscatter change of 1 dB with an accuracy of approximately 79% (Rignot and van Zyl, 1993). The only way to improve this accuracy is by further reducing the speckle level of the input images. A simple method of doing so is by averaging backscatter values of neighbouring pixels. However, in the present study this was not considered as it would reduce the effective spatial resolution of the input images. The maximum possible spatial resolution was required to optimise the chances of detecting the relatively small canopy openings resulting from selective logging.

Change maps like the one in Figure V.9b accurately show locations with changed backscatter properties. However, detection of change is just an initial step in a forest monitoring procedure. The real monitoring problem is that of change management. For the management of detected changes, information on the nature of the changes is indispensable. It is particularly important to know whether changes are due to human intervention or natural processes. At the local spatial level, in an environment managed like Mabura Hill it is often difficult to make this distinction. In this respect change maps are of little help. In fact there is considerable change in areas of Figure V.9b where loggers have never been near. This problem in discriminating human and natural disturbances is primarily due to the fact that they are of a similar scale. Moreover, the scale of these disturbances (intrinsic scale) is small in comparison to

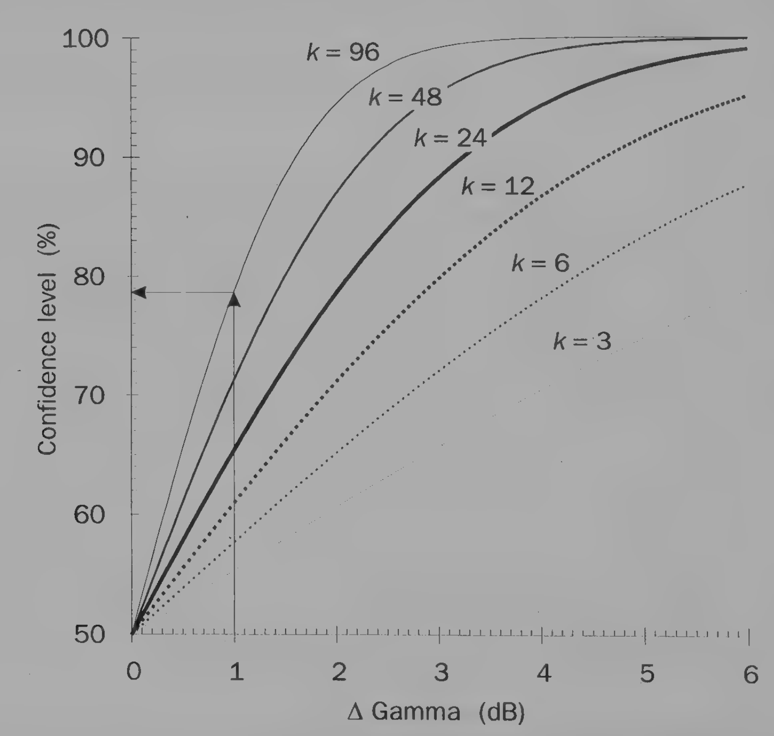



**Figure 7.6** Confidence level of image ratioing technique for detecting change in backscatter Δ Gamma between two observation dates, for a number of looks *k* ranging from 3 to 96. (Adapted from Rignot and van Zyl, 1993.)

the spatial resolution (measurement scale) of ERS-1. This implies that possible spatial particulars of human and/or natural disturbance go unobserved. The statement by Baltaxe (1987) that "monitoring becomes progressively more difficult and therefore less reliable as the individual areas of change to be detected, mapped and measured become smaller" is very much applicable to the situation in Mabura Hill. *At spatial levels where selective logging or other small scale human disturbances are an issue, automated monitoring with ERS-1 is not a simple procedure. It requires a sophisticated approach that uses contextual information and field knowledge.*

In addition to image ratioing Rignot and van Zyl (1993) propose a change detection method based on the temporal decorrelation of speckle. In section 3.1.3 speckle was mentioned to result from the interference of radar echoes from different scatterers within a resolution cell. Provided that scatterers do not change in nature or position over time, repeat-pass radar measurements will have identical speckle. However, if for some reason scatterers do change, images from successive dates will have different or decorrelated speckle. Hence, temporal decorrelation of speckle is an indicator of change in the observed object. The proposed decorrelation method was not tested in this study because image speckle is not expected to remain correlated in images from forests or other types of vegetation. Certainly not over time intervals as long as those in the available ERS-1 data set. Important causes of speckle decorrelation in images from vegetated terrain are growth and wind movement.

In section 7.2.1 roads were concluded to be the best observable indicators of selective logging in ERS-1 images. Detection of new or changed road networks in ERS-1 images could be the first step in procedures that aim to monitor forest resources notably at the national spatial level. In the present study, techniques for automated detection and extraction of roads from SAR images were not examined. The interested reader is referred to literature e.g. Touzi et al. (1988), Adair and Guindon (1990), Samadani and Vesecky (1990) and Hellwich (1994).

## 7.3 Conclusions

Analysis of the multi-temporal ERS-1 SAR Precision data leads to the following conclusions.

- Temporal variations in ERS-1 SAR backscatter measurements of tropical rain forests can be of the order of 1 dB.

- Temporal variations in ERS-1 SAR backscatter measurements of tropical rain forests result primarily from daily and seasonal fluctuations in rainfall.

➤ *ERS-1 SAR images acquired during dry conditions show better contrast between non-forest and primary or secondary forest than ERS-1 SAR images acquired during wet conditions.*

- ERS-1 SAR images acquired during dry conditions show marginally better contrast between logged-over forest and primary forest than ERS-1 SAR images acquired during wet conditions.

- ERS-1 SAR images acquired during wet conditions show marginally better contrasts between differing primary forest types than ERS-1 SAR images acquired during dry conditions.

➤ *Multi-temporal ERS-1 SAR data sets do not offer substantially better opportunities for discriminating among primary tropical forest types than mono-temporal ERS-1 SAR data sets.*

- ERS-1 SAR Precision (PRI) images clearly show physiographic terrain characteristics such as topography and drainage and can therefore support road planning in poorly known tropical forest areas.

➤ *Multi-temporal ERS-1 SAR PRI images make a good basis for monitoring tropical forest cover disturbances resulting from the construction of roads.*

- Averaging of ERS-1 SAR PRI images from different acquisition dates improves the chances for detecting roads. The need to do so depends on the local conditions and the scale of the logging operations.

➤ *Enhanced ERS-1 SAR PRI image products show the larger of the canopy openings resulting from selective logging. However, monitoring of forest cover disturbance due to selective logging will require an approach that uses contextual information and field knowledge.*

# 8 Radar remote sensing to support tropical forest management: General conclusions and recommendations

Radar remote sensing has long been known as a useful source of information in support of tropical forest management. In fact, much of the data acquired by the earliest airborne radar programmes in the humid tropics were used for this purpose (see section 2.2.3). Since that time, radar remote sensing technology and hence the application potential of radar data have improved considerably. The introduction of the following are examples of some of the important technological advances that have been made: digital recording techniques, synthetic aperture radar, satellite radar, multi-frequency and/or -polarization radar. In parallel with the refinement of radar technology, increasingly sophisticated facilities and techniques for digital analysis of radar images have been developed. The radar systems that acquired the data analysed in the present study largely represent the 'state-of-the art' in radar technology. Their potential for application to tropical forest management is evaluated in section 8.1. Recently, however, airborne radar systems with enhanced spatial resolutions and three dimensional imaging capabilities have been introduced. The application potential of these new types of radars is currently being studied by researchers of the Wageningen Agricultural University at sites in Indonesia.

Potential users will have to consider the information content of radar data and decide whether radar remote sensing is an attractive option for them or not. Information requirements will be the primary motive in this decision process. Other important considerations concern the availability of: alternatives to obtain the required information, time to fulfil the requirements, financial resources, human resources, facilities for data analysis and expertise. Once the decision to apply radar remote sensing has been made, users at different spatial levels must follow differing strategies to acquire radar data in attempt to fulfil their information needs. Data acquisition strategies for the global, national and local spatial level are discussed, in general terms, in section 8.2.1. Section 8.2.2 discusses strategies for radar data analysis, i.e. for extracting information on tropical forests from radar data. Section 8.3 concludes this text with some final remarks.

## 8.1 Potential of radar to fulfil user requirements

### 8.1.1 Applicability at the global level

Due to the enormous extent of the area of interest, *radar satellite systems are the only radar systems with good potential for application to tropical forest management at the global spatial level.* To date, the optical satellites in the NOAA AVHRR series have been the main source of data for this purpose (see section 2.2.2). The preference for these data can be explained by the fact that the NOAA AVHRR satellites were the only ones capable of providing up-to-date and world-wide coverage of usable (cloud-free) data. However, with the introduction of operational radar satellite systems the monopoly of the NOAA AVHRR satellites as providers of

remotely sensed data for application to global assessment and monitoring of tropical forest resources has come to an end. Early evidence of this can be found in the TREES ERS-1 Central Africa mosaic project CAMP of the Space Applications Institute of the European Commission Joint Research Center. In this project over 400 ERS-1 images were assembled to map the forests in the Central African tropical belt (De Grandi et al., 1997).

In section 2.1.1 the information requirements of the parties operating at the global spatial level were shown to be governed by major environmental issues. Moreover, it was shown that the emphasis is on information for the purpose of forest resource monitoring rather than forest resource assessment. To enable effective monitoring the remote sensing data that are to be used should be available for an extended period of time. Hence, *only satellite systems for which successors are foreseen make good bases for operational monitoring of the world's tropical (and non-tropical) forest resources.* This qualifies two out of the three currently orbitting radar satellites, namely ERS-1/2 and RADARSAT, but disqualifies the third one, i.e. JERS-1.

Table 2.1 in section 2.1.1 lists the parameters on which parties involved in the management of (tropical) forests at the global spatial level require information. Table 8.1 re-lists these parameters and shows appraisals of the possibilities for assessing and/or monitoring them on the basis of ERS-1/2 SAR Precision data. The most important parameters are shown in a bold typeface. These are parameters that according to Table 2.1 are rated "essential" in relation to two or more global environmental issues. Results in section 6.2 indicate that the use of time-averaged ERS-1/2 SAR Single Look Complex (SLC) data could enhance the possibilities for assessing parameters that are reflected in image texture, e.g. actual forest vegetation type. However, at the global spatial level in particular, it is not practical to apply such images since the production is involved and their geometrical properties are adverse. Table 8.1 lists a brief comment on each parameter and/or the appraisal given. These comments are elaborated upon in the paragraphs following.

With respect to the parameter 'logged areas' a distinction should be made between areas of selectively logged or logged-over forest and areas of clear-cut. Results, notably in section 7.2.1, indicate that multi-temporal ERS-1 image products can show forest disturbance resulting from selective logging. At the global spatial level, however, operational monitoring of selective logging is not deemed to be feasible. The most important reason being that it requires considerable knowledge of local conditions and practices. *Unlike detection of logging gaps, detection of road networks requires minimal local knowledge.* Roads are very distinctive indicators of foregoing and/or forthcoming (selective) logging and other human activities. Information on recently established roads is critical to those involved in forest management as roads identify locations where, unless appropriate actions are taken, the continued existence of the forest is at risk. The capacity of ERS-1/2 to support the monitoring of road networks is therefore of great importance (see section 7.2.1).

The difficulties in detecting areas of logged-over forest result primarily from the fact that the disturbance in forest cover is small in comparison to the resolution cell size of the ERS-1/2 SAR sensor. Considering this, it is expected that ERS-1/2 images will

**Table 8.1** Parameters of interest to parties involved in (tropical) forest management at the **global spatial level**; indication of the possibility for assessing each of the parameters specified based on ERS-1/2 SAR Precision data. Key: '++' good, '+' possible, '+/-' difficult, '-' impossible, '~~RS~~' not assessable using remote sensing. *The most important parameters are shown in a **bold** typeface.*

| Parameter | Assessment /monitoring using ERS-1/2 | Comments |
|---|---|---|
| Ecofloristic zones | ~~RS~~ | Not assessable using remote sensing |
| Forest cover: | | |
| - **Forest / non-forest** | + | Evidence in this study |
| - **Burned areas** | + | Evidence in e.g. Hoekman (1997) |
| - **Logged areas** | +/- | Evidence in this study |
| - **Regeneration** | +/- | Evidence in this study |
| - **Biomass degraded areas** | - | ERS-1/2 radar little sensitive to biomass |
| - **Deforested** | + | Evidence in this study |
| Forest categories: | | |
| - Potential forest vegetation type | ~~RS~~ | Not assessable using remote sensing |
| - **Actual forest vegetation type** | +/- | Evidence in this study |
| - Administrative / legal status | ~~RS~~ | Not assessable using remote sensing |
| - Management type | ~~RS~~ | Not assessable using remote sensing |
| - **Plantation / natural** | +/- | Follows from difficulty in assessing 'actual forest vegetation type' |
| Fires (numbers, distribution) | - | Assessable using optical remote sensing |
| Percentage of vegetation cover | - | Follows from difficulty in assessing 'regeneration' |
| **Crown cover / leaf index** | - | Follows from difficulty in assessing 'regeneration' |
| Tree species composition | - | Follows from difficulty in assessing 'actual forest vegetation type' |
| Diameter distribution | - | Not assessable using ERS-1/2 images |
| Stand height | - | Assessable using airborne nadir looking scatterometer and Lidar systems |
| Stand architecture | +/- | This study shows that ERS-1/2 images mirror canopy roughness |
| Soil characteristics / topography: | | |
| - Soil organic matter | ~~RS~~ | Not assessable using remote sensing |
| - Texture and slope | -, + | Slope assessable not soil texture |
| **Socio-economic factors** | +/- | Mostly not assessable using remote sensing; roads are among the exceptions |

facilitate the monitoring of forest depletion resulting from clear-cut as long as the cleared areas are sufficiently large. According to Forster (1993) the minimum size of a feature to be displayed and interpreted is 1.2 mm at map scale. Given the ERS-1/2 compatible image map scale of smaller than or equal to 1:200,000 (see Table 2.6) it follows that clear-cuts can be mapped reliably if their size is greater than approximately 6 ha.

Table 8.1 indicates that *ERS-1/2 Precision images provide limited information on regenerating or secondary forests.* This can be explained by the short operating wavelength and the restricted spatial resolution of the radar onboard ERS-1/2. Due to its short wavelength the ERS-1/2 radar is not particularly sensitive to differences in aboveground biomass. Hence, the tonal appearance of closed secondary forests and primary forests is very similar. Secondary forests in early phases of regeneration, i.e. non-closed secondary forests, are easily confused with non-forest cover types. Apart from differing biomass levels, secondary and primary forests have different canopy architectural properties. Canopy roughness, which is a parameter of canopy architecture, is mirrored in radar images in the spatial variation of image tone, i.e. in image texture. However, in ERS-1/2 Precision images the textural differences between secondary and primary forests are often small because of the relatively low spatial resolution of the radar. Evidence of this can be found in section 6.2.1 of the present text.

In contrast to single-date ERS-1/2 images, long-term series of these images can contain significant information on the location, extent and/or age of secondary forests. Image areas that appear deforested at one point in time and forested at a subsequent point in time must correspond to areas of secondary forest. Hence, *inter-comparison of images from differing years facilitates the identification of newly developed secondary forests.* Moreover, it enables the estimation of their year of origin and hence age.

ERS-1/2 is of limited value for the assessment and monitoring of a parameter denoted in Table 8.1 as the 'actual forest vegetation type'. Results in section 6.2.1 show that *ERS-1/2 Precision images make modest bases for classifying tropical land cover at the level of primary forest, logged-over forest, secondary forest and non-forest but poor bases for classifying different primary forest types.* Of all classes named, non-forest was found to be most easy to identify. These results hold for classification per region rather than per pixel. Compared to classification per pixel, classification per region will yield better results. However, the region-based approach assumes a capability to delimit regions of interest using automated image segmentation techniques. Hence, the success of this approach depends strongly on the success of the segmentation technique. Computerised definition of logged-over forest regions will be problematic since these regions are far from homogeneous and do not usually have clear boundaries. Attempts to segment areas of primary forest into regions representing different forest types will meet similar problems. Like discriminating between differing 'actual forest vegetation types', discriminating between 'plantation forest' and 'natural forest' will be difficult. The key to identifying forest plantations is expected to be in their homogeneous nature and man-made geometry, e.g. presence of straight boundaries.

The assessment possibility for 'stand architecture' is rated 'difficult' in Table 8.1. Because of its short operating wavelength the ERS-1/2 radar mainly observes the forest canopy. Hence, ERS-1/2 images do not contain information on stand architectural parameters other than those relating to the architecture of the canopy. Results in section 6.2.2 indicate that *textural attributes computed from ERS-1/2 images can be used to rank land cover types according to the degree of canopy roughness.* Canopy roughness, which is a parameter of canopy architecture, has been *identified as an indicator of species diversity* by Oldeman (1983a), Brünig and Huang (1989) and Brünig and Mohren (1989).

Unlike the majority of the parameters listed in Table 8.1, 'socio-economic factors' do not relate to the state of the forest ecosystem but rather to the social system interacting with the forest. Most socio-economic factors do not present themselves spatially at the Earth's surface and therefore cannot be assessed and/or monitored using remote sensing techniques. Infrastructural facilities such as roads are among the exceptions. The importance of roads in relation to tropical forest management and the capability of ERS-1/2 to support road monitoring were discussed earlier in this section.

The assessment possibility for the parameters listed in Table 8.1 can be seen to range from 'impossible' to 'possible'. Higher ratings, i.e. 'good', are lacking. This can be explained by the fact that the *ERS-1/2 radar system was not specifically developed for application to (tropical) forest resource assessment and/or monitoring.* The main application fields foreseen, relate to oceans and sea-ice rather than land surface areas. As a rule, the capabilities of ERS-1/2 will be adversely affected by the presence of large topographic variations. Apart from geometrical effects these variations induce differences in image tone that can easily be confused with tonal differences resulting from, for example, cover type transitions. Topographic variations therefore complicate the interpretation and application of radar images.

The applicability of RADARSAT data, although not evaluated in the present study, is expected to be comparable to that of ERS-1/2 data. Compared to ERS-1/2, RADARSAT offers more flexibility from an operational point of view. However, the information content of ERS-1/2 Precision and RADARSAT Standard beam images will be comparable since the spatial resolution is essentially the same and the signals of both radars interact with forest in a very similar manner. Like ERS-1/2, RADARSAT was primarily developed with a view to ocean and sea-ice applications.

### 8.1.2 Applicability at the national level

The *information requirements associated with tropical forest management at the national spatial level can best be fulfilled by a combination of spaceborne and airborne radar systems.* Spaceborne systems have good potential to support forest resource monitoring over extended areas but are (presently) unable to provide the spatial detail required for forest resource assessment. Airborne systems, on the other hand, have good potential to enable forest resource assessment at the

commonly required map scale of 1:50,000 but are less cost effective tools to monitor expansive forest areas.

As at the global spatial level, the information needs for forest resource monitoring at the national spatial level focus on the primary indicators of the forest's state, i.e. on parameters relating to forest cover and forest categories (see section 2.1.2). Section 8.1.1 discussed the potential of the currently available ERS-1/2 and RADARSAT satellites for application to forest resource monitoring at the global level. The potential of these systems to support the monitoring of tropical forests at the national level is comparable since the national and global information requirements for monitoring are essentially the same. Both ERS-1/2 and RADARSAT provide sufficient spatial detail to enable monitoring at the minimally required map scale of 1:250,000. The option to deploy airborne radar systems allows for refinement of national procedures for forest resource monitoring as it creates opportunities to 'zoom in' on areas where forest disturbance is suspected and/or expected. This approach is discussed in more detail in section 8.2.1.

Although airborne radar systems may be used to support the monitoring of national forest resources, their main asset is the potential for application to forest resource assessment. Currently available airborne radars have differing technical specifications and hence different potential for application to forest management. In view of application, the operating wavelength of the radar is the most important characteristic as it dominates the information content of the resulting images. Images from radar systems that operate with short wavelengths mostly contain information on the surface of the forest canopy, whereas images from radar systems that operate with long wavelengths contain information on lower lying forest quarters. In accordance with Table 2.2, Table 8.2 lists parameters of interest to parties involved in tropical forest management at the national spatial level. The most important parameters are shown in a bold typeface. Table 8.2 also shows appraisals of the possibilities for assessing the parameters listed on the basis of two types of high resolution, airborne radar data, i.e. short wavelength data (X-, C-band) and long wavelength data (L-, P-band). The studied CCRS SAR data are examples of the former type of data, whereas the studied NASA/JPL AIRSAR data are examples of the latter data type.

Results in section 6.1 of the present study clearly showed that texture rather than backscatter is the most important source of information for identifying tropical forest cover types in short wavelength radar images. *The appraisals of the possibilities for assessing forest cover on the basis of X- or C-band radar images therefore assume the use of textural information.* Due to the greater depth of vertical penetration of microwaves with long wavelengths the textural information content of L- and P-band radar images is limited. Hence, *the use of backscatter information is assumed in the case of the L- and P-band data.* The appraisals in Table 8.2 typically assume the assessment to be based on information contained in a single radar band. The following paragraphs elaborate upon some of the shown appraisals and/or comments.

**Table 8.2** Parameters of interest to parties involved in (tropical) forest management at the **national spatial level**; indication of the possibility for assessing each of the parameters specified based on high resolution, short wavelength (X-, C-band) and long wavelength (L-, P-band) airborne radar data. Key: '++' good, '+' possible, '+/-' difficult, '-' impossible, '~~RS~~' not assessable using remote sensing. *The most important parameters are shown in a* ***bold*** *typeface.*

| | Assessment using radar operating in | | |
|---|---|---|---|
| Parameter | X-, C-band | L-, P-band | Comments |
| Forest cover: | | | |
| - **Forest / non-forest** | + | ++ | Evidence in this study |
| - **Logged-over forest** | ++ | + | Evidence in this study |
| - **Secondary forest** | + | ++ | Evidence in this study |
| - **Primary forest types** | ++ | + | Evidence in this study |
| Forest categories: | | | |
| - **Administrative / legal status** | ~~RS~~ | ~~RS~~ | Not assessable using remote sensing |
| - **Management type** | ~~RS~~ | ~~RS~~ | Not assessable using remote sensing |
| - **Plantation / natural** | + | + | Geometrical features of plantations should enable identification |
| Tree species composition | - | - | Not feasible due to large number of species in most natural tropical forests |
| Timber volume/woody biomass | - | +/- | Evidence in this study |
| Biodiversity indicators: | | | |
| - Canopy roughness | ++ | - | Evidence in this study |
| - Terrain physiography | ++ | ++ | Terrain physiography well represented in radar images (see Figure V.1) |
| - Cover fragmentation | + | + | Follows from capabilities for assessing forest cover parameters |
| - Road density | ++ | ++ | Roads clearly visible in high resolution radar images (see Figure V.1) |
| - Net primary production | - | - | Assessable using optical remote sens. |
| - Actual evapotranspiration | - | - | Assessable using optical remote sens. |
| - Leaf chemistry | - | - | Assessable using optical remote sens. |
| - Leaf biomass, leaf area index | - | - | Assessable using optical remote sens. |
| **Socio-economic factors** | +/- | +/- | Mostly not assessable using remote sensing; roads are among the exceptions |

Generally speaking, *both the textural information in X- and C-band radar images and the backscatter information in L- and P-band radar images enable discrimination between forest and non-forest.* The latter image types, however, have the best capabilities for this purpose since the L- and P-band backscatter contrasts between forest and non-forest usually exceed the X- and C-band textural contrasts. Using texture, non-forest cover types are easily confused with secondary forests. L- and P-band radar images were shown to offer comparable capabilities for forest / non-forest identification (see sections 6.1.1 and 6.3.2).

*The key to identifying logged-over forests is in texture and not in backscatter.* Results in sections 6.1.1 and 6.3.2 show that the X- and C-band textural contrasts between logged-over and intact forest are large, whereas the L- and P-band backscatter contrasts are small. Unlike textural attributes computed from individual X- and C-band images, backscatter values computed from individual L- and P-band images do not enable reliable classification of logged-over forest. Classification of logged-over forest based on backscatter was shown to require observations in a minimum of two C-, L- and/or P-band radar channels with high radiometric resolutions. Channel combinations including two P-band images, one of which has HH polarization, were shown to be most suited for identifying logged-over forest.

In single date X- and C-band images from Mabura Hill, the texture of logged-over forests was found to be easily confused with that of a primary forest type known as Mora forest. However, this does not obstruct the identification of logged-over forests over time since forest types do not change from one year to another and logging is concentrated in forest types other than Mora forest. Consequently, a forest area with the textural appearance of, for example, Mixed forest in one year and with the textural appearance of either logged-over or Mora forest in the year following must have been subject to selective logging. In those cases where multi-temporal data are lacking the identification of logged-over and Mora forest can be greatly facilitated by the use of contextual information. Logged-over forests generally occur as patches and are always found in the vicinity of logging roads. The riparian Mora forests, on the other hand, are elongated and always found in connection with streams. Both roads and the locations of streams can be clearly observed in high resolution airborne radar images (see Figure V.1).

In Table 8.2 *L- and P-band radar images are shown to offer better opportunities for identifying secondary forests than X- and C-band radar data.* Using the texture present in X- and C-band images, secondary forests up to about 15 years in age were regularly confused with non-forest cover types in particular (see section 6.1.1). Linear cross-polarized (VH) L- and P-band images were found to make the most suitable bases for detecting secondary forests. Image combinations including L-band VH or P-band VH and C-band (any polarization) offer even better opportunities for this application (see section 6.3.2). The strong capabilities to map secondary forests using backscatter measurements in L- and P-band can be explained by the sensitivity of these radar bands to aboveground biomass (see section 6.3.3).

Backscatter in L- and P-band increases with increasing biomass until it saturates at a certain threshold level. Findings in literature indicate that the thresholds for L- and P-band correspond to total aboveground *dry* biomass levels of about 100 t $ha^{-1}$ and

200 t $ha^{-1}$, respectively. Roughly speaking, L- and P-band radar images will enable discrimination between secondary forests and non-forest cover types as long as the biomass levels of the secondary forests exceed those of the non-forest cover types. Similarly, L- and P-band radar images will enable discrimination between secondary forests and primary forests as long as the biomass levels of the secondary forests are below the thresholds at which backscatter saturates. The biomass levels of primary forest types are often well above the indicated threshold levels.

*Due to the restricted sensitivity to biomass, L- and P-band radar systems are only able to map the biomass of tropical forests in early phases of development.* Although this limits the application potential of radar to forest inventory, it does not so much constrain the potential of radar to support studies that aim to model the global carbon cycle. For these types of studies, the capability to map forests in early developmental phases is most important since such forests represent locations where biomass accumulation and carbon intake are at a maximum. The limited sensitivity of L- and P-band radars to biomass was the reason for appraising the associated assessment possibility for 'timber volume / woody biomass' as 'difficult'. Biomass estimation is further complicated by the fact that the backscatter in L- and P-band is not only a function of biomass but also of forest architecture, species composition and soil moisture content.

In general, the differing primary forest types are by far the most difficult to identify. This is partly due to the fact that tropical rain forests do not generally consist of a collection of homogeneous, well-defined forest types with distinct boundaries. In fact, a high variability in species composition and architecture, the presence of transitional forest types as well as of transitions between forest types are more characteristic. Results in sections 6.1.1 and 6.3.2 show that, similar to the case of logged-over forest, *image texture and not backscatter offers the best opportunity for identifying primary forest types.* Relative to textural attributes computed from individual X- and C-band images, backscatter values computed from individual L- and P-band images make considerably less reliable bases for primary forest type classification. Field checked image interpretations of texturally enhanced X- and C-band radar images showed that the existing 1:50,000 forest type map of Mabura Hill was incorrect at several locations (see section 6.1.3). Reliable identification of primary forest types using backscatter was shown to require observations in a minimum of three C-, L- and/or P-band radar channels with high radiometric resolutions. The best performing combinations were found to consist of the following channels: C,P,P or C,C,P or C,L,P or P,P,P. Combinations that include linear cross-polarized or circular like-polarized channels are most suitable (see section 6.3.2).

*The appraisals in Table 8.2 and the above discussion lead to the general conclusion that textural patterns in high resolution X- or C-band radar images and backscatter levels in L- or P-band radar images make equally suitable but complementary sources of information for assessing the land cover types studied.*

High resolution radar images, regardless of wavelength, are able to support the assessment of biodiversity indicators such as terrain physiography, cover fragmentation and road density. *Information on canopy roughness,* however, *is restricted to X- and C-band radar images.* The absence of this type of information in L-

and P-band images can be explained by the greater depth of vertical penetration of microwaves with long wavelengths. Results in section 6.1.2 of the present text show that the textural attributes computed from high resolution X- and C-band images can be used to rank cover types according to the degree of canopy roughness. In particular cases, textural attributes were also shown to enable quantification of canopy architectural properties, i.e. average logging gap size and average height difference between emergent trees and the main canopy.

### 8.1.3 Applicability at the local level

Parties involved in the management of tropical forests at the local level typically need information of a fine spatial detail. The review in section 2.1.3 indicates that the minimum required scales of maps for use in support of forest assessment and forest monitoring are of the order of 1:10,000 and 1:25,000, respectively. Mapping at such large scales requires deployment of radar systems with very high spatial resolutions (ca. 1 to 3 m). Consequently, *the only radars with real potential for application to tropical forest management at the local spatial level are airborne radars.* This holds true both for application to forest resource assessment and forest resource monitoring. It is evident that descending from the global to the local spatial level the application potential of satellite radar systems decreases, whereas the application potential of airborne radar systems increases.

Radar systems with very high spatial resolutions are a recent development. In fact, neither of the airborne imaging radars deployed over the sites presently studied offer such spatial resolutions. As shown in section 8.1.2, analysis of the available radar data has resulted in considerable knowledge of the capabilities of airborne radar to fulfil the information requirements associated with tropical forest management at the national spatial level. This knowledge makes a good *basis for formulating prognoses* concerning the potential of airborne radar to fulfil the information requirements of parties involved in tropical forest management at the local spatial level. After all, the information requirements at the national and local spatial level are often closely related.

Images from radar systems with spatial resolutions that are higher than those of the systems studied make improved information sources and hence support more applications (assuming comparable radiometric resolutions). This holds more strongly for X- and C-band images than for L- and P-band images. As explained previously, texture is the most important information source in X- and C-band images, whereas most of the information in L- and P-band images is contained in the backscatter level. Both the textural and the backscatter information contents of a radar image are a function of the properties of the incident microwaves as well as of the properties of the object observed. However, the textural information content also depends heavily on the spatial resolution of the deployed radar system. This explains why a higher spatial resolution will enhance the application potential of X- and C-band radar images, in particular.

**Table 8.3** Parameters of interest to parties involved in (tropical) forest management at the **local spatial level**; *prognosis* of the possibility for assessing each of the parameters specified based on very high resolution, short wavelength (X-, C-band) and long wavelength (L-, P-band) airborne radar data. Key: '++' good, '+' possible, '+/-' difficult, '-' impossible, '~~RS~~' not assessable using remote sensing.

| | Assessment /monitoring using radar operating in | | |
|---|---|---|---|
| Parameter | X-, C-band | L-, P-band | Comments |
| Terrain characteristics: | | | |
| - Topography | ++ | ++ | Well represented in radar images |
| - Water courses and drainage patterns | ++ | ++ | Well represented in radar images |
| - Infrastructure | ++ | ++ | Will be clearly visible due to very high spatial resolution |
| Forest cover: | | | |
| - Primary forest types | ++ | + | Same rating as at national level |
| - Logged-over forest | ++ | + | Same rating as at national level |
| - Clear-cuts | ++ | ++ | Large textural/backscatter contrasts will enable identification |
| - (Natural) regeneration | +/- | +/- | Nature of regrowth difficult to establish |
| - Burned areas | ++ | ++ | Large textural/backscatter contrasts will enable identification |
| Forest categories: | | | |
| - Management type | ~~RS~~ | ~~RS~~ | Not assessable using remote sensing |
| - Plantation / natural | ++ | ++ | Geometrical features of plantations will enable identification |
| Forest composition and structure: | | | |
| - Tree species composition | +/- | - | Difficult due to large number of Species in most natural tropical forests |
| - Diameter distribution | - | - | Not feasible for natural tropical forests |
| - Standing volume (by species) | +/- | - | Species identification will be difficult |
| - Growth rates | ~~RS~~ | ~~RS~~ | Not assessable using remote sensing |
| - Harvestable volume | ~~RS~~ | ~~RS~~ | Not assessable using remote sensing |
| - Positions of harvestable trees | ~~RS~~ | ~~RS~~ | Not assessable using remote sensing |
| Site class | +/- | +/- | Only partially assessable using remote sensing |
| Sustainable management indicators | | | Please refer to Table 8.4 |

In accordance with Table 2.3, Table 8.3 lists the parameters of interest to parties involved in tropical forest management at the local spatial level. Table 8.3 also shows *prognoses* of the possibilities for assessing these parameters on the basis of two types of very high resolution, airborne radar data, i.e. short wavelength data (X-, C-band) and long wavelength data (L-, P-band). The actual applicability of very high resolution X- and C-band radar is currently being studied at sites in Indonesia. As in Table 8.2, the use of textural information is assumed in relation to X- and C-band radar data, whereas in the case of the L- and P-band data the use of backscatter information is assumed. The prognoses in Table 8.3 typically assume the assessments to be based on the information contained in a single radar band. The following paragraphs elaborate upon some of the shown prognoses and/or comments.

Compared to the X- and C-band data studied, *very high resolution X- and C-band radar data will offer enhanced capabilities for identifying primary forest types and logged-over forests.* The wealth of textural information present in these images may, for example, enable detection of logged-over forests with different logging histories (e.g. different years of logging, differing intensities of logging). Very high resolution L- and P-band images will offer enhanced capabilities for identifying primary forest types in the sense that due to the finer spatial detail the transitions between forest types can be established more accurately. The higher resolution, however, does not enhance the differences between the mean backscatter values for the various primary forest types.

Due to the manner in which mean backscatter is computed, the *higher spatial resolution can be expected to enhance the difference in the mean backscatter values for logged-over and intact forest.* Logging gaps of given sizes occupy more pixels in a very high resolution image than in an image with a lower spatial resolution. If it is assumed that the individual pixels in the two images represent an equal number of backscatter measurements or looks (see section 3.1.3), than it follows that gaps represent more backscatter measurements in the very high resolution image than in the image with the lower resolution. In other words, in the very high resolution image gaps contribute a larger proportion of the measurements required to accurately compute the mean backscatter value for logged-over forest (see section 5.2.1). In general, backscatter measurements corresponding to gaps will resemble those of non-forest and hence be low in value. Due to the high proportion of low backscatter measurements, the mean backscatter values for logged-over forests computed from very high resolution images will be relatively low. The mean backscatter values for intact primary forests, on the other hand, will be largely unaffected by spatial resolution. Consequently, a higher spatial resolution results in enhanced differences in the mean backscatter values for logged-over forests and intact primary forests.

*Detection of clear-cuts and burned forest areas in very high resolution X-, C-band and L-, P-band radar images is not expected to create problems.* After all, the radar data studied were shown to be suitable bases for discriminating between forest and non-forest cover types (see section 8.1.2). Both clear-cuts and burned areas can be seen as special cases of non-forest. In Table 8.3 the assessment possibility for '(natural) regeneration' is rated to be 'difficult'. Unlike for most other forest cover parameters, the main interest with respect to regeneration is not so much in the

location and extent of the regrowing forests but in the success with which preferred (possibly planted) species establish themselves. *Although very high resolution radar images are expected to show the establishment of vegetation, these images are not likely to provide the detail required to discern whether or not this vegetation is comprised of the preferred species.*

The parameters listed in Table 8.3 under the heading 'Forest composition and structure' differ from most others in the sense that their assessment requires information at the level of individual trees. *Forest composition and structural parameters* have long been assessed in conventional forest inventories by means of extensive fieldwork. *Very high resolution radar images, like large scale aerial photographs* (see Swellengrebel, 1959; Loetsch et al., 1973), *cannot be expected to substantially facilitate the assessment of such parameters in natural tropical forests.* The backscatter levels in L- and P-band images, for example, do not relate to properties of individual trees but rather to properties of the forest as a whole. Although microwaves with long wavelengths are sensitive to biomass, L- and P-band radar images of mature tropical forests will often show very little biomass differences because many of these forests have biomass levels in excess of the level of backscatter saturation (see section 6.3.3 or 8.1.2).

Similar to aerial photographs, very high resolution X- and C-band radar images will show canopy architectural properties. However, due to the complexity of this architecture and the high diversity in species, individual tree crowns will be difficult to observe and identify. Hence, *tree species composition will be at least difficult to assess.* This prognosis is supported by the fact that investigators who attempted to identify tropical tree species on stereoscopic, large scale aerial photographs have met with little success (see Swellengrebel, 1959 and Loetsch et al. 1973). For similar reasons *it will be difficult to measure tree crown diameters on very high resolution radar images.* These measurements in combination with allometric equations provide the basis for assessing other structural parameters such diameter at breast height, crown base height and bole volume. *Growth rates, harvestable volume or locations of harvestable trees cannot be derived from any type of remote sensing data.* Calculation of growth rates requires accurate in situ measurements of tree diameters. Assessment of harvestable volume and positions of harvestable trees involves judgements concerning the qualities of tree trunks (e.g. bole form, presence of rot). Such judgements can be made in the field only.

Both X-, C-band and L-, P-band radar images contain information on terrain characteristics and forest types. Hence, these images have potential to support forest management in assessing 'site classes'. However, radar images lack sufficient information on other relevant parameters such as species composition, proportion of harvestable trees, physical and chemical soil properties. For this reason the associated assessment possibility is rated in Table 8.3 as 'difficult'.

Table 8.4 lists a subset of the *indicators of sustainable forest management* as given in Table 2.4. Results presented in sections 6.1 and 6.3 of this text indicate that the airborne radar data studied would make good bases for assessing and/or monitoring the indicators shown. Hence it may be assumed that comparable radar data of an even higher spatial resolution, i.e. data that are better suited for application at the

**Table 8.4** Examples of indicators of **sustainable forest management** that can be readily assessed and/or monitored with the use of very high resolution X-, C-, L- and P-band radar images. The indicators are categorised on the basis of related sustainability principles.

The forest resource shall be sustained.
- Area and percentage of forest; not further classified.
- Area and percentage of forest affected by fire and storm beyond the range of historic variation [1].
- Extent of illegal exploitation and encroachment [2].
- Rate of conversion of forest cover to other uses (e.g. mining, ranching, energy, infrastructure).

The protection function of the forest shall be sustained.
- Infrastructure (primary and secondary roads, timber yards, skidding tracks) is located on natural benches, ridges and flatter slopes.
- Sizes of infrastructure are reduced to the barest minimum possible.
- Presence of infrastructure or logging gaps in buffer zones around watercourses or areas of protected forest [2].

Yields of forest products (timber and non-timber) shall be sustained.

The biodiversity of the forest shall be sustained.
- Extent of forest disturbance due to logging (e.g. gap size and frequency).
- Presence of representative protected areas [2].
- Presence of ecological infrastructure (e.g. corridors of unlogged forest).

The long-term social and economic well-being of local communities shall be sustained.
- Sites of special cultural, ecological, economic or religious significance to indigenous peoples are excluded from forestry operations [2].

1) Assessment requires additional historic data.
2) Assessment requires maps showing data on management/legal status of forest areas.

local spatial level, make equally suitable or even better bases for assessing and/or monitoring these indicators. As indicated in Table 8.4 the assessment of certain indicators may require ancillary (map) information. Indicators listed in Table 2.4 but not in Table 8.4 are not necessarily impossible but at least more difficult to assess and/or monitor with the use of radar remote sensing. This is especially true of indicators that relate to the sustainability principle 'Yields of forest products (timber and non-timber) shall be sustained'. As in the case of the 'Forest composition and structure' parameters in Table 8.3, assessment of these indicators often requires information at the level of individual trees.

## 8.2 Implementation of radar remote sensing

### 8.2.1 Data acquisition strategies

Data acquisition strategies will be discussed at the global, national and local spatial levels. *At present, only two truly operational radar satellites are in orbit with potential for application to tropical forest management at the global level*, i.e. ERS-1/2 and

RADARSAT. RADARSAT offers more flexibility from an operational point of view when compared to ERS-1/2. It has, for example, the capability to acquire so-called ScanSAR images. These images are of a low but adequate spatial resolution for application at the global spatial level and have the advantage of covering an area 25 times the size of the area covered by a RADARSAT standard image or an ERS-1/2 image (see Table 2.6). As a rule, the use of data with an unnecessarily high spatial resolution and hence an unnecessarily small spatial coverage should be avoided because of the high costs involved in both data acquisition and analysis.

RADARSAT ScanSAR data are expected to make a suitable source of information for the first phase of a procedure for the world-wide assessment and/or monitoring of tropical forest resources. In the second phase of such a procedure, selected areas can be observed in more detail using ERS-1/2 data or RADARSAT Standard beam data. The selected areas can represent sub-samples for use in a multistage or permanent sampling procedure or 'hot spots', i.e. areas where forest cover change is either suspected or expected. In a possible third phase the spatially more detailed RADARSAT Fine beam data may be put to use. ERS-1/2 Single Look Complex data are less suited for this purpose because of poor geometric properties. Both RADARSAT Fine beam and ERS-1/2 Single Look Complex data have unfavourable radiometric properties.

The traditional frequency for collecting information on the world's forest resources is once every five years. Results in section 7.1 of the present text indicate that images acquired during the dry season are most suited for discriminating between forest and non-forest cover types. *From an application point of view it is important that the data become available in a regular, consistent and timely manner.* Unfortunately, this was not found to be the case for the ERS-1 data analysed in the present study. This was not due to problems in the functioning of the satellite but rather of the ground stations in South America. With onboard data storage facilities like those available on RADARSAT these problems can be largely overcome. The successor of ERS-1/2, i.e. ENVISAT-1, will also carry an onboard recorder for SAR data. The capabilities of this satellite which is scheduled for launch in 1999 resemble those of RADARSAT in other ways as well.

Alternative systems that can provide global coverage at a low spatial resolution are the NOAA AVHRR satellite, the ERS-1/2 thermal infrared radiometer and the ERS-1/2 windscatterometer. Although of comparable resolution, the data from the Landsat and SPOT satellites cannot be considered as genuine alternatives for ERS-1/2 and RADARSAT standard beam data. Notably for areas in the humid tropics, Landsat and SPOT will often fail to provide the required data due to the presence of clouds or smoke. However, if available the data from these satellites can greatly complement the information present in satellite radar data (see section 2.2.2). It should be noted that since RADARSAT is a relatively new satellite system its exact capabilities for the application studied are still under investigation. Due to their history as sites for radar remote sensing research, Mabura Hill and San José del Guaviare would make good locations for RADARSAT studies.

*The information needs associated with the management of tropical forests at the national spatial level can best be fulfilled by a combination of spaceborne and*

*airborne radar data.* Both ERS-1/2 data and RADARSAT Standard beam data provide the spatial detail required for monitoring. For 'hot spots' additional information can be obtained with the help of RADARSAT Fine beam and/or airborne radar data. Good examples of 'hot spots' are areas where new or changed road networks are detected (see sections 7.2.1 and 8.1.1). The preferred observation frequency for monitoring is once every two years. Airborne data acquired to enable detailed monitoring can also be put to use in ongoing forest assessment procedures. To meet the requirements associated with forest resource assessment, airborne radars should be deployed over areas of interest with a frequency of once every five to ten years. At present, the potential of airborne radar to support forest assessment over extended areas is restrained by the available data processing capacity in particular. As at the global spatial level, available Landsat and SPOT data can be used to complement radar data sets.

*Forest managers operating at the local spatial level typically need data acquired by airborne radar systems with very high spatial resolutions.* The only local application for which the information in radar and/or optical satellite data is of real value is the reconnaissance inventory. Data for use in forest resource monitoring can be of a lower spatial resolution (ca. 3 m) than data for use in forest resource assessment (ca. 1 m). Forest monitoring requires annual data takes over the management unit at large. Assessment of specific forest areas requires overflights with a time-interval of five years. Most likely, however, differing parts of the management unit will need to be assessed in different years (see section 2.1.3). To reduce costs, the yearly data takes in support of monitoring and assessment can best be carried out concurrently. The data intended for forest monitoring can support the activities of both forest managers and organisations involved in the control of forestry operations and/or the certification of forest products.

The results discussed in the present text illustrate that radar systems with differing technical specifications (e.g. wavelengths, polarizations, spatial resolutions) offer different capabilities for application to tropical forest management. An important aspect of any data acquisition strategy is therefore the choice of a particular radar system or combination of systems. The number of available airborne radar systems largely exceeds the number of available satellite radar systems. Moreover, the airborne systems offer a much wider range of capabilities than the satellite systems. Hence, *users with the option to apply airborne data have a better chance of satisfying their information needs by means of radar remote sensing than users that are dependent on satellite data.* Unfortunately, airborne radars that operate with long wavelengths such as L- and P-band are mostly experimental and hence not yet readily available for operational use.

Both of the currently available, truly operational, radar satellite systems have a largely comparable but modest potential for application to tropical forest management (see section 8.1.1). With the development of a dedicated system, the applicability of satellite radar could be enhanced greatly. *The two user requirements that make the highest demands on the technical specifications of such a system are the assessment and/or monitoring of primary forest types and logged-over forests.* Results of the present study indicate that radar satellites in order to be able to fulfil both these requirements must carry a system that either acquires multi-look, high

resolution (ca. 5 m) data in a single X- or C-band channel or multi-look data in a minimum of three channels with differing wavelengths and/or polarizations. Inclusion of at least one P-band channel is essential for the latter type of radar. Given the current status of the technology for (non-military) spaceborne radars, the development of either of these systems will be very challenging. Requirements relating to the assessment of forest/non-forest cover types and the monitoring of forest/non-forest conversion are less demanding and can be readily fulfilled by a system operating in a single L- or P-band channel.

### 8.2.2 Data analysis strategies

Following acquisition, the radar data must be analysed in order to obtain the information required. Although some users may be able to fully analyse the data themselves, others will depend at least partly on services of remote sensing specialists. Notably users at the local spatial level will often lack the required image processing facilities and/or expertise. For these users radar remote sensing will only be an option if others can provide them with dedicated image products for visual analysis and/or extracted thematic information (e.g. thematic maps, statistical data).

In practice, forest resource assessment and monitoring procedures require that the information obtained from radar images be evaluated prior to use. It can then be used to formulate and/or revise forest management plans. *Evaluation of the remotely sensed information must include verification by means of field observations.* Often, the remote sensing information will need to be complemented with information from other existing sources such as maps and statistical data. The need for integrated analysis of mostly georeferenced information from differing sources links remote sensing supported forest assessment and/or monitoring with the Geographic Information System (GIS) concept. Information on, for example, slope, aspect and elevation residing in geographically-referenced data bases can also be used to facilitate the extraction of information from radar images.

To ensure compatibility of extracted information from one forest area to another as well as for successive points in time, there is a need to standardise methods for radar data analysis. *Standardised analysis,* in other words, *is a prerequisite for aggregating extracted information for use at higher spatial levels as well as for effective monitoring.* Clearly, standardisation of methods for radar data analysis will require standardisation of procedures for data acquisition and hence continued availability of the preferred radar remote sensing data. Sections 8.1.1 through 8.1.3 reviewed the information content of the radar data studied. The remainder of the present section describes methods for extracting this information from the radar images.

Of the radar systems studied, the first European remote sensing satellite ERS-1 is most suited for the monitoring of global and national forest resources and likewise for the assessment of global forest resources. Although ERS-1 operates with a short wavelength, results reported in section 6.2.1 showed that most of the information in its images is contained in backscatter and not in texture. The absence of substantial

textural information in ERS-1 images can be explained by the systems limited spatial resolution and small angle of incidence. *ERS-1 images mainly provide information on the location and extent of forest, non-forest and roads.* Since roads mark areas of potentially significant deforestation ERS-1 can fulfil a deforestation alert function. The strongest point of the ERS-1 satellite is its capacity to routinely image every part of the Earth's surface at fixed time intervals. A series of ERS-1 images from different dates comprises substantially more information than a single date ERS-1 image. The information in a time-series of ERS-1 images not only enables the monitoring of forest resources but also allows for improved assessment of forest resources.

Extraction of information from the ensemble of backscatter measurements in ERS-1 images (i.e. the pixels) is complicated by the presence of backscatter differences that do not relate to the cover types observed but rather to the presence of image speckle (see section 3.1.3). Due to the confusing effect of speckle, pixel-by-pixel classification of forest and non-forest will meet with little success. Pixel-by-pixel detection of forest/non-forest conversion (or the opposite) using ERS-1 images from two different dates will fail for similar reasons. In single date images *the adverse effects of speckle can be reduced either by means of specially designed speckle filters (e.g. Gamma-Gamma MAP filter; see section 5.3.3) or the averaging of adjacent backscatter measurements.* Both techniques will improve the chances of success for subsequent forest/non-forest classification and, if applied to images from differing dates, for subsequent detection of change. Compared to speckle filtering, averaging of adjacent pixels is more economical because it requires less computer time. In particular for application at the global spatial level this is a distinct advantage. Unfortunately, spatial averaging of pixels is accompanied by a loss in spatial detail. Following averaging over a window of $8 \times 8$ pixels (resulting pixel size is $100 \times 100$m), however, assessment and monitoring of forest/non-forest at the required mapping scales of $\leq$ 1:250,000 is still feasible.

An *alternative method* for analysis of single date ERS-1 images for the purpose of forest/non-forest mapping *involves: automated image segmentation*, computation of average backscatter per image segment and subsequent classification of segments using averaged backscatter values. This method which is illustrated in Bijker (1997) is similar to the region based approach adopted in the present study. In the present study, however, the regions (or segments) were defined interactively using a priori knowledge (see section 5.2.1). Backscatter values resulting from this method are mostly free of speckle effects and hence make a good basis for classification. The success of the method, however, depends strongly on the success with which the segmentation algorithm applied identifies the boundaries between forest and non-forest areas. Like speckle filtering, image segmentation has the disadvantage of requiring much computer time.

Similar to forest/non-forest identification, detection of roads is complicated by the presence of image speckle. In the present study the visibility of roads in ERS-1 image products was enhanced by the averaging of images from different dates (see section 7.2.2). Unlike spatial averaging, temporal averaging of backscatter measurements does not adversely affect the spatial detail in the images (assuming they have been co-registered accurately). Temporal averaging, however, only yields distinctive

backscatter measurements for features that remain essentially unchanged over the period considered. Hence, speckle reduction by means of temporal averaging is not a suitable method for analysis of images from highly dynamic environments. *Techniques for automated detection and extraction of roads from radar satellite images deserve further investigation because of the potentially important role of roads in procedures for forest resource monitoring.*

The method described for enhancing road detection illustrates the value of multi-temporal data sets for the purpose of forest resource assessment. Availability of images from multiple dates also improves the chances of cover type classification as differing cover types may well display differing backscatter behaviours as a function of time. Hence, temporal variation in backscatter may make a valuable basis for discriminating cover types. For example in San José del Guaviare, the temporal variation in the backscatter of the non-forest cover types was shown to be distinctly different from that of the forest cover types (see Figure 7.1).

Procedures for forest resource monitoring require information on changes in forest cover, in particular. *The preferred method for detecting change in backscatter measurements represented in multi-temporal linearly scaled ERS-1 images is that of image ratioing.* Image ratioing at the linear scale translates to image differencing at the logarithmic (dB) scale. Following the ratioing or differencing of images from differing dates, a grey-level thresholding algorithm can be used to generate a change map, i.e. a map showing locations where backscatter levels have increased, decreased and/or remained the same (see Figure V.9b). Depending on local circumstances the optimum threshold value may differ. Results for the Mabura Hill study area indicate that backscatter changes up to ca. 1 dB may result from changing environmental conditions rather than disturbance of forest cover (see section 7.1). Hence, a threshold value of 1 dB is the lower limit for detecting forest cover change at this site. The level of confidence for detecting change in backscatter measurements by means of image ratioing increases with a decreasing speckle level. According to Figure 7.6 in section 7.2.2 the probability of detecting a 1 dB backscatter change in ERS-1 images with standard speckle levels (3 looks) is only 55%. To ensure more accurate detection of change the outlined method should be preceded by one of the earlier described techniques for reduction of speckle.

*Detection of change can be seen as the first step in a procedure for forest resource monitoring. The real monitoring problem, however, is that of change management.* This requires additional information, i.e. information on the nature of the changes detected. Information showing whether changes detected result from human intervention or natural processes is of particular importance. In some cases, the cause of the change will be deducible from radar image information. In others, establishment of the cause will require information from sources other than remote sensing data. Examples of indicators of human intervention in radar images are deforested areas with straight boundaries, presence of roads and presence of population centres.

Like in ERS-1 images, *the information in L- and P-band radar images is mainly contained in backscatter.* The procedure for extracting information from these types of images therefore in essence agrees with the one described earlier for analysis of

single date ERS-1 images. The main components of this procedure are reduction of image speckle effects and classification of cover types of interest. To reduce costs of data analysis, users with access to multi-frequency, multi-polarization images will have to select the images best expected to meet their information needs. The results presented in sections 6.3.2 and 6.3.3 of this text can support this selection process. Certain multi-frequency and/or multi-polarization image combinations were shown to contain considerable information on forest types. Pixel-by-pixel classification of image combinations with reduced speckle levels is expected to be the most practical computerised approach to extract forest type information. Analysis by means of automated image segmentation and subsequent classification of segments will meet with little success. Image segmentation is likely to fail since tropical rain forests do not generally consist of homogeneous, well-defined forest types with clear boundaries. Computerised generation of image segments representing areas of logged-over forest will fail for similar reasons.

*L- and P-band radar images can be applied to estimate the aboveground biomass of forests in early phases of development* (see section 6.3.3). Extraction of biomass information from radar images requires models that describe the relationship between the level of backscatter and the level of biomass. To date, universally applicable models for estimating biomass from radar backscatter are lacking. Development of such models is being hampered by the fact that the backscatter in L- and P-band not only depends on aboveground biomass but also on forest architecture and, if biomass levels are low, on the moisture status of the forest soil.

*Most of the information on tropical forests in high resolution X- and C-band radar images is contained in texture.* Radar intensity images with logarithmic scaling were shown to be more fit for use in textural analysis procedures than radar intensity (or radar amplitude) images with linear scaling (see section 5.1.2). When cover types of interest display textural characteristics that are distinctly different, both grey level co-occurrence (GLCO) statistics and standard deviation of gamma (in dB) make equally suitable bases for analysis. However, in general, GLCO statistics are more powerful descriptors of image texture because they are sensitive to the spatial organisation of the pixels, i.e. pattern. The standard deviation of gamma, on the other hand, is merely determined by the average difference in grey level between pixels and their mean. Unlike other GLCO statistics, GLCO-CONT (Contrast) and GLCO-COR (Correlation) can be directly related to the statistics of radar images (see section 6.1.2). Moreover, these two textural attributes are more sensitive to canopy architecture than most other GLCO attributes. Plots showing the variability of these attributes as a function of displacement length do in fact reflect physical properties of the canopies observed. In summary, *GLCO-COR and GLCO-CONT are the most explanatory GLCO descriptors of texture in radar images from tropical forests.* Hence, these two attributes are most suited for use in analysis of texture according to the GLCO approach.

Analysis of image texture according to the grey level co-occurrence approach involves a number of choices. One of these, i.e. the choice of a particular GLCO attribute, was discussed above. Other choices concern displacement direction, displacement length and, for analysis by means of a moving window, window size. Displacement direction is of particular importance for analysis of textures from cover types with directionally

organised canopies, e.g. plantation forests. Although, canopies of natural tropical forests tend to be organised isotropically most textural information was obtained using displacement in range direction (i.e. the direction perpendicular to the line of flight) (see Appendix I, section I.3). This can be explained by the side-looking measurement geometry of radar systems and holds as long as the spatial resolution and pixel size in range and azimuth direction are comparable.

Displacement length has to be chosen in accordance with the textures of the cover types of interest and the GLCO attribute applied. The discriminating capability of the GLCO-COR attribute was found to deteriorate rapidly for displacement lengths exceeding one pixel. The performance of GLCO-CONT, on the other hand, improves up to a certain displacement length and then saturates. To enable a well founded decision on the displacement length for GLCO-CONT, an assembly of training data is recommended. This involves the generation of GLCO-CONT textural signatures for image areas representing cover types of interest, i.e. training areas. The training process is commensurable with the Gross Textural Analysis (GTA) approach adopted in the present study (see section 5.1.3). Training results in textural signatures showing the variation in GLCO-CONT values as a function of displacement length and cover type. These signatures will be of a form comparable to the plots shown in, for example, Figure 6.3b. At displacement lengths suitable for use in further textural analysis the sum of the differences in the GLCO-CONT values for the various cover types must be at or near maximum.

In the present study image texture was analysed according to two complementary approaches, i.e. Gross Textural Analysis (GTA) and Moving Window Analysis (MWA). GTA is intended to quantify the texture for predefined image regions while MWA is meant to do so for a relatively small spatial window around each image pixel. In general, GTA yields considerably better textural descriptions than MWA. In practice, however, the applicability of GTA will often be hampered by the fact that its use requires a priori information on boundaries of cover types of interest. This type of information may be available in existing geographically-referenced data bases. If this is not the case, then use of GTA is feasible only if one is able to delimit regions of interest with the help of automated image segmentation techniques. Given the complex nature of tropical forests, however, such techniques have little chance of success. Incidentally, for an image segmentation technique to have any chance of success in a tropical forest environment it will have to make use of textural information.

Textural analysis by means of a moving spatial window (MWA) involves an additional choice, i.e. the choice of a window size. The window should be large enough to enable the textural attribute used to capture the essence of the grey level patterns present and yet be small enough to avoid that the window consistently encloses image areas with differing textures and hence cover types. In general, the optimum window size will vary as a function of the spatial resolution of the radar used, the architecture of the forest and the capability of the textural attribute applied. In the present study MWA's were carried out using windows $11 \times 11$ and $25 \times 25$ pixels in size. The larger window size yielded the best overall results (see section 6.1.3). GLCO-COR (using displacement length of one pixel) was found to be more sensitive to local variations in canopy architecture (textural noise) than GLCO-CONT (using

displacement length of five pixels). Consequently, GLCO-COR has more difficulty in capturing the essence of textures if small windows are used (see Appendix I, section I.5). Due to the heterogeneous nature of tropical forests, moving window analysis of texture followed by automated classification of forest types on a pixel-by-pixel basis yields modest results. However, *texturally processed radar image products make a good basis for assessment of tropical forest types by means of visual interpretation* (see Appendix V, Figures V.3 through V.6).

Results in sections 6.2.1 and 6.2.3 of the present text illustrate that ERS-1 Single Look Complex (SLC) images are more suitable for use in textural analysis than ERS-1 Precision (PRI) images. In an operational environment, however, textural analysis of ERS-1 SLC images is not recommended because the results will usually be out of proportion to the analysis effort required.

## 8.3 To conclude

In this study the capabilities and limitations of modern radar sensors for application to tropical forest management at global, national and local spatial levels were discussed. The findings illustrate that radar sensor systems have considerable potential for this purpose. Although the implementation of radar remote sensing in tropical forest management was addressed, much work in the development of tailor-made data acquisition and analysis strategies remains to be done. To be successful, the development of such strategies must be undertaken in close cooperation with forest managers. Work also remains to be done in background research because the technical capabilities of both spaceborne and airborne radar systems are being expanded constantly. The recently-introduced, very high resolution airborne SAR systems which have interferometric capabilities are examples of radars whose application potential deserves further investigation.

Meanwhile, forest managers may be able to adjust their procedures and information requirements in such a way that they are better matched with the capabilities of radar remote sensing. However, it should be noted that radar data alone can never provide a complete basis for a forest assessment or monitoring procedure. Assessment and/or monitoring of certain forest properties will require auxiliary information but, more importantly, the information extracted from radar images should always be verified by ground data. Furthermore, *it should be emphasised that radar is only a tool for collecting information. In the end, the differing parties involved in tropical forest management will have to judge all the information obtained and decide whether or not to act upon it.*

# Summary


## Radar remote sensing to support tropical forest management

The objective of the present study is to assess the potential of radar or microwave remote sensing for application to the management of tropical rain forests. To this end, the information content of images acquired by different radar systems is evaluated and compared to the information requirements of parties involved in tropical forest management. The study makes use of existing techniques for radar image analysis and investigates how these techniques can be optimised for the application studied.

Radar images have potential to support forest resource assessment as well as forest resource monitoring procedures. Forest resource assessment involves the collection, processing and presentation of forest data to obtain a description of the location, extent and/or constitution of a certain forest area *at a particular point in time*. Forest resource monitoring, on the other hand, is a *continuous process* involving the collection, processing and presentation of data on the location, extent, nature, cause and rate of change. Data that result from monitoring enable the inference of the forest's state at any point in time and provide a basis for planning and guiding future change. Forest resource assessment and monitoring are essential parts of procedures for sustainable forest management.

Individuals and organisations involved in the management of tropical forest resources presently operate at the global, national and local spatial levels. Descending from the global to the local level the following trends in information requirements of these managing parties can be observed. First, the area for which information is needed decreases. Second, the information required is of an increasingly fine spatial detail. Third, the information needs diversify and become more specific. Because of their need for spatial information, the parties involved in tropical forest management can be considered potential users of radar remote sensing data.

Parties operating at the global spatial level typically require information for use in forest resource monitoring procedures. Their requirements, which are usually inspired by major environmental issues, concentrate on parameters relating to: forest cover (e.g. forest, non-forest, logged), forest categories (e.g. vegetation type, administrative / legal status) and socio-economic factors (e.g. population density, infrastructure) (see Table 2.1). Nationally operating parties also require information on forest cover, forest category and socio-economic factors. Moreover, these parties have a growing need for information on indicators of biodiversity (see Table 2.2). Depending on their objectives, locally operating parties may require information on a variety of parameters relating to forest cover, forest category, terrain physiography, infrastructure, forest composition, forest structure and site class. Due to pressure of consumers, environmental and social groups, those involved in forest industry have a (future) need for information on indicators of sustainable management (see Tables 2.3 and 2.4).

Remote sensing systems as tools for collecting information offer some distinct advantages for application in extensive and/or inaccessible areas, in particular. First, these systems are able to acquire data in a synoptic, systematic and repetitive manner. Second, remotely sensed data can be geographically-referenced. In contrast to optical sensor systems, radar systems are able to acquire usable images when atmospheric conditions are poor due to the presence of moisture, clouds and/or smoke. In environments where tropical rain forests occur, adverse atmospheric conditions are in fact prevalent. Consequently, radar systems are the preferred remote sensing systems for application to tropical forest management. Nevertheless, in cases where data from optical sensor systems are available, these data can greatly complement the information present in radar remote sensing data. This is explained by the fact that optical and radar sensor systems operate in different parts of the electromagnetic spectrum. To illustrate the information on tropical forests present in optical and radar remote sensing data, the sections 2.2.2 and 2.2.3 of the present text review a selection of earlier publications.

To create an image, radar systems transmit electromagnetic waves towards the object of interest and subsequently record the waves that are reflected back towards the sensor. Waves reflected by the object in the direction of the sensor are referred to as the radar return signal or radar backscatter. The information content in radar images of a given forest area depends strongly on the properties of the wave signal with which the sensor operates. Relevant wave parameters include: frequency (or wavelength), polarization, incidence angle and viewing geometry. If wave parameters are fixed by system design and flight plan, then the received backscatter will only vary as a function of the scattering properties of the objects observed. Variables known to govern the radar return signal from the forest soil are: random surface roughness, periodic surface patterns and relative dielectric constant. The backscatter from the forest vegetation volume is a function of the volume's thickness and the densities, sizes, shapes, orientations and the relative dielectric constants of the component particles (e.g. leaves, branches and trunks). The relative dielectric constants of the forest soil and the vegetation particles are primarily determined by the water content. The principles of radar remote sensing and the interaction of radar waves with forest are discussed in detail in Chapter 3.

The radar data studied were acquired over tropical rain forest areas near the township of Mabura Hill in Guyana (5°10' N, 58°42' W) and the city of San José del Guaviare in Colombia (2°34' N, 72°38' W). The Mabura Hill study area is comprised of differing intact, primary forest types and forests that have been subject to industrial selective logging. Primary forests free of human impact are a rare occurrence in San José del Guaviare. Instead, this study area is characterised by the presence of secondary forests and a variety of non-forest cover types such as pastures, agricultural crops, burned areas and bare soils. In 1992 both study areas were imaged by the high resolution, X- and C-band airborne synthetic aperture radar (SAR) from the Canada Centre for Remote Sensing (CCRS). The year following, both sites were imaged by the high resolution, C-, L- and P-band airborne radar polarimeter from the Jet Propulsion Laboratory (JPL) of the National Aeronautics and Space Administration (NASA). Moreover, the data sets for the two study areas include time series of images acquired by the C-band SAR onboard the first European remote sensing satellite ERS-1. A collection of low altitude, nadir-looking, X-band measurements by the ERASME scatterometer system complements the data set for

Mabura Hill. Detailed descriptions of the study areas and available radar data can be found in Chapter 4.

To assess the information content of the available data, the study makes use of three fundamentally different information sources from the radar return signal: its strength (backscatter), polarization and phase, and spatial variability. Parameters concerning these sources of information are computed for predefined image regions and/or individual pixels. Spatial variations of the radar return signal are conceived as image texture. Texture in radar images of forests relates to canopy roughness which is a parameter of canopy architecture. In the present study, analysis of texture is largely based on the grey level co-occurrence (GLCO) technique. Use of this technique results in textural descriptors or attributes that represent grey level second-order statistics of pixel pairs. Like other methods and techniques, the method of textural analysis according to the GLCO technique is elaborated in Chapter 5.

Chapter 6 discusses the results of investigations into the potential of radar remote sensing to support forest resource assessment. The emphasis is on the application of radar to land cover type classification because this usually makes up the first step in assessment procedures. The paragraphs following summarise the results of the analysis of data acquired by the CCRS SAR, ERS-1, NASA/JPL AIRSAR and ERASME, respectively.

Analysis of images acquired by the CCRS airborne SAR shows that texture and not backscatter is the key to identifying tropical land cover types in high resolution, high frequency radar images. Region-based analysis of texture followed by classification of land cover at the level of primary forest types yields modest to good results. The combination of textural analysis and classification of images on a pixel-by-pixel basis yields less satisfactory results. However, texturally enhanced, high resolution and high frequency radar images make good bases for mapping of primary tropical forest types by means of visual interpretation. The textural appearance of the logged-over forest present in Mabura Hill is very similar to that of a riparian primary forest type known as Mora forest. In mono-temporal images the two forest types can only be discriminated by means of contextual information. Textural attributes enable the ranking of forest types according to the degree of canopy roughness. Moreover, certain textural attributes allow for quantification of canopy architectural properties. Findings by Oldeman (1983a), Brünig and Huang (1989) and Brünig and Mohren (1989) show that canopy roughness is an indicator of species diversity.

Textural attributes and backscatter values computed per region from mono-temporal ERS-1 SAR Precision (PRI) images are equivalent sources of information for identifying tropical land cover types. The two variables make modest bases for classifying at the level of primary forest, logged-over forest, secondary forest and non-forest and poor bases for classifying at the level of primary forest types. Textural attributes computed per region from time-averaged ERS-1 SAR Single Look Complex (SLC) images make modest bases for classifying tropical land cover at the level of primary forest types. The difference between the results for the ERS-1 PRI and time-averaged ERS-1 SLC images can be explained by the higher spatial resolution of the latter images. Neither texturally enhanced ERS-1 PRI images nor texturally enhanced time-averaged ERS-1 SLC images make an adequate basis for the mapping of tropical primary forest types by means of visual interpretation. In fact, a large

proportion of the coarse textures in these images results from relief and not from canopy architecture. Despite differences in measurement scale, the canopy roughness of the land cover types studied presents itself in a like manner in the texture of ERS-1 SAR and CCRS SAR images.

Analysis of the NASA/JPL AIRSAR data shows that backscatter measurements in radar bands with long wavelengths (i.e. L- and P-band) make considerably better bases for classifying tropical land cover types than backscatter measurements in radar bands with short wavelengths (i.e. C-band). Yet, comparison of results associated with the CCRS SAR and NASA/JPL AIRSAR data sets indicates that backscatter values computed from L- and P-band radar data and textural attributes computed from high resolution X- and C-band radar data are equally suitable bases for region-based classification at the level of primary forest types. The chances of classifying tropical land cover can be improved by the combined use of backscatter measurements in different frequency bands and/or polarizations. In general, measurements in either a single L- or P-band radar channel suffice for region-based classification at the forest / non-forest level. Reliable classification of secondary forest and logged-over forest requires measurements in a minimum of two radar channels. Similarly, reliable classification of primary forest types requires backscatter measurements in a minimum of three radar channels. For classification of primary forest types, inclusion of at least one P-band channel is essential. C-band channels are valuable for classifying primary forest types but not for classifying secondary and logged-over forests. The primary forest types studied have aboveground biomass levels over the threshold at which the backscatter in C-, L- and P-band saturates. This suggests that the potential of radar systems to map biomass is limited to tropical rain forests in early developmental phases.

Data from the ERASME scatterometer system contain information on the vertical and horizontal architecture of the forest. Hence, these data can support the analysis of forest architecture and forest dynamics and contribute to the development of forest management procedures. The capability of systems like ERASME to locate sources of scattering leads to a better notion of the scattering behaviour of the forest and can therefore support backscatter modelling studies.

Chapter 7 reports on investigations into the potential of radar remote sensing to support forest resource monitoring. These investigations are based on images acquired by the first European remote sensing satellite ERS-1. The paragraphs following summarise the most important results.

Results of analysis of the available time-series of ERS-1 SAR PRI images suggest that daily and seasonal fluctuations in rainfall can cause the backscatter of forests free of natural disturbance and human impact to vary by approximately 1 dB. Knowledge of daily and seasonal variations in the forest's backscatter allows for better founded decisions on the cause of backscatter changes observed and hence supports the application of radar in monitoring procedures. Images acquired during dry conditions show the most contrast between non-forest and primary and/or secondary forest and are therefore best suited to mapping (change in) the extent and location of forest and non-forest cover types. Availability of multi- rather than a mono-temporal ERS-1 data does not in essence improve the chances of discriminating between primary forest cover types.

ERS-1 SAR PRI images make a good basis for road detection. This is of great importance in view of the potential role of these images in forest monitoring procedures as roads are very distinctive indicators of foregoing and/or forthcoming human activities, including (selective) logging. Roads do in fact mark locations where the continued existence of the forest is at risk unless appropriate action is taken. Enhanced ERS-1 image products show the larger of the canopy openings resulting from selective logging. Yet, monitoring of selective logging is complicated by the fact that logging gaps often appear very similar to natural gaps. Monitoring of logging related disturbance in forest cover requires an approach that makes use of contextual information and field knowledge. Indicators of logging are the clustered and/or systematic occurrence of gaps and the presence of gaps in the vicinity of roads.

Considering the user requirements and the data analysis results, Chapter 8 elaborates upon the application and implementation of radar remote sensing to tropical forest management at the global, national and local spatial level. The final chapter of this text can be summarised as follows.

Table 8.1 shows appraisals of the potential of ERS-1 and equivalent systems to support the assessment and/or monitoring of the parameters of interest to parties involved in tropical forest management at the global spatial level. Based on ERS-1 SAR PRI images the assessment and/or monitoring of forest, non-forest, burned areas, deforested areas, clear-cuts and roads is judged to be 'possible'. Assessment and/or monitoring of logged-over forest, regenerating forest, actual forest vegetation type, plantation / natural forest and stand architecture is deemed to be 'difficult'.

The national and global information requirements associated with the monitoring of tropical forests are essentially the same. Hence, the capacities of the SAR onboard ERS-1 to support monitoring at national spatial level are comparable to those at the global spatial level. Assessment of national forest resources will often require data from airborne radar systems. Table 8.2 shows appraisals of the potential of two types of high resolution airborne radar data for this purpose, i.e. data acquired by systems operating in short wavelengths such as X- and C-band and long wavelengths such as L- and P-band. Appraisals relating to X- and C-band data assume the use of textural information, whereas appraisals concerning L- and P-band data assume the use of backscatter information. Both data types are judged to have 'good' potential for assessing terrain physiography and road density. Using either type of data, assessment of plantation / natural forest and cover fragmentation is deemed to be 'possible'. High resolution, short wavelength and long wavelength airborne radar data make equally suitable but complementary sources of information for identifying the cover types studied. Because of a limited sensitivity of L- and P-band radar signals to biomass, the possibilities for estimating timber volume and woody biomass are rated as 'difficult'.

Parties involved in forest management at the local spatial level require information of a very fine spatial detail. Prognoses of the potential of very high resolution X- or C-band and L- or P-band radar data for locally operating forest managers are given in Table 8.3. Based on either data type, the possibilities for assessing and/or monitoring of terrain characteristics, clear-cuts, burned areas and plantation / natural

forests are rated 'good'. Very high resolution X- and C-band radar data are judged to make better bases for the assessment and/or monitoring of primary forest types and logged-over forest than very high resolution L- and P-band data. Using either type of data, assessment and/or monitoring of (natural) regeneration is deemed to be 'difficult' because the data are not likely to provide the detail required to discern whether or not a regrowing vegetation is comprised of the preferred species. Assessment and/or monitoring of parameters relating to forest composition and forest structure requires information at the level of individual trees. In a natural tropical forest environment, radars operating with very high resolutions will at best have difficulty to provide this type of information. This also holds true for large scale (stereoscopic) aerial photography. Table 8.4 complements Table 8.3 and lists indicators of sustainable forest management with good potential to be assessed and/or monitored by very high resolution radars.

Forest managers who decide to make use of radar remote sensing data will have to follow different strategies to acquire the data most suited to their purposes. In turn, the radar data type selected will direct the strategy to be followed to extract the information desired. In the development of a data acquisition strategy it is important to consider: the spatial level, the nature of the required information and the requested observation time and frequency. These variables determine the choice of the data from a particular radar system or a combination of systems. The number of available airborne radar systems largely exceeds the number of available satellite radar systems. Moreover, the airborne systems offer a much wider range of technical capabilities than the satellite systems. Currently available radar satellite systems were not specifically developed for application to tropical forest management and therefore have only modest potential for this purpose. In general, forest managers with the option to apply airborne data have a better chance of satisfying their information needs by means of radar remote sensing than forest managers who are dependent on satellite data.

To ensure compatibility of information extracted from radar data from one forest area to another as well as for successive points in time, there is a need to standardise methods for radar data analysis. Strategies for analysis of the radar data as studied are the topic of section 8.2.2. The analysis strategy for a particular type of radar data is directed by the dominant source of information. Hence, analysis of data acquired by the ERS-1 satellite and airborne radars operating with long wavelengths focuses on backscatter, whereas analysis of data acquired by high resolution airborne radars operating with short wavelengths focuses on texture.

The findings of the present study illustrate that radar sensor systems offer considerable potential for application to tropical forest management. Radar data alone, however, can never provide a complete basis for a forest assessment or monitoring procedure. Assessment and/or monitoring of certain forest properties will require auxiliary information but more importantly the information extracted from radar images should always be verified by ground data. It should also be emphasised that radar is only a tool for collecting information. In the end, the differing parties involved in tropical forest management will have to judge all the information obtained and decide whether or not to act upon it.

## References

Adair, M. and B. Guindon, 1990. 'Statistical edge detection operators for linear feature extraction in SAR images'. *Canadian Journal of Remote Sensing*, vol.16, no.2, pp.10-19.

Ahern, F.J., T. Erdle, D.A. Maclean and I.D. Kneppeck, 1991. 'A quantitative relationship between forest growth rates and Thematic Mapper reflectance measurements'. *International Journal of Remote Sensing*, vol.12, no.3, pp.387-400.

Ahern, F.J., R.K. Raney, R.V. Dams and D. Werle, 1990. 'A review of remote sensing for tropical forest management to define possible RADARSAT contributions'. In: *Proceedings of the ISPRS symposium on primary data acquisition*, Manaus, 24-29 June 1990, pp.41-157.

Ahuja, N. and A. Rosenfeld, 1981. 'Mosaic models for textures'. *IEEE Transactions on Pattern Analysis and Machine Intelligence*, vol.3, no.1, pp.1-11.

Aiba, H., K. Murata and H. Iwashita, 1988. 'Experimental results of L-band microwave penetration properties of tropical and subtropical trees'. In: *Proceedings of the 8th Japan Conference on Remote Sensing*, pp.51-54.

Alder, D., 1980. *Forest volume estimation and yield prediction: vol. 2 - yield prediction.* Rome (FAO), FAO forestry paper no. 22/2, 194 p.

Andrade, A. and A. Etter, 1987. *Levantamiento ecológico del área de colonización de San José del Guaviare. Informe y memoria explicativa a los mapas.* Bogotá (Corporación de Araracuara), Proyecto Dainco-Casam.

Ardö, J., 1992. 'Volume quantification of coniferous forest compartments using spectral radiance recorded by Landsat Thematic Mapper'. *International Journal of Remote Sensing*, vol.13, no.9, pp.1779-1786.

Aronoff, S., 1982. 'Classification accuracy: a user approach'. *Photogrammetric Engineering and Remote Sensing*, vol.48, no.8, pp.1299-1307.

Attema, E.P.W. and F.T. Ulaby, 1978. 'Vegetation modelled as a water cloud'. *Radio Science*, vol.13, pp.357-364.

Balladares, C., R. Lazo and A.M. Martinez, 1997. 'Cover. Fire emissions from the Orinoco river delta'. *International Journal of Remote Sensing*, vol.18, no.5, pp.1007-1008.

Baltaxe, R., 1980. *The application of Landsat data to tropical forest surveys*. Rome (FAO), Document FOR: TF/INT/333 (SWE), 122 p.

Baltaxe, R., 1987. 'The application of remote sensing to tropical forest cover monitoring: a review of practices and possibilities'. In: Cracknell, A. and L. Hayes (eds.), *Remote sensing yearbook 1987*. London etc. (Taylor & Francis), pp.33-51.

Baraldi, A. and F. Parmiggiani, 1995. 'An investigation of the textural characteristics associated with gray level co-occurrence matrix statistical parameters'. *IEEE Transactions on Geoscience and Remote Sensing*, vol.33, no.2, pp.293-304.

Bass, S., D. Poore and B. Romijn, 1992. *ITTO and the future in relation to sustainable development*. Amsterdam (AIDEnvironment), report prepared by AIDEnvironment and International Institute for Environment and Development, 95 p.

Bayer, T. and R. Winter, 1990. 'Correction of relief effects in SAR-images of vegetated areas'. In: *Proceedings IGARSS'90, Remote Sensing Science for the Nineties*. Maryland, 20-24 May 1990, pp.2215-2218.

Beaudoin, A., T. Le Toan, E. Mougin, D.H. Hoekman and M. Wooding, 1992. 'Observation and modelling of pine forest responses and mapping of forest land-use type'. In: *Final Workshop MAESTRO-1/AGRISCATT; Radar techniques for forestry and agricultural applications.* Noordwijk, March 6-7 1992, ESA WPP-31, pp.183-188.

Benson, A.S. and SD DeGloria, 1985. 'Interpretation of Landsat-4 Thematic Mapper and Multispectral Scanner data for forest surveys'. *Photogrammetric Engineering and Remote Sensing*, vol.51, no.9, pp.1281-1289.

Bercha, F.G., 1992. *Revised SAREX-92 data acquisition report. SAR data acquisition and processing.* Calgary (Bercha International Inc.), ESTEC contract no.9643/91/NL/S2, 30 p. + appendices.

Bernard, R., P. Lancelin and G. Laurant, 1987. *Radar observation of the Guyana rain forest.* Issy-les-Moulineaux (Centre de Recherches en Physique de l'Environnement Terrestre et Planetaire), note technique CRPE/156, 76 p.

Bernard, R. and D. Vidal-Madjar, 1989. 'C-band radar cross section of the Guyana rain forest: possible use as a reference target for spaceborne SAR'. *Remote Sensing of Environment*, vol.27, no.1, pp.25-36.

Bijker, W., 1997. *Radar for rain forest - A monitoring system for land cover change in the Colombian Amazon.* Wageningen (Wageningen Agricultural University), PhD thesis, 192 p.

Bijker, W. and D.H. Hoekman, 1996. 'Monitoring of tropical rain forests and pastures with ERS-1. TREES ERS-1 '94 study: LAM-8'. In: van der Sanden, J.J., D.H. Hoekman and W. Bijker, *Radar remote sensing of tropical rain forests: ERS-1 studies in Guyana and Colombia. Final report.* Delft (BCRS, Netherlands Remote Sensing Board), BCRS report no.96-09, pp.29-33.

Bishop, Y.M.M., S.E. Fienberg and P.W. Holland, 1984. *Discrete multivariate analysis: theory and practice.* 8th printing. Cambridge etc. (The MIT Press), 557 p.

Boekee, D.E. and I.J. Boxma, 1976. *Theorie van de stochastische signalen.* Delft (Delft Technical University), 128 p.

Booth, W., 1989. 'Monitoring the fate of the forests from space'. *Science*, vol.243, no.4897, pp.1428-1429.

Box, E.O., B.N. Holben and V. Kalb, 1989. 'Accuracy of the AVHRR Vegetation Index as a predictor of biomass, primary productivity and net $CO_2$ flux'. *Vegetatio*, vol.80, no.2, pp.71-89.

Box, G.E.P. and G.M. Jenkins, 1970. *Time series analysis: forecasting and control.* San Francisco etc. (Holden-Day), 553 p.

Brils, C.A.J. and E.A. Laan, 1995. *Gaps and damage inflicted by directional felling in a tropical rain forest in Guyana.* Wageningen (Wageningen Agricultural University, The Tropenbos Foundation), M.Sc. thesis, 56 p + appendices.

Brockhaus, J.A. and S. Khorram, 1992. 'A comparison of SPOT and Landsat-TM data for use in conducting inventories of forest resources'. *International Journal of Remote Sensing*, vol.13, no.16, pp.3035-3043.

Brouwer, L.C., 1996. *Nutrient cycling in pristine and logged tropical rain forest.* Utrecht (Elinkwijk), Tropenbos-Guyana Series no.1, PhD thesis, 224 p.

Brünig, E.F. and Huang Y-W., 1989. 'Patterns of tree species diversity and canopy structure and dynamics in humid tropical evergreen forests on Borneo and in China'. In: Holm-Nielsen, L.B., I.C. Nielsen and H. Balslev (eds.), *Tropical forests. Botanical dynamics, speciation and diversity.* London etc. (Academic Press), pp. 75-88.

Brünig, E.F. and G.M.J. Mohren, 1989. 'Patterns in forest research'. In: Schmidt, P., R.A.A. Oldeman and A. Teller (eds.), *Unification of European forest pattern research.* Wageningen (Pudoc), pp.19-20.

Buiten, H.J. and J.G.P.W. Clevers (eds.), 1993. *Land observation by remote sensing. Theory and applications.* Amsterdam (Gordon and Breach Science Publishers), 642 p.

Busink, R.L., 1981. *Stand structure and phytomass in unexploited forest at Kabo: (experiments 78/21 and 78/22), 1978/1979: interim report of the first results.* Wageningen (Wageningen Agricultural University), M.Sc. thesis, 42 p. + appendices.

Cailliez, f., 1980. *Forest volume estimation and yield prediction: vol. 1 - volume estimation.* Rome (FAO), FAO forestry paper no. 22/1, 98 p.

Cannell, M.G.R., 1982. *World forest biomass and primary production data.* London etc. (Academic Press), 391 p.

CCRS, 1997. *Canada Centre for Remote Sensing Remote Sensing Glossary.* Web site.

Cihlar, J., T.J. Pultz and A.L. Gray, 1992. 'Change detection with synthetic aperture radar'. *International Journal of Remote Sensing*, vol.13, no.3, pp.401-414.

Cohen, W.B., T.A. Spies and G.A. Bradshaw, 1990. 'Semivariograms of digital imagery for analysis of conifer canopy structure'. *Remote Sensing of Environment*, vol.34, no.2, pp.167-178.

Colwell, R.N. (ed.), 1983. *Manual of Remote Sensing.* Falls Church, Virginia (American Society of Photogrammetry), 2nd edition, 2 volumes, 2440 p.

Congalton, R.G., R.G. Oderwald and R.A. Mead, 1983. 'Assessing Landsat classification accuracy using discrete multivariate analysis statistical techniques'. *Photogrammetric Engineering and Remote Sensing*, vol.49, no.12, pp.1671-1678.

Conners, R.W. and C.A. Harlow, 1980. 'A theoretical comparison of texture algorithms'. *IEEE Transactions on Pattern Analysis and Machine Intelligence*, vol.2, no.3, pp.204-222.

Conway, J.A., M.M. Leysen and A.J. Sieber, 1994. 'Evaluating multi-temporal ERS-1 SAR data for tropical forest mapping: data selection, processing and target identification'. In: *Proceedings of the Second ERS-1 Symposium - Space at the Service of our Environment.* Hamburg, 11-14 October 1993, ESA SP-361, pp.441-446.

Cross, A.M., 1990. 'AVHRR as a data source for a GIS: deforestation in Amazonia'. In: *Proceedings IGARSS'90, Remote Sensing Science for the Nineties.* Maryland, 20-24 May 1990, pp.223-226.

Cross, A.M., J.J. Settle, N.A. Drake and R.T.M. Päivinen, 1991. 'Subpixel measurement of tropical forest cover using AVHRR data'. *International Journal of Remote Sensing*, vol.12, no.5, pp.1119-1129.

Curlander, J.C. and R.N. McDonough, 1991. *Synthetic Aperture Radar. Systems and signal processing.* New York etc. (John Wiley & Sons, Inc.), 647 p.

Curran, P.J., 1985. *Principles of remote sensing.* Hong Kong etc. (Longman Group (FE) Ltd), 282 p.

Dams, R.V., D. Flett, M.D. Thompson and M. Lieberman, 1987. 'SAR (STAR-1) image analysis for Costa Rican tropical forestry applications'. In: *Proceedings II Simposyum Latinoamericano de Sensores Remotos*, Bogotá, 16-20 November 1987, pp.23-32.

Davis, T.A.W. and P.W. Richards, 1933. 'The Vegetation of Moraballi Creek, British Guinana: An Ecological Study of a Limited Area of Tropical Rain Forest. Part I'. *Journal of Ecology*, Vol.21, no.2, pp.350-384.

Davis, T.A.W. and P.W. Richards, 1934. 'The Vegetation of Moraballi Creek, British Guinana: An Ecological Study of a Limited Area of Tropical Rain Forest. Part II'. *Journal of Ecology*, Vol.22, no.1, pp.106-155.

de Graaf, N.R., 1986. *A silvicultural system for natural regeneration of tropical rain forest in Suriname.* Wageningen (Wageningen Agricultural University), PhD thesis, 250 p.

De Grandi, F., J.P. Malingreau, M. Leysen, M. Simmard and P. Mayaux, 1997. 'With radar global mapping of the tropical forest: new avenues from the TREES ERS-1 Central Africa mosaic'. In: *Proceedings of the third ERS symposium*, in preparation.

de Hoop, A.T., 1975. *Theorie van het elektromagnetische veld*. Delft (Delftse Universitaire Pers), 351 p.

de Oliveira, F., 1990. 'Deforestation of the Brazilian Amazon forest evaluated by remote sensing techniques'. *INPE Space News*, vol.1, no.1, pp.3-4.

de Vries, P.G., 1986. *Sampling theory for forest inventory A teach-yourself course*. Berlin etc. (Springer-Verlag), 399 p.

Dechambre, M., 1994. 'Radar measurements over the French Guiana mangrove'. In: *Proceedings of the IGARSS 1994 symposium; Surface and Atmospheric Remote Sensing: Technologies, Data Analysis and Interpretation*. Pasadena, California, 8-12 August 1994, pp.1057-1059.

Dechambre, M. and M. Bourdeau, 1996. 'Forest classification by means of pattern recognition method applied to scatterometer data'. In: *Proceedings of the IGARSS 1996 symposium; Remote Sensing for a Sustainable Future*. Lincoln, Nebraska, 27-31 May 1996, pp.833-835.

Dechambre, M., P. Lancelin and G. Laurant, 1993. *ERASME operations during the SAREX-92 campaign. Final report*. Velicy (CRPE), 30 p.

Dobson, M.C., F.T. Ulaby, T. Le Toan, A. Beaudoin, E.S. Kasischke and N. Christensen, 1992. 'Dependence of radar backscatter on conifer forest biomass'. *IEEE Transactions on Geoscience and Remote Sensing*, vol.30, no.2, pp.412-415.

Droesen, W.J., D.H. Hoekman, H.J.C. van Leeuwen, J.J. van der Sanden, B.A.M. Bouman, D. Uenk, M.A.M. Vissers and G.G. Lemoine, 1989. *MAESTRO 89 ground data collection Horsterwold / Speulderbos / Flevoland (NL)*. Wageningen (Wageningen Agricultural University), 57 p. + appendices.

Dubé, C., H. Proulx and K.P.B. Thompson, 1986. 'Analysis of the spatial structure of synthetic aperture radar (SAR) imagery for a better separability of cereal crops, wheat and barley'. In: *Proceedings of the IGARSS 1986 symposium; Remote sensing today's solutions for tomorrow's information needs*. Zürich, 8-11 September 1986, ESA SP-254, pp.745-750.

Duivenvoorden, J.F. and J.M. Lips, 1995. *A land-ecological study of soils, vegetation, and plant diversity in Colombian Amazonia*. Wageningen (The Tropenbos Foundation), Tropenbos Series no.12, PhD thesis University of Amsterdam, 437 p.

Eden, M.J., 1986. 'Monitoring indigenous shifting cultivation in forest areas of Southwest Guyana using aerial photography and Landsat'. In: Eden, M.J. and J.T. Parry (eds.), *Remote sensing and tropical land management*. London (John Wiley & Sons Ltd.), pp. 255-277.

Ehrlich, D., J.E. Estes and A. Singh, 1994. 'Applications of NOAA-AVHRR 1 km data for environmental monitoring'. *International Journal of Remote Sensing*, vol.15, no.1, pp.145-161.

ESA, 1992a. *ERS-1 System*. Noordwijk (ESA/ESTEC), ESA SP-1146, 87 p.

ESA, 1992b. *ESA ERS-1 Product Specification*. Frascati (ESA/ESRIN), ESA SP-1149, 7 p. + appendices.

ESA, 1993. *ERS User Handbook*. Noordwijk (ESA/ESTEC), ESA SP-1148, revision 1, 128 p.

Estes, J.E., 1982. 'Remote sensing and geographic information systems coming of age in the eighties.' In: *Proceedings of the Pecora VII Symposium. Remote sensing: an input to geographic information systems in the 1980's*, Sioux Falls, 18-21 October 1981, pp.23-40.

Etter, A. and A. Andrade, 1987. 'Seguimiento de la colonizacion en la Amazonia Colombiana el caso de San José del Guaviare (1973-1986)'. In: *Proceedings II Simposyum Latinoamericano de Sensores Remotos*, Bogotá, 16-20 November 1987, pp.145-152.

Eva, H.D., G. D'Souza and J.P. Malingreau, 1995. 'Potential of ATSR-1 data for detection of clearings within dense humid tropical forest'. *International Journal of Remote Sensing*, vol.16, no.11, pp.2071-2079.

Evans, D.L., T.G. Farr, J.J. van Zyl and H.A. Zebker, 1988. 'Radar polarimetry: analysis tools and applications'. *IEEE Transactions on Geoscience and Remote Sensing*, vol.26, no.6, pp.774-789.

Fanshawe, D.B., 1952. *The Vegetation of British Guiana. A Preliminary Review.* Oxford (Imperial Forestry Institute, University of Oxford), 96 p.

FAO, 1966. *Report on the soil survey project of British Guiana - Volume III Reconnaissance soil survey of British Guiana.* Rome (FAO) report no. MR/28627, part 1 137 p., part 2 160 p.

FAO, 1981. *Manual of forest inventory: with special reference to mixed tropical forests.* Rome (FAO), FAO forestry paper no. 27, 200 p.

FAO, 1993. *Forest resources assessment 1990 - Tropical countries.* Forestry Paper no.112, 61 p. + appendices.

Fearnside, P.M., A.T. Tardin, L.G.M. Filho, 1990. 'Deforestation rate in Brazilian Amazonia'. In: *Proceedings of the ISPRS Commission VII Mid-term Symposium.* Victoria, 17-21 September 1990, pp.539-547.

Foody, G.M., 1994. 'Ordinal-level classification of sub-pixel tropical forest cover'. *Photogrammetric Engineering and Remote Sensing*, vol.60, no.1, pp.61-65.

Foody, G.M., R.M. Green, R.M. Lucas, P.J. Curran, M. Honzak and I. Do Amaral, 1997. 'Observations on the relationship between SIR-C radar backscatter and the biomass of regenerating tropical forests'. *International Journal of Remote Sensing*, vol.18, no.3, pp.687-694.

Ford, J.P. and D.J. Casey, 1988. 'Shuttle radar mapping with divers incidence angle in the rainforest of Borneo'. *International Journal of Remote Sensing*, vol.9, no.5, pp.927-943.

Forster, B.C., 1993. 'Satellite remote sensing for land information in developing countries'. *Geocarto International*, vol.8, no.1, pp.5-15.

Forstreuter, W., 1988. 'Inventory of tropical rainforest in the southern provinces of the republic of Guinea based on Landsat TM data and GIS processing'. In: *Proceedings of the IUFRO subject group 4.02.05 meeting. Satellite imageries for forest inventory and monitoring; experiences, methods, perspectives.* Helsinki, 29 August - 2 September 1988, pp.158-162.

Freeman, A., B. Chapman and M. Alves, 1993. *MAPVEG software user's guide.* Pasadena (Jet Propulsion Laboratory), JPL document D-11254.

Freeman, A and S. Durden, 1992. 'A three-component scattering model to describe polarimetric SAR data'. In: *Proceedings of the radar polarimetry workshop*, SPIE vol. 1748, pp.213-224.

Freeman, A., S. Durden and R. Zimmerman, 1992. 'Mapping sub-tropical vegetation using multi-frequency, multi-polarization SAR data'. In: *Proceedings of IGARSS'92, International Space Year: Space Remote Sensing.* Houston, 26-29 May 1992, pp.1686-1689.

Fung, A.K., 1994. *Microwave scattering and emission models and their applications.* Boston (Artech House), 573 p.

Furley, P.A., 1986. 'Radar surveys for resources evaluation in Brazil: an illustration from Rondônia'. In: Eden, M.J. and J.T. Parry (eds.), *Remote sensing and tropical land management.* London (John Wiley & Sons Ltd.), pp.79-99.

Garcia, M.C. and R. Alvarez, 1994. 'TM digital processing of a tropical forest region in southeastern Mexico'. *International Journal of Remote Sensing*, vol.15, no.8, pp.1611-1632.

Gates, D.M., 1991. 'Water relations of forest trees'. *IEEE Transactions on Geoscience and Remote Sensing*, vol.29, no.6, pp.836-842.

Gelens, M.F., 1983. *Een vergelijking van twee bosprofieltekenmethodes (Experiment 82/14). Een beschouwing van bosstructuren binnen expt. 67/9a.* Paramaribo (CELOS), CELOS report no.135, 29 p.

Gerbrands, J.J., 1986. *Inleiding in de digitale beeldverwerking.* Delft (Delft Technical University), 141 p.

Gilruth, P.T., C.F. Hutchinson and B. Barry, 1990. 'Assessing deforestation in the Guinea highlands of West Africa using remote sensing'. *Photogrammetric Engineering and Remote Sensing*, vol.56, no.10, pp.1375-1382.

Givnish, T.J., 1984. 'Leaf and canopy adaptations in tropical forests'. In: Medina E., H.A. Mooney and C. Vázquez-yánes (eds.): *Proceedings of an international symposium on: Physiological ecology of plants of the wet tropics*, Oxatepec/los Tuxtlas, Mexico, June 29 - July 6 1983, pp.51-61.

Gräfe, W., 1981. *Struktur- und dynamikuntersuchungen in jungen zweitwuchbeständen der westlichen Llanos Venezuelas.* Göttingen (Georg-August-Universität), PhD thesis, 150 p.

Green, D.R., J.J. van der Sanden and J.A.T. Young, 1988. 'Communication: the key to integrating remote sensing and GIS.' In: *Proceedings of IGARSS'88, Remote sensing: moving towards the 21st century.* Edinburgh, 12-16 September 1988, pp.107-109.

Groot, J.S., 1991. *Introduction to radar polarimetry.* The Hague (TNO Physics and Electronics Laboratory), report no.FEL-91-B122, 68 p.

Guyana Forest Department, 1970. *Guyana Forest type map. The Great Falls area, Upper Demerara River.* Scale 1:50,000.

Hallé, F., R.A.A. Oldeman and P.B. Tomlinson, 1978. *Tropical trees and forests. An architectural analysis.* Berlin etc. (Springer-Verlag), 441 p.

Hammond, D.S., 1997. Personal communication.

Hammond, D.S. and V.K. Brown, 1992. *The ecological basis of recruitment and maintenance of timber species in the forests of Guyana 5.* Ascot, UK (Imperial College), Interim Group Report DSH5, 15 p.

Hammond, D.S. and V.K. Brown, 1995. 'Seed size of woody plants in relation to disturbance, dispersal, soil type in wet neotropical forests'. *Ecology*, vol.76, no. 8, pp.2544-2561.

Haralick, R.M., 1979. 'Statistical and structural approaches to texture'. In: *Proceedings of the IEEE*, vol.62, no.5, pp.763-768.

Haralick, R.M., 1986. 'Statistical image texture analysis'. In: T.Y. Young and K. Fu (eds.). *Handbook of pattern recognition and image processing*, chapter 11, pp.247-279. New York etc. (Academic Press, Inc.), 705p.

Haralick, R.M. and W.F. Bryant, 1976. *Documentation on procedures for textural/spatial pattern recognition techniques.* Lawrence (University of Kansas, Remote Sensing Laboratory), RSL Technical Report 278-1, 204 p.

Haralick, R.M., K. Shanmugan and I. Dinstein, 1973. 'Textural features for image classification'. *IEEE Transactions on Systems, Man and Cybernetics*, vol.SMC-3, no.4, pp.610-621.

Hawkins, R.K. and L.D. Teany, 1992. 'SAREX 1992 data calibration'. In: *Proceedings of the South American Radar EXperiment (SAREX-92) final workshop*, December 6-8 1993, ESA WPP-76, pp.41-53.

Heinsdijk, D. and A. de Miranda Bastos, 1963. *Inventários florestais na Amazônia.* Rio de Janeiro (Ministério da Agricultura, Serviço Florestal), boletim no.6, 100 p.

Heinsdijk, D. and A. de Miranda Bastos, 1965. *Report to the government of Brazil on forest inventories in the Amazon.* Rome (FAO), report no.2080, 78 p.

Helfert, M.R. and K.P. Lulla, 1990. 'Mapping continental-scale biomass burning and smoke palls over the Amazon Basin as observed from the Space Shuttle'. *Photogrammetric Engineering and Remote Sensing*, vol.56, no.10, pp.1367-1373.

Hellwich, O., 1994. 'Detection of linear objects in ERS-1 SAR images using neural network technology'. In: *Proceedings of the IGARSS 1994 symposium; Surface and Atmospheric Remote Sensing: Technologies, Data Analysis and Interpretation.* Pasadena, California, 8-12 August 1994, pp.1886-1888.

Hendrison, J., 1990. *Damage-controlled logging in managed tropical rain forest in Suriname.* Wageningen (Wageningen Agricultural University), PhD thesis, 204p.

Hess, L.L., J.M. Melack and D.S. Simonett, 1990. 'Radar detection of flooding beneath the forest canopy: a review'. *International Journal of Remote Sensing*, vol.11, no.7, pp.1313-1325.

Hoekman, D.H., 1985. 'Texture analysis of SLAR images as an aid in automated classification of forested areas'. In: *Proceedings of the EARSEL Workshop on Microwave remote sensing applied to vegetation.* Amsterdam, 10-12 December 1984, ESA SP-227, pp.99-109.

Hoekman, D.H., 1987. 'Measurements of the backscatter and attenuation properties of forest stands at X-, C- and L-band'. *Remote Sensing of Environment*, vol.23, no.3, pp.397-416.

Hoekman, D.H., 1990. *Radar remote sensing data for applications in forestry.* Wageningen (Wageningen Agricultural University), PhD thesis, 277 p.

Hoekman, D.H., 1991. 'Speckle ensemble statistics of logarithmically scaled data'. *IEEE Transactions on Geoscience and Remote Sensing*, vol.29, no.1, pp.180-182.

Hoekman, D.H., 1996. 'ERS-1 observations of tropical rain forests in Araracuara, Colombia. TREES ERS-1 '94 study: LAM-6'. In: van der Sanden, J.J., D.H. Hoekman and W. Bijker, *Radar remote sensing of tropical rain forests: ERS-1 studies in Guyana and Colombia. Final report.* Delft (BCRS, Netherlands Remote Sensing Board), BCRS report no.96-09, pp.9-19.

Hoekman, D.H., 1997. 'Radar monitoring for sustainable forest management in Indonesia'. Paper presented at seminar on: *Radar technology for sustainable forest management.* Jakarta, 3 April 1997, 17 p.

Hoekman, D.H., 1997. Lecture notes on theory of remote sensing. Wageningen (Wageningen Agricultural University), in prep.

Hoekman, D.H., M. van der Linden and J.J. van der Sanden, 1994. 'Application of ERS-1 in forest management'. In: Nieuwenhuis, G.J.A. and W.W.L. van Rooij (eds.), *Application of ERS-1 SAR data in agriculture and forestry.* Delft (BCRS, Netherlands Remote Sensing Board), BCRS report no.94-34, Chapter 5, pp.107-123.

Hoekman, D.H., J.J. van der Sanden and W. Bijker, 1994. *Radar remote sensing of tropical rain forests: The SAREX-92 campaign in Guyana and Colombia. First interim report.* Delft (BCRS, Netherlands Remote Sensing Board), BCRS report no.94-01, 34 p. + 4 appendices.

Hoekman, D.H., J.J. van der Sanden and W. Bijker, 1996. *Radar remote sensing of tropical rain forests: The AIRSAR-93 campaign in Guyana and Colombia.* Delft (BCRS, Netherlands Remote Sensing Board), BCRS report no.96-02, 59 p.

Hoffer, R.M., S.E. Davidson, P.W. Mueller and D.F. Lozano-Garcia, 1985. 'A comparison of X- and L-band radar data for discriminating forest cover types'. In; *Proceedings Pecora 10: Remote sensing in forest and range resource management.* Falls Church, Colorado, 20-22 August 1985, pp.439-440.

Hoffer, R.M., S. Maxwell and H. Ochis, 1995. *Use of radar for forestry applications*. Salt Lake City (USDA Forest Service), CSU project no.53-8800, 78 p.

Holdridge, L.R., W.C. Grenke, W.H. Hatheway, T. Liang and J.A. Tosi, 1971. *Forest environments in tropical life zones; a pilot study*. Oxford etc. (Pergamon Press), 747 p.

Howard, J.A., 1991. *Remote sensing of forest resources. Theory and application*. London etc. (Chapman & Hall), 420 p.

Husch, B., 1971. *Planning a forest Inventory*. Rome (FAO), Forestry and Forest Products Studies no.17, 120 p.

Hussin, Y.A., R.M. Reich and R.M. Hoffer, 1991. 'Estimating slash pine biomass using radar backscatter'. *IEEE Transactions on Geoscience and Remote Sensing*, vol.29, no.3, pp.427-431.

IEEE Antennas and Propagation Society, 1983. IEEE standard definitions of terms for antennas (IEEE std 145-1983). *IEEE Transactions on Antennas and Propagation*, vol.AP-31, no.6, part II of two parts, 29 p.

Imhoff, M.L., 1995. 'A theoretical analysis of the effect of forest structure on synthetic aperture radar backscatter and the remote sensing of biomass'. *IEEE Transactions on Geoscience and Remote Sensing*, vol.33, no.2, pp.341-352.

Imhoff, M., M. Story, C. Vermillion, F. Kahn and F. Polcyn, 1986. 'Forest canopy characterization and vegetation penetration assessment with space-borne radar'. *IEEE Transactions on Geoscience and Remote Sensing*, vol.GE-24, no.4, pp.535-542.

Isaaks, E.H. and Srivastava, R.M., 1989. *Applied geostatistics*. New York etc. (Oxford University Press), 561 p.

ITTO, 1991. *ITTO guidelines for the establishment and sustainable management of planted tropical forest*. Yokohama (International Tropical Timber Organisation), 38 p.

ITTO, 1992. *Criteria for the measurement of sustainable tropical forest management*. Yokohama (International Tropical Timber Organisation), ITTO - Policy Development Series no.3, 5 p.

Jacobs, M., R. Kruk and R.A.A. Oldeman, 1988. *The tropical rain forest: a first encounter*. Berlin etc. (Springer), 295 p.

Jensen, J.R., 1986. *Introductory digital image processing. A remote sensing perspective*. Englewood Cliffs (Prentice-Hall), 379 p.

Jetten, V.G., 1994. *Modelling the effects of logging on the water balance of a tropical rain forest. A study in Guyana*. Wageningen (The Tropenbos Foundation), Tropenbos Series no.6, PhD thesis University of Utrecht, 196 p.

Jonkers, W.B.J., 1987. *Vegetation structure, logging damage and silviculture in a tropical rain forest in Suriname*. Wageningen (Wageningen Agricultural University), PhD thesis, 172p.

Jorritsma, M., 1993. *SAREX-92 Araracuara: radar observation of tropical forests*. Wageningen (Wageningen Agricultural University), M.Sc. thesis, 73 p.

Journel, A.G. and C.J. Huijbregts, 1978. *Mining geostatistics*. London etc. (Academic Press Inc.), 600 p.

Joyce, A.T. and S.A. Sader, 1986. 'The use of remotely sensed data for the monitoring of forest change in tropical areas'. In: *Proceedings of the Twentieth International Symposium on Remote Sensing of Environment*. Nairobi , 4-10 December 1986, pp.363-378.

Kahn, Z., S. Paul and D. Cummings, 1980. *Mabura Hill, Upper Demerara forestry project. Soils investigation report no.1*. Mon Repos, Guyana (Ministry of Agriculture), 39 p. + appendices.

Kamaruzaman, J. and M.R.A. Manaf, 1995. 'Satellite remote sensing of deforestation in the Sungai Buloh Forest Reserve, Peninsular Malaysia'. *International Journal of Remote Sensing*, vol.16, no.11, pp.1981-1997.

Keil, M., R. Winter and H. Hönsch, 1994. 'Tropical rainforest investigation in Brazil using ERS-1 SAR data'. In: *Proceedings of the Second ERS-1 Symposium - Space at the Service of our Environment*. Hamburg, 11-14 October 1993, ESA SP-361, pp.481-484.

Kennett, R.G. and F.K. Li, 1989. 'Seasat over-land scatterometer data, Part II: selection of extended area land-target site for the calibration of spaceborne scatterometers'. *IEEE Transactions on Geoscience and Remote Sensing*, vol.27, no.6, pp.779-788.

Kilpelä, E. and J. Heikkilä, 1990. 'Comparison of some texture classifiers'. In: *Proceedings of the ISPRS Symposium; Commission 7*. Victoria, Canada, 17-21 September 1990, pp.333-339.

King, P.B., 1994. 'The value of ground resolution, spectral range and stereoscopy of satellite imagery for land system and land-use mapping of the humid tropics'. *International Journal of Remote Sensing*, vol.15, no.3, pp.521-530.

Kong, J.A. (ed.), 1990. *Polarimetric remote sensing*. New York etc. (Elsevier), 520 p.

Koop, H., 1989. *Forest Dynamics; SILVI-STAR: A comprehensive monitoring system*. Berlin etc. (Springer-Verlag), 229 p.

Koorevaar, P., G. Menelik and C. Dirksen, 1983. Elements of soil physics. Amsterdam etc. (Elsevier), 3rd edition, 230 p.

Kummer, D.M., 1992. 'Remote sensing and tropical deforestation: A cautionary note from the Philippines'. *Photogrammetric Engineering and Remote Sensing*, vol.58, no.10, pp.1469-1471.

Kuntz, S. and F. Siegert, 1994. 'Evaluation of ERS-1 SAR data for tropical rainforest monitoring'. *Earth observation quarterly*, no.45, September 1994, pp.1-5.

Kushwaha, S.P.S., S. Kuntz and G. Oesten, 1994. 'Applications of image texture in forest classification'. *International Journal of Remote Sensing*, vol.15, no.11, pp.2273-2284.

Kux, H.J.H., F.J. Ahern and R.W. Pietsch, 1995. 'Evaluation of radar remote sensing for natural resource management in the tropical rainforests of Acre state, Brazil'. *Canadian Journal of Remote Sensing*, vol.21, no.4, pp.430-440.

Lammerts van Bueren, E.M. and E.M. Blom, 1997. *Hierarchical framework for the formulation of sustainable forest management standards*. Wageningen (The Tropenbos Foundation), 82 p.

Lanly, J.P., 1992. 'Forestry issues at the United Nations Conference on Environment and Development'. Unasylva, vol.43, no.171.

Laur, H., 1992. *ERS-1 SAR calibration. Derivation of backscattering coefficient* $\sigma^{\circ}$ *in ERS-1.SAR.PRI products*. Frascati (ESA), ESA/ESRIN Technical Note, Issue 1, Rev.0, 16 p.

Laur, H., P. Meadows, J.I. Sanchez and E. Dwyer, 1993. 'ERS-1 SAR radiometric calibration'. In: *Proceedings of the CEOS SAR Calibration Workshop*. Noordwijk, 20-24 September 1993, ESA WPP-048, pp.257-281.

Le Toan, T., A. Beaudoin, J. Riom and D. Guyon, 1992. 'Relating forest biomass to SAR data'. *IEEE Transactions on Geoscience and Remote Sensing*, vol.30, no.2, pp.403-411.

Le Toan, T., F. Ribbes, T. Hahn, N. Floury and U.R. Wasrin, 1996. 'Use of ERS-1 data for forest monitoring in South Sumatra'. In: *Proceedings of the IGARSS 1996 symposium; Remote Sensing for a Sustainable Future*. Lincoln, Nebraska, 27-31 May 1996, pp.842-844.

Leberl, F.W., 1990. *Radargrammetric image processing*. Norwood (Artech House Inc.), 595 p.

Lescure, J.P., 1978. 'An architectural study of the vegetation's regeneration in French Guiana'. *Vegetatio*, vol.37, no.1, pp.53-60.

Lescure, J.P., H. Puig, B. Riera, D. Leclerc, A. Beekman and A. Beneteau, 1983. 'La phytomasse épigée d'une forêt dense en Guyane française'. *Acta Oecologica / Oecologia Generalis*, vol.4, no.3, pp.237-251.

Leysen, M.M., J.A. Conway and A.J. Sieber, 1994. 'Evaluating multi-temporal ERS-1 SAR data for tropical forest mapping: regional mapping and change detection applications'. In: *Proceedings of the Second ERS-1 Symposium - Space at the Service of our Environment.* Hamburg, 11-14 October 1993, ESA SP-361, pp.447-452.

Lichtenegger, J., 1996. 'ERS-1 SAR images - mirror of thunderstorms'. *Earth Observation Quarterly*, no.53, pp.7-9.

Lillesand T.M. and R.W. Kiefer, 1994. *Remote sensing and image interpretation.* New York etc. (John Wiley & Sons, Inc.), 3rd edition, 750 p.

Lo, C.P., 1986. *Applied remote sensing.* Hong Kong etc. (Longman Group (FE) Ltd), 393 p.

Loetsch, F., F. Zöhrer and K.E. Haller, 1973. *Forest inventory.* München etc. (BLV Verlagsgesellschaft), Vol.2, 469 p.

Lopes, A. and E. Nezry, 1991. *Refined Gamma-Gamma Maximum A Posteriori filter for detected SAR images.* Toulouse (Centre d'étude spatiale des rayonnements; CESR), 56 p.

Lopes, A., E. Nezry, R. Touzi and H. Laur, 1993. 'Structure detection and statistical adaptive speckle filtering in SAR images'. *International Journal of Remote Sensing*, vol.14, no.9, pp.1735-1758.

Loubry, D., 1994. *Déterminisme du comportement phénologique des arbres en forêt tropicale humide de Guyane française (5° lat. N.).* Paris (University of Paris), PhD thesis, 387 p.

Loubry. D., 1994. 'La phénologie des arbres caducifoliés en forêt guyanaise (5° de latitude nord): illustration d'un déterminisme à composantes endogène et exogène'. *Canadian Journal of Botany*, vol.72, no.12, pp.1843-1857.

Lucas, R.M., M. Honzak, G.M. Foody, P.J. Curran and C. Corves, 1993. 'Characterizing tropical secondary forests using multi-temporal Landsat sensor imagery'. *International Journal of Remote Sensing*, vol.14, no.16, pp.3061-3067.

Luckman, A.J., J. Baker, T.M. Kuplich, C.C.F. Yanasse and A.C. Frery, 1997. 'A study of the relationship between radar backscatter and regenerating tropical forest biomass for spaceborne SAR instruments'. *Remote Sensing of Environment*, vol.60, no.1, pp.1-13.

Malingreau, J.P. and N. Laporte, 1988. 'Global monitoring of tropical deforestation. AVHRR observations over the Amazon Basin and West Africa'. In: *Proceedings of the Forest Signatures Workshop.* Ispra, 7-9 September 1988, 33 p.

Malingreau, J.P., Stephens, G. and L. Fellows, 1985. 'Remote sensing of forest fires: Kalimantan and North Borneo in 1982-83'. *Ambio*,vol.14, no.6, pp.314-321.

Malingreau, J.P. and C.J. Tucker, 1990. 'Ranching in the Amazon basin. Large-scale changes observed by AVHRR'. *International Journal of Remote Sensing*, vol.11, no.2, pp.187-189.

Marceau, D.J., P.J. Howarth, J.-M. M. Dubois and D.J. Gratton, 1990. 'Evaluation of the grey-level co-occurrence matrix method for land-cover classification using SPOT imagery'. *IEEE Transactions on Geoscience and Remote Sensing*, vol.28, no.4, pp.513-519.

Marjuni, H. (ed.), 1990. *ITTO Guidelines for the sustainable management of natural tropical forests.* Yokohama (ITTO), ITTO Technical Series no.5, 18 p.

Matson, M. and B. Holben, 1987. 'Satellite detection of tropical burning in Brazil'. *International Journal of Remote Sensing*, vol.8, no.3, pp.509-516.

McDonald, K.C., M.C. Dobson and F.T. Ulaby, 1991. 'Modeling multi-frequency diurnal backscatter from a walnut orchard'. *IEEE Transactions on Geoscience and Remote Sensing*, vol.29, no.6, pp.852-863.

Meier, E., F. Holecz and D. Nüesch, 1992. 'Radiometric corrections in slant range and geocoded SAR images considering topographic effects'. In: *Proceedings of IGARSS'92, International Space Year: Space Remote Sensing*. Houston, 26-29 May 1992, pp.620-622.

Mennega, E.A., W.C.M. Tammens-de Rooij and M.J. Jansen-Jacobs (Eds.), 1988. *Check-list of woody plants of Guyana*. Ede (The Tropenbos Foundation), Tropenbos Technical Series no.2, 281 p.

Miranda, F.P., J.A. MacDonald and J.R. Carr, 1992. 'Application of the semivariogram textural classifier (STC) for vegetation discrimination using SIR-B data for Borneo'. *International Journal of Remote Sensing*, vol.13, no.12, pp.2349-2354.

Moghaddam, M., S. Durden and H. Zebker, 1994. 'Radar measurement of forested areas during OTTER'. *Remote Sensing of Environment*, vol.47, no.2, pp.154-166.

NASA, 1993. *AIRSAR South American Deployment. Operation Plan version 4.0*. Pasadena (NASA/JPL), 42 p.

Nelson, R. and B. Holben, 1986. 'Identifying deforestation in Brazil using multiresolution satellite data'. *International Journal of Remote Sensing*, vol.7, no.3, pp.429-448.

Nelson, R., N. Horning and T.A. Stone, 1987. 'Determining the rate of forest conversion in Mato Grosso, Brazil, using Landsat MSS and AVHRR data'. *International Journal of Remote Sensing*, vol.8, no.12, pp.1767-1784.

Nezry, E., E. Mougin, A. Lopes, J.P. Gastellu-Etchegorry and Y. Laumonier, 1993. 'Tropical vegetation mapping with combined visible and SAR spaceborne data'. *International Journal of Remote Sensing*, vol.14, no.11, pp.2165-2184.

Nyyssönen, A. (ed.), 1993. *Proceedings of FAO/ECE meeting of experts on global forest resources assessment in co-operation with UNEP and with support of FINNIDA (Kotka II). Kotka May 3-7 1993*. Helsinki (Gummerus Printing), Finnish Forest Research Institute research paper no.469, 214 p.

Ohler, F.M.J., 1980. *Phytomass and mineral content in untouched forest: onderzoeksproject 78/22: N, P, K, Ca en Mg gehalten in het ecosysteem ongestoord altijd groen seizoens-regenbos te Kabo*. Paramaribo (University of Surinam), Celos report no.132, 43 p. + appendices.

Oldeman, R.A.A., 1974. *L'architecture de la foret Guyanaise*. Paris (ORSTROM), Mémoires ORSTROM no.73, 204 p.

Oldeman, R.A.A., 1983a. 'Tropical rain forest, architecture, silvigenesis and diversity'. In: Sutton, S.L., T.C. Whitmore and A.C. Chadwick (eds.), *Tropical rain forest: ecology and management*. Oxford etc. (Blackwell Scientific Publications), pp. 139-150.

Oldeman, R.A.A., 1983b. *Veldgidsje transecttekenen*. Wageningen (Wageningen Agricultural University), 68 p.

Oldeman, R.A.A., 1990. *Forests: elements of silvology*. Berlin etc. (Springer-Verlag), 624 p.

Oldeman, R.A.A., 1996. Personal communication.

Oza, M.P., V.K. Srivastava, and P.K. Devaiah, 1992. 'Estimating the mean canopy diameter of teak plantations from Landsat MSS'. *International Journal of Remote Sensing*, vol.13, no.12, pp.2363-2369.

Oza, M.P., V.K. Srivastava, B.S. Pariswad and K.R.V. Setty, 1989. 'Relationship between Landsat MSS data and forest tree parameters'. *International Journal of Remote Sensing*, vol.10, no.11, pp.1813-1819.

Päivinen, R.T.M. and R.G. Witt, 1988. 'Application of NOAA/AVHRR data for tropical forest cover mapping in Ghana'. In: *Proceedings of the IUFRO subject group 4.02.05 meeting. Satellite imageries for forest inventory and monitoring; experiences, methods, perspectives.* Helsinki, 29 August - 2 September 1988, pp.163-170.

Paradella, W.R., M.F.F. Da Silva, N. De A. Rosa and C.A. Kushigbor, 1994. 'A geobotanical approach to the tropical rain forest environment of the Caraja's Mineral province (Amazon region, Brazil), based on digital TM-Landsat and DEM data'. *International Journal of Remote Sensing*, vol.15, no.8, pp.1633-1648.

Pardé, J. and J. Bouchon, 1988. *Dendrométrie.* Nancy (École nationale du Génie rural des Eaux et des Forêts), 2nd edition, 328 p.

Parry, D.E. and J.W. Trevett, 1979. 'Mapping Nigeria's vegetation from radar'. The Geographical Journal, vol. 145, no.2, pp.265-281.

Pereira, M.C. and A.W. Setzer, 1993a. 'Spectral characteristics of deforestation fires in NOAA/AVHRR images'. *International Journal of Remote Sensing*, vol.14, no.3, pp.583-597.

Pereira, M.C. and A.W. Setzer, 1993b. 'Spectral characteristics of fire scars in Landsat-5 TM images of Amazonia'. *International Journal of Remote Sensing*, vol.14, no.11, pp.2061-2078.

Peterson, D.L., W.E. Westman, N.J. Stephenson, V.G. Ambrosia, J.A. Brass and M.A. Spanner, 1986. 'Analysis of forest structure using Thematic Mapper Simulator data'. *IEEE Transactions on Geoscience and Remote Sensing*, vol.GE-24, no.1, pp.113-120.

Polak, A.M., 1992. *Major timber trees of Guyana: a field guide.* Wageningen (The Tropenbos Foundation), Tropenbos Series no.2, 272 p.

Poore, D., P. Burgess, J. Palmer, S. Rietbergen and T. Synnott, 1989. *No timber without trees. Sustainability in the tropical forest. A study for ITTO.* London (Earthscan Publications Ltd), 252 p.

Pope, K.O., J.M. Rey-Benayas and J.F. Paris, 1994. 'Radar remote sensing of forest and wetland ecosystems in the Central American tropics'. *Remote Sensing of Environment*, vol.48, no.2, pp.205-219.

PRORADAM, 1979. *La Amazonia Colombiana y sus recursos.* Bogotá D.E. (Proyecto Radargrametrico del Amazonas), 590 p.

Pulliainen, J.T., 1994. *Investigation on the backscattering properties of Finnish boreal forests at C- and X-band: a semi-empirical modeling approach.* Helsinki (Helsinki University of Technology), PhD thesis, report 19, 119 p.

Randall, R.E., 1978. *Theories and techniques in vegetation analysis.* Oxford (Oxford University Press), 61 p.

Ranson, K.J. and G. Sun, 1994. 'Mapping biomass of a northern forest using multifrequency SAR data'. *IEEE Transactions on Geoscience and Remote Sensing*, vol.32, no.2, pp.388-396.

Raunkiaer, C., 1934. *The life forms of plants and statistical plant geography, being the collected papers of C. Raunkiaer.* Oxford (Clarendon Press), 632 p.

Richards, P.W., 1952. *The tropical rain forest. An ecological study.* Cambridge (University Press), 450 p.

Richards, J.A., 1990. 'Radar backscatter modelling of forests: a review of current trends'. *International Journal of Remote Sensing*, vol.11, no.7, pp.1299-1312.

Richards, M, 1996. 'Stabilising the Amazon frontier: technology, institutions and policies'. *Natural Resource Perspectives*, no.10, series published by the Overseas Development Institute, 4 p.

Richards, J.A., P.W. Woodgate and A.K. Skidmore, 1987. 'An explanation of enhanced radar backscattering from flooded forests'. *International Journal of Remote Sensing*, vol.8, no.7, pp.1093-1100.

Riéra, B., M. Philippe, M. Dosso, R. Bernard, D. Vidal-Madjar and M. Dechambre, 1994. 'Étude du système sol végétation en forêt tropicale Guyanaise à l'aide d'observations radar en visée verticale'. *Revue d'ecologie*, continuation of; *La terre et la vie: revue d'ecologie appliquee*, vol.49, pp.357-377.

Rignot, E.J.M. and J.J. van Zyl, 1993. 'Change detection techniques for ERS-1 SAR data.' *IEEE Transactions on Geoscience and Remote Sensing*, vol.31, no.4, pp.896-906.

Rignot, E., J.J. van Zyl and R. Zimmermann, 1994. 'Inference of forest biomass using P-band circular-polarized radar signals'. In: *Proceedings of IGARSS'94; Surface and Atmospheric Remote Sensing: Technologies, Data Analysis and Interpretation.* Pasadena, August 8-12 1994, pp.2467-2469.

Rignot, E., W.A. Salas and D.L. Skole, 1997. 'Mapping deforestation and secondary growth in Rondonia, Brazil, using imaging radar and Thematic Mapper data'. *Remote Sensing of Environment*, vol.59, no.2, pp.167-179.

Rignot, E.J., R. Zimmermann and J.J. van Zyl, 1995. 'Spaceborne Applications of P band imaging radars for measuring forest biomass'. *IEEE Transactions on Geoscience and Remote Sensing*, vol.33, no.5, pp.1162-1169.

Rollet B., C. Hoegermann and I. Roth, 1990. *Stratification of tropical forests as seen in leaf structure.* The Hague etc. (Dr W. Junk Publishers), Tasks for vegetation science vol. 6, part 2, 246 p.

Roth, I. 1984. *Stratification of tropical forests as seen in leaf structure.* The Hague etc. (Dr W. Junk Publishers), Tasks for vegetation science vol. 6, part 1, 521 p.

Roy, P.S., R.N. Kaul, M.R. Sharma Roy and S.S. Garbyal, 1985. 'Forest-type stratification and delineation of shifting cultivation areas in the eastern part of Arunachal Pradesh using LANDSAT MSS data'. *International Journal of Remote Sensing*, vol.6, no.3-4, pp.411-418.

Roy, P.S., B.K. Ranganath, P.G. Diwakar, T.P.S. Vohra, S.K. Bhan, I.J. Singh and V.C. Pandian, 1991. 'Tropical forest type mapping and monitoring using remote sensing'. *International Journal of Remote Sensing*, vol.12, no.11, pp.2205-2225.

Saatchi, S.S., J.V. Soares and D.S. Alves, 1997. 'Mapping deforestation and land use in Amazon rainforest by using SIR-C imagery'. *Remote Sensing of Environment*, vol.59, no.2, pp.191-202.

Sabins, F.F. Jr., 1987. *Remote sensing. Principles and interpretation.* New York (W.H. Freeman and Company), 2nd edition, 449 p.

Sader, S.A., 1987. 'Forest biomass, canopy structure and species composition relationships with multipolarization L-band synthetic aperture radar data'. *Photogrammetric Engineering and Remote Sensing*, vol.53, no.2, pp.193-202.

Sader, S.A., T.A. Stone and A.T. Joyce, 1990. 'Remote sensing of tropical forests: an overview of research and applications using non-photographic sensors'. *Photogrammetric Engineering and Remote Sensing*, vol.56, no.10, pp.1343-1351.

Sader, S.A., R.B. Waide, W.T. Lawrence and A.T. Joyce, 1989. 'Tropical forest biomass and successional age class relationships to a vegetation index derived from Landsat TM data'. *Remote Sensing of Environment*, vol.28, no.1, pp.143-156.

Salas, W.A., J.K. Ranson, B.N. Rock and K.T. Smith, 1994. 'Temporal and spatial variations in dielectric constant and water status of dominant forest species from New England'. *Remote Sensing of Environment*, vol.47, no.2, pp.109-119.

Samadani, R. and J.F. Vesecky, 1990. 'Finding curvilinear features in speckled images'. *IEEE Transactions on Geoscience and Remote Sensing*, vol.28, no.4, pp.669-673.

Schanda, E., 1986. *Physical fundamentals of remote sensing.* Berlin etc. (Springer-Verlag), 187 p.

Schimper, A.F.W., 1935. *Pflanzengeographie auf physiologischer Grundlage; Volume I.* Jena (Fischer), 3rd edition, 588 p.

Shelton, R.L. and J.E. Estes, 1981. 'Remote sensing and geographic information systems: an unrealized potential'. *Geo-Processing*, vol.1, no.3, pp.395-420.

Shimabukuro, Y.E., B.N. Holben and C.J. Tucker, 1994. 'Fraction images derived from NOAA AVHRR data for studying the deforestation in the Brazilian Amazon'. *International Journal of Remote Sensing*, vol.15, no.3, pp.517-520.

Shimada, M., 1993. 'An estimation of JERS-1's SAR antenna elevation pattern using the Amazon rain forest images'. In: *Proceedings of the CEOS SAR Calibration Workshop.* Noordwijk, 20-24 September 1993, ESA WPP-048, pp.185-207.

Sicco Smit, G., 1975. 'Will the road to the green hell be paved with SLAR ? A case study of tropical rainforest type mapping in Colombia'. *ITC Journal*, 1975, no.2, pp.245-266.

Sicco Smit, G., 1978. 'SLAR for forest type classification in a semi-deciduous tropical region'. *ITC Journal*, 1978, no.3, pp.385-401.

Sicco Smit, G., 1988. 'A practical application of radar imagery for tropical rain forest vegetation mapping'. In: Küchler A.W. and I.S. Zonneveld (eds.), *Vegetation mapping.* Dordrecht (Kluwer Academic Publishers), pp.249-263.

Sieber, A.J., 1985. 'Forest signatures in imaging and non-imaging microwave scatterometer data'. *ESA Journal*, vol.9, no.4, pp.431-448.

Simonett, D.S., A.H. Strahler, G.-Q. Sun and Y. Wang, 1987. 'Radar forest modeling: potentials, problems, approaches, models'. In: *Proceedings of the 13th Annual Conference of the Remote Sensing Society; Advances in Digital Image Processing.* Nottingham, September 13-16 1987, pp.256-270.

Singh, A., 1986. 'Change detection in the tropical forest environment of Northeastern India using Landsat'. In: Eden, M.J. and J.T. Parry (eds.), *Remote sensing and tropical land management.* London (John Wiley & Sons Ltd.), pp.237-254.

Singh, A., 1987. 'Spectral separability of tropical forest cover classes'. *International Journal of Remote Sensing*, vol.8, no.7, pp.971-979.

Singh K.D., P. Reichert and R. Baltaxe, 1986. 'The role of remote sensing for global forest inventory'. In: *Proceedings of the 20th International Symposium on Remote Sensing of Environment.* Nairobi, 4-10 December 1986, pp.347-361.

Skolnik, M. I., 1980. *Introduction to radar systems.* 2nd edition. Tokyo etc. (McGraw-Hill Kogakusha, Ltd.), 581 p.

St-Onge, B.A. and F. Cavayas, 1995. 'Estimating forest stand structure from high resolution imagery using the directional variogram'. *International Journal of Remote Sensing*, vol.16, no.11, pp.1999-2021.

Stokes, G., 1852. 'On the composition and resolution of streams of polarized light from different sources'. In: *Proceedings of the Cambridge Philosophical Society.* Cambridge, 1852, pp.140-147.

Stoms, D.M. and J.E. Estes, 1993. 'A remote sensing research agenda for mapping and monitoring biodiversity'. *International Journal of Remote Sensing*, vol.14, no.10, pp.1839-1860.

Stone, T.A. and G.M. Woodwell, 1988. 'Shuttle imaging radar: an analysis of land use in Amazonia'. *International Journal of Remote Sensing*, vol.9, no.1, pp.95-105.

Stone, T.A., G.M. Woodwell and R.A. Houghton, 1989. 'Tropical deforestation in Pará, Brazil: analysis with Landsat and Shuttle Imaging Radar-A'. In: *Proceedings IGARSS'89, Quantitative Remote Sensing: An Economic Tool for the Nineties*. Vancouver, 10-14 July 1989, pp.192-195.

Swain, P.H. and S.M. Davis (eds.), 1978. *Remote sensing the quantitative approach*. New York etc. (McGraw-Hill, Inc.), 396 p.

Swellengrebel, E.J.G., 1959. 'On the value of large scale aerial photographs in British Guiana forestry'. *The Empire Forestry Review*, vol.38, no.95-98, pp.54-64.

Tanaka, S., H. Kimura and Y. Suga, 1983. 'Preparation of 1:25000 Landsat map for assessment of burnt area of Etajima Island'. *International Journal of Remote Sensing*, vol.4, no.4, pp.17-31.

ter Steege, H., 1990. *A monograph of Wallaba, Mora and Greenheart*. Ede (The Tropenbos Foundation), Tropenbos Technical Series no.5, 141 p.

ter Steege, H., 1993. *Patterns in tropical rain forest in Guyana*. Wageningen (The Tropenbos Foundation), Tropenbos Series no.3, PhD thesis University of Utrecht, 159 p.

ter Steege, H., R.G.A. Boot, L.C. Brouwer, J.C. Ceasar, R.C. Ek, D.S. Hammond, P.P. Haripersaud, P. van der Hout, V.G. Jetten, A.J. van Kekem, M.A. Kellman, Z. Kahn, A.M. Polak, T.L. Pons, J. Pulles, D. Raaimakers, S.A. Rose, J.J. van der Sanden and R.J. Zagt, 1996. *Ecology and logging in a tropical rain forest in Guyana. With recommendations for forest management*. Wageningen (The Tropenbos Foundation), Tropenbos Series no.14, 123 p.

ter Welle, B.J.H., M.J.A. Werger and J.T. Lambers (eds.), 1988. *Tropenbos Guyana. Report identification mission*. Ede (The Tropenbos Foundation), 71 p.

Thompson, M.D. and R.V. Dams, 1990. 'Forest and land cover mapping from SAR: a summary of recent tropical studies'. In: *Proceedings of the 23rd International Symposium on Remote Sensing of Environment*. Bangkok, 18-25 April 1990, pp.509-548.

Tittley, B., 1992. *A literature review of tropical American forests: description, management and remote sensing*. Ottawa (Energy Mines and Resources, Canada Centre for Remote Sensing), 45 p.

Touzi R., A. Lopes and P. Bousquet, 1988. 'A statistical and geometrical edge detector for SAR images'. *IEEE Transactions on Geoscience and Remote Sensing*, vol.26, no.6, pp.764-773.

Townshend, J.R.G., C.O. Justice, C. Gurney and J. McManus, 1992. 'The impact of misregistration on change detection'. *IEEE Transactions on Geoscience and Remote Sensing*, vol.30, no.5, pp.1054-1060.

Trevett, J.W., 1986. *Imaging radar for resources surveys*. London, New York (Chapman and Hall), 313 p.

Tropenbos, 1991a. *Guyana and Tropenbos*. Ede (The Tropenbos Foundation), 14 p.

Tropenbos, 1991b. *Colombia and Tropenbos*. Ede (The Tropenbos Foundation), 16 p.

Tucker, C.J., J.R.G. Townshend and T.E. Goff, 1985. 'African land-cover classification using satellite data'. *Science*, vol.227, no.4685, pp.369-375.

Tuomisto, H., A. Linna and R. Kalliola, 1994. 'Use of digitally processed satellite images in studies of tropical rain forest vegetation'. *International Journal of Remote Sensing*, vol.15, no.8, pp.1595-1610.

Ulaby, F.T., 1992. *Modeling radar backscatter from vegetation*. Ann Arbor (University of Michigan), Notes for short course at DLR, Oberpfaffenhofen, December 15-16, 1992, 175 p.

Ulaby, F.T. and C. Elachi (eds.), 1990. *Radar polarimetry for geoscience applications*. Norwood (Artech House Inc.), 364 p.

Ulaby, F.T. and M.A. El-Rayes, 1987. 'Microwave dielectric spectrum for vegetation - Part II: Dual-Dispersion Model'. *IEEE Transactions on Geoscience and Remote Sensing*, vol.GE-25, no.5, pp.550-557.

Ulaby, F.W., D. Held, M.C. Dobson, K.C. McDonald and T.B.A. Senior, 1987. 'Relating polarization phase difference of SAR signals to scene properties'. *IEEE Transactions on Geoscience and Remote Sensing*, vol.GE-25, no.1, pp.83-92.

Ulaby, F.W., F. Kouyate, B. Brisco and T.H. Lee Williams, 1986a. 'Textural information in SAR images'. *IEEE Transactions on Geoscience and Remote Sensing*, vol.GE-24, no.2, pp.235-245.

Ulaby, F.T., R.K. Moore and A.K. Fung, 1981. *Microwave remote sensing. Active and passive; Volume I Microwave remote sensing fundamentals and radiometry.* Norwood (Artech House Inc.), 456 p.

Ulaby, F.T., R.K. Moore and A.K. Fung, 1982. *Microwave remote sensing. Active and passive; Volume II Radar remote sensing and surface scattering and emission theory.* Norwood (Artech House Inc.), 608 p.

Ulaby, F.T., R.K. Moore and A.K. Fung, 1986b. *Microwave remote sensing. Active and passive; Volume III From theory to applications.* Norwood (Artech House Inc.), 1098 p.

Ulaby, F.T., K. Sarabandi, K. McDonald, M. Whitt and M.C. Dobson, 1990. 'Michigan microwave canopy scattering model'. *International Journal of Remote Sensing*, vol.11, no.7, pp.1223-1253.

Ulander, L.M.H., 1996. 'Radiometric slope correction of synthetic-aperture radar images'. *IEEE Transactions on Geoscience and Remote Sensing*, vol.34, no.5, pp.1115-1122.

UNCED, 1992. *Report of the United Nations conference on environment and development.* Rio de Janeiro, 3-14 June 1992, UNCED A/Conf.151/26, 5 volumes.

UNEP/FAO, 1993. *Report of the UNEP/FAO expert consultation on environmental parameters in future global forest assessments. Nairobi December 1-3 1992.* Nairobi (UNEP/GEMS), GEMS report series no.17, 262 p.

Unni, N.V.M., 1994. 'Space and forest management in India'. In: Mehrotra, A. and R.K. Suri (eds.), *Remote sensing for environment and forest management.* New Delhi (Indus Publishing Company), chapter 6, pp.94-116.

Unni, N.V.M., P.S. Roy and V. Parthasarathy, 1985. 'Evaluation of Landsat and airborne multispectral data and aerial photographs for mapping forest features and phenomena in a part of the Godavari Basin'. *International Journal of Remote Sensing*, vol.6, no.3-4, pp.419-431.

van den Hurk, B.J.J.M., 1996. *Sparse canopy parameterizations for meteorological models.* Wageningen (Wageningen Agricultural University), PhD thesis, 271 p.

van der Hout, P., 1996. *Effects of logging with different intensities of low impact harvesting.* Georgetown (Tropenbos-Guyana Programme), Tropenbos Guyana report 96-1, 71 p.

van der Meer, 1995. *Canopy dynamics of a tropical rain forest in French Guiana.* Wageningen (Wageningen Agricultural University), PhD thesis, 149 p.

van der Sanden, J.J., 1990. *Radar remote sensing of tropical forests. A literature review.* Delft (Netherlands Remote Sensing Board), BCRS report no.90-05b, 32 p.

van der Sanden, J.J. and D.H. Hoekman, 1994. 'The AIRSAR-93 campaign in Mabura Hill, Guyana; first results'. In: *Proceedings of PIERS'94.* Noordwijk (ESTEC), 11-15 July 1994, CD-ROM pp.814-819.

van der Sanden, J.J. and D.H. Hoekman, 1995. 'Multiband polarimetric SAR in support of tropical forest resources assessment'. In: *Proceedings of the IGARSS 1995 symposium; Quantitative Remote Sensing for Science and Applications.* Florence, 10-14 July 1995, pp.1207-1209.

van Dijk, A., M.A.M. Vissers, A. Tjalma, D.H. Hoekman and M. Verschoor, 1994. *The usefulness of ERS-1 data in monitoring the Amazon forest*. Delft (Netherlands Remote Sensing Board), BCRS report no.93-17, 55 p.

van Kekem, A.J., J.H.M. Pulles and Z. Kahn, 1996. *Soils of the rainforest in Central Guyana*. Georgetown (Tropenbos-Guyana Programme), Tropenbos-Guyana Scientific Series no. 2, 160 p. + one 1:100.000 landforms and soils map.

van Rompaey, R.S.A.R., 1993. *Forest gradients in West Africa. A spatial gradient analysis*. Wageningen (Wageningen Agricultural University), PhD thesis, 142 p.

van Zyl, J.J., 1989. 'Unsupervised classification of scattering behaviour using radar polarimetry data'. *IEEE Transactions on Geoscience and Remote Sensing*, vol.GE-27, no.1, pp.36-45.

van Zyl, J.J. 1993. 'The effect of topography on radar scattering from vegetated areas'. *IEEE Transactions on Geoscience and Remote Sensing*, vol.31, no.1, pp.153-160.

van Zyl, J.J., R. Carande, Y. Lou, T. Miller and K. Wheeler, 1992. 'The NASA/JPL three-frequency polarimetric AIRSAR system'. In: *Proceedings of IGARSS'92; International Space Year: Space Remote Sensing*. Houston, May 26-29 1992, Volume I, pp.649-651.

van Zyl, J.J., H.A. Zebker and C. Elachi, 1987. 'Imaging radar polarization signatures: theory and observation.' *Radio Science*, vol.22, no.4, pp.529-543.

Vester, H.F.M., 1997. The trees and the forest. *The role of tree architecture in canopy development; a case study in secondary forests (Araracuara, Colombia)*. Amsterdam (University of Amsterdam), PhD thesis, 182 p.

Viskne, A., T.C. Liston and C.D. Sapp, 1970. 'SLR reconnaissance of Panama'. *Photogrammetric Engineering*, vol.36, no.3, pp.253-259.

Vissers, M.A.M. and J.J. van der Sanden, 1993. *Groundtruth collection for the JPL-SAR and ERS-1 campaign in Flevoland and the Veluwe (NL) 1991*. Delft (Netherlands Remote Sensing Board), BCRS report no.92-26, 71 p.

Waide, R.B. and A.E. Lugo, 1992. 'A research perspective on disturbance and recovery of a tropical montane forest'. In: Goldammer, J.G. (ed.), *Tropical forests in transition. Ecology of natural and anthropogenic disturbance processes*, pp.173-190.

Wang, Y., L.L. Hess, S. Filoso and J.M. Melack, 1994. 'Canopy penetration studies: modeled radar backscatter from Amazon floodplain forests at C-, L- and P-band'. In: *Proceedings of IGARSS'94; Surface and Atmospheric Remote Sensing: Technologies, Data Analysis and Interpretation*. Pasadena, August 8-12 1994, pp.1060-1062.

Webb, L.J., 1968. 'Environmental relationships of the structural types of Australian rain forest vegetation'. *Ecology*, vol.49, no.2, pp.296-311.

Weber, J.A. and S.L. Ustin, 1991. 'Diurnal water relations of walnut trees: implications for remote sensing'. *IEEE Transactions on Geoscience and Remote Sensing*, vol.29, no.6, pp.864-874.

Webster, R. and M. Oliver, 1990. *Statistical methods in land and resource survey*. Oxford (Oxford University Press), 316 p.

Werle, D., 1989. 'Potential application of imaging radar for monitoring the depletion of tropical forests'. In: *Proceedings IGARSS'89, Quantitative Remote Sensing: An Economic Tool for the Nineties*. Vancouver, 10-14 July 1989, pp.1383-1386.

Westinga, E., W.J. Looijen, D.H. Hoekman and C. Racaut, 1993. *Consultation on user needs for RESPAS*. Delft (BCRS, Netherlands Remote Sensing Board), report no.93-15, 79 p.

Westman, W.E. and J.F. Paris, 1987. 'Detecting forest structure and biomass with C-band multipolarization radar: physical model and field tests'. *Remote Sensing of Environment*, vol.22, no.2, pp.249-269.

Weszka, J.S., C.R. Dyer and A. Rosenfeld, 1976. 'A comparative study of texture measures for terrain classification'. *IEEE Transactions on Systems, Man, and Cybernetics*, vol.SMC-6, no.4, pp.269-285.

Whitmore, T.C., 1990. *An introduction to tropical rain forests*. Oxford (Clarendon Press), 226 p.

Wilkie, D.S., 1990. 'Establishing the Okapi rain forest reserve: avoiding human land-use conflicts using satellite image analysis'. In: *Proceedings IGARSS'90, Remote Sensing Science for the Nineties*. Maryland, 20-24 May 1990, pp.233-236.

Wismann, V., A. Cavanie, D. Hoekman, I. Woodhouse, K. Boehnke and C. Schmullius, 1996. *Land surface observations using the ERS-1 windscatterometer*. Wedel (Institute for Applied Remote Sensing), Final report for ESA contract no.11103/94/NL/CN, 57 p.

Wood, E.F. (ed.), 1991. *Land surface-atmosphere interactions for climate modeling. Observations, models and analysis*. Dordrecht (Kluwer Academic Publishers), 314 p.

Woodcock, C.E., A.H. Strahler and D.L.B. Jupp, 1988a. 'The use of variograms in remote sensing: I. Scene models and simulated images'. *Remote Sensing of Environment*, vol.25, no.3, pp.323-348.

Woodcock, C.E., A.H. Strahler and D.L.B. Jupp, 1988b. 'The use of variograms in remote sensing: II. Real digital images'. *Remote Sensing of Environment*, vol.25, no.3, pp.349-379.

Wooding, M.G., A.D. Zmuda and E. Attema, 1992. 'An overview of SAREX-92 data acquisition and analysis of the tropical forest environment'. In: *Proceedings of the South American Radar EXperiment (SAREX-92) final workshop*, December 6-8 1993, ESA wpp-76, pp.3-14.

Wu, S.-T., 1987. 'Potential application of multipolarization SAR for the pine plantation biomass estimation'. *IEEE Transactions on Geoscience and Remote Sensing*, vol.GE-25, no.3, pp.403-409.

Wu, S.-T., 1990. 'Assessment of tropical forest stand characteristics with multipolarization SAR data acquired over a mountainous region in Costa Rica'. *IEEE Transactions on Geoscience and Remote Sensing*, vol.28, no.4, pp.752-755.

Wu, S.-T and S.A. Sader, 1987. 'Multipolarization SAR data for surface feature delineation and forest vegetation characterization'. *IEEE Transactions on Geoscience and Remote Sensing*, vol.GE-25, no.1, pp.67-76.

Yanasse, C.C.F., S.J.S. Sant'Anna, A.C. Frery, C.D. Rennó, J.V. Soares and A.J. Luckman, 1997. 'Exploratory study of the relationship between tropical forest regeneration stages and SIR-C L and C data'. *Remote Sensing of Environment*, vol.59, no.2, pp.180-190.

Yanasse, C.C.F., A.C. Frery, S.J.S. Sant'Anna, P.H. Filho and L.V. Dutra, 1994. 'Statistical analysis of Sarex data over Tapajós Brazil'. In: *Proceedings of the SAREX-92 Workshop*. Paris December 6-8 1993, ESA WPP-76, pp.25-40.

Zagt, R.J., 1995. *Population structure, dynamics and reproduction of tropical tree species*. Georgetown (Tropenbos-Guyana Programme), Tropenbos Guyana report 95-1, 40 p.

Zebker, H.A., J.J. van Zyl, S.L. Durden and L. Norikane, 1991. 'Calibrated imaging radar polarimetry: technique, examples and applications'. *IEEE Transactions on Geoscience and Remote Sensing*, vol.29, no.6, pp.942-961.

Zhan, C.-X., 1986. *Gray level dependence texture measures: sensitivity and stability problems and applications in remote sensing*. Santa Barbara (University of California), PhD dissertation, 99 p.

# APPENDIX I
# Details of GLCO textural analysis

The value of texture as a source of information in high frequency, high resolution radar images of forested terrain in the humid tropics was clearly illustrated in sections 6.1 and 6.2. *Analysis of image texture according to the grey level co-occurrence (GLCO) approach involves choices concerning: GLCO attribute, displacement direction, displacement length and, for analysis by means of a moving spatial window, window size.* The current appendix discusses the effects of these choices on the potential of GLCO textural descriptors to identify the land cover types studied. The results presented relate to the X-band HH CCRS SAR and the ERS-1 SLC-av data sets. Unless stated differently, the image data had the 'standard' scaling, i.e. pixels values ranging from 0 to 127 (see section 5.2.2). The effects of radar frequency, polarization, incidence angle and the number of grey levels (scaling) of the input image are also discussed.

## I.1 Texture as a function of frequency, polarization and incidence angle

Depending on frequency, polarization and/or incidence angle, radar images of one and the same area may contain differing amounts of textural information. The higher the textural information content, the better the chances for GLCO attributes to discriminate classes. Figure I.1 illustrates the differences in the textural information content of the radar bands present in the CCRS SAR data set. The value on the ordinate represents the total number of class pairs that is discriminated successfully by all GLCO attributes studied (see section 5.2.4). The data sets for the radar bands shown in Figure I.1a include six classes (Secondary forest and Non-forest are excluded). These six classes make up 15 different class pairs for each GLCO attribute to discriminate. The total number of available GLCO attributes equals 90, i.e. nine statistical parameters each computed for 10 displacement lengths. Hence, the maximum number of class pairs that can possibly be discriminated is 1350. The data sets for the bands shown in Figure I.1b include five classes (Secondary forest, Non-forest and Logged-over forest excluded) and for those shown in Figure I.1c eight classes (no classes excluded). Consequently, the maximum number of class pairs is 900 in Figure I.1b and 2520 in Figure I.1c.

The results in Figure I.1 should be interpreted with care since, apart from frequency and polarization, there are other possible methodological causes for the apparent differences in textural information content. Only the results for the following band combinations can be compared directly: XHH/XVH, XHV/XVV, CHH/CVH and CHV/CVV. Results for HH or VH polarized bands cannot be compared directly with those for HV or VV polarized bands since these data were acquired along different flight lines. Consequently, the samples in the HH/VH and HV/VV data sets do not relate to exactly the same areas on the ground. Also, certain areas of interest may be located at varying range distances in images from differing flight lines. Hence, these areas may be observed at different angles of incidence which in turn may change the

textural appearance. Both facts induce unwanted variation in the textural characteristics of the sample points in the HH/VH and HV/VV data sets. This influences the discriminating capacity of the GLCO attributes and obstructs the direct comparison of the corresponding transformed divergence analysis results. Likewise, the results for X-band cannot be compared directly with those for C-band because the pixels in these data sets are of a slightly different size (see Table 4.5).

Most striking in Figure I.1a is the difference in the performance of the GLCO attributes associated with the HH/VH and HV/VV data sets. The apparent difference for the VH and HV polarized bands is in conflict with the reciprocity principle (see section 3.1.6). Further study reveals that these differences are mostly due to variations in the textural appearance of Logged-over forest regions. In the HV/VV polarized bands the within class variation for Logged-over forest is larger than in the HH/VH polarized bands. Comparison of the Figures I.2a and I.2b show this to result from the fact that the Logged-over sample plots in X-band HV (likewise in: XVV, CHV and CVV) occupy a larger incidence angle range than in X-band VH (likewise in: XHH, CVH, CHH). Because of the larger within class variation, Logged-over forest is more easily confused with other classes (notably Mora forest and Mixed forest) in the HV/VV polarized bands than in the HH/VH polarized bands. This artefact can easily be 'compensated' for by excluding all class pairs involving Logged-over forest. The results of this procedure are shown in Figure I.1b. The noted artefact illustrates the importance of incidence angle in relation to textural analysis. The effect of incidence angle on the textural attributes will be discussed in more detail below.

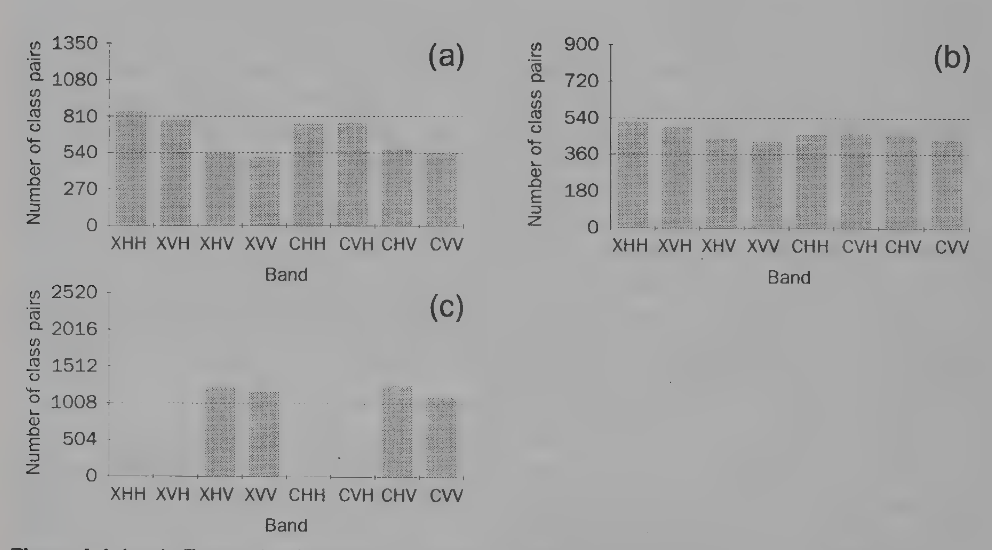



**Figure I.1 (a-c)** Textural information content of radar bands present in the **CCRS SAR** data set. The columns represent the total number of class pairs that is discriminated successfully by all of the GLCO attributes studied: (**a**) class pairs comprising Secondary forest and Non-forest excluded (**b**) class pairs comprising Secondary forest, Non-forest and Logged-over forest excluded (**c**) no class pairs excluded. The maximum number of class pairs that can possibly be discriminated is 1350 in the case of **a**, 900 in the case of **b** and 2520 in the case of **c.**

Despite the aforementioned complications, Figure I.1 allows the following observations. Overall, the differences in the suitability of the various radar bands for textural analysis appear small. In X-band the results for HH are slightly better than those for VH, likewise those for HV are better than those for VV. If one equates the results for the two cross polarizations, the results for HH are better than for VV. *In descending order, the suitability of the various X-band channels for textural analysis is therefore: HH, VH/HV and VV. In C-band, HH and VH/HV are equally suitable and both somewhat more suited for use in analysis of texture than VV.* The question whether X- or C-band is more suited for textural analysis is addressed below.

Texture in high frequency, high resolution radar images of forested areas (on flat terrain) is governed by the roughness of the canopy surface which is a parameter of the canopy's architecture. Consider two radar systems imaging the same stretch of forest. Of these two systems, the one operating with the highest frequency (shortest wavelength) is likely to produce the image with the highest textural information content since its signal penetrates the canopy surface to a lesser depth. Similarly, the radar image with the highest spatial resolution and/or smallest pixel size can be expected to contain the most textural information because it gives the most detailed representation of canopy roughness. This holds as long as the radar systems in question have the same radiometric resolution. In practice, this may not be the case because a higher spatial resolution can usually be achieved at the expense of radiometric resolution only. The CCRS SAR X- and C-band images are acquired by one and the same radar system, i.e. using identical spatial and radiometric resolutions. However, the X-band images are processed to a smaller pixel size than the C-band images (see Table 4.5). Given that the X-band images have both a shorter wavelength and a smaller pixel size than the C-band images, one would assume the X-band images to contain the most textural information. Yet, the results in Figure I.1 do not show evidence of such. Indeed, the results for XHH/XVH are slightly better than those for CHH/CVH, but the results for XHV/XVV are in fact somewhat poorer than for CHV/CVV. *It follows that there is no distinct difference in the suitability of X- and C-band radar data for use in analysis of texture.*

The most important causes of texture in high frequency, high resolution radar images are the geometrical effects that occur when a radar observes terrain with varying relief, e.g. an irregular forest canopy (see section 3.1.3). The nature and extent of these effects depends strongly on the geometry of the observed surface and the elevation and/or incidence angle (see Figure 3.8). A forest canopy of a given roughness will be conceived differently at small incidence angles than at large incidence angles. The effects of radar "shadowing" and "foreshortening" become more pronounced as the incidence angle increases, whereas the effects of "layover" decrease with an increasing incidence angle. Texture in radar images is the result of all these effects. Hence, *the textural appearance of a forest with a specific canopy roughness changes with a change in incidence angle.* Moreover, changes in ground range resolution give rise to changes in texture as a function of incidence angle (see Equation 3.1, section 3.1.1). At higher incidence angles, a radar system is capable of imaging a forest canopy with more spatial detail. This affects the canopy's textural appearance.

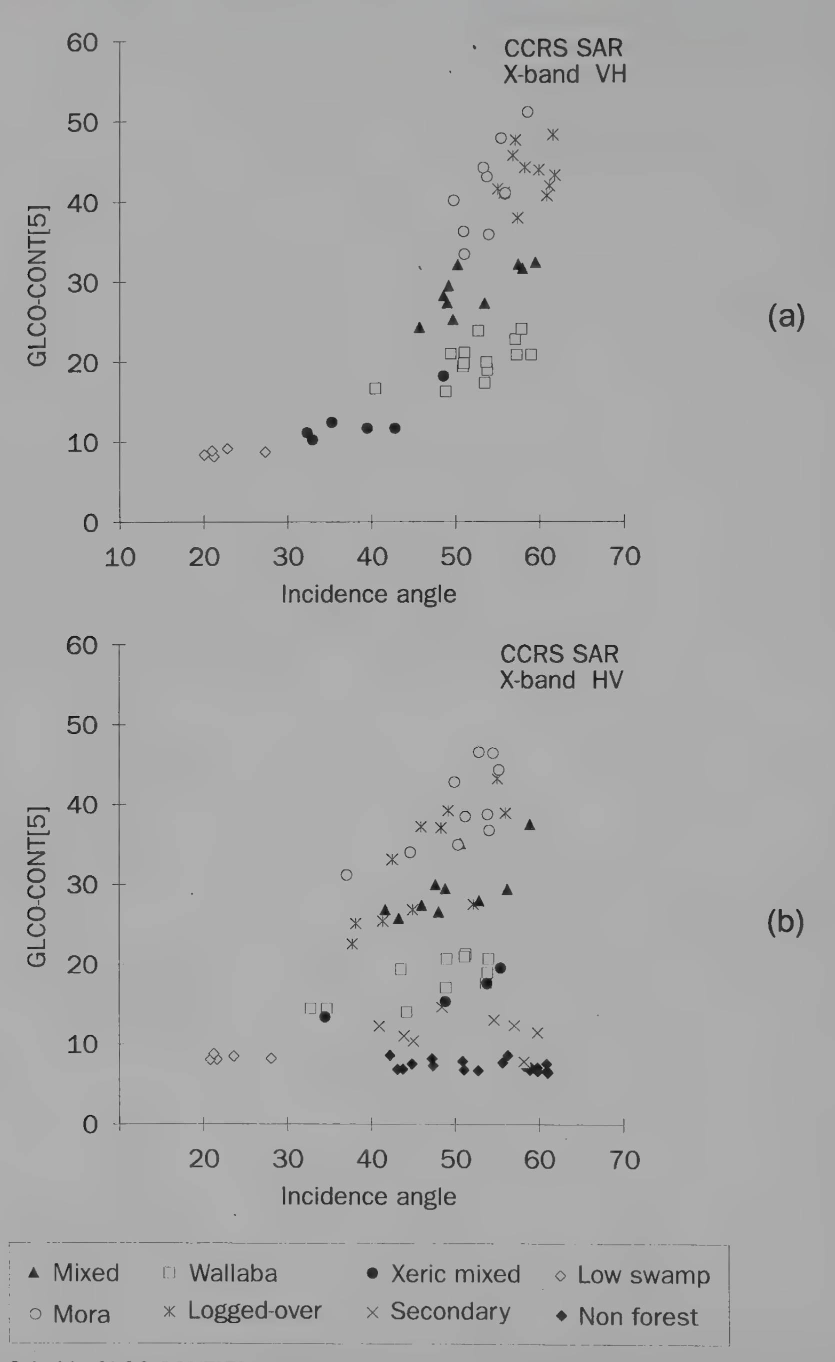



**Figure I.2 (a-b)** GLCO-CONT[5] textural values for image regions representing cover types studied as a function of incidence angle: (**a**) texture computed from the X-band VH CCRS SAR image (**b**) texture computed from the X-band HV CCRS SAR image.

Figure I.2 illustrates the changes induced by the incidence angle in the GLCO-CONT[5] textural attribute for the land cover types present in the X-band VH and HV images. The texture of forest types with rough upper canopies (Mora, Mixed and Logged-over forest) is shown to depend strongly on the angle of incidence. In contrast, the texture of Non-forest and forest types with smooth upper canopies (Low swamp and Secondary forest) can be seen to be almost independent of the incidence angle. Wallaba forest and Xeric mixed forest take up intermediate positions in the sense that their textures do not vary as much with the incidence angle as for the rough cover types, but more so than for the smooth ones. The differences in the effect of incidence angle on the textural appearance of the cover types studied can be

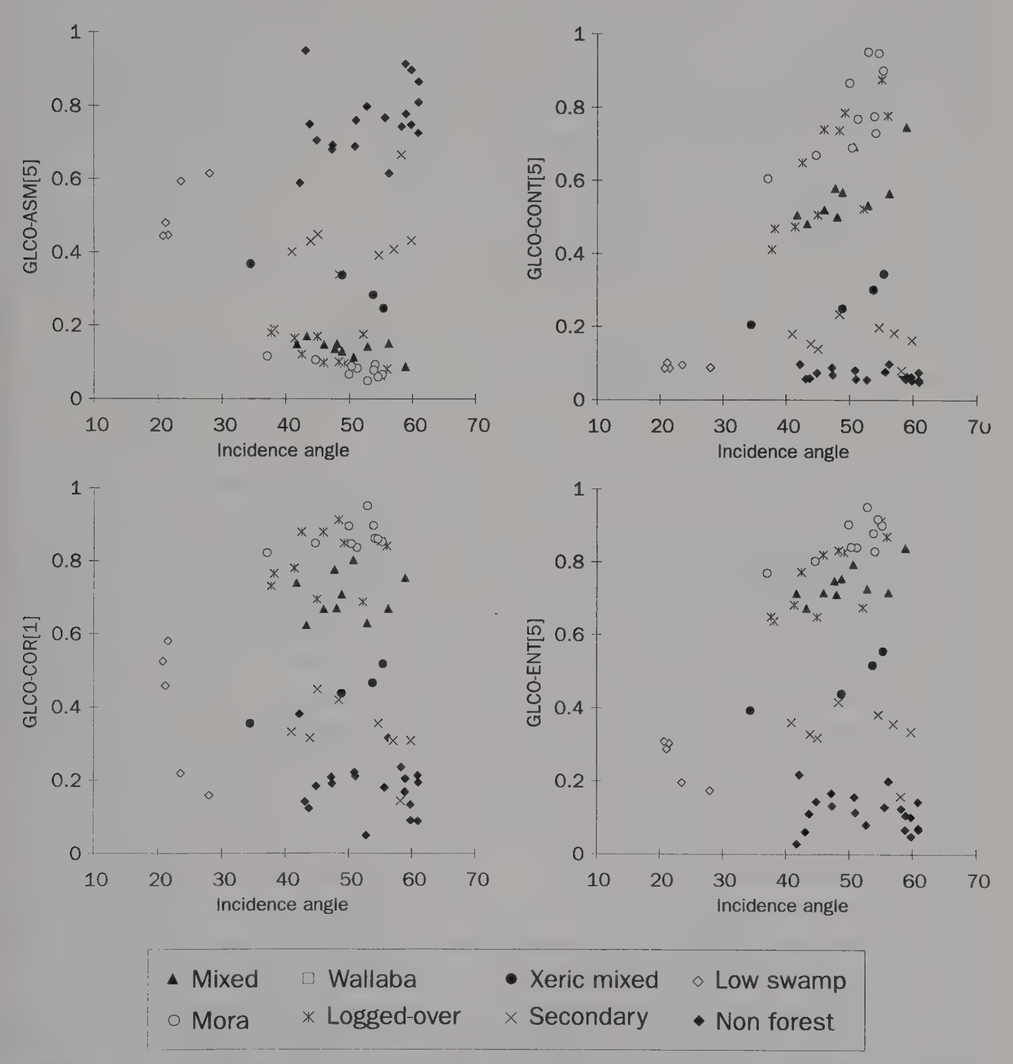



**Figure I.3** Different GLCO textural values and sd($\gamma$) for image regions representing cover types studied as a function of incidence angle. The textural attributes shown were computed from the X-band HV CCRS SAR image.

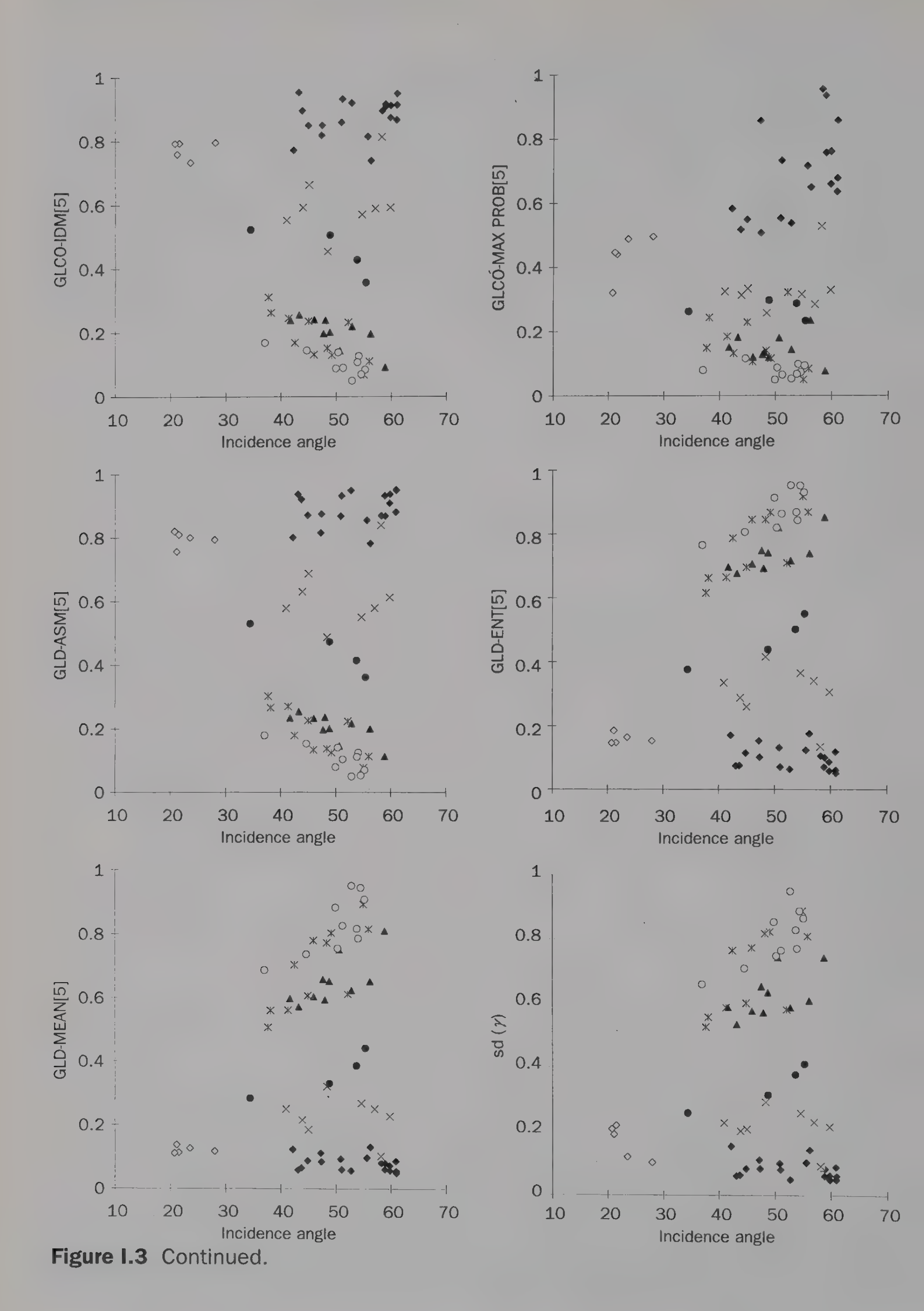



**Figure I.3** Continued.

explained by differences in the relative importance of the geometrical effects. In the imaging of rough canopies, these effects play a major role, whereas in the imaging of smooth canopies, these effects are almost absent. The implication of the incidence angle effect for the analysis of texture is twofold. On the one hand, it complicates the analysis of images that cover a wide incidence angle range. In certain cases, however, one may be able to take advantage of the incidence angle effect. For example, Figure I.2b shows that *the textural differences between the cover types studied are largest at large angles of incidence.* Therefore, by selecting images acquired at large incidence angles, one can facilitate the discrimination of these cover types. It also follows that the small incidence angle of the ERS-1 SAR system is not beneficial for the textural information content of its images.

In Figure I.2 a representation was chosen that shows the GLCO-CONT[5] data points derived from the X-band VH and HV data. Plots of data points associated with C-band or other polarizations and textural attributes (including sd($\gamma$)) would have allowed similar observations. Figure I.3 holds additional plots of textural attributes versus incidence angle for X-band HV. These plots illustrate that GLCO-CONT[5] is among the attributes most sensitive to incidence angle. This can be explained by the fact that this attribute measures the sharp grey level transitions resulting from "layover", "foreshortening" and "shadowing" (see section 5.1.1). The GLCO-COR[1] attribute appears to be the least sensitive to incidence angle effects.

## I.2 Texture as a function of the number of grey levels

The relationship between the number of grey levels (image scaling) and the textural information content is assumed to be reflected in the discriminating capacity of the GLCO attributes studied. Figure I.4 shows the results of a scaling experiment with the X-band HH CCRS SAR data. The value on the ordinate represents the total number of class pairs that is discriminated successfully by the statistical parameter in question, regardless of displacement length. The maximum number of class pairs that can possibly be discriminated by the GLCO attributes equals 150, since there are 15 class pairs and 10 displacement lengths. For sd($\gamma$) the maximum value is equal to 15. Similarly, Figure I.5 shows the results of a scaling experiment with the ERS-1 SLC-av data. In this particular case the maximum number of class pairs that can possibly be discriminated by the GLCO attributes equals 100 since there are only 10 class pairs. In the present study it was chosen to rescale the radar images prior to textural analysis. Alternatively, rescaling may be incorporated in the textural analysis procedure.

The backscatter input range for the scaling of the CCRS SAR and ERS-1 SLC-av image was fixed at 51 and 18 dB, respectively. Rescaling of the CCRS SAR image to 8 grey levels therefore results in backscatter steps of $51/8 \approx 6.4$ dB. In the ERS-1 SLC-av image with 8 grey levels each level represents a backscatter step of ca. 2.4 dB. Backscatter steps for images with a different number of grey levels can be calculated accordingly. The figures illustrate that a reduction in the number of grey levels does

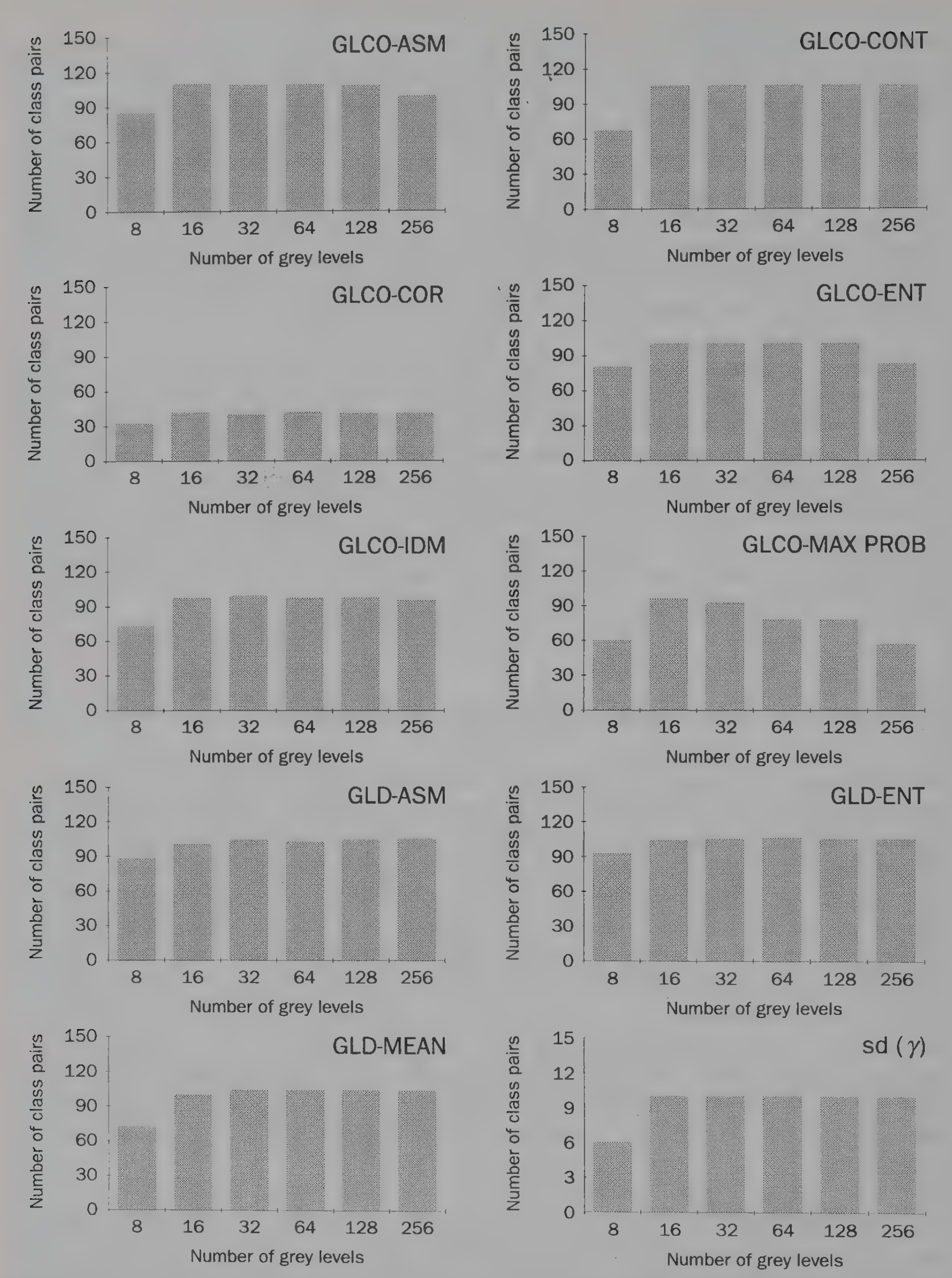



**Figure I.4** Effect of the number of grey levels in the **X-band HH CCRS SAR** image on the discriminating capacity of the textural attributes studied. Discriminating capacity is expressed in terms of the number of class pairs that can be discriminated successfully. The maximum number of class pairs that can possibly be discriminated equals 150 in the case of the GLCO attributes and 15 in the case of sd($\gamma$).

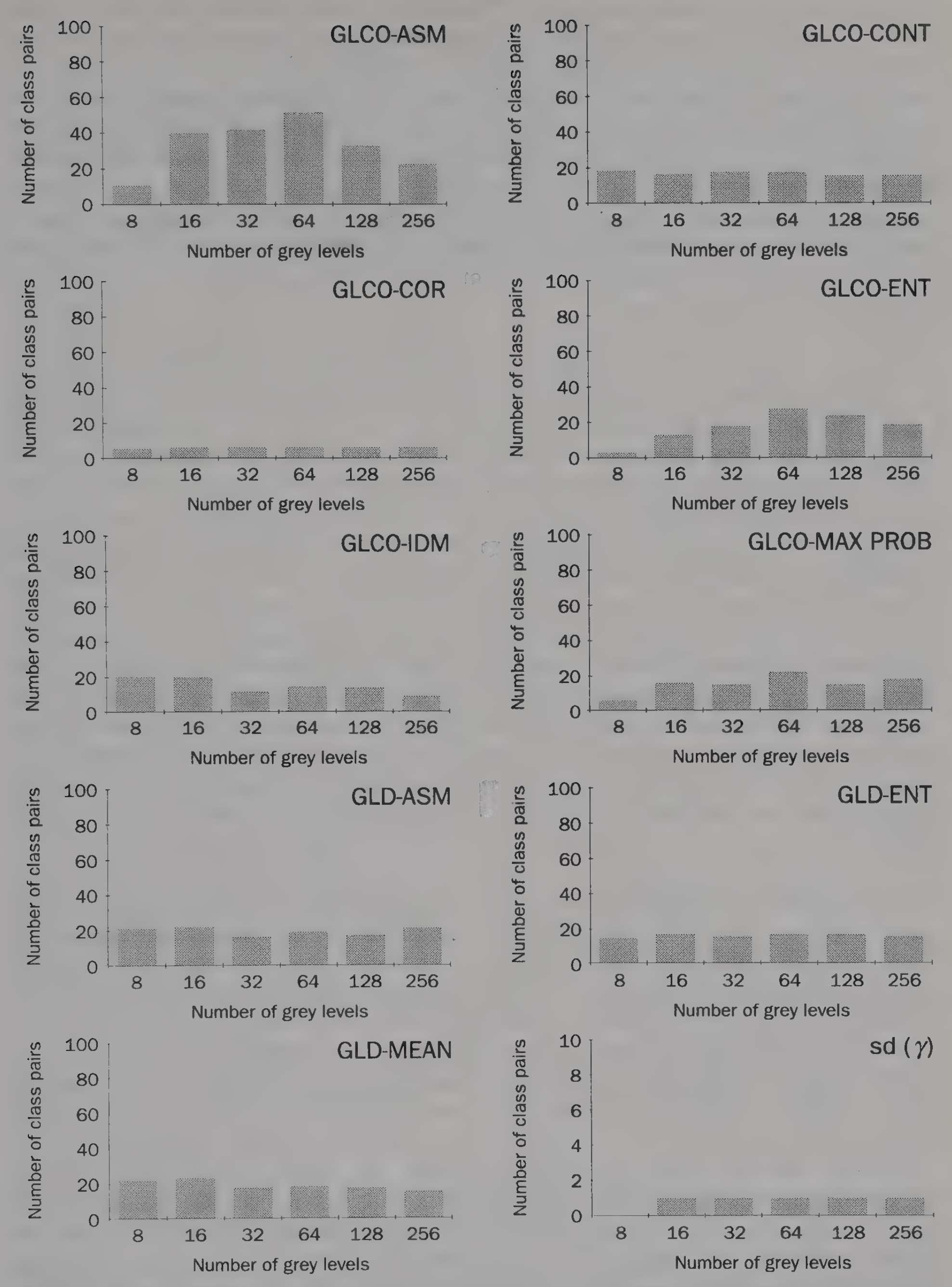



**Figure I.5** Effect of the number of grey levels in the **ERS-1 SLC-av** image on the discriminating capacity of the textural attributes studied. Discriminating capacity is expressed in terms of the number of class pairs that can be discriminated successfully. The maximum number of class pairs that can possibly be discriminated equals 100 in the case of the GLCO attributes and 10 in the case of sd($\gamma$).

not necessarily diminish the discriminating capacity of the GLCO attributes. In other words, rescaling of data to a lower number of grey levels does not automatically result in a loss of textural information. This is of importance in view of the operational use of methods for textural analysis, in particular for those that make use of a moving spatial window. A low number of grey levels reduces the computational load considerably, so textural analysis becomes more economical. It is the author's experience that textural processing by means of a moving window of images as acquired by the CCRS SAR can easily take three days on a SUN workstation (specifications system: SUN IPX, 32 Mbyte RAM; specifications scene/processing: size $2048 \times 10000$, 128 grey levels, window $11 \times 11$, attribute GLCO-CONT[5], displacement in range direction).

The results in Figure I.4 indicate that the X-band HH CCRS SAR data *could have been rescaled to 16 rather than 128 grey levels* (128 is standard in the present study; see section 5.2.2) *without noticeable loss of textural information.* In this case each grey level would have represented a backscatter step of ca. 3.2 dB, which is equal to about 1/6 of the backscatter range of the individual forest pixels. Further rescaling from 16 to 8 grey levels makes textural attributes lose the ability to discriminate between forest types with more comparable canopy architectures, e.g. Low swamp/Xeric mixed, Low swamp/Wallaba and Wallaba/Xeric mixed. This can be explained by the fact that after rescaling to 8 grey levels, image regions representing these forest types no longer comprise backscatter differences and hence become textureless. Following rescaling to 8 grey levels, only image regions that contain backscatter differences in excess of 6.4 dB will remain to show texture. In general, such large differences in backscatter result from radar "layover", "foreshortening" and/or "shadowing" effects. Hence, such backscatter differences are concentrated in image regions representative of forest areas with rough canopy surface. Discriminating between forest types with rough and smooth canopy surfaces has thus become a matter of distinguishing between regions with and without texture.

Most attributes associated with the ERS-1 SLC-av data demonstrate a discriminating capacity that is essentially independent of the number of grey levels (see Figure I.5). This includes GLCO-COR, GLCO-CONT and GLD-MEAN, i.e. the GLCO attributes most sensitive to canopy architecture (see section 6.1.2). Exceptions are those measuring textural uniformity (GLCO-ASM, GLCO-MAX PROB) or disorder (GLCO-ENT). The performance of these attributes is hampered by both excessively high and low numbers of grey levels. This is illustrated most clearly in Figure I.5 but can also be seen in Figure I.4. The adverse effects of too high a number of grey levels can be explained by the fact that the attributes only relate to the relative frequency and not to the grey levels of pixel pairs. A large number of grey levels (a GLCO matrix with many elements) causes the differences in the relative frequencies of pixel pairs to be small. Consequently, the GLCO-ASM, GLCO-MAX PROB and GLCO-ENT values of differing textures are less discriminative. Because of the sensitivity to under- and over-scaling the application of the named attributes is more complex. In the case of the ERS-1 SLC-av data the performance is best if the number of grey levels equals 64, i.e. if each grey level represents a backscatter step of ca. 0.3 dB. Figure I.5 illustrates that of all attributes studied, GLCO-ASM is the best performing one. This is

due to the fact that its performance, unlike that of most other attributes, shows little dependence on displacement length (see section I.4, Figures I.10 and I.11).

Comparison of the Figures I.5 and I.4 shows that *the discriminating capacities of the textural attributes associated with the ERS-1 SLC-av data are considerably poorer than of those associated with the X-band HH CCRS SAR data.* There appears to be a clear discrepancy in the textural information content of the two data types. This *can be explained by differences in spatial resolution and angle of incidence.* Both these parameters are much more determining for the textural information content of an image than scaling.

## I.3 Texture as a function of displacement direction

The GLCO-matrices used in the GTA approach were standard computed with consecutive displacements in *both* azimuth *and* range direction (see section 5.2.2). An experiment was carried out to compare the efficiency of this approach to one with displacement in *either* azimuth *or* range direction. Figure I.6 illustrates the results for the X-band HH CCRS SAR data, while Figure I.7 does so for the ERS-1 SLC-av data.

In the case of the X-band HH data consecutive displacements in azimuth and range direction yield results that are as good as or better than those from displacement in azimuth or range direction only. This holds true for each of the GLCO attributes applied. One profits most from two directional displacements when using attributes that measure textural uniformity (GLCO-ASM, GLCO-MAX PROB) or disorder (GLCO-ENT). Otherwise, the benefits of this approach are negligible since equally good results may be obtained by displacement in range direction. Needless use of displacement in two directions should be avoided as it increases the computational load. Left-over computer time is better spent on the computation of additional textural attributes. Economical use of computer time is especially of importance in textural analysis by means of a moving window approach.

For GLCO-ASM, GLCO-MAX PROB and GLCO-ENT displacement in range or azimuth direction yields comparable results. Other GLCO attributes perform better when displacement is in range direction. *In range direction the grey tone patterns are most prominent and therefore most easily described by textural attributes.* This may be explained by the side-looking measurement geometry of imaging radar systems (see section 3.1.1).

The statement that grey tone patterns are most prominent in range direction assumes the spatial resolution in range direction to be higher than or equal to the spatial resolution in azimuth direction. Moreover, it assumes the pixel size in range direction to be smaller than or equal to the pixel size in azimuth direction. This holds true for the CCRS SAR X-band HH image but not for the ERS-1 SLC-av image. In the latter case, the range and azimuth size of the pixels are in the proportion of 2 to 1. Consequently, the ERS-1 SLC-av image has a relatively low textural information content in range direction and a relatively high textural information content in azimuth direction. This is reflected in Figure I.7 by the fact that displacement in azimuth

direction can result in a better discriminating capacity than displacement in range direction.

In the case of the ERS-1 SLC-av image, consecutive displacements in azimuth and range direction generally lead to poorer and not to better discriminating capacities. In this respect the results for this image differ from those for the X-band HH image (see Figure I.6). Nevertheless, both directions contain textural information. The reduced discriminating capacities most likely result from the fact that identical displacement lengths are used for both the azimuth and range direction. The optimum length for displacement in azimuth and range direction must be different because of the smaller pixel size in the former direction (see also Figures I.10 and I.11). Application of two attuned displacement lengths is expected to yield results that are at least as good as those from displacement in azimuth direction. Usage of non-optimal displacement lengths just introduces 'textural noise' and therefore has a negative impact on the results.

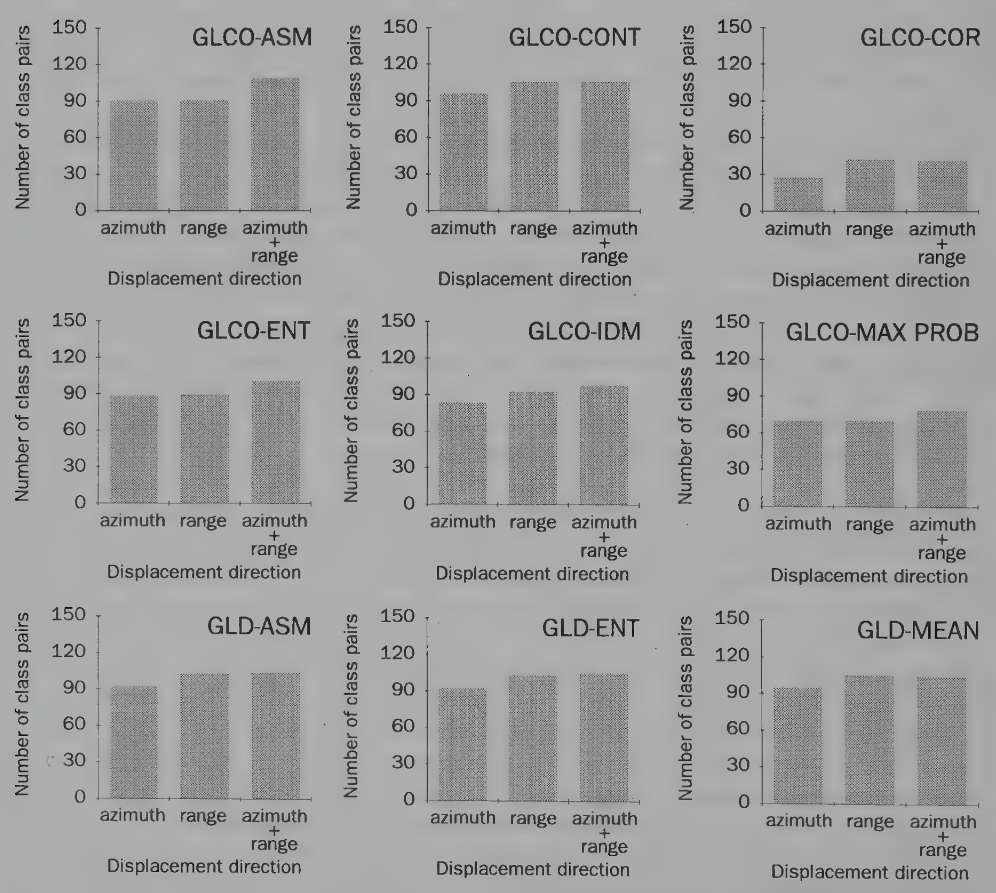



**Figure I.6** Effect of displacement direction on the discriminating capacity of GLCO textural attributes computed from the **X-band HH CCRS SAR** image. Discriminating capacity is expressed in terms of the number of class pairs that can be discriminated successfully. The maximum number of class pairs that can possibly be discriminated equals 150.

*In the case of the ERS-1 SLC-av data there is no agreement as to which displacement direction is preferred for GLCO textural analysis.* Despite the higher spatial detail, displacement in azimuth direction does not necessarily result in a better discriminating capacity. GLCO-CONT and GLCO-COR, i.e. the attributes that reflect canopy architecture best and are most closely related to radar image statistics (see section 6.1.2), yield the best results if displacement is in azimuth direction. This also holds for GLCO-ENT. Yet, GLCO-IDM, GLCO-MAX PROB and all of the GLD parameters perform best if displacement is in range direction. GLCO-ASM is an exception, it performs equally well with displacement in either direction. GLCO-MAX PROB is the only parameter that benefits from consecutive displacements in azimuth and range direction.

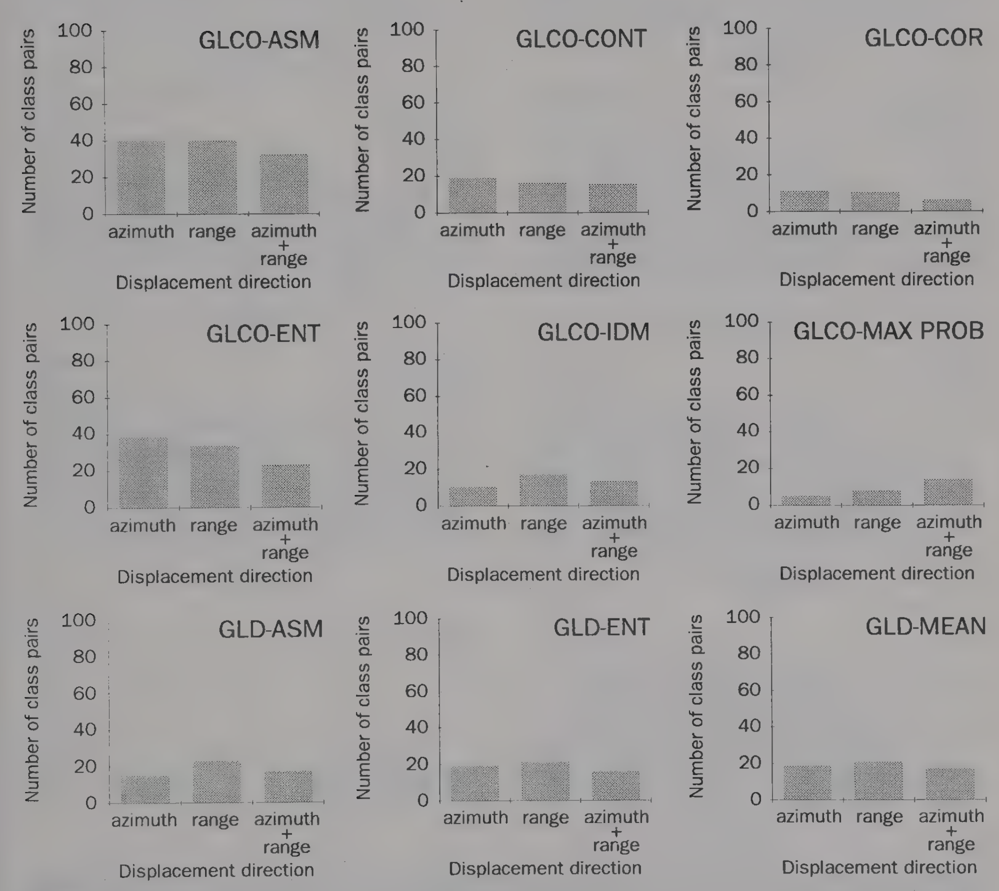



**Figure I.7** Effect of displacement direction on the discriminating capacity of GLCO textural attributes computed from the **ERS-1 SLC-av** image. Discriminating capacity is expressed in terms of the number of class pairs that can be discriminated successfully. The maximum number of class pairs that can possibly be discriminated equals 100.

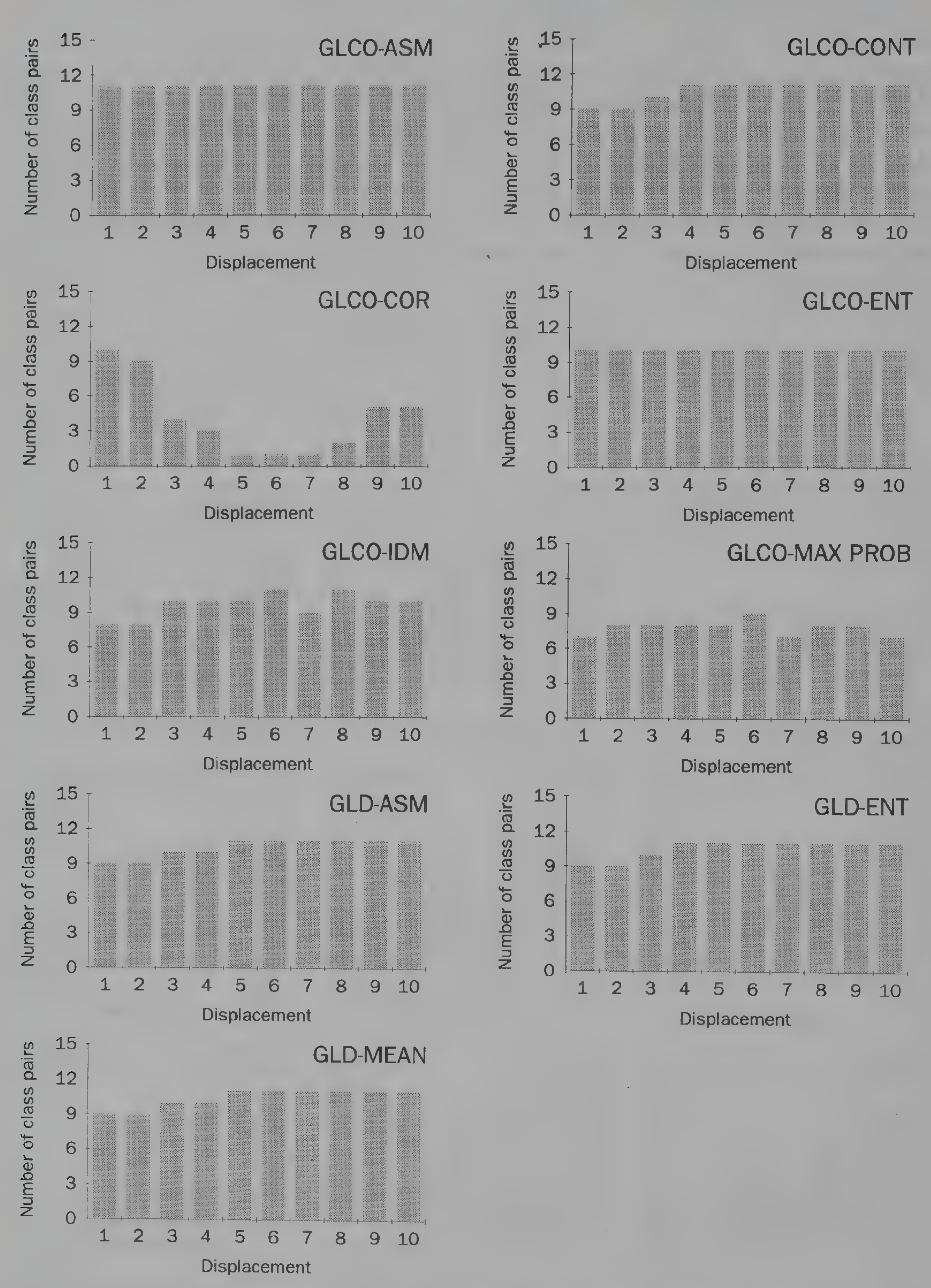



**Figure I.8** Effect of displacement length on the discriminating capacity of GLCO textural attributes computed from the **X-band HH CCRS SAR** image. Computation using *consecutive displacements in both azimuth and range direction*. Discriminating capacity is expressed in terms of the number of class pairs that can be discriminated successfully. The maximum number of class pairs that can possibly be discriminated equals 15.

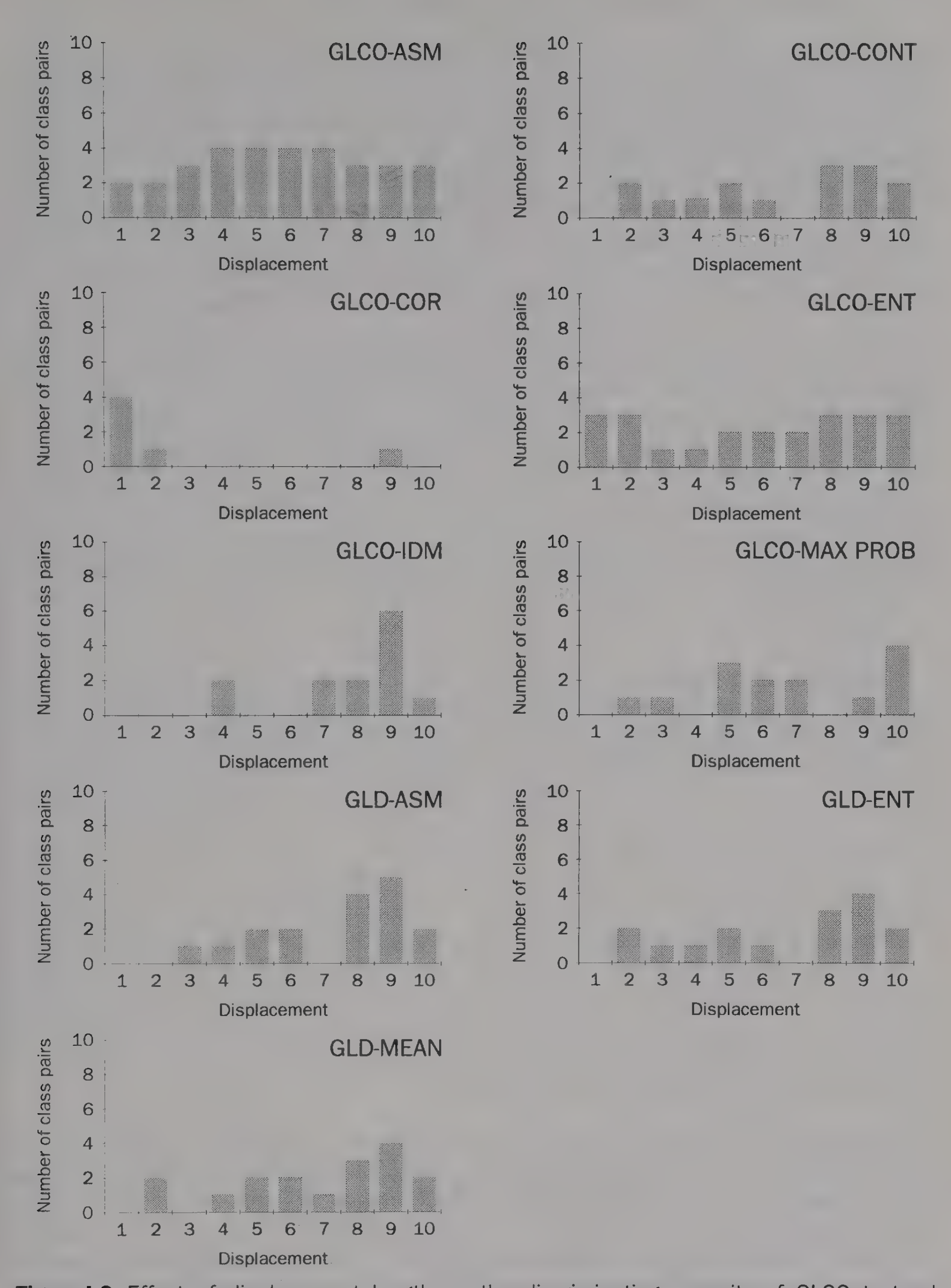



**Figure I.9** Effect of displacement length on the discriminating capacity of GLCO textural attributes computed from the **ERS-1 SLC-av** image. Computation using *consecutive displacements in both azimuth and range direction.* Discriminating capacity is expressed in terms of the number of class pairs that can be discriminated successfully. The maximum number of class pairs that can possibly be discriminated equals 10.

## I.4 Texture as a function of displacement length

The way in which textural patterns are being described by GLCO statistical parameters depends strongly on the displacement length used. A given statistical parameter can only discriminate forest types for which the displacement length adopted renders unique textural descriptions. Displacement length must be chosen in accordance with the statistical parameter used and the textural appearance of the cover types of interest. In situations like in the present study where one wants to discriminate more than two cover types, the preferred displacement length is the one yielding the best *overall* results. The preferred length of displacement is not necessarily the best choice for identifying each of the cover types involved.

The effect of displacement length on the capacity of GLCO statistical parameters to discriminate between the cover types studied is illustrated in the Figures I.8 and I.9. Figure I.8 illustrates this capacity for parameters derived from the X-band HH CCRS SAR data, while Figure I.9 does so for parameters derived from the ERS-1 SLC-av data. The results shown relate to the 'standard' GTA approach, i.e. the approach with consecutive displacements in both range and azimuth direction. In the case of the ERS-1 SLC-av data the most effective lengths for displacement in azimuth and range direction were presumed to be different (see section I.3). Therefore, Figures I.10 and I.11 show the results obtained for this data set with displacement in either azimuth or range direction.

*Of all statistical parameters shown in Figure I.8, GLCO-COR is clearly the one most sensitive to displacement length.* Its discriminating capacity is best when the displacement length equals one pixel and deteriorates rapidly when the displacement is over a length of more than two pixels. It can be shown that this is due to the fact that the variability in the GLCO-COR values for the differing classes increases strongly with an increase in displacement length. The effect of displacement length on the discriminating capacity of the other statistical parameters is much less pronounced or, like in the case of GLCO-ASM and GLCO-ENT, absent. Parameters that express grey level contrast statistics (GLCO-CONT, GLD-ASM, GLD-ENT and GLD-MEAN) perform best when the displacement length is greater than or equal to approximately five pixels. The relationship between displacement length and the discriminating capacity of GLCO-IDM and GLCO-MAX PROB is not well defined. Most statistical parameters prove to possess comparable discriminating capacities, provided that an appropriate displacement length is used. GLCO-MAX PROB is shown to be least capable of discriminating the classes studied.

The Figures I.9, I.10 and I.11 show that *the effect of displacement length on the discriminating capacity of most GLCO parameters associated with the ERS-1 SLC-av data is dramatic but poorly defined.* It should be noted that due to the discrete nature of the approach adopted to evaluate the separability of class pairs (see section 5.2.4) the shown effect of displacement length on overall discriminating capacity is probably exaggerated. In the case of Figure I.9 the poor relationship between length of displacement and discriminating capacity is at least in part due to the earlier noted difference in the size of the pixels in azimuth and range direction. However, in the case of Figure I.10 and I.11, i.e. when displacement is restricted to one direction

only, the relationships are not any clearer. It follows that the preferred displacement length for analysis of texture in ERS-1 SLC-av data is difficult to identify. The observed dramatic changes in the discriminating capacity of GLCO parameters as a function of displacement length seem to indicate that *the SLC-av data are only marginally suited for use in GLCO textural analysis.* More evidence of such can be found in the fact that the within class variability in GLCO parameters derived from the SLC-av data is often large in comparison to the between class variability in these parameters. In Figure 6.9b (section 6.2.2) this was illustrated using GLCO-CONT data for Logged-over forest and Low swamp forest.

Given a GLCO parameter, the classification potential associated with a certain displacement length depends strongly on the spatial resolution and/or pixel size of the radar data used and the canopy architecture of the cover types of interest. Consequently, *the findings discussed cannot be used as guidelines for studies that deal with different radar data sets and/or different cover types.* The presented results, however, clearly illustrate the importance (and difficulty) of selecting the 'optimum' displacement length. In analysis of texture according to the GTA approach, it is feasible to compute one or more textural parameters using a series of displacement lengths. Subsequent evaluation of the discriminating capacity of the extracted textural attributes enables the selection of the preferred length of displacement for each parameter computed. This GTA approach was illustrated in the present section. However, a similar a posteriori approach to resolve the 'optimum' length of displacement is neither practical nor economical in textural analysis by means of a moving window (MWA). This is due to the fact that MWA requires a considerable amount of computer time (see section I.2). A more *efficient approach is to carry out a GTA prior to a MWA and use the obtained results to optimise the MWA procedure.* GTA in this case can be seen as a training procedure, i.e. a procedure aimed at determining the optimum displacement length for further textural analysis and classification.

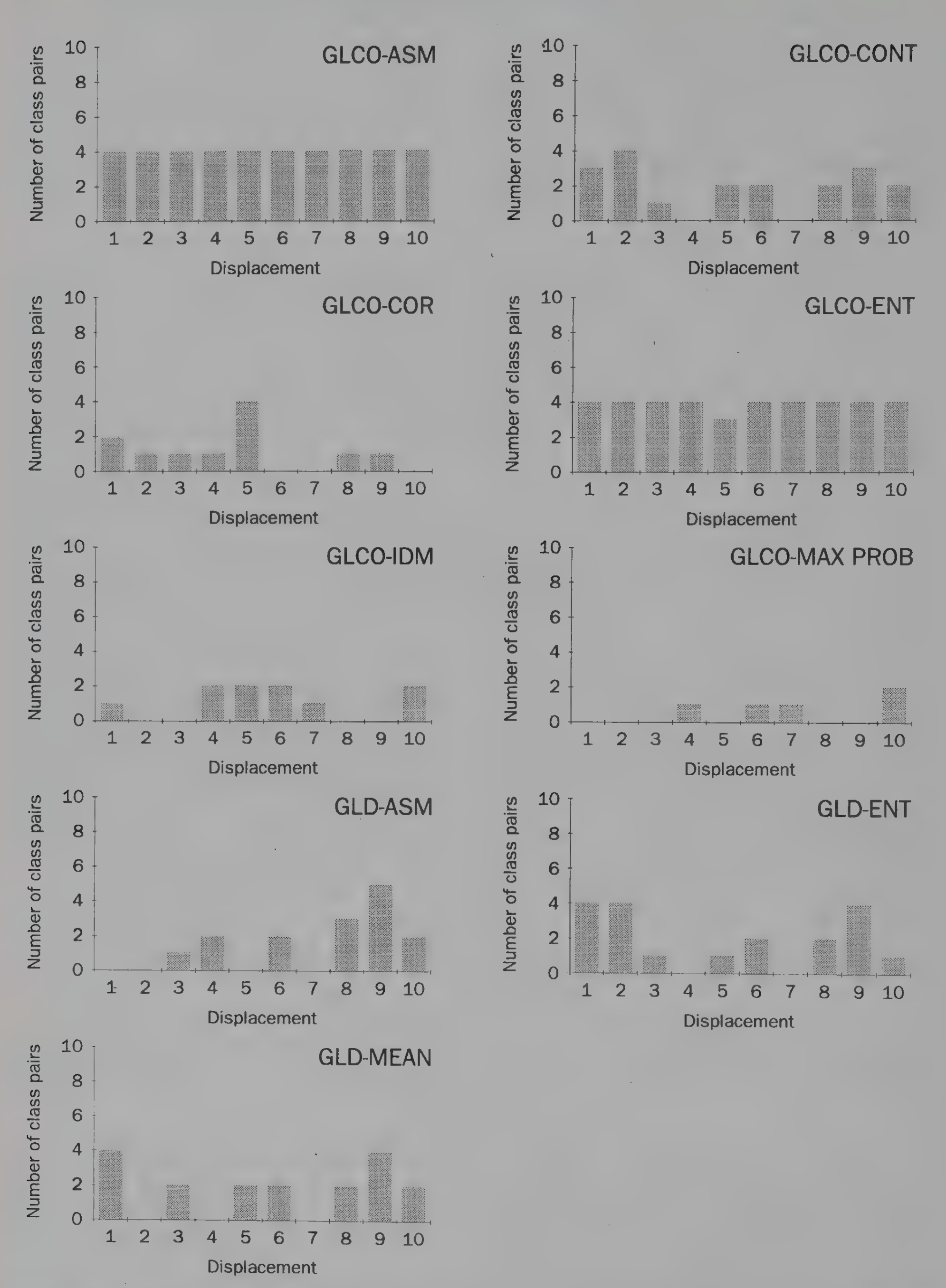



**Figure I.10** Effect of displacement length on the discriminating capacity of GLCO textural attributes computed from the **ERS-1 SLC-av** image. Computation using *displacement in azimuth direction*. Discriminating capacity is expressed in terms of the number of class pairs that can be discriminated successfully. The maximum number of class pairs that can possibly be discriminated equals 10.

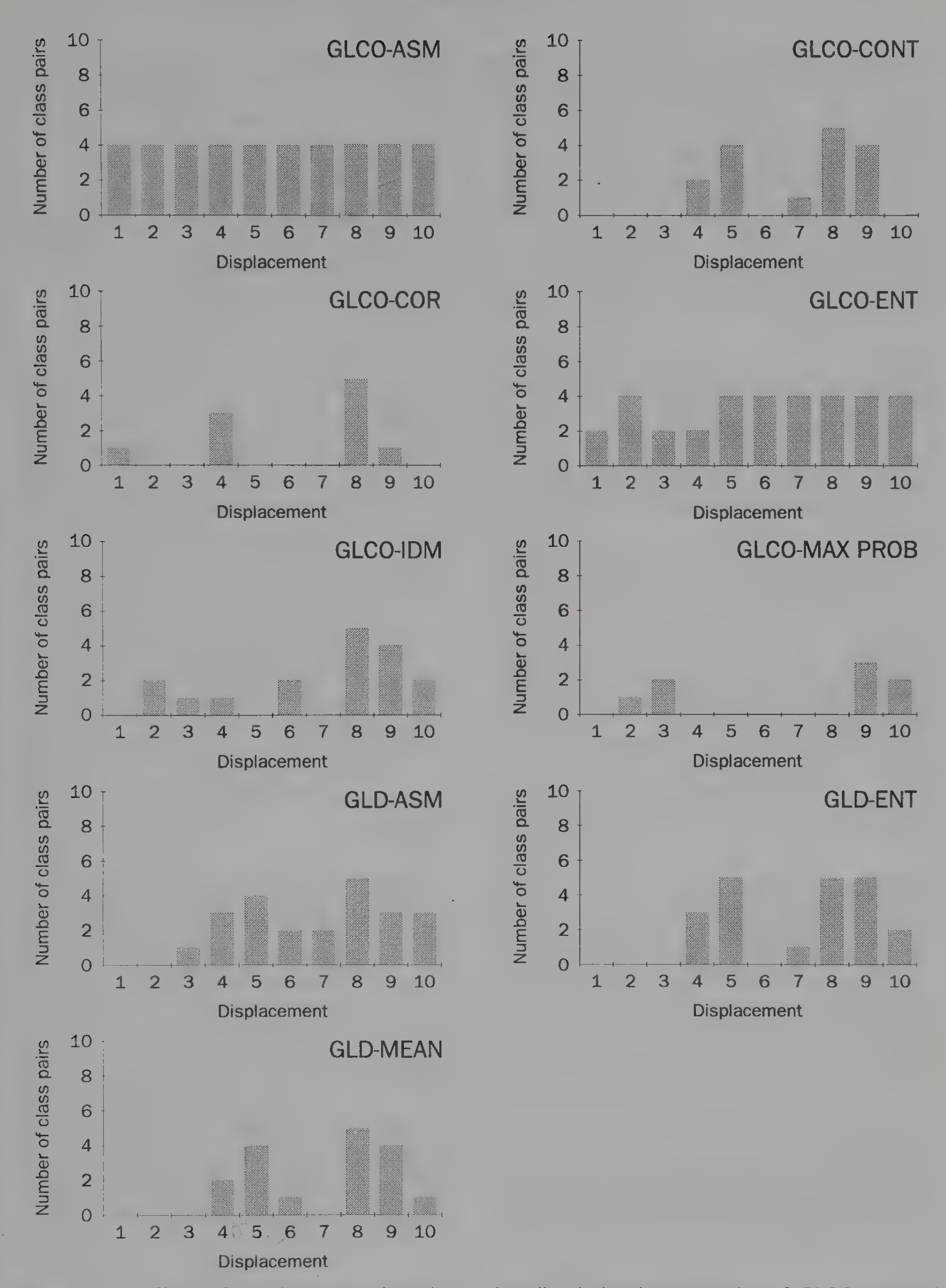



**Figure I.11** Effect of displacement length on the discriminating capacity of GLCO textural attributes computed from the **ERS-1 SLC-av** image. Computation using *displacement in range direction.* Discriminating capacity is expressed in terms of the number of class pairs that can be discriminated successfully. The maximum number of class pairs that can possibly be discriminated equals 10.

## I.5 Texture as a function of window size

For textural analysis according to the moving window approach (MWA), one needs to decide on the size of the required spatial window. *The size of this window must be attuned to the spatial resolution and the pixel size of the image used, the architecture of the forest under scrutiny and the capability of the textural attribute applied.* On the one hand, the window should be large enough to enable the textural attribute to describe the essence of the grey level patterns present in an accurate and unique manner. Yet, on the other hand, the window should be small enough to avoid that the window consistently encloses image areas corresponding to differing textures (and hence differing cover types).

In the present study the effect of window size on the capacity of textural attributes to identify textural patterns was evaluated with the help of the X-band HH CCRS SAR data. To this end, a single window of a size varying from $3 \times 3$ to $63 \times 63$ pixels was located within the boundaries of each of the earlier defined regions of interest (see section 5.1.3). Next, the texture within these windows was computed according to the GTA approach and the discriminating capacity of the resulting attributes evaluated with the help of the pairwise transformed divergence measure (see section 5.2.4). Figure I.12 shows the results for a limited selection of GLCO attributes and for sd($\gamma$). Since a displacement length of one pixel was found to be most discriminative in connection with the GLCO-COR statistical parameter it was chosen to present the results for GLCO-COR[1] (see section I.4). For similar reasons, the results shown for the other GLCO parameters correspond to a displacement length of five pixels. GLCO-COR[1] and sd($\gamma$) were computed for the full range of window sizes. GLCO attributes with displacements of five pixels were only computed for windows with sizes larger than or equal to $7 \times 7$ pixels. The results of the 'standard' GTA approach in which texture is computed for the image regions at large are also presented.

*An increase in window size is shown to result in improved discriminating capacities for all textural attributes concerned.* The results of analysis by means of spatial windows only match those of analysis by means of image regions if the window size equals $63 \times 63$ pixels and provided that GLCO-COR[1], GLCO-ENT[5] or GLCO-MAX PROB[5] is used. The effect of window size on the discriminating capacity of *GLCO-CONT[5] and sd($\gamma$)* is relatively small. These two attributes *perform considerably better than the others in case of small window sizes.* If computed using a window $7 \times 7$ pixels in size both GLCO-CONT[5] and sd($\gamma$) can discriminate 6 out of 15 class pairs. This is over 50% of the number of class pairs these attributes can discriminate if computed by means of image regions. GLCO-COR[1] is shown to have difficulty in identifying textural patterns if small spatial windows are used. It requires an image window of at least $15 \times 15$ pixels to discriminate any of the textures of the classes studied.

Larger spatial windows generally improve the discriminating capacities of GLCO attributes. This can be explained by the fact that larger windows comprise more pixel pair realisations (grey level co-occurrences) and hence yield more accurate

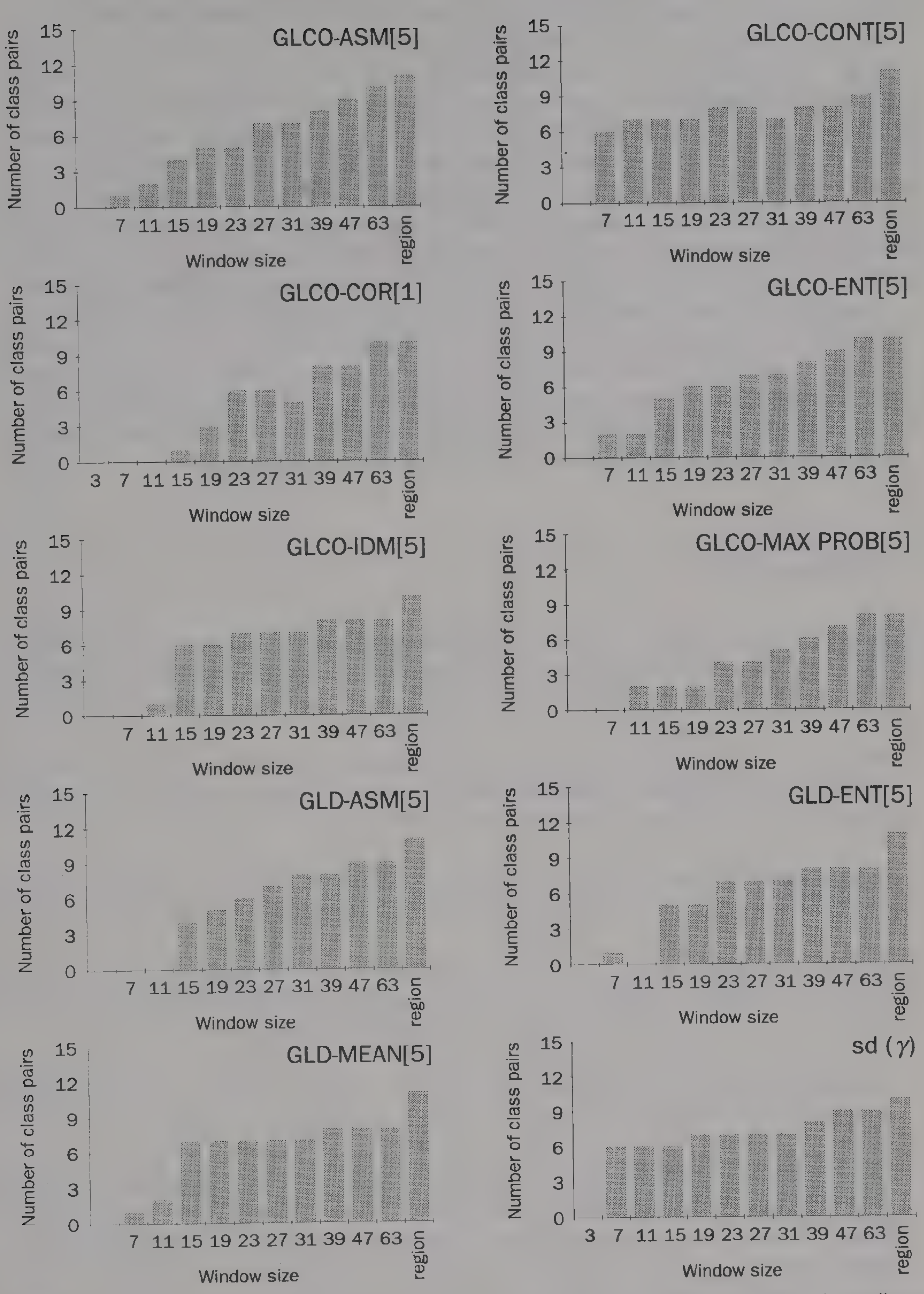



**Figure I.12** Effect of window size on the discriminating capacity of textural attributes computed from the **X-band HH CCRS SAR** image. Discriminating capacity is expressed in terms of the number of class pairs that can be discriminated successfully. The maximum number of class pairs that can possibly be discriminated equals 15.

representations of textural patterns. Results in section 6.1.3 of the present text suggest that the *differences in the performance of the textural attributes as a function of window size primarily result from the fact that some attributes are more sensitive to the presence of 'textural noise' than others.* Textural noise originates from local variations in canopy architecture, e.g. the presence of openings in a predominantly homogeneous and closed canopy. Radar images from tropical rain forests can be expected to contain considerable textural noise because these forests are of a heterogeneous nature. The extent to which textural noise shows up in textural descriptions depends on the window size and the attribute applied. Textural descriptions computed using large spatial windows (or image regions) are less affected by textural noise because this noise will be mostly averaged out. This contributes to the noted increase in discriminating capacity of textural attributes with an increasing window size. Similarly, the effects of textural noise will be less disturbing if the applied attribute is less susceptible to noise or, in other words, is more stable. It follows that more stable attributes require less large window sizes to produce identifiable textural descriptions. According to the results shown in Figure I.12, *GLCO-CONT[5] and sd($\gamma$) are among the most stable textural attributes, whereas GLCO-COR[1] is one of the least stable textural attributes.*

## I.6 Conclusions

Evaluation of the effects of radar image properties and analysis settings on the potential of GLCO attributes and sd($\gamma$) to identify the textures of the land cover types studied leads to the following conclusions.

➤ *High resolution, X- and C-band radar data with linear like- and cross-polarizations make equally suitable bases for use in textural analysis aimed at identifying tropical land cover types including primary forest types.*

- Large angles of incidence enhance the differences in the textural appearance of tropical land cover types in high resolution, high frequency radar images.

➤ *Rescaling of radar images to a lower number of grey levels does not necessarily reduce the images' textural information content and hence is a good method to reduce the computational load associated with textural analysis.*

➤ *The range direction is the preferred direction of displacement for GLCO textural analysis of high frequency and high resolution airborne radar images.*

- Results of GLCO textural analysis of high frequency and high resolution airborne radar images do not generally improve when consecutive displacements in both range and azimuth direction rather than displacement in range direction is implemented.

➤ *The preferred direction of displacement for GLCO textural analysis of the ERS-1 SLC-av depends on the attribute used. GLCO-COR and GLCO-CONT, i.e. the attributes that reflect canopy architecture best and are most closely related to radar image statistics, perform best when displacement is in azimuth direction.*

- GLCO textural analysis of ERS-1 SLC-av images using a fixed displacement length for consecutive displacements in both range and azimuth direction yields poorer results than analysis using an identical displacement length but a single displacement in either range or azimuth direction.

- Relative to that of most other GLCO attributes, the capacity of GLCO-COR to identify the textural patterns of tropical land cover types in high frequency, high resolution airborne radar images is more strongly dependent on displacement length.

- The effect of displacement length on the discriminating capacity of most GLCO parameters associated with the ERS-1 SLC-av data is dramatic but poorly defined. Hence, the preferred length of displacement for analysis of texture in ERS-1 SLC-av data is difficult to identify.

➤ *Discriminating capacities of textural attributes computed by means of a moving spatial window increase with an increase in window size.*

- Compared to other textural attributes, GLCO-CONT[5] and sd($\gamma$) require smaller spatial windows to identify the land cover types studied. In contrast, GLCO-COR[1] requires relatively large spatial windows.

# APPENDIX II
## Alphabetical list of vernacular names used in the text

Names and authorities are according to Mennenga et al. (1988).

| Vernacular name | Scientific name | Family |
|---|---|---|
| Aromata | *Clathrotropis brachypetala* (Tul.) Kleinhoonte | Papilionaceae |
| Clump wallaba | *Dicymbe altsonii* Sandw. | Caesalpiniaceae |
| Crabwood | *Carapa guianensis* Aublet | Meliaceae |
| Greenheart | *Chlorocardium rodiei* (Schomb.) Rohwer, Richter & v.d.Werff | Lauraceae |
| Guava skin | *Eschweilera alata* A.C. Smith | Lecythidaceae |
| Itikiboro | *Pterocarpus officinalis* Jacq. | Papilionaceae |
| Ituri wallaba | *Eperua grandiflora* (Aublet) Benth. | Caesalpiniaceae |
| Kakaralli | *Lecythis* spp. | Lecythidaceae |
| Mora | *Mora excelsa* Benth. | Caesalpiniaceae |
| Morabukea | *Mora gonggrijpii* (Kleinhoonte) Sandw. | Caesalpiniaceae |
| Soft wallaba | *Eperua falcata* Aublet | Caesalpiniaceae |
| Uriridan | *Pithecellobium collinum* Sandw. | Mimosaceae |
| Wamara | *Swartzia leiocalycina* Benth. | Papilionaceae |
| – | *Micrandra elata* (Didr.) Muell. Arg. | Euphorbiaceae |

## APPENDIX III
## Data on structure of primary forest types in Mabura Hill

**Table III.1a** Summary of structural data for **Mixed forest**; number density and basal area of trees per diameter class.

| | Stems $ha^{-1}$ 1) | | Std. deviation | Basal area 2) | Std. deviation |
|---|---|---|---|---|---|
| dbh class | Palm trees | Other trees | stems $ha^{-1}$ 1) | ($m^2$ $ha^{-1}$) | basal area 2) |
| 2 - 5 | 20 | 2140 | 980 | 1.0 | 0.5 |
| 5 - 10 | 20 | 680 | 330 | 2.5 | 1.0 |
| 10 - 15 | 0 | 210 | 90 | 2.5 | 1.0 |
| 15 - 25 | 0 | 135 | 30 | 4.0 | 1.0 |
| 25 - 35 | 0 | 90 | 40 | 6.0 | 2.5 |
| 35 - 45 | 0 | 40 | 20 | 5.0 | 2.0 |
| 45 - 55 | 0 | 25 | 20 | 4.5 | 3.5 |
| 55 - 65 | 0 | 20 | 15 | 6.0 | 4.5 |
| 65 - 75 | 0 | 5 | 5 | 2.0 | 2.0 |
| ≥ 75 | 0 | 15 | 10 | 8.5 | 6.0 |
| all classes | 40 | 3360 | 1155 | 42.5 | 5.0 |

1) numbers rounded off to nearest multiple of 5.
2) numbers rounded off to nearest multiple of 0.5.

**Table III.1b** Summary of structural data for **Mixed forest**; number density of stemless palms and lianas.

| Life form | Number $ha^{-1}$ 1) | Std.deviation 1) |
|---|---|---|
| Stemless palms with height ≥ 2 m | 10 | 10 |
| Stemless palms with height ≥ 5 m | 0 | 0 |
| Lianas with ∅ < 10 cm | 100 | 140 |
| Lianas with ∅ ≥ 10 cm | 10 | 15 |

1) numbers rounded off to nearest multiple of 5.

**Table III.2a** Summary of structural data for **Mixed forest with Greenheart dominance**; number density and basal area of trees per diameter class.

| | Stems $ha^{-1}$ 1) | | Std. deviation | Basal area 2) | Std. deviation |
|---|---|---|---|---|---|
| dbh class | Palm trees | Other trees | stems $ha^{-1}$ 1) | ($m^2$ $ha^{-1}$) | basal area 2) |
| 2 - 5 | 15 | 2330 | 410 | 1.0 | 0.0 |
| 5 - 10 | 0 | 500 | 225 | 2.0 | 0.5 |
| 10 - 15 | 0 | 130 | 45 | 1.5 | 0.5 |
| 15 - 25 | 0 | 150 | 35 | 4.0 | 1.0 |
| 25 - 35 | 0 | 50 | 30 | 3.5 | 2.0 |
| 35 - 45 | 0 | 30 | 20 | 4.0 | 2.5 |
| 45 - 55 | 0 | 20 | 15 | 4.0 | 2.5 |
| 55 - 65 | 0 | 15 | 10 | 4.0 | 2.5 |
| 65 - 75 | 0 | 15 | 15 | 6.5 | 4.5 |
| ≥ 75 | 0 | 30 | 10 | 25.0 | 17.0 |
| all classes | 15 | 3280 | 325 | 55.5 | 16.5 |

1) numbers rounded off to nearest multiple of 5.
2) numbers rounded off to nearest multiple of 0.5.

**Table III.2b** Summary of structural data for **Mixed forest with Greenheart dominance**; number density of stemless palms and lianas.

| Life form | Number $ha^{-1}$ 1) | Std.deviation 1) |
|---|---|---|
| Stemless palms with height ≥ 2 m | 0 | 0 |
| Stemless palms with height ≥ 5 m | 0 | 0 |
| Lianas with ∅ < 10 cm | 85 | 155 |
| Lianas with ∅ ≥ 10 cm | 5 | 10 |

1) numbers rounded off to nearest multiple of 5.

**Table III.3a** Summary of structural data for **Wallaba forest**; number density and basal area of trees per diameter class.

| | Stems ha$^{-1}$ 1) | | Std. deviation | Basal area 2) | Std. deviation |
|---|---|---|---|---|---|
| dbh class | Palm trees | Other trees | stems ha$^{-1}$ 1) | (m$^2$ ha$^{-1}$) | basal area 2) |
| 2 - 5 | 50 | 3715 | 1865 | 2.5 | 1.0 |
| 5 - 10 | 0 | 1285 | 405 | 4.0 | 1.0 |
| 10 - 15 | 0 | 190 | 30 | 2.0 | 0.5 |
| 15 - 25 | 0 | 210 | 55 | 6.0 | 1.5 |
| 25 - 35 | 0 | 105 | 25 | 7.0 | 1.5 |
| 35 - 45 | 0 | 65 | 10 | 7.5 | 1.5 |
| 45 - 55 | 0 | 40 | 15 | 7.5 | 3.0 |
| 55 - 65 | 0 | 10 | 10 | 2.0 | 2.0 |
| 65 - 75 | 0 | 5 | 10 | 2.0 | 3.5 |
| ≥ 75 | 0 | 0 | 0 | 0.0 | 0.0 |
| all classes | 50 | 5625 | 2200 | 41.0 | 4.5 |

1) numbers rounded off to nearest multiple of 5.
2) numbers rounded off to nearest multiple of 0.5.

**Table III.3b** Summary of structural data for **Wallaba forest**; number density of stemless palms and lianas.

| Life form | Number ha$^{-1}$ 1) | Std.deviation 1) |
|---|---|---|
| Stemless palms with height ≥ 2 m | 0 | 0 |
| Stemless palms with height ≥ 5 m | 0 | 0 |
| Lianas with ∅ < 10 cm | 135 | 150 |
| Lianas with ∅ ≥ 10 cm | 15 | 10 |

1) numbers rounded off to nearest multiple of 5.

**Table III.4a** Summary of structural data for **Xeric mixed forest**; number density and basal area of trees per diameter class.

| dbh class | Stems $ha^{-1}$ 1) Palm trees | Stems $ha^{-1}$ 1) Other trees | Std. deviation stems $ha^{-1}$ 1) | Basal area 2) ($m^2$ $ha^{-1}$) | Std. deviation basal area 2) |
|---|---|---|---|---|---|
| 2 - 5 | 0 | 3050 | 495 | 2.0 | 0.5 |
| 5 - 10 | 0 | 1000 | 430 | 3.5 | 1.5 |
| 10 - 15 | 0 | 490 | 125 | 5.5 | 1.5 |
| 15 - 25 | 0 | 370 | 40 | 9.5 | 1.0 |
| 25 - 35 | 0 | 85 | 5 | 6.0 | 0.5 |
| 35 - 45 | 0 | 40 | 25 | 5.0 | 3.5 |
| 45 - 55 | 0 | 20 | 15 | 3.5 | 2.5 |
| 55 - 65 | 0 | 5 | 5 | 0.5 | 1.0 |
| 65 - 75 | 0 | 0 | 0 | 0.0 | 0.0 |
| ≥ 75 | 0 | 0 | 0 | 0.0 | 0.0 |
| all classes | 0 | 5050 | 700 | 35.0 | 2.5 |

1) numbers rounded off to nearest multiple of 5.
2) numbers rounded off to nearest multiple of 0.5.

**Table III.4b** Summary of structural data for **Xeric mixed forest**; number density of stemless palms and lianas.

| Life form | Number $ha^{-1}$ 1) | Std.deviation 1) |
|---|---|---|
| Stemless palms with height ≥ 2 m | 0 | 0 |
| Stemless palms with height ≥ 5 m | 0 | 0 |
| Lianas with ∅ < 10 cm | 75 | 150 |
| Lianas with ∅ ≥ 10 cm | 10 | 10 |

1) numbers rounded off to nearest multiple of 5.

**Table III.5a** Summary of structural data for **Mora forest**; number density and basal area of trees per diameter class.

| | Stems $ha^{-1}$ 1) | | Std. deviation | Basal area 2) | Std. deviation |
|---|---|---|---|---|---|
| dbh class | Palm trees | Other trees | stems $ha^{-1}$ 1) | ($m^2$ $ha^{-1}$) | basal area 2) |
| 2 - 5 | 0 | 2050 | 340 | 1.0 | 0.0 |
| 5 - 10 | 15 | 500 | 185 | 1.5 | 0.5 |
| 10 - 15 | 0 | 95 | 60 | 1.0 | 0.5 |
| 15 - 25 | 0 | 70 | 30 | 2.0 | 1.0 |
| 25 - 35 | 0 | 70 | 40 | 4.5 | 2.5 |
| 35 - 45 | 0 | 25 | 20 | 3.0 | 2.0 |
| 45 - 55 | 0 | 15 | 15 | 3.0 | 2.5 |
| 55 - 65 | 0 | 15 | 20 | 3.5 | 4.5 |
| 65 - 75 | 0 | 15 | 5 | 5.5 | 2.0 |
| ≥ 75 | 0 | 20 | 10 | 17.5 | 9.0 |
| all classes | 15 | 2870 | 415 | 42.5 | 4.5 |

1) numbers rounded off to nearest multiple of 5.
2) numbers rounded off to nearest multiple of 0.5.

**Table III.5b** Summary of structural data for **Mora forest**; number density of stemless palms and lianas.

| Life form | Number $ha^{-1}$ 1) | Std.deviation 1) |
|---|---|---|
| Stemless palms with height ≥ 2 m | 50 | 80 |
| Stemless palms with height ≥ 5 m | 0 | 0 |
| Lianas with ∅ < 10 cm | 35 | 80 |
| Lianas with ∅ ≥ 10 cm | 5 | 5 |

1) numbers rounded off to nearest multiple of 5.

# APPENDIX IV
## Classification potential of backscatter measurements in two frequencies and/or polarizations

**Table IV.1** Potential of the $\overline{\gamma}$ values for dual frequency and/or polarization combinations for the classification per region of **primary forest types**. The values given represent the number of class pairs that can be successfully discriminated, i.e. the number of class pairs out of a **total of 10** for which $TD_{ij} \geq 1900$.

| | Combination | | | | | | | | | | | | | | | | | | | |
|---|---|---|---|---|---|---|---|---|---|---|---|---|---|---|---|---|---|---|---|---|
| | C HH | C VH | C VV | C RR | C RL | C LL | C TP | L HH | L VH | L VV | L RR | L RL | L LL | L TP | P HH | P VH | P VV | P RR | P RL | P LL |
| C VH | 2 | | | | | | | | | | | | | | | | | | | |
| C VV | 0 | 3 | | | | | | | | | | | | | | | | | | |
| C RR | 1 | 2 | 4 | | | | | | | | | | | | | | | | | |
| C RL | 0 | 4 | 0 | 1 | | | | | | | | | | | | | | | | |
| C LL | 2 | 2 | 2 | 2 | 3 | | | | | | | | | | | | | | | |
| C TP | 0 | 4 | 0 | 1 | 4 | 2 | | | | | | | | | | | | | | |
| L HH | 0 | 1 | 0 | 1 | 0 | 2 | 0 | | | | | | | | | | | | | |
| L VH | 0 | 1 | 0 | 1 | 0 | 2 | 0 | 0 | | | | | | | | | | | | |
| L VV | 4 | 4 | 4 | 4 | 4 | 4 | 4 | 4 | 3 | | | | | | | | | | | |
| L RR | 1 | 3 | 2 | 2 | 1 | 3 | 2 | 4 | 1 | 4 | | | | | | | | | | |
| L RL | 0 | 2 | 0 | 1 | 0 | 2 | 0 | 0 | 0 | 4 | 4 | | | | | | | | | |
| L LL | 0 | 2 | 0 | 1 | 0 | 2 | 0 | 4 | 2 | 4 | 1 | 0 | | | | | | | | |
| L TP | 0 | 2 | 0 | 1 | 1 | 2 | 0 | 4 | 1 | 4 | 4 | 1 | 0 | | | | | | | |
| P HH | 1 | 4 | 3 | 4 | 1 | **5** | 3 | 0 | 2 | 3 | 1 | 1 | 0 | 1 | | | | | | |
| P VH | 0 | 2 | 0 | 2 | 0 | 2 | 0 | 0 | 0 | 3 | 0 | 0 | 0 | 0 | 0 | | | | | |
| P VV | 0 | 3 | 3 | 3 | 0 | 3 | 0 | 0 | 0 | 3 | 0 | 0 | 0 | 0 | 0 | 1 | | | | |
| P RR | 0 | 3 | 2 | 3 | 0 | **6** | 0 | 0 | 0 | 3 | 1 | 0 | 0 | 0 | 0 | 1 | 0 | | | |
| P RL | 0 | 4 | 3 | 4 | 1 | 4 | 3 | 0 | 2 | 4 | 2 | 1 | 1 | 1 | 0 | 3 | 0 | 0 | | |
| P LL | 0 | **6** | 2 | 4 | 0 | 4 | 0 | 0 | 0 | 3 | 0 | 0 | 0 | 0 | 0 | 1 | 0 | 0 | **5** | |
| P TP | 0 | **6** | 3 | 3 | 0 | **6** | 1 | 0 | 0 | 3 | 1 | 0 | 0 | 0 | 0 | 2 | 0 | 0 | 1 | 3 |

**Table IV.2** Potential of the $\overline{\gamma}$ values for dual frequency and/or polarization combinations for the classification per region of **Logged-over forest.** The values given represent the number of class pairs that can be successfully discriminated, i.e. the number of class pairs out of a **total of 7** for which $TD_{ij} \geq 1900$.

| | Combination | | | | | | | | | | | | | | | | | | | |
|---|---|---|---|---|---|---|---|---|---|---|---|---|---|---|---|---|---|---|---|---|
| | C HH | C VH | C VV | C RR | C RL | C LL | C TP | L HH | L VH | L VV | L RR | L RL | L LL | L TP | P HH | P VH | P VV | P RR | P RL | P LL |
| C VH | 2 | | | | | | | | | | | | | | | | | | | |
| C VV | 1 | 2 | | | | | | | | | | | | | | | | | | |
| C RR | 0 | 1 | 2 | | | | | | | | | | | | | | | | | |
| C RL | 1 | 2 | 1 | 1 | | | | | | | | | | | | | | | | |
| C LL | 1 | 1 | 2 | 0 | 2 | | | | | | | | | | | | | | | |
| C TP | 1 | 1 | 1 | 1 | 2 | 2 | | | | | | | | | | | | | | |
| L HH | 1 | 1 | 1 | 1 | 1 | 2 | 1 | | | | | | | | | | | | | |
| L VH | 3 | 2 | 2 | 3 | 2 | 3 | 2 | 3 | | | | | | | | | | | | |
| L VV | 2 | 2 | 2 | 2 | 2 | 2 | 2 | 2 | 2 | | | | | | | | | | | |
| L RR | 2 | 2 | 2 | 2 | 2 | 2 | 2 | 2 | 3 | 2 | | | | | | | | | | |
| L RL | 2 | 2 | 2 | 2 | 2 | 2 | 2 | 2 | 3 | 2 | 2 | | | | | | | | | |
| L LL | 2 | 2 | 2 | 2 | 2 | 2 | 2 | 2 | 3 | 2 | 2 | 2 | | | | | | | | |
| L TP | 2 | 2 | 2 | 2 | 2 | 2 | 2 | 2 | 3 | 2 | 2 | 2 | 2 | | | | | | | |
| P HH | 5 | 5 | 5 | 5 | 5 | 5 | 5 | 4 | 5 | 5 | 4 | **6** | 4 | 5 | | | | | | |
| P VH | 2 | 3 | 2 | 3 | 2 | 3 | 2 | 2 | 3 | 3 | 3 | 2 | 3 | 3 | **6** | | | | | |
| P VV | 4 | 3 | 3 | 3 | 3 | 3 | 3 | 3 | 2 | 2 | 2 | 5 | 3 | 3 | **6** | 2 | | | | |
| P RR | 4 | 5 | 3 | 4 | 3 | 5 | 4 | 4 | 3 | 3 | 3 | 3 | 3 | 3 | **6** | **6** | 4 | | | |
| P RL | 3 | 4 | 3 | 3 | 3 | 4 | 3 | 3 | 3 | 3 | 3 | 4 | 3 | 3 | **6** | 4 | 4 | 4 | | |
| P LL | 4 | 4 | 4 | 5 | 5 | 4 | 5 | 4 | 3 | 3 | 3 | 4 | 3 | 4 | 5 | **6** | 5 | 3 | 5 | |
| P TP | 4 | 4 | 3 | 4 | 3 | 4 | 4 | 4 | 3 | 3 | 3 | 4 | 3 | 3 | **6** | 4 | 5 | 4 | 5 | 5 |

**Table IV.3** Potential of the $\overline{\gamma}$ values for dual frequency and/or polarization combinations for the classification per region of **Secondary forest.** The values given represent the number of class pairs that can be successfully discriminated, i.e. the number of class pairs out of a **total of 7** for which $TD_{ij} \geq 1900$.

| | Combination | | | | | | | | | | | | | | | | | | | |
|---|---|---|---|---|---|---|---|---|---|---|---|---|---|---|---|---|---|---|---|---|
| | C HH | C VH | C VV | C RR | C RL | C LL | C TP | L HH | L VH | L VV | L RR | L RL | L LL | L TP | P HH | P VH | P VV | P RR | P RL | P LL |
| C VH | 1 | | | | | | | | | | | | | | | | | | | |
| C VV | 0 | 1 | | | | | | | | | | | | | | | | | | |
| C RR | 0 | 1 | 1 | | | | | | | | | | | | | | | | | |
| C RL | 0 | 1 | 1 | 0 | | | | | | | | | | | | | | | | |
| C LL | 1 | 1 | 1 | 1 | 1 | | | | | | | | | | | | | | | |
| C TP | 0 | 1 | 0 | 0 | 2 | 1 | | | | | | | | | | | | | | |
| L HH | 1 | 1 | 0 | 1 | 0 | 3 | 0 | | | | | | | | | | | | | |
| L VH | **7** | 6 | 5 | **7** | 6 | **7** | 6 | 5 | | | | | | | | | | | | |
| L VV | 5 | 4 | 4 | 4 | 4 | 4 | 4 | 4 | 5 | | | | | | | | | | | |
| L RR | 4 | 3 | 3 | 3 | 3 | 4 | 3 | 4 | 6 | 5 | | | | | | | | | | |
| L RL | 5 | 2 | 2 | 2 | 2 | 3 | 2 | 4 | 5 | 5 | 4 | | | | | | | | | |
| L LL | 4 | 3 | 3 | 3 | 3 | 4 | 3 | 4 | 6 | 4 | 3 | 4 | | | | | | | | |
| L TP | 5 | 3 | 3 | 3 | 3 | 4 | 3 | 4 | 6 | 5 | 4 | 4 | 3 | | | | | | | |
| P HH | 4 | 4 | 3 | 4 | 4 | 4 | 4 | 3 | 6 | 5 | 3 | 5 | 4 | 5 | | | | | | |
| P VH | **7** | **7** | 6 | **7** | 6 | **7** | **7** | 4 | 5 | 5 | 4 | 5 | 5 | 5 | 4 | | | | | |
| P VV | 5 | 4 | 3 | 4 | 3 | 5 | 4 | 3 | 5 | 4 | 3 | 4 | 3 | 3 | 4 | 6 | | | | |
| P RR | **7** | 5 | 4 | 5 | 4 | 5 | 5 | 4 | 5 | 4 | 3 | 3 | 3 | 3 | 4 | 5 | 3 | | | |
| P RL | 4 | 4 | 3 | 4 | 3 | 3 | 3 | 2 | 4 | 4 | 3 | 4 | 3 | 3 | 4 | 6 | 5 | 4 | | |
| P LL | **7** | 5 | 5 | **7** | 5 | 5 | **7** | 4 | 4 | 4 | 3 | 4 | 3 | 4 | 4 | 6 | 4 | 3 | 5 | |
| P TP | **7** | 5 | 4 | 5 | 4 | 5 | 5 | 4 | 4 | 4 | 3 | 4 | 3 | 3 | 4 | 5 | 4 | 3 | 4 | 5 |

**Table IV.4** Potential of the $\overline{\gamma}$ values for dual frequency and/or polarization combinations for the classification per region of **Non-forest**. The values given represent the number of class pairs that can be successfully discriminated, i.e. the number of class pairs out of a **total of 7** for which $TD_{ij} \geq 1900$.

| | Combination | | | | | | | | | | | | | | | | | | | |
|---|---|---|---|---|---|---|---|---|---|---|---|---|---|---|---|---|---|---|---|---|
| | C HH | C VH | C VV | C RR | C RL | C LL | C TP | L HH | L VH | L VV | L RR | L RL | L LL | L TP | P HH | P VH | P VV | P RR | P RL | P LL |
| C VH | 3 | | | | | | | | | | | | | | | | | | | |
| C VV | 3 | 4 | | | | | | | | | | | | | | | | | | |
| C RR | 0 | 5 | 5 | | | | | | | | | | | | | | | | | |
| C RL | 6 | 6 | 5 | 6 | | | | | | | | | | | | | | | | |
| C LL | 1 | 6 | 6 | 1 | 6 | | | | | | | | | | | | | | | |
| C TP | 3 | 1 | 4 | 6 | **7** | 6 | | | | | | | | | | | | | | |
| L HH | **7** | 6 | 6 | **7** | 6 | **7** | 6 | | | | | | | | | | | | | |
| L VH | **7** | **7** | **7** | **7** | **7** | **7** | **7** | 6 | | | | | | | | | | | | |
| L VV | 6 | 6 | 6 | 6 | 6 | 6 | 6 | 6 | **7** | | | | | | | | | | | |
| L RR | 6 | 6 | 6 | 6 | 6 | **7** | 6 | 6 | **7** | **7** | | | | | | | | | | |
| L RL | **7** | 6 | 6 | 6 | 6 | **7** | 6 | 6 | 6 | **7** | 6 | | | | | | | | | |
| L LL | 6 | 6 | 6 | 6 | 6 | **7** | 6 | 6 | **7** | 6 | 6 | 6 | | | | | | | | |
| L TP | **7** | 6 | 6 | 6 | 6 | **7** | 6 | 6 | **7** | **7** | 6 | 6 | 6 | | | | | | | |
| P HH | 6 | 6 | 6 | 6 | 6 | 6 | 6 | 6 | **7** | 6 | 6 | 6 | 6 | 6 | | | | | | |
| P VH | **7** | **7** | 6 | **7** | 6 | **7** | **7** | 6 | 6 | 6 | 6 | 6 | 6 | 6 | 6 | | | | | |
| P VV | 5 | 6 | 6 | 6 | 6 | **7** | 6 | 6 | **7** | 6 | 6 | 6 | 6 | 6 | 6 | 6 | | | | |
| P RR | **7** | **7** | 6 | **7** | 6 | **7** | **7** | 6 | **7** | 6 | 6 | 6 | 6 | 6 | 6 | 6 | 6 | | | |
| P RL | 6 | 6 | 6 | 6 | 6 | 6 | 6 | 6 | 6 | 6 | 6 | 6 | 6 | 6 | 6 | 6 | 6 | 6 | | |
| P LL | **7** | **7** | **7** | **7** | 6 | **7** | **7** | 6 | 6 | 6 | 6 | 6 | 6 | 6 | 6 | 6 | 6 | 6 | 6 | |
| P TP | **7** | **7** | 6 | **7** | 6 | **7** | **7** | 6 | 6 | 6 | 6 | 6 | 6 | 6 | 6 | 6 | 6 | 6 | 6 | 6 |

# APPENDIX V
## Coloured figures

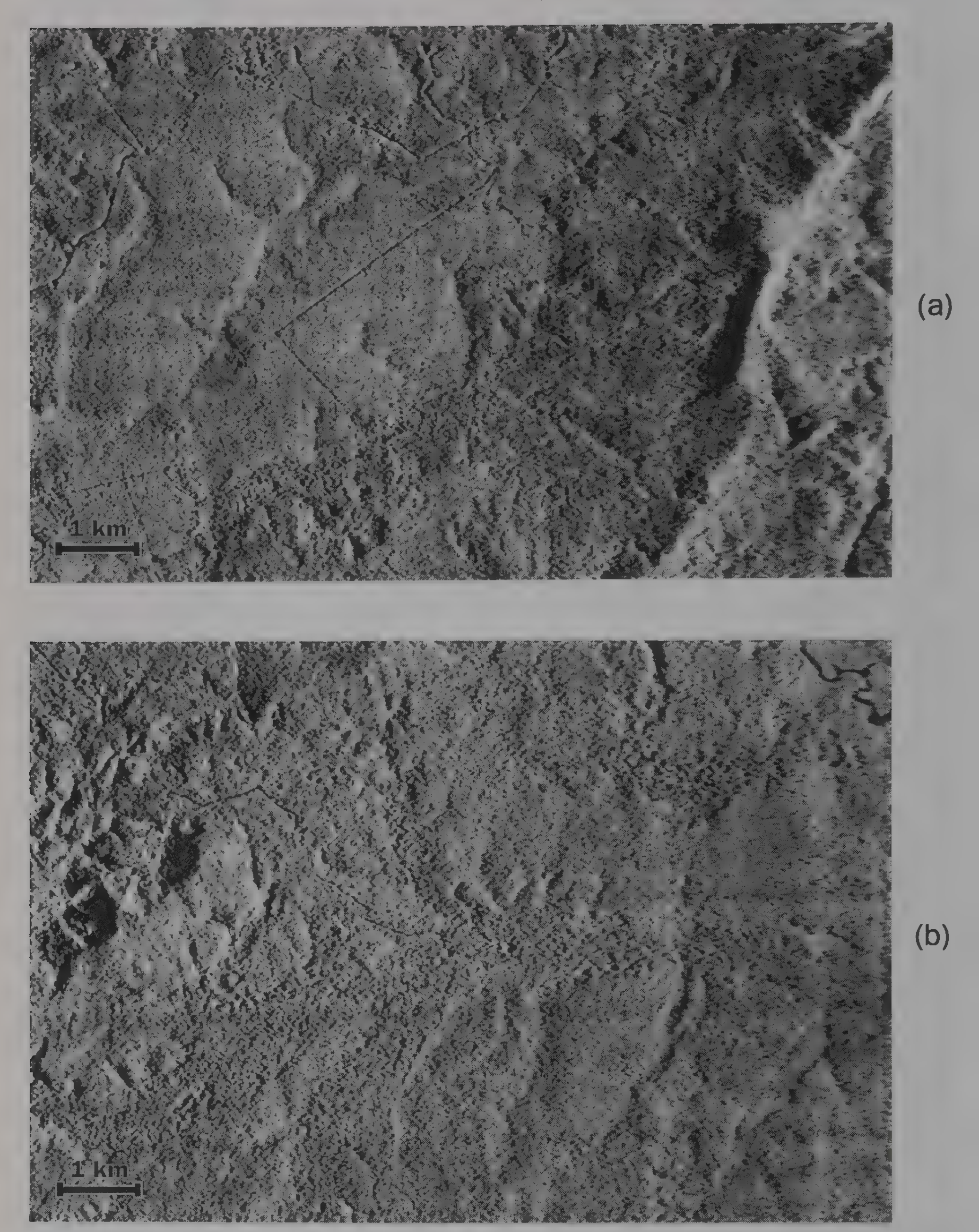



**Figure V.1 (a-b)** Subsets of the **X-band HH CCRS SAR** image: (**a**) image showing the Tropenbos ecological reserve and its surroundings (**b**) image showing the West Pibiri compartment.

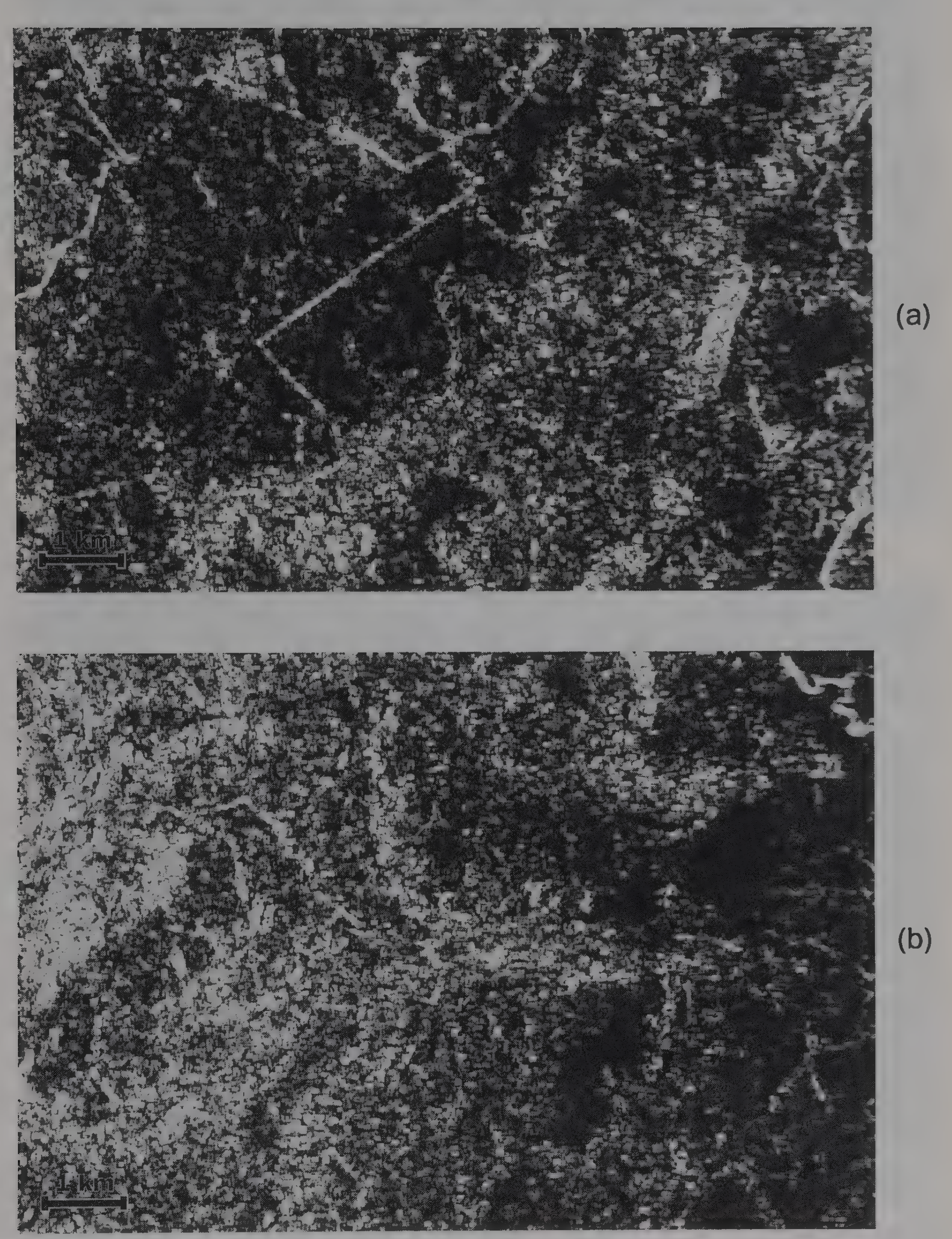



**Figure V.2 (a-b)** Texturally transformed images resulting from moving window textural analysis of images in Figure V.1 using GLCO-CONT[5] and a window of 11x11 pixels: (**a**) image showing the Tropenbos ecological reserve and its surroundings (**b**) image showing the West Pibiri compartment.

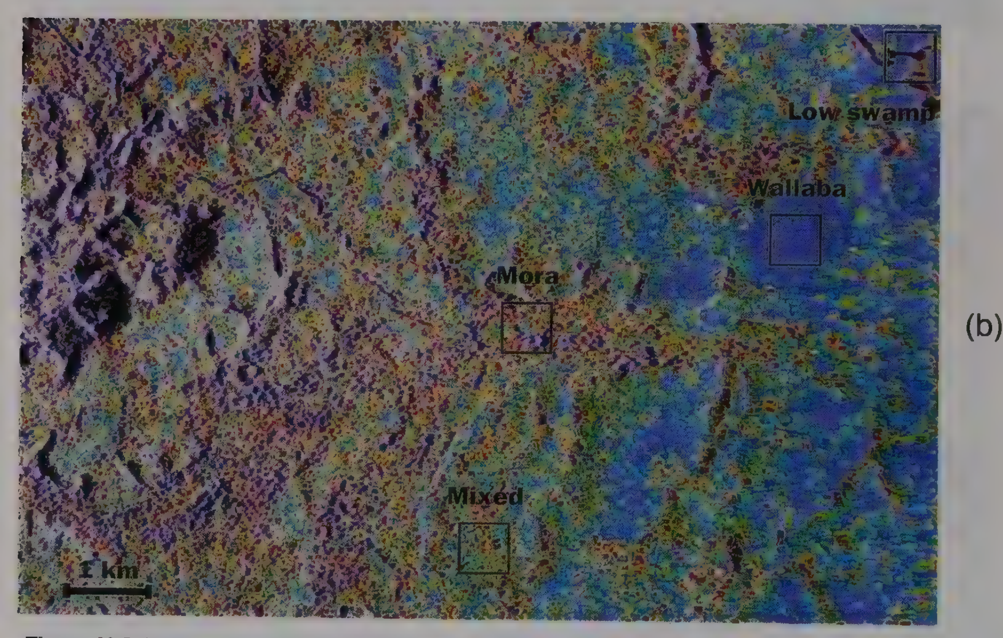



**Figure V.3 (a-b)** Texturally enhanced composite images resulting from Red-Green-Blue colour space transformation of SAR images (Figure V.1) in combination with **GLCO-CONT[5]** textural transforms (Figure V.2) and grey channels: (**a**) image showing the Tropenbos ecological reserve and its surroundings (**b**) image showing the West Pibiri compartment. The colours mirror the roughness of the forest canopy. Blue colours indicate a low degree of canopy roughness, green/yellow colours an intermediate degree of canopy roughness and red colours a high degree of canopy roughness. The areas marked by squares demonstrate the appearance of the forest types studied.




**Figure V.4 (a-b)** Subsets of the landforms and soils map for the Mabura Hill area. (**a**) subset showing the Tropenbos ecological reserve and its surroundings (**b**) subset showing the West Pibiri compartment. Mixed forests occur on landform/soil types labelled H1, H2, H3, Pe3, Pe4, Ps4, Ps5, Ps6 and Ps8. Wallaba forests dominate on Ps1, Xeric mixed forests on Pe2, Low swamp forests on A2 and Mora forests on A1. For a description of the landform/soil types please refer to original map by van Kekem et al. (1996).

(a)




**Figure V.5 (a-b)** Texturally enhanced composite images resulting from Red-Green-Blue colour space transformation of SAR images (Figure V.1) in combination with **GLCO-COR[1]** textural transforms and grey channels: (**a**) image showing the Tropenbos ecological reserve and its surroundings (**b**) image showing the West Pibiri compartment. The significance of the colours conforms to Figure V.4. The areas marked by squares demonstrate the appearance of the forest types studied.

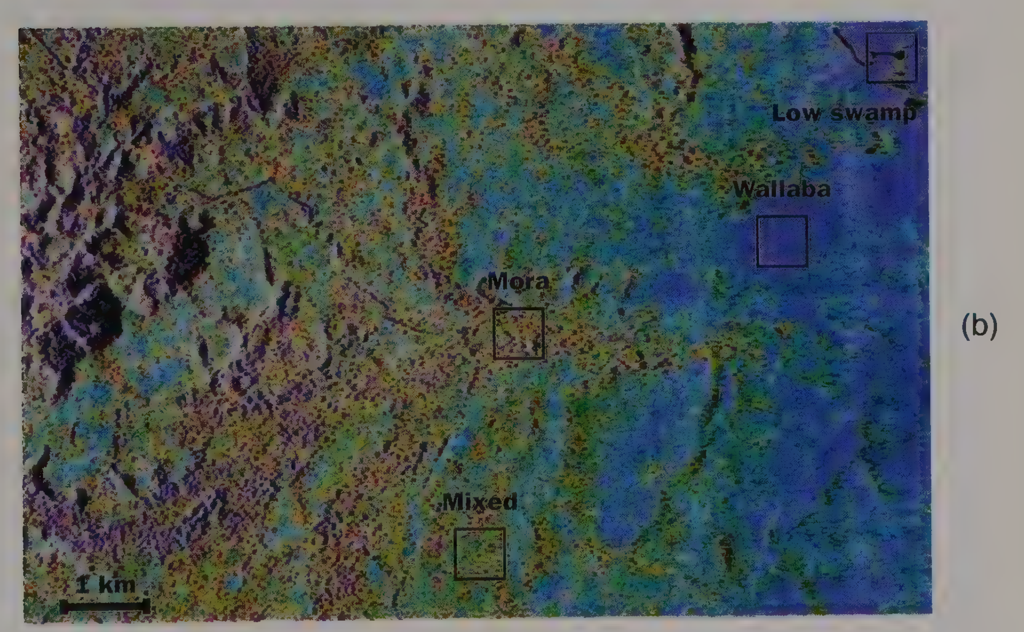



**Figure V.6 (a-b)** Texturally enhanced composite images resulting from Red-Green-Blue colour space transformation of SAR images (Figure V.1) in combination with **sd(** $\gamma$ **)** textural transforms and grey channels: (**a**) image showing the Tropenbos ecological reserve and its surroundings (**b**) image showing the West Pibiri compartment. The significance of the colours conforms to Figure V.4. The areas marked by squares demonstrate the appearance of the forest types studied.

**Figure V.7 (a-b)** Texturally enhanced composite images showing the West Pibiri compartment: (**a**) Red-Green-Blue transformed image produced from **ERS-1 PRI** image in combination with GLCO-CONT[5] textural transform and grey channel (**b**) Red-Green-Blue transformed image produced from **ERS-1 SLC-av** image in combination with GLCO-CONT[5] textural transform and grey channel. The significance of the colours conforms to Figure V.4. The areas marked by squares demonstrate the appearance of the forest types studied.

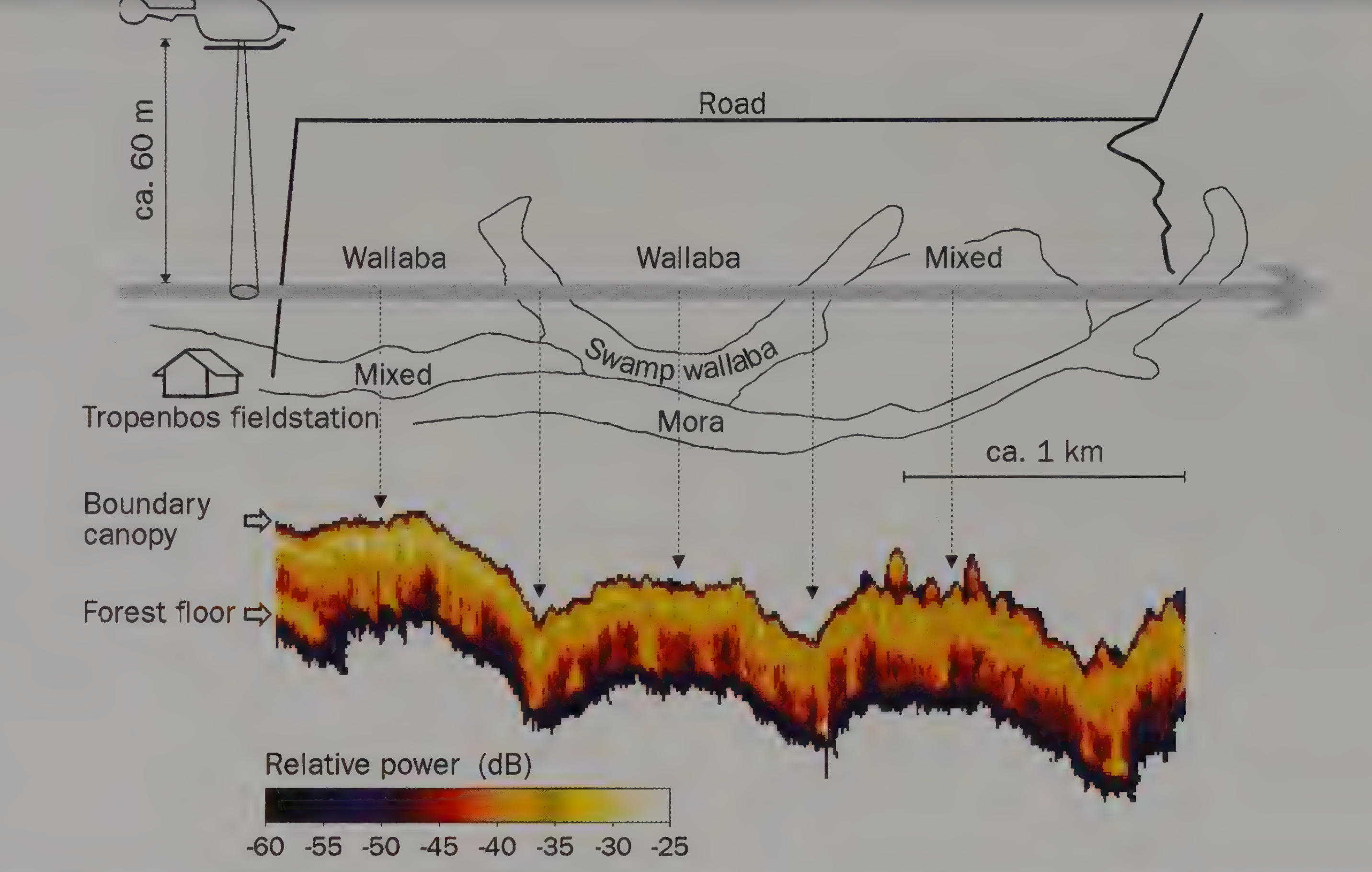



**Figure V.8** Representation of the deployment of the ERASME scatterometer over the Tropenbos ecological reserve and the resulting transect of radar measurements. The first radar return signal at a particular location along the flight path flown corresponds to the upper boundary of the forest canopy. Successive return signals from the same location result from consecutive observation layers. The radar return signals are colour coded to express their relative strength.

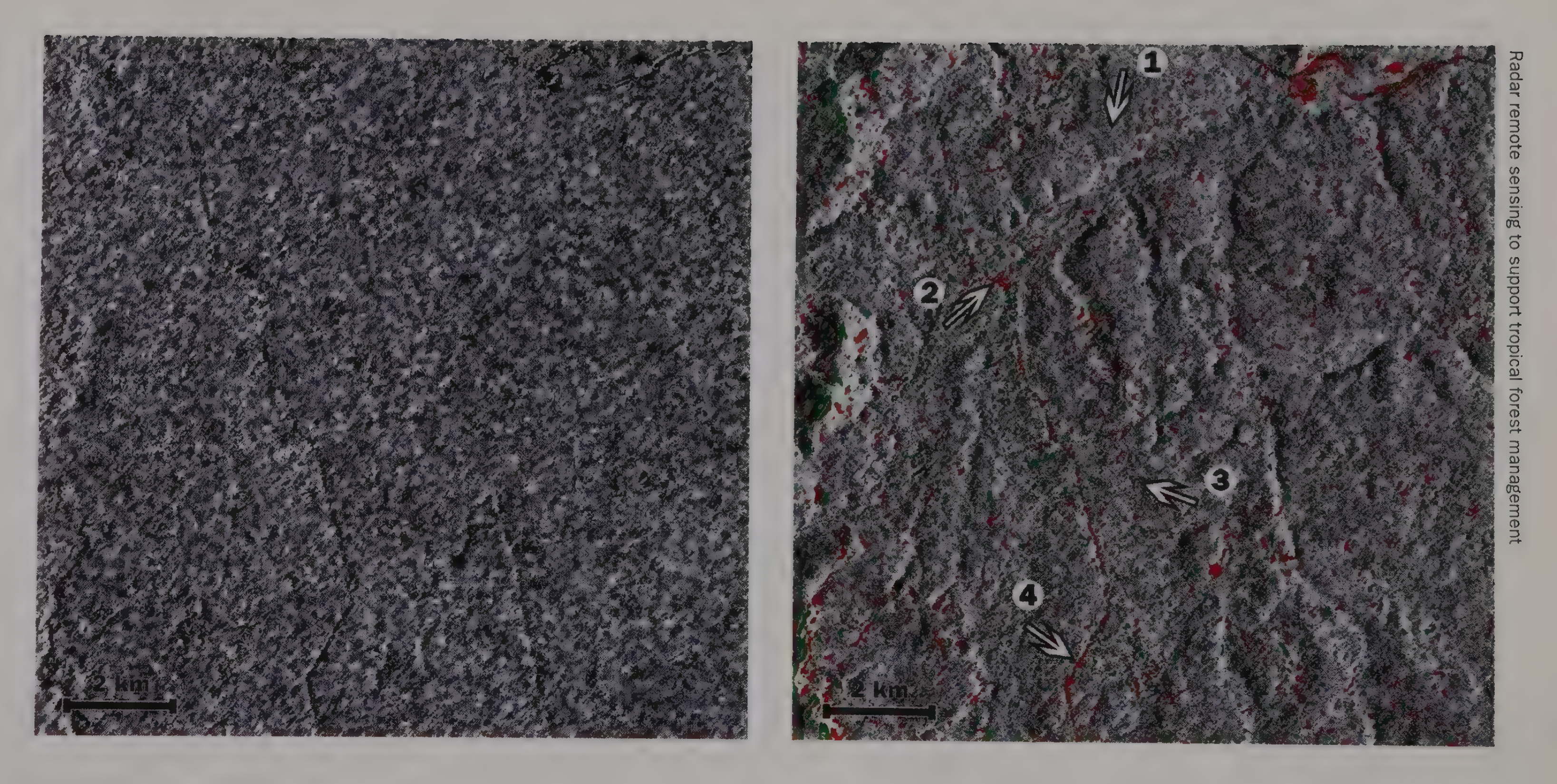



**Figure V.9 (a-b)** Processed ERS-1 SAR PRI image products showing forest cover change in **Mabura Hill**'s West Pibiri compartment: (**a**) ratio of time averaged PRI image products for 1992 and 1994 (**b**) time averaged PRI image product for 1994 with superimposed change map. The change map was generated from ratio image shown in **a**. In this map red colours indicate image regions for which the backscatter over the 1992-1994 time period decreased by > 1 dB. Similarly, green colours indicate image regions with a > 1 dB increase in backscatter. Arrow 1 marks a new road, arrow 2 and 3 log-markets and arrow 4 the widened and extended main access road.

# Samenvatting

## Radar remote sensing ter ondersteuning van tropisch bosbeheer

Het doel van de huidige studie is de potentiële mogelijkheden van radar remote sensing, ofwel aardobservatie met behulp van radar, voor toepassing in het beheer van tropisch regenwoud te bepalen. Hiertoe wordt de informatie-inhoud van verschillende typen radarbeelden beoordeeld en vergeleken met de informatiebehoeften van partijen betrokken in het tropisch bosbeheer. De studie maakt gebruik van bestaande technieken voor de analyse van radarbeelden en gaat na hoe deze technieken geoptimaliseerd kunnen worden voor de beoogde toepassing.

Radarbeelden bieden potentiële mogelijkheden ter ondersteuning van procedures voor zowel het inventariseren als het monitoren van bossen. Bosinventarisatie omvat het verzamelen, verwerken en presenteren van gegevens ten einde een beschrijving van de locatie, omvang en/of samenstelling van een zeker bosgebied *op een bepaald tijdstip* te verkrijgen. Bosmonitoring, daarentegen, is een *continu proces* dat bestaat uit het verzamelen, verwerken en presenteren van gegevens met betrekking tot de locatie, omvang, aard, oorzaak en snelheid van veranderingen. Uit gegevens, die door middel van monitoring worden verkregen kan op ieder gewenst tijdstip de toestand van het bos worden afgeleid. Tevens vormen deze gegevens een basis voor het plannen en sturen van toekomstige veranderingen. Bosinventarisatie en -monitoring zijn essentiële onderdelen van procedures voor duurzaam bosbeheer.

Mensen en organisaties, die betrokken zijn bij het beheer van tropisch bos, opereren op het mondiale, nationale en lokale ruimtelijke niveau. Afdalend van het mondiale naar het lokale niveau kunnen de volgende tendensen in de informatiebehoeften van betrokken beheerders worden waargenomen. Ten eerste: De omvang van het gebied waarvoor informatie nodig is neemt af. Ten tweede: De benodigde informatie dient in ruimtelijke zin steeds gedetailleerder te worden. Ten derde: De informatiebehoeften gaan verder uiteenlopen en worden steeds specifieker. Vanwege hun behoefte aan ruimtelijke informatie kunnen de partijen, die betrokken zijn in het beheer van tropisch bos gezien worden als potentiële gebruikers van radar remote sensing data.

Kenmerkend voor partijen, die opereren op het mondiale niveau is de behoefte aan informatie ten behoeve van bosmonitoringsprocedures. De informatiebehoeften op dit niveau zijn veelal ingegeven door belangrijke milieuvraagstukken en richten zich op parameters aangaande het bosareaal (b.v. oppervlakte bos, niet-bos en gekapt bos), boscategoriën (b.v. vegetatie type en administratieve c.q. wettelijke status) en sociaal-economische factoren (b.v. bevolkingsdichtheid en infrastructuur) (zie Tabel 2.1). Nationaal opererende partijen hebben ook behoefte aan informatie met betrekking tot bosareaal, boscategoriën en sociaal-economische factoren. Bovendien hebben deze partijen een groeiende behoefte aan informatie omtrent indicatoren van biodiversiteit (zie Tabel 2.2). Afhankelijk van hun doelstellingen kunnen lokaal opererende partijen behoefte hebben aan verscheidene parameters met betrekking tot bosareaal, boscategoriën, fysiografische terreinkenmerken, infrastructuur,

bossamenstelling, bosstruktuur en terreinklasse. Als gevolg van druk uitgeoefend door consumenten, milieu- en maatschappelijke groeperingen hebben, dan wel krijgen, zij die betrokken zijn bij industriële bosbouw behoefte aan informatie betreffende indicatoren van duurzaam beheer (zie Tabellen 2.3 en 2.4).

Toepassing van remote sensing systemen, als hulpmiddelen voor het verzamelen van informatie, biedt met name voordelen in uitgestrekte en/of moeilijk toegankelijke gebieden. Ten eerste: Deze systemen zijn in staat data te verzamelen op overzichtelijke, systematische en periodieke wijze. Ten tweede: Remote sensing data kunnen eenvoudig van een geografisch referentiekader worden voorzien. In tegenstelling tot optische sensorsystemen kunnen radarsystemen bruikbare beelden verwerven indien de toestand van de atmosfeer slecht is door aanwezigheid van vocht, wolken en/of rook. In gebieden waar tropisch regenwoud voorkomt zijn ongunstige atmosferische condities in feite overheersend. Bijgevolg zijn radarsystemen de meest geschikte remote sensing systemen voor toepassing in het beheer van tropisch regenwoud. Evengoed kunnen voorhanden zijnde optische en radar remote sensing data elkaar, wat betreft aanwezige informatie, in belangrijke mate aanvullen. Dit kan verklaard worden uit het feit dat optische en radar sensorsystemen in verschillende delen van het elektromagnetische spectrum werken. Ter illustratie van de informatie-inhoud van optische en radar remote sensing data met betrekking tot tropische bossen, geven de secties 2.2.2 en 2.2.3 van de huidige tekst een overzicht van een selectie van eerder verschenen publikaties.

Om beelden te vormen, zenden radarsystemen eerst elektromagnetische golven uit in de richting van het te registreren object. Vervolgens leggen ze de door het object in de richting van de sensor weerkaatste golven vast. Deze golven worden aangeduid als het radar-ontvangstsignaal of de radarbackscatter. De informatie-inhoud van radarbeelden voor een bepaald bosgebied hangt sterk af van de eigenschappen van het golfsignaal waarmee de radar werkt. Relevante golfparameters zijn: frequentie (of golflengte), polarisatie, invalshoek en kijkrichting. Indien de golfparameters vastgesteld zijn door een systeemontwerp en door een vluchtplan, dan zal het radar-ontvangstsignaal nog slechts als een functie van de reflectiekarakteristieken van de waargenomen objecten veranderen. Variabelen, waarvan bekend is, dat zij de radarbackscatter van de bosbodem in sterke mate beïnvloeden zijn: willekeurige oppervlakte-ruwheid, regelmatige oppervlakte-patronen en relatieve diëlektrische constante. De backscatter van het volume, zoals gevormd door de bosvegetatie, is een functie van de dikte van dit volume en de dichtheid, afmetingen, vormen, oriëntaties en relatieve diëlektrische constanten van de samenstellende deeltjes (b.v. bladeren, takken en stammen). De relatieve diëlektrische constanten van de bosbodem en de vegetatie deeltjes worden voornamelijk bepaald door de aanwezige hoeveelheid water. De principes van aardobservatie met behulp van radar en de interactie van radargolven met bos worden in detail beschreven in Hoofdstuk 3.

De bestudeerde radardata werden verworven op locaties in tropisch regenwoud nabij het dorp Mabura Hill in Guyana (5°10' N, 58°42' W) en de stad San José del Guaviare in Colombia (2°34' N, 72°38' W). Het Mabura Hill studiegebied omvat verschillende typen ongeschonden, primair bos, alsmede bossen die op industriële wijze selectief gekapt zijn. Primaire bossen welke niet door de mens zijn beschadigd,

komen in San José del Guaviare maar zelden voor. Dit studiegebied wordt daarentegen gekenmerkt door de aanwezigheid van secondaire bossen en verscheidene niet-bos vegetatietypen zoals graslanden, landbouwgewassen, verbrande gebieden en kale gronden. In 1992 werden beide studiegebieden geregistreerd met behulp van de hoge resolutie, X- en C-band synthetische apertuur (SAR) vliegtuigradar van het "Canada Centre for Remote Sensing" (CCRS). Het daarop volgend jaar werden ze vastgelegd door de polarimetrische, hoge resolutie, C-, L- en P-band vliegtuigradar van het "Jet Propulsion Laboratory" (JPL) van de "National Aeronautics and Space Administration" (NASA). De datapakketten van de twee studiegebieden omvatten bovendien tijdseries van beelden geregistreerd door de C-band SAR aan boord van de eerste Europese remote sensing satelliet ERS-1. Een verzameling van door het ERASME scatterometersysteem verticaal uitgevoerde, X-band radarmetingen complementeert de dataset voor Mabura Hill. Uitgebreide beschrijvingen van de beide studiegebieden en de beschikbare radardata zijn gegeven in Hoofdstuk 4.

Om de informatie-inhoud van de beschikbare data te bepalen, maakt de studie gebruik van drie fundamenteel verschillende bronnen van informatie in het radar-ontvangstsignaal: signaalsterkte (backscatter), polarisatie, fase en ruimtelijke variabiliteit. Parameters met betrekking tot deze informatiebronnen zijn berekend voor vooraf gedefinieerde beeldsegmenten en/of voor individuele beeldelementen oftewel pixels. De ruimtelijke variabiliteit van het radar-ontvangstsignaal wordt in de beelden waargenomen als textuur. Textuur in radarbeelden van bossen houdt verband met de ruwheid van het kronendakoppervlak, welke op haar beurt een parameter is van de kronendakarchitectuur. In de huidige studie wordt voor analyse van textuur voornamelijk gebruik gemaakt van een techniek die is gebaseerd op de grijswaarden van pixelparen. De textuurbeschrijvingen of -attributen, die deze zogenaamde GLCO techniek oplevert, vertegenwoordigen tweede orde statistieken. Overeenkomstig andere methoden en technieken, wordt de GLCO techniek uitgebreid beschreven in Hoofdstuk 5.

Hoofdstuk 6 behandelt de resultaten van onderzoek naar het vermogen van radar remote sensing om bosinventarisatie te ondersteunen. De nadruk ligt hierbij op het gebruik van radar voor classificatie van typen landbedekking, omdat dit veelal de eerste stap vormt in inventarisatieprocedures. De paragrafen hierna vatten achtereenvolgens de resultaten samen van de analyse van de CCRS SAR, ERS-1, NASA/JPL AIRSAR en ERASME data.

Analyse van beelden vastgelegd door de CCRS vliegtuigradar, toont aan dat niet backscatter, maar textuur de sleutel is tot herkenning van tropische landbedekkingstypen in hoog frequente radarbeelden met een hoge resolutie. Segmentsgewijze analyse van textuur, gevolgd door classificatie van landbedekking op het niveau van primaire bostypen, levert bescheiden tot goede resultaten op. Pixelgewijze analyse van textuur en classificatie levert minder bevredigende resultaten op. Desalniettemin vormen hoog frequente radarbeelden met hoge resolutie, die met behulp van de GLCO techniek zijn bewerkt, een goede basis voor visuele interpretatie gericht op het karteren van primaire tropische bostypen. De textuur van het in Mabura Hill aanwezige selectief gekapt bos lijkt sterk op die van een rivierbegeleidend bostype, dat bekend staat als Mora bos. In beelden van één

bepaalde opnamedatum kunnen de twee bostypen slechts onderscheiden worden met behulp van contextuele informatie. Textuurattributen maken het mogelijk bostypen te rangschikken overeenkomstig de mate van ruwheid van het kronendakoppervlak. Bovendien kunnen op basis van bepaalde textuurattributen architecturele eigenschappen van het kronendak gekwantificeerd worden. Resultaten van Oldeman (1983a), Brünig en Huang (1989) en Brünig en Mohren (1989) duiden erop dat de ruwheid van het kronendakoppervlak een indicatie vormt voor de diversiteit aan soorten.

Textuurattributen en backscatterwaarden, segmentsgewijs berekend uit ERS-1 SAR "Precision" (PRI) beelden van één bepaalde opnamedatum, vormen gelijkwaardige bronnen van informatie voor identificatie van tropische landbedekkingstypen. De twee variabelen vormen een bescheiden basis voor classificatie op het niveau van primair bos, selectief gekapt bos, secondair bos en niet-bos en een slechte basis voor classificatie op het niveau van primaire bostypen. Textuurattributen, segmentsgewijs berekend uit tijdsgemiddelde ERS-1 SAR "Single Look Complex" (SLC) beelden, vormen een bescheiden basis voor classificatie van tropische landbedekkingstypen op het niveau van primaire bostypen. Het verschil tussen de resultaten behaald met de ERS-1 PRI beelden en de tijdsgemiddelde ERS-1 SLC beelden kan verklaard worden uit de hogere ruimtelijke resolutie van de laatstgenoemde beelden. Aan texturele analyse onderworpen ERS-1 PRI en ERS-1 SLC beelden vormen geen geschikte basis voor visuele interpretatie gericht op het karteren van primaire tropische bostypen. Een groot deel van de ruwe texturen in deze beelden resulteert in feite van reliëf en niet van de architectuur van het kronendak. Ondanks verschillen in de schaal waarmee gemeten wordt, toont de ruwheid van het kronendak van de bestudeerde landbedekkingstypen zich op vergelijkbare wijze in de textuur van de ERS-1 SAR en CCRS SAR beelden.

Analyse van de NASA/JPL AIRSAR data toont dat backscattermetingen in radarbanden met lange golflengten (d.w.z. L- en P-band) een aanzienlijk betere basis vormen voor classificatie van tropische landbedekkingstypen dan backscattermetingen in radarbanden met korte golflengten (d.w.z. C-band). Vergelijking van resultaten voor de NASA/JPL AIRSAR met die voor de CCRS SAR duidt er echter op dat backscatterwaarden berekend uit L- en P-band radardata en textuurattributen berekend uit hoge resolutie X- en C-band radardata gelijkwaardige bases vormen voor segmentsgewijze classificatie op het niveau van primaire bostypen. De mogelijkheden voor classificatie van tropische landbedekkingstypen kunnen worden verbeterd door gecombineerd gebruik van backscattermetingen in verschillende frequentie banden en/of polarisaties. Metingen in een enkel L- of P-band radarkanaal zijn over het algemeen voldoende voor segmentsgewijze classificatie op het niveau van bos / niet-bos. Betrouwbare classificatie van secondair bos en selectief gekapt bos vereist metingen in tenminste twee radarkanalen. Backscattermetingen in een minimum van drie radarkanalen zijn vereist voor betrouwbare classificatie van primaire bostypen. Tenminste een van deze drie kanalen moet een P-band kanaal zijn. C-band kanalen zijn nuttig voor classificatie van primaire bostypen maar niet voor classificatie van secondair en selectief gekapt bos. De bovengrondse biomassa van de bestudeerde typen primair bos ligt boven het niveau waarbij verzadiging van de backscatter in C-, L- en P-band optreedt. Dit doet vermoeden dat de potentie van radarsystemen voor het karteren van de biomassa

van tropisch regenwoud zich beperkt tot bossen die zich in een vroeg ontwikkelingsstadium bevinden.

De data zoals geregistreerd door het ERASME scatterometersysteem bevatten informatie met betrekking tot de verticale en horizontale architectuur van het bos. Derhalve kunnen deze data van nut zijn in de analyse van de architectuur en de dynamiek van het bos en tevens bijdrage leveren aan de ontwikkeling van procedures voor bosbeheer. Het vermogen van systemen, zoals ERASME om objecten te lokaliseren die invallende radargolven reflecteren, leidt tot een beter begrip van het backscattergedrag van het bos. Het toepassen van dergelijke systemen kan als zodanig van nut zijn voor studies gericht op het modelleren van de radarbackscatter van bossen.

Hoofdstuk 7 doet verslag van onderzoek naar de mogelijkheden, die radar remote sensing biedt om het monitoren van bossen te ondersteunen. Dit onderzoek is gebaseerd op beelden geregistreerd door de eerste Europese remote sensing satelliet ERS-1. De volgende paragrafen vatten de meest belangrijke bevindingen samen.

De resultaten van analyse van de beschikbare tijdreeks ERS-1 SAR PRI beelden duiden erop dat dagelijkse en seizoensgebonden schommelingen in regenval de backscatter van bossen, welke vrij zijn van natuurlijke verstoring of menselijk invloed, met circa 1 decibel kunnen doen variëren. Kennis van dagelijkse en seizoensgebonden variaties in de backscatter van het bos maakt beter overwogen beslissingen met betrekking tot de oorzaak van waargenomen backscatter veranderingen mogelijk en ondersteunt dus het gebruik van radar in bosmonitoringsprocedures. Beelden, die zijn geregistreerd gedurende droge periodes tonen het meeste contrast tussen niet-bos en primair c.q. secondair bos en zijn daarom het geschiktst voor het karteren van (veranderingen in) de omvang en locatie van bos en niet-bos landbedekkingstypen. Beschikbaarheid van ERS-1 data, die zijn vastgelegd op meerdere tijdstippen, in plaats van data vastgelegd op één enkel tijdstip, leidt niet tot essentieel betere kansen voor het onderscheiden van primaire bostypen.

ERS-1 SAR PRI beelden vormen een goede basis voor de detectie van wegen. Dit is van groot belang met het oog op de mogelijke rol van deze beelden in bosmonitoringsprocedures, omdat wegen bijzonder markante indicatoren zijn van voorbije en/of toekomstige menselijke activiteiten met inbegrip van (selectieve) kap. Wegen markeren in feite locaties waar, tenzij gepaste actie wordt ondernomen, het voortbestaan van het bos op het spel staat. ERS-1 beelden die met behulp van beeldbewerkingstechnieken zijn verbeterd, tonen de grotere van de kroonopeningen die ontstaan door selectieve kap. Het monitoren van selectieve kap wordt echter bemoeilijkt door het feit dat kapgaten vaak sterk lijken op natuurlijke gaten. Monitoring van door kap veroorzaakte verstoring in het bos vereist een benaderingswijze, die gebruik maakt van contextuele informatie en veldkennis. Indicatoren van kap zijn het gegroepeerd en/of stelselmatig voorkomen van gaten dan wel de aanwezigheid van gaten in de nabijheid van wegen.

In Hoofdstuk 8 worden de gebruikersbehoeften en de analyse resultaten nader beschouwd en wordt ingegaan op de toepassingsmogelijkheden van radar voor en de invoering van radar in het tropische bosbeheer op het mondiale, nationale en lokale ruimtelijke niveau. Het laatste hoofdstuk van deze tekst kan als volgt worden samengevat.

Tabel 8.1 toont taxaties van het vermogen van ERS-1 en vergelijkbare satellietsystemen om hulp te bieden bij de inventarisatie c.q. het monitoren van parameters van interesse voor partijen, die betrokken zijn in het beheer van tropisch bos op het mondiale ruimtelijke niveau. Op basis van ERS-1 SAR PRI beelden wordt inventarisatie en/of monitoring van wegen, bos, niet-bos, alsmede van verbrande, ontboste en kaalgekapte gebieden 'mogelijk' geacht. Inventarisatie en/of monitoring van selectief gekapt bos, bosvegetatietype, plantage / natuurlijk bos en opstandsarchitectuur wordt als 'moeilijk' beoordeeld.

De nationale en mondiale informatiebehoeften voor het monitoren van tropisch bos zijn vrijwel identiek. De mogelijke rol van de ERS-1 SAR bij het monitoren op nationaal niveau is daarom vergelijkbaar met die op mondiaal niveau. Inventarisatie van nationale bosbezittingen vraagt vaak om gebruik van data van vliegtuig-radarsystemen. Tabel 8.2 toont taxaties van de mogelijkheden, die twee typen hoge resolutie vliegtuig-radardata voor dit doel bieden, dat wil zeggen van data zoals geregistreerd door systemen werkend met korte golflengten zoals X- en C-band en lange golflengten zoals L- en P-band. Taxaties met betrekking tot de X- en C-band data veronderstellen het gebruik van informatie in textuur, terwijl taxaties betreffende L- en P-band data het gebruik van informatie in backscatter veronderstellen. De mogelijkheden die de twee datatypen bieden voor inventarisatie van fysiografische terreinkenmerken en wegen worden als 'goed' beoordeeld. Met gebruikmaking van beide datatypen wordt inventarisatie van plantage / natuurlijk bos en van versnippering van bosareaal 'mogelijk' geacht. Hoge resolutie vliegtuig-radardata met korte dan wel lange golflengten vormen gelijkwaardige maar aanvullende bronnen van informatie voor het onderscheiden van de bestudeerde landbedekkingstypen. Vanwege de beperkte gevoeligheid van L- en P-band radarsignalen voor biomassa, wordt het schatten van houtvolume en houtige biomassa op basis van L- en P-band data als 'moeilijk' beoordeeld.

Bosbeheerders, die opereren op het lokale niveau, hebben behoefte aan ruimtelijk uiterst gedetailleerde informatie. Prognoses van de mogelijkheden, die zeer hoge resolutie X- of C-band en L- of P-band radardata bieden voor lokale bosbeheerders worden gegeven in Tabel 8.3. De mogelijkheden, die de beide datatypen bieden voor inventarisatie dan wel monitoring van terreinkenmerken, plantage / natuurlijk bos en kaalgekapte c.q. verbrande gebieden worden als 'goed' beoordeeld. X- en C-band radardata met zeer hoge resoluties worden geacht betere bases te vormen voor inventarisatie en/of monitoring van primaire bostypen en selectief gekapt bos dan zeer hoge resolutie L- en P-band data. Het inventariseren en/of monitoren van (natuurlijke) regeneratie wordt als 'moeilijk' ingeschat, omdat de beide datatypen waarschijnlijk niet het ruimtelijke detail tonen dat vereist is om te kunnen zien of de hergroeiende vegetatie al dan niet bestaat uit gewenste soorten. Voor inventarisatie en/of monitoring van parameters met betrekking tot de samenstelling en de structuur van het bos is informatie vereist op het niveau van individuele bomen.

Radarsystemen, die worden toegepast in gebieden met natuurlijk tropisch bos zullen dergelijke informatie moeilijk kunnen verschaffen. Overigens kan dit type informatie ook moeilijk verkregen worden indien gebruik wordt gemaakt van luchtfotografie. Tabel 8.4 vult Tabel 8.3 aan en toont een lijst van indicatoren van duurzaam bosbeheer die naar verwachting goed met behulp van hoge resolutie radar kunnen worden geïnventariseerd en/of gemonitord.

Bosbeheerders die besluiten om van radar remote sensing gebruik te maken, zullen verschillende wegen moeten volgen om de voor hen meest geschikte data te bemachtigen. Het geselecteerde type radardata bepaalt op zijn beurt de bewerkingen die zullen moet worden uitgevoerd om de gewenste informatie te verkrijgen. Bij het ontwikkelen van een strategie om geschikte data te verkrijgen is het belangrijk dat men nadenkt over: het ruimtelijke niveau, het benodigde type informatie, het vereiste opnametijdstip en de noodzakelijke opnamefrequentie. Op basis van deze variabelen zal een keuze gemaakt moeten worden voor data van één of meerde radarsystemen. Het aantal beschikbare vliegtuig-radarsystemen is aanmerkelijk groter dan het aantal beschikbare satelliet-radarsystemen. Bovendien bieden vliegtuigsystemen veel meer technische mogelijkheden dan satellietsystemen. De satelliet-radarsystemen, die op dit moment beschikbaar zijn, werden niet ontwikkeld voor toepassing in het tropisch bosbeheer en bieden daarom slechts bescheiden mogelijkheden voor dit doel. Bosbeheerders, die de mogelijkheid hebben vliegtuigdata te gebruiken, hebben in het algemeen een betere kans om hun informatiebehoeften met behulp van radar remote sensing te vervullen dan bosbeheerders, die afhankelijk zijn van satellietdata.

Om de compatibiliteit van informatie, zoals verkregen voor verschillende bosgebieden en/of opnametijdstippen, te kunnen verzekeren is het nodig methoden voor analyse van radardata te standaardiseren. Strategieën voor de analyse van de bestudeerde typen radarbeelden worden besproken in sectie 8.2.2. De te volgen analyse strategie wordt bepaald door de belangrijkste bron van informatie in het radar-ontvangstsignaal. Daarom ligt bij de analyse van ERS-1 satelliet data en van vliegtuigradar data met lange golflengten de nadruk op backscatter. Daarentegen ligt bij de analyse van data geregistreerd door hoge resolutie vliegtuig-radarsystemen met korte golflengten de nadruk op textuur.

De resultaten van de studie tonen aan dat radarsystemen het beheer van tropisch regenwoud in belangrijke mate kunnen ondersteunen. Op zichzelf vormen radar data echter geen afdoende basis voor bosinventarisatie- en bosmonitoringsprocedures. Voor de inventarisatie en/of het monitoren van bepaalde boskarakteristieken kan additionele geografische informatie benodigd zijn. Daarnaast is er ter controle van uit radarbeelden verkregen informatie altijd behoefte aan veldgegevens. Het is belangrijk dat men zich realiseert dat radar slechts een hulpmiddel is voor het verzamelen van bosinformatie. Uiteindelijk zijn het de partijen die betrokken zijn bij het beheer van tropisch bos die deze informatie moeten beoordelen. Op basis van hun bevindingen zullen deze partijen moeten besluiten of ingrijpen gewenst is en vervolgens zullen ze overeenkomstig hun besluit moeten handelen.

## About the author

Josephus Johannes (Joost) van der Sanden was born in Breda, The Netherlands, on 2 December 1960. In 1980 he finished his secondary education and started his studies at the Wageningen Agricultural University. From this university he received his B.Sc. and M.Sc. degrees in Forestry in 1984 and 1987, respectively. The M.Sc. study was completed with distinction. It consisted of a teachers training course and research projects in the fields of forest economics, town and country planning and remote sensing. His first introduction to tropical rain forests was in 1986 when he was involved in the preparations for a radar campaign initiated by the European Space Agency in the Brazilian Amazon. Upon completion of his studies in Wageningen he was awarded a scholarship by the British Council. This enabled him to enrol in an M.Sc. programme in Environmental Remote Sensing at Aberdeen University in Scotland (UK). In 1988 he graduated from Aberdeen University and returned to The Netherlands to take a position at the Wageningen Agricultural University.

At the Wageningen Agricultural University he was mainly involved in research but also lectured and tutored at both undergraduate and post-graduate levels. His research focused on the application of radar remote sensing to forestry. A five-year project that started in 1991 constituted the basis for his doctoral research. The results of this are presented in the current text. In the course of the project he spent a period of six months as a visiting scientist with the Canada Centre for Remote Sensing. During this time he worked on the analysis of the airborne radar data which was acquired in the framework of the 1992 South American Radar Experiment.

In early 1997 he resigned his position at the Wageningen Agricultural University and moved to Canada. Following the defence of his doctoral research he intends to begin working at the Canada Centre for Remote Sensing on a visiting fellowship awarded by the Natural Sciences and Engineering Research Council of Canada.

# Glossary

**Aggradation phase**: The phase in the development of a forest eco-unit which commences when woody plants close the canopy (Oldeman, 1990).

**Amplitude**: The maximum deviation of the electrical field of an electromagnetic wave; an indication of the strength of an electromagnetic wave.

**Angle of incidence**: See Incidence angle.

**Architecture**: See Forest architecture.

**Azimuth direction**: In radar images, the direction in which the aircraft or satellite is heading; also called flight direction.

**Backscatter**: See Radar backscatter.

**Biostatic phase**: The phase in the development of a forest eco-unit during which the average formation and dieback of living mass are equal to each other (Oldeman, 1990).

**Calibration**: See Radiometric calibration.

**Channel**: See Spectral band.

**Classification**: The arrangement of individual pixels or groups of pixels into classes and the assignment of a label (class name) to each of these pixels (Buiten and Clevers, 1993).

**Deforestation**: Change of land use with depletion of tree crown cover to less than 10 % (FAO, 1993).

**Degradation phase**: The phase in the development of a forest eco-unit when biostasis breaks down and loss of living mass exceeds its formation. This phase enables the forest to re-enter the innovation phase (Oldeman, 1990).

**Dielectric constant**: See Relative dielectric constant.

**Differential radar cross-section**: The radar cross-section per unit of area (of the region illuminated by radar) (Buiten and Clevers, 1993). See also Radar cross section.

**Eco-unit**: See Forest eco-unit.

**Electromagnetic spectrum**: The total wavelength range of electromagnetic waves (Buiten and Clevers, 1993).

**Foreshortening**: See Radar foreshortening.

**Forest architecture**: The visible, morphological, expression of the genetic blueprint of organic growth and development (Hallé et al., 1978).

**Forest degradation**: Changes within the forest class (from close to open forest), which negatively affect the stand or site and, in particular, lower the production capacity (FAO, 1993).

**Forest eco-unit**: Every surface on which at one moment in time a vegetation development has begun, of which the architecture, ecophysiological functioning and species composition are ordained by one set of trees until the end (Oldeman, 1990).

**Forest structure**: The mathematical expression of structure of the trees in a forest sample plot, e.g. as expressed by size (diameter or height) class distribution.

**Forest**: An ecosystem with a minimum of 10 % crown cover of trees and / or bamboos, generally associated with wild flora, fauna and natural soil conditions, and not subject to agricultural practices (FAO, 1993).

**Frequency**: The number of recurrences of a periodic phenomenon per unit of time. Electromagnetic waves are usually specified in Hertz (Hz), which is a unit of frequency equal to one cycle per second. See also Wavelength.

**Frequency band**: See Spectral band.

**Gamma** ($\gamma$): See Radar cross-section per unit projected area.

**Geographical-referencing**: Registration of images to the reference geometry of a map; also called georeferencing or geocoding (After Buiten and Clevers, 1993).

**Grazing angle**: Angle of viewing relative to the horizontal at the point of the object observed (Buiten and Clevers, 1993).

**Ground range distance**: The distance along the earth's surface from the nadir point to the object observed.

**Image**: A (usually latent) two-dimensional representation (in a formal sense) of the spatial structure of an object with respect to its spectral features, also called image raster (grid) (After Buiten and Clevers, 1993).

**Image segmentation**: The subdivision of an image in coherent parts or components, each being more or less homogeneous in a particular property. In addition, the neighbouring areas should be mutually different (Buiten and Clevers, 1993).

**Image texture**: The pattern of spatial distributions of grey tone (Haralick and Bryant, 1976).

**Incidence angle**: Angle of viewing relative to the vertical at the point of the object observed (After Buiten and Clevers, 1993).

**Innovation phase**: The phase in the development of a forest eco-unit which starts after the destruction of the original forest cover and which is characterised by the development of herbs, weedy climbers and tree seedlings (Oldeman, 1990).

**Interferometry**: Here SAR interferometry; a technique using the phase difference of two SAR observations of a same area on the ground taken from slightly different sensor positions. The interferogram derived from different observations has been demonstrated to be either a measure of terrain height (spatial interferometry) or of movement in the scene (time delay interferometry) (After CCRS, 1997).

**Layover**: See Radar layover.

**Look**: See Radar look.

**Microwave window**: No firm definition exists for the microwave window but a reasonable convention is that it is the window in the electromagnetic spectrum referring to radiation of wavelengths ranging from 0.1 to 100 cm (After Ulaby et al., 1981).

**Microwaves**: Electromagnetic radiation in the microwave window (Buiten and Clevers, 1993).

**Monitoring**: Following changes with the aim to correct them if necessary.

**Nadir point**: The point on the surface of the earth directly below the sensor system (After Lillesand and Kiefer, 1994).

**Optical sensor (system)**: Sensor system operating in the optical window of the electromagnetic spectrum.

**Optical window**: The window in the electromagnetic spectrum from ultraviolet to thermal infrared inclusive (wavelengths ranging from 0.30 to 14 μm) (Buiten and Clevers, 1993).

**Phenology**: Science of regular yearly patterns of visible events in a natural system, such as flowering, fruiting, leaf-fall and -flush and growth (After ter Steege, 1993).

**Pixel**: Acronym for picture element, the position of which is determined by means of the position in the image raster, and the appertaining numerical value is taken artificially from complete or partial resolution cells (Buiten and Clevers, 1993).

**Polarization**: The polarization of an electromagnetic wave describes the manner in which its electrical field vibrates. The electrical field can be seen as the vector sum of two components that vibrate in the horizontal and vertical plane, respectively. At any fixed point in space the electrical field vector is a function of time. As time changes, the tip of the electrical field vector traces a curve in the plane perpendicular to the direction of propagation. The nature of this curve can be defined by means of the ellipticity angle and orientation angle of the so-called polarization ellipse. When the curve is a straight line, the wave is said to be linearly polarized. When the curve is a circle, the wave is circularly polarized and when it forms an ellipse, the wave is elliptically polarized. In case of circular or elliptic polarization, the tip may move either clockwise or counter clockwise. To distinguish between the two, the wave is said to be right-handed polarized, when the right-hand thumb points in the direction of propagation while other fingers point in the direction of the tip motion. Similarly, if that description fits the left-hand thumb and fingers, the wave is left-hand polarized (After Ulaby et al., 1981).

**Power density**: The power incident on a surface, expressed per unit of area ($Wm^{-2}$) (Buiten and Clevers, 1993).

**Power**: The quantity of energy in the form of electromagnetic waves or photons moving from one point to another per unit of time. For a given signal, the power is proportional to the amplitude, squared, per unit of time (After Buiten and Clevers, 1993).

**Radar**: Acronym for radio detection and ranging; a device for transmitting microwaves and the subsequent recording of waves reflected by objects within its volume of coverage (After Buiten and Clever, 1993).

**Radar backscatter**: Radar echo; the process of scattering of microwave energy by an object in the direction of the radar antenna, after actively being irradiated by the radar source (Buiten and Clevers, 1993).

**Radar cross-section per unit projected area**: The radar cross-section per unit of area projected in the direction of transmission (Buiten and Clevers, 1993). See also Radar cross section.

**Radar cross-section**: A hypothetical area of an object of such an extent that if the power intercepted by this area is distributed isotropically over the space, it renders the same power density at the receiving antenna as the power density brought about in reality by the presence of the object. Usually the radar cross section concerning compound objects (distributed targets) is normalised: either as a radar cross section per unit of area (sigma nought or differential radar cross-section) or as a radar cross section per unit of area projected in the direction of transmission (gamma or radar cross-section per unit projected area) (Buiten and Clevers, 1993).

**Radar echo**: See Radar backscatter.

**Radar foreshortening**: The phenomenon by sideways-looking radar that the base of a sloped surface is imaged earlier than the top; the size of the sloped surface is compressed on the image (After Lillesand and Kiefer, 1994).

**Radar layover**: The phenomenon by sideways-looking radar that the top of a high object is imaged earlier than the foot, as the top is nearer to the antenna than the foot (or its fictitious vertical projection on to the ground reference plane) (Buiten and Clevers, 1993).

**Radar look**: A single measurement of the backscatter from an object observed.

**Radar sensor (system)**: Sensor system operating in the microwave window of the electromagnetic spectrum.

**Radar shadow**: The phenomenon that the terrain behind high objects cannot be observed by sideways-looking radar, so that no echo returns (Buiten and Clevers, 1993).

**Radiometric calibration**: The process of characterising the performance of the end-to-end radar system, in terms of its ability to measure the amplitude (and phase) of the backscattered signal (Curlander and McDonough, 1991).

**Radiometric resolution**: The smallest observable difference in energy in the form of electromagnetic waves or photons with respect to reflection, emission, temperature differences, power differences, etc. (After Buiten and Clevers, 1993).

**Range direction**: The direction in which pulses of microwave energy are transmitted by a radar system. The range direction is normal to the azimuth or flight direction.

**Relative dielectric constant**: Electrical property of material, relative to that of free space, partly determining the radar backscatter (After Buiten and Clevers, 1993)

**Remote sensing**: The instrumentation, techniques and methods to observe the earth's surface at a distance and to interpret the images or numerical values obtained in order to acquire meaningful information of particular objects on earth (Buiten and Clevers, 1993).

**Rescaling**: Application of a change of scale to observed values, where usually a linear mathematical function is employed (After Buiten and Clevers, 1993).

**Resolution cell**: In radar, a three-dimensional cylindrical volume surrounding each point in the scene. The cell range depth is slant range resolution, its width is azimuth resolution, and its height, which is conformal to the illumination wavefront, is limited only by the vertical beam width of the antenna pattern. Resolution cell often is defined with respect to the local horizontal (CCRS, 1997).

**Scatterer**: Any object capable of reflecting incident radar waves.

**Scatterometer**: In general, a non-imaging instrument to measure either the sigma nought or gamma (After Buiten and Clevers. 1993).

**Segmentation**: See Image segmentation.

**Sensor**: Instrument sensitive to a particular physical quantity (radiation). It is able to transpose this quantity into a photographical or electrical value (Buiten and Clevers, 1993).

**Sigma nought** ($\sigma^{\circ}$): See Differential radar cross-section.

**Silvigenesis**: Forest-making; the complex process by which forest architecture is built (Oldeman, 1983a).

**Slant range distance**: The direct distance from the radar to the object observed.

**Spatial resolution**: A theoretical measure of the smallest detail that can be detected (or the smallest spatial distance between two objects, usually expressed in radians or metres) (After Buiten and Clevers, 1993).

**Speckle**: The phenomenon of a strong variation of echo signals from one resolution cell to another occurring in radar, because the echo received consists of the summation of the contributions of a collection of scatterers in each resolution cell, in continuously changing combinations (interference) (After Buiten and Clevers, 1993).

**Spectral band**: A well-defined continuous range (interval) of wavelengths in the electromagnetic spectrum; wavelength band, frequency band, channel (Buiten and Clevers, 1993).

**Sustainable forest management**: The process of managing permanent forest land to achieve one or more clearly specified objectives of management with regard to the production of a continuous flow of desired forest products and services without undue reduction of its inherent values and future productivity and without undue undesirable effects on the physical and social environment (ITTO, 1992).

**Synthetic aperture radar** (SAR): radar system with a high spatial resolution in the flight direction as every terrain element observed in the flight direction for a longer time. Each return signal is recorded in amplitude and phase for a slight displacement of the antenna in the flight direction. The effect of a considerable larger antenna is obtained synthetically by storing and combined processing of these multiple echoes. The SAR method operates only when the radar radiation is coherent (Buiten and Clevers, 1993).

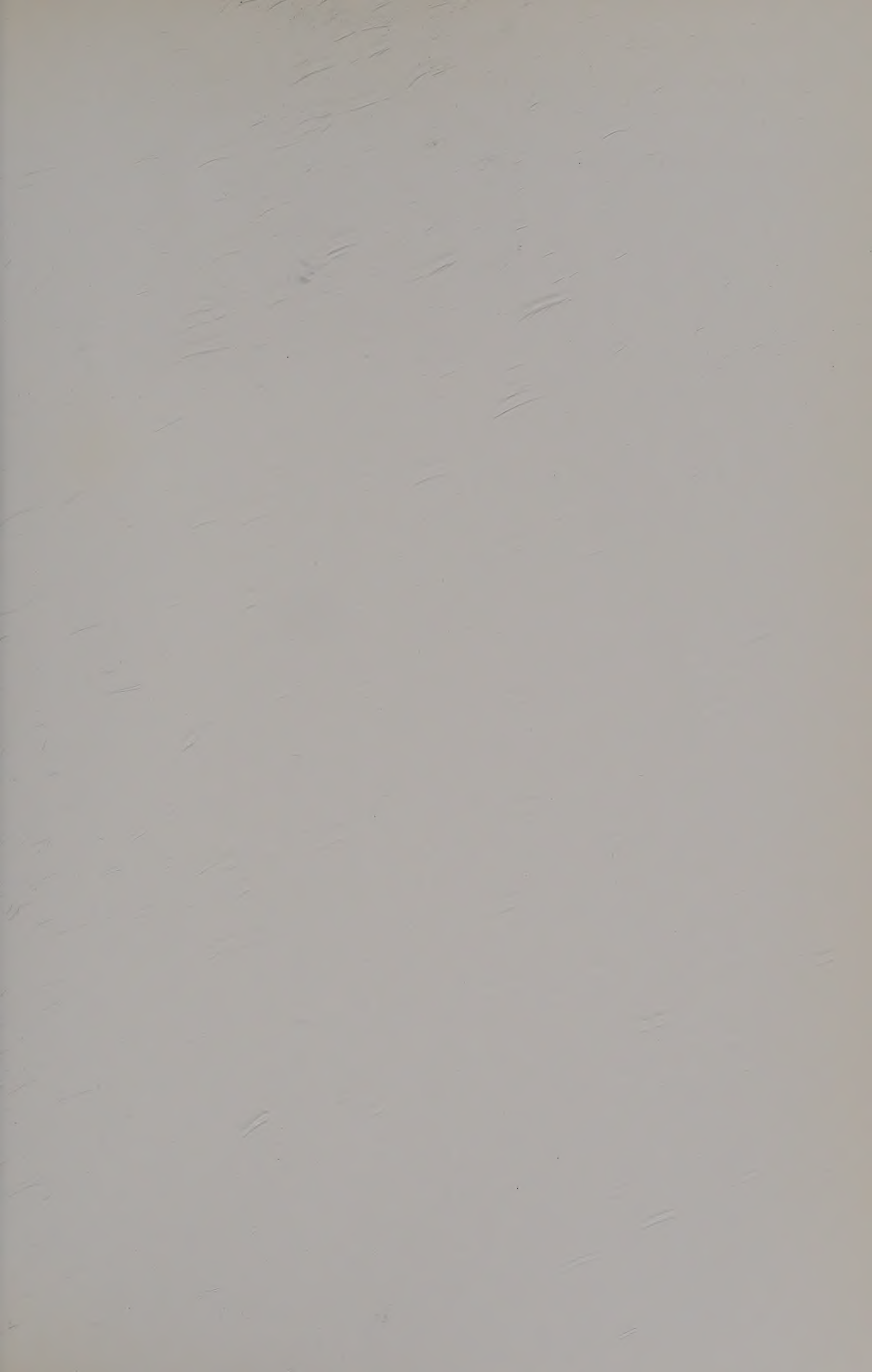
**Textural attribute**: Function assigning a numerical value to the original image texture (After Buiten and Clevers, 1993).

**Texture**: See Image texture.

**Transmission**: The process of transmitting electromagnetic waves (Buiten and Clevers, 1993).

**Wavelength**: The distance a wave will travel in the time required to generate one cycle. The distance between two consecutive wave peaks (or other reference points) in space. See also Frequency.

**Wavelength band**: See Spectral band.










ISBN
90-5485-778-1